Spring 2015

Origin and stratigraphic architecture of the Middle Permian lower and upper Quanzijie low-order cycles, Bogda Mountains, NW China

Jonathan Obrist-Farner
Missouri University of Science and Technology, obristj@mst.edu

Department: Geosciences and Geological and Petroleum Engineering

ORIGIN AND STRATIGRAPHIC ARCHITECTURE OF THE MIDDLE PERMIAN LOWER AND UPPER QUANZIJIE LOW-ORDER CYCLES, BOGDA MOUNTAINS, NW CHINA

by

JONATHAN OBRIST FARNER

A DISSERTATION

Presented to the Faculty of the Graduate School of the

MISSOURI UNIVERSITY OF SCIENCE AND TECHNOLOGY

In Partial Fulfillment of the Requirements for the Degree

DOCTOR OF PHILOSOPHY

in

GEOLOGY AND GEOPHYSICS

2015

Approved by

Wan Yang, Advisor
John P. Hogan
David J. Wronkiewicz
Francisca Oboh-Ikuenobe
Neil Tabor

PUBLICATION DISSERTATION OPTION

This dissertation has been prepared in publication format. Section 1, pages 1 to 3, introduce the project. Paper I, pages 4 to 60, is titled "Nonmarine Time Stratigraphy in a Rift Setting: An Example from the Mid-Permian Lower Quanzijie Low-Order Cycle, Bogda Mountains, NW China," and was prepared for publication in the Journal of Palaeogeography, Volume 4, Number 1, in 2015. Paper II, pages 61 to 133, is titled "Loess and Fluvial Deposits and Their Implications on Paleoclimatic Conditions During an Icehouse-Hothouse Transition, Capitanian Upper Quanzijie Low-Order Cycle, Bogda Mountains, NW China," and was written in the form of a manuscript to be submitted to Sedimentology. Paper III, pages 134 to 195, is titled "Provenance and Depositional Conditions of Fluvial Sandstones and Their Controlling Processes in a Rift Setting, Mid-Permian Lower and Upper Quanzijie Low-Order Cycles, Bogda Mountains, NW China," and was written in the form of a manuscript to be submitted to Journal of Sedimentary Research.

ABSTRACT

This study is carried out in the Bogda Mountains, NW China, and aims to provide a detailed sedimentary, stratigraphic, environmental, and paleoclimatic reconstruction in the paleo-mid-latitude along the east coast of Pangea. The Middle Permian lower and upper Quanzijie low-order cycles (QZJ LCs) provide a nearly complete sedimentary record in an area were little is known. In the first part of this work, the previously-established QZJ LC is divided into two LCs on the basis of regional stratigraphic correlation and major changes in depositional environments and tectonic and climatic processes. The newly-established lower QZJ LC is mainly composed of meandering streams and associated overbank deposits that formed under a semiarid climate with strong precipitation seasonality and its delineation demonstrates that a process-response approach is effective in time-stratigraphic analysis of complex nonmarine fluvial-lacustrine strata. In the second part of this work, the depositional environments of the upper QZJ LC are interpreted as a mixture of meandering and ephemeral stream and loess deposits. Loess in the region is poorly-documented and its presence indicates persistent arid to semiarid conditions during upper QZJ LC. The uppermost part of the upper QZJ LC records a major climatic change to humid-subhumid as a result of the global icehouse to hothouse transition. Finally, the fluvial conglomerates and sandstones in the lower and upper QZJ LCs are interpreted as being derived from the northern Tian Shan volcanic arc to the south and from local rift shoulders. This study provides a detailed sedimentologic, stratigraphic, environmental, and paleoclimatic reconstruction in an area were little is known and aims to provide a record in an important time period in the Earth's history when major climatic and biotic changes occurred.

ACKNOWLEDGMENTS

I would like to express my deep appreciation to my advisor Dr. Wan Yang for his knowledge, support, advice, life lessons, and motivation during the completion of this degree. Without him, this work would have not been possible. I would like to thank all the members of my committee and the entire Geology and Geophysics faculty and staff for their help, support, and encouragement. I thank the Donald Radcliffe Trust, Alfred Spreng Award, AAPG, GSA, and GCSSEPM for funding my studies and fieldwork in China.

Special thanks to my fellow graduate students Zhixin Li, Wei Guan, Angelica Alvarez, Dr. Carlos Sanchez, Robert Haselwander, Bin Sun, Abdullah Nabhan, Dr. Ahmed Elsheikh, and Abdurraouf Okok for their help, patience, and insightful conversations and/or assistance during my work, and to Drs. J. Wang, M.L. Wan, Y. Yang, Y. Liu, X. Luo, Q. Feng, and S.S. Wang, and J.J. Liu, T. Foster, J.J. Li, L.L. Cheng, C.C. Zhou, and Y.M. Gao for field assistance, funding, and/or logistic help.

Special thanks to my parents, my brothers' and sisters' family, and my family-in-law for their continued support and encouragement. Without them, this work would have not been possible.

Finally, and most importantly, I would like to thank my beautiful wife and daughters for their support, encouragement, and love. Their sacrifice was a source of inspiration during the long days of work. This is for them.

TABLE OF CONTENTS

LIST OF ILLUSTRATIONS

Page

PAPER I

PAPER II

LIST OF TABLES

Page

PAPER II

PAPER III

1. INTRODUCTION

Permian terrestrial sedimentary records provide important clues on paleoclimatic conditions and their changes during the last icehouse to hothouse transition in a vegetated planet and a deep time perspective into the driving mechanisms and possible outcomes of such transition (Isbell et al., 2008). However, scarcity of Permian sedimentary records in NE Pangea (e.g., Metcalfe et al., 2009; Yang et al., 2010; Thomas et al., 2011; Sheldon et al., 2014) have hampered the overall understanding of the climatic conditions and changes that occurred during this time in the Earth's history. Moreover, these terrestrial records are difficult to correlate because they are stratigraphically complex, with abundant erosional surfaces, rapid lateral and vertical facies and thickness changes, multiple sediment sources, and poor biostratigraphic and geochronologic resolution (Miall, 1996; Talbot and Allen, 1996; Olsen, 1997; Blum and Törnqvist, 2000; Lowenstein et al., 2003). The complexity makes time-stratigraphic correlation difficult, which is needed for accurate sedimentologic, paleoclimatic, and paleogeographic reconstructions.

This study focuses on the Middle Permian lower and upper Quanzijie low-order cycles (abbreviated as QZJ LC) that are superbly-exposed in the Tarlong-Taodonggou and Dalongkou areas of the Bogda Mountains, NW China. The QZJ LCs were deposited in the Greater Turpan-Junggar Basin. The tectonic setting and evolution of the basin, however, are poorly understood. Proposed models vary from extension, transtension, and collision, with a volcanic arc to the south (Hsu, 1988; Carroll et al., 1990; Allen et al., 1995; Shao et al., 2001; Wartes et al., 2002; Greene et al., 2005). Structural complexities in the region, with abundant reactivated orogenic belts and long thrust and strike-slip

faults (e.g., Carroll et al., 1995; Carroll et al., 2010), hinder the overall understanding of the history of the basin. Compositional and textural characteristics of sandstones have been commonly used to interpreted depositional and paleoclimatic conditions, basin types, and tectonic settings (Dickinson and Suczek, 1979; Dickinson et al., 1983; Dickinson, 1985; Suttner and Dutta, 1986). Therefore, the sandstones deposited in the Turpan-Junggar Basin can provide clues about the depositional conditions, tectonic setting, and evolution of the Turpan-Junggar basin during the Middle Permian.

Field, petrographic, and geochemical observations and results are collected from seven stratigraphic sections; six sections from the Tarlong-Taodonggou area and one section from the Dalongkou area. The previously established QZJ LC (e.g., Yang et al., 2007; 2010) is subdivided into two LCs using a process-response approach combining multiple sedimentologic and stratigraphic proxies. This is achieved by a high-resolution cyclostratigraphic correlation among six stratigraphic sections in a 60 km^2 study area. The lower QZJ LC is composed mainly of meandering streams and associated overbank deposits and formed under persistent semiarid conditions with strong precipitation seasonality. The upper QZJ LC is composed mainly of ephemeral braided-streams deposits, coarse-grained meandering-streams with associated overbank deposits, and loess deposits and formed under persistent semiarid to arid conditions. Loess in the region indicates that persistent aridity, eolian processes, and trapping mechanisms existed in NE Pangea during Capitanian time to transport, deposit, and trap a large volume of silt and clay as loess. The uppermost part of the upper QZJ LC recorded a dramatic climatic shift to humid-subhumid conditions. The shift is interpreted to correspond to warmer and

wetter conditions that resulted from the demise of the Late Paleozoic Ice Age at the end of the Capitanian (Fielding et al., 2008).

Compositional and textural characteristics of the lower and upper QZJ sandstones remain constant. A slight increase in compositional maturity and increase in pedogenic features in the sandstones from the upper part of the upper QZJ LC in Tarlong-Taodonggou could be caused by a change from arid to humid conditions. In addition to the well-known volcanic arc source to the south of the Turpan-Junggar basin (e.g., Shao et al., 2001; Greene et al., 2005), rift shoulders are identified as secondary sources for the sandstones in the Tarlong-Taodonggou area and as main sources for the Dalongkou sandstones. The petrographic results substantiate previous interpretations that the basin during Middle Permian was a rift basin with abundant sediments derived from rocks exposed in rift shoulders.

This study demonstrates that a process-response approach is effective in identifying regional time surfaces in fluvial-lacustrine settings. It improves the overall understanding of the climatic conditions and changes in NE Pangea during the Middle Permian. The results provide clues about the controlling processes on the compositional and textural characteristics of the sandstones and on the tectonic setting and paleogeography of the Turpan-Junggar basin during Middle Permian.

PAPER

I. NONMARINE TIME-STRATIGRAPHY IN A RIFT SETTING: AN EXAMPLE FROM THE MID-PERMIAN LOWER QUANZIJIE LOW-ORDER CYCLE, BOGDA MOUNTAINS, NW CHINA

Jonathan Obrist-Farner and Wan Yang

Abstract

Sedimentological and stratigraphic study of seven stratigraphic sections of Permian Hongyanchi and Quanzijie low-order cycles (LCs) in Tarlong-Taodonggou half graben and Dalongkou area in Bogda Mountains, NW China, demonstrate effective approaches and methodology in cyclo- and time-stratigraphic analyses of complex fluvial-lacustrine deposits in an intracontinental rift setting. A new synchronous stratigraphic unit, the lower Quanzijie LC was defined. The lower and upper boundaries of the cycle are regionally correlative disconformity, erosional unconformity, and conformity, across which significant and abrupt changes in paleoenvironments and tectonic and climatic conditions occurred. The lower boundary is an erosional unconformity and disconformity with a high-relief topography that juxtaposes lacustrine deposits of underlying Hongyanchi LC with overlying meandering stream deposits of lower Quanzijie LC, and was caused by a regional tectonic uplift. The upper boundary is a disconformity and local erosional unconformity and conformity, juxtaposing stacked paleosols developed on fluvial sediments with overlying fluvial and loessial deposits of the upper Quanzijie LC. The paleosols indicate landscape stability and a prolonged period of subaerial exposure and minimal deposition and suggest that climatic condition was semi-arid with strong precipitation seasonality in the Tarlong-Taodonggou area and

subhumid in Dalongkou area. The fluvial-loessial deposits indicate a renewed tectonic uplift and a change in the atmospheric circulation pattern. The newly-defined lower Quanzijie LC facilitates accurate paleogeographic reconstruction in the study area during a period of major tectonic and climatic changes. The interpreted tectonic and climatic conditions provide a critical data point in the mid-latitude east coast of NE Pangea during the mid-Permian icehouse-hothouse transition. The results demonstrate that a process-response approach is effective in time-stratigraphic analysis of complex fluvial-lacustrine strata in a highly-partitioned rift basin.

1. Introduction

Continental deposits are stratigraphically complex, caused by abundant erosional surfaces, rapid lateral and vertical facies and thickness changes, multiple sediment sources, and a poor biostratigraphic resolution (Miall, 1996; Talbot and Allen, 1996; Olsen, 1997; Blum and Törnqvist, 2000; Lowenstein et al., 2003). This intrinsic complexity makes time-stratigraphic correlation difficult, which is needed for accurate paleogeographic reconstructions. A time-stratigraphic approach to fluvial-dominated but marine-influenced strata has been successfully applied (Shanley and McCabe, 1994) because the processes controlling the formation of correlative sedimentary packages and associated surfaces can be related to shoreline shifts (Catuneanu, 2006). However, the approach to intracontinental fluvial-lacustrine settings is not effective due to interplay of allogenic and autogenic controls on fluvial-lacustrine sedimentation not associated with shoreline shift (Shanley and McCabe, 1994; Catuneanu, 2006). Previous studies in nonmarine sequence stratigraphy have used a wide variety of evidence, for example, fluvial styles (Legarreta and Uliana, 1998), petrographic data (Miall and Arush, 2001)

and paleosols (Bown and Kraus, 1987; Kraus and Bown, 1988; Kraus, 1999) to subdivide valley fills into correlative sequences. But successful studies are limited.

This study focuses on the transition interval between the Hongyanchi (HYC) and Quanzijie (QZJ) low-order cycles (LCs) in the Tarlong-Taodonggou half graben in southern Bogda Mountains and the Dalongkou area in the north, NW China (Yang et al., 2010). We demonstrate the complexities in fluvial valley fills and establish a time-stratigraphic correlation using a process-response approach combining multiple sedimentologic and stratigraphic proxies. A new regional time-stratigraphic surface is identified, resulting in the definition of a new time-stratigraphic unit – the lower QZJ LC. This is achieved by a high-resolution cyclostratigraphic correlation among six stratigraphic sections in a 60-km^2 study area. Otherwise, miscorrelation would be inevitable. The lower cycle boundary is mainly of a tectonic origin, whereas the upper boundary a mixed climatic and tectonic origin. The paleogeographic evolution of the study interval is clearly depicted. This study improves the understanding of basin-filling processes in half grabens.

2. Geological Background

The Permian Hongyanchi and Quanzijie formations are widely present in the outcrops and the subsurface of the greater Turpan-Junggar rift basin, NW China (Figs. 1, 2, 3). This study focuses on the Tarlong-Taodonggou and Dalongkou areas in the southern and northern foothills of Bogda Mountains, respectively, in southeastern Kazakhstan Plate, NE Pangea, between ~40 to 50^0 N paleo-latitude (Fig. 1A; Allen et al., 1995; Carroll et al., 1995; Sengor and Natal'in, 1996; Scotese, 2002; Yang et al., 2010). The basin has many grabens formed by intracontinental rifting since the latest

Carboniferous (Yang, 2008; Yang et al., 2013). The Tarlong-Taodonggou area was interpreted as a half graben on the basis of rapid lateral facies changes of uppermost Carboniferous to Lower Triassic deposits (Yang et al., 2010).

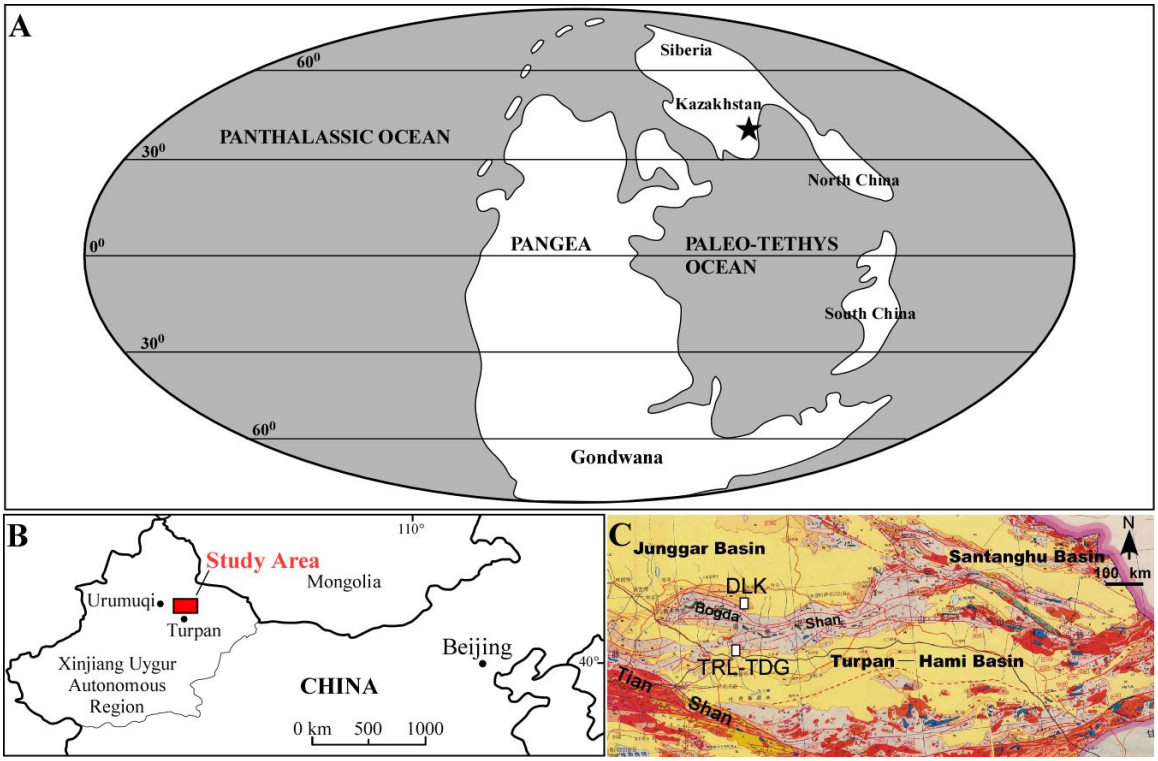

Figure 1. A) Global paleogeographic reconstruction for the Late Permian. Modified from Scotese (2002). The location of the study area is marked with a black star. B) Location of the study area in Xinjiang Uygur Autonomous Region, NW China. C) Geological map of eastern Xinjiang, showing locations of Tarlong-Taodonggou (TRL-TDG) and Dalongkou (DLK). Modified from XBGMR (1993).

The Hongyanchi (HYC) and Quanzijie (QZJ) low-order cycles (LCs) are informal cyclostratigraphic units defined on the basis of long-term trends of environmental, tectonic, and climatic conditions by Yang et al. (2007; 2010), and correlative largely to the Hongyanchi and Quanzijie formations (Fig. 3; XBGMR, 1993; Cai, 1999; Zhu et al., 2005). The chronostratigraphy is poorly constrained by bio- and litho-stratigraphy

(Wartes et al., 2002; Zhu et al., 2005; Metcalfe et al., 2009). Recent U-Pb zircon IDTIMS ages from Yang et al. (2010) constrain the HYC LC to a Sakmarian-Artinskian age. They also placed the QZJ LCs as Capitanian and estimated that the hiatus represented by the HYC-QZJ unconformity may span up to ~14 Ma. Finally, they interpreted the disconformity on top of stacked Calcisols in north Tarlong and Taodonggou and a channel base in southeast Tarlong as the boundaries between the HYC and QZJ LCs. The north Tarlong and Taodonggou sections were described in detailed in their study. With five additional sections, the present contribution rectifies a miscorrelation made by Yang et al. (2010), and establishes two new low-order cycles, namely, the lower and upper QZJ LCs in the interval from the upper part of HYC and the lower part of QZJ LCs of Yang et al. (2010).

3. Data and Methodology

Seven stratigraphic sections from the upper part of the HYC LC to the lower part of the QZJ LC, both of which were defined previously by Yang et al. (2010), are measured at a cm-dm scale, including six sections in the Tarlong-Taodonggou half graben, and one in the Dalongkou area (Fig. 2). Lithology, sedimentary structures and texture, fossil content, boundary relationship, and stratal geometry of individual rock units from each section are studied. The lateral thickness and lithological variations of the individual units are described and, in some cases, measured, across outcrops commonly 50-300 m wide. The data is used to define lithofacies; their characteristics, combined with thickness and lithologic stacking patterns and lateral variations, are used to interpret depositional environments.

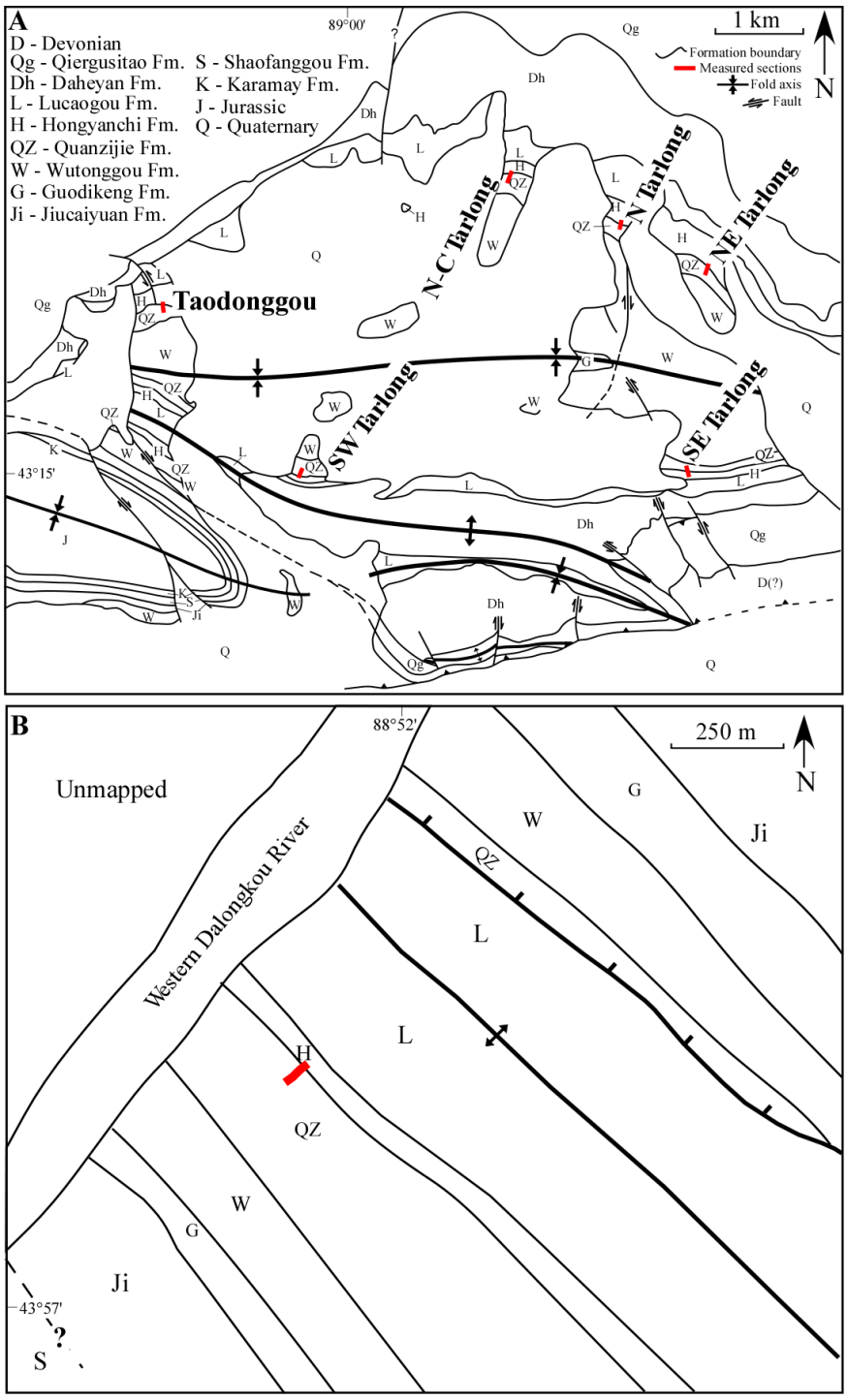

Figure 2. Geologic maps of Tarlong-Taodonggou (A) and Dalongkou (B) areas showing names and location (red lines) of measured sections. The former is modified from Yang et al. (2010).

Subsequently, sedimentary cycles are delineated using the criteria and methodology of Yang et al. (2010), who recognized three orders of cycles in the Tarlong-Taodonggou area. A high-order cycle (HC) is defined by repetitive changes of interpreted depositional environments commonly associated with lake expansion and contraction, or repetitive changes between erosion/nondeposition and deposition as the case of fluvial erosion and deposition (Yang et al., 2010). HCs are regarded as basic cyclostratigraphic entities and provide a framework to facilitate interpretations of processes and factors controlling erosion, nondeposition, deposition, and environmental changes. A low-order cycle is defined by a group of HCs showing similar environmental variations and formed under persistent tectonic and/or climatic conditions, and bounded by low-order cycle boundaries across which major tectonic and/or climatic changes and associated environmental shifts occurred. These boundaries should be correlative graben-wide or basinwide. Yang et al. (2010) also defined intermediate-order cycles, where systematic stacking of HCs can be linked clearly with lake expansion and contraction. However, definition of intermediate-order cycles is not the focus of this study and is not carried out.

In addition, a total of 19 thin sections of sandstone, shale, mudstone, calcitic nodule, and limestone samples from the study interval are studied under a petrographic microscope. Grain composition, size, sorting, roundness, and contact, matrix-to-grain ratio, and type of cement are documented. The information is used to supplement and substantiate field observations in lithofacies definition and environmental interpretation.

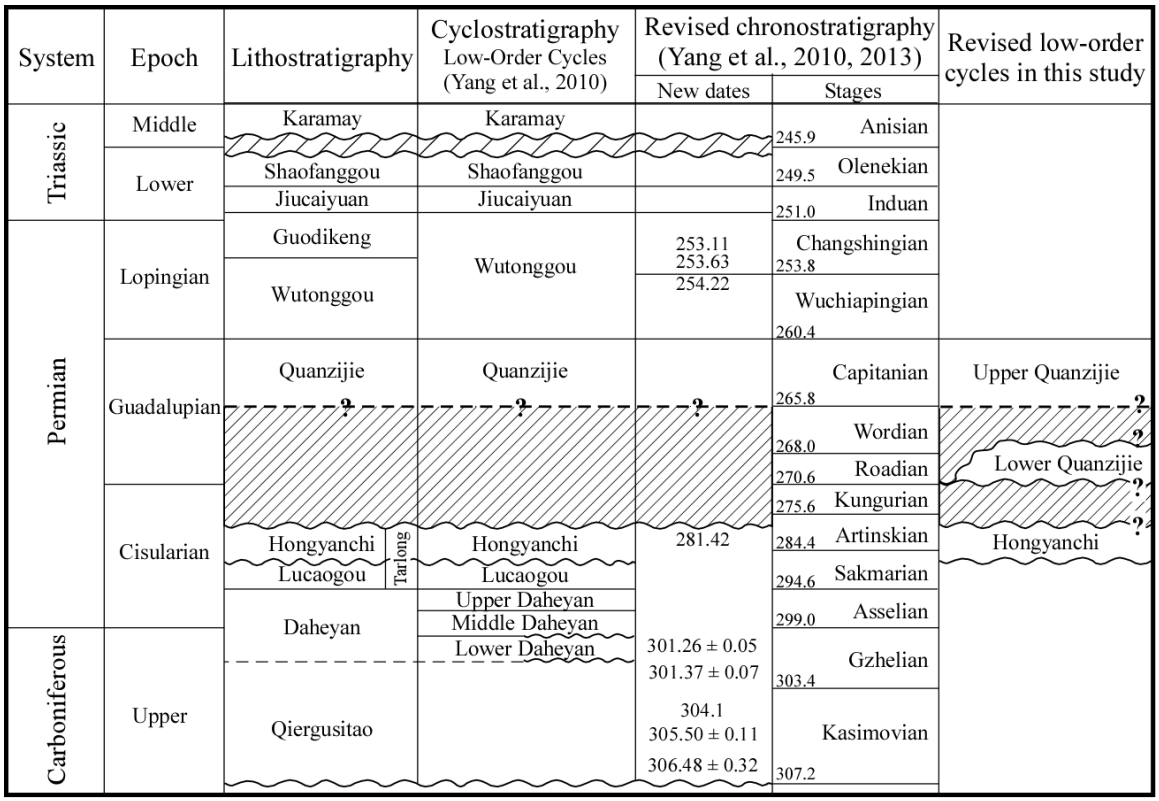

Figure 3. Chrono-, litho-, and cyclostratigraphy of Upper Carboniferous-Lower Triassic strata in the Tarlong-Taodonggou area. The newly-defined lower Quanzijie low-order cycle is bounded by disconformities and erosional unconformities, but its age is poorly constrained. Wavy lines are major unconformities; dashed lines disconformity; and hatched areas missing strata. Absolute ages at stage boundaries from Gradstein et al. (2004). Modified from Yang et al. (2010, 2013).

4. Lithofacies and Their Depositional Environment

Five lithofacies are identified in the study interval and were interpreted as fluvial, lacustrine, or eolian deposits. Their characteristics, stacking patterns, and interpreted depositional environments are essential to subsequent cyclostratigraphic analysis and interpretation of major autogenic and allogenic processes controlling sedimentation.

4.1 Lithofacies 1 – Clast-Supported Conglomerate

Clast-supported conglomerates are common in the study interval. Those in the Tarlong-Taodonggou half graben are dominantly igneous, whereas those in Dalongkou mainly sedimentary. The gravels range from cobble to granule size, mainly pebble size. They are moderately to well sorted and angular to subrounded. A sandy matrix is common. The gravels are commonly imbricated or parallel to bedding plane. Large-scale tabular and trough cross beddings are common. The base of the conglomerates is erosional and concave upward, whereas the top is commonly flat and gradational. Three types of conglomerates are differentiated on the basis of stratal geometry, sedimentary structure, and grain size trend. The first type is 2-5 m thick, has a clear fining-upward grain size trend, a high-relief erosional base, and is laterally persistent for 100s of m (Fig. 4A). The second type is 0.5-2 m thick, does not have a clear fining-upward trend but a low-relief erosional base, and is laterally persistent for 10s of m. The second type changes abruptly to the overlying mudrocks with minimal or no sandstones, and is encased in mudrocks (Fig. 4B). The third type is rare, 0.2-0.5 m thick, has no clear grain size trend but a sharp base, and is laterally persistent for 100s of m. It is well sorted and rounded, and commonly overlain by dark gray shales with a sharp to gradational contact.

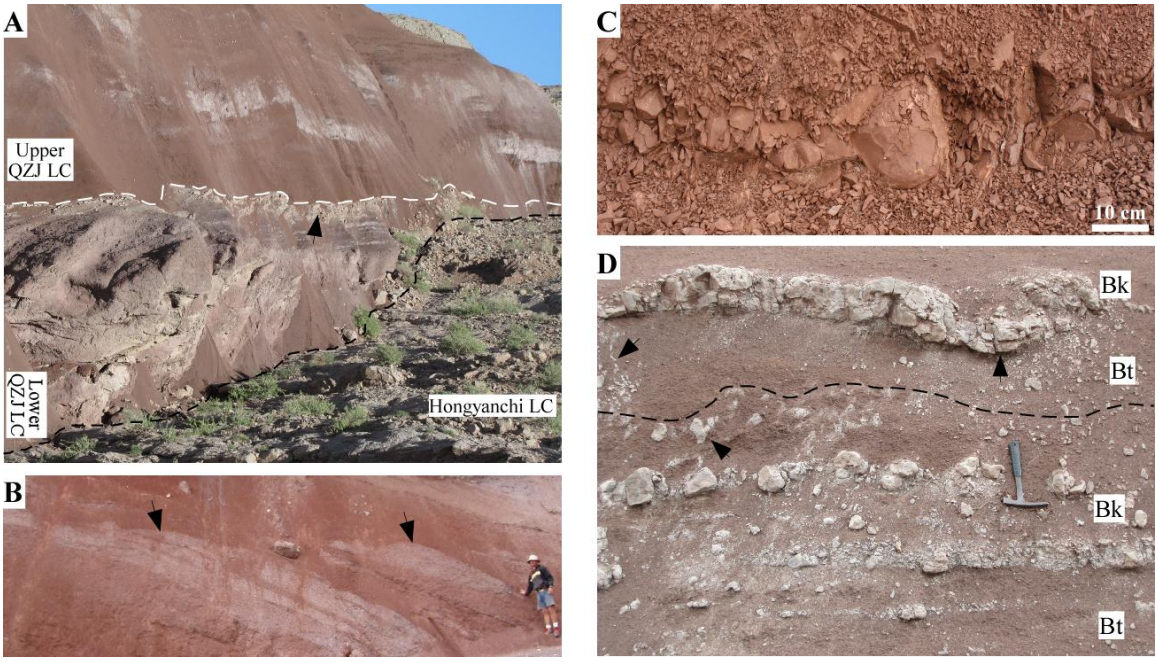

Figure 4. Field photographs showing features of some lithofacies. A) Western section in northeastern Tarlong showing a meandering stream channel cutting into underlying algal-laminated wackestone of Hongyanchi LC with a 5-m relief, forming an erosional unconformity (black dashed line) as the boundary between the HYC and lower QZJ LCs. The channel-fill conglomerate and sandstone change laterally into thin overbank deposits to the right (west), both of which are capped by a thin white-gray calcrete of the upper Calcisol (arrow; see text). The upper part is reddish purple loessite encasing thin and narrow, gray conglomerate bodies with a sharp base as ephemeral-stream channel fills in basal upper QZJ LC. White dashed line is the boundary between lower and upper QZJ LCs. B) Basal upper QZJ LC showing small gray ephemeral-stream channel-fill conglomerate bodies with a sharp base (arrows) encased in reddish purple loessite. The beds are overturned; stratigraphic-up is to lower left. Person is 1.9 m tall. Taodonggou section. C) A trench profile in basal upper QZJ LC, showing reddish purple to brown, blocky, massive loessite containing multi-faceted peds. The overall stratal dip is to the left, but no bedding is present in the loessite. Stratigraphic up is to the left (north). Southeastern Tarlong section. D) Two stacked Calcisols separated by a black dashed line in the eastern section of northeastern Tarlong, showing Bk horizons rich in light gray calcitic nodules and calcretes and Bt horizons rich in illuvial clay. Crude antiforms and synforms (arrows) can be discerned by geometry of calcretes and preferential alignment of nodules. The top of the upper calcrete is the boundary between lower and upper QZJ LCs. Hammer is 24 cm long.

The clast supported fabric, erosional base, tabular and trough cross bedding, imbricated gravels, and overall fining-upward grain size trend indicates that the first two types of conglomerates are stream channel deposits. The large thickness and high-relief erosional base of the first type underlie sandstones and mudrocks and is interpreted as channel-lag and point-bar deposits in meandering streams. In contrast, the thin and laterally-limited conglomerates of the second type were likely deposited in small, poorly-defined stream channels poor in sand and mud, mostly commonly associated with ephemeral gravelly braided streams (Miall, 1996). The third type of conglomerates is interpreted as lacustrine beach or littoral deposits on the basis of their sheet-like geometry and mature texture.

4.2 Lithofacies 2 – Sandstones

Sandstones in the studied sections are lithic wackes to arenites. Framework grains range from very fine to very coarse sand, with floating granules and pebbles, and are subangular to rounded. Basaltic lithics dominate in Tarlong-Taodonggou, whereas sedimentary lithics in Dalongkou. The sandstone lithofacies is subdivided into three subfacies on the basis of their depositional environments interpreted based on their textural and structural characteristics, fossil content, stratal geometry of individual sandstone units, vertical and lateral variations in grain size and thickness, boundary relation, and stacking pattern with adjacent lithofacies.

4.2.1 Lithofacies 2a – Fluvial Sandstone Subfacies

Three types of fluvial sandstones are distinguished. The first type has limited lateral extent and overlies ephemeral-stream conglomerates. The sandstones are lithic subarenite to wacke, and contain medium to very coarse sands with common floating granules and pebbles. The grains are subangular to subrounded. Internal erosional surfaces, plane beds, and trough and low-angle tabular cross beds are common. This type of sandstone is thin and occurs sporadically. The second type is thick lithic arenite to subarenite and occurs in fining-upward conglomerate-sandstone-mudrock successions. Sand grains are medium to very coarse, subangular to subrounded, and moderately to poorly sorted. Internal erosional surfaces and trough and tabular cross beds are common. Accretionary surfaces are apparent in many cases. Finally, the third type consists of very fine to fine-grained lithic wackes, and commonly occurs as thin, lenticular beds in mudrock-rich intervals.

The first type of fluvial sandstones is interpreted as waning-flow sandy deposits associated with ephemeral-stream conglomerates. The second type is interpreted as laterally-accreting point-bar deposits associated with underlying channel-lag conglomerate and overlying shale of an overbank origin (see below). The third type of sandstones is interpreted as deposits in a mud-rich meandering stream overbank environment.

4.2.2 Lithofacies 2b – Lakeplain-Littoral Sandstone Subfacies

This subfacies contains lithic arenite and subarenite. Sand grains are very fine to medium, with scattered floating granules, moderately well to very well sorted, and

subangular to subrounded. Climbing ripple cross laminations, hummocky cross stratifications, and tabular cross beds are common; mottling and burrowing are present. The sandstones are moderately calcareous, thin, and laterally persistent. The high textural maturity and thin sheet-like geometry suggest a well-washed origin in a lacustrine beach or littoral environment.

4.2.3 Lithofacies 2c – Deltaic Sandstone Subfacies

This subfacies includes lithic arenite to subarenite and forms an upward-coarsening trend within the subfacies and, in many cases, with the underlying shale and/or overlying conglomerate. Sand grains range from very fine to very coarse, with occasional floating granules. The sandstones are commonly well sorted and moderately to well rounded, contain low-angle tabular cross beds, climbing ripple cross laminations, ripple marks, burrows, and plant remains. They are 10s of cm to several m thick and laterally persistent for 100s m. The distinctive coarsening upward trend and absence of an erosional base suggest that this subfacies is delta front deposits.

4.3 Lithofacies 3 – Mudrocks

Mudrocks in the study interval have diverse characteristics formed in different environments. Three subfacies are identified on the basis of their vertical and lateral extent, grain size trends, bedding types, fossil content, and stacking pattern with vertically adjacent lithofacies.

4.3.1 Lithofacies 3a – Shale Subfacies

Shale is commonly green, gray, to black, some brown to maroon, commonly well laminated in thin beds, and contains thin sandstone stringers. It contains abundant disseminated plant remains, common to sparse ostracods, gastropods, and other fossil debris. It is variably tuffaceous, locally silty and sandy, and commonly non-calcareous. The thickness of shale intervals varies from several centimeters up to several meters.

Shale that occurs in the lower part of a coarsening upward succession is interpreted as prodeltaic deposits. In some cases, shales are overlain by lacustrine limestones rich in fauna, and are interpreted as sublittoral to profundal deposits. Some shales are sandwiched by tuffs. They are pure, thinly laminated, and contain common euhedral mineral crystals, and are interpreted as mud deposits in a volcanics-dammed lake (Yang et al., 2010). Finally, some other brown to maroon shales are thick laminated, variably silty and sandy, and locally massive with relict beddings. They occur in the upper part of fining-upward conglomerate-sandstone-mudrock successions. They are interpreted as overbank deposits in a meandering stream environment.

4.3.2 Lithofacies 3b – Mudstone Subfacies

Mudstones are massive mudrocks without clear laminations. Some mudstones are brown, silty and sandy, moderately to non-calcareous. They contain relict laminations and sparse equant to irregular calcitic nodules, suggesting some degree of pedogenesis. They are 0.2-1 m thick and occur in the upper part of coarsening-upward shale-sandstone-conglomerate successions or fining upward conglomerate-sandstone-shale successions. The subfacies can be alternatively interpreted as a Protosol (see Paleosol

below; Mack et al., 1993; Yang et al., 2010). They are interpreted as delta plain or overbank deposits.

4.3.3 Lithofacies 3c – Massive Mudrock Subfacies

This subfacies is a special type of mudrock of unique characteristics. It is brown, maroon, red, or purple, variably silty, laterally persistent for 100s of m in individual sections, and persistent throughout the two studied areas. The most unique characteristic of the mudrocks is the persistent multi-modal grain-size distribution ranging from clay to very fine sand, mainly from clay to fine silt (Obrist et al., 2013). It is commonly hackly and contains poorly to moderately defined blocks or peds several 10s of cm in size. Thin, discontinuous illuvial clay coats and poorly-defined multi-faceted slickensides occur sparsely in some intervals. However, distinctive pedogenic structures and relict laminations were not observed (Fig. 4C). This subfacies commonly overlies thin conglomerates of an ephemeral-stream origin or fining-upward conglomerate-sandstone-shale successions of a meandering stream origin. It may be interpreted as a Protosol, and the original parent materials are likely not overbank deposits associated with the underlying fluvial deposits (cf. Yang et al., 2010). This unique mudrock facies is interpreted as loessite by Obrist et al. (2013). Similar textural and structural characteristics were found in some mudrocks overlying thick channel lag and point bar deposits. This type of mudrock is interpreted as resedimented loess. The loess deposits indicate climatic aridity where the availability of surface water and atmospheric moisture was limited and an atmospheric circulation pattern favored dust entrainment, transport, and deposition (Bagnold, 1941; Pye, 1987).

4.4 Lithofacies 4 – Limestones

Carbonate lithofacies include mudstone, wackestone, and grainstone in the HYC LC. They are gray and greenish gray, and 0.2-2.6 m thick. Allochems include ooids, skeletal fragments, intraclasts, and peloids. Mudstone and wackestone are algal laminated; some are stromatolitic. The stromatolites are mostly hemispherical with a diameter of up to 20 cm. The uppermost limestones in HYC LC underneath an erosional unconformity contain microfractures and micro-karsts filled with brown silt and clay. All the limestones are interpreted to have formed in a shallow lacustrine environment. The mudstones and wackestones were deposited in a restricted, quiet environment, whereas the grainstones in a high energy environment. The microfractures and micro-karst features indicate that the limestones were subaerially exposed and pedogenetically altered during the formation of the unconformity.

4.5 Lithofacies 5 – Paleosols

Calcisol, Vertisol, Argillisol, and Protosol (Mack et al., 1993) are identified in the study interval. Soil horizons are described following Retallack (2001) and include illuvial clay-rich Bt horizons, illuvial calcite-rich Bk horizons, heavily slickensided Bss horizons, and largely pedogenically unmodified C horizons. Paleosol development indicates a prolonged period of landscape stability and subaerial exposure, when nondeposition dominated. Readers are referred to detailed descriptions by Yang et al. (2010, their Table 2; see also Thomas et al., 2011) covering the entire uppermost Carboniferous to Lower Triassic interval in Tarlong and Taodonggou. The four types of paleosols observed in this study are described briefly below.

4.5.1 Lithofacies 5a – Calcisol

Calcisols are characterized by a zone of calcitic accumulation of a pedogenic origin (Mack et al., 1993). They occur in red, brown and maroon mudstone matrix, and contain a poorly-defined zone rich in calcitic nodules. The nodules have variable shapes and, in some cases, coalesce to form discontinuous layers of calcrete. The calcretes contain microbial laminations, pisoids, and detrital grains. In some places, antiforms and synforms are present in the nodule-rich horizons, manifested by calcite-filled cracks, representing vertic features (Fig. 4D). The mudstones contain blocky to rounded peds and subvertical slickensides.

The Calcisols developed in well-drained sediments in a semi-arid to arid climate (Mack et al., 1993; Mack and James, 1994). The vertic features suggest precipitation seasonality, causing shrinkage and expansion cracks in the soil. Well-developed and stacked Calcisols, as observed in Tarlong-Taodonggou, signify a long period of subaerial exposure (Alonso-Zarza and Wright, 2010), during which landscape stability persisted.

4.5.2 Lithofacies 5b – Vertisol

Two Vertisols occur in the studied sections; one in the northern and one in the north-central Tarlong section. The Vertisol in the northern Tarlong section contains abundant slickensides, which may be coated by illuvial clay as argillic or pedogenic calcite as calcitic. It occurs in a reddish purple to gray mudstone matrix. Peds are rounded to subangular and mm in size. The mudstone is slightly calcareous. The Vertisol in the north-central Tarlong section is similar. It contains scattered calcitic nodules and abundant slickensides and clay coats and occurs in a brown to maroon mudstone matrix.

Vertisols form in a strongly seasonal climate, with common precipitation (Mack and James, 1994).

4.5.3 Lithofacies 5c – Argillisol

Three stacked Argillisols occur in Dalongkou. They are brown to dark purple, sandy or silty, and contain common illuvial clay films and slickensides, diffuse color mottles, and angular prismatic peds 1-5 cm in size. The parent mudrocks are interpreted as resedimented loess deposits of meandering streams. In some places, the clay films are thin and discontinuous and interpreted as relatively immature proto-Argillisols. The lowest Argillisol developed distinct soil horizons (cf. Retallack, 2001), as indicated by abundant clay films in the lower part, the Bt Horizon, which become scarce in the uppermost part. Argillisols commonly form under a climate of a strong precipitation seasonality with a moderate to high annual precipitation (Mack and James, 1994).

4.5.4 Lithofacies 5d – Protosol

Protosols are characterized by a massive structure and lack of distinctive soil horizons. They are commonly red, brown, to purple, indicating an oxidizing environment. Poorly-developed illuvial clay films, slickensides, and/or calcitic accumulations are common in Protosols, but not distinctive and abundant enough to better define the paleosols. Protosols suggest incipient soil development on a relatively stable landscape during a short time period of subaerial exposure, which ended by renewed sedimentation.

5. High-Order Sedimentary Cycles

The sedimentary deposits in the study interval are cyclic as defined by repetitive changes in depositional environments or between erosional and depositional processes (Yang et al., 2010). The former is termed as environmental cycles, the latter erosion-deposition cycles. In addition to the five types of HCs identified by Yang et al. (2010), a new type, the fluvial-loessial HC, is identified and described here in detail.

5.1 Lacustrine Deltaic HCs

Lacustrine deltaic HCs are a type of environmental cycle and consist of an upward-coarsening succession from fossil-bearing, well-laminated prodeltaic shale of Lithofacies 3a (LF 3a) to lithic arenite and subarenite of LF 2c, which are commonly overlain by silty and sandy fluvial shale of LF 3a and delta plain mudstone of LF 3b. In some cases, a basal thin, well sorted arenite and subarenite of LF 2b is present, indicating initial lake transgression and deepening. This type of HCs formed during an episode of initial lake expansion followed by contraction and progradational infilling.

5.2 Lacustrine Fluctuating Profundal Mixed Carbonate and Siliciclastic HCs

This type of HCs are environmental cycles and commonly consist of a basal transgressive sandstone of LF 2b formed during lake transgression, a sublittoral to profundal shale of LF 3a, a limestone of LF 4, and a capping mudstone of LF 3b or Protosol of LF 5d deposited in a lake-margin environment. The limestones may be lime mudstone, wackestone, or grainstone; and the upper part of some limestones is pedogenically altered. This type of HC indicates an episode of lake expansion and contraction where siliciclastic influx was insignificant (Yang et al., 2010).

5.3 Lakeplain-Littoral Siliciclastic HCs

The lakeplain-littoral HCs are largely similar to the fluctuating profundal mixed carbonate and siliciclastic HCs, but the profundal shale and carbonate facies are absent. The carbonate facies is replaced by a well-washed lakeplain-littoral arenite of LF 2b or, in rare cases, beach-littoral conglomerates of LF 1. This type of HCs indicates an episode of lake expansion and contraction of a small magnitude. A special variety of this type of HC occurs in southwestern Tarlong section, which comprises an interval of shales sandwiched by tuffs. The shales are well-laminated and, in some cases, have an upward-coarsening trend marked by an upward increase in the amount of sand grains. Yang et al. (2010) interpreted the shales as littoral to sublittoral or prodeltaic deposits in a volcanics-dammed lake.

5.4 Meandering Stream HCs

Meandering stream HCs are a type of erosion-deposition cycles, and are characterized by a high-relief erosional base overlain by channel-fill conglomerates of LF 1 and sandstones of LF 2a, overbank mudrocks of LF 3a and 3b, paleosols of LF 5a, 5b, and 5c, and minor sandstones of LF 2a. This type of HCs signifies perennial streams in a subhumid climate. However, in some cases, the cycles are capped by Calcisols, suggesting intra-cycle climatic variations from a subhumid condition during stream deposition to a semi-arid condition during pedogenesis (Yang et al., 2010).

5.5 Fluvial-Loessial HCs

The definition of this new type of HCs results from reinterpretation of the depositional environments of some mudrocks of LF 3c as loessite, which were tentatively interpreted as overbank deposits by Yang et al. (2010; cf. Obrist et al., 2013). The loessite interpretation is further supported by the wide distribution of the loess deposits in the study area, similar to the Pleistocene loess blankets in the Chinese Loess Plateau (e.g., Pye, 1987). This type of HCs is a combination of erosion-deposition and environmental cycles. Two subtypes can be differentiated. The first subtype is characterized by a low-relief erosional base overlain by thin ephemeral-stream channel-fill conglomerates of LF 1 and, in rare cases, thin fluvial channel-fill sandstones of LF 2a. The conglomerates are overlain directly by thick loessite of LF 3c. The other subtype is similar, but has a fining-upward meandering stream succession in the lower part. As a result, the thick massive loessite of LF 3c in the upper part of the cycle may contain some intercalated overbank sandstones and mudrocks. The fluvial-loessial HCs signify alternating fluvial and eolian deposition. Climatic aridity may have persisted through the entire cycle for the ephemeral stream-loessial cycles. On the other hand, for the meandering stream-loessial cycles, climatic conditions may have changed from subhumid during the meandering stream deposition to arid during loess deposition.

6. Depositional Environmental Trends and Sequence of Events

Systematic variations of depositional environments and stacking of HCs in individual sections show minor and major shifts in depositional environments, which can be used to delineate the sequence of events during which major changes in processes controlling cyclic sedimentation had occurred. The boundaries where the major changes

occurred are the candidates for low-order cycle boundaries. Subsequent cyclostratigraphic correlation among individual sections will confirm the low-order cycle boundaries to establish a cyclo- and time-stratigraphic framework of the study interval.

6.1 Northeastern Tarlong

The composite northeastern Tarlong section is composed of two sections 100 m apart (Fig. 5). The eastern section is 4 m thick and covers the uppermost part of the HYC LC of Yang et al (2010; Fig. 2). The lower part of the interval is a fluctuating profundal HC. The upper part is a wackestone with stromatolite heads up to 20 cm wide. The uppermost 0.3 m of the wackestone is highly brecciated, where fractures are commonly filled with sparry calcite. The brecciated wackestone may be the C horizon of a paleosol, of which the shallower horizons may have been eroded later. A mudrock interval overlies the wackestone with a sharp contact. It is interpreted as overbank deposits of three meandering stream HCs in the western section (see below; Fig. 5).

The mudrock interval contains two stacked Calcisols. Each has a lower part composed of a dark reddish brown mudstone containing well developed peds, thick illuvial clay coats, and abundant slickensides, which are classified as the Bt and Bss horizons (Retallack, 2001). This mudstone is overlain by a mudstone interval containing abundant calcitic nodules. The nodules are commonly 1-10 cm long and increase in abundance upward. In the uppermost part, nodules coalesce, forming one or two beds of calcretes. The calcretes are gray, locally microbially laminated, laterally continuous, and vary from 1-10s cm thick. Antiforms and synforms occur in the nodular interval as

defined by crude alignment of elongate and tabular calcitic nodules. They also occur as undulating forms in the calcrete zone.

Both Calcisols can be traced to the western section, where the lower Calcisol terminates against fluvial channel-fill deposits and the upper Calcisol persists and caps the channel deposits. The lacustrine deposits of the HYC LC in the western section are lithologically similar to those in the eastern section (Fig. 5). Three meandering stream HCs overlie the limestone with a sharp contact. Physical tracing indicates that the contact is concave upward, at least 300 m wide from east to west, and has a high relief of three meters through stratigraphic correlation between the eastern and western sections. The lower two HCs do not contain mudrocks, which were likely eroded by subsequent channeling. The uppermost part of the third HC is a Calcisol correlative to the upper Calcisol in the eastern section (Fig. 5).

A fluvial-loessial HC overlies the Calcisol (Fig. 5). It does not have a basal ephemeral stream conglomerate, which is present laterally away from the line of measured section. This is the first occurrence of loess deposits in the upper QZJ LC. Upward is a meandering stream HC, where an argillic and calcitic Protosol is present, containing sparse clay-lined rootlets, steles, and incipient calcitic nodules. The next is an ephemeral stream-loessial HC. In the upper overbank deposits of the ephemeral stream succession, a calcareous vertic Protosol occurs, containing abundant slickensides and sparse-common equant, micro-brecciated calcitic nodules. This Protosol was overlain gradationally by a 40-cm-thick interval with three light green calcrete beds. Each bed is 1-5 cm thick, and contains locally abundant microbial encrusting and coating and, in some places, embedded detrital grains and small pisoids. The calcrete beds change to a

nodular zone 50 m to the west. They are interpreted as a palustrine limestone deposited on the floodplain or, alternatively, the Bk horizon of a Calcisol. The loessite interval in the upper part of this HC is 6.4 m thick, structurally massive and texturally monotonic, and contains a variable amount of thin discontinuous illuvial clay coats. Fluvial-loessial HCs dominate in the rest of the QZJ LC for 65.7 m to the base of overlying Wutonggou LC (Fig. 2), where the first lacustrine deltaic deposits occur (Yang et al., 2010).

The fluctuating-profundal lacustrine deposits of the upper HYC LC juxtapose abruptly with overlying meandering stream deposits with a concave erosional contact (Fig. 5). The contact resembles a broad fluvial valley floor, where meandering stream channel-fills were deposited; and overbank sediments were deposited outside the valley. The stratigraphic juxtaposition suggests a series of events: lake withdrawal and termination of lacustrine sedimentation, erosion and development of a fluvial valley, pedogenesis of lacustrine sediments, especially outside the valley, and ensuing subsidence and fluvial deposition. Tectonic uplift is interpreted as the major controlling process. The erosional surface may represent a significant time span where those processes had occurred and is interpreted as an unconformity.

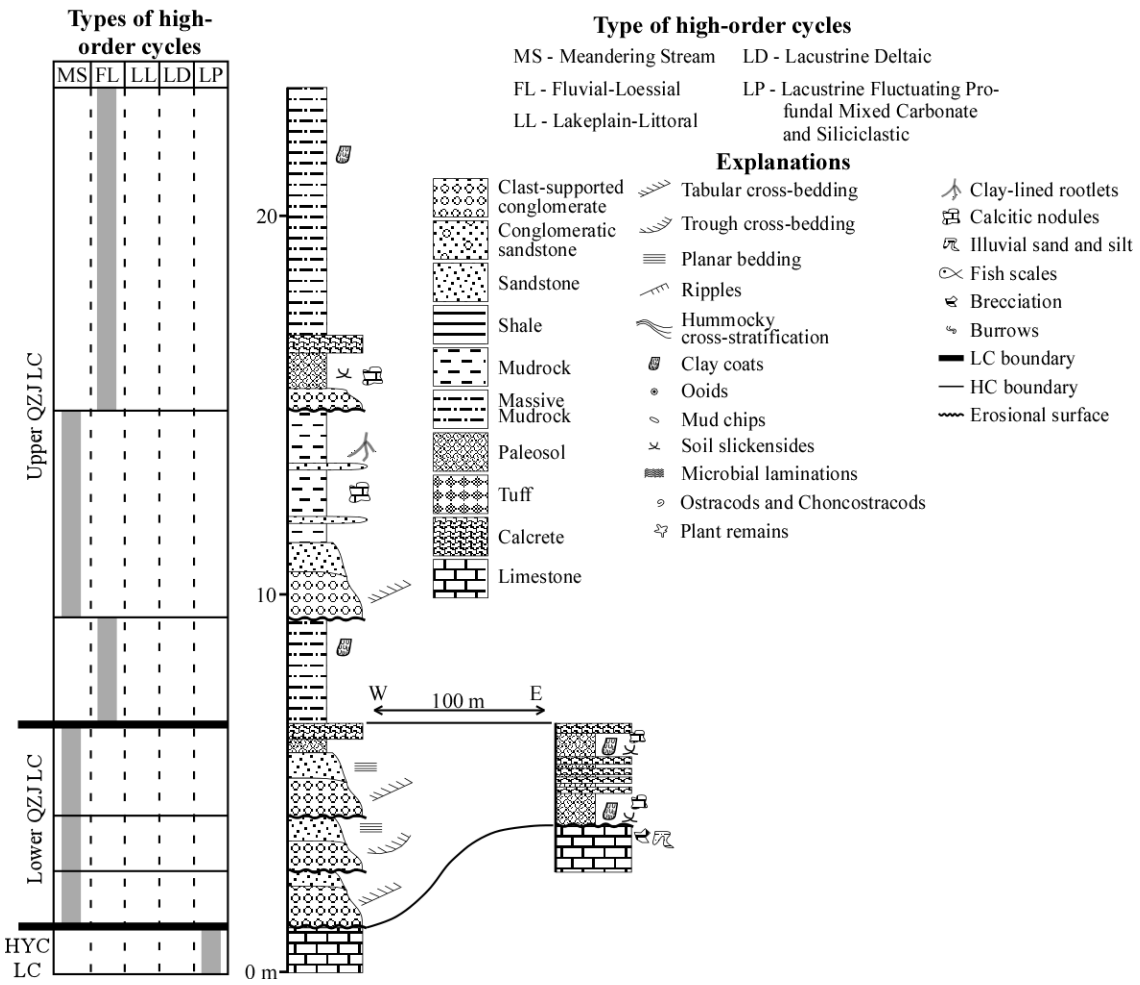

Figure 5. Highly-simplified lithologic column (middle panel), sedimentary structures (right panel), and high-order cycle types (left panel) of the HYC and lower and upper QZJ LCs of the northeastern Tarlong section. Fluvial channel-fill conglomerates and sandstones of lower QZJ LC in the western section change to overbank mudstone hosting two Calcisols to the east. See Fig. 2 for location of measured section.

The formation of two stacked Calcisols outside the valley, one of which also developed on the overbank sediments inside the valley, suggests an episode of prolonged tectonic quiescence after fluvial valley filling. The valley filling resulted in a subdued topography and a stable landscape, upon which pedogenesis occurred. The upper Calcisol signifies a prolonged period of non-deposition. The stacked fluvial-loessial HCs above the Calcisols suggest a drastic change in drainage basin morphology, provenance,

depositional environment, and atmospheric circulation pattern, and renewed moderate tectonic activity, although climatic aridity persisted. Hence, the surface separating the Calcisols and overlying fluvial-loessial HCs is a disconformity.

6.2 Northern Tarlong

The northern Tarlong section (Fig. 6) has a similar stratigraphy to that in the eastern section in northeastern Tarlong, although it is ~1 km to the WNW. The upper HYC consists of fluctuating profundal mixed carbonate and siliciclastic, lacustrine deltaic, and lakeplain-littoral HCs in the lower part. Calcisols and calcitic Protosols developed in the upper parts of the HCs. The uppermost limestone is algal laminated, stromatolitic, and moderately pedogenetically altered. Overlying the lacustrine deposits is a red mudstone interval that is 6.4 m thick and contains four stacked paleosols. The lower three paleosols are vertic and argillic Calcisols. Each of them has a highly-slickensided argillic lower part with large antiforms and synforms, and a calcitic nodule-rich horizon with local calcretes in the upper part. The uppermost paleosol is a weakly calcareous argillic Vertisol, containing abundant slickensides. Atop of the stacked paleosols is a coarse-grained meandering stream HC, followed by two fluvial-loessial HCs. The rest of the QZJ LC cannot be observed in detail because of limited outcrop exposure, but appears to be similar to that in northeastern Tarlong, composed of many fluvial (meandering stream or ephemeral stream)-loessial HCs for 53.5 m to the base of overlying Wutonggou LC (Yang et al., 2010).

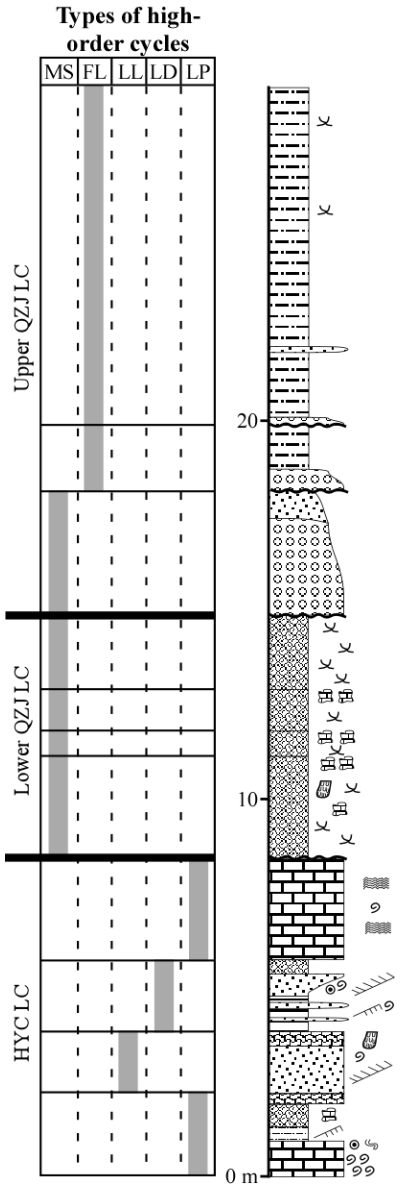

Figure 6. Highly-simplified lithologic column, sedimentary structures, and high-order cycle types of the HYC and lower and upper QZJ LCs of the northern Tarlong section. Overbank mudstone hosts three Calcisols and one Vertisol in the lower QZJ LC. See Fig. 5 for explanations and Fig. 2 for location of measured section.

The lacustrine deposition of the upper HYC LC terminated abruptly. The overlying overbank mudstone indicates a drastic environmental change. The pedogenic features in the uppermost limestone of HYC indicate a possible episode of pedogenesis before fluvial deposition, or may have been formed by pedogenesis of the overlying mudstone. However, a comparison with the similar record in the northeastern Tarlong section suggests a likely event of pedogenesis after lake withdrawal and before overbank deposition. Lake withdrawal may have been caused by a tectonic uplift. Above all, the boundary separating the lacustrine and overbank deposits is likely to be a disconformity. The occurrence of four stacked mature Calcisols and Vertisol suggests great landscape stability and minimal deposition in an overbank environment. The overlying fluvial-loessial HCs signify renewed deposition under different environmental and atmospheric conditions. A significant time span is represented by those paleosols and the surface separating the stacked paleosols from overlying fluvial-loessial HCs. Hence, this surface is also a disconformity.

6.3 North-Central Tarlong

The north-central Tarlong section (Fig. 7) has a similar stratigraphic record to those in northeastern and northern Tarlong sections and is 1.4 km to the WNW of the northern Tarlong section. The two HCs in the upper part of the HYC LC are fluctuating-profundal mixed carbonate and siliciclastic cycles. Ostracods and conchostracans are common in limestones and sandstones. The uppermost limestone is rich in conchostracans. It juxtaposes abruptly with overlying fluvial deposits rich in paleosols. The paleosol-rich interval is 19.5 m thick and contains at least five paleosols in six

meandering stream HCs (Fig. 7). The HCs contain channel-fill sandstones and overbank mudrock and sandstones with an erosional base, and are thin, except the uppermost HC. Four vertic and argillic Calcisols developed in the lower and middle parts of the fluvial deposits. A thick, mature calcitic and argillic Vertisol developed in the uppermost HC. Pedogenesis is pervasive in both channel-fill sandstones and conglomerates and overbank deposits in the six HCs. The paleosol-rich fluvial deposits juxtapose sharply with an overlying 4-m thick loessite and a possible fluvial-loessial HC. The rest of the QZJ LC is not exposed in this location, but possibly similar to those in the other sections in Tarlong-Taodonggou based on field reconnaissance and correlation (Yang et al., 2010).

The abrupt juxtaposition of lacustrine deposits with overlying fluvial deposits and paleosols suggests lake withdrawal. Two observations also suggest erosion: first, no pedogenic features are present in the uppermost limestone; and second, the limestone rich in conchostracans may be correlative to a similar limestone in the northern Tarlong section. Such a correlation indicates that the top of the limestone is approximately 7.5 m below the top of the uppermost stromatolitic limestone in northern Tarlong, suggesting fluvial erosion of at least 7.5 m relative to the limestone top in the northern Tarlong section. Hence, the contact between the uppermost limestone of HYC and overlying fluvial-paleosol deposits is likely a disconformity or erosional unconformity. Tectonic uplift may have caused lake withdrawal and fluvial downcutting, followed by fluvial infilling.

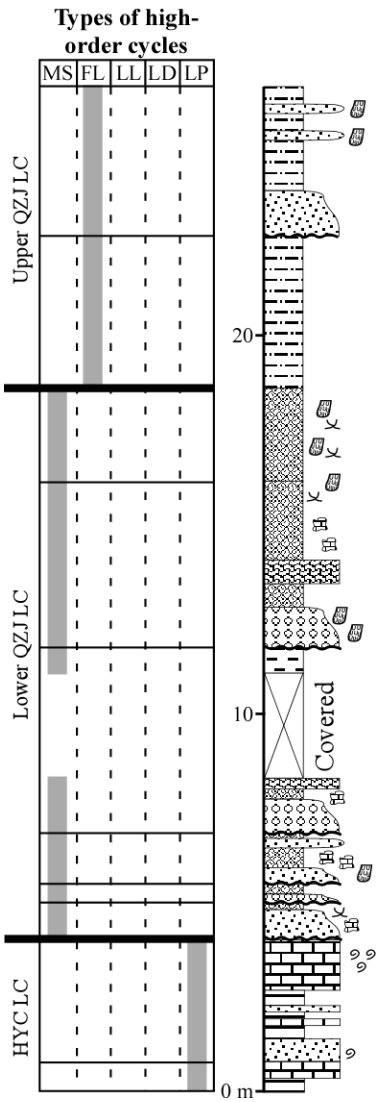

Figure 7. Highly-simplified lithologic column, sedimentary structures, and high-order cycle types of the HYC and lower and upper QZJ LCs of the north-central Tarlong section. Four vertic and argillic Calcisols and one argillic Vertisol developed in small tributary streams and overbank deposits in the lower QZJ LC. See Fig. 5 for explanations and Fig. 2 for location of measured section.

The fluvial HCs overlying the disconformity are thin and highly pedogenically altered. This suggests fluvial deposition by small tributary streams in floodplain lows, where deposition was slow and pedogenesis was pervasive. Alternatively, the deposition could have occurred in the peripheral part of a fluvial valley, although stratigraphic correlation does not support this scenario (see below). The thick muddy Vertisol suggests

completion of fluvial infilling and a prolonged period of nondeposition and landscape stability. The thick loessite overlying the Vertisol and subsequent fluvial and loess deposits signify renewed active sediment deposition under environmental and atmospheric conditions different from those below. As a result, the contact separating the stacked paleosols and overlying fluvial-loessial deposits is a disconformity.

6.4 Taodonggou

Three sections, eastern, central, and western, in the Taodonggou area show the stratigraphic characteristics of the upper part of HYC and lower QZJ LCs along a 100-m transect (Fig. 8). The section is located 4 km WSW from the north-central Tarlong section. In the eastern section, three fluctuating profundal mixed carbonate and siliciclastic HCs occur in the upper HYC. Fossil fish scales are present. The lime mudstone in the uppermost HC is highly brecciated and fractured with infiltrating red-brown silt. Lateral physical tracing indicates that an erosional surface with a relief of ~ 2 m separates the limestone from overlying mudstone. The mudstone contains abundant calcitic nodules and is interpreted as an overbank deposit, within which a Calcisol developed. In the central section, the uppermost HYC LC has a 0.4-m thick, blackish gray to purple shale containing disrupted laminations and scattered clasts of altered lacustrine limestone. An erosional surface, the same as that in the eastern section, separates the shale from overlying meandering stream HC. The lower part of the HC is a 0.3-m thick calcareous sandstone containing pure to sandy calcitic nodules; the upper part is a 0.4-m thick red to purple mudstone. The mudstone contains scattered calcitic nodules in the lower 15 cm, a discontinuous, massive to laminated calcrete in the middle 10 cm,

and a hackly calcareous mudstone in the upper 15 cm. Two thin Calcisols are interpreted on the basis of calcitic horizons. The Bk horizon of the lower Calcisol is in the sandstone, whereas that of the upper Calcisol is the calcretes. The superimposed Calcisol interval is overlain by a fluvial-loessial HC with an erosional contact. The HC has a gravelly sandstone in the lower part, which changes abruptly into a red, massive loessite (Fig. 8).

In the western section, the uppermost HYC has a 0.5-m thick greenish gray shale, of which the upper part is altered into gray-purple blocky mudstone. The shale is overlain by a meandering stream-loessial HC with an erosional contact of a 0.5-m relief. The channel fill is a fining-upward succession of conglomerate and sandstone, where the conglomerate contains common limestone and shale clasts. The upper part is a 0.7-m thick red, massive, silty loessite. Physical correlation indicates that this channel eroded the Calcisol in the central section (Fig. 8). Upward, three ephemeral stream-loessial HCs occur. The rest of the QZJ LC is composed of similar repetitive fluvial-loessial HCs and is 86.4 m thick to the base of overlying Wutonggou LC (Yang et al., 2010).

The fluctuating profundal lacustrine deposition of the HYC LC was terminated by a lake withdrawal. However, the altered deposits in the uppermost part suggest an episode of pedogenesis before significant fluvial erosion. Alternatively, the pedogenic alteration may be the downward extension of overlying Calcisols. The first scenario suggests that the top of the lacustrine deposits is a significant erosional unconformity. Both lake withdrawal and fluvial erosion suggest an episode of tectonic uplift. Thin fluvial channel-fill and overbank deposits above the erosional unconformity suggest an overall overbank environment where small tributaries developed. Mature Calcisols developed in the fluvial sediments and signify the completion of fluvial valley infilling

followed by a long period of tectonic quiescence, landscape stability, and pedogenesis. Subsequently, renewed fluvial erosion and fluvial and loess deposition occurred as observed in the western section, and persisted throughout the rest of QZJ LC. The contact separating the Calcisols from overlying fluvial and loess deposits indicates a prolonged hiatus and transition where tectonic, atmospheric, and environmental conditions changed. Thus, this contact is likely a significant erosional unconformity. Finally, the two erosional unconformities in the eastern and central sections merge as one in the western section because of the significant channel downcutting as indicated by physical tracing of these surfaces in the field.

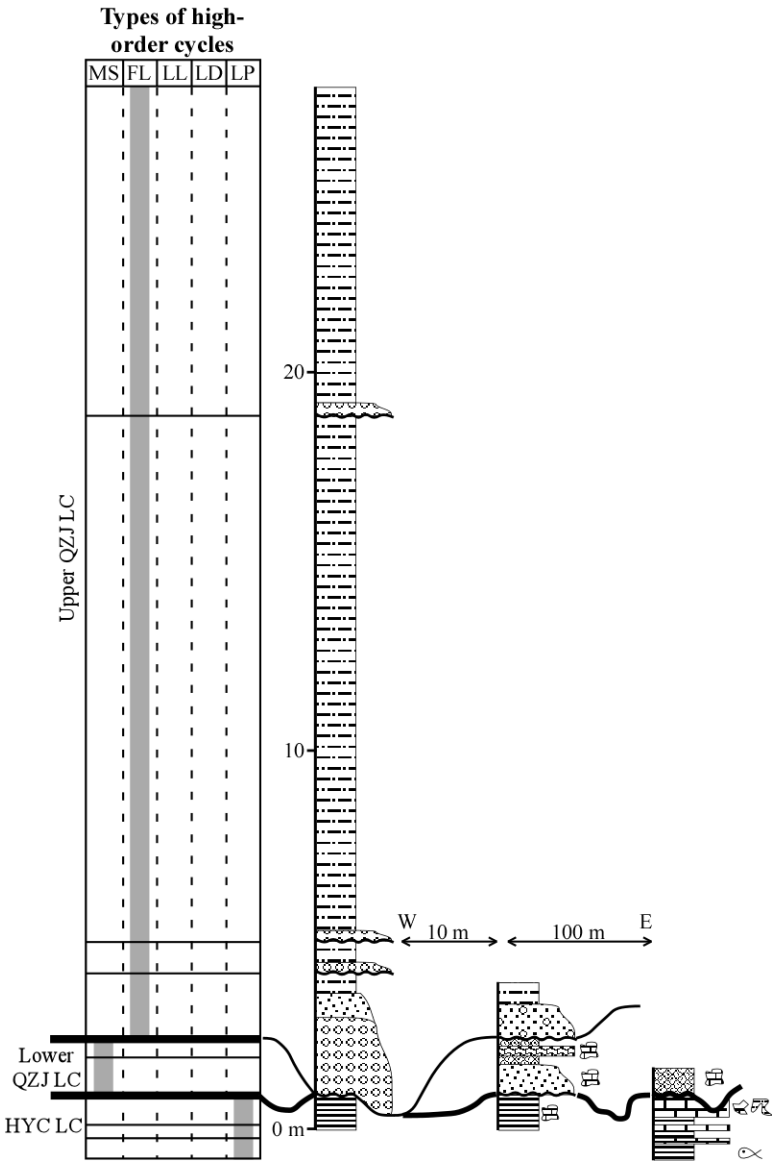

Figure 8. Highly-simplified lithologic column, sedimentary structures, and high-order cycle types of the HYC and lower and upper QZJ LCs of the Taodonggou section. Small tributary stream and associated overbank deposits dominate the lower QZJ LC and thick loessite dominates in the upper QZJ LC. The lower QZJ LC was eroded in the western section. See Fig. 5 for explanations and Fig. 2 for location of measured section.

6.5 Southwestern Tarlong

The southwestern Tarlong section is thick and complex and located 3 km to the SE of the Taodonggou section (Fig. 9). The upper HYC LC contains three lakeplain-littoral HCs. In general, each HC has an upward-coarsening progradational littoral sandstone facies in the lower part and a lacustrine limestone or a tuffaceous sandstone in the upper part. The limestone in the uppermost HC has common algal laminations, ooids, and spar-filled vugs; and is highly brecciated and filled with infiltrating silts and sands in the uppermost one meter. Some brecciated clasts are coated by calcans and argillans. The characteristics of the brecciated limestone suggests that extensive mechanical and chemical alterations had occurred after the deposition and were probably caused by pedogenic processes, such as fracturing associated with variations in temperature and wet-dry conditions, chemical dissolution and infiltration, all in the vadose zone. The lacustrine deposits are separated from overlying meandering stream HCs by an erosional surface. The interval above this surface is 51.3 m thick, consists of 17 meandering-stream HCs and one lacustrine deltaic HC in the middle. The meandering-stream HCs are composed of thick conglomerates and gravelly sandstones as channel fills in the lower part and thin interbedded sandy shale and sandstone as overbank deposits in the upper part. Cobbles and pebbles are common in the conglomerates. In many cases, younger channels cut into underlying channel-fill deposits. The deltaic HC is 3.5 m thick and contains a basal transgressive gravelly sandstone, prodeltaic shale and siltstone, and delta-front sandstone in the upper part. In addition, there is a 3-m thick interval of sandy and shaly tuff and tuffaceous shale in the upper part of a meandering stream HC. They were interpreted as subaerial ashflow deposits.

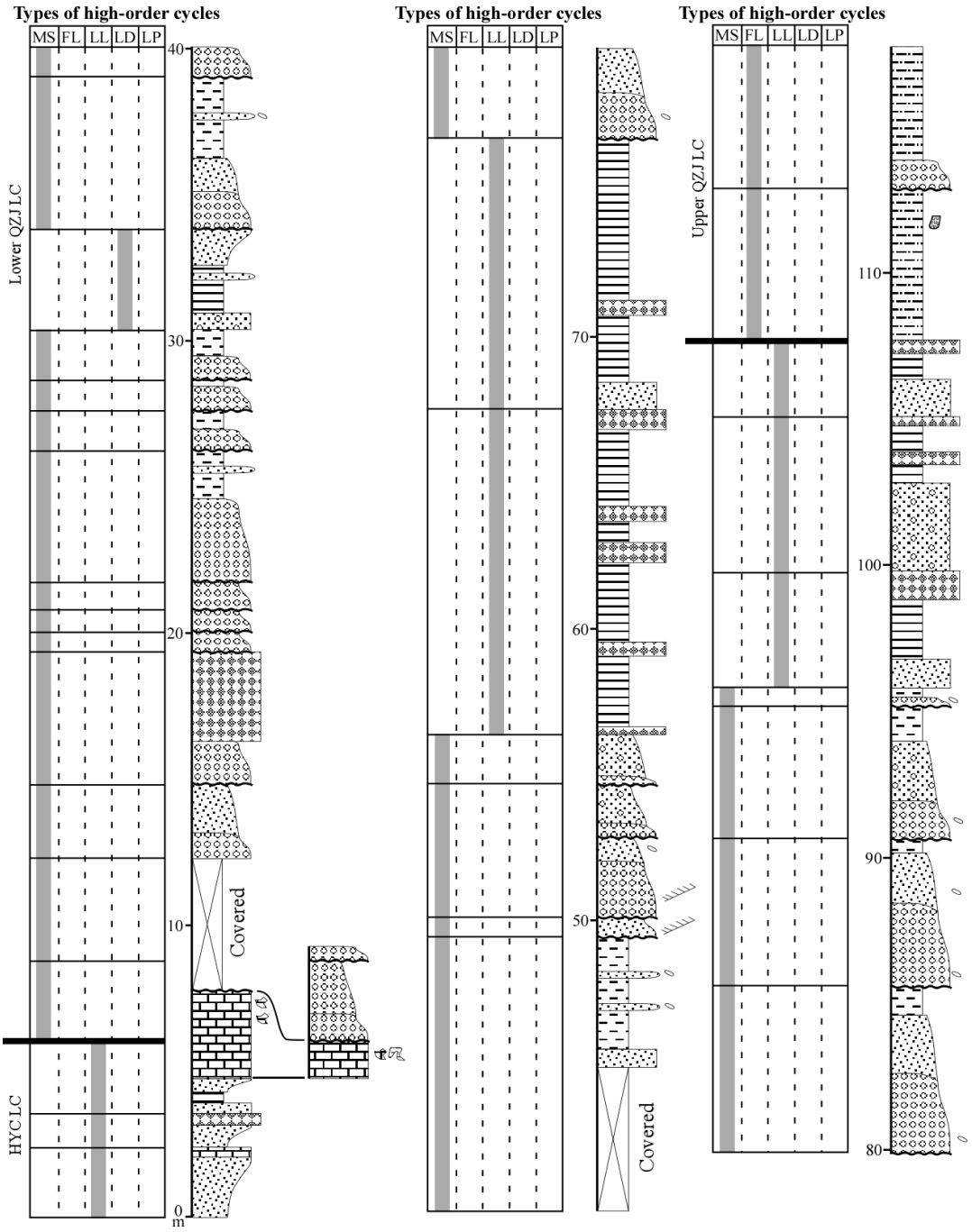

Figure 9. Highly-simplified lithologic column, sedimentary structures, and high-order cycle types of the HYC and lower and upper QZJ LCs of the southwestern Tarlong section. Thick meandering stream and minor lacustrine deposits dominate the lower QZJ LC, which are overlain conformably by ephemeral stream and loess deposits of the upper QZJ LC. See Fig. 5 for explanations and Fig. 2 for location of measured section.

Overlying the meandering stream deposit-dominated interval are two lakeplain-littoral HCs, formed in volcanics-dammed lakes, as interpreted by Yang et al. (2010). Well-laminated tuffaceous shale and siltstone dominate. Thin tuffs are numerous at the basal, middle, and top of the HCs. Overlying the lake deposits are five coarse-grained meandering stream HCs, similar to those below the lake deposits. One of the channels has a basal relief of 1.5 m. Further up are three volcanics-dammed lake HCs which are similar to those below, but thinner and contain more sandstones. Overlying the lake deposits are two fluvial-loessial HCs. The lower HC does not have a basal stream channel deposit and is composed entirely of massive muddy and silty loessite. The upper part of the loessite contains scarce clay coats, suggesting slight pedogenic alteration. The rest of the QZJ LC consists of similar fluvial-loessial HCs, with a thickness of 76 m to the first delta of the Wutonggou LC (Yang et al., 2010).

The southwestern Tarlong section presents an extraordinary record of events and depositional environmental changes. Termination of lacustrine deposition of HYC LC indicates a lake withdrawal and subaerial exposure of the uppermost limestone, which were probably caused by a tectonic uplift. An episode of intense pedogenesis formed the Calcisol hosted in the limestone, which suggests a period of tectonic quiescence and landscape stability. Afterward, a renewed tectonic uplift must have occurred as indicated by the fluvial erosional surface separating the Calcisol from overlying meandering stream deposits. Alternatively, fluvial erosion followed lake withdrawal. Subsequently, erosion stopped and pedogenesis of the uppermost HYC limestone took place. Afterward, meandering stream erosion and deposition ensued. In either case, the erosional surface

separating the HYC lacustrine and QZJ fluvial deposits is likely an unconformity of a significant time span.

Fluvial erosion during the unconformity had generated a major fluvial valley in the southwestern Tarlong region, where thick and coarse-grained meandering stream systems were deposited. This interpretation is supported by the sporadic occurrence of lacustrine deposits in the valley fill. Active tectonic uplift must have been intense during the period of major meandering stream deposition as indicated by abundant coarse conglomerates and repetitive downcutting of younger channels into underlying channel-fill deposits. Finally, active meandering stream deposition was replaced by fluvial-loessial deposition. The transition signifies the completion of fluvial valley filling, reduced tectonic uplift, a change in atmospheric circulation pattern, and a major change in depositional environment. These changes seemingly took place without a major gap in the southwestern Tarlong record. Thus, the boundary separating the fluvial-loessial deposits from underlying meandering stream-dominated interval is a conformity or disconformity.

6.6 Southeastern Tarlong

The southeastern Tarlong section is 4 km due east of the southwestern Tarlong section (Fig. 10). The uppermost part of the HYC LC contains four cycles. The lower three are wave-dominated lacustrine deltaic HCs, each of which is composed of well laminated shale in the lower part and well cross-stratified lithic arenite in the upper part. The uppermost HC contains only a 2-m thick thinly-laminated, pure to silty, black shale with two thin tuffs, and could be the prodeltaic deposit of a deltaic HC. An erosional

surface with a 10s-cm relief separates the shale from two overlying meandering stream HCs. The two HCs are thick and laterally persistent for at least 200 m. The lower parts are composed of thick gray conglomerates and sandstones; and the upper parts gray to maroon thick-laminated and variably sandy shales. Clasts of a small boulder and cobble size are not uncommon in the conglomerates. No pedogenic features are evident in these deposits. Upward, four fluvial-loessial HCs occur, among which, the lower HC is a meandering stream-loessial cycle, the other three are ephemeral stream-loessial cycles.

The juxtaposition of black lacustrine shale of HYC LC with meandering stream deposits of the QZJ LC indicates lake withdrawal and fluvial erosion and deposition. The lack of pedogenic alteration of the black shale and the large gravel size in the channel-fill conglomerates suggest that significant fluvial erosion had occurred and was probably caused by significant tectonic uplift. Thus, this erosional surface is interpreted as an erosional unconformity of a prolonged time span. Meandering stream deposition changed to fluvial-loessial deposition rather quickly and continuously. This is supported by the facts that no paleosols are present in these deposits and the first fluvial-loessial HC has a meandering-stream succession in the lower part. The rest of the QZJ LC contains similar repetitive fluvial and loessite deposits (see supplemental sections in Yang et al., 2010) and is 77.2 m thick to the base of overlying Wutonggou LC (Yang et al., 2010).

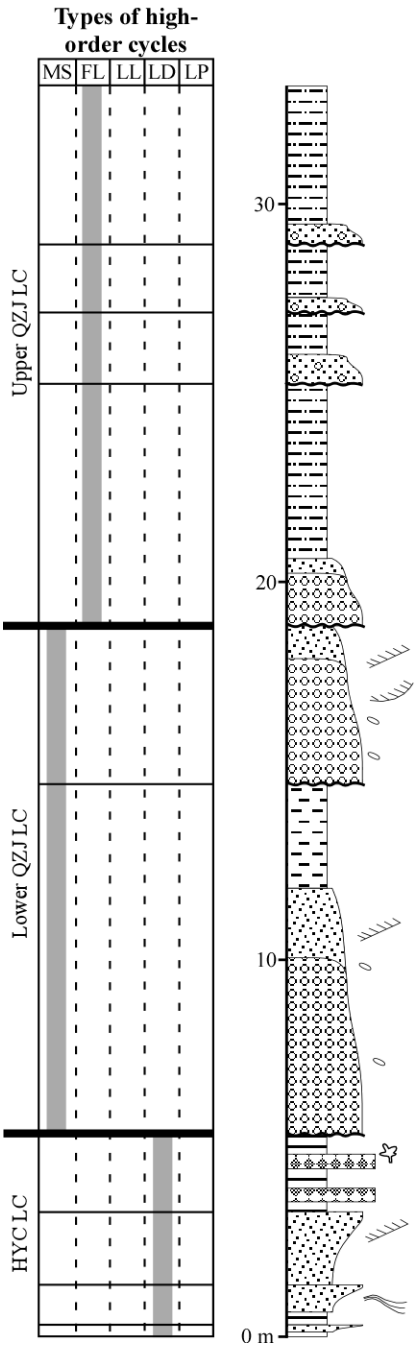

Figure 10. Highly-simplified lithologic column, sedimentary structures, and high-order cycle types of the HYC and lower and upper QZJ LCs of the southeastern Tarlong section. Thick coarse-grained meandering stream deposits dominate the lower QZJ LC and change rapidly to fluvial-loessial deposits in the upper QZJ LC. See Fig. 5 for explanations and Fig. 2 for location of measured section.

6.7 Dalongkou

The Dalongkou section (Fig. 11) in the northern Bogda Mountains offers a record far from the Tarlong-Taodonggou area for a regional perspective on delineation and correlation of low-order cycles. The uppermost HYC is composed of two lacustrine deltaic HCs. The deltaplain deposits in the upper HC are slightly pedogenically altered. They are in a high-relief erosional contact with overlying three meandering stream HCs of the lower QZJ LC. Younger channels cut into underlying channel-fill conglomerates and sandstones with a high relief. The conglomerates are pebble to cobble-sized; and only the upper HC has overbank mudstone, siltstone, shale, and minor sandstone, total 2.3 m thick. The overbank deposits are color mottled, contain common clay coats, slickensides, and wedge-shaped peds and are interpreted as an Argillisol. Particle size distribution of four samples in the overbank deposits is similar to that of loessite in the Tarlong-Taodonggou area (Obrist et al., 2013). The three samples in the lower and middle parts of the overbank deposits have an elevated percentage of the very-fine sand fraction and were interpreted as resedimented loess (cf. Péwé, 1955, 1975) mixed with some non-loess sand grains.

Upward, two thin fluvial-loessial HCs occur. The ephemeral stream channel-fill sandstones in the lower part are thin; and the loessites in the upper part are relatively thick. Furthermore, illuvial clay coats and slickensides are common in the loessites of both HCs. Overlying are three meandering-stream HCs, of which the overbank deposits are devoid of any pedogenic features. The rest of the QZJ LC consists of a mixture of fluvial-loessial and meandering stream HCs. Some of the overbank deposits and loessites contain weakly to moderately developed Protosols.

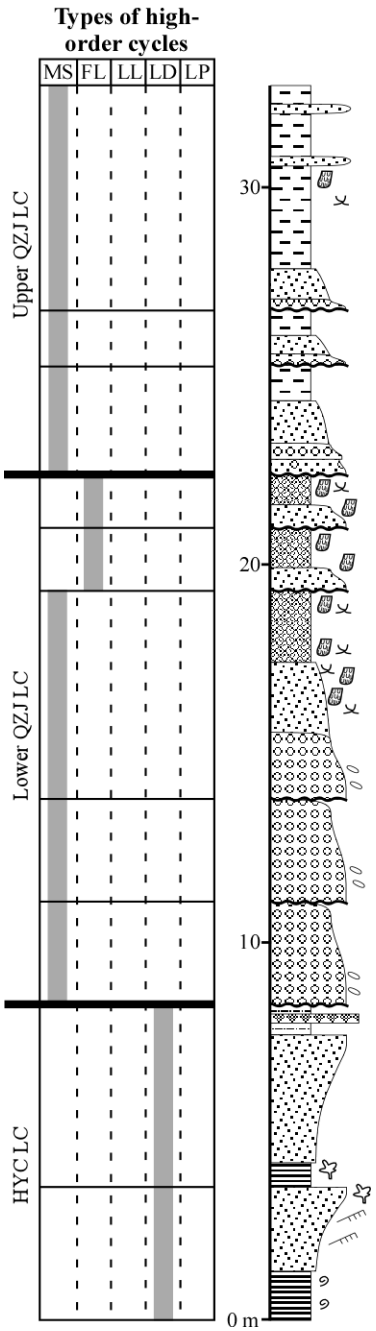

Figure 11. Highly-simplified lithologic column, sedimentary structures, and high-order cycle types of the HYC and lower and upper QZJ LCs of the Dalongkou section. Meandering stream and overbank deposits dominate in the lower QZJ LC with minor loess deposits. Three Argillisols occur in the upper part. See Fig. 5 for explanations and Fig. 2 for location of measured section.

The juxtaposition of lacustrine deposits of the upper HYC LC with thick and coarse meandering stream deposits of QZJ LC suggests lake withdrawal and fluvial downcutting and deposition, probably caused by a major tectonic uplift. The slight pedogenic alteration of deltaplain deposits in the uppermost HYC may or may not have developed after lake withdrawal. The erosional surface separating HYC from QZJ deposits is interpreted as an erosional unconformity, although the amount of erosion is unknown. The three meandering stream HCs in basal QZJ and the Argillisols in the uppermost part indicates fluvial infilling on the erosional unconformity. As a result, the landscape was stabilized for pedogenesis to proceed. The landscape stability and pedogenesis had persisted through the deposition of the overlying two thin ephemeral stream-loessial HCs. The Argillisols probably developed under a subhumid climate (Mack and James, 1994). Afterwards, continuous fluvial and loessial deposition persisted without major interruptions as evidenced by the lack of mature paleosols throughout the rest of QZJ LC. The top of the Argillisol-rich interval was interpreted as a disconformity across which mixed fluvial and loessial deposition dominated, suggesting a renewed tectonic uplift and change of atmospheric circulation pattern. Finally, the Argillisols developed on the resedimented loess deposits, suggesting that the change in atmospheric circulation pattern initiated concurrently during the period of landscape stability and pedogenesis, but persisted and intensified across the disconformity.

7. Delineation and Stratigraphic Correlation of Low-Order Cycle Boundaries

The geological events and processes interpreted from individual sections are similar and systematic, and form the foundation for stratigraphic correlation of the study interval (Fig. 12). A pure lithostratigraphic correlation is not possible because of the

lithological and stratigraphic complexities of the records. The trends of interpreted depositional environmental changes and major controlling processes that caused these changes are used to establish process-response relationships, all of which facilitate the delineation of the lower QZJ LC and its time-stratigraphic correlation.

7.1 Uppermost HYC LC

The widespread lacustrine deposition of the uppermost HYC LC in the Tarlong-Taodonggou half graben and Dalongkou area indicates a dominantly lacustrine environment in both areas. However, the uppermost HYC deposits are not synchronous due to the variable amount of subsequent erosion and, thus, a detailed paleoenvironmental and paleogeographic reconstruction at the end of the HYC time cannot be done. A series of events may have occurred during the widespread disconformity and erosional unconformity capping the HYC lacustrine deposits. A lake withdrawal probably was caused by a tectonic uplift because of sedimentary evidence in the uppermost HYC and basal QZJ deposits did not record significant drying (Yang et al., 2010). An episode of pedogenesis of the uppermost HYC sediments may have occurred locally. Variable degrees of pedogenesis occurred in most sections, except the southeastern Tarlong section. The pedogenic features may be the downward extension of overlying paleosols where they are in direct contact with the altered HYC lacustrine deposits; or may have formed before the lake withdrawal and subaerial exposure, because Calcisols are common in the upper HYC LC (Yang et al., 2010). Fluvial erosion is evident in all sections after the lake withdrawal, but the depth of downcutting varies greatly among sections. Two data were used in stratigraphic correlation to estimate the

minimum topographic variations caused by fluvial erosion. The first datum is the top of the stacked paleosol interval in the basal QZJ in northeastern, northern, and north-central Tarlong, Taodonggou, and Dalongkou. The second is the base of the first fluvial-loessial HC in southeastern and southwestern Tarlong section where the paleosol interval is absent. The top of paleosol intervals coincides with the base of the fluvial-loessial HCs in four other Tarlong-Taodonggou sections (Fig. 12), thus, it is reasonable to use the data to correlate the seven sections. In addition, a correlation of the conchostracan-rich bed in upper HYC between north-central and northern Tarlong sections indicates the erosional surface in north-central Tarlong is 7.5 m lower than that in northern Tarlong. Correlation using aforementioned data indicates that the greatest downcutting is in southwestern and southeastern Tarlong and Dalongkou sections at 101.6, 14, and 13.9 m, respectively. Similar topographic variations of the surface were reached by using the maximum-flooding surface in lower HYC LC (Yang et al., 2010) or the base of first deltaic deposits in overlying Wutonggou LC. The pattern of topographic variations suggests that a major fluvial valley is present in southwestern and southeastern Tarlong area and oriented approximately east to west (Fig. 12). An episode of intense tectonic uplift is interpreted from the extensive fluvial erosion and rugged topography in the Tarlong-Taodonggou half graben and from the thick channel-fill complex in Dalongkou. These facts and interpretation suggest that the disconformity-erosional unconformity capping the uppermost HYC lacustrine deposits is regional and significant, across which major changes in environmental, tectonic, and climatic conditions occurred. Hence, the surface is a low-order cycle boundary, namely the base of the newly-defined lower QZJ low-order cycle. Yang et al. (2010) did not identify this surface as a low-order cycle

boundary, because their interpretation was mainly based on data from northern Tarlong and Taodonggou sections.

7.2 Lower QZJ LC

Meandering stream deposits filled the topographic lows at the lower boundary of the lower QZJ LC. Rugged topography and copious sediment supply, both of which were probably driven by intense tectonic uplift, resulted in thick and extensive meandering stream deposits. Stream channels concentrated in the valleys in northeastern, southwestern, and southeastern Tarlong areas as well as in Dalongkou, whereas overbank and small tributaries occupied areas outside the valley in the eastern part of northeastern Tarlong, northern and north-central Tarlong, and Taodonggou. Slow sediment accumulation in overbank environments promoted pedogenesis, forming stacked paleosols. The rapid lateral facies and thickness changes are best demonstrated between the eastern and western sections in northeastern Tarlong and Taodonggou (Figs. 5, 8). Repeated downcutting by younger streams into older channel fills supports the interpretation of episodic intense tectonic activities, which had limited the fluvial accommodation space. The vicinity of southwestern Tarlong is probably the lowest area, where small, short-lived lakes developed by volcanic damming. The large amount of tuffs suggests a nearby volcanic source to southwestern Tarlong.

The intense meandering stream deposition eventually tapered, signifying a reduced topographic gradient, stable landscape, and likely an enlarged drainage basin, which were probably caused by fluvial infilling, headwater erosion, and tectonic quiescence. Intense pedogenesis expanded from the overbank area to the fluvial valleys,

covering most Tarlong-Taodonggou and the Dalongkou area, except southeastern and southwestern Tarlong. Stacked mature vertic Calcisols and calcareous Vertisols in Tarlong-Taodonggou suggest a semi-arid to arid climate with strong precipitation seasonality. However, vertic Argillisols in Dalongkou suggest a different climate than that in Tarlong-Taodonggou. The interpretation is less certain due to the limited amount of data. It is speculated that the Argillisols formed on a subhumid climate with strong seasonality, which may have been caused by local climatic variations, such as an orographic rain shadow effect, or regional climatic change because Dalongkou section is ~70 km to the north. Pedogenesis is minimal in the overbank deposits of meandering stream HCs in southeastern and southwestern Tarlong, where overbank deposition was more active than in the other areas. Nonetheless, the widespread occurrence of stacked mature paleosols suggests a significant time period of minimal deposition and nondeposition, landscape stability, and tectonic quiescence. Hence, the top surface of the paleosol interval is likely a regional disconformity, which, locally, changes to a correlative erosional unconformity in Taodonggou and a conformity in southwestern Tarlong. Yang et al. (2010) identified this surface as the boundary between HYC and QZJ LCs. Their interpretation is supported by this study and the surface now defines the upper boundary of the lower QZJ LC and the lower boundary of the rectified upper QZJ LC.

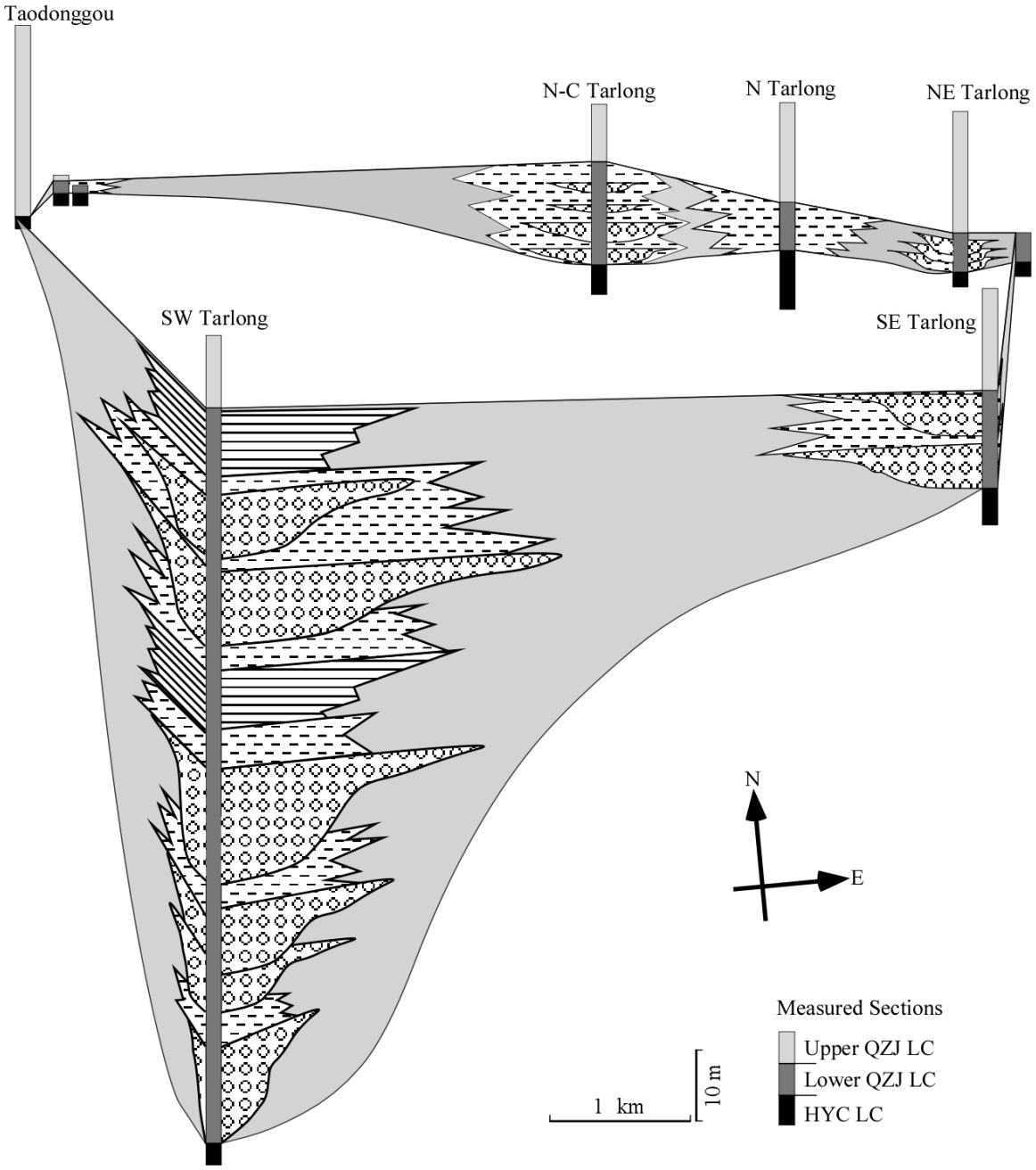

Figure 12. Fence diagram of the lower QZJ LC and adjacent strata in the Tarlong-Taodonggou half graben, showing lateral changes in thickness and lithofacies of fluvial valley and overbank deposits. The boundary between lower and upper QZJ LCs is the datum. Distance between measured sections is to scale.

7.3 Basal Upper QZJ LC

Renewed sedimentary deposition of alternating fluvial and loessial sediments occurred on top of the upper boundary of the lower QZJ LC in Tarlong-Taodonggou and Dalongkou areas. The common occurrence of ephemeral stream and loessial deposits suggests a dominantly semi-arid climate. In addition, the common loessites suggest a change of atmospheric circulation patterns that affected regional wind regime. Loess accumulation may have started during the deposition of the uppermost part of the lower QZJ LC in Dalongkou, earlier than in Tarlong-Taodonggou. The difference may be caused by spatial variations in wind regimes and source areas for loessial sediments or, alternatively, the lack of detailed analysis of host sediments of Calcisols in Tarlong-Taodonggou area. Future studies shall clarify the cause of the difference. In addition, tectonic activities intensified during the renewed deposition of basal upper QZJ LC, but were likely much less intense than those during the formation of the boundary between HYC and lower QZJ LCs and deposition of thick meandering stream systems in the lower part of the lower QZJ LC. Finally, we adapt Yang et al.'s (2010) definition of the upper boundary of the upper QZJ LC, which separates the fluvial-loessial deposits of the upper QZJ LC from the lacustrine deltaic and meandering stream deposits of the Wutonggou LC.

8. Discussion

The criteria for establishing a low-order cycle should be its duration, regional correlatability, and magnitude of changes in depositional environments and controlling processes across the cycle boundary, not its thickness (Fig. 13). Yang et al. (2010) stated that "*Low-order cycles are defined on the basis of similarity in types of HCs and ICs*

(intermediate-order cycles), which reflects the long-term trend of environmental changes and long-term stability of tectonic and/or climatic conditions. Low-order cycles are demarcated by regional unconformities and/or conformities, across which major changes in environment and tectonic and/or climatic conditions occurred." The newly-defined lower QZJ LC meets these criteria. The lower boundary of the lower QZJ LC is a regional erosional unconformity and disconformity, where a significant amount of erosion had occurred. It should represent a large amount of geological time. The processes that formed and occurred during the unconformity include lake withdrawal, fluvial incision, and tectonic uplift, and are regional in scale. The upper boundary of the lower QZJ LC has similar attributes to those of the lower boundary, including regional fluvial infilling resulting in a subdued topography and landscape stability and pedogenesis signifying a prolonged period of tectonic quiescence. The HCs within the lower QZJ LC are all dominated by meandering stream deposits, representing active fluvial infilling followed by paleosol formation. The thickness of the low-order cycle varies over a wide range as determined by the rugged depositional topography and uneven distribution of stream channels and overbank environments, which are the norm of terrestrial environments in a rift setting. In addition, sedimentary environments and tectonic and/or climatic conditions changed drastically across both the lower and upper boundaries. Finally, the duration of the two boundaries and the lower QZJ LC is unknown but probably significant. Yang et al. (2010) interpreted the unconformable boundary between their HYC and QZJ LCs to have a maximum duration of ~14 Ma, on the basis of a U/Pb zircon age of 281.42 ± 0.10 Ma of the tuff at the uppermost HYC at the southeastern Tarlong section and previous chronostratigraphic ages of the QZJ

Formation. The new stratigraphic data and interpretations in this study suggest that the maximum 14-Ma duration is likely distributed among the lower and upper boundaries and the rocks of the lower QZJ LC. All the above evidence supports the establishment of the lower QZJ LC.

The identification of the newly-defined lower QZJ LC provides insights into the profound changes and evolution of sedimentary environments and the mechanisms of major allogenic processes that had caused such changes. These changes and processes were recorded in a relatively thin and highly complex time-stratigraphic unit, the lower QZJ LC, in a highly-partitioned rift basin. This study demonstrates that only through detailed observations and careful sedimentological and stratigraphic analyses can such a significant time-stratigraphic unit be identified, and the process-response approach is effective in nonmarine time-stratigraphic analysis. Finally, the lower QZJ LC provides an important tectonic and climatic record at the mid-latitude of NE Pangea during the mid-Permian icehouse-hothouse transition (Scotese, 2001; Fielding et al., 2008).

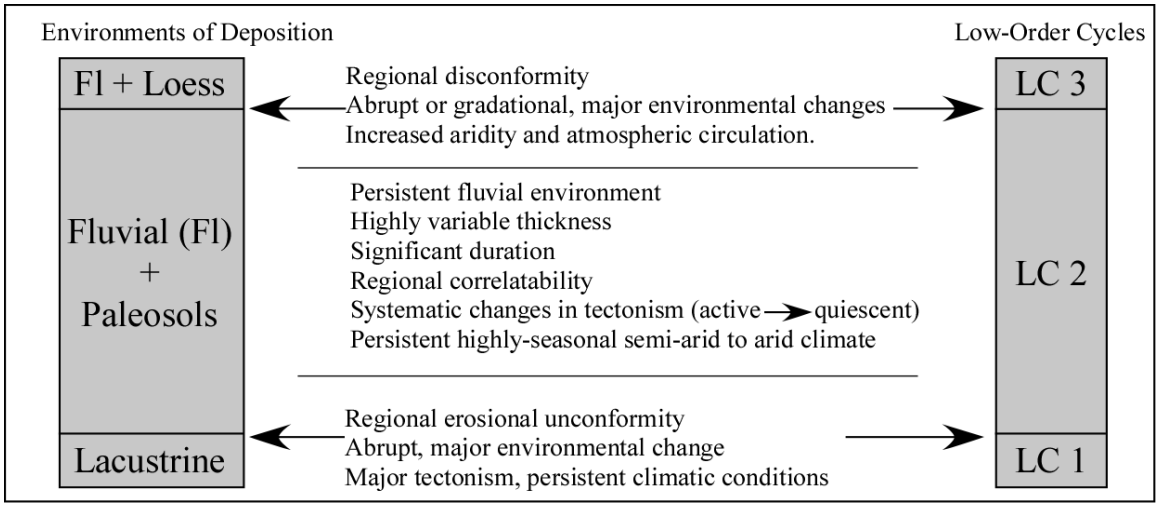

Figure 13. Schematic diagram showing the rationale behind the identification of low-order cycles (LC) and their boundaries on the basis of magnitude of changes in environments of deposition, nature of stratigraphic surfaces as cycle boundaries, and trends of environmental change and tectonic and climatic conditions.

9. Conclusions

A new synchronous cyclo-stratigraphic unit, the Middle-Permian lower QZJ LC, is defined in the Tarlong-Taodonggou half graben at the southern foothills and the Dalongkou area ~70 km to the north at the northern foothills of Bogda Mountains, NW China. It was the uppermost part of the previously-defined HYC LC, and consists of meandering stream deposits and stacked mature Calcisols and minor Argillisols and Vertisols in the upper part. Its lower boundary is a regional erosional unconformity separating the lacustrine deposits of the HYC LC from the overlying meandering stream deposits, and represents a regional lake withdrawal and significant fluvial incision, driven by an episode of intense tectonic uplift. Its upper boundary is a regional disconformity and correlative local erosional unconformity and conformity, separating the mature paleosols from overlying ephemeral and meandering stream and loessial deposits of the upper QZJ LC, and represents a prolonged episode of pedogenesis, tectonic quiescence, and a change of atmospheric circulation pattern. The lower QZJ LC is a significant time-

stratigraphic unit of a significant duration, albeit its highly variable thickness ranging from 0 to 102 m.

Intense tectonic uplift occurred during the formation of the lower boundary and deposition of meandering stream systems of the lower QZJ LC. Tectonic uplift decreased during the deposition of the upper part of the lower QZJ LC and tectonic quiescence occurred during pedogenesis and the formation of the upper boundary. Tectonic activities increased moderately afterward.

The climatic conditions had been semi-arid with strong precipitation seasonality in the Tarlong-Taodonggou area during the formation of the lower QZJ LC, whereas the conditions had been subhumid with strong precipitation seasonality in the Dalongkou area, which may have been caused by its northern location or local orographic effects. Atmospheric circulation pattern and wind regime changed in both areas after the formation of the upper boundary when loess deposition became dominant. The lower QZJ record serves as an important data point for tectonic and climatic conditions in the mid-latitude east coast of NE Pangea during the mid-Permian icehouse-hothouse transition.

This study demonstrates that a process-response approach, combined with detailed field observations and interpretation of controlling processes in a cyclostratigraphic context, is effective in identifying regional time surfaces and encompassing synchronous time-stratigraphic units of complex fluvial-lacustrine deposits in a rift setting.

Acknowledgements

We would like to thank Drs. J. Wang and M.L. Wan of Nanjing Institute of Geology and Paleontology of Chinese Academy of Sciences, Dr. Y. Yang of Xi'an Petroleum University, Dr. X. Luo of Institute of Geology and Geophysics, Chinese Academy of Sciences, Dr. Q. Feng of Shandong University of Science and Technology, S.S. Wang, J.J. Liu, T. Foster, Z.X. Li, J.J. Li, L.L. Cheng, C.C. Zhou, Y.M. Gao, and B. Sun for field, funding, and/or logistic assistance. This research was partially supported by four student research grants from Geological Society of America, Ed Picou/GCSSEPM, American Association of Petroleum Geologists, and the Al Spreng Graduate Research Grant from the Geology and Geophysics Program of Missouri University of Science and Technology to Jonathan Obrist-Farner, and by a research grant from University of Missouri Research Board and a research grant (No. 2011ZX05008-004-053) from Institute of Geology and Geophysics of Chinese Academy of Sciences to Wan Yang. Acknowledgement is made to the Donors of the American Chemical Society Petroleum Research Fund, for a grant to Wan Yang. We are grateful to Zengzhao Feng, Jingtai Han, and an anonymous reviewer for the constructive reviews that improved the quality of this contribution.

References

Allen, M. B., Sengor, A. M. C., and Natal'in, B. A., 1995, Junggar, Turfan and Alakol basins as Late Permian to Early Triassic extensional structures in a sinistral shear zone in the Altaid orogenic collage, central Asia: Journal of the Geological Society, v. 152, p. 327-338.

Alonso-Zarza, A. M., and Wright, V. P., 2010, Calcretes, In: Alonso-Zarza, A. M., and Tanner, L. H., (Ed.), Carbonates in continental settings: facies, environment, and processes. pp. 225-267.

Bagnold, R. A., 1941, The physics of blown sand and desert dunes, Methuen, London, 265 p.

Blum, M. D., and Törnqvist, T. E., 2000, Fluvial responses to climate and sea-level change: a review and look forward: Sedimentology, v. 47, p. 2-48.

Bown, T. M., and Kraus, M. J., 1987, Integration of channel and floodplain suits, I. Developmental sequence and lateral relations of alluvial paleosols: Journal of Sedimentary Petrology, v. 57, p. 587-601.

Cai, T., 1999, Stratigraphy of Xinjiang Uygur Autonomous Region, China University of Geosciences Press, 430 p.

Carroll, A. R., Graham, S. A., Hendrix, M. S., Ying, D., and Zhou, D., 1995, Late Paleozoic tectonic amalgamation of northwestern China: sedimentary record of the northern Tarim, northwestern Turpan, and southern Junggar Basins: Geological Society of America Bulletin, v. 107, p. 571-594.

Catuneanu, O., 2006, Principles of sequence stratigraphy, Elsevier, Oxford, 375 p.

Fielding, C. R., Frank, T. D., and Isbell, J. L., 2008, The late Paleozoic ice age - A review of current understanding and synthesis of global climate patterns, In: Fielding, C. R., Frank, T. D., and Isbell, J. L., (Ed.), Resolving the Late Paleozoic Ice Age in Time and Space. The Geological Society of America Special Paper 441, Boulder, pp. 343-354.

Kraus, J. M., and Brown, T. M., 1988, Pedofacies analysis: A new approach to reconstructing ancient fluvial sequences, In: Reinhardt, J., and Sigleo, W. R., (Ed.), Paleosols and Weathering Through Geologic Time: Principles and Applications. pp. 143-152.

Kraus, M. J., 1999, Paleosols in clastic sedimentary rocks: their geologic application: Earth-Science Reviews, v. 47, p. 41-70.

Legarreta, L., and Uliana, M. A., 1998, Anatomy of hinterland depositional sequences: Upper Cretaceous fluvial strata, Neuquen Basin, west-central Argentina, Relative Role of Eustasy, Climate, and Tectonism in Continental Rocks, SEPM Special Publication No. 59, p. 83-92.

Lowenstein, T. K., Hein, M. C., Bobst, A. L., Jordan, T. E., Ku, T. L., and Luo, S., 2003, An assessment of stratigraphic completeness in climate-sensitive closed-basin lake sediments: Salar de Atacama, Chile: Journal of Sedimentary Research, v. 73, p. 91-104.

Mack, G. H., and James, W. C., 1994, Paleoclimate and the global distribution of paleosols: The Journal of Geology, v. 102, p. 360-366.

Mack, G. H., James, W. C., and Monger, H. C., 1993, Classification of paleosols: Geological Society of America Bulletin, v. 105, p. 129-136.

Metcalfe, I., Foster, C. B., Afonin, S. A., Nicoll, R. S., Mundil, R., Xiaofeng, W., and Lucas, S. G., 2009, Stratigraphy, biostratigraphy and C-isotopes of the Permian-Triassic non-marine sequence at Dalongkou and Lucaogou, Xinjian Province, China: Journal of Asian Earth Sciences, v. 36, p. 503-520.

Miall, A. D., 1996, The geology of fluvial deposits: sedimentary facies, basin analysis, and petroleum geology, Springer, New York, 582 p.

Miall, A.D., and Arush, M., 2001, The Castlegate sandstone of the Book Cliffs, Utah: sequence stratigraphy, paleogeography, and tectonic controls: Journal of Sedimentary Research, v. 71, p. 537-548.

Obrist, J., Yang, W., and Feng, Q., 2013, Mixed fluvial and loess deposits in an intracontinental rift basin, Mid-Permian (Wordian-Capitanian) Quanzijie Low-Order Cycle, Bogda Mountains, NW China: AAPG Annual Meeting, Pittsburgh.

Olsen, P. E., 1997, Stratigraphic record of the Early Mesozoic breakup of Pangea in the Laurasia-Gondwana rift system: Annual Review of Earth and Planetary Sciences, v. 25, p. 337-401.

Péwé, T. L., 1955, Origin of the upland silt near Fairbanks, Alaska: Geological Society of America Bulletin, v. 66, p. 699-724.

Péwé, T. L., 1975, Quaternary Geology of Alaska: Geological Survey Professional Paper 835, 145 p.

Pye, K., 1987, Aeolian dust and dust deposits, Academic Press Inc., London, 334 p.

Retallack, G. J., 2001, Soils of the past: An introduction to paleopedology, Blackwell Science, London, 404 p.

Scotese, C. R., 2001, Atlas of Earth history, Volume 1, PALEOMAP Project, Arlington, Texas, 52 p.

Scotese, C. R., 2002, PALEOMAP website http://www.scotese.com.

Sengor, A. M. C., and Natal'in, B. A., 1996, Paleotectonics of Asia: fragments of a synthesis, In: Yin, A., and Harrison, T. M., (Ed.), The tectonic evolution of Asia. New York, Cambridge University Press, pp. 486-640.

Shanley, K. W., and McCabe, P. J., 1994, Perspectives on the sequence stratigraphy of continental strata: AAPG Bulletin, v. 78, p. 544-568.

Talbot, M. R., and Allen, P. A., 1996, Lakes, In: Reading, H. G., (Ed.), Sedimentary environments: processes, facies and stratigraphy. Blackwell Science, London, pp. 83-124.

Thomas, S. G., Tabor, N. J., Yang, W., Myers, T. S., Yang, Y., and Wang, D., 2011, Paleosol stratigraphy across the Permian-Triassic boundary, Bogda Mountains, NW China: implications for palaeoenvironmental transition through earth's largest mass extinction: Palaeogeography, Palaeoclimatology, Palaeoecology, v. 308, p. 41-64.

Wartes, M. A., Carroll, A. R., and Greene, T. J., 2002, Permian sedimentary record of the Turpan-Hami basin and adjacent regions, northwest China: constraints on postamalgamation tectonic evolution: Geological Society of America Bulletin, v. 114, p. 131-152.

XBGMR, 1993, Regional geology of Xinjiang Uygur Autonomous Region. Geological Memoirs, Series 1, No. 32, Xinjiang Bureau of Geology and Mineral Resources: Beijing, Ministry of Geology and Mineral Resources, Geological Publication House, p. 762.

Yang, W., 2008, Depositional systems analysis within a seismic sequence stratigraphic framework, Turpan-Hami basin, NW China: Internal Report, Tu-Ha Petroleum Bureau, v. PetroChina, p. 49 pp.

Yang, W., Crowley, J. L., Obrist-Farner, J., Tabor, N. J., Feng, Q., and Liu, Y. Q., 2013, A marine back-arc origin for the Upper Carboniferous basement of intracontinental greater Turpan-Junggar basin - Volcanic, sedimentary, and geochronologic evidence from southern Bogda Mountains, NW China: Geological Society of America Annual Meeting, GSA Abstract with Programs, Vol. 45, No. 1, Denver, Colorado.

Yang, W., Feng, Q., Liu, Y., Tabor, N., Miggins, D., Crowley, J. L., Lin, J., and Thomas, S., 2010, Depositional environments and cyclo- and chronostratigraphy of uppermost Carboniferous-Lower Triassic fluvial-lacustrine deposits, southern Bogda Mountains, NW China - A terrestrial paleoclimatic record of mid-latitude NE Pangea: Global and Planetary Change, v. 73, p. 15-113.

Yang, W., Liu, Y., Feng, Q., Lin, J., Zhou, D., and Wang, D., 2007, Sedimentary evidence of Early-Late Permian mid-latitude continental climate variability, southern Bogda Mountains, NW China: Palaeogeography, Palaeoclimatology, Palaeoecology, v. 252, p. 239-258.

Zhu, H. C., Ouyang, S., Zhan, J. Z., and Wang, Z., 2005, Comparison of Permian palynological assemblages from the Junggar and Tarim basins and their phytoprovincial significance: Review of Palaeobotany and Palynology, v. 136, p. 181-207.

II. LOESS AND FLUVIAL DEPOSITS AND THEIR IMPLICATIONS ON PALEOCLIMATIC CONDITIONS DURING AN ICEHOUSE-HOTHOUSE TRANSITION, CAPITANIAN UPPER QUANZIJIE LOW-ORDER CYCLE, BOGDA MOUNTAINS, NW CHINA

Jonathan Obrist-Farner, Wan Yang, Edgar Martinez

Abstract

Permian terrestrial sedimentary records provide important clues on paleoclimatic conditions and their changes during the last icehouse to hothouse transition in a vegetated planet. Seven stratigraphic sections of Middle Permian upper Quanzijie low-order cycle (QZJ LC) in Bogda Mountains, NW China, are studied to interpret the depositional environments and paleoclimatic conditions within a multi-order stratigraphic framework. The upper QZJ LC is characterized by laterally persistent, thick, and massive red mudrocks interbedded with laterally discontinuous conglomerates. The massive mudrocks are interpreted as loess deposits on the basis of their massive structure, uniform grain size distribution, lateral extent, mineral composition, and geochronological characteristics. Thin conglomerates with a low-relief erosional base are interpreted as ephemeral braided stream deposits, whereas thick conglomerates with a high-relief base as meandering stream deposits. In Tarlong-Taodonggou, Protosols are common in loess deposits and indicate fast dust accumulation under arid to semiarid conditions; Gleysols are common in loess in the upper part of the studied sections and indicate humid to subhumid conditions at the end of upper QZJ time. In Dalongkou, climatic conditions are subhumid with semiarid episodes during most of the upper QZJ time. The data strongly suggests that persistent aridity, eolian processes, and trapping mechanisms existed in NE Pangea during Capitanian time to transport, deposit, and trap a large volume of silt and

clay as loess. The gradual but dramatic climatic change from semiarid to subhumid conditions as late as Roadian-Wordian to the end of Capitanian correlates to the global demise of the Late Paleozoic Ice Age.

1. Introduction

Permian sedimentary records have been extensively studied to interpret paleoenvironment, paleogeography, paleoclimate, tectonics, and their changes at many locations across Pangea (e.g., Soreghan et al., 2007; Fielding et al., 2008a; Tabor and Poulsen, 2008; Sweet et al., 2013). It is well known that during the assemblage of Pangea, extreme climatic changes occurred from Carboniferous to Triassic (Kutzbach and Gallimore, 1989; Parrish, 1993; Tabor and Poulsen, 2008). However, most of Permian sedimentary records used to infer these climatic conditions are located in central (e.g., Tabor and Montañez, 2002, 2004; Tabor and Poulsen, 2008) and southern Pangea (e.g., Fielding et al., 2008a; 2008b; 2010) because Permian terrestrial records are limited in northern mid- to high-latitude Pangea (e.g., Metcalfe et al., 2009; Yang et al., 2010; Thomas et al., 2011).

In this study, the terrestrial Middle Permian upper Quanzijie low-order cycle (abbreviated as QZJ LC in this paper; Yang et al., 2007, 2010; Obrist-Farner and Yang, 2015) in Tarlong-Taodonggou and Dalongkou areas of Bogda Mountains, NW China (Fig. 1A, B), is investigated to interpret the depositional environments and paleoclimatic conditions through field and petrographic observations. This work focuses on detailed interpretation of lithofacies, depositional environments, and cyclostratigraphy of upper QZJ deposits in southern and northern Bogda Mountains. The results show that the upper QZJ LC is composed of mixed deposits mainly in ephemeral braided-stream, coarse-

grained meandering-stream, and eolian environments. Arid climatic conditions predominated during the deposition of most of upper QZJ LC, and changed to humid condition gradually during the deposition of the uppermost part of upper QZJ LC. The climatic change correlates and is similar to that documented from southern mid- to high-latitude Pangea (e.g., Retallack et al., 2006) and is interpreted to correspond to warmer and wetter conditions that resulted from the demise of the Late Paleozoic Ice Age (Ziegler et al., 1997; Fielding et al., 2008a). The findings in this study serve as a critical data point for future quantitative paleoclimatic modeling as well as regional and global stratigraphic correlation of Middle Permian terrestrial records across Pangea.

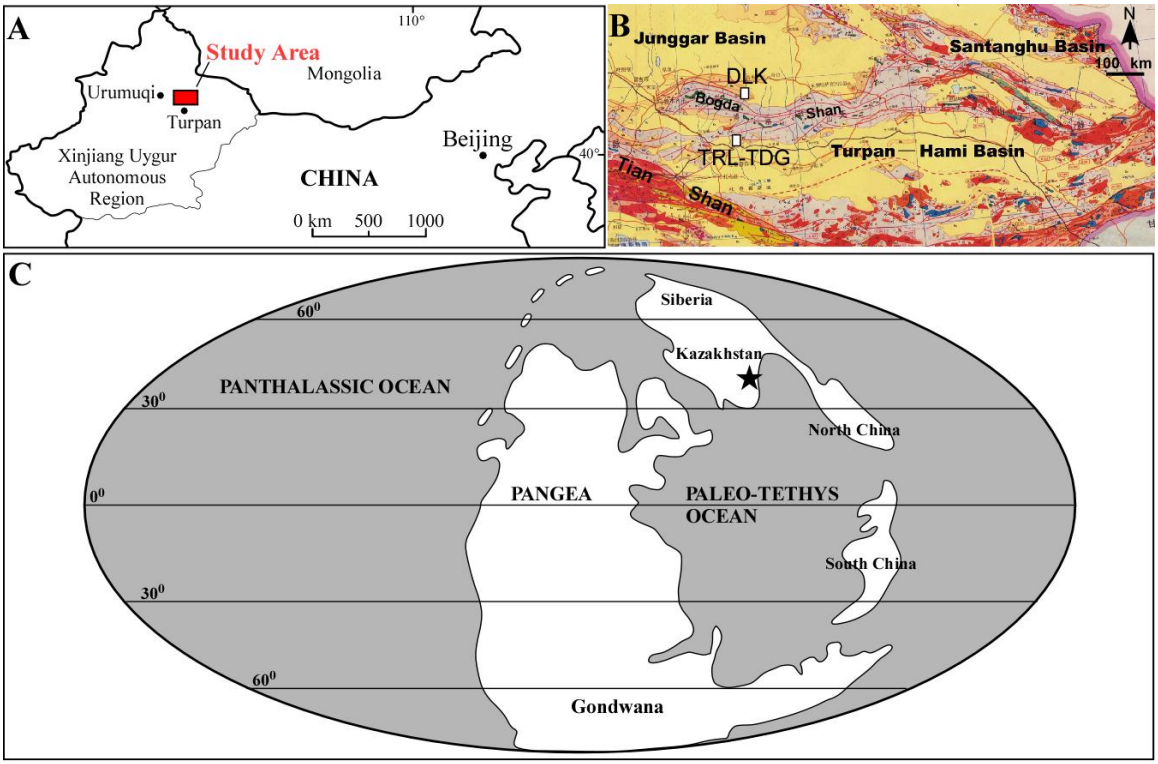

Figure 1. A) Location of the study area in Xinjiang Uygur Autonomous Region, NW China. B) Geological map of eastern Xinjiang, showing locations of Tarlong-Taodonggou (TRL-TDG) and Dalongkou (DLK). Modified from XBGMR (1993). C) Global paleogeographic reconstruction for the Late Permian. Modified from Scotese (2002). The location of the study area is marked with a black star.

2. Geological Background

The studied upper QZJ LC is exposed in the Tarlong-Taodonggou and the Dalongkou areas at the southern and northern foothills of Bogda Mountains, respectively (Figs. 1A, B; 2). It was deposited in the intra-continental greater Turpan-Junggar rift basin in northwestern China during the Middle Permian (Allen et al., 1995; Sengor and Natal'in, 1996; Yang et al., 2010; cf. Carroll et al., 1990, 1995, 2010). The Bogda Mountains is in southeastern Kazakhstan Plate, NE Pangea (Fig. 1C), which migrated northward to ~40-50^0 N paleo-latitude during Kungurian-Wuchiapingian epochs (Sengor and Natal'in, 1996; Scotese, 2001). This plate reconstruction places the Bogda Mountains in the mid-latitude east-coast temperate humid climatic belt during the Permian according to modern climatic zonation (Chumakov and Zharkov, 2003; Yang et al., 2010). Yang (2008) interpreted the Tarlong-Taodonggou area as a half graben, based on lateral facies and thickness changes and basin geometries on seismic sections from the adjacent Turpan-Hami Basin. Moreover, Yang et al. (2013) suggests that a marine back-arc basin in the Tarlong-Taodonggou area was progressively filled up in the latest Carboniferous; final plate amalgamation and formation of the Turpan-Junggar continental crust are represented by the deposition of a thick felsic ignimbrite capping the marine deposits at 301.37 Ma. Rifting occurred almost immediately after the closure of the back-arc basin and formation of the Turpan-Junggar continental crust (Yang et al., 2013). Alluvial, fluvial, and lacustrine deposition ensued and persisted throughout Permian and Early Triassic, filling the half grabens and grabens in the intra-continental Turpan-Junggar basin (XBGMR, 1993; Cai, 1999; Yang, 2008; Metcalfe et al., 2009; Yang et al., 2010).

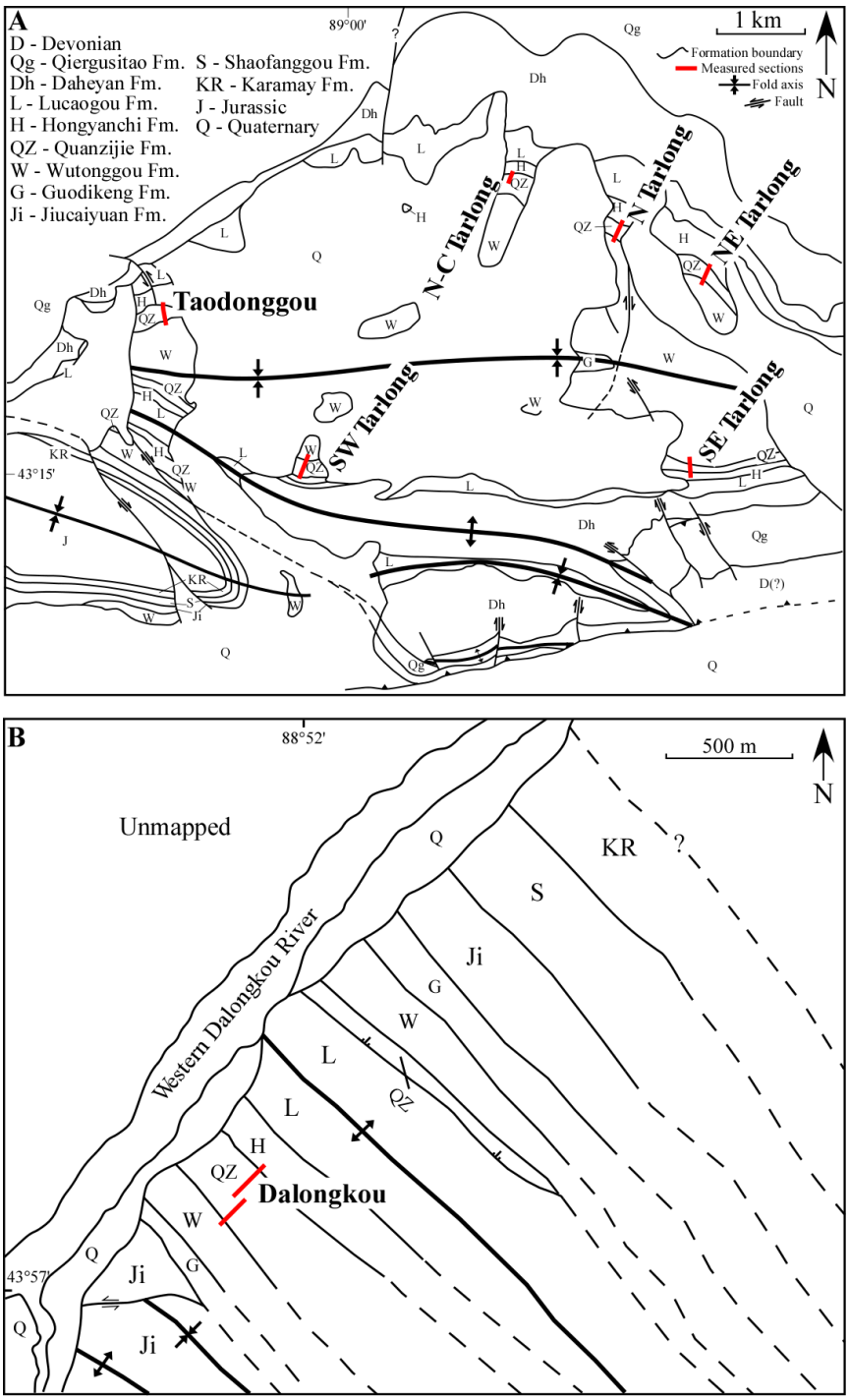

Figure 2. Geologic maps of Tarlong-Taodonggou (A) and Dalongkou (B) areas showing names and location (red lines) of measured sections. Modified from Yang et al. (2010) and Obrist-Farner and Yang (2015).

The upper QZJ LC is an informal cyclostratigraphic unit defined by Obrist-Farner and Yang (2015; see also Yang et al., 2007, 2010) on the basis of major environmental trends in the Tarlong-Taodonggou and Dalongkou areas (Fig. 3). It correlates largely with the Quanzijie Formation (XBGMR, 1993; Cai, 1999), which occurs in present Junggar Basin and Turpan Basin in the subsurface and in the foothills of Bogda Mountains and northern Tianshan in the outcrop (Fig. 1B). Exposure of the upper QZJ LC is commonly subdued due to the abundance of muddy deposits. Yang et al.'s (2010) field study of two QZJ sections in southern Bogda Mountains interpreted preliminarily the depositional environments and large-scale paleoclimatic and tectonic trends. They stated that the origin of common structureless mudrocks is enigmatic, which were tentatively interpreted as fluvial overbank deposits. In the Tarlong-Taodonggou area, the upper QZJ LC contains red, drab, and gray conglomerate, sandstone, mudrocks, and paleosols, overlies fluvial and lacustrine deposits of the lower QZJ LC unconformably and conformably (Obrist-Farner and Yang, 2015), and grades upward into lacustrine deltaic and lake-margin deposits of the Wutonggou LC conformably (Fig. 4A; Yang et al., 2010). The upper QZJ LC shows an overall fining-upward trend, as indicated by a decrease in clast size of conglomerate and an increase in the amount of mudrock. Paleoclimatic conditions changed from arid and semiarid as indicated by the occurrence of Calcisols to subhumid-humid as indicated by the occurrence of Gleysols (Yang et al., 2010).

The age of upper QZJ LC is poorly constrained and was interpreted as Capitanian by Obrist-Farner and Yang (2015; see also XBGMR, 1993; Cai, 1999; Zhu et al., 2005; Wartes et al., 2002; Yang et al., 2010). Yang et al. (2010) placed the Hongyanchi LC as Artinskian in age on the basis of a U/Pb zircon age of 281.42 ± 0.10 Ma of a tuff found at

the uppermost part of the Hongyanchi LC. Obrist-Farner and Yang (2015) estimated the bounding surfaces and the strata of the lower QZJ LC to have a combined maximum duration of ~ 14 Ma (cf. Yang et al., 2010). Hence, a Capitanian age is used for the upper QZJ LC in this study.

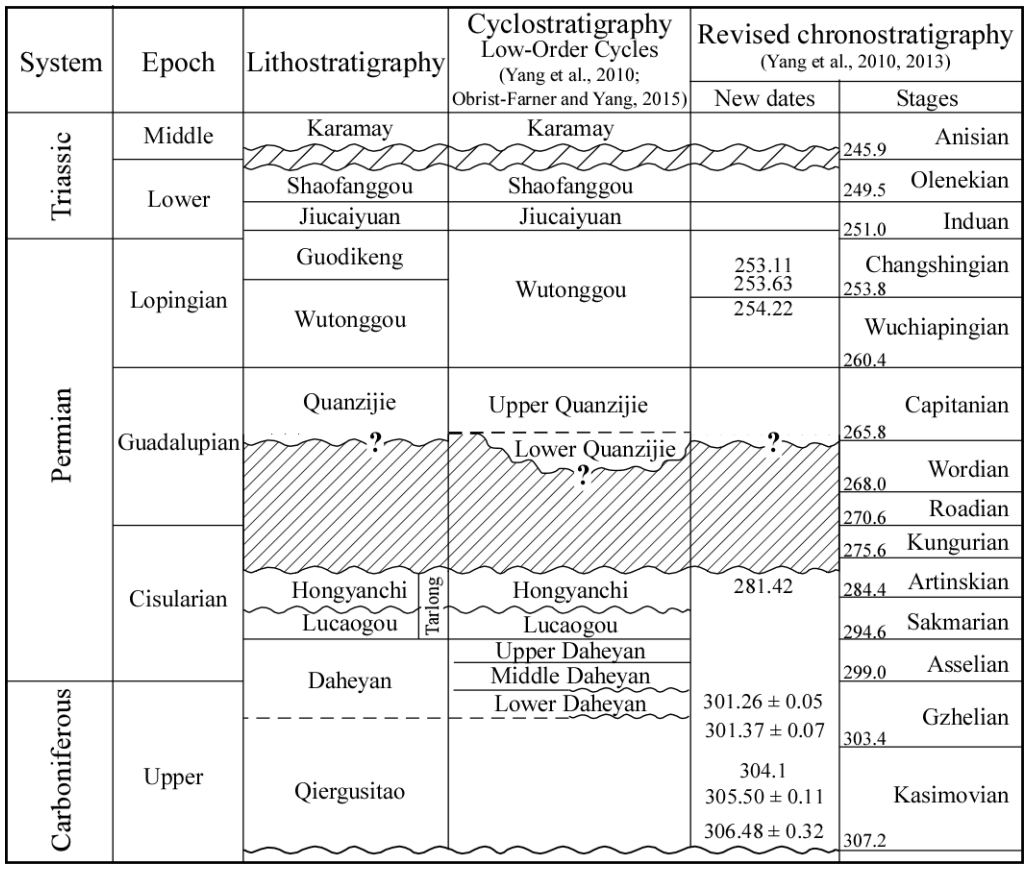

Figure 3. Chrono-, litho-, and cyclostratigraphy of Upper Carboniferous-Lower Triassic strata in the Tarlong-Taodonggou area. Wavy lines are major unconformities; dashed lines disconformity; and hatched areas missing strata. Absolute ages at stage boundaries from Gradstein et al. (2004). Modified from Yang et al. (2010, 2013) and Obrist-Farner and Yang (2015).

3. Data and Methodology

Field and laboratory observations and analyses along seven measured outcrop sections are conducted to characterize and identify lithofacies and their vertical and lateral associations, from which their depositional environments and paleoclimatic conditions are interpreted. Five of the sections are first reported in detail here; the other two, the northern Tarlong and Taodonggou sections, were reported by Yang et al. (2010) but reinterpreted here. Six of the sections, the northern, northeastern, southeastern, southwestern, and north-central Tarlong sections and the Taodonggou section, are in the Tarlong-Taodonggou half-graben; and one section is in the Dalongkou area (Fig. 2). Lithology, sedimentary texture and structure, fossil content, stratal geometry and boundary relationship, and lateral thickness and lithologic changes of sedimentary units are described at a cm-dm scale and used to define lithofacies. Subsequently, the characteristics of individual lithofacies, lithofacies associations, and their vertical and lateral stacking patterns are used to interpret the depositional environments. In addition, the texture and composition of 1688 gravels from 16 different conglomerates are examined to identify their lithologies for provenance interpretation. Dip directions and angles of a total of 327 imbricated pebbles from 16 conglomerates are measured. The measurements are corrected using the software Stereonet v.8.6.6 of Allmendinger et al. (2013) to determine the paleocurrent directions. Finally, paleosols are differentiated on the basis of lithology, color, and ped texture and structure and classified using Mack et al.'s (1993) scheme.

Thin sections for 42 medium- to coarse-grained sandstones are studied under a petrographic microscope. Each thin section is stained for calcite and 400 points are counted using the Gazzi-Dickinson method (Gazzi, 1966; Dickinson, 1970). Grain

composition, size, sorting, roundness, and contact, matrix-to-grain ratio, and type of cement are documented. The results are used to substantiate field observations and interpretations of lithology and depositional conditions.

Grain size analysis of 69 mudrock samples is conducted to aid in environmental interpretation. It is done using the laser diffraction particle size analyzer (LS 13 320 series) in the Beckman Coulter Particle Characterization Laboratory, Miami, Florida, U.S.A. 2 grams of a sample are placed in 1 mL of 1M HCl solution in a 150 mL beaker to loosen and disperse the grains. 60 mL of deionized water and one mL of 10% sodium hexametaphosphate (Calgon) are added into the beaker. The sample solution is probe-sonicated for four minutes at 100 watts, and then transferred into the LS 13 320 Aqueous Liquid Module to carry out the standard operation procedure. Each sample is processed and analyzed for three rounds to ensure the reliability of the measurements. The results are presented as an average of the three measurements and are reported as volume percentages. In addition, to test whether 2 grams are representative of an entire sample, two larger samples weighing 40 grams are disaggregated following the aforementioned procedure and analyzed under standard conditions. The results are similar to those obtained from the smaller samples, indicating that results from 2-gm samples are representative.

A total of 10 sandstone and mudrock samples are grounded in a mortar and pestle. The grounded samples are loaded as randomly oriented powder for X-ray diffraction (XRD) analysis using a PANalytical X'Pert Pro Multi-Purpose Diffractometer with Cu-Kα radiation from 4° to 80° 2Θ at a scanning speed of 2º 2Θ/min. The results are used to substantiate field observations and interpretations of mineral composition.

U-Pb detrital zircon geochronology is used to aid in environmental and provenance interpretations. Zircons are separated using standard techniques and annealed at 900°C for 60 hours in a muffle furnace. Randomly selected grains are mounted in epoxy and polished until their centers are exposed. Cathodoluminescence (CL) images are obtained with a JOEL JSM-1300 scanning electron microscope and Gatan MiniCL. The zircons are analyzed by a laser ablation inductively couple plasma mass spectrometer (LA-ICPMS) using a ThermoElectron X-Series II quadrupole ICPMS and New Wave Research UP-213 Nd:YAG UV laser ablation system at Boise State University. A total of 544 zircons are analyzed from nine samples; three samples from Tarlong-Taodonggou and six from Dalongkou.

Three orders of sedimentary cycles are delineated on the basis of repetitive changes of interpreted depositional environments and controlling processes (Yang et al., 2010). A high-order cycle (HC) is the basic cyclostratigraphic entity. The stacking pattern of HCs is used to interpret environmental and paleoclimatic conditions and changes. A low-order cycle is defined by the stacking of HCs showing similar environmental variations that formed under persistent climatic and tectonic processes and is bounded by low-order cycle boundaries across which major climatic or tectonic changes and associated environmental changes occur. Yang et al., (2010) also defined intermediate-order cycles as a group of HCs that are linked to lake expansion and contraction. However, delineation of intermediate cycles is not the focus of this study and, thus, not carried out.

Finally, climatic conditions and tectonic movement are interpreted using the aforementioned cyclostratigraphic framework. The climatic conditions for individual

cycles are qualitatively interpreted with respect to the precipitation (P) to evaporation (E) ratio as arid (P/E<<1), semiarid (<1), subhumid (>1), and humid (>>1) (Yang et al., 2010). Tectonic uplift is interpreted to occur when channels are amalgamated and minimal overbank and loess deposits are present, quiescence when paleosols developed, and subsidence when thick overbank and loess deposits are preserved. The tectonic influence on sedimentation and possible effects on lithofacies and depositional environments is filtered to consider the sedimentary record as an optimal reflection of climatic conditions (e.g., Lowenstein et al., 2003; Yang et al., 2010).

4. Lithofacies and Their Depositional Environments

Five types of lithofacies are identified in the upper QZJ LC and interpreted as fluvial and eolian deposits. The environments and their stratigraphic trends are used to delineate sedimentary cycles and interpret paleoclimatic conditions.

4.1 Lithofacies 1 – Clast-Supported Conglomerates

Clast-supported conglomerates are common and account for ~11% of upper QZJ LC in thickness. They occur in the lower part of fining-upward successions. In the lower part of the Tarlong-Taodonggou sections, mafic and intermediate volcanic and shallow-intrusive igneous gravels dominate and sandstone and shale gravels are minor; the latter increases in the upper part of the sections (Table 1). On the other hand, sandstone and shale gravels dominate with minimal igneous gravels throughout the Dalongkou section. The gravels in all sections are moderately to well sorted and angular to subrounded. They are mostly in contact with each other and embedded in a sandy matrix. The percentage of gravels in the conglomerates is 30-100%. In a few cases, such as a 5-m thick

conglomerate in the upper part of the Dalongkou section, dark gray to black dolomitic shale gravels (Fig. 4B) dominate and are similar in lithology to the underlying shales of the Lucaogou LC (Yang et al., 2010). The gravels in all sections are commonly imbricated or parallel to bedding plane. Large-scale low-angle tabular cross beddings are rare. The base of conglomerates is concave and erosional, whereas the top is commonly flat and gradational with overlying sandstones.

Table 1. Composition of 1688 gravels in 16 conglomerates beds.

Sections	Stratigraphic Location	Igneous	Sedimentary	Metamorphic
Northeastern	Lower QZJ LC	80	20	0
	Middle upper QZJ LC	81	19	0
	Upper upper QZJ LC	33	67	0
Southeastern	Lower QZJ LC	92	8	0
	Middle upper QZJ LC	83	17	0
	Upper upper QZJ LC	42	58	0
Southwestern	Lower QZJ LC	38	62	0
	Lower QZJ LC	76	24	0
	Lower upper QZJ LC	25	75	0
Taodonggou	Lower upper QZJ LC	70	30	0
	Middle upper QZJ LC	57	33	10
	Upper upper QZJ LC	60	33	7
Dalongkou	Lower QZJ LC	4	96	0
	L. Middle upper QZJ LC	3	97	0
	U. Middle upper QZJ LC	8	92	0
	Upper upper QZJ LC	6	94	0

Note: All results are in percentage.

Two types of conglomerates are differentiated on the basis of their stratal geometry, grain size trend, and sedimentary structures. The first type is 2-5 m thick on average, has a channel form with a high-relief erosional base up to several meters, and is laterally persistent for several hundreds of meters. Several channel-forms may stack

successively and are filled with conglomerates and sandstones. The channel fill contains common internal erosional surfaces. This type of conglomerate occurs mainly in the Dalongkou section and rarely in the Tarlong-Taodonggou sections. The second type of conglomerates are 0.1-2 m thick on average, have an erosional base with a low-relief base of 10s cm and an abrupt top with overlying mudrocks, and are laterally continuous for 1-10s m and encased in mudrocks. They dominate in the Tarlong-Taodonggou sections and are rare in the Dalongkou section.

The ratio between lateral extent and measured thickness of 18 conglomerate units in the northeastern Tarlong section and 25 conglomerate units in the Dalongkou section are used to estimate the width-depth ratios of channel forms. No decompaction is considered to restore the original thickness. Thus, the width/depth estimates are the upper limits. The lateral extent for the upper QZJ channels is assumed to represent a single channel fill. In addition, where channel fills contain sandstones, their thickness is regarded as a part of the total thickness of the channel fill. The lateral extent of the channels in northeastern Tarlong ranges from 7.3-102.2 m, and is 44.1 m on average; the thickness of channel fills from 0.4-1.9 m, and 0.8 m on average; the resulting width-depth ratio from 9.1-175.2, and 60.4 on average. The channels in Dalongkou extend 7-258 m, and 77.5 m on average; the thickness from 0.3-11.2 m, and 2.17 m on average; the resulting width-depth ratio from 6.36-286.0, and 59.1 on average. A fining-upward trend is evident in the thick conglomerates, where gravels decrease in size gradationally into sand. The trend, however, is crude to nonexistent in most thin conglomerates. Overall, the abundance, thickness, and maximum size of gravels of conglomerates decrease upsection in the upper QZJ LC.

The erosional base, imbricated gravels, tabular cross-beds, and overall fining-upward trend of conglomerates indicate that they are stream deposits. The great thickness of the first type of conglomerates, the overlying gravelly very coarse to coarse lithic sandstones and thin mudrock (see descriptions below), and the high-relief erosional base suggest that the thick conglomerates are channel-fill deposits of coarse-grained meandering streams. On the other hand, the small thickness of the second type of conglomerates, their large width-depth ratio, low-relief erosional base, limited to no overlying sandstones, and abrupt juxtaposition with overlying mudrocks suggest that this type of conglomerates were deposited in small, shallow, poorly-defined, sand and mud-poor streams. In addition, their limited lateral extent and isolated occurrences as bodies encased in thick mudrocks suggest that the streams are likely ephemeral gravelly braided streams generated by episodic flash floods (Miall, 1996).

4.2 Lithofacies 2 – Sandstones

Sandstones in the upper QZJ LC make up ~21% in thickness of all measured upper QZJ LC and include texturally and compositionally immature to submature lithic wackes and lithic arenites. Grain size ranges from very fine to very coarse sand. Framework grains are angular to rounded, with common rounded floating granules and pebbles. Basaltic lithics and plagioclase feldspars dominate in Tarlong-Taodonggou. Sedimentary lithics, potassium and plagioclase feldspars, and quartz dominate in Dalongkou, with rare basaltic lithics. Zeolite cements are abundant in Tarlong-Taodonggou but are not present in Dalongkou. Finally, framework grains are commonly

coated by illuvial clays in the upper part in Tarlong-Taodonggou, whereas the grains are commonly coated throughout in Dalongkou.

Three types of sandstones are recognized on the basis of their measured thickness, lateral extent, grain size trend, and boundary relationship with underlying and overlying lithofacies. The first type of sandstones have a thickness range of 0.1-3.1 m, 0.5 m on average, and have a limited lateral extent. In the upper QZJ LC, it occurs sporadically and overlies ephemeral-stream conglomerates across a gradational boundary and underlies mudrocks across a sharp boundary, forming a crude upward-fining trend. The sandstones are lithic arenites to wackes and mainly medium to very coarse-grained. Internal erosional surfaces, plane beds, trough and low-angle tabular cross beds are rare. The association of this subtype with ephemeral stream conglomerates and the crude fining upward trend indicate that the sandstones are waning-flow deposits during flash floods.

The second type is similar to the first type in composition but thicker, with a thickness range of 0.3-3.3 m; 0.9 m on average. The sandstones overlie conglomerates across a gradational boundary and underlie mudrocks across a gradational boundary, forming an overall fining-upward conglomerate-sandstone-mudrock succession. This type is rare in Tarlong-Taodonggou but common in Dalongkou. Faint large-scale accretionary surfaces and illuvial clays are common in Dalongkou but rare in Tarlong-Taodonggou. The association of the second type of sandstones with thick fining-upward conglomerate-sandstone-mudrock successions and the presence of accretionary surface argue for a point-bar origin for the sandstones.

The third type of sandstones is very fine to fine-grained lithic wackes. It occurs as 0.1-0.2 m thick beds that have a lenticular geometry and are encased in mudrock-rich

intervals. In Dalongkou, this type of sandstones contains abundant illuvial clays. They are interpreted as sandy overbank deposits.

4.3 Lithofacies 3 – Mudrocks

Mudrocks are the most common lithofacies in the upper QZJ LC and the most diverse with respect to their environments of deposition. They account for ~69% in thickness of the low-order cycle. Four subfacies are identified on the basis of grain size trend, sedimentary structures, vertical and lateral extent, and facies association.

4.3.1 Lithofacies 3a – Shale

Shale occurs sporadically throughout the upper QZJ LC, forming the upper part of many fining-upward successions. It is maroon to brown and, in a few cases, gray to greenish gray. The shales are silty, sandy, or pure, and non-calcareous. They contain rip-up mud chips and are locally tuffaceous. Subrounded to rounded floating sand grains are rarely present. Pedogenic features, such as clay coats and slickensides, are absent or poorly developed. No fossils are found; plant remains are absent in the lower and middle parts but common in the uppermost part of the measured sections. Sandstone stringers and bentonites occur and are 1-10s cm thick. The shales have a gradational contact with underlying conglomerate or sandstone and a sharp or erosional contact with overlying conglomerate or sandstone. They are interpreted as overbank deposits of meandering stream systems.

4.3.2 Lithofacies 3b – Mudstone

Mudstones are brown mudrocks, silty and sandy, and moderately to non-calcareous. They are distinguished from shales by the lack of laminations and from massive mudrocks (see below) by the presence of floating coarse grains. The mudstones are rare in Tarlong-Taodonggou but common in Dalongkou. The mudstones contain rounded to angular floating sand and granule size grains and mud clasts, and are mottled with root halos. All the mudstones occur in the upper part of fining-upward conglomerate-sandstone-mudrock successions. The massiveness and mottling suggest postdepositional modification. Therefore, the facies could be interpreted as a Protosol (see below). The mudstones are interpreted as overbank deposits of meandering stream systems.

4.3.3 Lithofacies 3c – Massive mudstone interpreted as ancient loess deposits (see next section "The Massive Mudstone Lithofacies (LF 3c and its Loessial Origin")

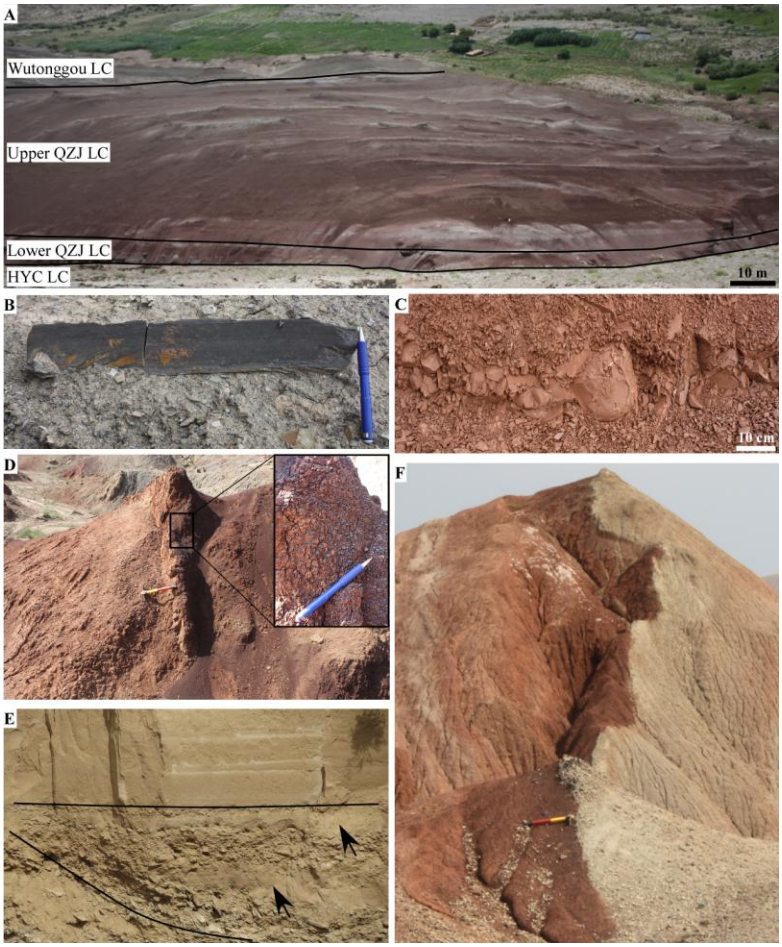

Figure 4. Field photographs showing features of the upper QZJ LC, some lithofacies, and modern loess. A) Northeastern Tarlong section showing persistent reddish purple loessite encasing thin and narrow, gray conglomerate bodies with a sharp base as ephemeral-stream channel fills in the entire upper QZJ LC. The strata dips to the south at ~ 60°. View is to the south. The upper QZJ LC in this section is 80 m thick. B) Lucaogou shale clast as a channel-lag deposit. Dalongkou section. Pen is 15 cm long and pointing stratigraphically up. C) A trench profile in basal upper QZJ LC, showing reddish purple to brown, blocky, massive loessite containing multi-faceted peds. The overall stratal dip is to the left, but no bedding is present in the loessite. Stratigraphic up is to the left (north). Southeastern Tarlong section. D) Highly-oxidized and lithified Gleysol bearing well-developed Fe-Mn pisoids in the Dalongkou section. View is to the west, beds dip at ~70° to the north. Backhole is 40 cm long. Inset photo shows well-developed Fe-Mn pisoids. Pen is 15 cm long and pointing stratigraphically up. E) Loess profile in the Chinese Loess Plateau encasing conglomerate bodies with an erosional base and sharp top. Notice common mud lenses as part of the channel fill (arrows). View is close to 2 m. F) Erosional contact between the highly-oxidized Gleysols of the upper QZJ LC and the well-washed littoral conglomerates of the Wutonggou LC in the Dalongkou section. View is to the east. Backhole is 40 cm long.

4.3.4 Lithofacies 3d – Bentonite

Some mudrocks occur as thin (5-20 cm) and laterally persistent beds intercalated with other muddy lithologies throughout the upper QZJ LC. They are dark brown to dark gray, ductile, and intensely slickensided. The basal and top contacts are sharp to slightly gradational. This subfacies is interpreted as bentonite of altered volcanic ash deposits in overbank and loess environments.

4.4 Lithofacies 4 – Paleosols

Gleysols and Protosols (Mack et al., 1993) are identified in the upper QZJ LC and are interpreted with respect to landscape and climatic conditions (e.g., Mack and James, 1994).

4.4.1 Lithofacies 4a – Gleysol

Gleysols (Mack et al., 1993) occur in the uppermost part of the upper QZJ LC in all measured sections (Yang et al., 2010). The matrix is red, gray, brown to maroon mud. Color mottling and thick clay coats are common. Soil horizons are well developed. The lower horizon is normally brown to maroon, 50-200 cm thick, and contains thick clay coats with common slickensides. The middle horizon is gray, maroon, or variegated, and 50-150 cm thick, and contains abundant Fe-Mn pisoids (Fig. 4D). Individual pisoids range from 0.5-20 mm in size and have wavy and concentric cortices and a core composed of black to dark brown iron oxide-rich mud. In Dalongkou and southwest Tarlong, pisoids are coalesced to form a well-cemented ironcrete 5 to 50 cm thick (Fig. 4D). The upper horizon is red, brown to maroon, 50-100 cm thick, contains scattered

clay coats and slickensides and, in many cases, is highly oxidized. Gleysols usually form in a water-logged environment, probably associated with a raised groundwater table, which could have been caused by lake transgression and/or a climatic change to a more humid condition (Mack and James, 1994; Yang et al., 2010).

4.4.2 Lithofacies 4b – Protosol

Protosols are characterized by a massive structure and lack of soil horizons (Mack et al., 1993; Yang et al., 2010). They occur in red to brown mudstones and, less commonly, in dark brown and purple mudstones. The red color indicates a possible oxidizing soil environment. Discontinuous thin clay coats with small slickensides are rare in Tarlong-Taodonggou, but are more common and, in some cases, extend into the underlying sandstones in Dalongkou. In few cases in Dalongkou, where faint soil horizons are observed, the paleosols are interpreted as argillic Protosols or immature Argillisols. Protosols occur mainly in the massive mudrock subfacies (Lithofacies 3c). They cannot provide reliable information on climatic conditions, but indicate incipient soil development on a relatively stable landscape. Slow but continuous deposition may have hampered soil formation. Finally, the argillic Protosols in Dalongkou suggest a possible humid climate.

4.5 Lithofacies 5 – Calcrete

A calcrete occurs in the lowermost part of the northeastern Tarlong section. It contains three light gray beds, each of which is 1-5 cm thick. It contains common microbially coated detrital grains and small calcareous pisoids. The beds are laterally

discontinuous and change to a nodular zone 50 m to the west. They are interpreted as a palustrine limestone deposited in an overbank environment or the Bk horizon of a Calcisol (Obrist-Farner and Yang, 2015).

5. Massive Mudstones Lithofacies and its Loessial Origin

The massive mudstones (Lithofacies 3c) in the upper QZJ LC have peculiar sedimentological, stratigraphic, geochemical, and geochronological characteristics. The evidence presented below is to substantiate the interpretation of a loess origin by describing the characteristics of the mudrocks of the upper QZJ LC and comparing them with those of Quaternary loess deposits.

5.1 Sedimentary Structures and Stratigraphic Attributes

This subfacies of mudrocks is the most common rock type in the upper QZJ LC and the focus of this study. It accounts for ~57% in thickness of all the measured sections, ~75% in Tarlong-Taodonggou and only ~7% in Dalongkou. The facies is brown, maroon, red, purple, green, or gray, variably silty, and laterally persistent for 100s m on outcrops (Fig. 4A). Individual mudrock intervals range in thickness from 0.1-16.5 m; most of the mudrock intervals range in thickness from 0.1-1 m and from 1-2 m, with 32% and 28% respectively. The mudrocks are massive, and contains no invertebrate fossils and evidence of bioturbation, such as color mottling, rootlets, or animal burrows (Fig. 4C).

The observed lateral continuity in the field (Fig. 4A), consistent vertical distribution and similar sedimentological attributes throughout the measured sections, and massive structure supports a loess origin for the mudrocks. The presence of stream

deposits of Lithofacies 1 (LF1) and LF2 throughout the measured sections suggests a possible genetic linkage between the streams and mudrock deposits (e.g., Yang et al., 2010). However, the large width/depth ratio of the channels, the poorly-defined fining-upward grain size trend, and the sharp boundary separating LF1 and LF2 from this type of mudrock indicate that the two are not genetically related. Moreover, massive mudrock to channel ratio is 0.3-84.2, 5.73 on average. The large ratio is rare for ephemeral braided stream systems because this type of stream commonly have no or small amount of suspension load and therefore do not deposit thick overbanks (Miall, 1996). The massive mudrock facies do not contain intercalated overbank sandstones of LF2, do not have floating coarse sand and granule size grains, and are not laminated as commonly observed in overbank deposits (e.g., Miall, 1985). Hence, the massive mudrocks are likely not overbank deposits of the ephemeral streams, even though they are vertically adjacent. Stream processes ceased before deposition of the mudrocks by a non-fluvial process. A viable subaerial process for mudrock deposition is eolian process. Alternating fluvial and eolian processes are common in the accumulation of Holocene loess of Alaska (e.g., Muhs et al., 2004) and Pleistocene loess of China (e.g., Porter et al., 2005). An example of alternating fluvial channel fills and loess in Pleistocene deposits as observed on the outcrop of the Chinese Loess Plateau during a field reconnaissance study supports a possible loess origin of the massive mudrocks interbedded with stream deposits (Fig. 4E).

Only faint and crude pedogenic features are present in this facies in the lower and middle parts of the upper QZJ LC. They include poorly to moderately-defined prismatic peds, discontinuous and thin clay coats, and faint slickensides (Fig. 4C), and are

identified as Protosols of LF 4b. These features are slightly better developed in Dalongkou to form some argillic Protosols. However, the facies contains well-developed Gleysols of LF 4a in the uppermost 10-20 m of the low-order cycle (Fig. 4D). The lack of mature paleosols in this facies in the lower and middle parts differs from modern and recent loess. Soil formation and loess deposition are considered as competing processes in many modern loess environments (Muhs et al., 2004); if abundant loess is deposited, soil will not form, and vice versa. In addition, paleosol horizons in Pleistocene loess indicate warmer and wetter periods corresponding to interglacial times (e.g., Porter, 2001). Thus, a possible reason of the lack of mature paleosols in the massive mudrocks is that pedogenic processes were hampered by continuous accumulation of loess during the deposition of the lower and middle parts of upper QZJ LC. In some cases, illuvial clay coats occur in channel fill conglomerates and sandstones. This suggests a period of relatively wet climate during and after fluvial deposits but before the onset of loess deposition. In the upper part of the sections, the record is similar to modern loess deposits with the appearance of well-developed paleosols on loess deposits.

5.2 Particle Size Distribution

The most unique characteristic of the subfacies is the consistent multi-modal grain size distribution, which ranges from clay to very fine sand and is dominated by the clay and fine silt size fractions (see measured sections). A total of 69 samples from this subfacies are analyzed for grain size, among which 14 are from the lower part, 11 from the middle part, and 21 from the upper part in Tarlong and Taodonggou and 5 from the lower part, 15 from the middle part, and 3 from the upper part in Dalongkou (see

measured sections below for location of samples). The grain size distributions show four distinct modes at, in decreasing average percentage in volume, 2 μm, 5 μm, 11 μm, and 40-50 μm. The corresponding percentages of these modes range from 0.0-3.07%, 0.13% on average for very fine sand (3.0- 4.0 ϕ); 0.0-14.04%, 3.29% for coarse silt (4.0-5.0 ϕ); 2.62-14.49%, 8.81% for medium silt (5.0-6.0 ϕ); 6.45-14.96%, 10.21% for fine silt (6.0-7.0 ϕ); 15.14-22.01%, 18.66% for very fine silt (7.0-8.0 ϕ); and 45.96-70.89, 58.90% for clay (< 8.0 ϕ). All samples as a whole are poorly sorted with a graphic standard deviation (Folk and Ward, 1957; Folk, 1980) ranging from 1.34-2.13ϕ and 1.68 ϕ on average, and coarse skewed with a skewness ranging from -0.02 to -0.34 and -0.18 on average. Individual modes are moderately sorted to moderately well sorted; the 2 μm mode has a graphic standard deviation of 0.72ϕ, while the 5 μm, 11 μm, and 40-50 μm have a graphic standard deviation of 0.55ϕ, 0.53ϕ, and 0.52ϕ, respectively.

Minor trends of grain size decrease from the lower part to middle and upper parts in Tarlong-Taodonggou are discernable. The lower part contains an average of 1.2% more coarse silt, 1.3% more medium silt, and 3.0% less clay than the middle and upper parts. The content of very fine sand, medium silt, and very fine silt is constant throughout the QZJ LC. A similar trend also occurs in Dalongkou. The lower part contains an average of 0.8% more very fine sand than the middle and upper parts. The amount of coarse silt fraction decreases systematically from an average of 7.7% in the lower part, 5.0% in the middle part, to 0.7% in the upper part. Correspondingly, the clay content increases from an average of 55.8% in the lower part, 57.5% in the middle part, to 65.7% in the upper part. In summary, overall grain size of this subfacies decreases upsection in both Tarlong-Taodonggou and Dalongkou areas. This trend may have been

caused by several processes, for example, an overall change to a more humid condition with an increase in precipitation and, presumably, increased vegetation cover, and reduced wind speed and intensity.

Grain size difference between Tarlong-Taodonggou and Dalongkou areas is clear. For the lower part of upper QZJ LC, the Tarlong-Taodonggou samples contain an average of 0.8% less very fine sand, 4.5% less coarse silt, and 0.6% less medium silt, and an average of 2.3% more fine silt, 1.8% more very fine silt, and 1.8% more clay than the Dalongkou samples. This suggests a northward increase in overall grain size. For the middle part, the Tarlong-Taodonggou samples contain an average of 0.3% less very fine sand, 3.0% less coarse silt, and 1.5% less medium silt, and an average of 1.4% more fine silt, 2.0% more very fine silt, and 1.2% more clay than the Dalongkou samples, also showing an overall northward grain size increase. The trend, however, reverses for the upper part of the upper QZJ LC. The Tarlong-Taodonggou samples contain an average of 1.4% more coarse silt, 2.3% more medium silt, and 1.7% more fine silt, and an average of 0.2% less very fine silt and 5.2% less clay than the Dalongkou samples. The amount of very fine sand is negligible in the upper parts in both areas. In summary, grain size increases northward from Tarlong-Taodonggou to Dalongkou in the lower and middle parts of upper QZJ LC, and decreases northward in the upper part.

The consistent modes and grain size ranges in all samples suggest similar processes controlling the deposition of the mudrocks. In addition, the distribution and grain size range differ from those typical of modern overbank deposits, which tend to be heterogeneous (e.g., He and Walling, 1998) and contain a large portion of variable sand size fractions (e.g., Walling et al., 2004). Finally, the particle size distribution of a sample

from the overbank mudstones from the lower QZJ LC in northeast Tarlong (see measured section) is substantially different than those observed from the upper QZJ mudrocks. These differences suggest a non-fluvial overbank origin of the mudrocks in the upper QZJ LC.

The typical particle size range in Quaternary loess deposits is 20-50 μm (medium-coarse silt), but clayey and sandy loess is not uncommon (Pye, 1987). For example, loess in Nigeria contains abundant clay size particles (McTainsh et al., 1982; McTainsh, 1987) and is similar to modern dust from West Africa (Gillies et al., 1996; McTainsh et al., 1997). The Nigerian (McTainsh et al., 1982; McTainsh, 1987) and Negev loess (Crouvi et al., 2008; Israel et al., 2015) have a multimodal grain size distribution similar to that of the QZJ mudrocks. The similarities of grain size distribution and range of this facies to the Quaternary loess as well as its non-fluvial origin as discussed above strongly argue for a loessial origin for the massive mudrock facies.

Different modes in modern Nigeria and Negev loess are interpreted to represent either different sources (McTainsh, 1987; Crouvi et al., 2008; Israel et al., 2015) or deposition under different conditions (McTainsh, 1987; McTainsh et al., 1997), such as source distance or temporal changes in wind conditions. It is possible that the mudrocks of upper QZJ LC were derived from different source regions, with far and near-traveled components representing different modes (e.g., Bagnold, 1941; Tsoar and Pye, 1987). Daily or seasonal changes in wind intensity could also be responsible for the different modes observed (e.g., McTainsh, 1987; Gillies et al., 1996). Alternatively, interfingering between fluvial and loess deposits could result in a multimodal grain size distribution.

However, the lack of sand fractions coarser than very fine sand suggests that the interfingering is insignificant, as also indicated by the field observations.

Moreover, pedogenically-modified loess horizons in the Chinese Loess Plateau contain a high percentage of clay size particles when compared to unaltered loess horizons (Sun et al., 2006). The clay size fraction also increases with the distance of sediment transport from their sources (e.g., Tsoar and Pye, 1987; Muhs et al., 2004). By analogy, the great clay size fraction in the QZJ loess may have been introduced by downward illuviation after deposition. However, the weak pedogenesis in the majority of the upper QZJ LC, except the uppermost part, argues against a significant contribution of illuvial clay to the massive mudrocks. On the other hand, the QZJ loess could be distal eolian deposits, which typically contain a large amount of clay size particles (Pye, 1987; Tsoar and Pye, 1987).

Finally, grain size trends of the massive mudrock facies can be explained by climatic and regional factors assuming their loessial origin. First, the overall grain-size decrease upsection in both Tarlong-Taodonggou and Dalongkou areas may have been caused by several processes, for example, an overall change to a more humid condition in the uppermost part of the low-order cycle, which implies an increased vegetation cover that resulted in reduced wind speed and transport capacity and, thus, smaller dust grain size. Another possibility is that humid conditions increased soil moisture decreasing sediment availability (Bagnold, 1941). Second, the northward grain size increase of the facies from Tarlong-Taodonggou to Dalongkou in the lower and middle parts of upper QZJ LC, and a reverse trend in the upper part suggest that the prevailing wind during the deposition of the lower and middle parts had been from north to south, then reversed the

direction during the deposition of the upper part. The reversal may correspond to the overall shift to a more humid condition that ultimately developed into a full-fledged humid condition at the beginning of the overlying Wutonggou LC (Yang et al., 2010).

5.3 Mineralogy

The massive mudrocks are composed of quartz, feldspar, and clay minerals as revealed by XRD analysis of eight samples. The composition differs significantly from that of the conglomerates and sandstones of LFs 1 and 2, respectively (Table 1). Igneous gravels dominate in conglomerates and volcanic lithics and plagioclase feldspars are the most common framework grains in sandstones. Secondary grains in sandstones include K-feldspars, biotite, rutile, and opaque minerals. Both XRD and point-counting data (Obrist-Farner, 2015) indicate minimal to no quartz in 22 sandstone samples analyzed under a petrographic microscope and two samples analyzed with an XRD from Tarlong-Taodonggou. The disparity suggests that the mudrocks have a different provenance from that of the conglomerates and sandstones. The massive mudrocks are likely of a non-fluvial origin.

Conversely, the conglomerates and sandstones from Dalongkou are compositionally different to those in Tarlong-Taodonggou. Sedimentary gravels dominate in conglomerates and sandstones contain abundant quartz, feldspars, and sedimentary lithic grains. The mineralogical disparity seen in Tarlong-Taodonggou between the sandstones and conglomerates and mudrocks is not seen in Dalongkou.

5.4 Detrital Zircon Ages

A similar age spectrum of detrital zircon grains from nine samples from Tarlong-Taodonggou and Dalongkou provides an important clue for the origin of the facies (Fig. 5). Out of the 544 zircon grains analyzed, 38 are younger than 270 Ma, 381 have an age range from 270-320 Ma, 83 have an age range from 320 to 400 Ma, 28 have an age range from 400 to 500 Ma, 7 have an age range from 500 to 900 Ma, and 7 are older than 900 Ma. The concentrated ages around 300 Ma indicate that the zircon grains were derived from the same source rocks in the provenance or different provenances with source rocks of similar ages. In addition, samples from both Tarlong-Taodonggou and Dalongkou show similar age spectra. This similarity is significant in light of that the two areas are 70 km apart at the present (Fig. 1B). The distance should be greater than 70 km considering that the Bogda Mountains are a giant anticline and that the study area has undergone extensive shortening due to the India-Eurasia collision (Allen et al., 1993; 1995; Sengor et al., 1993; Carroll et al., 1995; Sengor and Natal'in, 1996). Thus, the similarity argues for a consistent transport agent and mechanism of mud and zircon particles in the massive mudrock facies. Fluvial processes are not adequate candidates because the presence of many half grabens and grabens forming small partitioned drainage basins in the greater Turpan-Junggar basin during the deposition of upper QZJ LC (e.g., Yang et al., 2010; Obrist-Farner and Yang, 2015). By default, eolian process is a viable candidate for the transport of the mud particles.

The dominant age of ~270-320 Ma suggests that the source rocks are of a latest Carboniferous to Early Permian age. An interesting fact is that the detrital zircon ages of sandstones and mudrocks in Dalongkou are similar (Fig. 5) and in agreement with those of mudrocks in Tarlong-Taodonggou. Datable zircons are not obtained from sandstones

in Tarlong-Taodonggou. The ages and agreement suggest that Dalongkou was close to and connected through a drainage network to the source region that provided zircon grains for both Dalongkou and Tarlong-Taodonggou areas and that Tarlong-Taodonggou area was in a different fluvial drainage basin from Dalongkou, assuming the fluvial sandstones in Tarlong-Taodonggou do not have zircons with similar ages to those in Dalongkou. Carboniferous and Permian orogens are present along the northern, western, and southern margins of the greater Turpan-Junggar basin (e.g., Xiao et al., 2010, 2013, 2014; Xiao and Santosh, 2014). A possibility is that these suture zones were the main source for the detrital zircons, which are dominantly Carboniferous to Permian in age with dominant zircon ages around 300 Ma (Han et al., 2011; see Figure 1 of Tang et al., 2014). Another possibility is that the source was the Carboniferous volcanic and volcaniclastic rocks that make up the basement of the Turpan-Junggar basin (e.g., Yang et al., 2013) that were exposed in rift shoulders during QZJ time.

6. High-Order Sedimentary Cycles

Sedimentation in the upper QZJ LC is apparently repetitive as best manifested by repetitive environmental changes. Yang et al. (2010) recognized two types of sedimentary cycles in Permian-Lower Triassic terrestrial deposits in Tarlong-Taodonggou. The first type is a erosion–deposition cycle, which has an erosional base and an overlying depositional system, representing repetitive changes between phases of erosion/nondeposition and deposition. Environments during the phase of deposition may not change repetitively, such as a meandering stream cycle. The second type is an environmental cycle, which is composed of several depositional systems showing a cycle of environmental shifts, such as lake expansion and contraction. Erosion may or may not

occur at the cycle base. Many sedimentary cycles are environmental cycles with an erosional/nondepositional base, as a combination of the two basic types (Yang et al., 2010). The cycles are regarded as basic cyclostratigraphic entities and termed high-order cycles (HCs). They provide a framework to facilitate interpretations of processes and factors controlling erosion, nondeposition, and deposition. A total of 172 HCs are interpreted in the upper QZJ LC. The HCs are classified into two types on the basis of types of facies associations and depositional systems. Readers are referred to Yang et al. (2010) and Obrist-Farner and Yang (2015) for detailed description of these types of HCs.

6.1 Meandering Stream High-Order Cycles

Meandering stream high-order cycles (Yang et al., 2010) are a type of erosion-deposition cycle and characterized by a high relief erosional base overlain by channel-fill conglomerates and sandstones of LFs 1 and 2, respectively, overbank mudrocks of LFs 3a and 3b with thin sandstones of LF 2, and paleosols of LF 4b, with occasional bentonites of LF 3d and palustrine carbonates of LF 5. The thickness of channel-fill and overbank deposits are similar, indicating classic meandering stream deposits (Miall, 1996). A total of 47 meandering stream HCs in the upper QZJ LC range from 0.42-6.92 m in thickness, 2.62 m on average. There are a total of 8 meandering stream HCs in Tarlong-Taodonggou and 39 in Dalongkou. Meandering stream cycles are common where topographic relief is low and/or river flow is perennial, suggesting a relatively large catchment basin and a likely humid or subhumid climate.

6.2 Fluvial-Loessial HCs

Fluvial-loessial HCs (Obrist-Farner and Yang, 2015) are the most common HCs in the upper QZJ LC in Tarlong-Taodonggou and are less common in Dalongkou. A total of 125 such HCs are delineated and range from 0.42-16.84 m in thickness and 3.82 m on average. They are a combination of erosional-depositional and environmental cycles. Two subtypes are identified. The first subtype contains thin ephemeral-stream conglomerates of LF 1 and rare fluvial sandstones of LF 2 with a low relief erosional base in the lower part and loessite of LF 3c and paleosols of LF 4b in the upper part. The contact between the lower and upper parts is sharp. In few cases, the ephemeral-stream conglomerates are absent due to lateral facies change; and the cycle boundary is the contact between underlying pedogenically-altered loessite and overlying unaltered loessite, which can be laterally traced and have contrasting colors. The loessites in 1-8 cycles in the uppermost part of the upper QZJ LC are pedogenically altered into Gleysols of LF 4a. There are a total of 83 ephemeral stream-loessial HCs in Tarlong-Taodonggou and 4 in Dalongkou. The second subtype has thick meandering-stream conglomerates of LF 1 and sandstones of LF 2 with a high-relief erosional base in the lower part. The thick loessite of LF 3c occur in the upper part of the cycle and is interbedded with overbank sandstones of LF 2, shales and mudstones of LF 3a and 3b, and paleosols of LF 4a and 4b. There are a total of 20 meandering stream-loessial HCs in Tarlong-Taodonggou and 18 in Dalongkou.

Fluvial-loessial HCs are the dominant type in the upper QZJ LC, suggesting that fluvial and eolian deposition alternated and dominated during the deposition of the low-order cycle. Semiarid-subhumid conditions prevailed during ephemeral stream deposition

and semiarid-arid conditions during loess deposition. Alternatively, climatic conditions did not change significantly between periods of ephemeral stream deposition and loess deposition. However, in the uppermost part of the upper QZJ LC, arid conditions during loess deposition dramatically changed to subhumid when loess is altered into Gleysols (Fig. 4D). Climatic conditions fluctuated for the meandering-stream and loess cycle from subhumid during the meandering stream deposition to semiarid to arid during loess deposition.

7. Environmental and Climatic Trends of the Upper QZJ LC

The variations and stacking of HCs in individual sections reveal minor and major changes in depositional environments and tectonic and paleoclimatic conditions. The changes in each section are described using a cyclostratigraphic framework to provide a detailed description of the processes controlling cyclic sedimentation.

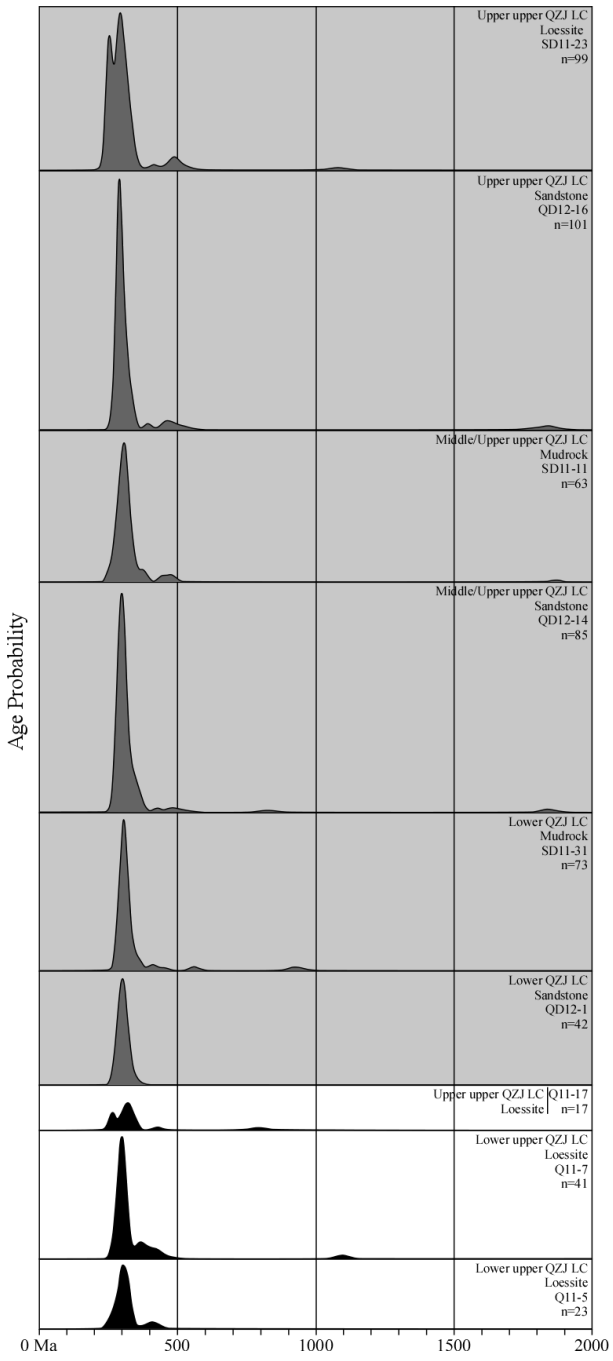

Figure 5. U-Pb relative age-probability diagrams for detrital zircons in the upper QZJ LC. Notice the similar peak at ~ 300 Ma for all samples. White boxes represent samples from the northeast Tarlong section, while gray boxes from the Dalongkou section. Samples are plotted in stratigraphic order. Stratigraphic position of the samples in the section, lithology, sample name, and number of zircons counted per sample are specified for each sample.

7.1 Northeastern Tarlong Section

The upper QZJ LC in the northeastern Tarlong section (Figs. 2A, 6) overlies the lower QZJ LC across a disconformity (Obrist-Farner and Yang, 2015) and underlies the Wutonggou LC across a gradational boundary. It is 81.0 m thick. 22 HCs include 17 ephemeral stream-loessial, four meandering stream-loessial, and one meandering-stream HCs. The ephemeral stream-loessial HCs are 1.21-9.06 m, 3.84 m on average in thickness; the meandering stream-loessial HCs are 1.63-4.30 m, 2.58 m on average in thickness. The meandering-stream HC is 5.4 m thick. There is no clear upsection cycle thickness trend of these HCs (Fig. 7). However, there is an overall increase upsection of loessite and decrease of conglomerate and sandstone content. The uppermost three HCs contain no basal conglomerates or sandstones (Fig. 7). 31 loessite samples from the lower, middle, and upper parts of the LC show a consistent multimodal grain size distribution with minimal variations between samples within and between HCs (Fig. 6). Paleocurrent direction of the ephemeral streams is to the SW and SE, similar to that observed from the underlying lower QZJ LC (Fig. 6). The amount of igneous gravels decreases from 80% in the lower part to 33% in the upper part (Table 1). The loessites in six out of the 21 fluvial-loessial HCs contain Protosols, whereas those in the uppermost four HCs contain well-developed Gleysols.

The persistent paleocurrent direction suggests a northern highland during the deposition of lower and upper QZJ LCs. The upsection decrease in thickness of conglomerate and sandstone and in the amount of igneous gravels suggests denudation of the northern highland and an enlarged catchment basin. Similar thickness of loessites and their grain size distributions suggest that loess deposition occurred under similar

processes. The Protosols in the majority of the section indicate mostly continuous loess accumulation that inhibited extensive pedogenesis, except in the uppermost part where Gleysols indicate significant periods of nondeposition and pedogenesis between episodes of loess accumulations.

Climate had alternated between a semiarid condition during deposition of ephemeral stream deposits to arid during the loess accumulation during the deposition of the lower and middle parts of the upper QZJ LC. The meandering stream HC in the lower part suggests a deviation to a short-term subhumid condition. However, during the deposition of the upper part, semiarid conditions persisted during loess deposition and changed dramatically to subhumid conditions during formation of Gleysols. Alternatively, the formation of Gleysols may have been caused by the elevation of groundwater table due to the approaching lake shoreline. The former interpretation is supported by the presence of Histosols in the basal part of the overlying Wutonggou LC (Yang et al., 2010).

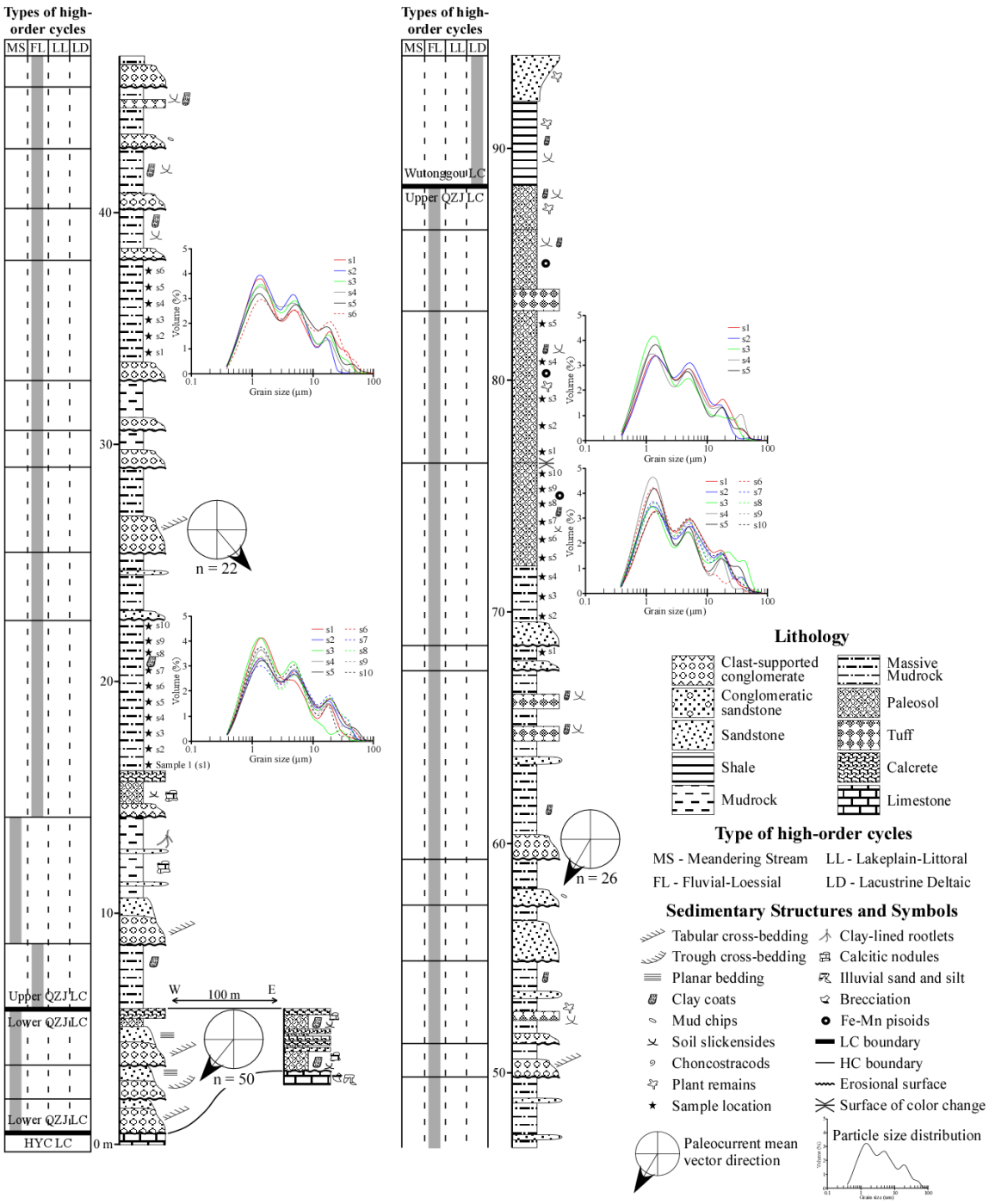

Figure 6. Highly simplified lithological column (middle panel), sedimentary textures and structures (right panel), and high-order cycle types (left panel) of the lower and upper QZJ LCs in northeastern Tarlong. Ephemeral streams and loessite deposits dominate throughout the section. Notice constant particle size in the loessite facies. See Figure 2 for location of the measured section.

7.2 Northern Tarlong Section

The poorly-exposed upper QZJ LC in the northern Tarlong section (Figs. 2A, 8A) has similar sedimentologic and stratigraphic characteristics to those in northeastern Tarlong. It overlies the lower QZJ LC with a disconformity (Obrist-Farner and Yang, 2015) and underlies the Wutonggou LC conformably (Yang et al., 2010). It is 66.4 m thick. Only eight HCs are delineated due to poor exposure: seven fluvial-loessial HCs with a thickness range of 1.73-15.83 m, 9.03 m on average; and one meandering-stream HC in the lower part with a 3.23 m thickness. No pedogenic features are observed in the lower and middle parts, mainly due to poor exposure. The uppermost HC contains a well-developed Gleysol. Ephemeral stream-loessial HCs dominate. They show an upward increase in loessite and a decrease in sandstone content (Fig. 7); the last two HCs do not contain basal sandstones.

The general decrease in sandstone thickness suggests a decrease in topographic gradient and an enlarged catchment basin. Thick loessites in the upper part suggest that conditions conducive to loess formation were better developed in the upper part. The climatic trend is likely to be similar to that in the northeastern Tarlong section.

7.3 North-Central Tarlong Section

The upper QZJ LC overlies the lower QZJ LC across a disconformity (Obrist-Farner and Yang, 2015) in north-central Tarlong. Only seven meters of the basal part of upper QZJ LC are well exposed (Figs. 2A, 8B). It is composed of two fluvial-loessial HCs that are 3.12 and 3.96 m thick, respectively (Fig. 7). The two HCs indicate that fluvial and eolian processes were active at the beginning of upper QZJ LC.

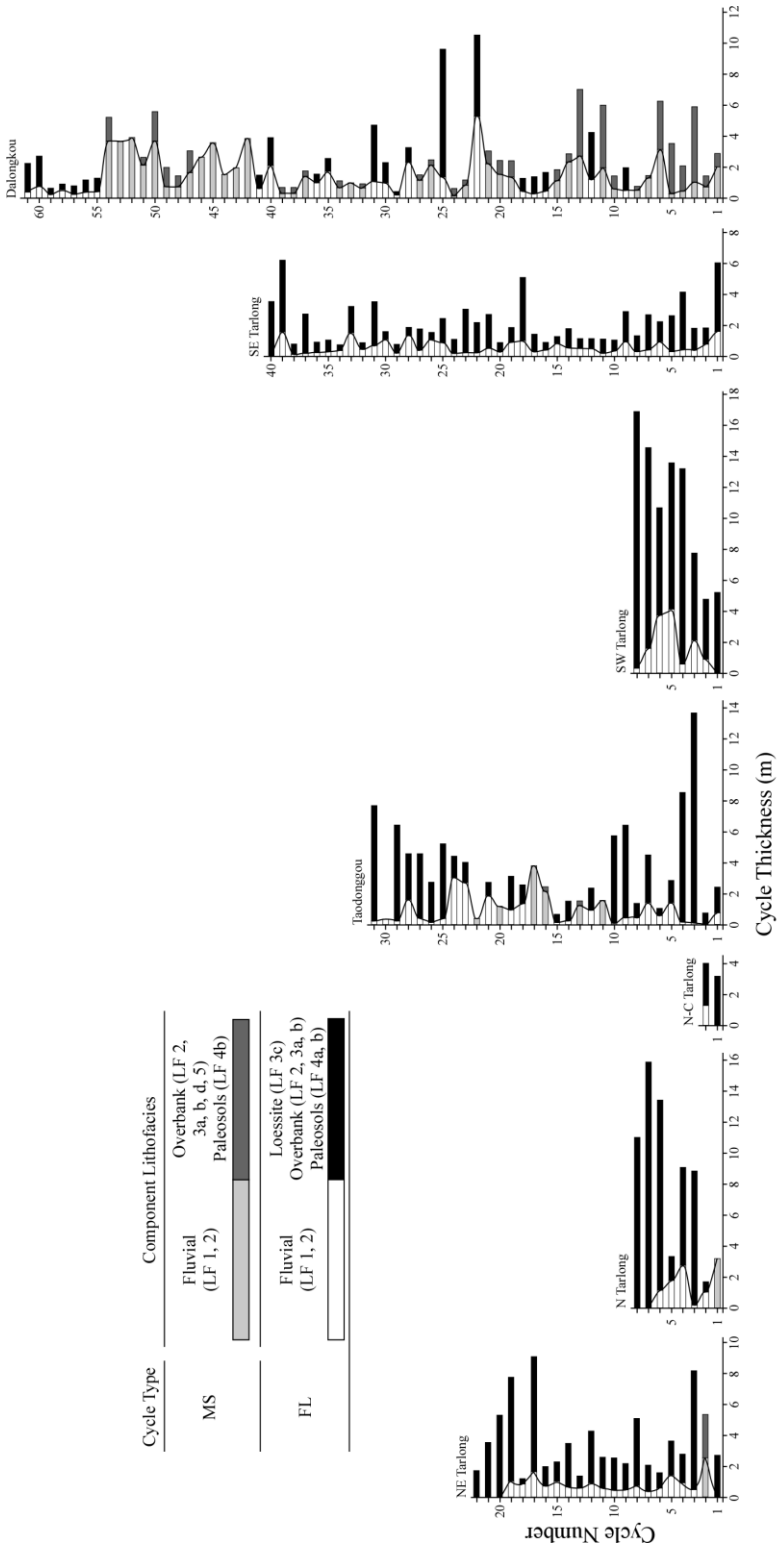

Figure 7. Cycle type, cycle thickness, and component lithofacies for all upper QZJ LC sections measured in this study. See text for details.

7.4 Taodonggou Section

The stratigraphic trends and sedimentological attributes of upper QZJ LC in the Taodonggou section (Figs. 2A, 9) mimic those in the northeastern Tarlong section. The Taodonggou section has 31 HCs with a total thickness of 110.4 m. The base of upper QZJ LC is an erosional unconformity (Obrist-Farner and Yang, 2015) and the top a conformity (Yang et al., 2010). 31 HCs include 19 ephemeral stream-loessial, six meandering stream-loessial, and six meandering-stream HCs. Ephemeral stream-loessial HCs dominate, while meandering-stream HCs are concentrated in the middle part of the section (Fig. 7). The ephemeral stream-loessial HCs are 0.42-13.64 m, 4.20 m on average in thickness; the meandering stream-loessial HCs 2.44-4.42 m, 3.25 m on average in thickness; and the meandering-stream HCs 0.42-3.84 m, 1.86 m on average in thickness. The thickness of HCs decreases from the lower to middle part and, then, increases to the upper part (Fig. 7). Six loessite samples from the upper part show similar multimodal grain size distributions (Fig. 9). Paleocurrent directions of ephemeral streams are to SE in the lower part, NE in the middle part, and E in the upper part (Fig. 9). The amount of igneous gravels remains consistent throughout the LC but the amount of metamorphic gravels increases in the upper part (Table 1). The thickness of loessites decreases from the lower to middle part, then increases to the upper part. Pedogenic alteration of loessites is minimal, except in the uppermost HC with a well-developed Gleysol.

Variations of paleocurrent directions upsection indicate changes in local topography with a paleo-highland to the west of Taodonggou area. The highland is composed of mainly igneous and minor metamorphic rocks. Processes of loess accumulation are similar to that in northeastern Tarlong as indicated by the similar grain

size distribution. However, the decrease in loessite in the middle part indicates conditions unfavorable for loess accumulation. Loess accumulation was continuous for most of the LC and interrupted only in the uppermost part. The overall climatic trend upsection from semiarid-arid to subhumid-humid conditions is similar to that in northeastern Tarlong. A period of subhumid conditions may have occurred in the middle part as indicated by the meandering-stream HCs. Alternatively, meandering streams were better developed in Taodonggou, which is located in the central part of the Tarlong-Taodonggou half graben and has a low topographic gradient.

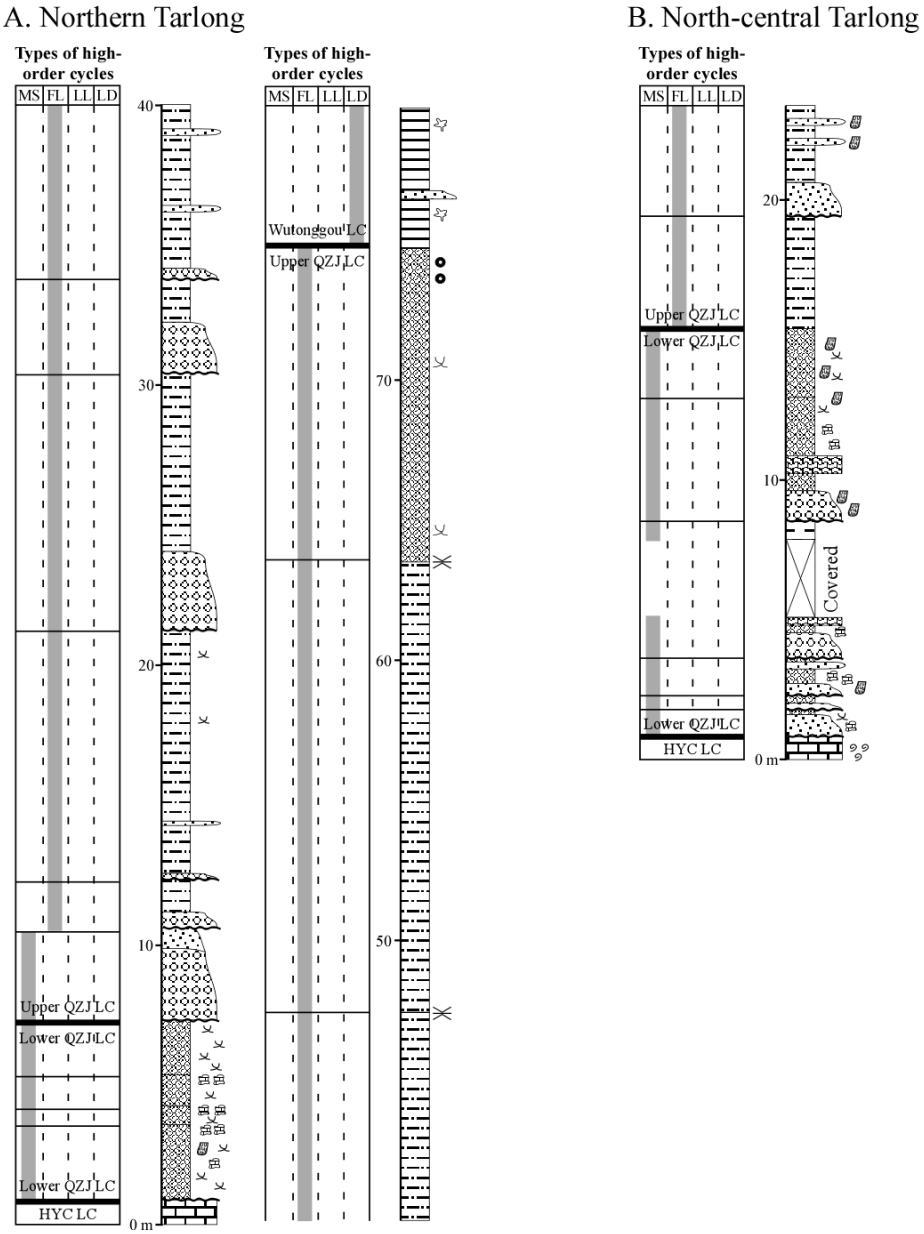

Figure 8. Highly simplified lithological column (middle panel), sedimentary structures (right panel), and high-order cycle types (left panel) of the lower and upper QZJ LCs of measured sections. A) Northern Tarlong. Loessite deposits are thick and dominate throughout the section. Notice the decrease in conglomerate and sandstone content upsection. B) North-central Tarlong. Thick loessite dominate in the lowermost part of the upper QZJ LC. See Figure 2 for location of the measured sections and Figure 5 for explanations.

7.5 Southwestern Tarlong Section

The upper QZJ LC in southwestern Tarlong (Figs. 2A, 10) overlies the lower QZJ LC across a conformity or disconformity (Obrist-Farner and Yang, 2015) and underlies the Wutonggou LC across a conformity. It is 86.7 m thick. All eight HCs are ephemeral stream-loessial HCs and are 4.81-16.84 m, 10.83 m on average in thickness. Their thickness increases upsection systematically (Fig. 7). Paleocurrent direction in the second HC from the base is to the NW (Fig. 10), similar to that in the underlying lower QZJ LC. Sedimentary gravels dominate, as in the lower QZJ LC (Table 1). Loessite in the basal three HCs contain Protosols, whereas those in the upper four HCs contain well-developed Gleysols. They thicken slightly upsection (Fig. 7).

The paleocurrent direction indicates a southeastern highland during the lower and upper QZJ time, which was mainly covered by sedimentary rocks as indicated by the abundant sedimentary gravels. Loess accumulation increased upsection in the upper QZJ time. However, the paleosol evidence suggests a similar upsection trend of processes in loess accumulation, including climatic conditions, to those in northern Tarlong and Taodonggou. The southwest Tarlong area was interpreted as the lowest place in the half graben during deposition of lower QZJ LC (Obrist-Farner and Yang, 2015) and may be the reason for an increase in sedimentary gravels and thicker and mature Gleysols.

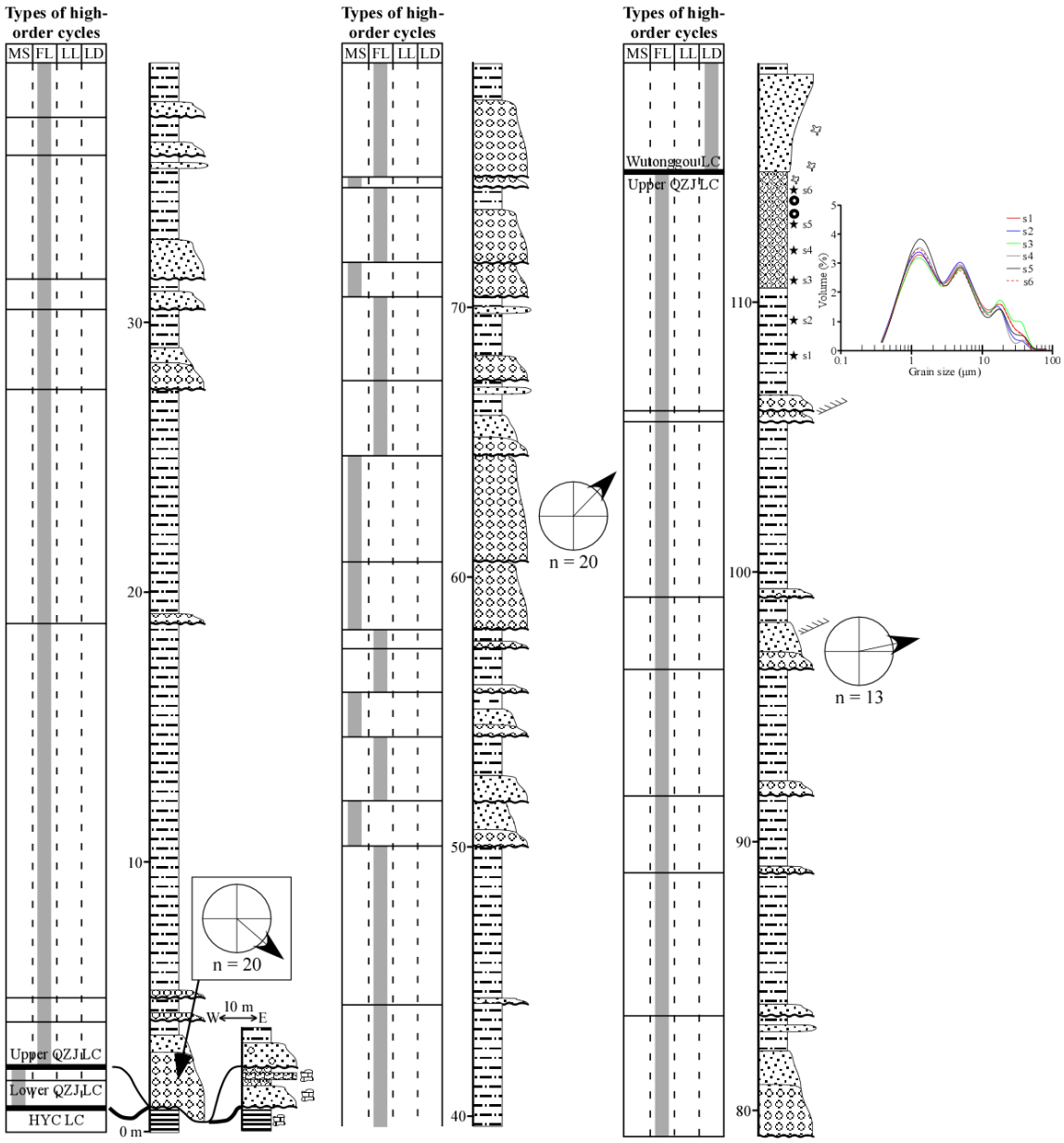

Figure 9. Highly simplified lithological column (middle panel), sedimentary textures and structures (right panel), and high-order cycle types (left panel) of the lower and upper QZJ LCs in Taodonggou. Ephemeral streams and loess deposits are present throughout the upper QZJ LC with occasional meandering streams. Notice constant grain size in the uppermost part of the section. See Figure 2 for location of the measured section and Figure 5 for explanations.

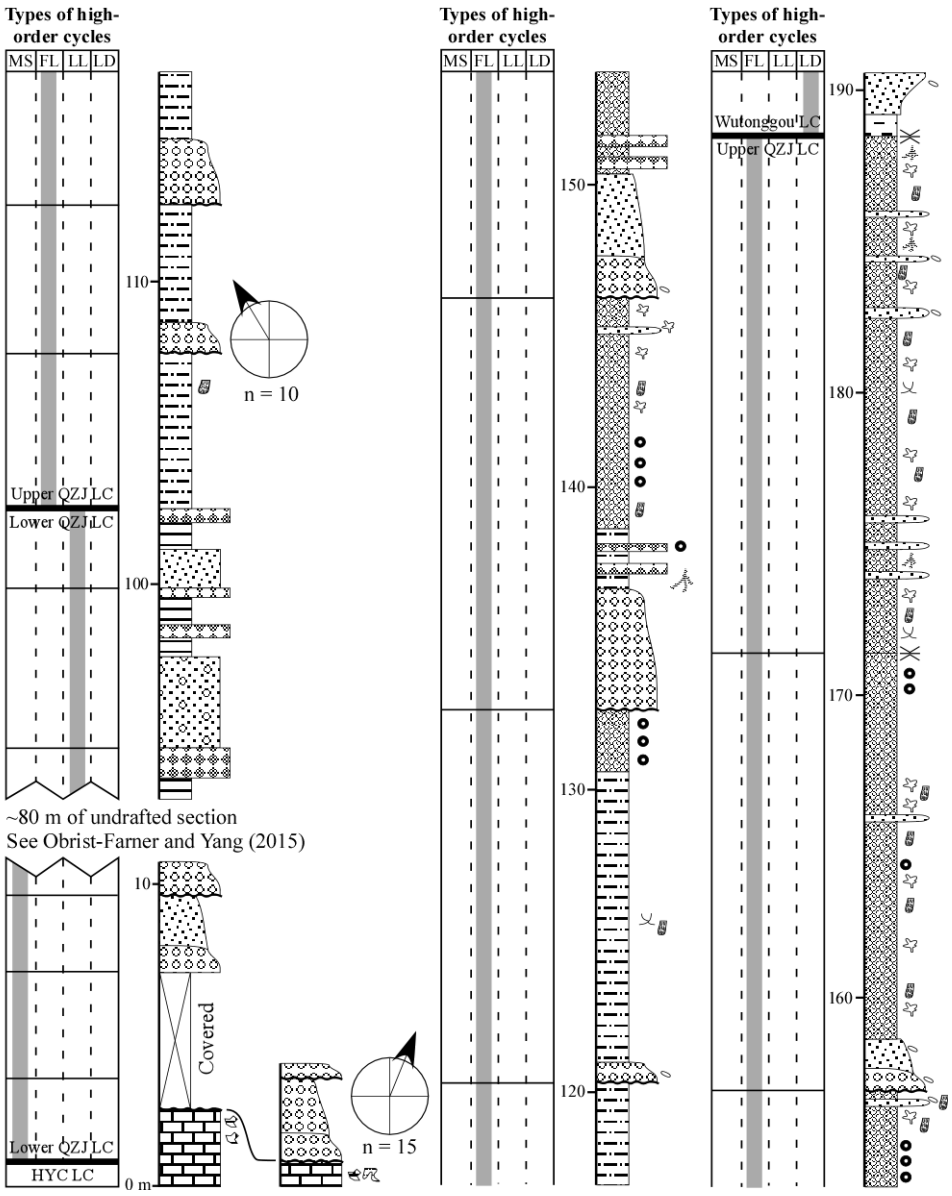

Figure 10. Highly simplified lithological column (middle panel), sedimentary structures (right panel), and high-order cycle types (left panel) of the lower and upper QZJ LCs in southwestern Tarlong. ~ 80 m of the lower QZJ LC are omitted. The upper QZJ LC contains thick loessite with occasional ephemeral streams. See Figure 2 for location of the measured section and Figure 5 for explanations.

7.6 Southeastern Tarlong Section

The southeastern Tarlong section (Figs. 2A, 11) shows a similar stratigraphic trend to that of northeastern Tarlong. The upper QZJ LC has a conformable base and top (Yang et al., 2010; Obrist-Farner and Yang, 2015). It is 85.53 m thick. 31 ephemeral stream-loessial and nine meandering stream-loessial HCs are delineated. The former are 0.66-4.10 m, 1.77 m on average in thickness and the latter 1.54-6.20 m, 3.39 m on average. There is no clear cycle thickness trend (Fig. 7). Grain size distributions in the lower and middle parts are consistent and multimodal (Fig. 11). Paleocurrent direction measured in the middle part is to the NE (Fig. 11), similar to that in the lower QZJ LC. Igneous gravels dominate in the lower QZJ LC; there is a decrease in igneous and increase in sedimentary gravels upsection (Table 1). Loessites show no clear thickness trend upsection (Fig. 7). Those in 33 HCs do not contain any pedogenic features, whereas five HCs contain Protosols with faint and poorly developed clay coats and slickensides and occur in the upper part of the section. The uppermost two HCs contain well-developed Gleysols.

The upper QZJ LC is dominated by ephemeral stream-loessial HCs. Paleocurrent direction indicates a southern highland during the lower and upper QZJ time, which was covered by mainly igneous rocks. The persistent occurrence of conglomerate and sandstone, general decrease in igneous gravels upsection, and consistent paleocurrent direction suggest continuous denudation of the southern highland. The consistent grain size distribution and the pedogenic characteristics suggest similar climatic conditions and processes controlling loess accumulation to those in other Tarlong-Taodonggou sections.

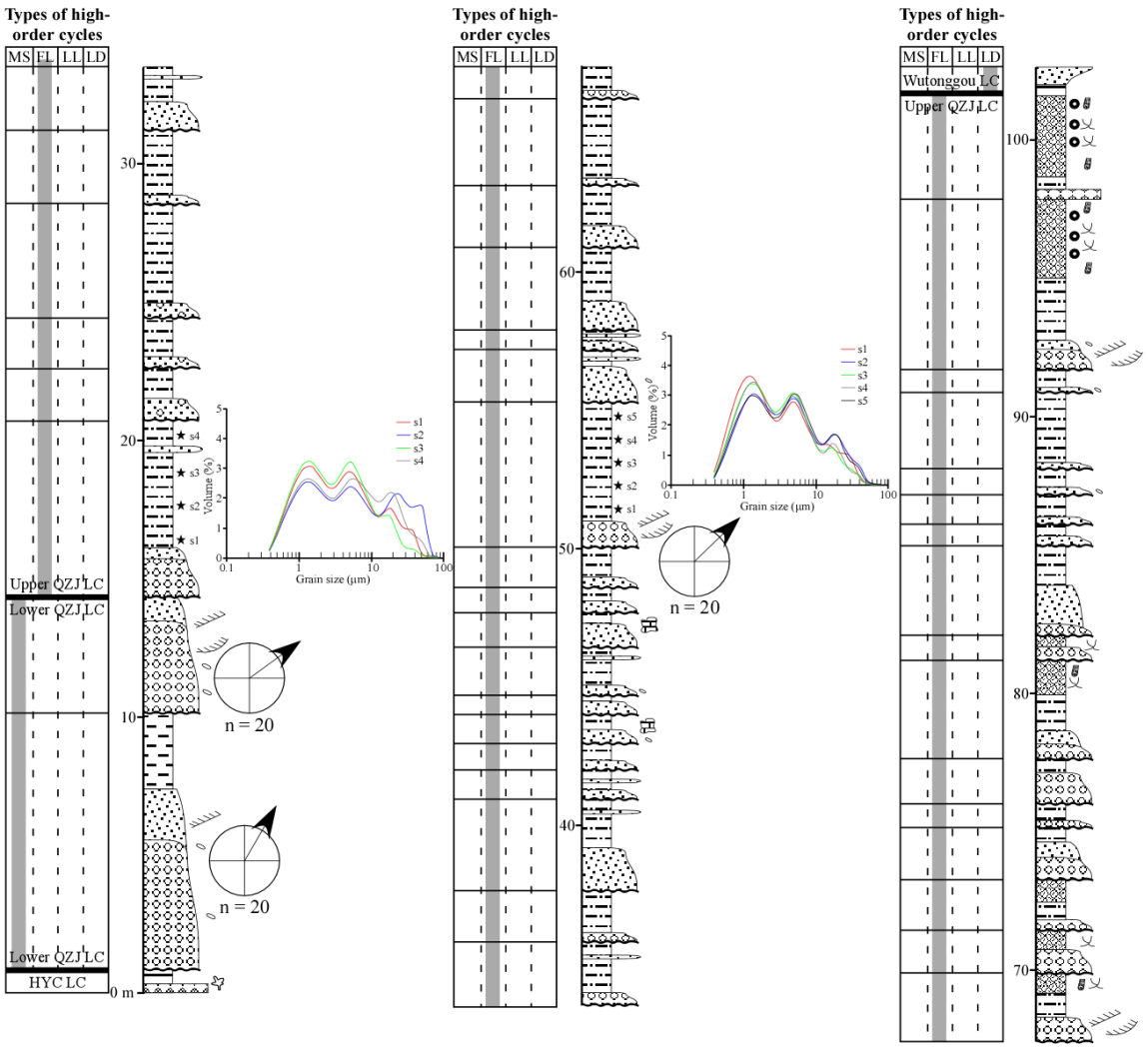

Figure 11. Highly simplified lithological column (middle panel), sedimentary textures and structures (right panel), and high-order cycle types (left panel) of the lower and upper QZJ LCs in southeastern Tarlong. The upper QZJ LC is dominated by ephemeral stream-loessial HCs. Notice constant grain size in the loessite facies. See Figure 2 for location of the measured section and Figure 5 for explanations.

7.7 Dalongkou

The Dalongkou section (Figs. 2B, 12) offers a record for regional correlation with those in Tarlong-Taodonggou. The upper QZJ LC in Dalongkou overlies the lower QZJ LC across a disconformity (Obrist-Farner and Yang, 2015) and underlies the Wutonggou LC across a lacustrine transgressive surface (Fig. 4F). The upper QZJ LC is 163.82 m thick. Four ephemeral stream-loessial, 18 meandering stream-loessial, and 39 meandering-stream HCs are delineated. The ephemeral stream-loessial HCs are 0.43-1.66 m, 1.29 m on average in thickness; the meandering stream-loessial HCs 0.60-10.48 m, 3.09 m on average; and the meandering-stream HCs 0.61-6.92 m, 2.65 m on average. There is no clear cycle thickness trend (Fig. 7). Two thick intervals of stacked meandering-stream HCs occur in the upper part, which contain common angular dolomitic shale pebbles, cobbles, and boulders in the channel deposits. Grain size distribution of 15 loessite samples from the middle part and three from the upper part are consistent and multimodal, similar to those in the underlying lower QZJ LC (Fig. 13). Paleocurrent direction measured from the meandering stream deposits in the lower and upper parts is to the NE (Fig. 12). Sedimentary gravels make up more than 90% of the gravels throughout the section (Table 1). Loessites occur sporadically throughout the section. The loessite, mudstones, and shales in the lower 53 HCs are Protosols with common root halos; and one contains an argillic Protosol. The uppermost 8 HCs contain well-developed Gleysols.

The paleocurrent direction suggests a highland to the southwest. The thick intervals of stacked meandering-stream HCs in the upper part suggest a well-developed meandering stream environment on gentle basin floor of a relatively large drainage basin.

The common sedimentary gravels throughout and shale gravels with similar lithology to the underlying Lucaogou LC (Yang et al., 2010) suggest a sedimentary source, possibly a horst where lithified Lower-Permian sediments were uplifted and eroded. Massive mudrock facies, that is, loessites, in the lower and upper QZJ LCs have similar grain size distributions, but those of lower QZJ LC contain more very fine sand and are interpreted as resedimented loess by Obrist-Farner and Yang (2015). Loessites in the uppermost seven meandering stream-loessial HCs have grain size distributions similar to those in the middle part (Fig. 13). However, they contain well-developed Gleysols, instead of Protosols. The grain size distributions of loessites similar to those in Tarlong-Taodonggou area suggest that processes controlling loess accumulation are similar in Tarlong-Taodonggou and Dalongkou areas.

The climate alternated between semiarid to subhumid conditions. However, the abundance of meandering stream deposits and predominance of meandering stream HCs suggest that the periods of subhumid conditions are prolonged. The overall climatic trend to subhumid-humid condition upsection is similar to that in Tarlong-Taodonggou, which turned into humid conditions in the Wutonggou LC with common Histosols throughout (unpublished data by the authors).

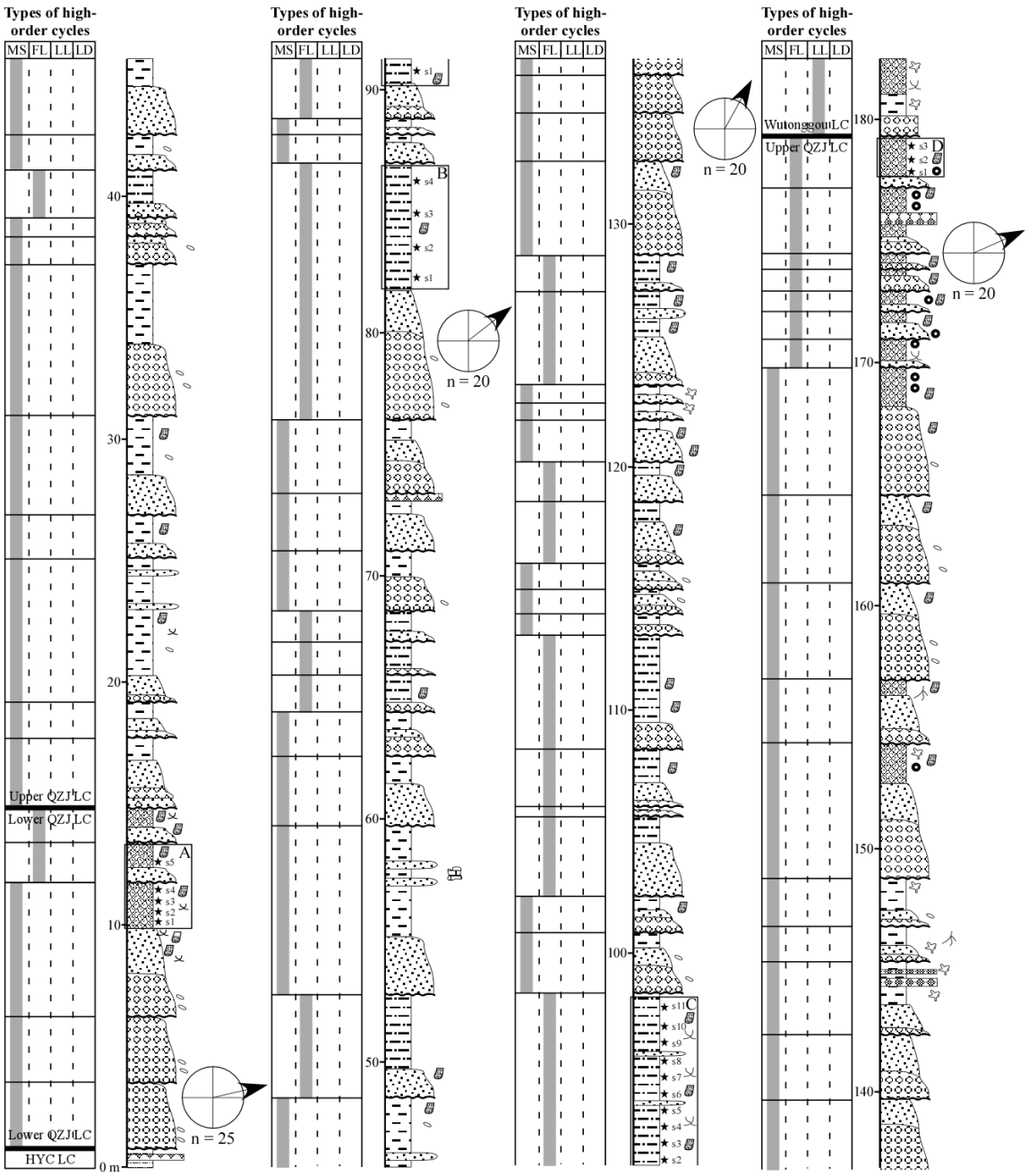

Figure 12. Highly simplified lithological column (middle panel), sedimentary structures (right panel), and high-order cycle types (left panel) of the lower and upper QZJ LCs in Dalongkou. The upper QZJ LC is dominated by meandering streams, with occasional loess deposits. Intervals with grain size analysis are highlighted with a black box. See Figure 13 for results of grain size analysis, Figure 2 for location of measured section, and Figure 5 for explanations.

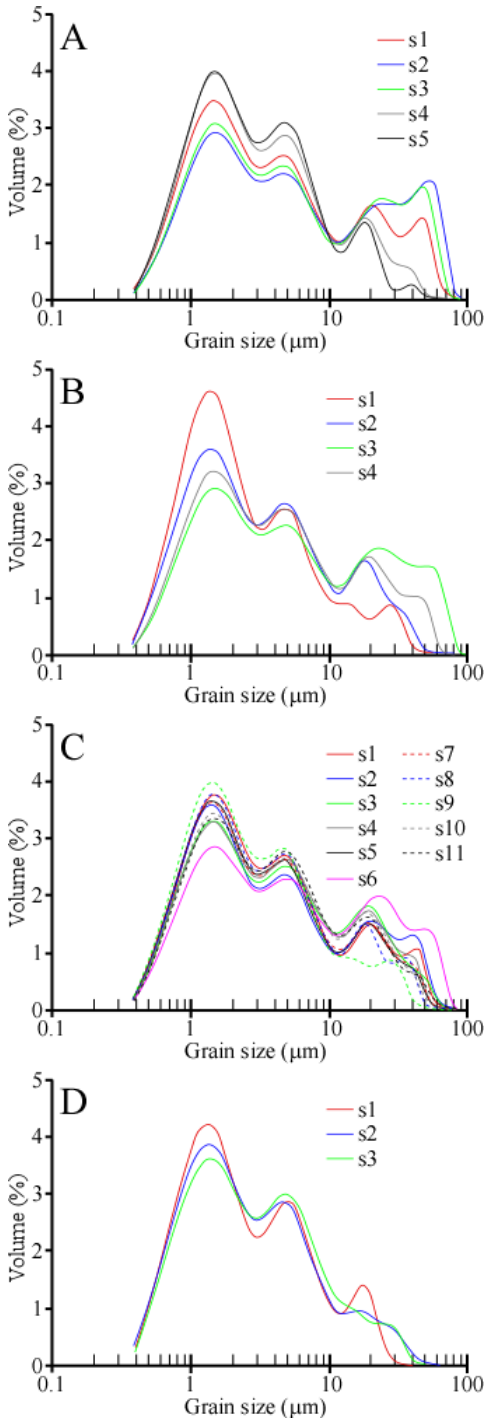

Figure 13. Grain size analysis results for the loessite facies from the Dalongkou section. Notice the constant grain size and the similar grain size distribution to that from Tarlong-Taodonggou. Sampling intervals A) lower part, B) lower-middle part, C) upper-middle part, and D) upper part. See Figure 12 for location of samples and sampling intervals.

8. Discussion

8.1 Environmental Evolution of the Upper QZJ LC

Individual lithofacies, facies associations, and high-order cycles in multiple sections of Tarlong-Taodonggou and Dalongkou offer the records of sedimentary environments and conditions that can be used to understand environmental evolution and controlling processes and factors during the deposition of the upper QZJ LC.

In the Tarlong-Taodonggou area, the upper QZJ LC is dominated by thin ephemeral stream and thick loess deposits with rare thin meandering stream deposits. The abundance of igneous gravels, basaltic lithics, and plagioclase feldspars in the lower and middle parts, where coarse lithofacies are common, suggests a major mafic igneous source in local horsts or distant suture zones surrounding the greater Turpan-Junggar basin, such as the northern Tianshan to the south (e.g., Shao et al., 2001; Greene et al., 2005; Guan et al., 2010; Yang et al., 2010; Obrist-Farner, 2015). The overall decrease in grain size, increase in sedimentary gravels, and decrease in basaltic lithics upsection suggest source denudation and an enlarged catchment basin, or a gradual change in provenance lithology. In contrast, the Dalongkou record contains common meandering stream, and some ephemeral stream and loess deposits. The abundance of sedimentary gravels and lithics suggests a sedimentary source, likely local horsts where Lower Permian sedimentary rocks were uplifted and eroded. The contrast in fluvial styles between Taodonggou and Dalongkou may reflect the differences in drainage basin size, topography, and climatic conditions. The Dalongkou area, presently situated about 1^{o} latitude north of Tarlong-Taodonggou area, may have been in a relatively large drainage basin with a more gentle slope and humid climate, in comparison to the Tarlong-Taodonggou area.

The dominance of ephemeral streams in Tarlong-Taodonggou and meandering streams in Dalongkou suggests a possible paleotopographic and/or climatic control on stream types. A higher topographic location in a relatively small drainage basin, couple with persistent arid to semiarid conditions lead to ephemeral stream development in Tarlong-Taodonggou. A gentler slope on a relatively larger drainage basin increasing water availability promoted the formation of better developed streams in Dalongkou.

The high percentage of clay size particles in the upper QZJ loessites is similar to modern and recent loess that are deposited far away from its source (e.g., Kes, 1984; Pye, 1987; Tsoar and Pye, 1987; McTainsh et al., 1997). Alternatively, it may be partially originated from subsequent pedogenesis after deposition (e.g., Sun et al., 2006; Jacobs and Mason, 2007). However, the poorly-developed paleosols in most loessites and their consistent grain-size distribution in individual sections and among all sections suggest a distant source for the clay size particles. The slight overall grain size decrease upsection suggests a decrease in wind intensity during the deposition of the upper QZJ LC. It is perceivable that illuvial clay in Gleysols in the upper part of upper QZJ LC had contributed to the higher clay content. Finally, the increase in very fine sand and coarse silt content in Dalongkou (Fig. 13) may have resulted from local contributions from overbank deposits of contemporary meandering streams.

The multimodal grain size distribution observed in the upper QZJ loessites is similar to modern loess with diverse provenances (e.g., McTainsh et al., 1982, 1997; Crouvi et al., 2008; Israel et al., 2015). The presence of abundant clay size particles indicates a distant source and the coarse fraction a nearby source. Alternatively, daily or

seasonal changes in wind intensity could have caused mixing of different grain sizes (e.g., Gillies et al., 1996).

The increase in the coarser fraction observed in Dalongkou in the lower and middle parts of the upper QZJ LC indicate a proximity to the source and a downwind decrease in grain size towards the Tarlong-Taodonggou area. This pattern of downwind grain size change is observed in the Pleistocene loess of China (e.g., Kes, 1984; Pye, 1987) and in modern dust studies (e.g., Gillies et al., 1996). This indicates that a possible source for the loess was located to the north of the Dalongkou area. A reversal of the winds must have occurred in the upper part of the upper QZJ LC, possibly caused by a change to humid conditions in the two study areas. Alternatively, the increase in grain size observed in the lower and middle parts of Dalongkou could have been caused by interfingering between fluvial and eolian processes.

The loessites indicate that a significant quantity of dust had been delivered, trapped, and accumulated in the Bogda Mountains during the mid-Permian time, when the Earth experienced one of the dustiest times in its history (Soreghan et al., 2008). Rift shoulders served as topographic obstacles to reduce wind speed and trap the dust. The less abundant loess deposits in Dalongkou suggest that the area may not have the best conditions for loess accumulation, an orographic barrier to the south, and/or too far from a possible dust source. Finally, the well-developed Gleysols in the uppermost part suggest a prolonged period of landscape stability at the end of upper QZJ deposition. It is on this stable and subdued landscape that lake transgression and deposition of overlying Wutonggou LC took place (Yang et al., 2010).

8.2 Paleoclimatic and Tectonic Trends

Paleosols, loessites, and other climatically-sensitive lithofacies and interpreted environmental changes provide clues to climatic changes and areal variations in the Bogda Mountains area during Middle Permian. Semiarid conditions with a strong precipitation seasonality prevailed in Tarlong-Taodonggou during the deposition of the lower QZJ LC, as interpreted from paleosols and lithofacies by Obrist-Farner and Yang (2015). The climate changed to dominantly arid conditions during the deposition of upper QZJ LC, as indicated by the accumulation of multiple intervals of loessites (Fig. 14). Arid conditions are conducive to dust entrainment, transport, and deposition (Bagnold, 1941; Pye, 1987; Tsoar and Pye, 1987), as commonly in modern arid environments (e.g., Reheis et al., 1995; Singer et al., 2003; Evans et al., 2004). The arid conditions were interrupted by semiarid conditions, under which intervening ephemeral and meandering stream sediments were deposited. During these semiarid periods, the climate may have been slightly wetter, similar to the conditions where paleosol horizons have formed in Quaternary loess deposits (e.g., Porter, 2001). The intervening semiarid conditions changed rather abruptly to subhumid conditions during the deposition of the uppermost part of the upper QZJ LC (Fig. 14). Mature Gleysols developed in thick parent loess sediments indicate semiarid-arid conditions during loess deposition followed by subhumid conditions during Gleysol formation.

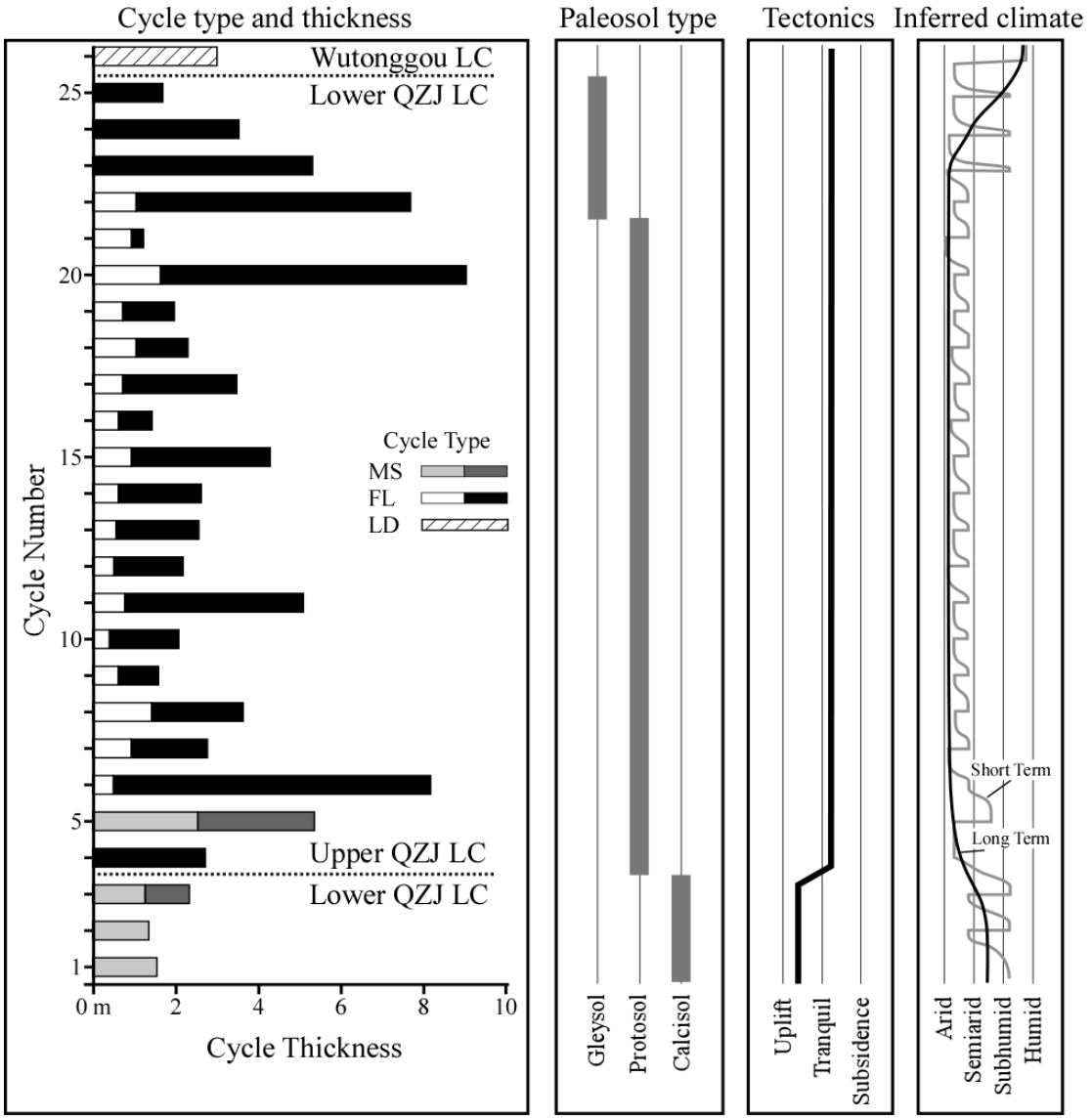

Figure 14. High-order cycle and paleosol types, and tectonic and climatic interpretations for the lower and upper QZJ LC in northeastern Tarlong. A similar record is found in all other sections measured in Tarlong-Taodonggou. Notice the abrupt climatic shift in the upper part of the section. See Figure 2 for location of measured section, and Figure 6 and 7 for cycle type abbreviations and component lithofacies.

The Dalongkou record to the north, on the other hand, shows a dominantly subhumid-humid condition during the deposition of the upper QZJ LC, as indicated by common thick meandering stream deposits throughout the section and Gleysols in the uppermost part (Fig. 15). Well-developed meandering streams indicate perennial water flows supplied by persistent precipitation and groundwater discharge, both of which require frequent and large atmospheric precipitation. However, semiarid-arid periods interrupted the subhumid-humid trend, as indicated by loessites interspersed among meandering stream deposits. The wetter conditions as indicated by mature Gleysols occurred during the deposition of the uppermost part of QZJ LC, similar to the Tarlong-Taodonggou records.

The Tarlong-Taodonggou and Dalongkou paleoclimatic records have a similar overall upward-increasingly humid trend and repeated variations between arid-semiarid and subhumid-humid conditions at the HC scale. However, the oscillations between two types of conditions at the HC-scale are reciprocal with respect to the dominance of arid-semiarid and subhumid-humid conditions. The areal variation may have been caused by paleolatitude and paleo-altitude differences, and an orographic barrier. An orographic barrier could have placed the Tarlong-Taodonggou in the rain shadow to experience an arid climate. However, no such barrier with a significant relief was reported and is unlikely within the great Turpan-Junggar intracontinental rift basin. Alternatively, the orographic barrier could be the Tian Shan arc to the south, increasing aridity in Tarlong-Taodonggou which is closer to the arc. Similarly, the Dalongkou area could have been located at a much higher altitude than the Tarlong-Taodonggou area and experienced a subhumid-humid highland climate. However, no such significant highland was reported

and is unlikely inside a great rift basin. In addition, a highland topography is in conflict with the well-developed meandering stream environment, which commonly develops in subdued topography. Finally, a ~1^{o} latitudinal difference may have placed the two areas in two contrasting climatic zones, assuming a zonal climate pattern at a paleolatitude of ~40^{o}N, for instance, Tarlong-Taodonggou in an arid desert zone, and Dalongkou in a subhumid-humid meso-microthermal zone. The boundary between the two contrasting climatic zones would be located close to 40^{o}N in NE Pangea (e.g., Chumakov and Zharkov, 2003). However, the presence of an arid climate region at the mid-latitude east coast, where the study area was located according to current plate tectonic reconstruction (Sengor and Natal'in, 1996; Scotese, 2001), is in conflict with the modern global climatic zonation (Yang et al., 2010). The conflict is probably caused by the megamonsoon circulation on the supercontinent Pangea during Middle Permian (Kutzbach and Gallimore, 1989; Parrish, 1993). During the mid-Permian, the northern boundary of the semiarid climatic belt in the northern hemisphere may have shifted gradually northward due to the presence of the paleo-Tethys ocean to the south and east (Chumakov and Zharkov, 2003). In summary, the observed climatic changes in and between Tarlong-Taodonggou and Dalongkou during the deposition of the Middle Permian upper QZJ LC are a dilemma. More regional data and knowledge are needed to provide insights into the causes of these variations. However, the contrasting reciprocal climate conditions between the Tarlong-Taodonggou and Dalongkou areas did not exist during the deposition of underlying Hongyanchi LC under a highly seasonal arid-semiarid condition and during the deposition of overlying Wutonggou LC under a weakly subhumid-humid condition (Yang et al., 2010; unpublished data from the authors). It is speculated that the

contrasting climatic conditions suggest a steep latitudinal climate gradient at the paleo-mid-latitude, which may have been closely related to the icehouse-hothouse climatic transition during the Middle Permian (Fielding et al., 2008a; 2008b). Finally, the abrupt change to a weakly seasonal, humid to subhumid change in overlying Upper-Permian Wutonggou LC can be attributed to the demise of the continental glaciers in northern (Chumakov, 1994; Chumakov and Zharkov, 2003), and to a lesser extent, southern Pangea (Fielding et al., 2008a).

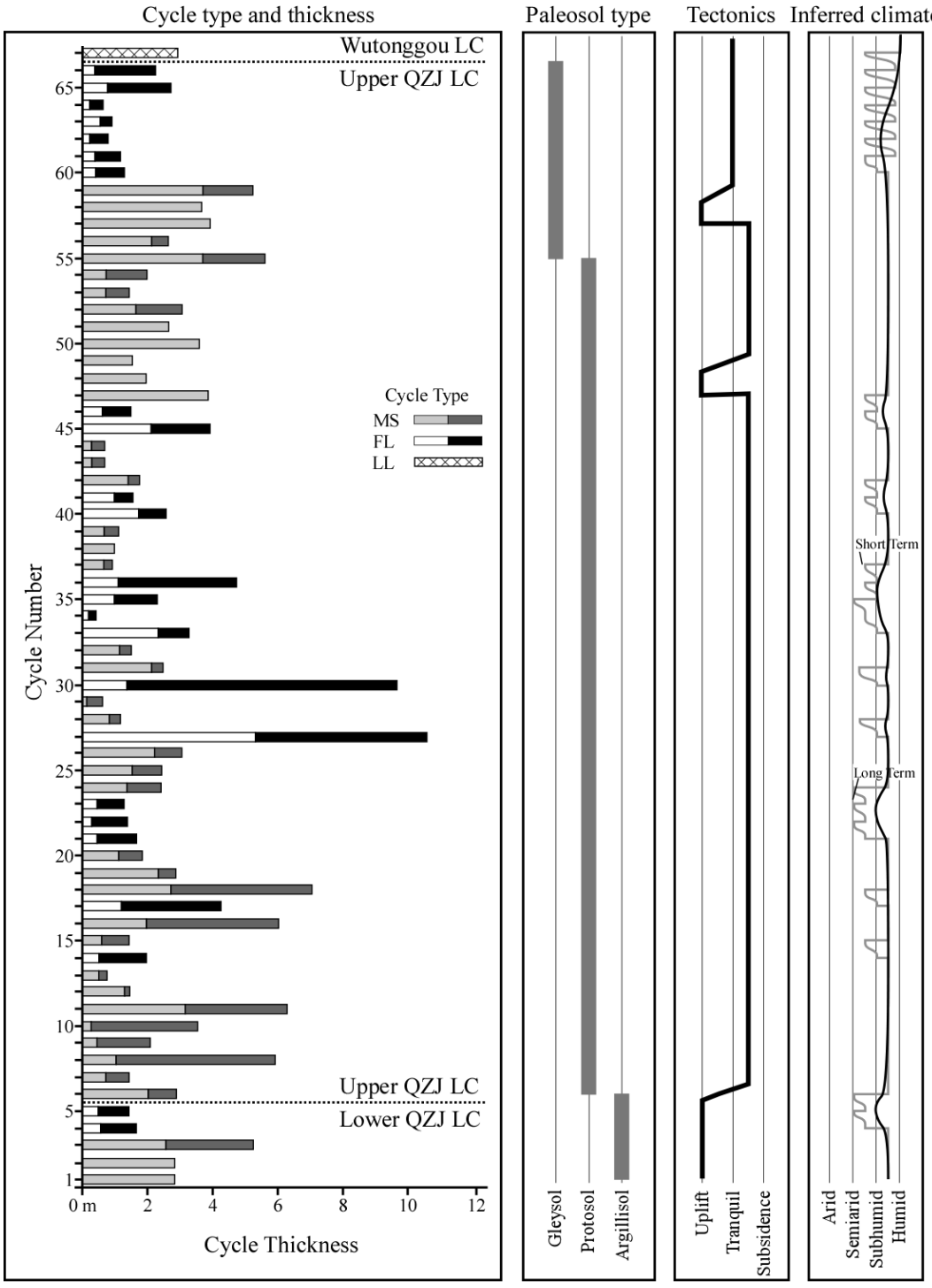

Figure 15. High-order cycle and paleosol types, and tectonic and climatic interpretations for the lower and upper QZJ LC in Dalongkou. A humid to subhumid climate persisted throughout the upper QZJ LC with occasional periods of arid climate. See Figure 2 for location of measured section, and Figure 6 and 7 for cycle type abbreviations and component lithofacies.

8.3 Comparison with Terrestrial Capitanian Records

Worldwide biotic (e.g., Wignall et al., 2009) and climatic (e.g., Fielding et al., 2008b) changes occurred in continental (e.g., Retallack et al., 2006) and marine (e.g., Wang et al., 2004) settings during Capitanian time. Fielding et al. (2008a) suggested that the demise of the late Paleozoic Ice Age occurred at the end of the Capitanian (Fig. 16) and, thus, global climate should have changed significantly during the icehouse-hothouse transition. Antarctica remained under cool, humid conditions during the transition (Sheldon et al., 2014; cf. Retallack et al., 2006). However, parts of South Africa in mid- to high-latitudes of southern Pangea had changed from dry conditions during Capitanian to warm and wet conditions during Wuchiapingian (Retallack et al., 2006). Niger remained under arid conditions during Middle and Late Permian (Tabor et al., 2011). Parts of the United States also were under well-documented arid conditions throughout the Permian (e.g., Parrish, 1993; Tabor and Montañez, 2002; 2004; Tabor and Poulsen, 2008). As a whole, it appears that arid and, in some instances extreme arid, conditions had prevailed (e.g., Benison and Goldstein, 2000; 2001; Zambito and Benison, 2013), in equatorial Pangea before, during, and after the icehouse-hothouse transition. The Bogda record shows a similar trend to that in South Africa, but differs from the equatorial Pangea trend. Nevertheless, arid conditions probably had occurred in a large part of Pangea during the late Capitanian icehouse-hothouse transition. The global zonal climatic pattern had been disrupted, signifying a great impact of continentality on global climate (Parrish, 1993). The shift to a subhumid-humid condition after the transition, on the other hand, indicates a somewhat restored zonal climate.

The subhumid-humid conditions in the uppermost part of the upper QZJ LC and overlying Wutonggou LC (Fig. 16) is in agreement with previous interpretations that NE Pangea was located in the northern tropical humid belt during the Late Permian (Chumakov and Zharkov, 2003). If latitudinal climatic variations are responsible for the contrasting climate observed in Tarlong-Taodonggou and Dalongkou, then the shift to humid climate in Tarlong-Taodonggou could indicate a southward expansion of the temperate humid belt by the end Capitanian. In addition, the possible presence of continental glaciers in the northernmost Siberia (Chumakov, 1994), which are reassigned as Capitanian in age based on paleomagnetic data (Chumakov and Zharkov, 2003), and have an uncertain distribution and timing (Fig. 16), may have impacted the global climate significantly.

Finally, the demise of southern Pangea continental glaciers at the end of Capitanian time has recently been attributed to a global greenhouse crisis (Retallack, 2013). The timing of the crisis seems to coincide with the arid-humid climatic transition in the uppermost upper QZJ LC, and in the southern mid-latitude regions of Pangea (e.g., Retallack et al., 2006). More data and observations are needed to reveal the intricate and feedback cause-effect mechanisms and relationships among climate proxies, attributes, and controlling factors. The climatic conditions and changes during the icehouse-hothouse transition at the end of Capitanian in the study area will serve as a critical data point for quantitative climate modelling (e.g., Gibbs et al., 2002; Winguth and Winguth, 2013) to understand the mechanisms and relationships at a global scale and the impact of the changes on the environmental and biotic (e.g., Retallack et al., 2006; Wignall et al., 2009) evolution on Pangea.

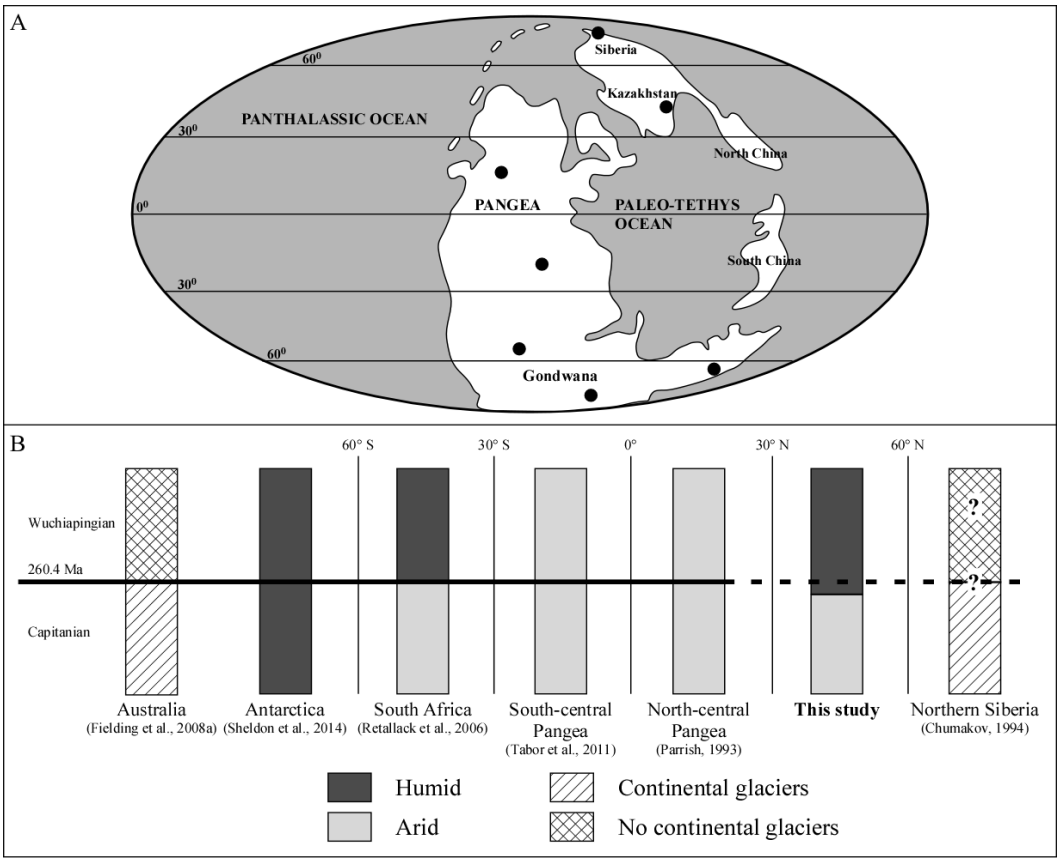

Figure 16. Permian paleogeographic map (A) showing the location (black circles) of studies of climate-sensitive sediments across Pangea with the interpreted climatic conditions (B) from Capitanian into Wuchiapingian. Notice the arid to humid climatic change in southern and northern mid-latitudes Pangea across the Capitanian boundary. Capitanian absolute age is from Gradstein et al., (2014). World map is modified from Scotese (2002). Location of study areas is approximated. See text for details.

9. Conclusions

Loessites in the Capitanian upper QZJ low-order cycle in Tarlong-Taodonggou and Dalongkou areas south and north of Bogda Mountains, NW China, respectively, are widespread. They alternate with mainly ephemeral-stream deposits and Protosols in Tarlong-Taodonggou and with mainly meandering stream deposits in Dalongkou. Mature Gleysols occur in the uppermost upper QZJ LC in both areas. The persistent

multimodal grain size distribution observed in all loessite samples indicates similar depositional conditions for all loessite samples in the upper QZJ LC. The multimodal distribution is attributed to temporal changes in wind conditions, to mixture of different sources, or to changes in distance for the source or sources.

The loessites suggest semiarid to arid conditions through much of the Capitanian and the Gleysols suggest a dramatic change to subhumid-humid conditions at the end of Capitanian. The common ephemeral stream deposits and Protosols in Tarlong-Taodonggou suggest prevailing arid-semiarid conditions, whereas the common meandering stream deposits and argillic Protosols in Dalongkou suggest humid-subhumid conditions. The pattern suggests that the two areas are in different climatic regions. Latitudinal difference may have played an important role.

The dramatic change from arid-semiarid to subhumid-humid conditions at the end of Capitanian corresponds to the final demise of continental glaciers and the icehouse-hothouse transition in late Paleozoic. The climatic record in NE Pangea is similar to that observed in southern mid- to high-latitudes and suggests a restored zonal climate for the Late Permian.

The results of this study provide two rare data points on paleoenvironmental and paleoclimatic conditions in the mid-high paleolatitude along the east coast of NE Pangea during the icehouse-hothouse transition, which will be critical to future quantitative paleoclimatic modelling. However, paleoclimatic speculations based on two data points might not be reliable. More data is needed to clarify the climatic differences observed in the two locations and provide a better understanding of the regional paleoenvironmental and paleoclimatic conditions and their changes during the Middle Permian.

Acknowledgments

We would like to thank Drs. J. Wang and M.L. Wan of Nanjing Institute of Geology and Paleontology of Chinese Academy of Sciences, Drs. Y. Liu and S.S. Wang of Northwest University of China, Dr. Y. Yang of Xi'an Petroleum University, Dr. X. Luo of Institute of Geology and Geophysics, Chinese Academy of Sciences, Dr. Q. Feng of Shandong University of Science and Technology, and J.J. Liu, T. Foster, Z.X. Li, J.J. Li, L.L. Cheng, C.C. Zhou, Y.M. Gao, and B. Sun for field and logistic assistance and funding. This research was partially supported by five student research grants from Geological Society of America, Ed Picou/GCSSEPM, American Association of Petroleum Geologists, and the Al Spreng Graduate Research Grant from the Geology and Geophysics Program of Missouri University of Science and Technology to Jonathan Obrist-Farner, and by a research grant from University of Missouri Research Board and a research grant (No. 2011ZX05008-004-053) from Institute of Geology and Geophysics of Chinese Academy of Sciences to Wan Yang. Acknowledgement is made to the Donors of the American Chemical Society Petroleum Research Fund, for a grant to Wan Yang.

References

Allen, M.B., Sengor, A.M.C., and Natal'in, B.A., 1995, Junggar, Turfan and Alakol basins as Late Permian to Early Triassic extensional structures in a sinistral shear zone in the Altaid orogenic collage, central Asia: Journal of the Geological Society, v. 152, p. 327-338.

Allen, M.B., Windley, B.F., Chi, Z., and Jinghui, G., 1993, Evolution of the Turfan Basin, Chinese central Asia: Tectonics, v. 12, p. 889-896.

Allmendinger, R.W., Cardozo, N.C., and Fisher, D., 2013, Structural geology algorithms: vectors and tensors: Cambridge, England, 289 pp.

Bagnold, R.A., 1941, The physics of blown sand and desert dunes: Methuen, London, 265 pp.

Benison, K.C., and Goldstein, R.H., 2000, Sedimentology of ancient saline pans: An example from the permian opeche shale, williston basin, north dakota, U.S.A: Journal of Sedimentary Research, v. 70, p. 159-169.

Benison, K.C., and Goldstein, R.H., 2001, Evaporites and siliciclastics of the Permian Nippewalla Group of Kansas, USA: A case for non-marine deposition in saline lakes and saline pans: Sedimentology, v. 48, p. 165-188.

Cai, T., 1999, Stratigraphy of Xinjiang Uygur Autonomous Region: China University of Geosciences Press, 430 pp. (In Chinese with English abstract).

Carroll, A.R., Graham, S.A., Hendrix, M.S., Ying, D., and Zhou, D., 1995, Late Paleozoic tectonic amalgamation of northwestern China: sedimentary record of the northern Tarim, northwestern Turpan, and southern Junggar Basins: Geological Society of America Bulletin, v. 107, p. 571-594.

Carroll, A.R., Graham, S.A., and Smith, M.E., 2010, Walled sedimentary basins of China: Basin Research, v. 2010, p. 17-32.

Carroll, A.R., Liang, Y., Graham, S.A., Xiao, X., Hendrix, M.S., Chu, J., and McKnight, C.L., 1990, Junggar basin, northwest China: trapped Late Paleozoic ocean: Tectonophysics, v. 183, p. 1-14.

Chumakov, N.M., 1994, Evidence of Late Permian Glaciation in the Kolyma River Basin: A Repercussion of the Gondwana Glaciations in Northeast Asia?: Stratigraphy and Geological Correlation, v. 2, p. 426-444.

Chumakov, N.M., and Zharkov, M.A., 2003, Climate during the Permian-Triassic biosphere reorganizations. Article 2. Climate of the Late Permian and Early Triassic: general inferences: Stratigraphy and Geological Correlation, v. 11, p. 361-375.

Crouvi, O., Amit, R., Enzel, Y., Porat, N., and Sandler, A., 2008, Sand dunes as a major proximal dust source for late Pleistocene loess in the Negev Desert, Israel: Quaternary Research, v. 70, p. 275-282.

Dickinson, W.R., 1970, Interpreting detrital modes of graywacke and arkose: Journal of Sedimentary Petrology, v. 40, p. 695-707.

Evans, R.D., Jefferson, I.F., Kumar, R., O'Hara-Dhand, K., and Smalley, I.J., 2004, The nature and early history of airborne dust from north Africa; in particular the lake Chad basin: Journal of African Earth Sciences, v. 39, p. 81-87.

Fielding, C.R., Frank, T.D., Birgenheier, L.P., Rygel, M.C., Jones, A.T., and Roberts, J., 2008a, Stratigraphic impring of the Late Paleozoic Ice Age in eastern Australia: a record of alternating glacial and nonglacial climate regime: Journal of the Geological Society, v. 165, p. 129-140.

Fielding, C.R., Frank, T.D., and Isbell, J.L., 2008b, The late Paleozoic ice age - A review of current understanding and synthesis of global climate patterns, *in* Fielding, C.R., Frank, T.D., and Isbell, J.L., eds., Resolving the Late Paleozoic Ice Age in Time and Space: The Geological Society of America Special Paper 441, Boulder, 343-354 pp.

Fielding, C.R., Frank, T.D., Isbell, J.L., Henry, L.C., and Domack, E.W., 2010, Stratigraphic signature of the late Palaeozoic Ice Age in the Parmeener Supergroup of Tasmania, SE Australia, and inter-regional comparisons: Palaeogeography, Palaeoclimatology, Palaeoecology, v. 298, p. 70-90.

Folk, R.L., 1980, Petrology of sedimentary rocks: Hemphill Publishing Company, Austin, Texas, 184 pp.

Folk, R.L., and Ward, W.C., 1957, Brazos River bar: a study in the significance of grain size parameters: Journal of Sedimentary Petrology, v. 27, p. 3-26.

Gastaldo, R.A., DiMichele, W.A., and Pfefferkorn, H.W., 1996, Out of the Icehouse into the Greenhouse: A Late Paleozoic Analogue for Modern Global Vegetational Change: GSA Today, v. 6.

Gazzi, P., 1966, Le Arenarie del Flysch Sopracretaceo dell'Appennino Modenese: Correlazioni con il Flysch di Monghidoro: Mineralogica e Petrografica Acta, v. 12, p. 69-97.

Gibbs, M.T., Rees, P.M., Kutzbach, J.E., Ziegler, A.M., Behling, P.J., and Rowley, D.B., 2002, Simulations of Permian climate and comparisons with climate-sensitive sediments: Journal of Geology, v. 110, p. 33-55.

Gillies, J.A., Nickling, W.G., and McTainsh, G.H., 1996, Dust concentrations and particle-size characteristics of an intense dust haze event: Inland Delta region, Mali, West Africa: Atmospheric Environment, v. 30, p. 1081-1090.

Gradstein, F.M., Ogg, J.G., and Smith, A.G., 2004, A geologic time scale 2004: Cambridge University Press, New York, 589 pp.

Greene, T.J., Carroll, A.R., Wartes, M.A., Graham, S.A., and Wooden, J.L., 2005, Integrated provenance analysis of a complex orogenic terrane: Mesozoic uplift of the Bogda Shan and inception of the Turpan-Hami basin, NW China: Journal of Sedimentary Research, v. 75, p. 251-267.

Guan, W., Yang, W., Jeffrey, B., Feng, Q., Liu, Y., Zhao, W., and Wang, Q.Y., 2010, Distinguishing source areas of Upper-Permian fluvial-lacustrine deltaic sediment fills of a half graben through petrographic study, southern Bogda Mountains, the Greater Turpan-Junggar basin, NW China: AAPG Annual Meeting, New Orleans, p. 95.

He, Q., and Walling, D.E., 1998, An investigation of the spatial variability of the grain size composition of floodplain sediments: Hydrological Processes, v. 12, p. 1079-1094.

Israel, M.B., Enzel, Y., Amit, R., and Erel, Y., 2015, Provenance of the various grain-size fractions in the Negev loess and potential changes in major dust sources to the Eastern Mediterranean: Quaternary Research, v. 83, p. 105-115.

Jacobs, P.M., and Mason, J.A., 2007, Late Quaternary climate change, loess sedimentation, and soil profile development in the central Great Plains: a pedosedimentary model: Geological Society of America Bulletin, v. 119, p. 462-475.

Kes, A.S., 1984, Zonation and faciality of loessic deposits, *in* Pecsi, M., ed., Lithology and Stratigraphy of Loess and Palaeosols: Hungarian Academy of Sciences, Budapest, 325 pp.

Kutzbach, J.E., and Gallimore, R.G., 1989, Pangaean Climates: Megamonsoons of the Megacontinent: Journal of Geophysical Research, v. 94, p. 3341-3357.

Lowenstein, T.K., Hein, M.C., Bobst, A.L., Jordan, T.E., Ku, T.L., and Luo, S., 2003, An assessment of stratigraphic completeness in climate-sensitive closed-basin lake sediments: Salar de Atacama, Chile: Journal of Sedimentary Research, v. 73, p. 91-104.

Mack, G.H., and James, W.C., 1994, Paleoclimate and the global distribution of paleosols: The Journal of Geology, v. 102, p. 360-366.

Mack, G.H., James, W.C., and Monger, H.C., 1993, Classification of paleosols: Geological Society of America Bulletin, v. 105, p. 129-136.

McTainsh, G., 1987, Desert loess in northern Nigeria: Zeitschrift fur Geomorphologie, v. 31, p. 145-165.

McTainsh, G.H., Nickling, W.G., and Lynch, A.W., 1997, Dust deposition and particle size in Mali, west Africa: Catena, v. 29, p. 307-322.

McTainsh, G.H., Walker, S., and Walker, P.H., 1982, Nature and distribution of Harmattan dust: Zeitschrift fur Geomorphologie, v. 26, p. 417-435.

Metcalfe, I., Foster, C.B., Afonin, S.A., Nicoll, R.S., Mundil, R., Xiaofeng, W., and Lucas, S.G., 2009, Stratigraphy, biostratigraphy and C-isotopes of the Permian-Triassic non-marine sequence at Dalongkou and Lucaogou, Xinjian Province, China: Journal of Asian Earth Sciences, v. 36, p. 503-520.

Miall, A.D., 1985, Architectural-element analysis: a new method of facies analysis applied to fluvial deposits: Earth-Science Reviews, v. 22, p. 261-308.

Miall, A.D., 1996, The geology of fluvial deposits: sedimentary facies, basin analysis, and petroleum geology: Springer, New York, 582 pp.

Muhs, D.R., McGeehin, J.P., Beann, J., and Fisher, E., 2004, Holocene loess deposition and soil formation as competing processes, Matanuska Valley, southern Alaska: Quaternary Research, v. 61, p. 265-276.

Obrist-Farner, J., 2015, Origin and stratigraphic architecture of the Middle Permian lower and upper Quanzijie low-order cycles, Bogda Mountains, NW China [Ph.D. dissertation]: Rolla, Missouri, Missouri University of Science and Technology, 390 pp.

Obrist-Farner, J., and Yang, W., 2015, Nonmarine time-stratigraphy in a rift setting - An example from the mid-Permian lower Quanzijie low-order cycle, Bogda Mountains, NW China: Journal of Palaeogeography, v. 4, p. 27-51.

Parrish, J.T., 1993, Climate of the Supercontinent Pangea: The Journal of Geology, v. 101, p. 215-233.

Porter, S.C., 2001, Chinese loess record of monsoon climate during the last glacial-interglacial cycle: Earth-Science Reviews, v. 54, p. 115-128.

Porter, S.C., and An, Z., 2005, Episodic gullying and paleomonsoon cycles on the Chinese Loess Plateau: Quaternary Research, v. 64, p. 234-241.

Pye, K., 1987, Aeolian dust and dust deposits: Academic Press Inc., London, 334 pp.

Reheis, M.C., Goodmacher, J.C., Harden, J.W., McFadden, L.D., Rockwell, T.K., Shroba, R.R., Sowers, J.M., and Taylor, E.M., 1995, Quaternary soils and dust deposition in southern Nevada and California: Geological Society of America Bulletin, v. 107, p. 1003-1022.

Retallack, G.J., 2013, Permian and Triassic greenhouse crises: Gondwana Research, v. 24, p. 90-103.

Retallack, G.J., Metzger, C.A., Greaver, T., Jahren, A.H., Smith, R.M.H., and Sheldon, N.D., 2006, Middle-Late Permian mass extinction on land: Bulletin of the Geological Society of America, v. 118, p. 1398-1411.

Scotese, C.R., 2001, Atlas of Earth history, Volume 1, PALEOMAP Project, Arlington, Texas, 52 pp.

Scotese, C.R., 2002, PALEOMAP website http://www.scotese.com.

Sengor, A.M.C., and Natal'in, B.A., 1996, Paleotectonics of Asia: fragments of a synthesis, *in* Yin, A., and Harrison, T.M., eds., The tectonic evolution of Asia: New York, Cambridge University Press, 486-640 pp.

Sengor, A.M.C., Natal'in, B.A., and Burtman, V.S., 1993, Evolution of the Altaid tectonic collage and Palaeozoic crustal growth in Eurasia: Nature, v. 364, p. 299-307.

Shao, L., Stattegger, K., and Garbe-Schoenberg, C.-D., 2001, Sandstone petrology and geochemistry of the Turpan basin (NW China): implications for the tectonic evolution of a continental basin: Journal of Sedimentary Research, v. 71, p. 37-49.

Sheldon, N.D., Chakrabarti, R., Retallack, G.J., and Smith, R.M.H., 2014, Contrasting geochemical signatures on land from the Middle and Late Permian extinction events: Sedimentology, v. 61, p. 1812-1829.

Singer, A., Ganor, E., Dultz, S., and Fischer, W., 2003, Dust deposition over the Dead Sea: Journal of Arid Environments, v. 53, p. 41-59.

Soreghan, G.S., Moses, A.M., Soreghan, M.J., Hamilton, M.A., Fanning, C.M., and Link, P.K., 2007, Paleoclimatic inferences from upper Palaeozoic siltstone of the Earp Formation and equivalents, Arizona-New Mexico (USA): Sedimentology, v. 54, p. 701-719.

Soreghan, G.S., Soreghan, M.J., and Hamilton, M.A., 2008, Origin and significance of loess in late Paleozoic western Pangaea: a record of tropical cold?: Palaeogeography, Palaeoclimatology, Palaeoecology, v. 268, p. 234-259.

Sun, Y., Lu, H., and An, Z., 2006, Grain size of loess, paleosol and Red Clay deposits on the Chinese Loess Plateau: Significance for understanding pedogenic alteration and palaeomonsoon evolution: Palaeogeography, Palaeoclimatology, Palaeoecology, v. 241, p. 129-138.

Sweet, A.C., Soreghan, G.S., Sweet, D.E., Soreghan, M.J., and Madden, A.S., 2013, Permian dust in Oklahoma: source and origin for Middle Permian (Flowerpot-Blaine) redbeds in western tropical Pangaea: Sedimentary Geology, v. 284-285, p. 181-196.

Tabor, N.J., and Montañez, I.P., 2002, Shifts in late Paleozoic atmospheric circulation over western equatorial Pangea: Insights from pedogenic mineral ^{18}O composition Journal of Geology, v. 30, p. 1127-1130.

Tabor, N.J., and Montañez, I.P., 2004, Morphology and distribution of fossil soils in the Permo-Pennsylvanian Wichita and Bowie Groups, north-central Texas, USA: implications for western equatorial Pangean palaeoclimate during icehouse-greenhouse transition: Sedimentology, v. 51, p. 851-884.

Tabor, N.J., and Poulsen, C.J., 2008, Palaeoclimate across the Late Pennsylvanian-Early Permian tropical palaeolatitudes: a review of climate indicators, their distribution, and relation to palaeophysiographic climate factors: Palaeogeography, Palaeoclimatology, Palaeoecology, v. 268, p. 293-310.

Tabor, N.J., Smith, R.M.H., Steyer, J.S., Sidor, C.A., and Poulsen, C.J., 2011, The Permian Moradi Formation of northern Niger: Paleosol morphology, petrography and mineralogy: Palaeogeography, Palaeoclimatology, Palaeoecology, v. 299, p. 200-213.

Tang, W., Zhang, Z., Li, J., Li, K., Chen, Y., and Guo, Z., 2014, Late Paleozoic to Jurassic tectonic evolution of the Bogda area (northwest China): evidence from detrital zircon U-Pb geochronology: Tectonophysics, v. 626, p. 144-156.

Thomas, S.G., Tabor, N.J., Yang, W., Myers, T.S., Yang, Y., and Wang, D., 2011, Paleosol stratigraphy across the Permian-Triassic boundary, Bogda Mountains, NW China: implications for palaeoenvironmental transition through earth's largest mass extinction: Palaeogeography, Palaeoclimatology, Palaeoecology, v. 308, p. 41-64.

Tsoar, H., and Pye, K., 1987, Dust transport and the question of desert loess formation: Sedimentology, v. 34, p. 139-153.

Walling, D.E., Fang, D., Nicholas, A.P., and Sweet, R.J., 2004, The grain size characteristics of overbank deposits on the flood plains of British lowland rivers, International Assocation of Hydrological Sciences, Volume 288: Sediment transfer through the fluvial system: Moscow, p. 226-234.

Wang, W., Cao, C., and Wang, Y., 2004, The carbon isotope excursion on GSSP candidate section of Lopingian–Guadalupian boundary: Earth and Planetary Science Letters, v. 220, p. 57-67.

Wartes, M.A., Carroll, A.R., and Greene, T.J., 2002, Permian sedimentary record of the Turpan-Hami basin and adjacent regions, northwest China: constraints on postamalgamation tectonic evolution: Geological Society of America Bulletin, v. 114, p. 131-152.

Wignall, P.B., Sun, Y., Bond, D.P.G., Izon, G., Newton, R.J., Védrine, S., Widdowson, M., Ali, J.R., Lai, X., Jiang, H., Cope, H., and Bottrell, S.H., 2009, Volcanism, mass extinction, and carbon isotope fluctuations in the middle permian of China: Science, v. 324, p. 1179-1182.

Winguth, A., and Winguth, C., 2013, Precession-driven monsoon variability at the Permian–Triassic boundary — Implications for anoxia and the mass extinction: Global and Planetary Change, v. 105, p. 160-170.

Xinjiang Bureau of Geology and Mineral Resources (XBGMR), 1993, Regional geology of Xinjiang Uygur Autonomous Region. Geological Memoirs, Series 1, No. 32, Ministry of Geology and Mineral Resources, Geological Publication House, Beijing, 762 pp (In Chinese with English abstract).

Xiao, W., Han, C., Liu, W., Wan, B., Zhang, J.e., Ao, S., Zhang, Z., Song, D., Tian, Z., and Luo, J., 2014, How many sutures in the southern Central Asian Orogenic Belt: Insights from East Xinjiang–West Gansu (NW China)?: Geoscience Frontiers, v. 5, p. 525-536.

Xiao, W., Huang, B., Han, C., Sun, S., and Li, J., 2010, A review of the western part of the Altaids: A key to understanding the architecture of accretionary orogens: Gondwana Research, v. 18, p. 253-273.

Xiao, W., and Santosh, M., 2014, The western Central Asian Orogenic Belt: A window to accretionary orogenesis and continental growth: Gondwana Research, v. 25, p. 1429-1444.

Xiao, W., Windley, B.F., Allen, M.B., and Han, C., 2013, Paleozoic multiple accretionary and collisional tectonics of the Chinese Tianshan orogenic collage: Gondwana Research, v. 23, p. 1316-1341.

Yang, W., 2008, Depositional systems analysis within a seismic sequence stratigraphic framework, Turpan-Hami basin, NW China: Internal Report, Tu-Ha Petroleum Bureau, v. PetroChina, p. 49 pp.

Yang, W., Crowley, J.L., Obrist-Farner, J., Tabor, N.J., Feng, Q., and Liu, Y.Q., 2013, A marine back-arc origin for the Upper Carboniferous basement of intracontinental greater Turpan-Junggar basin - Volcanic, sedimentary, and geochronologic evidence from southern Bogda Mountains, NW China: Geological Society of America Annual Meeting, GSA Abstract with Programs, Vol. 45, No. 1, Denver, Colorado.

Yang, W., Feng, Q., Liu, Y., Tabor, N., Miggins, D., Crowley, J.L., Lin, J., and Thomas, S., 2010, Depositional environments and cyclo- and chronostratigraphy of uppermost Carboniferous-Lower Triassic fluvial-lacustrine deposits, southern Bogda Mountains, NW China - A terrestrial paleoclimatic record of mid-latitude NE Pangea: Global and Planetary Change, v. 73, p. 15-113.

Yang, W., Liu, Y., Feng, Q., Lin, J., Zhou, D., and Wang, D., 2007, Sedimentary evidence of Early-Late Permian mid-latitude continental climate variability, southern Bogda Mountains, NW China: Palaeogeography, Palaeoclimatology, Palaeoecology, v. 252, p. 239-258.

Zambito, J.J., and Benison, K.C., 2013, Extremely high temperatures and paleoclimate trends recorded in Permian ephemeral lake halite: Geology, v. 41, p. 587-590.

Zhu, H.C., Ouyang, S., Zhan, J.Z., and Wang, Z., 2005, Comparison of Permian palynological assemblages from the Junggar and Tarim basins and their phytoprovincial significance: Review of Palaeobotany and Palynology, v. 136, p. 181-207.

Ziegler, A.M., Hulver, M.L., and Rowley, D.B., 1997, Permian world topography and climate, *in* Martini, I.P., ed., Late Glacial and Postglacial Environmental Changes: Pleistocene, Carboniferous-Permian, and Proterozoic: Oxford University Press, Oxford, 111-146 pp.

III. PROVENANCE AND DEPOSITIONAL CONDITIONS OF FLUVIAL SANDSTONES AND THEIR CONTROLLING PROCESSES IN A RIFT SETTING, MID-PERMIAN LOWER AND UPPER QUANZIJIE LOW-ORDER CYCLES, BOGDA MOUNTAINS, NW CHINA

Jonathan Obrist-Farner and Wan Yang

Abstract

This study investigates how provenance lithology, transport distance, and depositional and paleoclimatic conditions had affected the composition and texture of fluvial sandstones in the Middle Permian lower and upper Quanzijie low-order cycles, Bogda Mountains, greater Turpan-Junggar intracontinental rift basin, NW China. Composition and texture of 1688 gravels in16 conglomerate beds and thin sections of 42 sandstones define two petrofacies and five subfacies in Tarlong-Taodonggou area in southern Bogda and Dalongkou area 70 km to the north in northern Bogda. Petrofacies I occurs in Tarlong-Taodonggou and contains dominantly basaltic lithics, few sedimentary lithics, and are texturally immature, indicating the young Tian Shan arc to the south as the main sediment source, and rift shoulders as a local source. Sandstones deposited in ephemeral streams have abundant sedimentary lithics, whereas those deposited in meandering streams contain minimal sedimentary lithics; the sandstones deposited in both streams have similar texture. Compositional maturity increases from lower-middle part to upper part of the section; so are pedogenic features better developed in uppermost part. Petrofacies II occurs in Dalongkou and contains dominantly sedimentary lithics, which were likely derived from older rift sedimentary rocks exposed at rift shoulders. Hence, information on regional tectonic setting is not evident. The Dalongkou sandstones were deposited mainly in meandering streams, are consistently sedimentary-lithic rich

upsection, and contain abundant and well-developed pedogenic clay coats. In summary, the composition and texture of QZJ sandstones are mainly controlled by provenance lithology, and secondarily by depositional and paleoclimatic conditions and transport distance. The results substantiate the rift origin of the Turpan-Junggar basin in Middle Permian, which had many half-grabens and grabens and was bordered by a volcanic arc in the southern margin.

1. Introduction

Ancient fluvial sediments recorded tectonic, climatic, and depositional conditions on the Earth's surface (e.g., Basu, 1976; Mack and Suttner, 1977; Folk, 1980; Suttner et al., 1981; Basu, 1985; Suttner and Dutta, 1986; Grantham and Velbel, 1988; Garzanti et al., 2001, 2013; Roy and Roser, 2013). Among the factors controlling fluvial sedimentation, provenance lithology is regarded as the main control on sediment composition (Dickinson and Suczek, 1979; Dickinson et al., 1983; Dickinson, 1985). However, imprints from other factors, such as transport distance, physical and chemical weathering, topographic relief, and paleoclimatic conditions, complicate interpretations of provenance lithology (e.g., Suttner and Dutta, 1986; Johnsson and Stallard, 1989; Ingersoll, 1990; Garzanti et al., 2001, 2013; Van Loon and Mange, 2007).

This study focuses on the sedimentology and petrography of fluvial sandstones in the Middle Permian lower and upper Quanzijie low-order cycles (QZJ LCs) in the southern and northern Bogda Mountains, NW China, deposited in the greater Turpan-Junggar intracontinental rift basin (Figs. 1, 2). The QZJ LCs offer an opportunity to study compositional and textural characteristics of fluvial sandstones where lithology, fluvial processes, and tectonic and climatic conditions are reasonably well-documented (e.g.,

Carroll et al., 1992, 1995; Shao et al., 2001; Wartes et al., 2002; Greene et al., 2005; Yang et al., 2007, 2010; Metcalfe et al., 2009; Thomas et al., 2011; Obrist-Farner and Yang, 2015; Obrist-Farner, 2015). Field and petrographic data are used to document characteristics of framework grains to interpret provenance lithologies, transport distance, and paleoclimatic conditions. The results indicate that the sandstone composition is mainly controlled by provenance lithology and secondarily by depositional and paleoclimatic conditions and transport distance, and texture is mainly controlled by depositional processes and diagenetic modification.

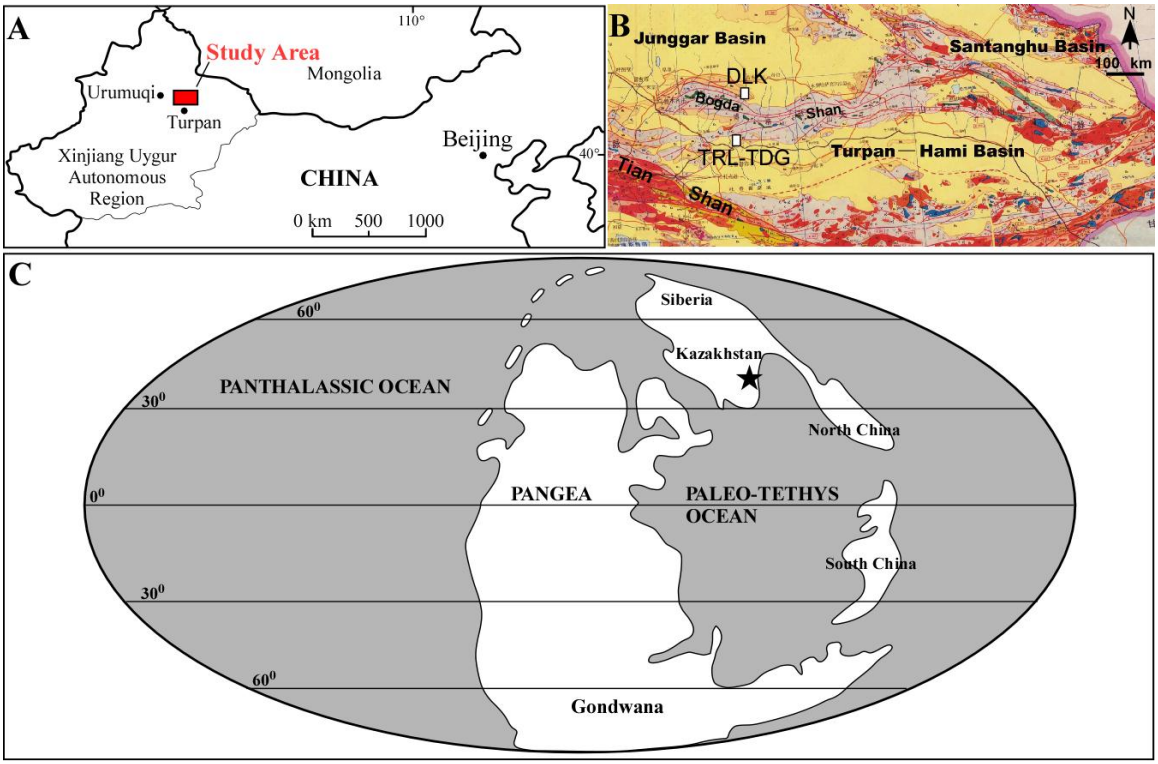

Figure 1. A) Location of the study area in Xinjiang Uygur Autonomous Region, NW China. B) Geological map of eastern Xinjiang, showing locations of Tarlong-Taodonggou (TRL-TDG) and Dalongkou (DLK). Modified from XBGMR (1993). C) Global paleogeographic reconstruction for the Late Permian. Modified from Scotese (2002). The location of the study area is marked with a black star.

2. Geological Background

The lower and upper QZJ LCs were deposited in the greater Turpan-Junggar intracontinental rift basin in northwestern China during the Middle Permian (Sengor and Natal'in, 1996; Allen et al., 1995, Yang et al., 2010; cf. Carroll et al., 1995; Carroll et al., 2010). The basin was developed on an Upper Carboniferous volcanic arc basement (Yang et al., 2010, 2013). This study focuses on the well-exposed QZJ LCs in Tarlong-Taodonggou and Dalongkou areas in the southern and northern foothills of the Bogda Mountains, respectively (Figs. 1, 3). The study area is in southeastern Kazakhstan Plate of NE Pangea (Fig. 1C), which migrated northward from ~40 to 50^0 N paleo-latitude during Kungurian-Wuchiapingian epochs (Sengor and Natal'in, 1996; Scotese, 2001). Yang (2008) and Yang et al., (2010) interpreted the Tarlong-Taodonggou area as a half graben, based on lateral facies and thickness changes in the outcrop and basin geometries on seismic sections from the adjacent Turpan-Hami Basin.

The QZJ LCs are informal cyclostratigraphic units first defined by Yang et al. (2007 and 2010) and refined by Obrist-Farner and Yang (2015). It largely correlates to the Quanzijie Formation (Fig. 2; XBGMR, 1993; Cai, 1999), which occurs in the subsurface of the greater Turpan-Junggar basin and in the foothills of Bogda Mountains and northern foothills of Tian Shan. The lower QZJ LC consists of meandering stream channel and overbank deposits, whereas the upper QZJ LC of alternating ephemeral and meandering stream and loess deposits. The low-order cycles are composed of stacked high-order cycles (HCs), as defined by repetitive changes in depositional conditions and environments. Four types were identified as meandering stream, fluvial-loessial, lakeplain-littoral, and lacustrine deltaic HCs (Yang et al., 2010; Obrist-Farner and Yang, 2015; Obrist-Farner, 2015). Both the lower and upper QZJ LCs are composed mainly of

meandering stream and fluvial-loessial HCs. A meandering stream HC is composed of a high-relief erosional base overlain by channel-fill conglomerate and sandstone, and overbank mudrock, paleosol, and thin sandstones. A fluvial-loessial HC has two subtypes: ephemeral stream-loessial and meandering stream-loessial. The former has a low-relief erosional base overlain by thin channel-fill conglomerate and thin sandstone, which are overlain sharply by thick loessite. The latter has a high-relief erosional base overlain by an upward-fining conglomerate-sandstone-mudrock succession of a meandering-stream origin in the lower part and a thick loessite in the upper part. Sedimentary and paleosol evidence in the Tarlong-Taodonggou area suggests a semiarid climate with strong precipitation seasonality during the deposition of lower QZJ LC, an arid-semiarid condition during the deposition of the lower and middle parts of the upper QZJ LC, and a humid-subhumid condition during the deposition of the uppermost part of the upper QZJ LC (Yang et al., 2007, 2010; Obrist-Farner and Yang, 2015). Climatic trend in the Dalongkou area is similar to that in Tarlong-Taodonggou. However, the condition during the deposition of the lower QZJ LC and the lower and upper part of upper QZJ LC appears to be dominantly semiarid to subhumid (Obrist-Farner and Yang, 2015).

The ages of the QZJ LCs are poorly constrained (Fig. 2). Regional geological survey placed the Quanzijie Formation as Capitanian on the basis of limited biostratigraphic data (e.g., XBGMR, 1993; Cai, 1999). Yang et al. (2010) placed the underlying Hongyanchi LC as Artinskian on the basis of a U/Pb zircon age of 281.42 ± 0.10 Ma. They estimated that the unconformity separating the Hongyanchi LC from the lower QZJ LC may represent a maximum duration of ~14 Ma. The age of the lower QZJ

LC should be similar to that of the upper QZJ LC, because the two LCs are separated by a disconformity (Obrist-Farner and Yang, 2015). Thus, it is speculated that the base of the lower QZJ LC may be within the Wordian (see also Wartes et al., 2002; Zhu et al., 2005). The boundary between upper QZJ LC and overlying Wutonggou LC is conformable, which has been designated as Wuchiapingian by regional survey and biostratigraphy (e.g., XBGMR, 1993; Cai, 1999; Zhu et al., 2005), which was substantiated by three zircon ages of Yang et al. (2010). In this study, a possible Kungurian to early Capitanian age is used for the lower QZJ LC, although a Wordian age for the base of lower QZJ LC may be more reasonable; and a Capitanian age for the upper QZJ LC (cf. Obrist-Farner and Yang, 2015).

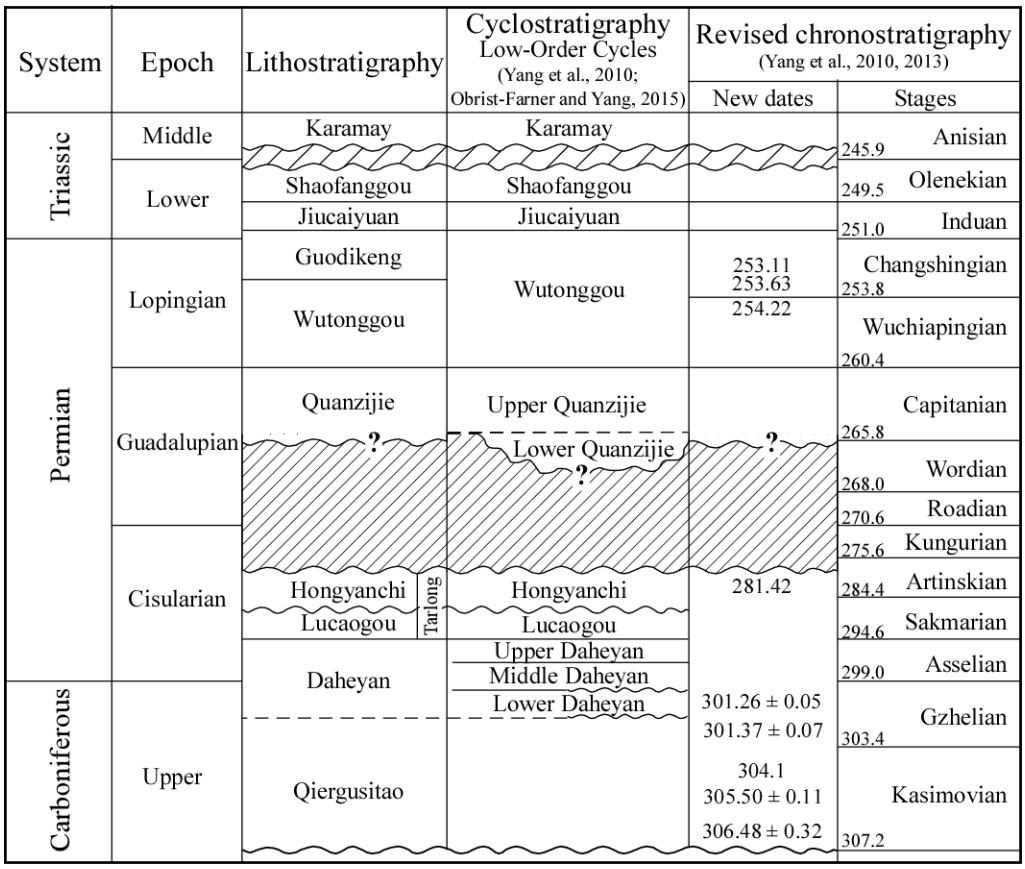

Figure 2. Chrono-, litho-, and cyclostratigraphy of Upper Carboniferous-Lower Triassic strata in the Tarlong-Taodonggou area. Wavy lines are major unconformities; dashed lines disconformity; and hatched areas missing strata. Absolute ages at stage boundaries from Gradstein et al. (2004). Modified from Yang et al. (2010, 2013) and Obrist-Farner and Yang (2015).

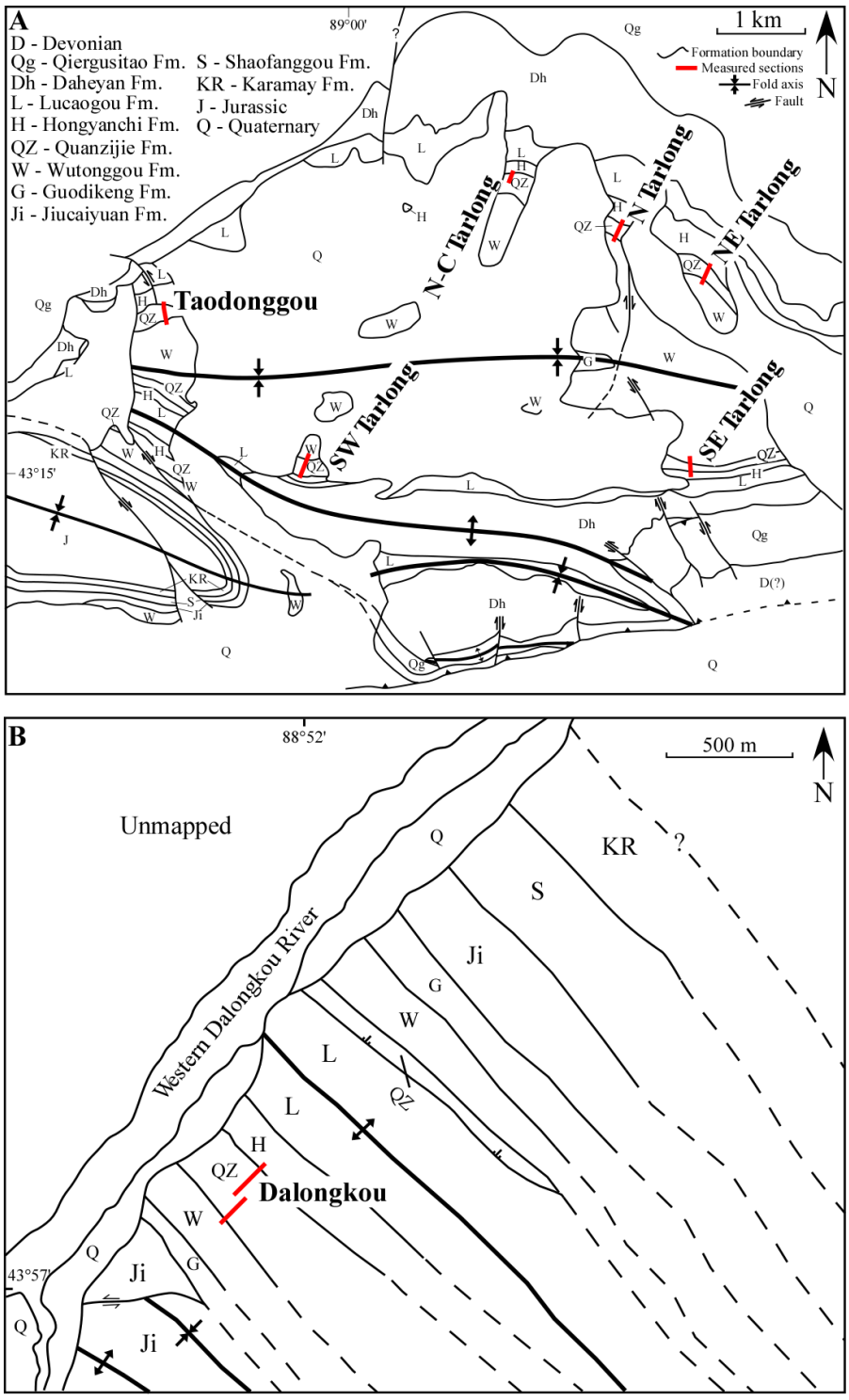

Figure 3. Geologic maps of Tarlong-Taodonggou (A) and Dalongkou (B) areas showing names and location (red lines) of measured sections. Modified from Yang et al. (2010) and Obrist-Farner and Yang (2015).

3. Data and Methodology

Field and petrographic observations of fluvial sandstones and conglomerates from the Tarlong-Taodonggou and the Dalongkou areas provide the basic data for this study. Composition and texture of a total of 1688 gravels from 16 conglomerate beds are collected and described in four measured sections in Tarlong-Taodonggou and one in Dalongkou. So are 42 sandstone samples, among which four samples are from the northeast Tarlong section, 18 samples from the southeast Tarlong section (Fig. 3A), and 20 samples from the Dalongkou section (Fig. 3B). 400 points on each standard thin section of sandstones are counted under a petrographic microscope using two methods: the Gazzi-Dickinson method (Gazzi, 1966; Dickinson, 1970; Ingersoll et al., 1984) and the traditional method (Suttner, 1974). The two methods differ mainly in the identification of lithic fragments and the inclusion of intrabasinal grains. For example, any plagioclase grain larger than 0.0625 mm in a basaltic lithic fragment is counted as a plagioclase framework grain with the Gazzi-Dickinson method, whereas the entire basaltic fragment is counted as a volcanic lithic grain with the traditional method. Suspected intrabasinal grains are excluded from the modal sandstone composition when using the Gazzi-Dickinson method but included in the traditional method. Point-counting data using the traditional method are used for sandstone compositional classification of Folk (1980); and those using the Gazzi-Dickinson method are used only for tectonic classification of sandstone of Dickinson (Dickinson and Suczek, 1979; Dickinson et al., 1983; Dickinson, 1985). Petrographic parameters used in the two classifications are defined in Table 1. Sandstone textural classification is modified based on the scheme of Dott (1964). The term arenite is used for sandstones with 0-5% matrix; subarenite with 5-15% matrix; and wacke with 15-50% matrix. The term subarenite is used to further

separate the classification scheme and provide a detailed description of sandstone characteristics. To characterize framework grain size, the grains are placed into 28 grain size bins equally distributed into 0.5ϕ bins to plot the grain size distribution to calculate graphic mean (M_Z), inclusive graphic standard deviation (σ_I), and inclusive graphic skewness (Sk_I; Folk and Ward, 1957; Folk, 1980). The grain size parameters are used to interpret differences in depositional processes among studied samples. Angular, subangular, subrounded, and rounded grain shape are differentiated according to Powers (1953). Rare very angular and well-rounded grains are combined with the angular and rounded grains, respectively. Subsequently, the compositional and textural characteristics of the studied sandstones are used to contrast sandstones deposited in ephemeral and meandering streams and to show the lateral and vertical stratigraphic trends in the QZJ LCs. Finally, provenance lithology, transport distance, and depositional and paleoclimatic conditions are interpreted to provide insights into fluvial sedimentation in an intracontinental rift setting.

Table 1. Grain types and modal parameters used in this study.

Symbol	Definition
Qnu	Nonundulose monocrystalline quartz
Qu	Undulose monocrystalline quartz
Qp	Polycrystalline quartz
Qm	Microcrystalline quartz
Qc	Chalcedony
K	Potassium feldspar
P	Plagioclase feldspar
Lvf	Felsitic
Lvv	Vitreous
Lvl	Lathwork
Lvm	Microlitic
Lvt	Trachytic
Lva	Amygdaloidal
Lvs	Shards
Lv	Lvf + Lvv + Lvl + Lvm + Lvt + Lva + Lvs
Lsm	Mud clasts
Lsr	Mudrock
Lsh	Shale
Lsc	Carbonate
Ls	Lsm + Lsr + Lsh + Lsc
Lm	Metamorphic
Calculated parameters for sandstone classification (Folk, 1980)	
Q	Qnu + Qu + Qp + Qm + Qc
F	K + P
L	Lv + Ls + Lm
Calculated parameters for Dickinson's ternary diagrams	
Q	Qnu + Qu + Qp + Qm + Qc
Qmo	Qnu + Qu
Qpo	Qp + Qm + Qc
F	K + P
L	Lv + Ls - Lsc - Lsm
Ls	Ls - Lsc - Lsm
Lt	L + Qpo

4. Results

4.1 Conglomerate Petrology

Class-supported conglomerates are common in the QZJ LCs. The gravels in Tarlong-Taodonggou are mostly mafic and intermediate volcanic and shallow intrusive, whereas those from Dalongkou are mainly sedimentary. On average, the gravels are pebble in size but range from granule to boulder. The gravels in all sections are moderately to well sorted and angular to subrounded. They are mostly in contact with each other and embedded in a sandy matrix. The percentage of gravels in the conglomerates is 30-100%.

In Tarlong-Taodonggou area, the composition of gravels in conglomerates varies significantly among sections and upward (Table 2). Gravels in the northeastern and southeastern Tarlong and Taodonggou sections (Fig. 3) are dominantly volcanic and shallow intrusive (66.3% on average) with some sedimentary (31.7%) and minor metamorphic (<1%) (Table 2). Gravels in the southwestern Tarlong section, on the other hand, contain much more sedimentary (53.5%) than volcanic and shallow intrusive (46.5%) gravels.

In addition, the composition of gravels changes gradually upsection. Gravels in the lower QZJ LC are mainly volcanic and shallow intrusive (71.3%) and sedimentary (28.7%) gravels (Table 2). The volcanic and shallow intrusive gravels are mainly intermediate (65.3%) and mafic (18.8%); 15.9% volcanic gravels are undifferentiated between intermediate to mafic in composition. Sedimentary gravels include clasts of sandstone (84.7%), mudrock (6.5%), limestone (7.3%), and chert (1.6%). Upward in the lower part of upper QZJ LC, the amount of sedimentary gravels (46.6%) increases slightly and that of volcanic and shallow intrusive gravels (53.4%) decreases (Table 2).

Volcanic and shallow intrusive gravels are intermediate (69.8%) to mafic (2.1%); 28.1% are undifferentiated. Sedimentary gravels are sandstone (90%), mudrock (3.6%), limestone (2.7%), and chert (3.6%). However, the percentage of volcanic and shallow intrusive gravels (73.4%) increases significantly and that of sedimentary gravels (23.1%) decreases in the middle part of upper QZJ LC (Table 2). Metamorphic gravels (3.5%) appear, for the first time, in this interval in the Taodonggou section. Volcanic and shallow intrusive gravels are dominated by intermediate and mafic compositions, with a total of 55.0% and 24.9%, respectively; 20.1% are undifferentiated. Sedimentary gravels are dominated by sandstone (80.6%) with mudrock (2.8%) and a relatively large amount of chert (16.7%). The gravel composition in the upper part of upper QZJ LC is similar to that in the lower part, as sedimentary (52.9%), volcanic and shallow intrusive (44.9%), and metamorphic (2.2%) (Table 2). Volcanic and shallow intrusive gravels are intermediate to mafic in composition, with a total of 62.4% and 12.1%, respectively; 25.5% are undifferentiated. Sedimentary gravels include sandstone (92.2%), mudrock (2.4%), and chert (5.4%).

In Dalongkou section, gravel composition shows no distinct stratigraphic trend, but is significantly different from that in Tarlong-Taodonggou (Table 2). Sedimentary gravels dominate with an overall average of 94.8%, whereas volcanic and shallow intrusive gravels only account for 4.8%. Sandstone gravels are the most abundant, with an average of 89.2% and mudrock and limestone gravels are rare. In addition, well-laminated dark gray dolomitic and organic-rich shale gravels similar to those in the underlying Lucaogou LC (Yang et al., 2010) appear in the middle and upper parts of the section. Volcanic gravels are all intermediate. All gravels are pebble in size and

subrounded to rounded, except the shale gravels in the middle and upper parts, which are cobble to boulder in size and angular.

The abundance of volcanic and shallow intrusive gravels in Tarlong-Taodonggou indicates an igneous source for the conglomerates; the sedimentary gravels suggest a secondary sedimentary source. The increase of sedimentary gravels in the lower and upper part of the upper QZJ LC indicates an increase in sediment supply from a sedimentary source. The increase in sedimentary lithics in the lower part of the upper QZJ LC is only observed in the southwestern Tarlong section because gravel composition and texture from the lower part of the upper QZJ LC was only described from the southwest section. The increase in sedimentary gravels in the upper part of the upper QZJ LC is observed in all studied sections. The variations in gravel composition between stratigraphic sections suggest variable lithology of provenances at different locations and of fluvial sediment influx into the Tarlong-Taodonggou half graben. This is supported by the variations in gravel angularity. The rounded to subrounded gravels indicate a long transport distance, whereas the angular to subangular gravels indicate a short distance.

The dominance of sedimentary gravels in Dalongkou indicates a prominent sedimentary provenance during the deposition of the lower and upper QZJ LCs, different from those in Tarlong-Taodonggou. The dominant rounded to subrounded shape indicates a long transport distance or a recycled origin. The angular Lucaogou shale gravels indicate that the Lower Permian Lucaogou deposits had been lithified and uplifted at the rift shoulders and eroded and transported for a short distance to the depositional site.

Table 2. Composition of gravels in the QZJ LCs.

Stratigraphic Section	Volcanic			Sedimentary					Metamorphic
	Intermediate	Mafic	Unknown	Sandstone	Mudrock	Limestone	Chert	Shale	
Tarlong-Taodonggou									
Northeast	142	23	35	103	2	0	6	0	0
Southeast	109	54	60	70	3	0	12	0	0
Southwest	118	16	18	152	6	12	5	0	0
Taodonggou	113	41	45	90	7	0	4	0	18
Dalongkou									
Dalongkou	20	0	2	379	2	6	1	14	0

Stratigraphic Location	Volcanic			Sedimentary					Metamorphic
	Intermediate	Mafic	Unknown	Sandstone	Mudrock	Limestone	Chert	Shale	
Tarlong-Taodonggou									
Lower QZJ LC	201	58	49	105	8	9	2	0	0
L. upper QZJ LC	67	2	27	99	4	3	4	0	0
M. upper QZJ LC	126	57	46	58	2	0	12	0	11
U. upper QZJ LC	88	17	36	153	4	0	9	0	7
Dalongkou									
Lower QZJ LC	2	0	2	106	0	1	1	0	0
L. upper QZJ LC	3	0	0	96	0	4	0	0	0
M. upper QZJ LC	9	0	0	79	1	0	0	14	0
U. upper QZJ LC	6	0	0	98	1	1	0	0	0

4.2 Sandstone Petrology

4.2.1 Framework Grain Types and Characteristics

The sandstones from Tarlong-Taodonggou and Dalongkou are compositionally different (Tables 3, 4). The former are feldspathic litharenites and litharenites (Folk, 1980), with a mean composition of $Q_4F_{23}L_{73}$ (Fig. 4). Matrix content in eight samples ranges from 0 to 5%, two from 5 to 15%, and 12 from 15 to 50% (Table 3). Volcanic lithics dominate, plagioclase is the most dominant feldspar, and monocrystalline quartz is the most dominant type of quartz. On the other hand, Dalongkou sandstones are lithic arkose and feldspathic litharenites (Folk, 1980) with a mean composition of $Q_{43}F_{30}L_{27}$ (Fig. 4). Matrix content in two samples ranges from 5 to 15% and 18 from 15 to 50% (Table 4). Content of quartz, sedimentary lithics, and feldspars is similar in all samples from Dalongkou.

Table 3. Raw point counting data and statistical grain size analysis for Tarlong-Taodonggou sandstones.

Sample No.	Qnu	Qu	Qp	Qm	Qc	K	P	Lvf	Lvv	Lvl	Lvm	Lvt	Lva	Lvs	Lsr	Lsm	Lsh	Lsc	Lm	M_Z	σ_I	Sk_I	Matrix
Southeast Tarlong																							
Q13-1	4	9	1	1	2	33	63	1	0	40	100	20	0	1	8	0	0	0	0	2.49	0.82	-0.02	29
Q13-2	0	1	2	1	0	20	67	0	5	47	101	23	9	1	0	0	0	0	0	2.44	0.94	-0.09	21
Q13-3	1	11	5	1	0	45	57	0	2	40	66	17	7	0	7	1	1	0	2	2.84	1.02	-0.38	29
Q13-4	3	4	3	6	0	17	53	20	3	26	49	31	0	0	2	13	0	0	0	2.97	0.70	-0.34	41
Q13-5	0	2	0	0	0	7	29	14	1	49	52	35	1	0	1	0	0	0	0	1.45	1.00	0.11	0
Q13-6	2	0	0	0	3	15	80	27	2	68	48	24	2	0	2	7	0	0	0	2.41	0.82	0.05	0
Q13-7	0	0	0	0	1	1	18	14	5	40	60	10	3	0	11	44	0	0	0	0.89	1.03	0.14	24
Q13-8	1	1	0	0	1	0	125	4	8	54	65	15	1	0	11	17	0	0	0	1.35	0.77	-0.04	0
Q13-9	0	0	1	1	12	1	15	9	1	53	73	27	3	0	19	50	0	0	0	1.80	0.89	-0.08	2
Q13-10	0	0	0	0	4	3	87	8	7	33	63	17	0	0	12	45	0	0	0	1.86	0.73	0.09	0
Q13-11	2	0	0	0	1	2	69	18	1	45	101	23	2	0	4	18	0	0	0	2.06	0.74	0.11	0
Q13-12	0	0	1	0	0	0	17	51	5	80	99	51	0	0	21	12	0	0	0	0.79	1.30	-0.15	14
Q13-13	0	0	0	0	0	0	5	4	5	37	95	44	0	0	15	5	0	0	0	0.25	1.60	0.06	0
Q13-16	3	3	3	1	5	0	10	2	3	19	60	20	0	0	93	0	0	0	0	0.50	0.85	0.13	20
Q13-17	8	4	5	8	8	3	61	1	0	14	43	7	0	0	52	5	0	0	0	1.64	0.88	0.14	22
Q13-18	14	2	3	3	1	6	62	0	4	22	81	8	0	0	57	0	0	0	0	1.72	1.02	0.00	30
Q13-19	0	3	1	1	3	2	9	0	3	14	102	28	0	0	44	0	0	0	1	0.88	0.60	0.11	27
Q13-20	5	3	1	1	5	3	26	2	0	5	34	10	0	0	50	2	0	0	1	1.52	0.73	-0.02	31
Northeast Tarlong																							
S10-3	0	0	0	0	0	0	35	0	1	11	79	8	0	0	0	0	0	0	0	1.19	0.69	0.04	0
S10-12	2	1	7	1	2	1	12	1	0	8	2	0	0	0	52	50	0	0	0	0.98	0.93	0.17	15
Q14-4	0	0	0	0	0	4	25	0	2	12	60	10	2	0	19	18	0	0	0	1.79	0.70	0.08	21
Q14-5	0	0	0	0	0	5	47	1	1	7	62	3	5	0	5	15	0	0	0	2.20	0.74	-0.11	21

Note. Samples with white background belong to petrofacies Ia, light gray background to petrofacies Ib, and dark gray background to petrofacies Ic. Mean grain size and sorting values are in ϕ units. Matrix is in percentage.

Table 4. Raw point counting data and statistical grain size analysis for Dalongkou sandstones.

Sample No.	Qnu	Qu	Qp	Qm	Qc	K	P	Lvf	Lvv	Lvl	Lvm	Lvt	Lva	Lvs	Lsr	Lsm	Lsh	Lsc	Lm	M_Z	σ_I	Sk_I	Matrix
Dalongkou																							
QD12-1	8	14	47	30	0	83	40	0	0	2	19	0	0	0	39	2	0	0	0	2.66	0.69	0.08	13
QD12-2	12	18	49	27	0	107	31	0	0	0	10	0	0	0	24	0	0	0	0	3.08	0.62	-0.17	29
SD11-2	16	10	31	46	0	20	68	0	0	4	12	0	0	0	43	15	0	0	0	2.36	0.72	0.04	34
QD12-3	6	14	62	27	1	52	25	0	0	0	7	0	0	0	49	0	0	0	0	2.51	0.75	-0.07	25
QD12-4	27	18	55	42	5	52	18	0	0	4	16	0	0	0	20	25	0	1	0	2.36	0.78	-0.02	22
QD12-5	28	14	54	27	1	58	34	0	0	4	17	0	0	0	26	3	0	0	0	2.51	0.78	0.11	29
QD12-6	28	18	34	30	5	73	70	0	0	7	16	0	0	0	20	6	0	0	0	2.49	0.80	0.06	24
QD12-7	20	14	30	20	3	27	36	0	0	1	12	0	0	0	23	6	0	0	0	2.46	0.80	0.03	25
QD12-8	18	18	66	12	4	37	33	0	0	12	9	0	0	0	68	8	1	0	0	2.15	1.00	-0.04	22
QD12-9	9	14	33	33	3	25	36	0	0	1	4	0	0	0	94	18	1	1	0	2.43	0.81	-0.02	32
QD12-10	13	18	56	26	1	18	41	0	0	5	7	0	0	0	71	38	6	0	0	1.90	1.16	-0.26	25
QD12-11	13	14	67	43	2	23	43	0	0	6	8	0	0	0	39	3	0	0	0	2.38	0.99	0.03	36
QD12-12	18	18	38	38	0	26	36	0	0	4	0	0	0	0	42	11	0	0	0	2.37	0.87	-0.09	44
SD11-9	22	13	27	32	1	29	62	0	0	3	11	0	0	0	31	2	0	0	0	2.28	0.64	0.00	38
QD12-13	34	11	44	56	0	42	55	0	0	3	7	0	0	0	41	30	0	0	0	2.37	0.60	0.02	19
QD12-14	32	6	42	40	0	24	48	0	0	4	1	0	0	0	51	23	0	0	0	2.39	0.75	0.02	29
QD12-15	24	2	28	36	2	42	40	0	0	1	3	0	0	0	89	12	0	0	0	2.31	0.99	-0.18	30
SD11-12	22	9	21	55	1	14	56	0	0	4	11	0	0	0	23	7	0	0	0	2.51	0.69	0.00	40
QD12-16	35	12	52	57	0	12	63	0	0	9	12	0	0	0	72	31	0	0	0	1.72	0.87	-0.03	12
SD11-13	17	31	26	59	0	12	26	0	0	2	4	0	0	0	75	41	9	0	0	1.18	1.27	-0.46	26

Note. Samples with white background belong to petrofacies IIa and light gray background to petrofacies IIb. Mean grain size and sorting values are in ϕ units. Matrix is in percentage.

4.2.1.1 Quartz

Five types of quartz grains (Q) are recognized in the two study areas: nonundulatory and undulatory monocrystalline quartz (Qnu, Qu, respectively), polycrystalline quartz (Qp), microcrystalline quartz (Qm), and chalcedony (Qc). The monocrystalline grains are typically clear with rare microlites. In rare cases, those in Tarlong-Taodonggou contain small embayments. Qu grains generally exhibit slight undulose extinction with a range of 5 to 10^0; the largest extinction angle occurs in Qu grains from Dalongkou. Qp grains are composed of non-oriented and welded quartz crystals. Qc grains have a feather-like texture and contain rounded edges.

Qnu, Qu, and Qc grains are common in Tarlong-Taodonggou samples; Qp and Qm grains are rare and variable (Table 3). The median grain size of quartz grains is medium sand, ranging from very fine to very coarse sand (Fig. 5A). On average, 31.3% and 37.9% of quartz grains are mainly angular and rounded, respectively (Table 5). Subangular and subrounded grains are less common, with averages of 15.4% and 15.4%, respectively (Table 5). Qm, Qp, Qnu, and Qu grains are common in Dalongkou samples; Qc grains are rare (Table 4). The median grain size is fine sand, ranging from very fine to very coarse sand (Fig. 5A). On average, 73.2% and 14.8% of the grains are rounded and subrounded, respectively (Table 5). Angular and subangular grains are less common, with average of 6.6% and 5.4%, respectively (Table 5).

In Tarlong-Taodonggou, the abundance of clear monocrystalline quartz grains and small embayments suggest a volcanic source. The rarity of quartz indicates a non-felsic or a carbonate source lithology. The rounded to subrounded grains indicate a long transport distance or a possible recycled origin, whereas the angular to subangular grains

indicate a relatively short distance. In Dalongkou, the dominance of all types of quartz and rounded shapes suggest a distant sedimentary source or a recycled origin.

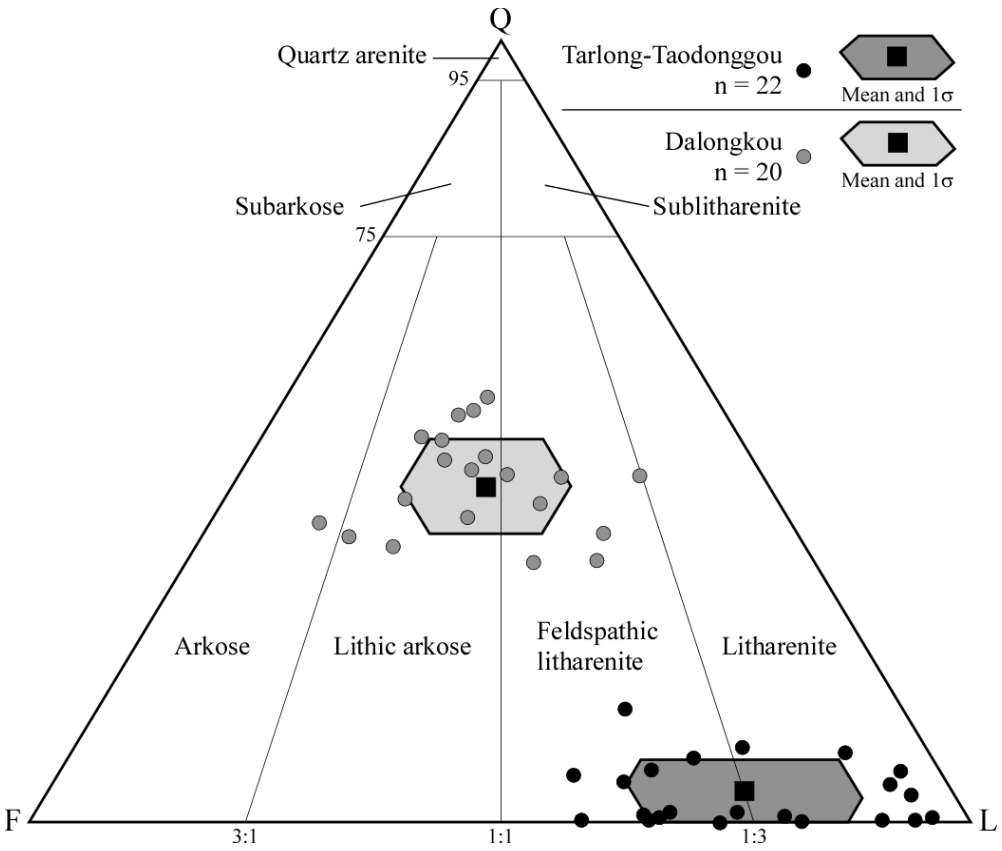

Figure 4. Composition of the Tarlong-Taodonggou and Dalongkou sandstones plotted in a QFL diagram after Folk (1980). Tarlong-Taodonggou sandstones are L rich, whereas Dalongkou sandstones have a similar mean distribution of Q, F, and L.

4.2.1.2 Feldspars

Feldspars (F) include microcline and orthoclase (K) and albite (P). In Tarlong-Taodonggou, albite dominates and has common compositional zoning (Table 3; Fig. 6A, B), with an average P/F ratio (Dickinson, 1970) of 0.85. Average median size of feldspar

grains is fine sand, ranging from very fine to very coarse sand (Fig. 5A). On average, 43.3% and 29.2% of feldspar grains are mainly angular and rounded, respectively (Table 5). Subangular and subrounded grains are less common, with averages of 13.4% and 14.0%, respectively (Table 5). In Dalongkou, the amount of P and K is similar (Table 4), with an average P/F ratio of 0.52. The average median grain size is fine sand, ranging from very fine to medium sand (Fig. 5A). On average, 18.8% and 59.9 % of feldspar grains are mainly subrounded and rounded, respectively (Table 5). Angular and subangular grains are less common, with averages of 14.1% and 7.2%, respectively.

The compositional zoning, large P/F ratio, and dominant angular shape of feldspar grains in Tarlong-Taodonggou suggest a dominant near volcanic source. On the other hand, the similar amount of P and K and dominant rounded shape of feldspar grains in Dalongkou suggest a distant source with a small influx of volcanic feldspars.

4.2.1.3 Lithics

Lithics (L) are the most common grains in the sandstones. 13 types of volcanic, sedimentary, and metamorphic lithics are identified.

Volcanic lithics (Lv) are differentiated on the basis of texture into vitreous (Lvv), lathwork (Lvl), microlitic (Lvm), trachytic (Lvt), felsitic (Lvf), amygdaloidal (Lva), and glass shard fragments (Lvs; Table 1). Lvv have a glassy, isotropic texture with rare to no microlites. Lvl contain elongated laths of albite encased in a finely crystalline groundmass which, in rare cases, is of a felsitic texture (Fig. 6C). Lvm contain needle-shaped plagioclase microlites encased in a finely crystalline or black groundmass (Fig. 6D). Lvm are similar to Lvl and are differentiated on the basis of the size of the

plagioclase phenocrysts; Lvm have phenocrysts smaller than 63 μm, whereas Lvl have phenocrysts larger than 63 μm. Lvt are similar to Lvm expect that the plagioclase phenocrysts show a preferred orientation. Lvf have a very fine-grained texture with anastomose grain boundaries and, in some cases, contain small plagioclase laths. They are differentiated from Qm by the presence of quartz and feldspar which are visible under plane light using the Becke line (e.g., Shelley, 1993). In rare cases, the Lvf grains contain euhedral high-birefringence zircon microlites (Fig. 6E, F). Lva contain vesicles that are filled by secondary minerals, such as zeolites or chalcedony (Fig. 7A). Lvs are composed entirely of shards with distinct embayed edges (Fig. 7B). Lvv, Lvl, Lvm, Lvt, and Lva grains are derived from a mafic source, whereas Lvf and Lvs from a felsic source.

In Tarlong-Taodonggou, Lv grains make up 78% of the lithics; 93% of the Lv grains are mafic and 7% are felsic in composition (Table 3). The average size of Lv grains is coarse sand on average, ranging from fine to very coarse sand (Fig. 5A). On average, 64.1% and 16.8% of the grains are rounded and subrounded, respectively (Table 5). Angular and subangular grains are rare, with averages of 11.8% and 7.3%, respectively. In Dalongkou, however, 17% of the lithics are Lv grains, which are all mafic (Table 4). The average grain size is fine sand, ranging from fine to very coarse sand (Fig. 5A). On average, 85.5% and 10.7% of the grains are rounded and subrounded, respectively (Table 5). Angular to subangular grains are rare, with averages of 2.3% and 1.5%, respectively.

In Tarlong-Taodonggou, the abundance of mafic Lv grains indicates a primary mafic volcanic source. The presence of Lvf and Lvs grains, however, suggest a secondary

felsitic source. In Dalongkou, the limited amount of Lv grains indicates a secondary mafic volcanic source.

Sedimentary lithics (Ls) include fragments of mudrock and carbonate rock. Three types of mudrock clasts are identified. First, some mudrock clasts have a dull matrix that exhibit high birefringence under cross-polarized light, suggesting clay-rich matrix. They have common embayed edges apparently caused by indentation by adjacent hard grains, indicating that these clasts were semi-consolidated during deposition and, thus, rip-up mud clasts (Lsm). Second, some mudrock clasts contain very fine sand and silt grains floating in a mud matrix and are subrounded to rounded with no embayed edges, which indicate the clasts were well lithified during deposition. They are interpreted as fragments of mudrock (Lsr) derived from old mudrocks. Finally, some other mudrock lithics show clear laminations, suggesting they were derived from lithified shale (Lsh). Lsh are present mainly in Dalongkou and show similar color, fissility, and composition as the underlying Lucaogou shale (Fig. 7C; Yang et al., 2010). Carbonate lithics (Lsc) are fragments of micrite and rare in the studied samples.

In Tarlong-Taodonggou, Ls grains account for 21% of all lithics (Table 3) and have an average grain size of coarse sand, ranging from very fine to very coarse sand (Fig. 5A). On average, 73% and 14.2% of the grains are rounded and subrounded, respectively (Table 5). Angular and subangular Ls grains are rare, with averages of 5.2% and 7.6%, respectively (Table 5). In Dalongkou, however, Ls grains account for 83% of all lithics (Table 4) and have an average grain size of coarse sand, ranging from very fine sand to pebble (Fig. 5A). 87.1% of the grains are rounded (Table 5). The small amount of Ls grains in Tarlong-Taodonggou suggests a secondary sedimentary source for the

sandstones. In contrast, the abundance of Ls grains in Dalongkou suggests a primary sedimentary source.

Metamorphic lithics (Lm) are rare (~1%) in Tarlong-Taodonggou (Table 3) and not present in Dalongkou (Table 4). They are medium to coarse, and subrounded to rounded. The rarity of Lm grains suggests that metamorphic rocks were likely not exposed in the Tarlong-Taodonggou and Dalongkou areas during deposition of the QZJ LCs.

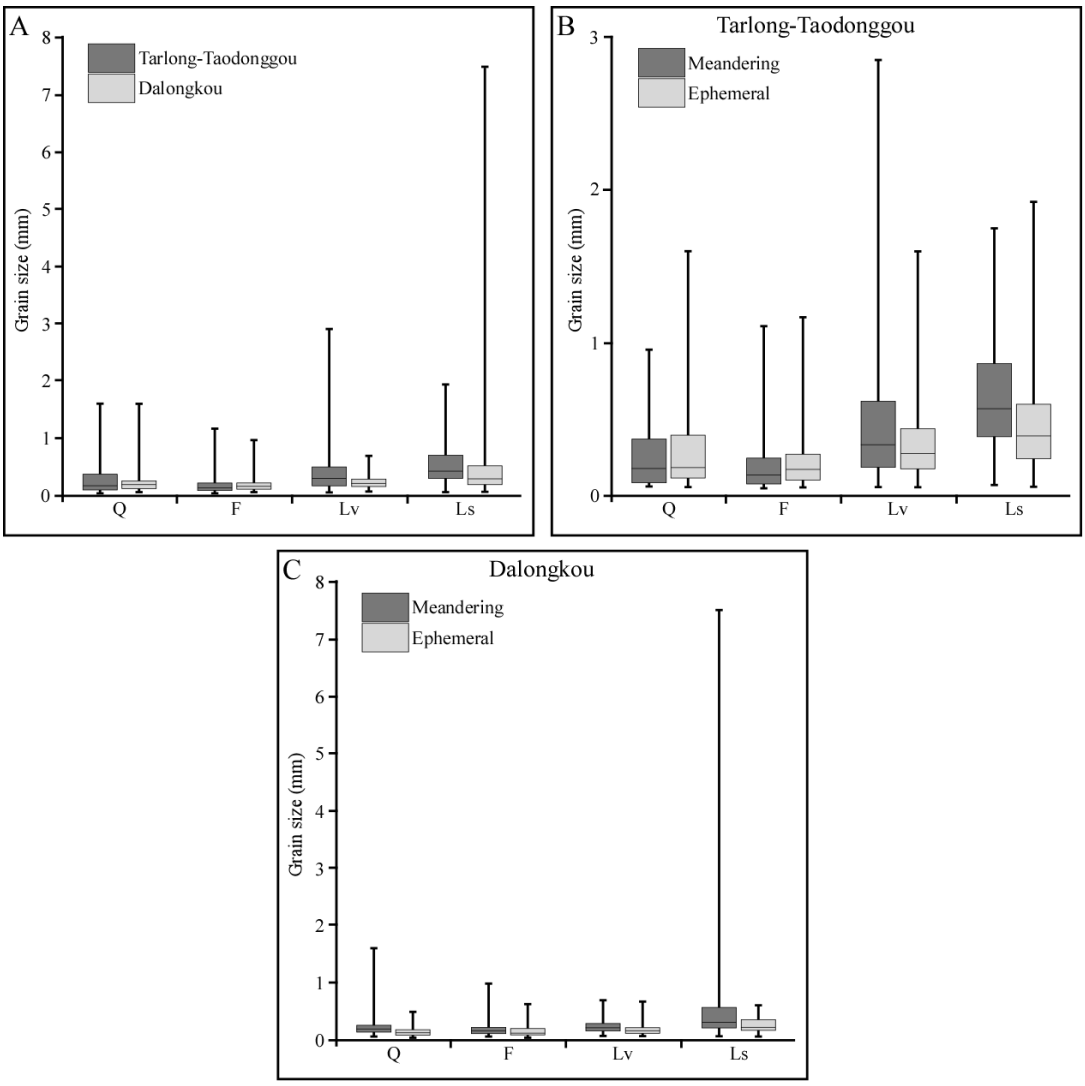

Figure 5. Box-and-whiskers plot of grain size for Q, F, Lv, and Ls grains. A) Grain size for the four main groups in Tarlong-Taodonggou and Dalongkou. Notice the increase in Lv grain size in Tarlong-Taodonggou and increase in Ls grain size in Dalongkou. B) Grain size for the four main groups in Tarlong-Taodonggou comparing meandering and ephemeral streams. Notice the increase in grain size in meandering streams in the Lv and Ls groups. C) Grain size for the four main groups in Dalongkou comparing meandering and ephemeral streams. Notice the similarities in Q, F, and Lv, and the increase in grain size range in meandering streams in the Ls group.

4.2.1.4 Accessory Minerals

A wide variety of accessory minerals are present and account for less than 1% on average of all framework grains. They are biotite, muscovite, rutile, amphibole, pyroxene, zircon, zeolites, and opaque minerals. Biotite, rutile, and zeolites are the most common in Tarlong-Taodonggou samples (Fig. 7D), whereas zircon and muscovite are common in Dalongkou. All grains are medium to fine sand in size and angular to subrounded in shape. No systematic trends in occurrence are identified.

Table 5. Grain shape data for the Tarlong-Taodonggou and Dalongkou sandstones.

Parameters	Tarlong-Taodonggou				Dalongkou			
	Angular	Subangular	Subrounded	Rounded	Angular	Subangular	Subrounded	Rounded
Grain type								
Q	61	30	30	74	153	125	343	1694
F	494	153	160	333	231	118	308	980
Ls	41	60	112	575	9	22	129	1080
Lv	345	213	491	1874	6	4	28	224
All	941	456	793	2856	399	269	808	3978
Petrofacies								
Ia/IIa	350	177	273	1175	276	148	474	2168
Ib/IIb	422	180	257	1153	129	123	336	1800
Ic	180	89	239	555	---	---	---	---
Stream type								
Meandering	433	277	377	1399	351	244	724	3592
Ephemeral	519	219	392	1484	54	27	86	376

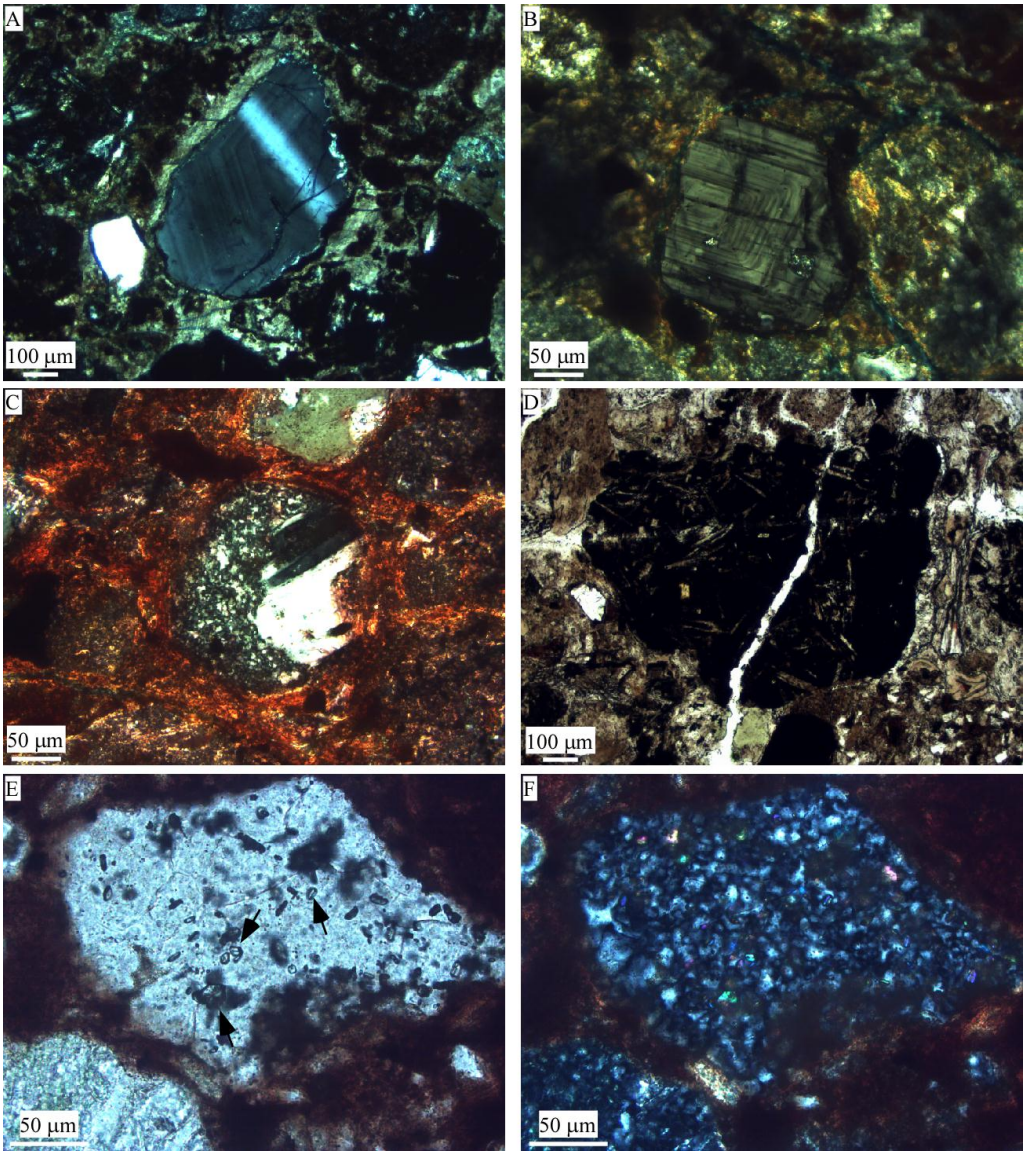

Figure 6. Photomicrographs of some typical grains in the QZJ LCs. A) Subrounded zoned plagioclase feldspar indicative of a volcanic origin under cross-polarized light (XP). Sample Q13-8 from southeast Tarlong. B) Angular zoned plagioclase feldspar indicative of a volcanic origin under XP. Notice the thin clay coats around the grain as an example of immature coats. Sample Q13-17 from southeast Tarlong. C) Rounded Lvl grain with a large plagioclase lath in a felsitic groundmass under XP. Notice the well-developed red clay coats around the grain and adjacent grains as an example of mature coats. Sample QD12-16 from Dalongkou. D) Rounded Lvm grain with thin and small plagioclase laths in a black groundmass under plane light (PL). Fracture in the middle is caused when thin section was made. Sample Q14-4 from northeast Tarlong. E) Subangular Lvf grain with small euhedral zircons (see arrows) in PL. Sample Q13-6 from southeast Tarlong. F) Same as E but under XP light to show felsitic texture and high birefringence euhedral zircons.

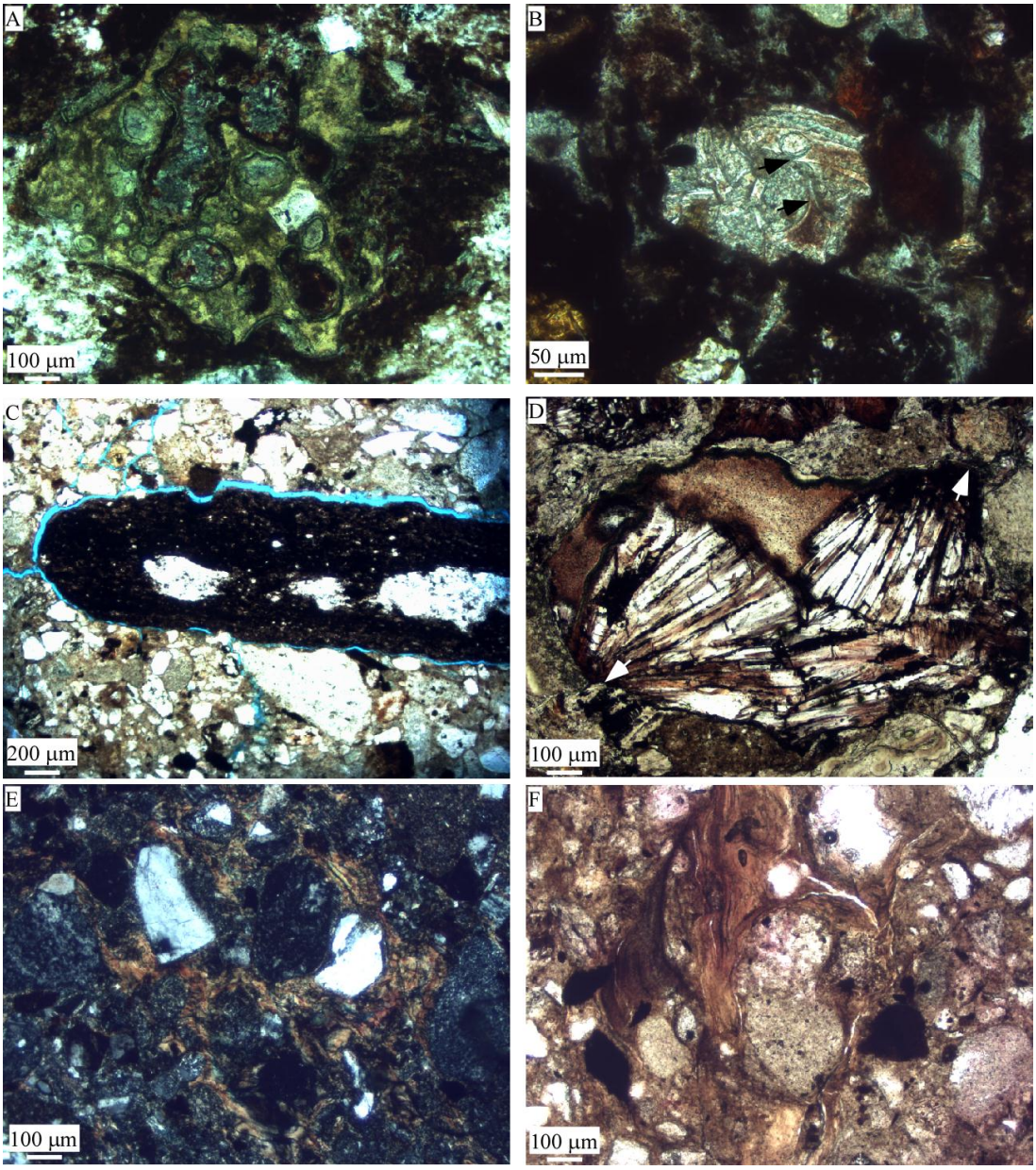

Figure 7. Photomicrographs of some typical grains and features in the QZJ LCs. A) Angular Lva grain with secondary zeolite filling the vesicles under XP. Sample Q13-7 from southeast Tarlong. B) Subangular Lvs grain with abundant features resembling shards (see arrows) under PL. Sample Q13-1 from southeast Tarlong. C) Rounded Lsh grain with similar lithology to the Lucaogou shale under PL. Grain is close to 7 mm long. White features are ripped up pieces during thin sectioning. Sample QD12-8 from Dalongkou. D) Rounded detrital zeolite with a radial texture under PL. Notice rounded edges of grain (see arrows) suggesting some degree of transportation. Sample Q13-8 from southeast Tarlong. E) Well-developed clay coats surrounding rounded to angular grains under XP. Sample QD12-14 from Dalongkou. F) Well-developed clay coats surrounding an Ls grain under PL. Notice the laminations and downward continuation of the coats. Sample SD11-12 from Dalongkou.

4.2.2 Textural Characteristics

Sandstones in Tarlong-Taodonggou and Dalongkou have similar textural characteristics. Sandstones in the southeast and northeast Tarlong sections (Figs. 8, 9) have consistent framework grain size of medium sand on average, ranging from very fine sand to granule (Table 3). On average, framework grains are moderately sorted, ranging from moderately well to poorly sorted (Table 3). On average 56% of the grains are rounded (Table 5) and the rest range from angular to subrounded. The sandstones in the upper part of the southeast Tarlong section appear to have a slight decrease in roundness (Fig. 8). Grains are dominantly in a line or point contact with an average of 51% and 36%, respectively, although concavo-convex, floating, and sutured contacts are present. Matrix content is 18% on average, ranging from 0 to 41% (Table 3).

Sandstones in the Dalongkou section (Fig. 10) have a consistent framework grain size throughout, which is medium sand on average, ranging from very fine sand to pebble (Table 4). Framework grains are moderately sorted on average, ranging from moderately well to poorly sorted (Table 4). 72.9% of the grains are rounded (Table 5) and the rest range from angular to subrounded. The roundness remains fairly consistent throughout the section (Fig. 10). Grains are dominantly in a line contact with an average of 70%; the rest are point, concavo-convex, and floating contacts. Matrix content is 28% on average, ranging from 12 to 44% (Table 4).

The persistent textural characteristics upsection in Tarlong-Taodonggou and Dalongkou suggest that transport distance and depositional processes had not changed significantly during the QZJ time. In comparison to sandstones in Tarlong-Taodonggou,

those in Dalongkou have a smaller average grain size and more rounded grains, suggesting a longer transport distance or a different source for the Dalongkou sandstones.

4.2.3 Pedogenic Characteristics

Pedogenetic processes may have altered the sandstones. Clay coats, or argillans (Brewer, 1976; Retallack, 2001), are the most common pedogenic features in the QZJ LCs (Yang et al., 2010; Obrist-Farner and Yang, 2015; Obrist-Farner, 2015). They occur in the uppermost five sandstones in the southeast Tarlong section, none in northeast Tarlong section, and all sandstones in Dalongkou section (Figs. 8, 9, 10). They are composed of preferentially-oriented aggregates of clay minerals with rare silts and are variably laminated. They are brown and, in three samples, dark red and highly birefringent. The coats envelope framework grains with a sharp contact. Some coats are very thin and discontinuous (Fig. 6A). Where the coats are ~10 μm thick, they are continuous and completely envelope a framework grain (Figs. 6C, 7E). Coats that are 50 μm or thicker have clear laminations and form a patch encasing several adjacent grains (Fig. 7F). In some cases, they can be traced for ~1000 μm on the thin section. Clay coats in four sandstones in southeast Tarlong section and in the lower part of Dalongkou section are thin and poorly to moderately developed (Fig. 8), whereas those in the middle and upper parts of Dalongkou are well developed (Fig. 10). The coats are normally brown (Fig. 7E, F) but change to dark red (Fig. 6C) in the uppermost three sandstones in Dalongkou.

The pedogenic clay coats indicate periods of nondeposition, landscape stability, and subhumid conditions, where illuvial clays accumulated in the sandstones by

percolating soil water. However, intense pedogenesis had occurred only in the lower QZJ LC and the uppermost part of the upper QZJ LC (Yang et al., 2010; Obrist-Farner and Yang, 2015), 2015), where distinct soil horizons are present. The increase in the thickness and continuity of clay coats reflects increasing intensity of pedogenesis. The laminations were formed by episodic illuviation of clay minerals on the grain surface. The presence of poorly to moderately-developed clay coats in the sandstones in the upper part of the southeast Tarlong section suggest illuviation under an increasingly humid climate, which culminated into a fully humid condition in the uppermost part of the upper QZJ LC, as evidenced by well-developed Gleysols (Yang et al., 2010; Obrist-Farner, 2015). The presence of moderately to well-developed clay coats in sandstones throughout the entire Dalongkou section indicate that subhumid conditions had persisted during the deposition of lower and upper QZJ LCs. The climatic condition during the deposition of the uppermost part of upper QZJ LC is likely humid, as indicated by the thick and continuous clay coats, Gleysols, and development of dark red ferruginous clay coats or ferrans (Retallack, 2001).

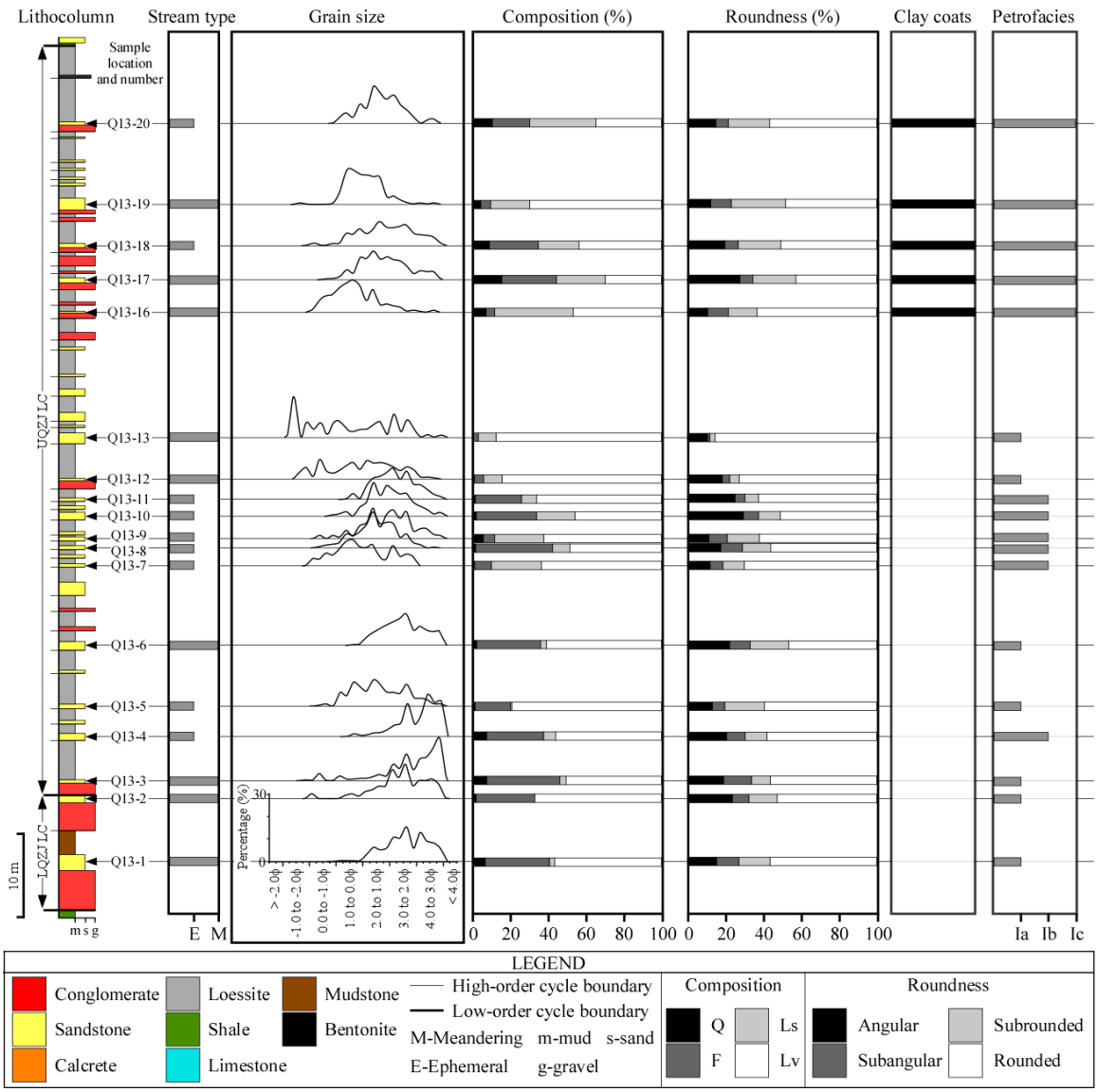

Figure 8. Highly-simplified lithologic column, sample name and location, stream type, grain size, composition, roundness, clay coat types, and petrofacies for the southeast Tarlong section. Stream type from Obrist-Farner and Yang (2015) and Paper II. See Figure 3A for location of measured section. See text for details.

4.2.4 Diagenetic Characteristics

Diagenesis is not the focus of the study, but is assessed to remove any diagenetic effects on depositional features of studied sandstones. Cements include quartz overgrowth, zeolites, and poikilotopic calcite. Quartz overgrowth is common in arenites. Zeolite is the most abundant cement in all samples in Tarlong-Taodonggou, but is not present in Dalongkou. It has a distinct red color under plane light, a euhedral form, and, in some cases, a radial growth pattern. It partially replaces volcanic grains and feldspars in Tarlong-Taodonggou sandstones. Poikilotopic calcite cement occurs in two sandstones in southeast Tarlong. Other diagenetic alterations include calcitization, vacuolization, and sericitization of feldspars. Sericitization is especially common in Dalongkou sandstones.

5. Petrofacies

Two petrofacies are recognized in the QZJ sandstones on the basis of their QFL composition (Fig. 11A) and textural characteristics described above. Petrofacies I has a mean composition of $Q_4F_{23}L_{73}$ and occurs in Tarlong-Taodonggou sandstones and Petrofacies II a mean composition of $Q_{43}F_{30}L_{27}$ and in Dalongkou. Petrofacies I is subdivided into three subfacies on the basis of Q, Lv, and Ls content, and Petrofacies II into two subfacies (Tables 3 and 4).

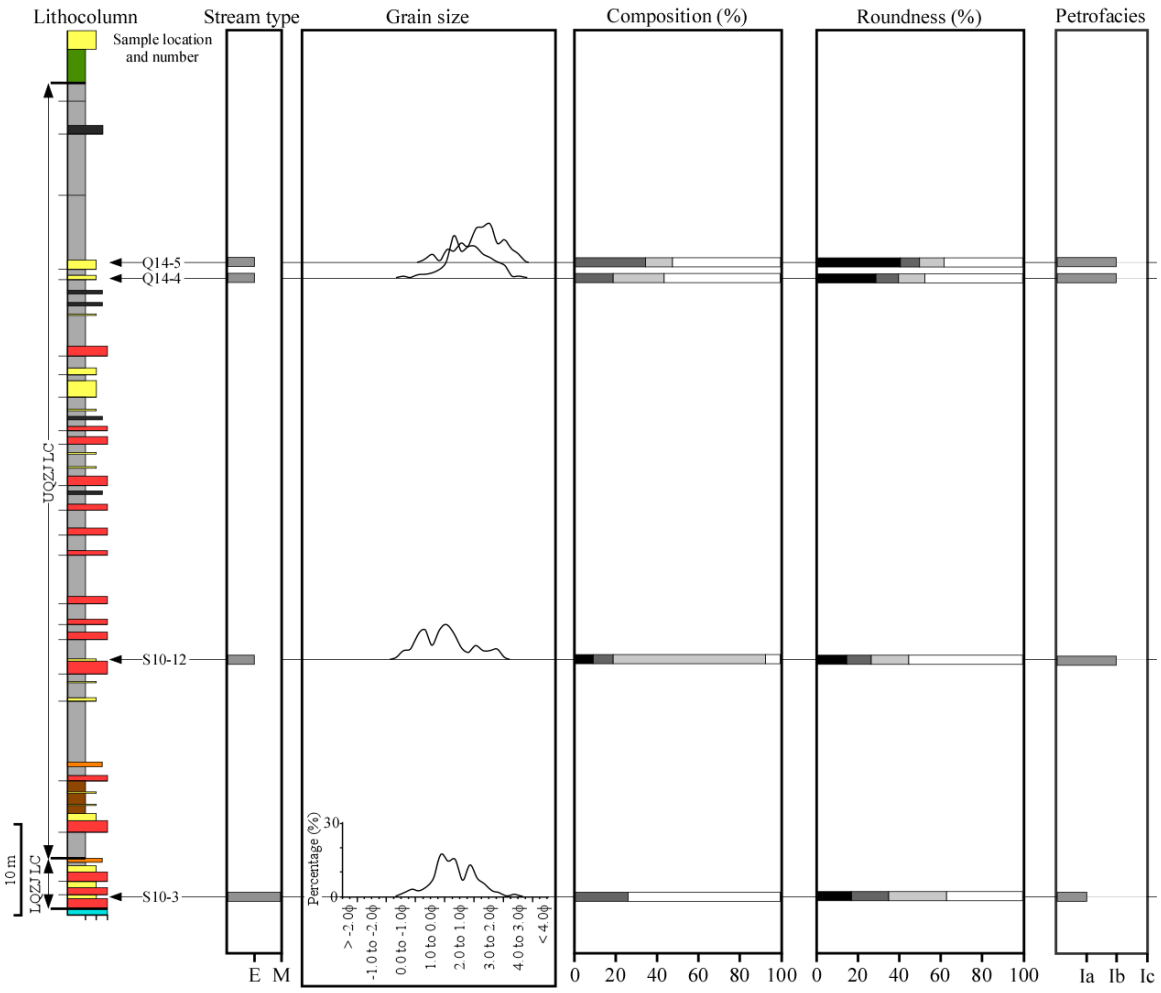

Figure 9. Highly-simplified lithologic column, sample name and location, stream type, grain size, composition, roundness, and petrofacies for the northeast Tarlong section. Stream type from Obrist-Farner and Yang (2015) and Paper II. See Figure 3A for location of measured section and Figure 8 for legend. See text for details.

5.1 Petrofacies I

Petrofacies I is characterized by a high percentage of lithic grains. Volcanic lithics dominate, with an average of 78.6%. Sedimentary lithics content is lower (21.2%) and metamorphic lithics are rare (<1%). Plagioclase feldspar dominates (85%) and all quartz types have similar average percentages. Grain size of Petrofacies I is medium sand on average, ranging from fine to coarse sand. Framework grains are moderately sorted overall, with a degree of sorting of 0.89ϕ. The distribution of framework grain size is near symmetrical with an average skewness value of 0.03. Rounded grains dominate, with an average of 57.1% and the rest range from angular to subrounded. Average matrix content is 17%, ranging from 0 to 41%.

Petrofacies Ia has a mean composition of $Q_2F_{24}L_{74}$ (Fig. 11A) and occurs in eight sandstones; seven in the southeast section and one in the northeast section (Figs. 8, 9; Table 3). Volcanic lithics dominate and account for 94% of all the lithics and include 7% felsitic and 93% mafic lithics. Sedimentary lithics (Ls) accounts for 5% and include mudrock (67.5%), mud clasts (31.3%) and shale lithics (1.2%). Metamorphic lithics account for 1% on average of the samples. Undulatory quartz grains (Qu) dominate (49%); all other quartz types have similar average percentages. Plagioclase feldspar dominates (75%). Grain size of Petrofacies Ia is medium sand on average, ranging from fine to coarse sand. Framework grains are poorly sorted overall, with a degree of sorting of 1.02ϕ. The distribution of framework grain size is near symmetrical with an average skewness value of -0.06. Rounded grains are the most dominant shape, with an average of 59.5%, and the rest range from angular to subrounded (Table 5). Average matrix content is 16%, ranging from 0 to 29%.

Petrofacies Ib has a mean composition of $Q_3F_{24}L_{73}$ (Fig. 11A) and occurs in nine sandstones; six in the southeast section and three in the northeast section (Figs. 8, 9; Table 3). It has a relatively large amount of sedimentary lithics (28%), although volcanic lithics still dominate (72%). 7% of the volcanic lithics are felsitic and 93% mafic. Mud clasts and mudrock dominate the sedimentary lithics, with 67% and 33% on average, respectively. All quartz types are present with similar average percentages. Plagioclase feldspars are the dominant feldspar type, 93% on average. In Petrofacies Ib, framework grain size is medium sand on average, ranging from fine to coarse sand. Framework grains are moderately sorted with a degree of sorting of 0.80ϕ. The distribution of framework grain size is near symmetrical with an average skewness of 0.08. 57.3% of grains are rounded and the rest range from angular to subrounded (Table 5). Finally, average matrix content is 14%, ranging from 0 to 41%.

Petrofacies Ic has a mean composition of $Q_9F_{17}L_{74}$ (Fig. 11A) and occurs in five sandstones in the upper part of the southeast section (Fig. 8; Table 3). It is characterized by the relatively large amount of quartz and presence of pedogenic clay coats. Volcanic lithics dominate, 61% on average among all lithics, where 1% of them are felsitic and 99% mafic. Mudrock lithics (Lsr) dominate among sedimentary lithics, 97.6% on average. Mud clasts are rare (2.3%). All quartz types are present with similar average percentages. Plagioclase feldspars dominate among all feldspar grains, 92% on average. In Petrofacies Ic, the size of framework grains is medium sand on average, ranging from medium to coarse sand. The framework grains are moderately sorted with a degree of sorting of 0.82ϕ. The size distribution is near symmetrical with an average skewness of

0.07. Rounded grains account from 52.2% and the rest range from angular to subrounded (Table 5). Average matrix content is 26%, ranging from 20 to 31%.

The large quantity of Lv grains and the dominance of rounded grains in Petrofacies I indicate a main volcanic source located far away from Tarlong-Taodonggou. The common volcanic lithics in Petrofacies Ia suggests a dominant volcanic source with minimal sediment supply from secondary sedimentary sources. The increase in mud clasts in Petrofacies Ib suggest contemporaneous overbank deposits as a local source. The increase in sedimentary lithics and a slight worsening in roundness in Petrofacies Ic indicate a nearby secondary sedimentary source. Finally, the presence of pedogenic clay coats in Petrofacies Ic indicates an environment of stable landscape and subhumid climate after deposition.

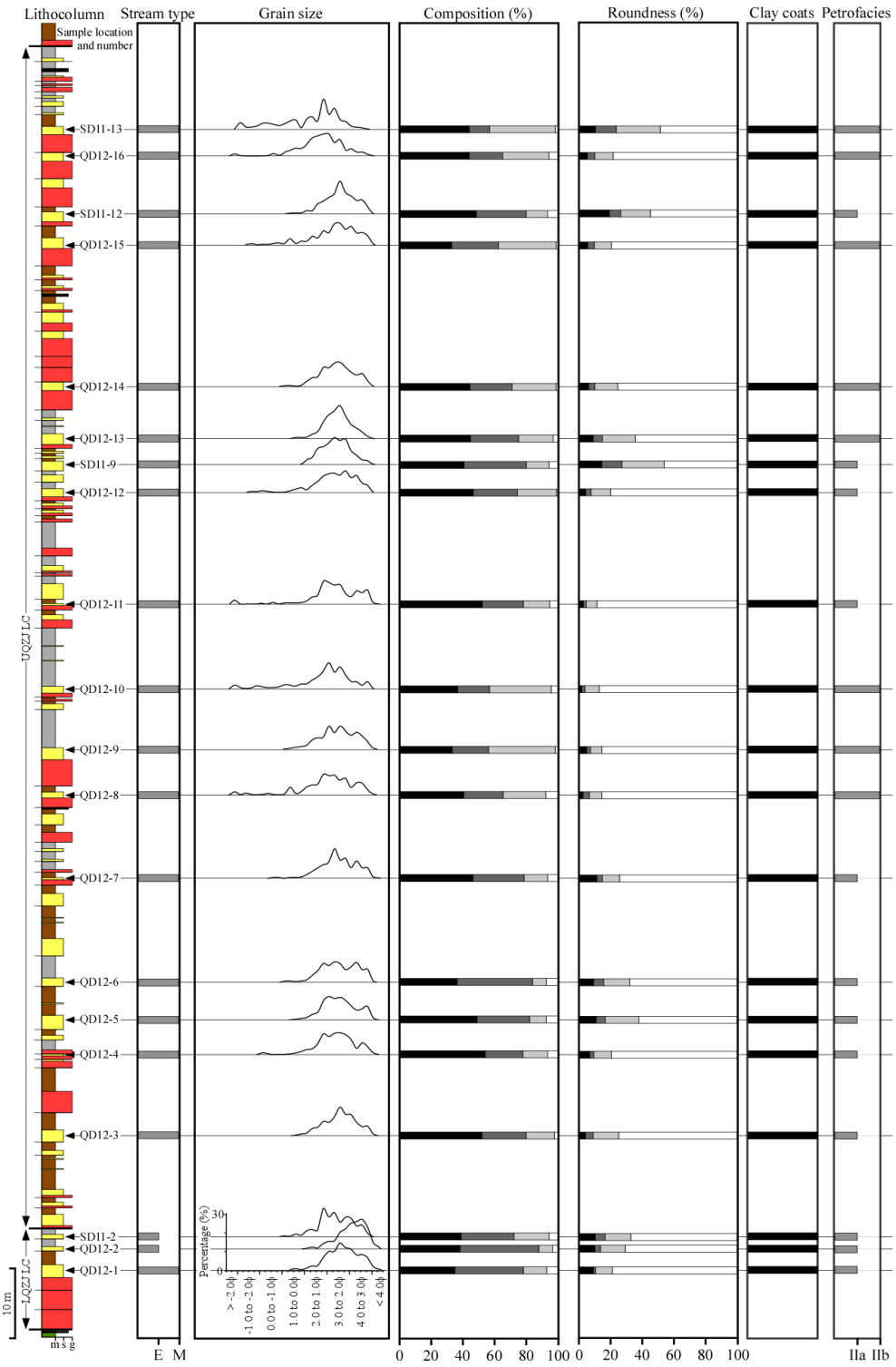

Figure 10. Highly-simplified lithologic column, sample name and location, stream type, grain size, composition, roundness, clay coat types, and petrofacies for the Dalongkou section. Stream type from Obrist-Farner and Yang (2015) and Paper II. See Figure 3B for location of measured section and Figure 8 for legend. See text for details.

5.2 Petrofacies II

Petrofacies II is characterized by a similar quartz, feldspar, and lithic content. Sedimentary lithics dominate the lithic content with an average percentage of 83%, among which mudrock and mud clasts are the most common at 75.8% and 22.7%, respectively. Volcanic lithic account for 17% and are all mafic. All quartz types are present, but micro- and polycrystalline quartz dominate at 32% and 37.2%, respectively. Potassium and plagioclase feldspars are 47.4% and 52.6%, respectively. Grain size of Petrofacies II is fine sand, ranging from very fine to medium sand. Framework grains are moderately sorted overall, with a degree of sorting of 0.83ϕ. The distribution of framework grain size is near symmetrical with an average skewness value of -0.05. Rounded grains dominate, with an average of 72.8% and the rest range from angular to subrounded. Average matrix content is 28%, ranging from 12 to 44%.

Petrofacies IIa has a mean composition of $Q_{45}F_{35}L_{21}$ (Fig. 11A) and occurs in 12 sandstones, mainly in the lower part of the Dalongkou section (Fig. 10; Table 4). Sedimentary lithics dominate the lithic content with an average percentage of 72%, among which mudrock lithics and mud clasts are the most common at 82.4% and 17.4%, respectively. Volcanic lithics account for 28% and are all mafic. All quartz types are present, but micro- and polycrystalline quartz dominate at 30% and 37%, respectively. Potassium and plagioclase feldspars are 52% and 48%, respectively. The size of framework grains is fine sand on average, ranging from very fine to fine sand. Framework grains are moderately sorted with a degree of sorting of 0.76ϕ. The size distribution is near symmetrical with an average skewness value of 0.00. Finally, rounded

grains dominate with an average percentage of 71% (Table 5) and the rest range from angular to subrounded. Average matrix content is 30%, ranging from 13 to 44%.

Petrofacies IIb has a mean composition of $Q_{40}F_{23}L_{36}$ (Fig. 11A) and occurs in eight sandstones, mainly located in the middle and upper parts of the Dalongkou sandstones (Fig. 10; Table 4). Sedimentary lithics dominate over the other lithics at an average percentage of 90%, where fragments of mudrock and mud clasts are the most common. Shale lithics occur but accounts for 2.2% on average of all sedimentary lithics. Only 10% of lithics are mafic volcanic grains. All quartz types are present. Micro- and polycrystalline quartz grains dominate at an average percentage of 33% and 36%, respectively. Plagioclase feldspar is more common than K feldspars, at 62% and 38% on average, respectively. Size of framework grains is fine sand on average, ranging from fine to medium sand. Framework grains are moderately sorted with a degree of sorting of 0.93ϕ. The size distribution is coarse skewed with an average skewness of -0.12, indicating an excessive coarse fraction. Rounded grains dominate with an average of 75% (Table 5) and the rest range from angular to subrounded. Average matrix content is 24%, ranging from 12 to 32%.

The common occurrence of quartz grains and sedimentary lithics and the similar amount between potassium and plagioclase feldspar grains suggest a primary sedimentary source and secondary basaltic source for the Dalongkou sandstones. The shale lithics in Petrofacies IIb probably were derived from the underlying Lucaogou LC (see descriptions above; Yang et al., 2010) exposed at rift shoulders. The large amount of rounded grains suggest a distant source.

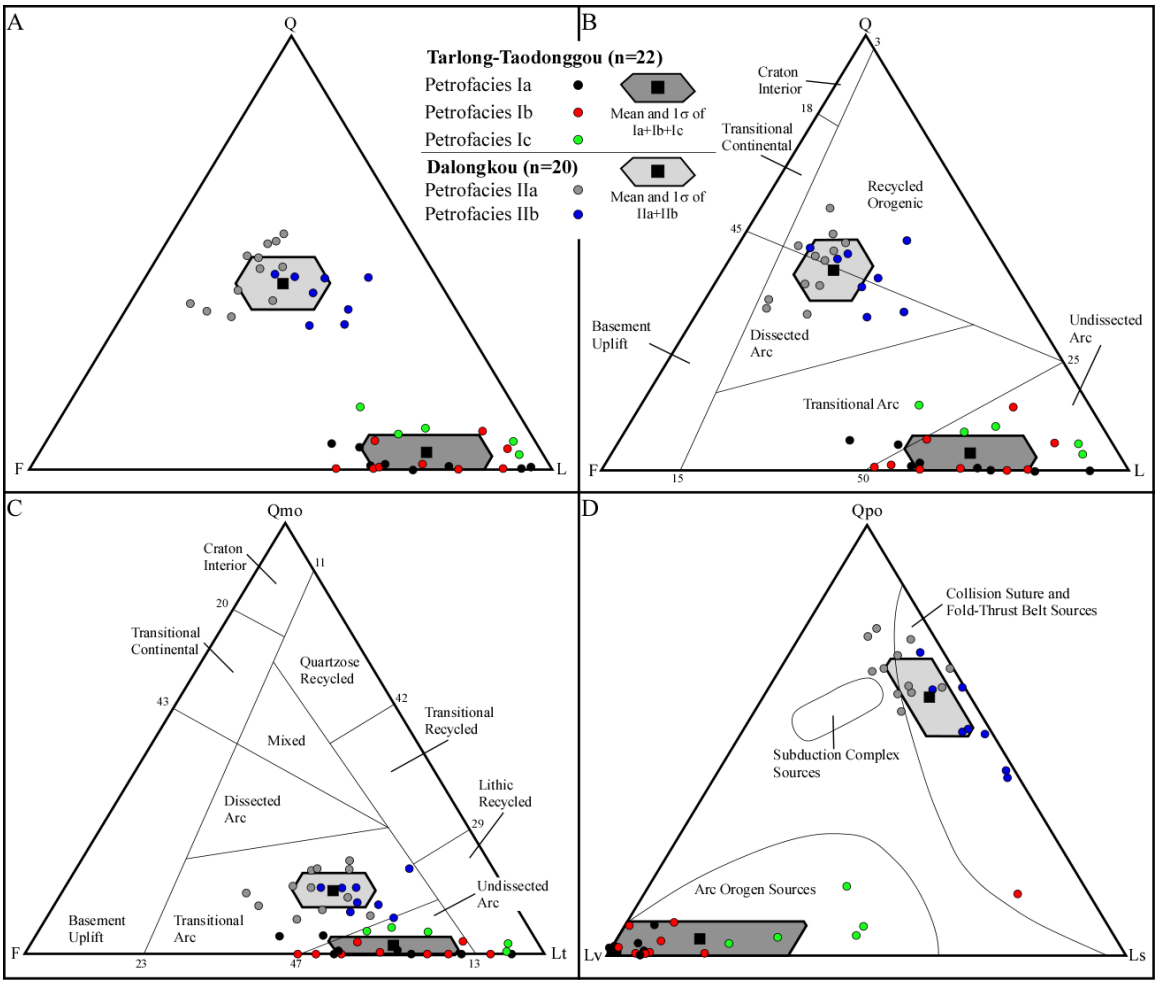

Figure 11. Ternary plots of modal sandstone grain composition for sandstones from Tarlong-Taodonggou and Dalongkou. A) QFL plot using the traditional point counting method. B) QFL plot. C) QmoFLt plot. D) QpoLvLs plot. Gazzi-Dickinson point counting method is used for B, C, and D. Provenance field in B, C, and D from Dickinson (1985). Point counting parameters are defined in Table 1. See text for details.

6. Sandstone Characteristics and Fluvial Processes

Topographic setting and processes of ephemeral and meandering streams differ from each other and, thus, should impart different petrographic characteristics of sandstones deposited by the two types of streams. However, 10 meandering-stream and 12 ephemeral-stream sandstones in Tarlong-Taodonggou have the same mean composition of $Q_4F_{23}L_{73}$. Minor differences do occur. Seven out of 10 meandering-stream sandstones belong to Petrofacies Ia; and three to Petrofacies Ic (Figs. 8, 9). Nine out of 12 ephemeral-stream sandstones belong to Petrofacies Ib; two to Petrofacies Ic; and one to Petrofacies Ia (Figs. 8, 9). The greatest variability between sandstones of the two types of streams lies in the amount of volcanic (Lv) and sedimentary (Ls) lithics. Lv grains are more common in meandering-stream sandstones (62% on average of all framework grains) than in ephemeral-stream sandstones (53%). On the other hand, Ls grains are less common in meandering-stream sandstones (11%) than in ephemeral-stream sandstones (20%). No major difference in average grain size, sorting, and skewness exists between the two types of sandstones. Degree of sorting of individual grain types, however, differ between the two types of sandstones. Q, F, and Ls grains in meandering-streams sandstones are better sorted than those in ephemeral-stream sandstones, vice versa for Lv grains (Fig. 5B). The amount of rounded framework grains is similar between the two types of sandstones at ~57% on average (Table 5).

The meandering- and ephemeral-stream sandstones in Dalongkou vary in different aspects from those in Tarlong-Taodonggou. In Dalongkou, the mean composition of meandering-stream sandstones ($Q_{43}F_{29}L_{28}$) is quite different from that of ephemeral-stream sandstones ($Q_{38}F_{42}L_{20}$). Ten out of 18 meandering-stream sandstones belong to Petrofacies IIa; and eight to Petrofacies IIb (Fig. 10). The two ephemeral-

stream sandstones belong to Petrofacies IIa. Average grain size, sorting, and skewness of framework grains are similar between the two types of sandstones. The attributes remain similar for individual grain types (Fig. 5C), except the sorting of Ls grains in meandering-stream sandstones is poorer than that in ephemeral-stream sandstones (Fig. 5C). Rounded grains dominate and account for ~70% of all framework grains in both types of sandstones (Table 5).

In Tarlong-Taodonggou, the predominance of Petrofacies Ia with a large amount of Lv grains in meandering-stream sandstones and the predominance of Petrofacies Ib with an increased amount of Ls grains, especially mud clasts, in ephemeral-stream sandstones suggest that the two types of sandstones have different provenances. The meandering-stream sandstones, with abundant rounded framework grains, were sourced from a distant volcanic provenance. On the other hand, the ephemeral-stream sandstones, with a slight decrease in grain roundness, were sourced from a volcanic provenance and a secondary local provenance of lithified sedimentary rocks and contemporary semi-consolidated sediments. Commonly, ephemeral streams are shorter in length and drain a much smaller catchment basin confined by rift shoulders exposed with underlying lithified sedimentary rocks. As a result, the contribution from local sedimentary rocks increases.

In Dalongkou, however, the two types of sandstones show no clear difference in petrographic attributes. A possible reason is that the ephemeral-stream sandstones are not statistically well-represented. Another possibility is that the Dalongkou area was located farther away from volcanic sources. Therefore, meandering and ephemeral streams had

similar sedimentary sources exposed in rift shoulders but at variable distances from Dalongkou.

7. Stratigraphic Trends

Systematic trends of compositional and textural characteristics of sandstones would provide clues on long-term changes in environmental conditions and elements of catchment basins. In the southeast Tarlong section, Petrofacies Ia occurs mainly in the lower part; Petrofacies Ib in the middle part; and Petrofacies Ic in the upper part (Fig. 8). This reflects several upsection trends of petrographic attributes. First, the size of framework grains increases upward from an average fine sand size to an average medium sand size (Fig. 12; Table 3). Second, sorting improves upward (Fig. 12). An exception, however, occurs with samples Q13-12, Q13-13, and Q13-16, which show upward increase in grain size and worsening in sorting (Fig. 12). Third, matrix content is high in the lower and upper parts of the section and decreases in the middle part of the section (Table 3). Fourth, the ratio between quartz and combined feldspar and lithics (Q/(F+L); Suttner and Dutta, 1986) increases upward (Fig. 12). Finally, plagioclase feldspar has dominated over other types of feldspars throughout the section.

The upsection grain size increase suggests a shrinking catchment basin, resulting in a steeper topographic gradient from the source to depositional site and a shorter transport distance. The trend could also be caused by an increase in sedimentary lithics from local sedimentary rocks, which tend to be larger in size due to the proximity of the source. The decrease in matrix content in the middle part of the section indicates a decrease in suspension load. The upward increase in Q/(F+L) ratio indicates an increasing compositional maturity upsection. This apparently contradicts with a shrinking

catchment basin. However, the increase in quartz content may have been caused by an increase in sediments from local sedimentary rocks with high quartz content. A reasonable scenario to explain the petrographic trends is that a local sedimentary source containing relatively quartz-rich lithologies was uplifted through normal faulting during the deposition of the upper part of the upper QZJ LC, and contributed sedimentary lithics and quartz grains with a relatively large grain size.

In the Dalongkou section, Petrofacies IIa occurs mainly in the lower parts; and Petrofacies IIb mainly in the middle and upper parts (Fig. 10). The size of framework grains increases upsection, along with worsening of sorting (Fig. 13). The Q/(F+L) ratio shows no trend upsection (Fig. 13). Finally, the overall content of plagioclase feldspar and sedimentary lithics increases upsection (Fig. 13).

The grain size increase suggests a shrinking catchment basin and decreased transport distance. The increased sedimentary lithics, especially shale lithics, in Petrofacies IIb in the middle and upper parts of the section suggests the presence of a local sedimentary source probably as an uplifted rift shoulder, which was eroded and insignificant during the deposition of the lower part of Upper QZJ LC. The general increase in Ls content in the upper part of the section indicates that a sedimentary source became more prominent in the upper part of the section.

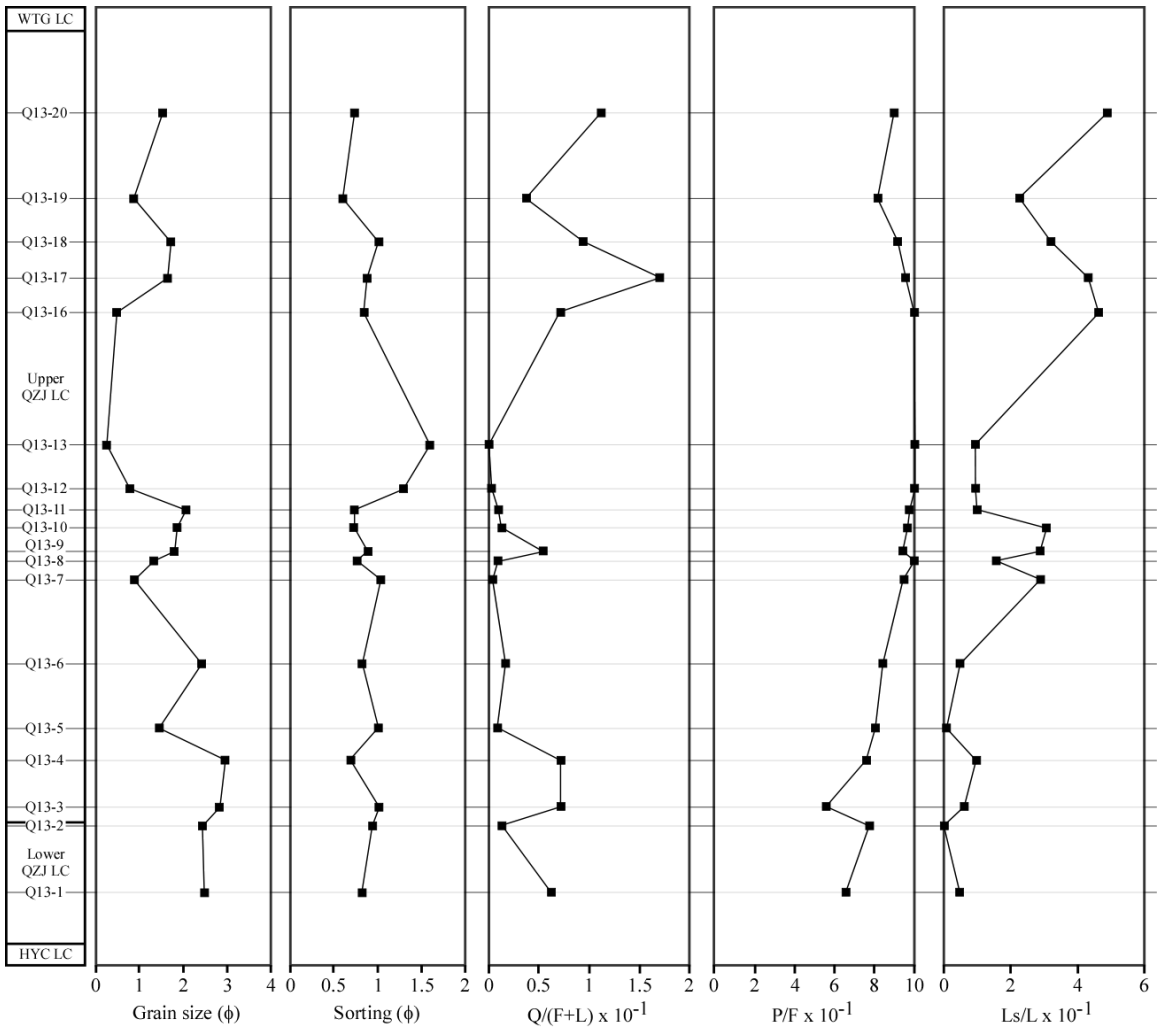

Figure 12. Stratigraphic variations in grain size, sorting, and composition of the QZJ sandstones in southeast Tarlong. Scale is the same as in Figure 8. See Figure 3A for location of measured section.

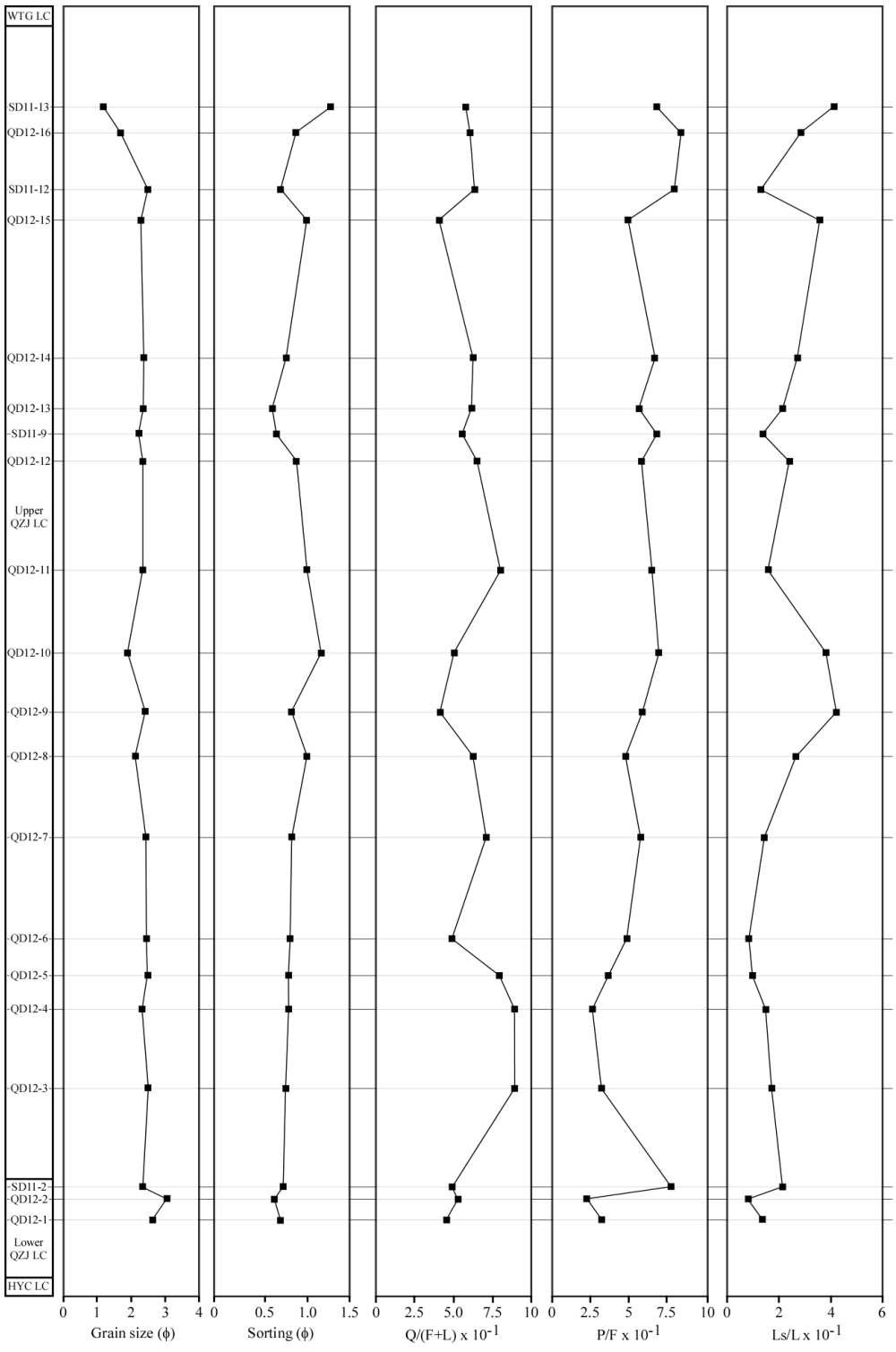

Figure 13. Stratigraphic variations in grain size, sorting, and composition of the QZJ sandstones in Dalongkou. Scale and sample location is the same as in Figure 10. See Figure 3B for location of measured section.

8. Tectonic Setting of Provenance

Modal sandstone composition is used for provenance analysis using three discriminant diagrams (Fig. 11; Dickinson and Suczek, 1979; Dickinson et al., 1983; Dickinson, 1985). In Tarlong-Taodonggou area, the modal composition of 19 of the 22 sandstones falls within the undissected arc field in the QFL diagram; and three within the transitional arc field (Fig. 11B). Similar results show on QmoFLt and QpoLvLs plots (Fig. 11C, D), where modal compositions of most sandstones fall in the undissected arc and arc orogenic fields, respectively. Only one point falls in the collision suture and fold-thrust belt field in the QpoLvLs plot (Fig. 11D). Gravel composition dominated by basalt points to a dominantly young arc source. In summary, framework grains in Tarlong-Taodonggou sandstones were likely derived mainly from a magmatic arc.

The modal compositions of eight sandstones in Dalongkou fall in the dissected magmatic arc field and those of 12 sandstones in recycled orogenic field (Fig. 11B). The compositions, however, suggest a different tectonic setting on QmoFLt and QpoLvLs plots (Fig. 11C, D), where most points fall in the transitional arc and collision suture and fold-thrust belt field. Moreover, the dominance of sandstone gravels suggests the presence of an additional sedimentary source. Thus, the primary source for the Dalongkou sandstones is probably sedimentary and the secondary source arc-related.

The young arc signature and the northward paleocurrent direction in southeast Tarlong (Obrist-Farner, 2015) suggest that the Late Carboniferous northern Tian Shan volcanic arc to the south is the primary provenance of the Tarlong-Taodonggou sandstones (Allen et al., 1992; Shao et al., 2001; Greene et al., 2005; Yang et al., 2013). The abundant rounded Lv grains indicate their compositional immaturity but textural maturity, suggesting that the Lv grains had survived a long transport distance (e.g.,

Garzanti et al., 2006; 2012). The angular zoned feldspars and Lv grains and common sedimentary gravels in other sections in Tarlong-Taodonggou indicate a close secondary source for the sandstones. The surrounding rift shoulders could have exposed underlying Upper Carboniferous oceanic arc basement basalts (Carroll et al., 1990; Graham et al., 1993; Yang et al., 2013) or Upper Carboniferous marine to Lower Permian nonmarine sedimentary rocks (Yang et al., 2010; 2013). The basement basalt is difficult to be identified because sediments derived from rift-shoulder basement basalts are similar to those in a mafic magmatic arc (e.g., Garzanti et al., 2013). The interpreted provenance tectonic setting of Tarlong-Taodonggou sandstones conform with that from previous studies in the Turpan-Junggar basin (e.g., Shao et al., 2001; Greene et al., 2005).

However, the interpreted setting for the Dalongkou sandstones is not in complete agreement with that for the Tarlong-Taodonggou sandstones, even though the sandstones in both areas formed in the greater Turpan-Junggar intracontinental basin. The difference between Dalongkou and Tarlong-Taodonggou sandstones and the mixed results in discriminant diagrams (Fig. 11) for the Dalongkou sandstones might be caused by the presence of diverse lithologies exposed in rift shoulders (e.g., Ingersoll, 1990; Garzanti et al., 2001; Garzanti et al., 2013). A nonmarine Lower Permian sedimentary source is evident for sandstones in Dalongkou, where angular shale boulders to sand-size framework grains (Fig. 7C) with similar lithology as the Lower Permian Lucaogou LC (e.g., Carroll, 1998; Yang et al., 2010) are observed. Nevertheless, the limited amount of Lv grains suggests that the northern Tian Shan arc was not the primary provenance. The arc may have been too far to the south and not connected to Dalongkou due to topographic barriers in the highly-partitioned intracontinental rift basin (Yang, 2008).

9. Discussion

9.1 Controls on Sandstone Characteristics

Many processes and factors have affected the composition and texture of sandstones in Tarlong-Taodonggou and Dalongkou, such as source rock lithology, transport distance, depositional environment and conditions, and tectonic and paleoclimatic conditions of catchment basin. It is their complex interplay that resulted in the diverse sandstone characteristics described above (e.g., Suttner, 1974; Folk, 1980; Johnsson, 1993; Garzanti et al., 2013).

Major differences between ephemeral- and meandering-stream sandstones include changes in the average lithic content and in degree of sorting of individual grain types. The differences observed between stream types are possibly caused by changes in paleoclimatic conditions, topographic relief, and provenance. Meandering streams developed on subhumid conditions and drained a larger catchment. It is speculated that the increase in atmospheric precipitation caused an increase in sediment flux from a distant volcanic source. On the other hand, ephemeral streams developed when arid to semiarid conditions persisted and on steep topography and are shorter and closer to source. It is speculated that a decrease in atmospheric precipitation caused a decrease in sediment flux from a distance volcanic source but an increase from local sedimentary sources. In summary, changes in paleoclimatic conditions seem to have a major control on stream types, sediment supply, and provenance.

Meandering streams that developed in Tarlong-Taodonggou and Dalongkou are compositionally and texturally different. Meandering streams in Tarlong-Taodonggou have a high percentage of lithic volcanic grains, whereas those in Dalongkou have a high percentage of lithic sedimentary grains and quartz. In addition, framework grain size is

medium size on average in Tarlong-Taodonggou, whereas fine size on average in Dalongkou. The compositional and textural differences are possibly caused by changed in provenance, suggesting that provenance lithology is a major control on sandstone characteristics.

The increase in quartz content in the upper part of the southeast Tarlong section, causing a relative increase in compositional maturity, is possibly caused by interplay between source rock lithology and/or climatic conditions. The increase in sedimentary gravels in all the sections in Tarlong-Taodonggou and the increase in sedimentary lithics in the sandstones from southeast Tarlong indicate a change in provenance lithology. The provenance could have contained higher quartz content, increasing compositional maturity in the Tarlong-Taodonggou sandstones. On the other hand, an overall change in climatic conditions occurred from dominantly arid-semiarid in the lower QZJ LC and lower and middle parts of the upper QZJ LC to humid-subhumid conditions in the upper part of the upper QZJ. The humid to subhumid conditions would have caused an increase in chemical weathering, destroying unstable lithic volcanic grains. This would have caused a relative increase in quartz, feldspars, lithic sedimentary grains, and pedogenic features. In Dalongkou, there is no change observed in the sandstone compositional maturity, possibly caused by persistent climatic conditions and low percentage of unstable lithic volcanic grains. The persistent subhumid conditions lead to an increase in pedogenic features in Dalongkou.

Tectonic movement in the source area may have caused major compositional and textural changes in the Tarlong-Taodonggou and Dalongkou sandstones. Tectonic uplift in the source area could have exposed Upper Carboniferous marine and Lower Permian

nonmarine lithified sedimentary rocks in rift shoulders. The exposed sedimentary rocks could have caused the increase in sedimentary lithics and quartz content in Tarlong-Taodonggou and the increase in sedimentary lithics with similar lithology as the Lucaogou LC (Yang et al., 2010) in the middle and upper parts of the section in Dalongkou.

In summary, the interactions and feedbacks of the processes controlling sandstone composition and texture are complex. A change in one of the processes could result in distinct compositional and textural characteristics. Provenance lithology seems to be the primary control on sandstone characteristics. However, the supply itself is controlled by paleoclimatic conditions, which in turn control the fluvial and pedogenic processes. A careful study of composition and its changes, texture, texture of different grain types, and pedogenic features help understand the roles that the different processes had on the final composition and texture of the sandstones.

9.2 Discerning Different Sediment Sources

Rift basins are not included in tectonic classification of sandstones by Dickinson (1985; see also Dickinson and Suczek, 1979; Dickinson et al., 1983) because of the diverse lithologies exposed in rift shoulders that generate contrasting results of tectonic settings (Ingersoll, 1990). Provenance information, however, is important to understand basin-filling processes and reconstruct paleogeography. A close examination of framework textural attributes may be useful to understand the processes controlling sandstone characteristics in a rift basin setting. The sandstones in Tarlong-Taodonggou and Dalongkou contain a range of grain shapes from angular to rounded. Assuming the

idea that angular to subangular grains have undergone minimal transport distance and rounded to subrounded grains have traveled further (e.g., Folk, 1951), then angular to subangular grains are possibly derived from local sources, whereas rounded to subrounded grains are derived from far away sources. Including all suspected contemporaneous and intrabasinal grains and artificially separating each sample into two groups of sandstones based on grain roundness (subangular/angular and rounded/subrounded groups), distinct sources can be interpreted in a QFL plot (Fig. 14). In Tarlong-Taodonggou, rounded to subrounded framework grains are dominantly lithics, whereas angular to subangular grains are mainly lithics or feldspar grains. The two groups have a small amount of quartz grains. In Dalongkou, angular to subangular grains have an equal percentage of Q, F, and L grains, whereas rounded to subrounded grains have a larger percentage of F and Q grains and a small percentage of L grains.

In Tarlong-Taodonggou, the rounded to subrounded group is dominated by lithic volcanic grains and is interpreted as being sourced from the Tian Shan arc to the south. The angular to subangular group is derived from a different provenance. A possibility for the angular-subangular L-rich subgroup is the uplifted Upper Carboniferous oceanic arc basement in rift shoulders because the grains seem to have been derived from local sources and traveled a short distance. The possible source for the angular-subangular F-rich subgroup is the oceanic arc basement with thick ignimbrite deposits, the first deposit when crustal amalgamation was completed and before major rifting occurred (Yang et al., 2013), or nearby volcanic fields that supplied the abundant zoned P feldspars common from volcanic sources (Dickinson, 1970), embayed quartz, Lvf, Lvs, and abundant volcanic ash beds throughout the QZJ LCs (Yang et al., 2010; Obrist-Farner and Yang,

2015). The rounded-subrounded group in Dalongkou indicates a distant source rich in feldspar and quartz, possibly granitoid plutons exposed in the region (Allen et al., 1992, 1993; Greene et al., 2005). The presence of abundant angular-subangular L grains in Dalongkou, shifting the angular-subangular group toward the L pole in the QFL diagram (Fig. 14), indicates a nearby source exposing sedimentary-rich rocks. Examination of framework grain types with respect to their roundness may be a useful tool to discriminate source or sources in rift basins.

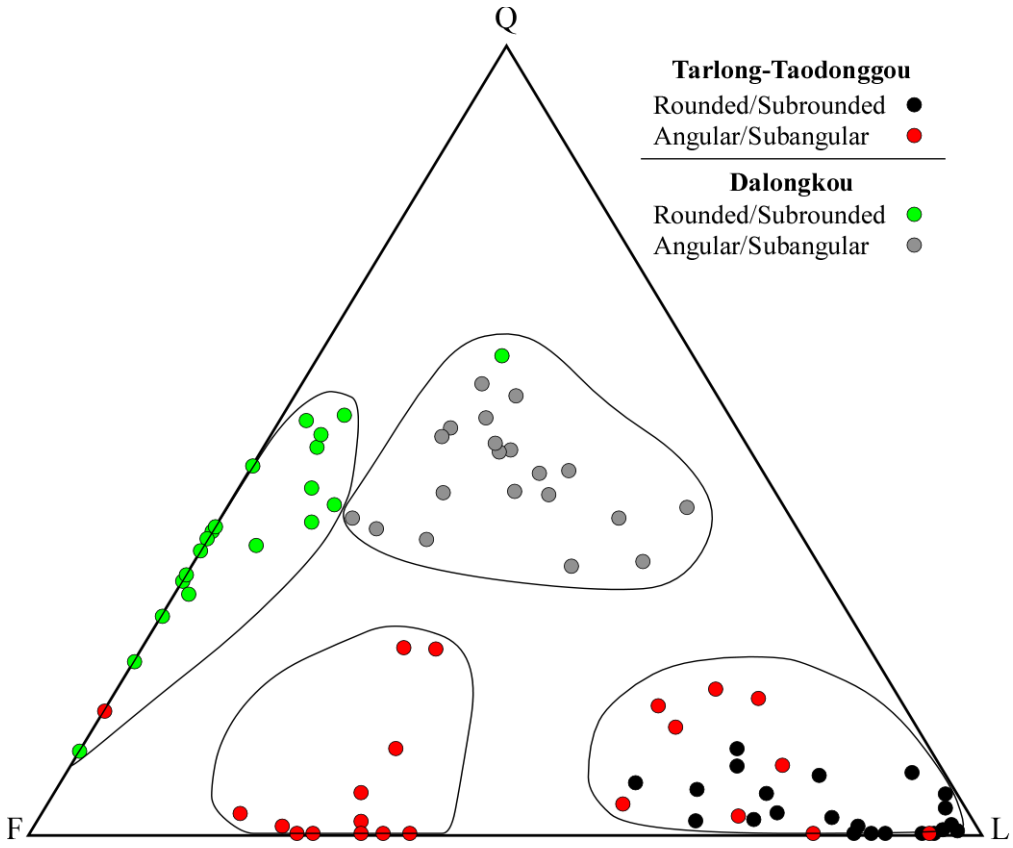

Figure 14. Composition of the Tarlong-Taodonggou and Dalongkou sandstones plotted in a QFL diagram. Notice the clear separation suggesting different sources for angular/subangular and rounded/subrounded grains. See text for details.

9.3 Paleogeography of the Turpan-Junggar Basin

The evidence in this study substantiates the interpreted origin of the Turpan-Junggar basin as an intracontinental rift basin during the Middle Permian (e.g., Allen et al., 1995; Yang, 2008; Yang et al., 2010). A modern analog is the Basin and Range Province in western U.S.A., with the Sierra Nevada acting as a volcanic arc source (e.g., Ingersoll and Eastmond, 2007) and the rift shoulders acting as secondary sources for individual grabens.

The Dalongkou area is presently ~70 km to the north of the Tarlong-Taodonggou area, and may be longer if the Bogda Mountain anticline is palinspastically restored. The great distance between the north Tianshan arc to Tarlong-Taodonggou area across many grabens and half grabens may have prevented streams from reaching the Tarlong-Taodonggou area. This effect would have been exacerbated for the Dalongkou area because it is even farther away from the arc. The distance is possibly responsible for the major differences in lithic volcanic content seen between the sandstones from the two study areas.

10. Conclusions

Field and petrographic study of conglomerates and sandstones from the Tarlong-Taodonggou and Dalongkou areas in the Bogda Mountains, NW China provides evidence on how provenance lithology, transport distance, and depositional and paleoclimatic conditions affect sandstone composition and texture. Changes in sandstone composition in Tarlong-Taodonggou and Dalongkou, and changes in composition between the sandstones in the two study areas indicate that the major control on sandstone

composition is provenance lithology. Transport distance, provenance lithology, and stream conditions are major controls on sandstone texture.

The inclusion of contemporaneous and intrabasinal grains and subdivision of grains based on different grain shapes aid in recognizing secondary sources, assuming that angular/subangular grains are derived from local sources and rounded/subrounded grains from distant sources. The secondary sources are interpreted as rift shoulders and help understand the basin-fill history and substantiate the previous interpretation of the Turpan-Junggar basin as a rift basin during Middle Permian.

The inferred paleoclimatic conditions and changes throughout the lower and upper QZJ LCs seem to have played an important role in composition and texture of sandstones in Tarlong-Taodonggou and Dalongkou. Changes from arid-semiarid conditions to subhumid-humid conditions seem to increase compositional maturity in Tarlong-Taodonggou. Pedogenic features also developed on sandstones that formed under persistent subhumid-humid conditions. Subhumid-humid conditions seem to have been persistent in Dalongkou and caused consistent compositional and textural characteristics and pedogenic features.

Lithological variations in a rift basin cause mixed results of tectonic settings of provenance in tectono-petrographic schemes. Distinct sources can be recognized by subdividing sandstones into groups based on grain shapes. The methodology can be used in other rift basins to help understand basin-filling processes and paleogeographic evolution.

Acknowledgements

We would like to thank Drs. J. Wang and M.L. Wan of Nanjing Institute of Geology and Paleontology of Chinese Academy of Sciences, Drs. Y. Liu and S.S. Wang of Northwest University of China, Dr. Y. Yang of Xi'an Petroleum University, Dr. X. Luo of Institute of Geology and Geophysics, Chinese Academy of Sciences, Dr. Q. Feng of Shandong University of Science and Technology, and J.J. Liu, T. Foster, Z.X. Li, J.J. Li, L.L. Cheng, C.C. Zhou, Y.M. Gao, and B. Sun for field and logistic assistance and funding. This research was partially supported by five student research grants from Geological Society of America, Ed Picou/GCSSEPM, American Association of Petroleum Geologists, and the Al Spreng Graduate Research Grant from the Geology and Geophysics Program of Missouri University of Science and Technology to Jonathan Obrist-Farner, and by a research grant from University of Missouri Research Board and a research grant (No. 2011ZX05008-004-053) from Institute of Geology and Geophysics of Chinese Academy of Sciences to Wan Yang. Acknowledgement is made to the Donors of the American Chemical Society Petroleum Research Fund, for a grant to Wan Yang.

References

Allen, M.B., Sengor, A.M.C., and Natal'in, B.A., 1995, Junggar, Turfan and Alakol basins as Late Permian to Early Triassic extensional structures in a sinistral shear zone in the Altaid orogenic collage, central Asia: Journal of the Geological Society, v. 152, p. 327-338.

Allen, M.B., Windley, B.F., and Chi, Z., 1992, Paleozoic collisional tectonics and magmatism of the Chinese Tien Shan, central Asia: Tectonophysics, v. 220, p. 89-115.

Allen, M.B., Windley, B.F., Chi, Z., and Jinghui, G., 1993, Evolution of the Turfan Basin, Chinese central Asia: Tectonics, v. 12, p. 889-896.

Basu, A., 1976, Petrology of Holocene fluvial sand derived from plutonic source rocks: Implications to paleoclimatic interpretations: Journal of Sedimentary Petrology, v. 46, p. 694-709.

Basu, A., 1985, Influence of climate and relief on (mineralogical) compositions of sands released at source areas, *in* Zuffa, G.G., ed., Provenance of arenites: R. Reidel Publishing Company, p. 1-18.

Brewer, R., 1976, Fabric and mineral analysis of soils: Krieger, New York, 482 pp.

Cai, T., 1999, Stratigraphy of Xinjiang Uygur Autonomous Region: China University of Geosciences Press, 430 pp. (In Chinese with English abstract).

Carroll, A.R., 1998, Upper Permian lacustrine organic facies evolution, Southern Junggar Basin, NW China: Organic Geochemistry, v. 28, p. 649-667.

Carroll, A.R., Brassell, S.C., and Graham, S.A., 1992, Upper Permian lacustrine oil shales, southern Junggar Basin, northwest China: American Association of Petroleum Geologists Bulletin, v. 76, p. 1874-1902.

Carroll, A.R., Graham, S.A., Hendrix, M.S., Ying, D., and Zhou, D., 1995, Late Paleozoic tectonic amalgamation of northwestern China: sedimentary record of the northern Tarim, northwestern Turpan, and southern Junggar Basins: Geological Society of America Bulletin, v. 107, p. 571-594.

Carroll, A.R., Graham, S.A., and Smith, M.E., 2010, Walled sedimentary basins of China: Basin Research, v. 2010, p. 17-32.

Carroll, A.R., Liang, Y., Graham, S.A., Xiao, X., Hendrix, M.S., Chu, J., and McKnight, C.L., 1990, Junggar basin, northwest China: trapped Late Paleozoic ocean: Tectonophysics, v. 183, p. 1-14.

Dickinson, W.R., 1970, Interpreting detrital modes of graywacke and arkose: Journal of Sedimentary Petrology, v. 40, p. 695-707.

Dickinson, W.R., 1985, Interpreting provenance relations from detrital modes of sandstones, *in* Zuffa, G.G., ed., Provenance of arenites: D. Reidel Publishing Company, p. 333-361.

Dickinson, W.R., Beard, L.S., Brakenridge, G.R., Erjavec, J.L., Ferguson, R.C., Inman, K.F., Knepp, R.A., Lindberg, F.A., and Ryberg, P.T., 1983, Provenance of North American Phanerozoic sandstones in relation to tectonic setting: Geological Society of America Bulletin, v. 94, p. 222-235.

Dickinson, W.R., and Suczek, C., 1979, Plate tectonics and sandstone composition: American Association of Petroleum Geologists Bulletin, v. 63, p. 2164-2182.

Dott, R.H., 1964, Wacke, graywacke and matrix - What approach to immature sandstone classification?: Journal of Sedimentary Petrology, v. 34, p. 625-632.

Folk, R.L., 1951, Stages of textural maturity in sedimentary rocks: Journal of Sedimentary Petrology, v. 21, p. 127-130.

Folk, R.L., 1980, Petrology of sedimentary rocks: Hemphill Publishing Company, Austin, Texas, 184 pp.

Folk, R.L., and Ward, W.C., 1957, Brazos River bar: a study in the significance of grain size parameters: Journal of Sedimentary Petrology, v. 27, p. 3-26.

Garzanti, E., Andò, S., Vezzoli, G., Ali Abdel Megid, A., and El Kammar, A., 2006, Petrology of Nile River sands (Ethiopia and Sudan): Sediment budgets and erosion patterns: Earth and Planetary Science Letters, v. 252, p. 327-341.

Garzanti, E., Andò, S., Vezzoli, G., Lustrino, M., Boni, M., and Vermeesch, P., 2012, Petrology of the Namib Sand Sea: Long-distance transport and compositional variability in the wind-displaced Orange Delta: Earth-Science Reviews, v. 112, p. 173-189.

Garzanti, E., Padoan, M., Andò, S., Resentini, A., Vezzoli, G., and Lustrino, M., 2013, Weathering and relative durability of detrital minerals in equatorial climate: Sand petrology and geochemistry in the east African rift: Journal of Geology, v. 121, p. 547-580.

Garzanti, E., Vezzoli, G., Andò, S., and Castiglioni, G., 2001, Petrology of rifted-margin sand (Red Sea and Gulf of Aden, Yemen): Journal of Geology, v. 109, p. 277-297.

Gazzi, P., 1966, Le Arenarie del Flysch Sopracretaceo dell'Appennino Modenese: Correlazioni con il Flysch di Monghidoro: Mineralogica e Petrografica Acta, v. 12, p. 69-97.

Gradstein, F.M., Ogg, J.G., and Smith, A.G., 2004, A geologic time scale 2004: Cambridge University Press, New York, 589 pp.

Graham, S.A., Hendrix, M.S., Wang, L.B., and Carroll, A.R., 1993, Collisional successor basins of western China: impact of tectonic inheritance on sand composition: Geological Society of America Bulletin, v. 105, p. 323-344.

Grantham, J.H., and Velbel, M.A., 1988, The influence of climate and topography on rock-fragment abundance in modern fluvial sands of the southern Blue Ridge Mountains, North Carolina: Journal of Sedimentary Petrology, v. 58, p. 219-227.

Greene, T.J., Carroll, A.R., Wartes, M.A., Graham, S.A., and Wooden, J.L., 2005, Integrated provenance analysis of a complex orogenic terrane: Mesozoic uplift of the Bogda Shan and inception of the Turpan-Hami basin, NW China: Journal of Sedimentary Research, v. 75, p. 251-267.

Ingersoll, R.V., 1990, Actualistic sandstone petrofacies: discriminating modern and ancient source rocks: Geology, v. 18, p. 733-736.

Ingersoll, R.V., Bullard, T.F., Ford, R.L., Grimm, J.P., Pickle, J.D., and Sares, S.W., 1984, The effect of grain size on detrital modes: a test of the Gazzi- Dickinson point-counting method (Holocene, sand, New Mexico, USA): Journal of Sedimentary Petrology, v. 54, p. 103-116.

Ingersoll, R.V., and Eastmond, D.J., 2007, Composition of modern sand from the Sierra Nevada, California, U.S.A.: Implications for actualistic petrofacies of continental-margin magmatic arcs: Journal of Sedimentary Research, v. 77, p. 784-796.

Johnsson, M.J., and Stallard, R.F., 1989, Physiographic controls on the composition of sediments derived from volcanic and sedimentary terrains on Barro Colorado Island, Panama: Journal of Sedimentary Petrology, v. 59, p. 768-781.

Mack, G.H., and Suttner, L.J., 1977, Paleoclimate interpretation from a petrographic comparison of Holocene sands and the Fountain Formation (Pennsylvanian) in the Colorado front range: Journal of Sedimentary Petrology, v. 47, p. 89-100.

Metcalfe, I., Foster, C.B., Afonin, S.A., Nicoll, R.S., Mundil, R., Xiaofeng, W., and Lucas, S.G., 2009, Stratigraphy, biostratigraphy and C-isotopes of the Permian-Triassic non-marine sequence at Dalongkou and Lucaogou, Xinjian Province, China: Journal of Asian Earth Sciences, v. 36, p. 503-520.

Obrist-Farner, J., and Yang, W., 2015, Nonmarine time-stratigraphy in a rift setting - an example from the mid-Permian lower Quanzijie low-order cycle, Bogda Mountains, NW China Journal of Palaeogeography.

Powers, M.C., 1953, A new roundness scale for sedimentary particles: Journal of Sedimentary Petrology, v. 23, p. 117-119.

Retallack, G.J., 2001, Soils of the past: An introduction to paleopedology: Blackwell Science, London, 404 pp. 2nd Edition.

Roy, D.K., and Roser, B.P., 2013, Climatic control on the composition of Carboniferous-Permian Gondwana sediments, Khalaspir basin, Bangladesh: Gondwana Research, v. 23, p. 1163-1171.

Scotese, C.R., 2001, Atlas of Earth history, Volume 1, PALEOMAP Project, Arlington, Texas, 52 pp.

Scotese, C.R., 2002, PALEOMAP website http://www.scotese.com.

Sengor, A.M.C., and Natal'in, B.A., 1996, Paleotectonics of Asia: fragments of a synthesis, *in* Yin, A., and Harrison, T.M., eds., The tectonic evolution of Asia: New York, Cambridge University Press, 486-640 pp.

Shao, L., Stattegger, K., and Garbe-Schoenberg, C.-D., 2001, Sandstone petrology and geochemistry of the Turpan basin (NW China): implications for the tectonic evolution of a continental basin: Journal of Sedimentary Research, v. 71, p. 37-49.

Shelley, D., 1993, Igneous and metamorphic rocks under the microscope: classification, textures, microstructures and mineral preferred orientations: Chapman & Hall, London, 445 pp.

Suttner, L.J., 1974, Sedimentary petrographic provinces: An evaluation: SEPM Special Publication No. 21, p. 75-84.

Suttner, L.J., Basu, A., and Mack, G.H., 1981, Climate and the origin of quartz arenites: Journal of Sedimentary Petrology, v. 51, p. 1235-1246.

Suttner, L.J., and Dutta, P.K., 1986, Alluvial sandstone composition and paleoclimate, I. Framework mineralogy: Journal of Sedimentary Petrology, v. 56, p. 329-345.

Thomas, S.G., Tabor, N.J., Yang, W., Myers, T.S., Yang, Y., and Wang, D., 2011, Paleosol stratigraphy across the Permian-Triassic boundary, Bogda Mountains, NW China: implications for palaeoenvironmental transition through earth's largest mass extinction: Palaeogeography, Palaeoclimatology, Palaeoecology, v. 308, p. 41-64.

Van Loon, A.J., and Mange, M.A., 2007, 'In Situ' Dissolution of Heavy Minerals through Extreme Weathering, and the Application of the Surviving Assemblages and their Dissolution Characteristics to Correlation of Dutch and German Silver Sands, *in* Mange, M.A., and Wright, D.T., eds., Developments in Sedimentology, Volume 58: Elsevier, Amsterdam, p. 189-213.

Wartes, M.A., Carroll, A.R., and Greene, T.J., 2002, Permian sedimentary record of the Turpan-Hami basin and adjacent regions, northwest China: constraints on postamalgamation tectonic evolution: Geological Society of America Bulletin, v. 114, p. 131-152.

Xinjiang Bureau of Geology and Mineral Resources, 1993, Regional geology of Xinjiang Uygur Autonomous Region. Geological Memoirs, Series 1, No. 32, Ministry of Geology and Mineral Resources, Geological Publication House, Beijing, 762 pp (In Chinese with English abstract).

Yang, W., 2008, Depositional systems analysis within a seismic sequence stratigraphic framework, Turpan-Hami basin, NW China: Internal Report, Tu-Ha Petroleum Bureau, v. PetroChina, p. 49 pp.

Yang, W., Crowley, J.L., Obrist-Farner, J., Tabor, N.J., Feng, Q., and Liu, Y.Q., 2013, A marine back-arc origin for the Upper Carboniferous basement of intracontinental greater Turpan-Junggar basin - Volcanic, sedimentary, and geochronologic evidence from southern Bogda Mountains, NW China: Geological Society of America Annual Meeting, GSA Abstract with Programs, Vol. 45, No. 1, Denver, Colorado.

Yang, W., Feng, Q., Liu, Y., Tabor, N., Miggins, D., Crowley, J.L., Lin, J., and Thomas, S., 2010, Depositional environments and cyclo- and chronostratigraphy of uppermost Carboniferous-Lower Triassic fluvial-lacustrine deposits, southern Bogda Mountains, NW China - A terrestrial paleoclimatic record of mid-latitude NE Pangea: Global and Planetary Change, v. 73, p. 15-113.

Yang, W., Liu, Y., Feng, Q., Lin, J., Zhou, D., and Wang, D., 2007, Sedimentary evidence of Early-Late Permian mid-latitude continental climate variability, southern Bogda Mountains, NW China: Palaeogeography, Palaeoclimatology, Palaeoecology, v. 252, p. 239-258.

Zhu, H.C., Ouyang, S., Zhan, J.Z., and Wang, Z., 2005, Comparison of Permian palynological assemblages from the Junggar and Tarim basins and their phytoprovincial significance: Review of Palaeobotany and Palynology, v. 136, p. 181-207.

Zuffa, G.G., 1980, Hybrid arenites: Their composition and classification: Journal of Sedimentary Petrology, v. 50, p. 21-29.

SECTION

2. CONCLUSIONS

The sedimentary and stratigraphic study presented in this work provides clues about the stratigraphic architecture, depositional conditions, tectonic and climatic processes, and provenance of the Middle-Permian lower and upper QZJ LCs exposed in the Tarlong-Taodonggou and Dalongkou areas in Bogda Mountains, NW China. A new synchronous cyclo-stratigraphic unit, the Middle-Permian lower QZJ LC, is defined in the Tarlong-Taodonggou half graben and the Dalongkou area ~70 km to the north. It was the uppermost part of the previously-defined HYC LC, and consists of meandering stream deposits and stacked mature Calcisols and minor Argillisols and Vertisols in the upper part. Its lower boundary is a regional erosional unconformity separating the lacustrine deposits of the HYC LC from the overlying meandering stream deposits, and represents a regional lake withdrawal and significant fluvial incision driven by an episode of intense tectonic uplift. Its upper boundary is a regional disconformity and correlative local erosional unconformity and conformity, separating mature paleosols from overlying ephemeral and meandering stream and loessial deposits of the upper QZJ LC, and represents a prolonged episode of pedogenesis, tectonic quiescence, and a change of atmospheric circulation pattern. The upper QZJ LC is dominated by ephemeral-streams and loessites in Tarlong-Taodonggou and meandering streams and occasional loessites in Dalongkou. The presence of Protosols throughout the upper QZJ LC indicates stable tectonic conditions but fast sedimentation. The presence of Gleysols in the upper part of the sections indicates prolonged periods of exposure and tectonic quiescence.

The climatic conditions had been semi-arid with a strong precipitation seasonality in the Tarlong-Taodonggou area during the formation of the lower QZJ LC, whereas the conditions had been subhumid with a strong precipitation seasonality in the Dalongkou area. Atmospheric circulation pattern and wind regime changed in both areas after the formation of the upper boundary when loess deposition became dominant. In Tarlong-Taodonggou, the presence of loess deposits suggests that a semiarid to arid climate persisted through much of the upper QZJ LC and changed dramatically to a subhumid-humid climate in the uppermost part of the upper QZJ LC. This interpretation is supported by an increase in compositional maturity and an increase in pedogenic features in the sandstones. The change is interpreted as a response to the icehouse-hothouse transition in the Middle Permian. The Dalongkou area remained under humid to subhumid conditions throughout and is corroborated by the presence of abundant illuvial clays in the sandstones. The climatic interpretation for the QZJ LCs provides a rare data point in NE Pangea and insights into climate change during the Middle Permian. It serves as groundtruth data for future quantitative paleoclimatic models.

Finally, field and petrographic study of conglomerates and sandstones of the lower and upper QZJ LCs provides evidence on how provenance lithology, transportation distance, and depositional and paleoclimatic conditions affect sandstone composition and texture. The consistent composition between the sandstones from Tarlong-Taodonggou and Dalongkou indicate that source rock lithologies did not change during QZJ time. Lithological variations in the Turpan-Junggar rift basin result in mixed interpretations in well-established tectono-petrographic schemes. Recognition of secondary sources and their implications in basin-filling history depends on the study of compositional and

textural characteristics of intrabasinal grains. By combining both compositional and textural characteristics, secondary sources are identified. The detailed study of the sandstones using different point counting techniques enhances the understanding of the basin-filling history and of the paleogeography of the Turpan-Junggar Basin during the Middle Permian. The findings in this study provide an example of time-stratigraphic analysis in fluvial-lacustrine deposits, serve as a critical data point for future quantitative paleoclimatic modeling as well as regional and global stratigraphic correlation of Middle Permian terrestrial records across Pangea, and aid in understanding the paleogeography and tectonic history of the Turpan-Junggar basin during the Middle Permian.

APPENDIX A
NORTHEAST TARLONG SECTION

LEGEND

LITHOLOGY

Clast-supported conglomerate
Matrix-supported conglomerate
Sandstone
Well-bedded sandstone
Well-laminated sandstone
Cross-bedded sandstone
Conglomeratic sandstone
Calcareous sandstone
Muddy sandstone
Interbedded sandstone and shale/siltstone
Shale
Siltstone, Silty Mudstone, Sandy Mudstone
Calcareous shale or mudstone
Dolostone
Shale, dolomitic.
Mudstone
Conglomeratic mudstone
Calcrete or altered palustrine limestone
Paleosol
Limestone with shale partings
Limestone
Arenaceous limestone
Argillaceous limestone
Oolitic packstone/grainstone
Volcanic Tuff/Bentonite

SEDIMENTARY TEXTURE AND STRUCTURE

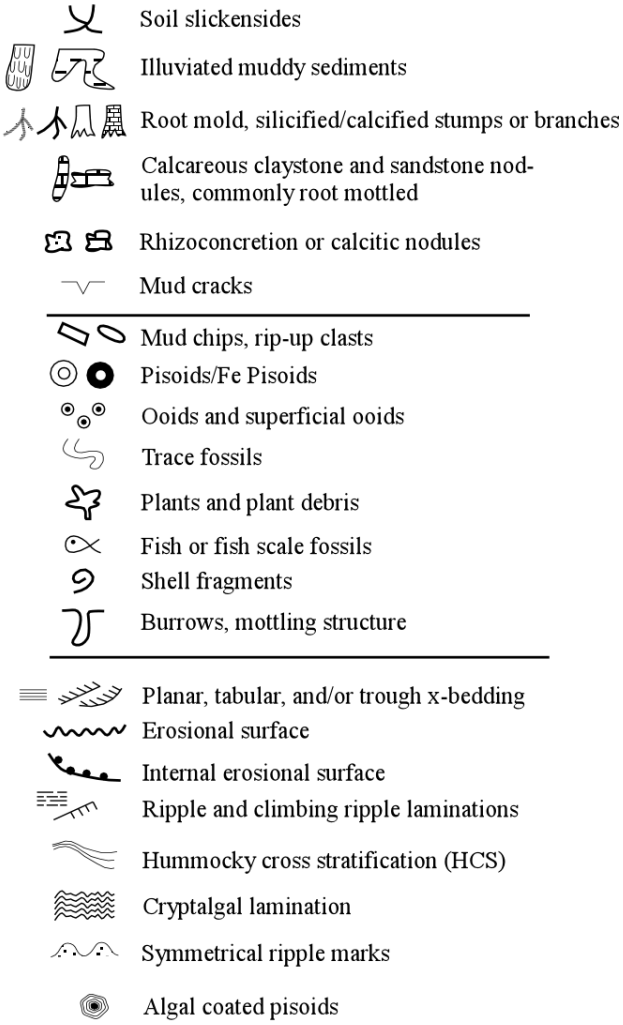

Soil slickensides
Illuviated muddy sediments
Root mold, silicified/calcified stumps or branches
Calcareous claystone and sandstone nodules, commonly root mottled
Rhizoconcretion or calcitic nodules
Mud cracks
Mud chips, rip-up clasts
Pisoids/Fe Pisoids
Ooids and superficial ooids
Trace fossils
Plants and plant debris
Fish or fish scale fossils
Shell fragments
Burrows, mottling structure
Planar, tabular, and/or trough x-bedding
Erosional surface
Internal erosional surface
Ripple and climbing ripple laminations
Hummocky cross stratification (HCS)
Cryptalgal lamination
Symmetrical ripple marks
Algal coated pisoids

High-order cycle boundary
Low-order cycle boundary
U QZJ xx — Cycle number
p-xxxx — Picture
sxx-xx, qxx-xx, trxx — Sample

Type of high-order cycles

MS - Meandering Stream
FL - Fluvial-Loessial
LL - Lakeplain-Littoral
LD - Lacustrine Deltaic
LP - Lacustrine Fluctuating Profundal Mixed Carbonate and Siliciclastic

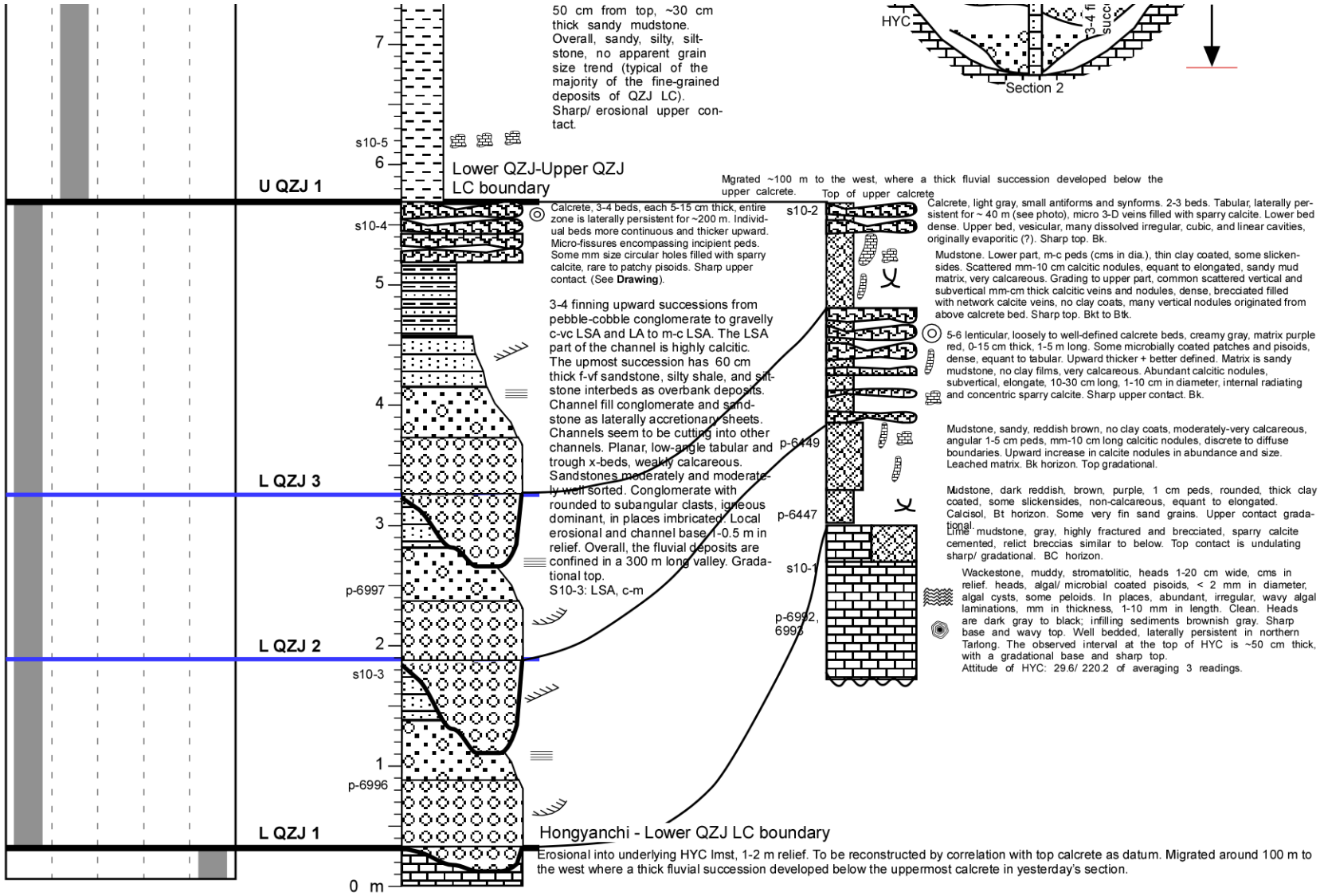
HYC
Section 2
50 cm from top, ~30 cm thick sandy mudstone. Overall, sandy, silty, siltstone, no apparent grain size trend (typical of the majority of the fine-grained deposits of QZJ LC). Sharp/ erosional upper contact.
s10-5
Lower QZJ-Upper QZJ LC boundary
U QZJ 1
s10-4
Calcrete, 3-4 beds, each 5-15 cm thick, entire zone is laterally persistent for ~200 m. Individual beds more continuous and thicker upward. Micro-fissures encompassing incipient peds. Some mm size circular holes filled with sparry calcite, rare to patchy pisoids. Sharp upper contact. (See **Drawing**).
3-4 finning upward successions from pebble-cobble conglomerate to gravelly c-vc LSA and LA to m-c LSA. The LSA part of the channel is highly calcitic. The upmost succession has 60 cm thick f-vf sandstone, silty shale, and siltstone interbeds as overbank deposits. Channel fill conglomerate and sandstone as laterally accretionary sheets. Channels seem to be cutting into other channels. Planar, low-angle tabular and trough x-beds, weakly calcareous. Sandstones moderately and moderately well sorted. Conglomerate with rounded to subangular clasts, igneous dominant, in places imbricated. Local erosional and channel base 1-0.5 m in relief. Overall, the fluvial deposits are confined in a 300 m long valley. Gradational top.
S10-3: LSA, c-m
L QZJ 3
p-6997
L QZJ 2
s10-3
p-6996
L QZJ 1
0 m
Migrated ~100 m to the west, where a thick fluvial succession developed below the upper calcrete.
Top of upper calcrete
s10-2
Calcrete, light gray, small antiforms and synforms. 2-3 beds. Tabular, laterally persistent for ~ 40 m (see photo), micro 3-D veins filled with sparry calcite. Lower bed dense. Upper bed, vesicular, many dissolved irregular, cubic, and linear cavities, originally evaporitic (?). Sharp top. Bk.
Mudstone. Lower part, m-c peds (cms in dia.), thin clay coated, some slickensides. Scattered mm-10 cm calcitic nodules, equant to elongated, sandy mud matrix, very calcareous. Grading to upper part, common scattered vertical and subvertical mm-cm thick calcitic veins and nodules, dense, brecciated filled with network calcite veins, no clay coats, many vertical nodules originated from above calcrete bed. Sharp top. Bkt to Btk.
5-6 lenticular, loosely to well-defined calcrete beds, creamy gray, matrix purple red, 0-15 cm thick, 1-5 m long. Some microbially coated patches and pisoids, dense, equant to tabular. Upward thicker + better defined. Matrix is sandy mudstone, no clay films, very calcareous. Abundant calcitic nodules, subvertical, elongate, 10-30 cm long, 1-10 cm in diameter, internal radiating and concentric sparry calcite. Sharp upper contact. Bk.
p-6449
Mudstone, sandy, reddish brown, no clay coats, moderately-very calcareous, angular 1-5 cm peds, mm-10 cm long calcitic nodules, discrete to diffuse boundaries. Upward increase in calcite nodules in abundance and size. Leached matrix. Bk horizon. Top gradational.
p-6447
Mudstone, dark reddish, brown, purple, 1 cm peds, rounded, thick clay coated, some slickensides, non-calcareous, equant to elongated. Calcisol, Bt horizon. Some very fin sand grains. Upper contact gradational.
s10-1
Lime mudstone, gray, highly fractured and brecciated, sparry calcite cemented, relict breccias similar to below. Top contact is undulating sharp/ gradational. BC horizon.
p-6992, 6993
Wackestone, muddy, stromatolitic, heads 1-20 cm wide, cms in relief. heads, algal/ microbial coated pisoids, < 2 mm in diameter, algal cysts, some peloids. In places, abundant, irregular, wavy algal laminations, mm in thickness, 1-10 mm in length. Clean. Heads are dark gray to black; infilling sediments brownish gray. Sharp base and wavy top. Well bedded, laterally persistent in northern Tarlong. The observed interval at the top of HYC is ~50 cm thick, with a gradational base and sharp top.
Attitude of HYC: 29.6/ 220.2 of averaging 3 readings.
Hongyanchi - Lower QZJ LC boundary
Erosional into underlying HYC lmst, 1-2 m relief. To be reconstructed by correlation with top calcrete as datum. Migrated around 100 m to the west where a thick fluvial succession developed below the uppermost calcrete in yesterday's section.

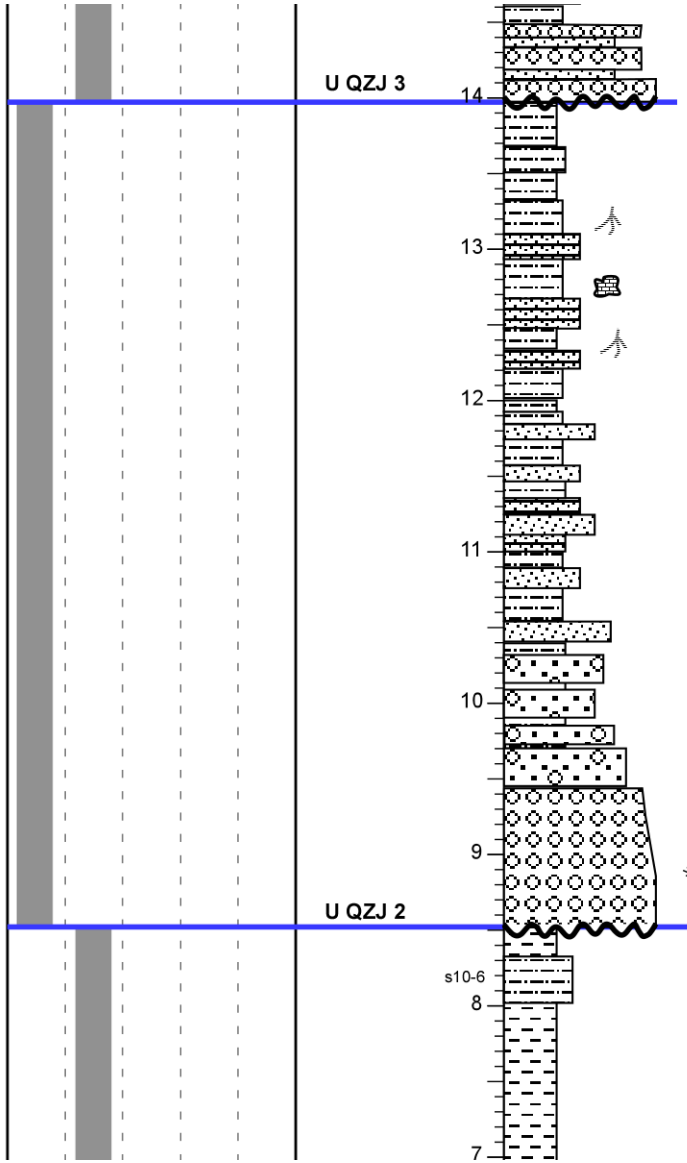

Conglomerate, light gray, granule to pebble, with stringers of sandstone and siltstone. Well rounded, moderately sorted. Intercalated with vc-c LW. Overall, fining upward. The QZJ conglomerate contains common pink, yellowish, transparent + translucent chert/jaspers, siliceous fragments, or QZJ crystals (all the above geode? fragments). Gradational top.

Siltstone, silty mudstone/shale, vf sandstone, sandy mudstone, maroon, blocky to platy, non-weakly calcareous, maroon. Interbeds of 10-30 cm. Low half, scattered clay-lined rootlets, mm in diameter. Middle part a 10 cm zone with incipient calcitic nodules. Sandy matrix with green steles (spots). Upper part, sandy mudstone/shale, siltstone, noncalcareous. Sharp/erosional upper contact.

Sandy shale, siltstone, mudstone, sandstone, interbedded, 10-20 cm beds, weakly to non-calcareous, platy to bulky, sharp to gradational contacts. Sandstone: LW , f-c, poorly sorted. Sharp/gradational top. Overbank facies.

LW, muddy conglomeratic, maroon to grayish maroon, well bedded, interbedded with sandy mudstone/shale, platy, m-vc, poorly sorted. Non-calcareous. Grains are igneous dominant. Gradational upper contact.

Conglomerate, light gray, granule to f-pebble, Grains are igneous dominant, well to subrounded, moderately well sorted, matrix c-vc sand, slightly and crudely fining upward. Tabular cross-bedded. Sharp low-relief erosional base. Gradational top.

Mudstone/ shale, reddish purple to purplish red, maroon, blocky to platy, sharp angular blocks, rare faint clay coats, weakly to non-calcareous. 50 cm from base a zone of scattered, discrete calcitic nodules (may not be pedogenic, S10-5). About 50 cm from top, ~30 cm thick sandy mudstone. Overall, sandy, silty, silt-

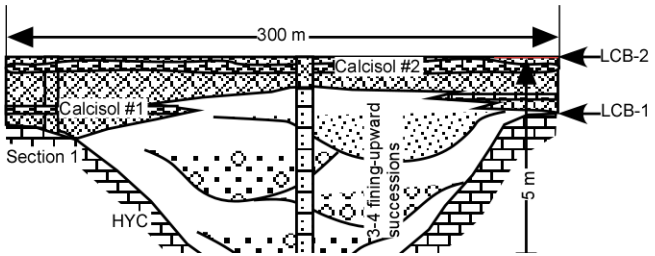

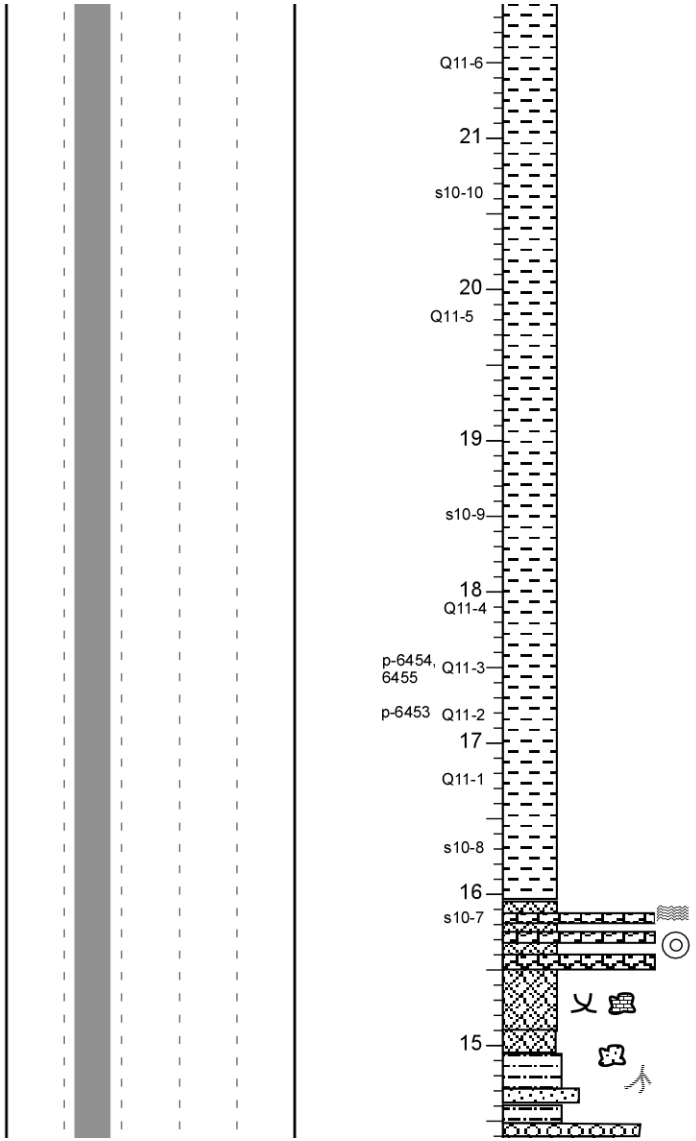

Lower part, maroon, gray, sandy mudstone, dense, blocky, angular, abundant slickensides and sparse-common calcitic nodules, equant, micro-brecciated. Upper part, gradational with lower part, light green, 1-5 cm, thin tabular calcrete. In places, abundant microbial encrusting and coating, in other places, embedded detrital grains and small pisoids. Calcrete zone, Bk. Palustrine limestone or calcrete. 50 meters to the west changes to a nodular zone. Gradational upper contact.

Siltstone, silty shale/mudstone, vf LW, maroon, platy-blocky, common equant sandy calcitic nods, mm-5 cm in size. Lower part, platy to blocky, upward increasingly blocky. Rare clay-filled rootlets. Gradational upper contact. Protosol, increasingly pedogenically altered upward.

Conglomerate, light gray, granule to pebble, with stringers of sandstone and siltstone. Well rounded, moderately sorted. Intercalated

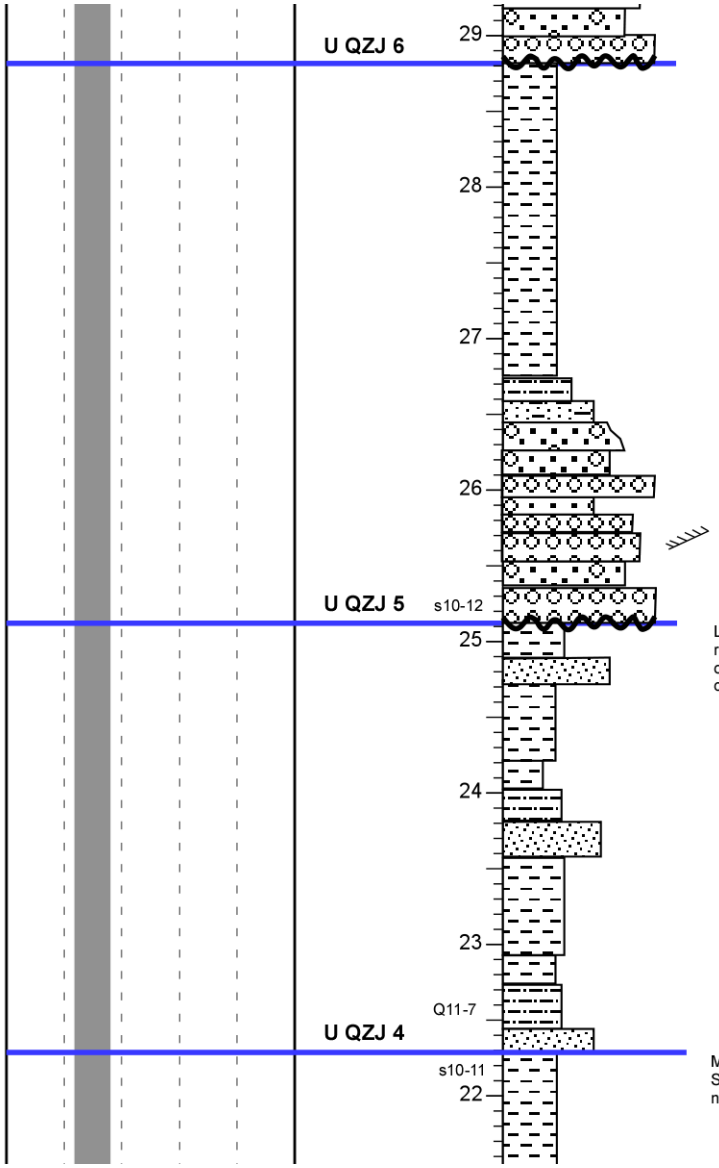

Mudstone, siltstone, silty and sandy, olive, olive gray, platy, monotonic, rare to no clay films. Non-calcareous. Typical QZJ mudstone. Sharp/erosional upper contact.

Sandstone, fining upward from gravelly c-vc to gravelly f-vf, LW throughout, muddier upward to very muddy LW or sandy mudstone, platy, non-calcareous, poor-moderately sorted, maroon to light gray, maroon in lower part. Gradational upper contact.

Conglomerate, pale gray, interbedded with conglomeratic LW, well bed, sharp erosional base, laterally persistent for ~ 30 meters. Conglomerate is granule to pebble size, rounded. Ss: m-vc, muddy LW, poorly sorted, subrounded to rounded. Large low-angle tabular cross-beds. No clear grain size trend. Gradational/sharp upper contact.
S10-12: crumbled sandstone.

LW, siltstone, silty mudstone, sandy mudstone interbeds, 10-30 cm thick beds. Sandstone: m-c, moderately sorted, subrounded to rounded, sharp base, gradational top. Mudrock: platy to blocky, dominantly platy. Rare clay films, dense, non-calcareous, massive to crudely laminated, massive dominant. Faster deposition than underlying mudstone interval. Sharp/erosional upper contact. Proximal overbank facies.

Mudstone, maroon, blocky-platy, peds f-m (1-5 cm), angular to subrounded, non to weakly calcareous. Silty, sandy, and siltstone. Sand is f-m. Massive, not laminated. No, sparse to some clay films (variable amount), thin, discontinuous. Monotonic, no laminations, no organic films. This is the enigma of QZJ. Sharp/gradational upper contact. Immature Argilisol or Argili-Protosol?

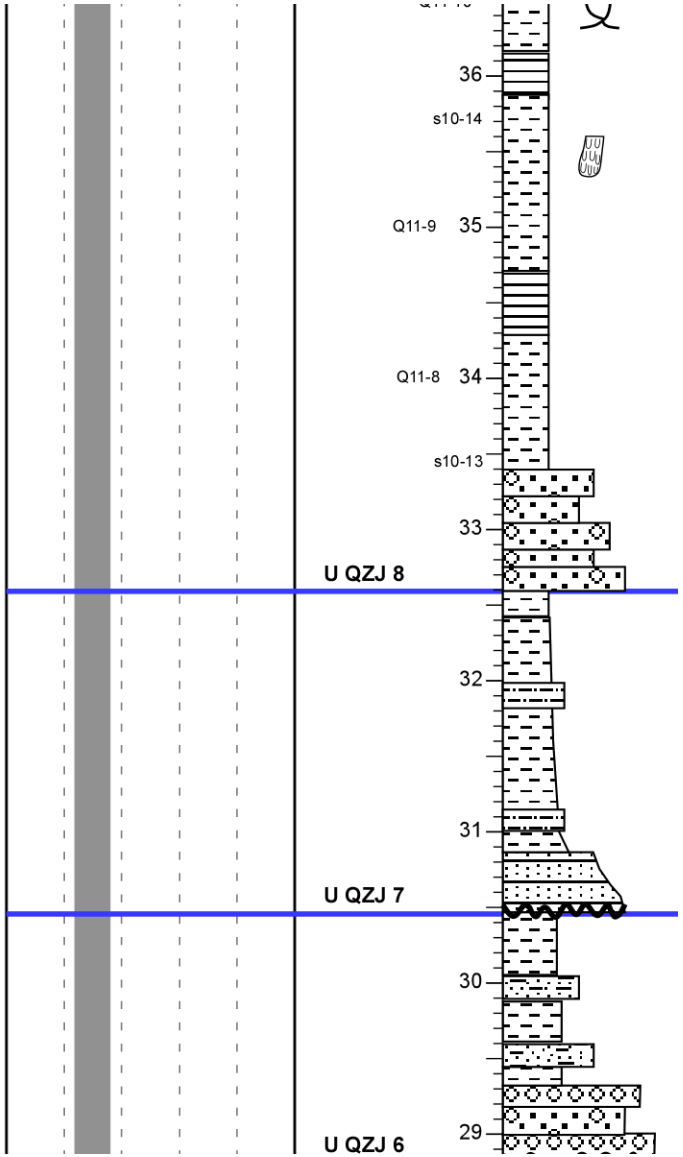

LW, light gray, well bedded, f-vc, moderately sorted, subrounded. Upper part, olive. Overall finning upward from m-vc to f-c.

Lower 40 cm, LW, m-vc, thickens to the W, moderately sorted. Grades to upper part, maroon-olive to olive, pebbly in places, siltstone, sandy and silty mudstone, purer mudstone to the top. Overall finning upward. A minor channel fill or edge of channel fill and overbank. Sharp/erosional upper contact.

Siltstone, silty mudstone, m-f LW, muddy, interbedded. Overall fining upward, maroon to olive. Sandstone dominant, poorly to moderately sorted, muddy, subrounded to rounded. Shard/ erosional upper contact. Overbank or upper channel fill facies.

Conglomerate + conglomeratic LW, light gray, laterally persistent for ~30 m. Gradational top.

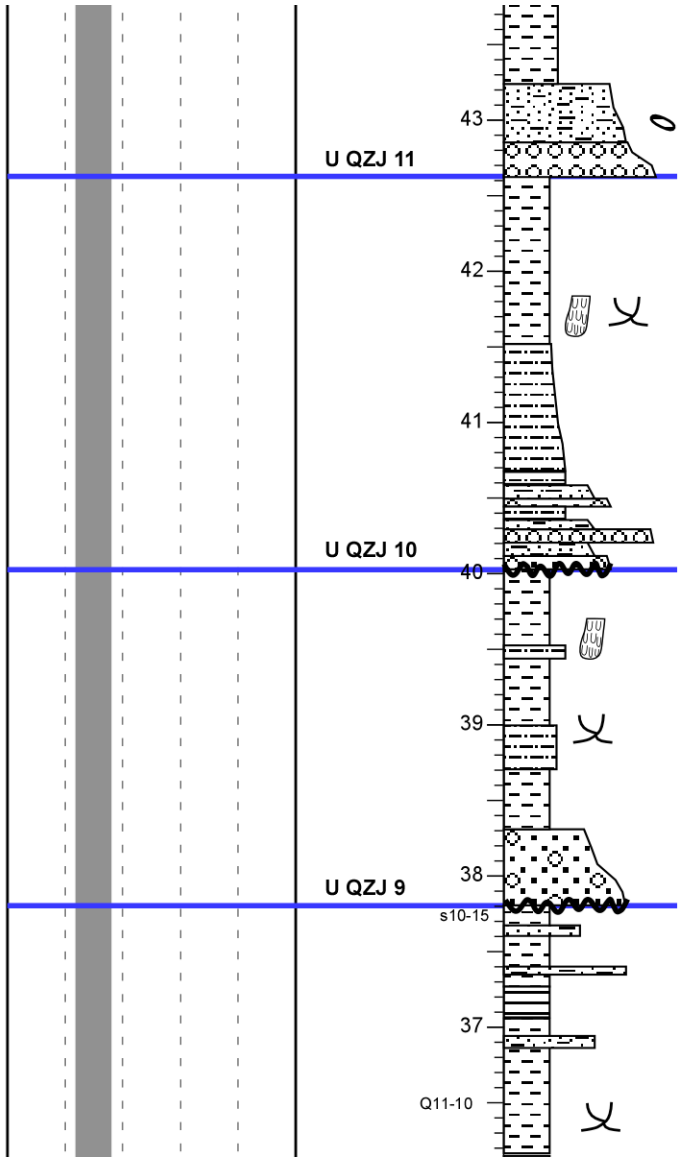

Conglomerate + conglomeratic LW, common mud clasts similar to below, angular, ~1 cm in size. Sandstone: c-vc, overall fining upward from conglomerate/ conglomeratic sandstone to muddy LW, poorly-moderately sorted, and weakly calcareous. Gradational upper contact.

Mudstone/shale, maroon, olive, to olive gray, platy. Overall fining upward from sandy to silty, to pure mudstone. Sparse to no clay films. Middle part, a 20 cm zone of common discontinuous clay films with slickensides. Upper part, sparse clay films. Protosol, slow but continuous deposition, thick lake margin mud flat. Sharp upper contact.

Sandstone, light gray in lower part, olive gray in upper part. Fining upward from gravelly c-vc LSA/LW to muddy LW to sandy mudstone. Clasts igneous dominant. Subrounded to rounded, many quartzose clasts. Laterally (~20 m) thickens to ~2-3 m. 2-3 fining upward units from gravelly sandstone or pebble conglomerate to sandstone. Sandstone non-calcareous. Gradational upper contact.

Mudstone, olive, platy to blocky, sparse clay films and slickensides, non-calcareous, silty, siltstone, sandy. Monotonic. Sharp upper contact.

LW, gray, conglomeratic, overall fining upward from c-vc, gravelly LW to muddy LW, f-m. Non-calcareous, well rounded. Gradational top.

Mudstone/shale, maroon to olive, rare clay films and slickensides, local abundant, thick, discontinuous clay films. Upper part, intercalated with thin 5-10 cm, f-vc LW, rounded to well rounded. Non-calcareous. Monotonic in general. Sharp/erosional upper contact.

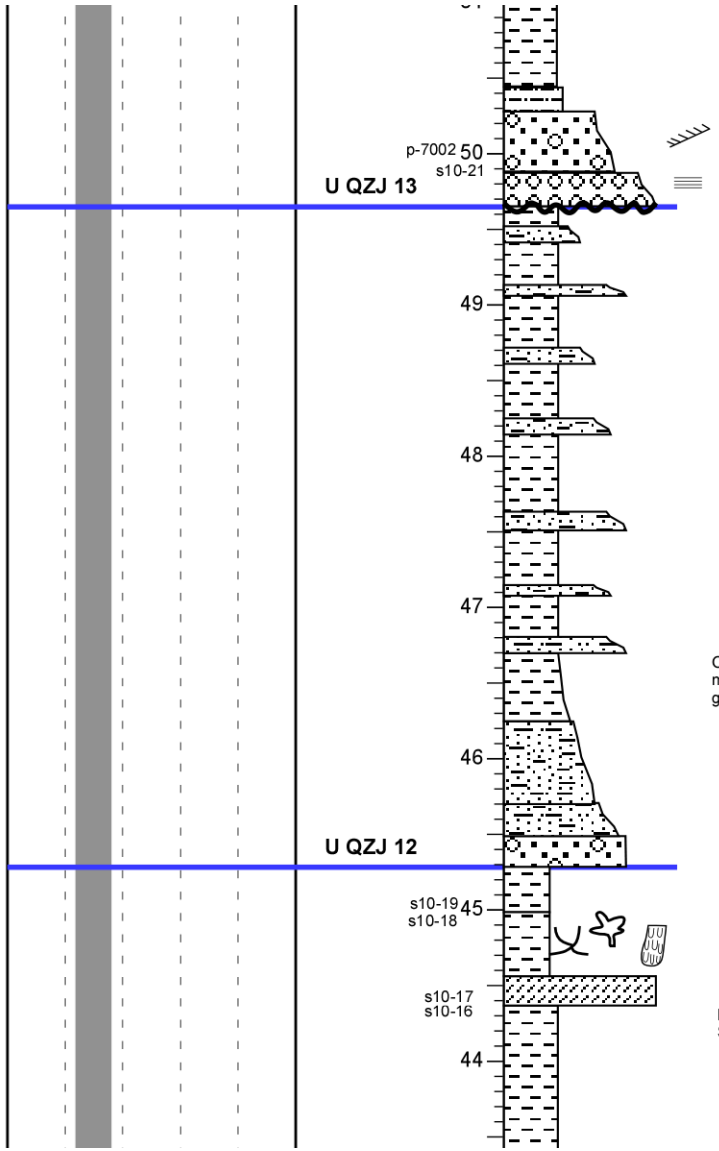

Sharp/ erosional upper contact.

Conglomerate and gravelly LSA/LW, light gray, fining upward to muddy LW, medium - large tabular and plane cross beddings. Intercalated with siltstone in upper part. Clasts igneous dominant, subrounded to rounded, moderately to moderately well sorted. Drastic lateral thickness change to 2.5 m 20 m to the west. Non-calcareous. (See photo for tabular bedding). Gradational upper contact.

Interbedded light gray LW (30%) and silty, sandy mudstone (~70%). LW is muddy, f-c/ vc, moderately to poorly sorted, sheet flood onto a mud flat, sharp based. LW beds are 5-15 cm thick, finning upward with a gradational top, variable sorting. Mudstone/ shale is platy - blocky. Sharp/ erosional upper contact.

Overall finning upward from muddy LW to sandy mudstone, maroon to olive gray, floating pebbles (common in all normal QZJ mudstone). They indicate occasional transport (wind or water) of pebbles onto mud flat or sandy mud flat of the subaerial lake margin. Sharp upper contact.

Fining upward from gravelly c-vc LW/ LSA to muddy m-c LW. Olive to maroon, non-calcareous. Gradational upper contact.

Mudstone, same as the normal QZJ mudstone underneath the volcanic deposits. Sharp top.

Mudstone, gray to greenish gray, platy, soft, pure, some carbonized plant remains. Common clay films + slickensides. Clay altered from volcanic ash or water-laid in a volcanics-dammed pond. Sharp upper contact.

Bentonite, pervasive abundant clay coatings, abundant to moderately calcitic plates, light gray. Intercalated with pure mudstone.

Mudstone, silty, sandy, platy to blocky, maroon, olive. Non-calcareous. Sand grains are variable in size, from f-c. Sharp upper contact.

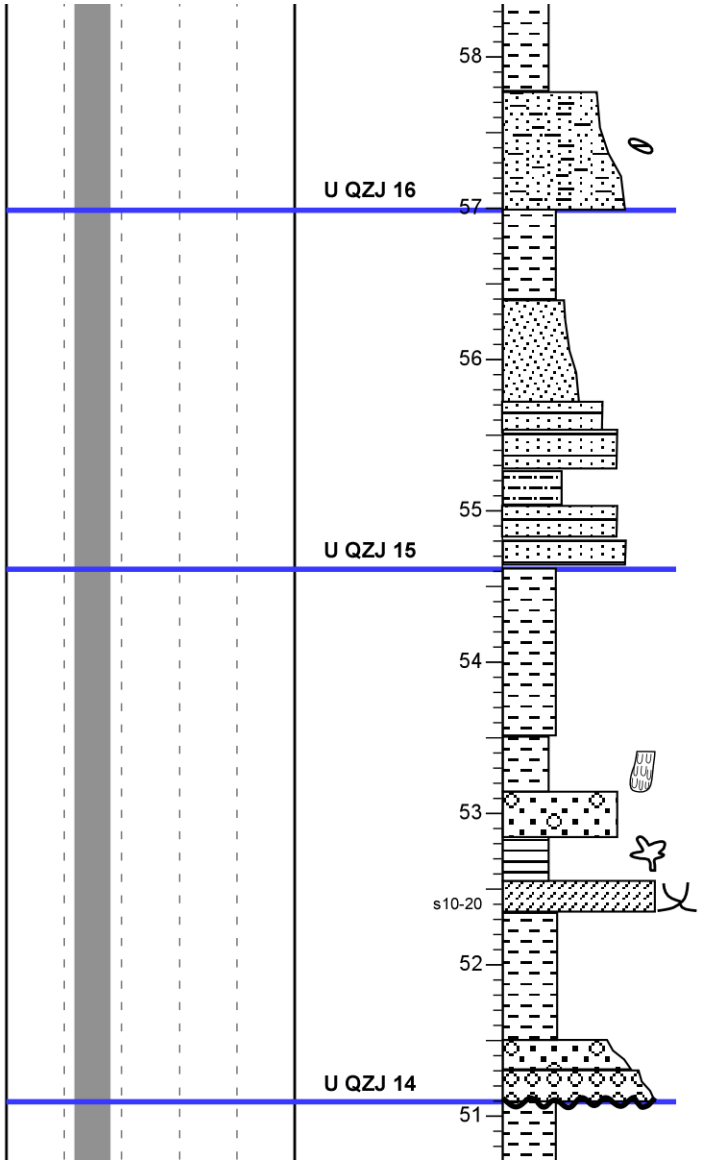

LW/LSA, pale gray in lower 1/3, upward to maroon, rounded to well rounded, non-calcareous. Upward finning and muddier from c-vc to m-c, common mud chips, especially in upper part. A 10-cm thick siltstone/silty mudstone in lower part. Upward changing again to a 20 cm bed of muddy LW, vc-f, rounded. Gradational upper contact.

Lower part muddy LW, brown, vf-f, rounded. Upward fining to a silty mudstone, brown, maroon, platy to blocky. Sharp upper contact.

LW/ LSA, c-vc, with a 20 cm siltstone/ mudstone in between, pale gray, fining upward overall. Gradational upper contact.

Normal QZJ mudstone, maroon, sandy to silty, with sparse clay films. Some parts contain concentrations of f-m grains, well rounded, non-calcareous. Sharp upper contact.

Mudstone/shale, greenish gray, mid part a 30 cm thick c-vc gravelly LSA. The pure mud may be deposited in volcanics-dammed lake. Clay films and plant remains sparse to common, decrease upward. Gradational upper contact.

Bentonite, dark greenish gray, pure, clay films and slickensides, modern calcite flakes/ plates. Carbonized plant remains. Gradational top.
Normal QZJ mudstone, brown, maroon, some small amount of sand grains, vf-f. Sharp upper contact.

Conglomerate and gravelly LSA, pale greenish gray, subrounded to rounded. Gradational top.

Mudstone, maroon to dark olive gray. Normal QZJ mudstone. Non-calcareous, contains some sand grains, mostly f-m. Sharp/ erosional upper contact.

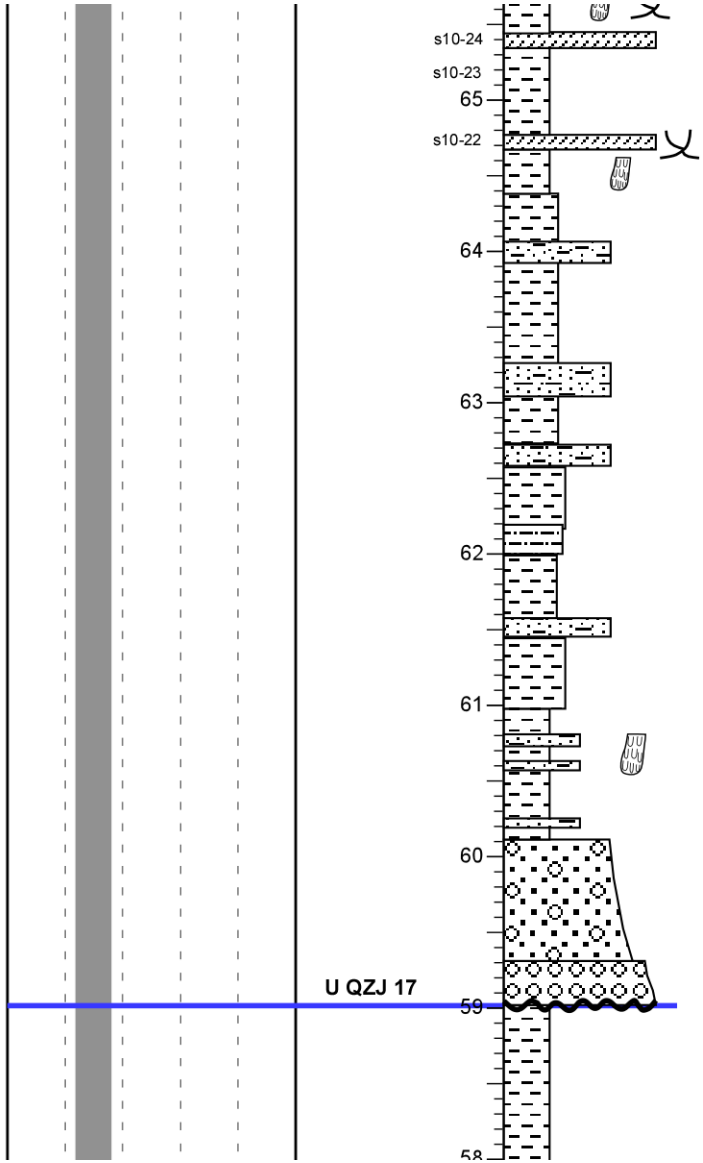

10 cm of bentonite. 30 m to the west, this and underlying bentonite coalesce to form a 1 m thick bentonite interval.

Mudstone, greenish gray, platy, crudely laminated, maybe bentonitic of mud in a volcanic dammed lake. Sharp/ gradational top.

10 cm of bentonite, maroon, ductile, heavily slickensided. Gradational/ sharp top.
~30 cm of mudstone, maroon, clay films common. Maybe related to above bentonite. Gradational top.

Normal QZJ mudstone, which is interbedded with sandy, silty mudstone, siltstone, very muddy LW. 4 beds of pale gray LW, m-c, 10-20 cm thick. One of the beds is mottled with maroon mudstone. Sharp/ gradational upper contact.

Normal/ typical QZJ mudstone, intercalated with muddy LW, maroon, platy to blocky, rare clay films locally. Sharp upper contact.

Fining upward from pebble - cobble conglomerate, light gray, to gravelly LW/LSA, c-vc, rounded to subrounded. Clasts igneous dominant, some chert. Some mud clasts. Gradational upper contact.

Normal QZJ mudstone, some compacted mud chips, probably healed desiccation chips. Brown, non-calcareous. Some sands. Sharp/ erosional upper contact.

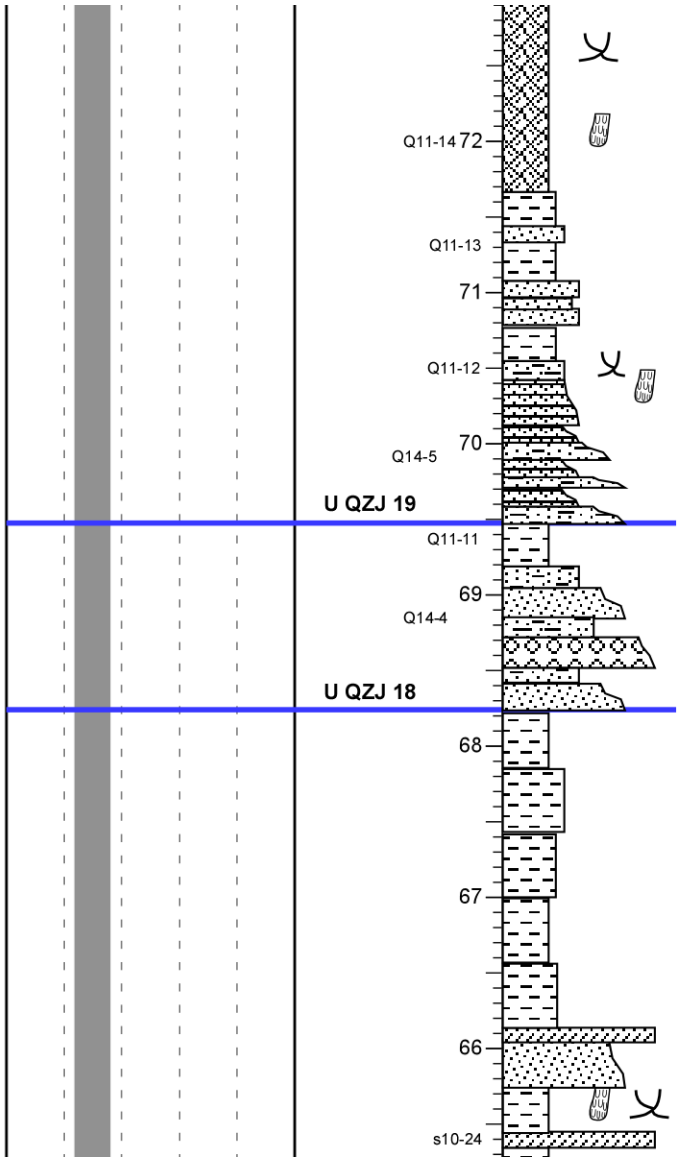

Mudstone, maroon to dark maroon, blocky, sandy, silty, siltstone. Some vf-f sands. Gradational upper contact.

LSA/LW, vf-f, well rounded, gray non-calcareous. moderately to moderately well sorted, subangular to subrounded. In places mottled. Gradational top.

Mudstone, maroon to olive gray, some clay coating + slickensides in upper middle part. Overall fining upward from vf-f LW to siltstone, silty and sandy mudstone. Sharp upper contact.

LW/LSA, pale gray to olive gray, intercalated with thin sandy and silty mudstone. 2-3 finning upward successions from m-vc sandstone to vf-f LSA or siltstone. Gradational upper contact.

Mudstone, maroon, rare to sparse clay coatings, non-calcareous. Gradational upper contact.

3 stacked finning upward successions from c-vc LSA/LW, gray, well rounded, to f-vf LW, muddy, maroon. The middle one from pebble conglomerate to m LW, pebbles well imbricated. Gradational upper contact.

Mudstone, typical of QZJ. Sandy, silty, with vf-f sand grains, well rounded, brown, maroon, non-calcareous. Sharp upper contact.

Bentonite.
Sandstone, vc-c, grains separated by bentonitic clay.

Mudstone, maroon, pure, some clay films and slickensides, volcanic-dammed lake?

10 cm of bentonite. 30 m to the west, this and underlying bentonite coalesce to form a 1 m thick bentonite interval.

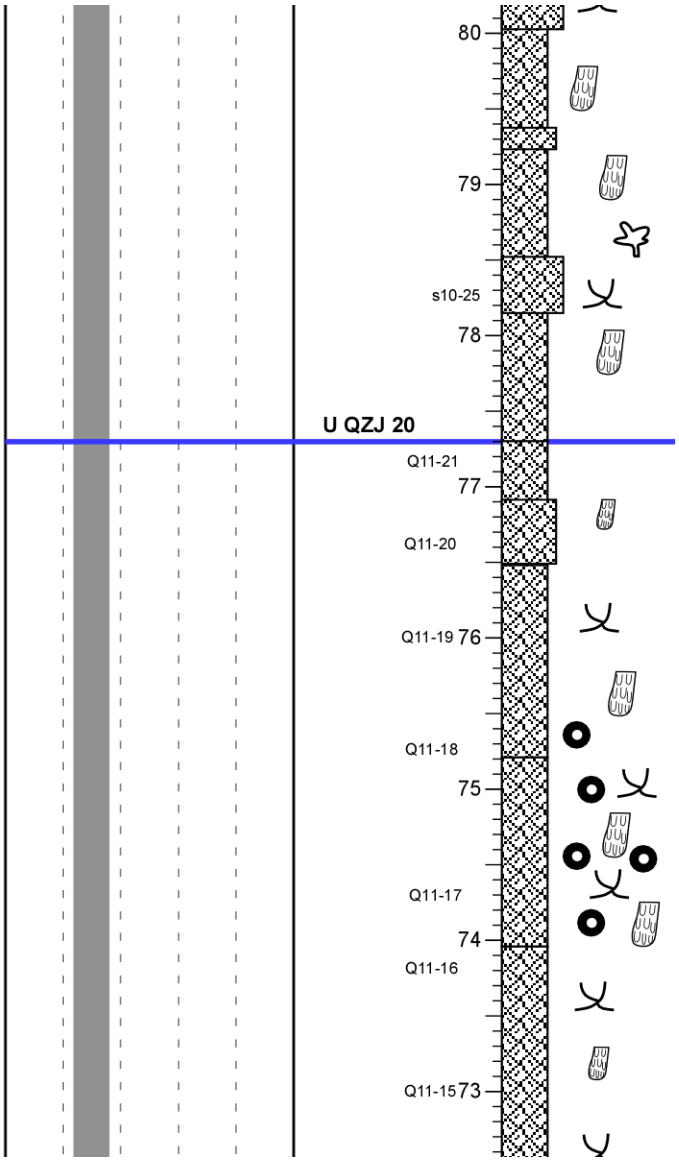

Mudstone, light brown in lower 20 cm, changing to greenish gray in upper part. Patchy, relict, discontinuous clay films, non-calcareous, silty in lower part, less in upper part. Some purple color on fresh surface. Peds increase upward in size from cms to 10s cm. Sharp upper contact. A horizon?

A surface of color contrast.
Mudstone, similar to below in color and clay films, some slickensides, but rare to no Fe pisoids. Sharp upper contact as a color contrast.

Mudstone, pale greenish gray, well-developed thick clay films. Lower 30 cm variegated, mixed with maroon, olive, and gray of underlying unit. Slickensided. Common and upward to abundant Fe pisoids, 0.2-15 mm in diameter. Abundance decreases in upper part. Waterlogged paleosol/Gleysol. Gradational upper contact.

Mudstone, olive gray, well developed peds, 1-5 cm in size, rounded, thick clay films + slickensides. Bt. Gradational upper contact.

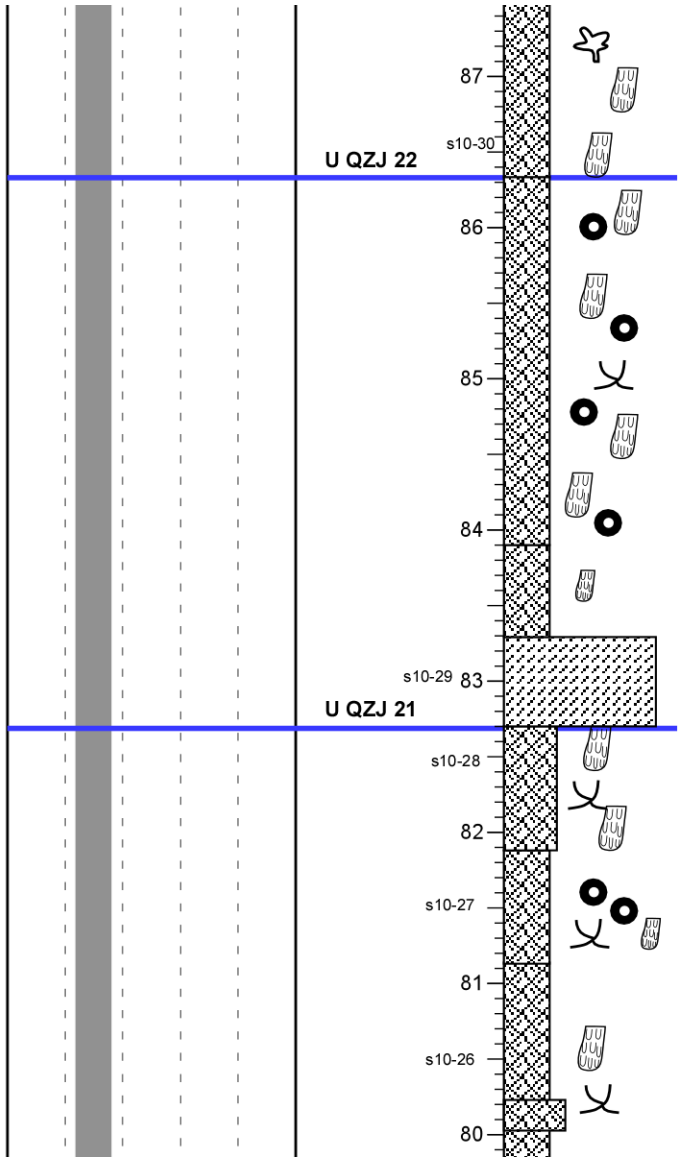

Mudstone, variegated, lower part, maroon dominant, greenish gray. Upper part, gray, yellow green dominant with maroon. Thick and continuous clay films, with or without slickensides. Fine (cm) peds. Common but not abundant Fe pisoids, yellow brown to steel gray, rounded 0.2 - 10 mm in diameter. Gradational upper contact.

Mudstone, maroon, to dark olive gray, blocky, thin and common clay coats. Non-calcareous. Gradational upper contact.

Bentonite, basal 10 cm green, gray, upward changing to maroon, highly clay coated and slickensided. Ductile. Sharp upper contact.

Mudstone, pure to variably silty, maroon to dark olive gray, common to abundant clay coats, increasing upward, probably related to bentonite above. Some slickensides. Sharp upper contact.

Mudstone, dark olive gray, to maroonish gray. Common small (<0.5 mm) Fe pisoids, most abundant in the middle part. Common discontinuous clay films, some slickensides. Gradational upper contact.

Mudstone, olive gray to maroon gray, pure to silty, common to abundant clay films, some slickensides. In places, intercalated with siltstone and sandy mudstone, moderately-well developed peds, cm in size. Rare to sparse plant remains, weakly to non-calcareous. Gradational upper contact.
S10-25: 1 m above base.
S10-26: 1 m below base.

Northeast Tarlong Section

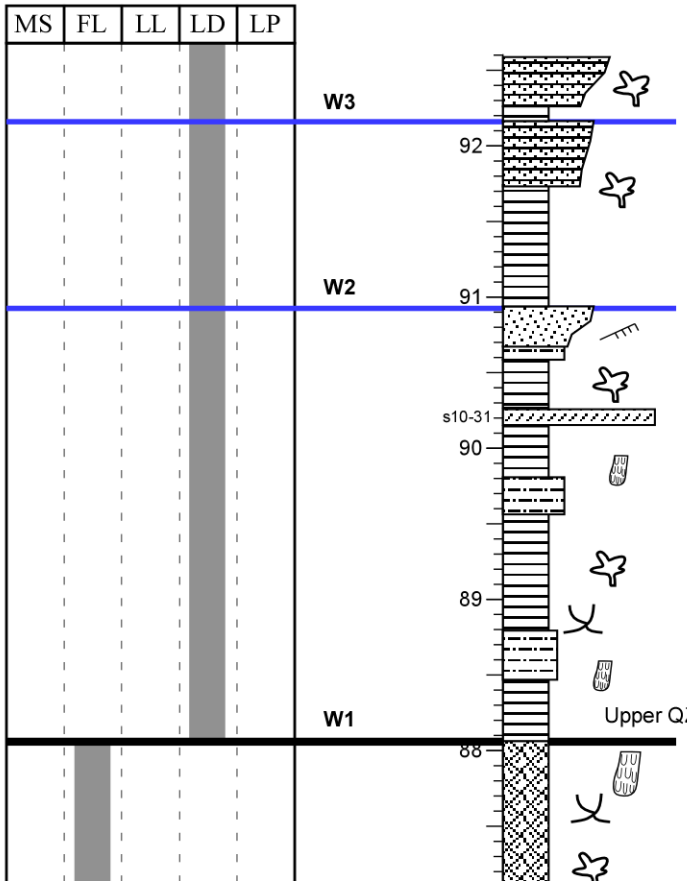

Basal 10 cm, maroon shale, silty, siltstone. Upward changing to f-m/ c pale gray LSA. Non-calcareous. Some plant remains on the bottom shale. Sharp upper contact.

Lower part, shale, long platy, olive gray, common minute/disseminated plant remains, variably silty. Uppermost 40 cm, f changes to m, well laminated LSA, coarsening upward. Gradational upper contact.

Coarsening upward from siltstone, f-vf to m LW/LSA, probable CRL, platy, abundant to common disseminated plant remains, moderately well to well sorted, subrounded. Greenish gray. 20 m to the west, the sandstone thickens to about 2 m, and coarsening from siltstone to pebble conglomerate, very large tabular cross beds and internal stratal surfaces, stratal geometry is concave base and convex top. Delta front. Sharp upper contact.

Shale/mudstone, olive gray, upward changing to greenish gray to dark grayish in upper 60 cm. Bentonite is black. Platy to strongly platy. Rare to sparse discontinuous clay films, mainly in lower part associated with bentonite. Upward increasing in plant remains. Variably silty and pure. 10 cm thick bentonite 30 cm below the top. Gradational top. Embayment or delta plain?

Upper QZJ-Wutonggou LC boundary

Lower part, mudstone, steel gray (the first such mudstone, typical of WTG LC), ~70 cm thick. Upward increasing clay films. Upper part gray, greenish gray, clay films, rare to sparse plant remains. Gradational to sharp top.

APPENDIX B
NORTH TARLONG SECTION

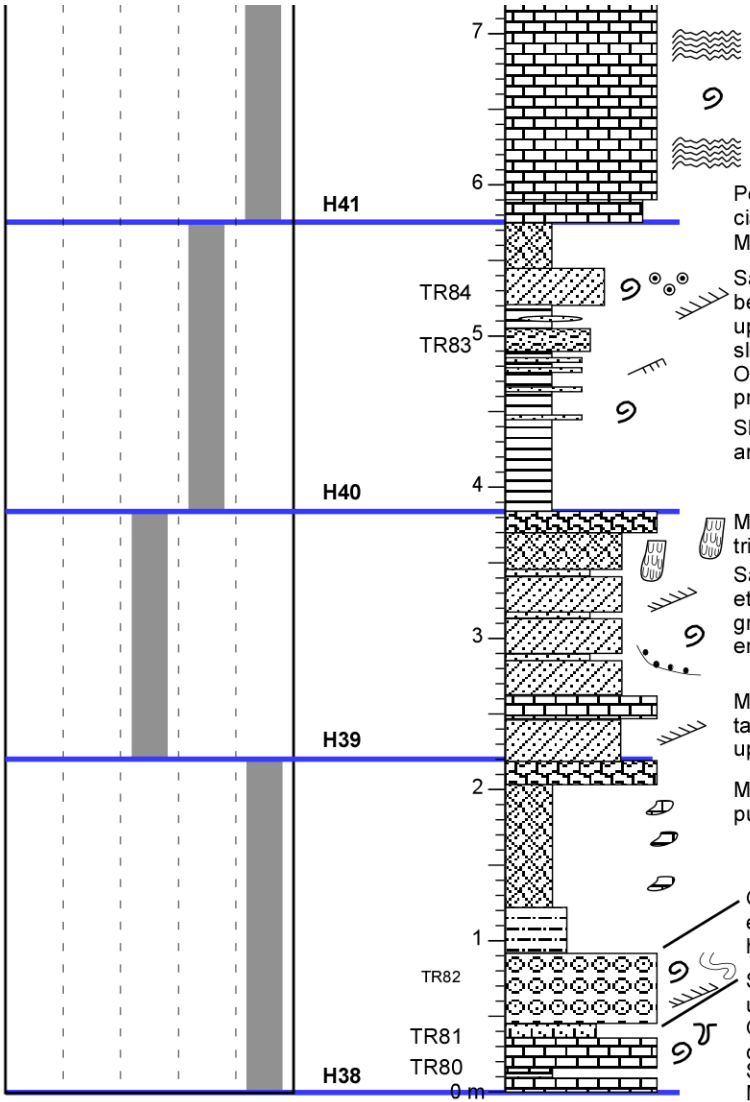

Peloidal wackestone to mudstone, gray, purple, variegated, dense, pure. Highly internally brecciated. Palustrine carbonate (pedogenetically altered lacustrine carbonate).
Mudstone, variegated, purple, gray, yellowish green. Fine (<1 cm), rounded to subangular peds.

Sandstone, gray, arenite, mixed lithic and skeletal grains, sparse ooids, very calcareous. 2 thick beds: lower bed has sets of ripple laminations with internal erosional or reactivation surfaces; upper bed, m-c, tabular x-bedded. Middle part, lithic wacke, f-m, and siltstone; laterally persistent, slight variation in thickness, lenses of fine-grained sandstone in a 15-cm thick mudstone/shale. Overall coarsening upward trend. Lower contact is gradational. This and the underlying units form progradational lake shore bodies.

Shale, gray to dark gray, platy, calcareous, some ostracods. Upward increasing sandstone beds and thickness from mm to cm.

Micrite, whitish gray, variegated, purplish. Illuviated with silt and mud, variable thickness. Palustrine carbonate or calcrete. Sharp lower and upper contacts.

Sandstone, greenish gray, c-vc subarenite to arenite, moderately sorted and rounded, some skeletal grains, well stratified, tabular x-bedded, internal erosional surfaces. Intercalated with dark gray f-m lithic wacke (1-5 cm thick). Upper 30 cm illuviated. Thickness varies from 80-200 cm, laterally persistent. Lake shore/beach aggradational and progradational succession.

Micrite, greenish gray in the upper part (~10 cm), Laterally persistent. Lower part (~ 25 cm), gray, tabular x-bedded, lithic arenite, c-vc, persistent, intercalated with well-laminated shale. Sharp upper and lower contacts.

Mudstone, reddish purple. Lower part (~30 cm), ripple-laminated siltstone; middle part, shale, purplish, platy; upper 15 cm, highly variegated, indurated, clayey, calcitic mudstone/calcrete.

Grainstone, oolitic, gray, dense, c-vc ooids, massive cortex, rounded to oval shape; sparse skeletal fragments. Tabular x-bedded. A 5-cm bed of highly concentrated trace fossils at the top, horizontal to subhorizontal (see Lin's photo).

Sandstone, calcareous, or arenaceous grainstone, grayish green, single bed, sand grains medium. Mottled, massive bedding.
Grainstone, gray, abundant half shells, ~1 cm in size, some 4-cm bivalves. Sparry cements. Gradational upper contact.
Shale, whitish green, very calcareous, platy, could be an argillaceous micrite.
Micrite, greenish gray, slightly silty, slightly mottled. Sharp lower contact.

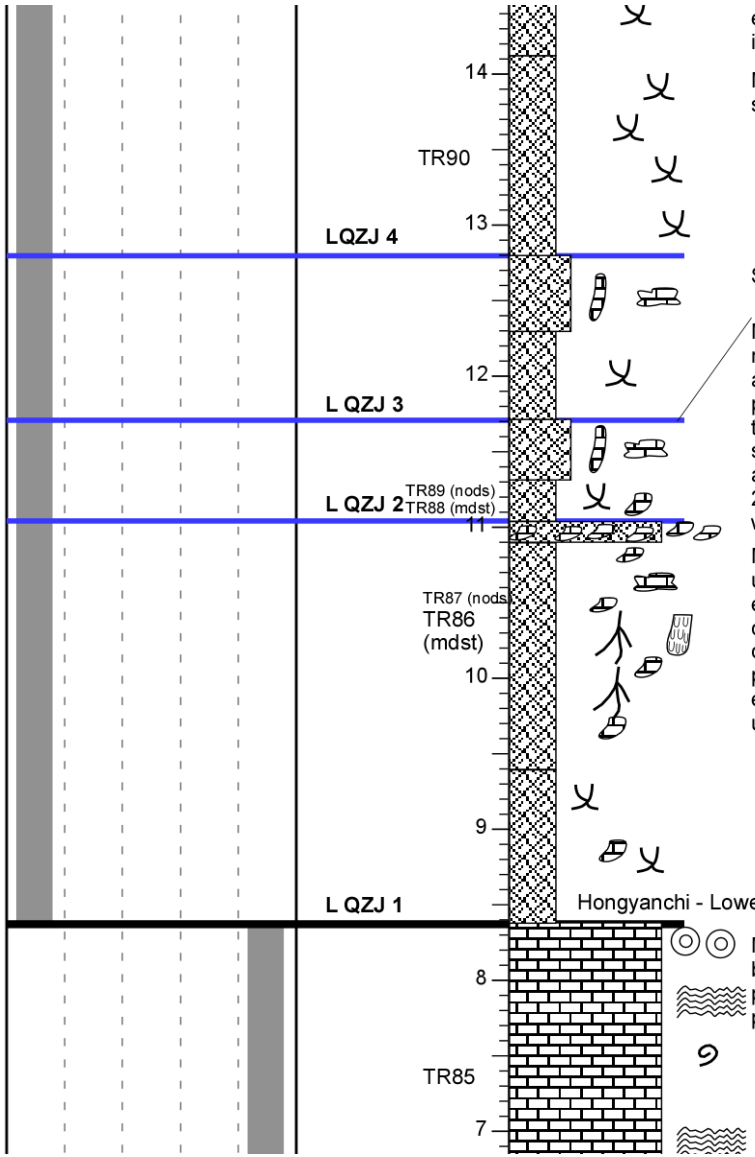

ensides. Not as much pedogenetically altered as below, transition to overlying overbank deposits and a more humid or seasonal climate. Immature Vertisol.

Mudstone, variegated, reddish purple, dark gray, diffuse color patches, mm peds, rounded to subangular, weakly calcareous, abundant slickensides. Vertisol.

Soil package #3, similar to #1 and #2. Plasma weakly to moderately calcareous.

Mudstone, purplish red. Upper 30 cm concentrated with calcitic nodules. Lower part, scattered nodules, slickensided, mm-size (< 2 mm) rounded peds, with sparse scattered nodules, may also be the original A Horizon of the underlying soil package which were modified during pedogenesis of soil package #2. Nodules tabular, 5-10 cm in diameter. Upper surface is gradational but clear. The lower contact of the nodule-concentrated interval is gradational. The upper surface of a soil package is temporarily placed on top of the nodule-concentrated interval (Bk), assuming the A Horizon is eroded. A Calcisol with vertic features. In this case, this interval is the 2nd soil package above the top of the nodule-concentrated interval of the 1st soil package, which was measured previously in the same location.

Mudstone, purplish red. Lower part, blocky peds (0.5-1 cm in size), subangular to rounded, upward increasing cm-scale slickensides. Middle part, upward increasing calcitic nodules, equant, tabular, or irregular, highly auto-brecciated with infiltrated silt and clay, and sparry calcite-filled cracks. Some m-scale subvertical slickensides (inferred from surface-lined tabular calcitic nodules). Peds <0.5 cm, rounded to subrounded, weakly to moderately calcareous. Upper part, a 15 cm interval concentrated with whitish green-gray calcitic nodules, 5-20 cm long, equant to irregular, tabular. Nodules amalgamated indicating multiple generations of calcitic nodule formation. Sharp lower contact, gradational internal contacts. A vertic Calcisol.

Hongyanchi - Lower QZJ LC boundary

Micrite, gray, algal laminated, mm thick, cms long, discontinuous cryptalgal laminae, parallel to bedding, pedogenetically altered. Apparent mounded geometry. Lower part (20-60 cm), dense, peloidal wackestone with skeletal grains, overlain by laminite. Uppermost part stromatolitic and pisolitic. Sharp upper boundary.

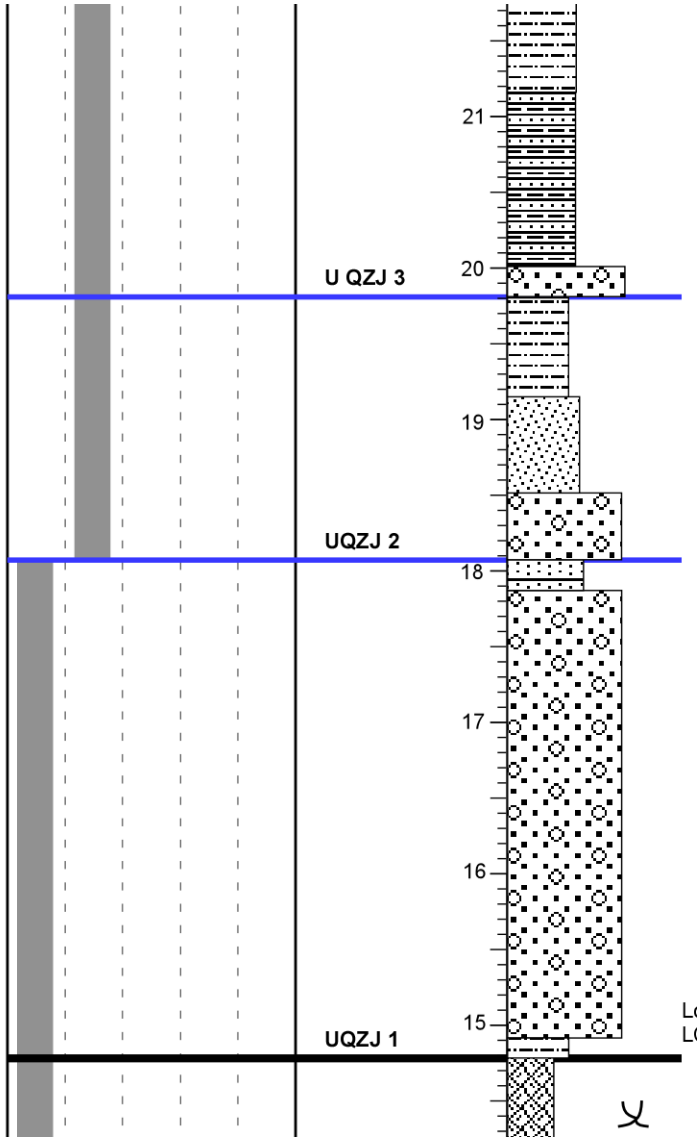

Sandstone, siltstone, and mudstone interbeds, reddish purple, non-calcareous. Sandstone f-vf, mudstone/shale sandy and platy. All sandstones below and in this interval in the fine/upper-part of the two-unit stream deposits are mud-rich lithic wackes; no pure mudstone/shale.

Sandstone, conglomeratic, gray to purplish gray. Clasts ~10-20%, up to 5 cm max., rapid lateral thickening and thinning. Channel fill.

Siltstone and sandstone, purplish red. Sandstone in the lower part, f-vf, poorly sorted; siltstone in the upper party, platy, sandy.

Sandstone, conglomeratic, whitish gray, c-vc, clasts up to 10 cm in diameter.

Siltstone and sandstone, vf, reddish purple, platy. Absence of mudstone. Coarse-grained meandering stream or braided stream.

Sandstone, conglomeratic, gray, c-vc, clasts granule to fine pebble (5 cm max.), common sedimentary clasts. Crude upward-fining trend. Rapid lateral facies changes. Coverage makes sedimentary structures not observable, likely superimposed multiple channel fill/bar deposits.

Lower QZJ-Upper QZJ
LC boundary

Mudstone, reddish purple in lower part, reddish gray to dark gray in the upper part, gradual color change. Slightly coarsening upward. Large peds to platy in the upper part. Lower part has slickensides. Not as much pedogenetically altered as below, transition to overlying overbank depos-

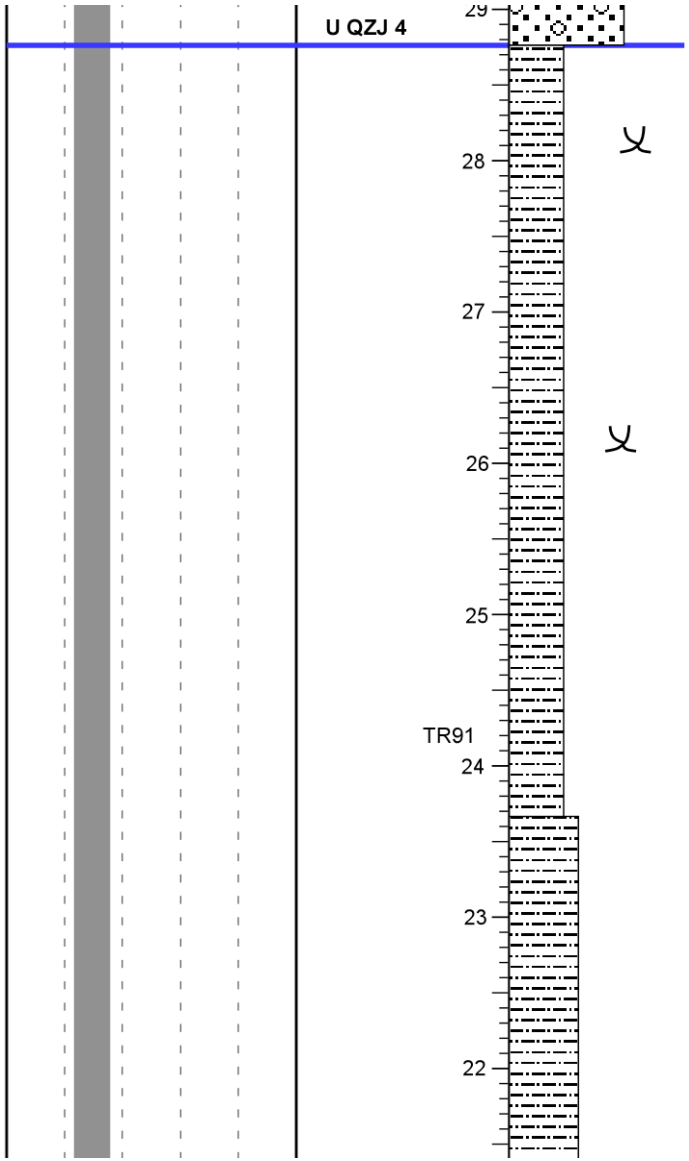

Mudstone/shale, and conglomeratic lenses. Lower 2.5 m, reddish sandy mudstone; upper part pure and silty mudstone/shale, not sandy or gravelly, platy, sparse slickensides, <1 cm peds. Several gray conglomeratic sandstone lenses (10s cm thick).

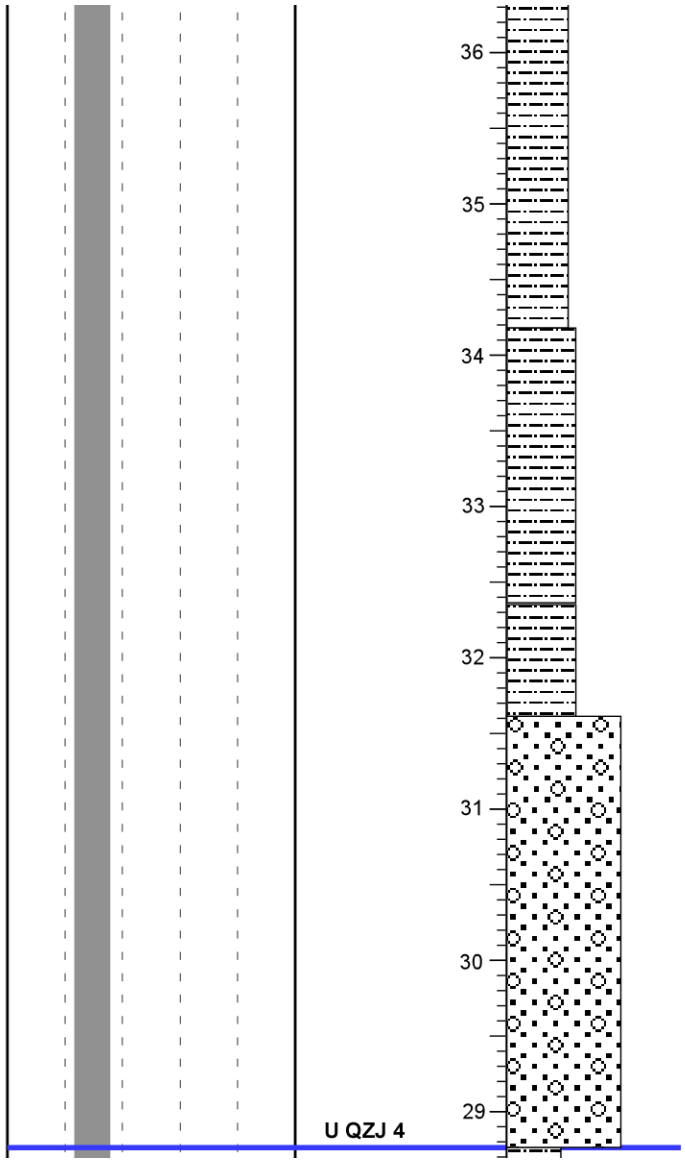

Sandstone, conglomeratic, whitish gray, lithic, clasts granule to fine pebble, <10% in content.

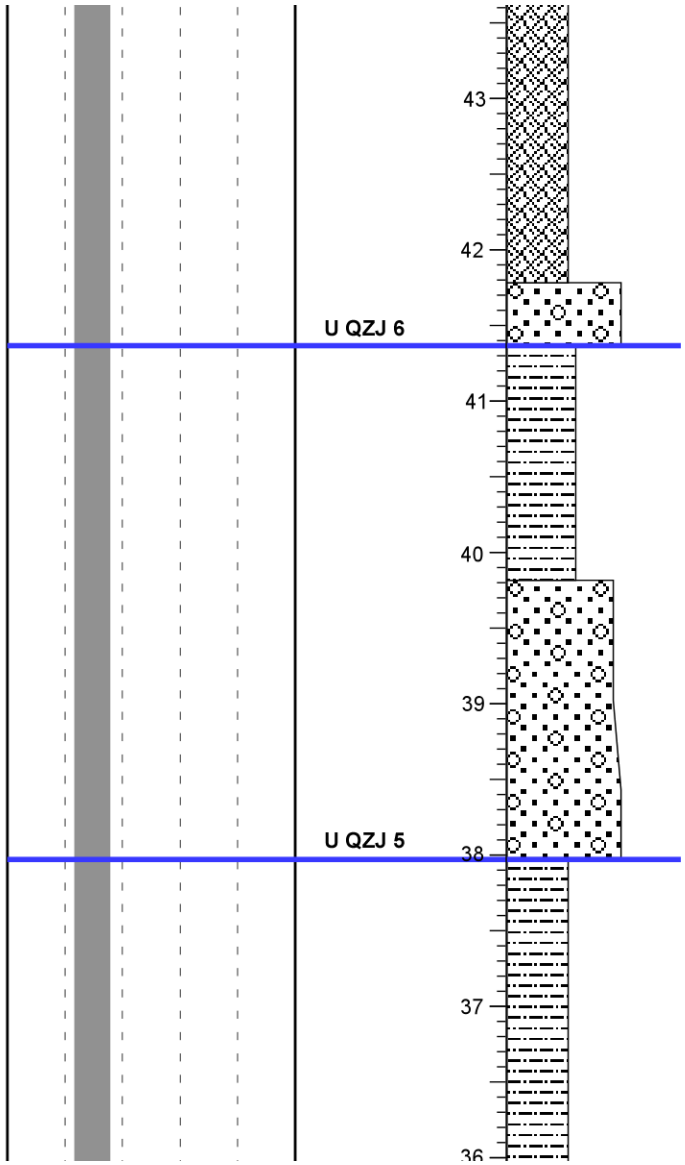

Sandstone, conglomeratic, lithic subarenite to wacke, common sedimentary clasts, <20% in content.

Mudstone/shale, sandy, and sandy siltstone, reddish purple, weakly calcareous, platy to granular.

Sandstone, conglomeratic, whitish gray, clasts <20%, granule to fine pebble. Few intercalated lithic wacke, c-vc. Fining upward into mud-rich wacke (c-vc).

Shale, sandy, grayish brown, in the lower part, grading into silty mudstone and mudstone in the upper part. Platy, weakly calcareous.

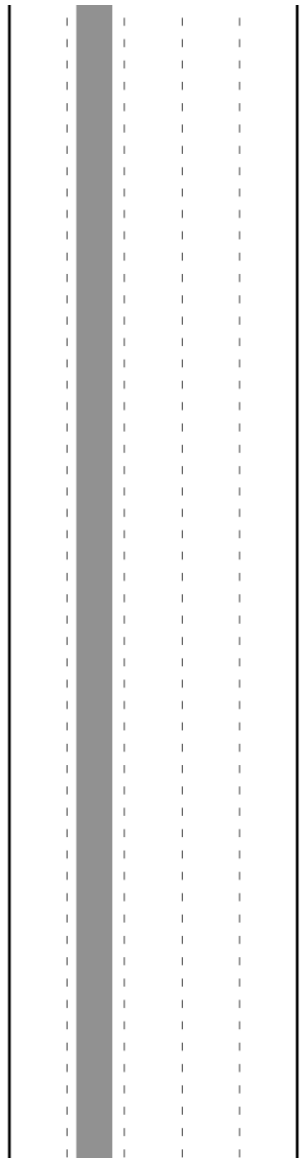

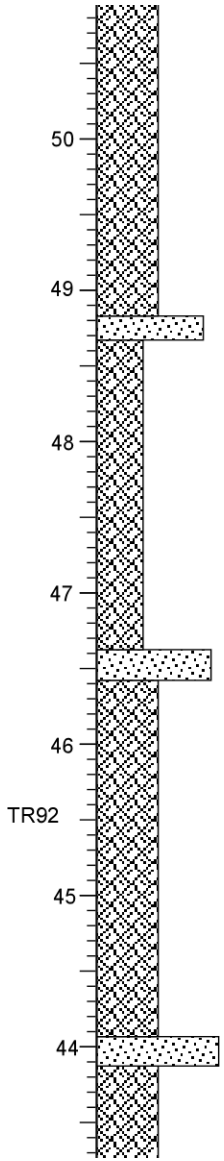

Sandstone, gray, muddy wacke, m-vc, poorly sorted. The muddy matrix suggests illuviation of clay (?).

Mudstone, reddish purple, platy to fine (<1 cm) peds, no slickensides, weakly calcareous.

Sandstone, gray, c-vc, arenite, not conglomeratic.

Mudstone, silty, reddish purple to dark reddish gray, weakly calcareous. Immature paleosol, Argillisol, not Calcisol or Vertisol, a subhumid climate paleosol.

Sandstone gray, c-vc, arenite.

Mudstone, silty, reddish purple, platy to fine peds, no slickensides. Immature paleosol, or an Argillisol.

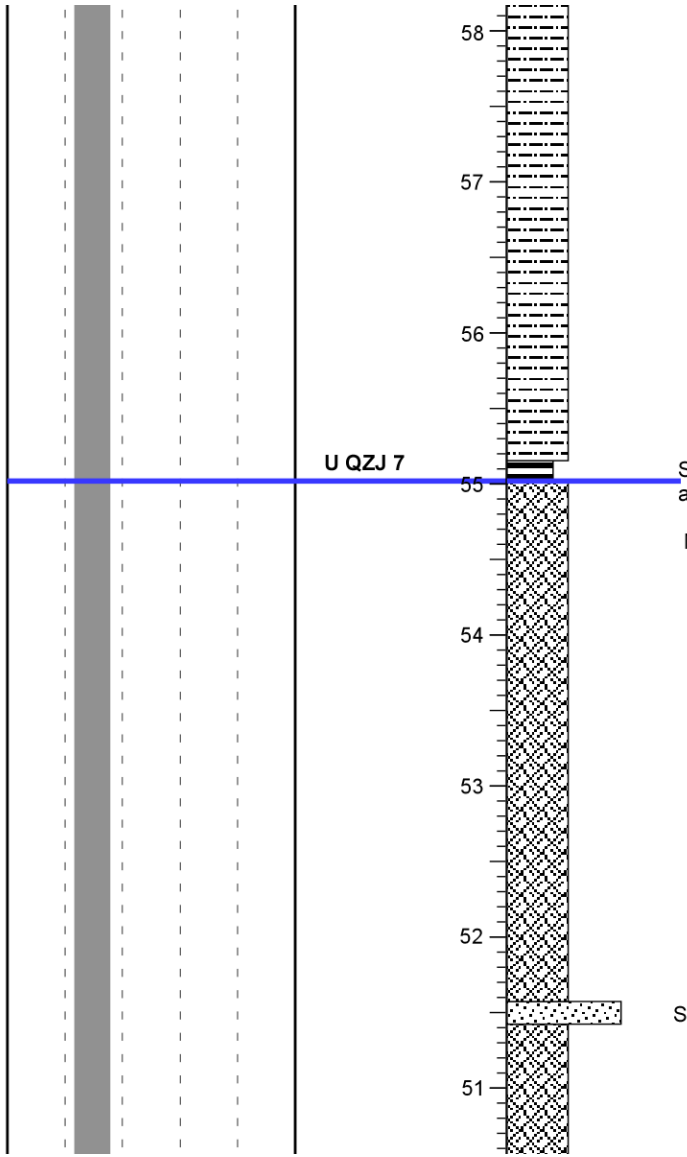

Shale/mudstone, blackish gray, laminated, some fine peds. Probably organic rich. Gradational upper and lower boundaries.

Mudstone, reddish brown to purple, upper part dark grayish red. Silty.

Sandstone, gray, muddy wacke will illuvial clay (?), c-vc.

Mudstone, silty or sandy, reddish brown to purple, platy to fine peds, weakly calcareous.

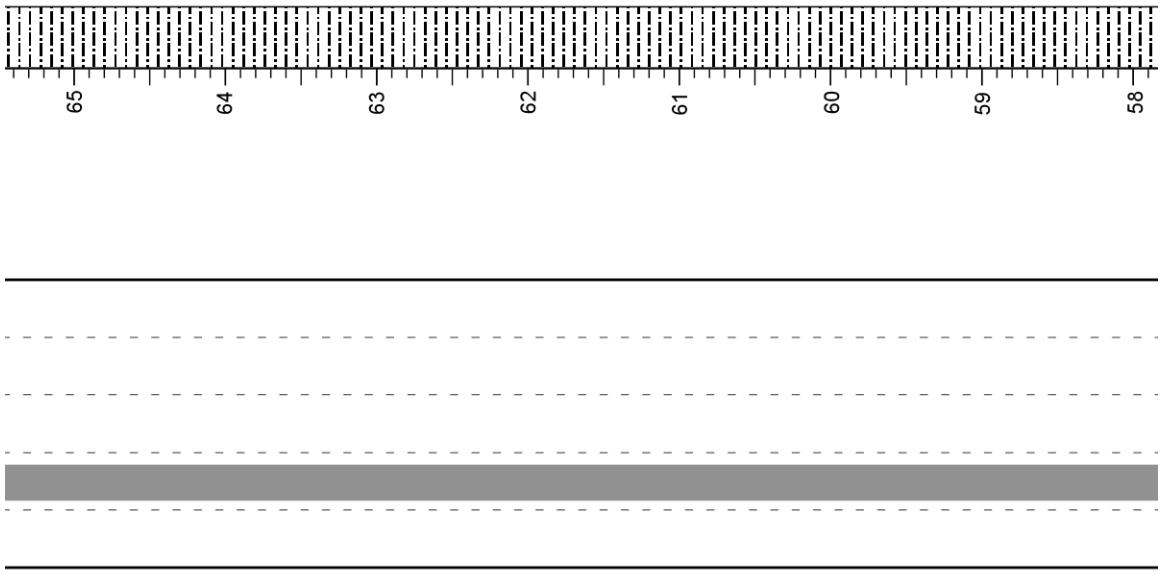
65
64
63
62
61
60
59
58

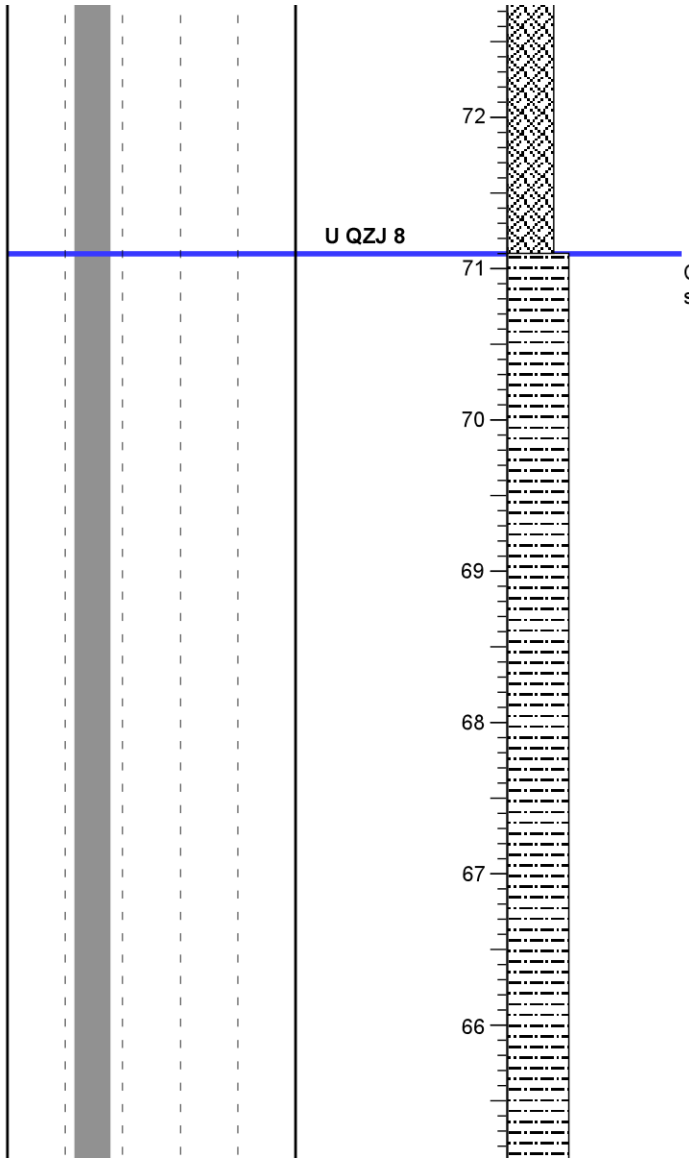

Covered to partially covered, probably silty mudstone dominant, similar to rocks below. No major sandstones, some lenses may be present. Dome dark grayish red layers are present (organic rich?).

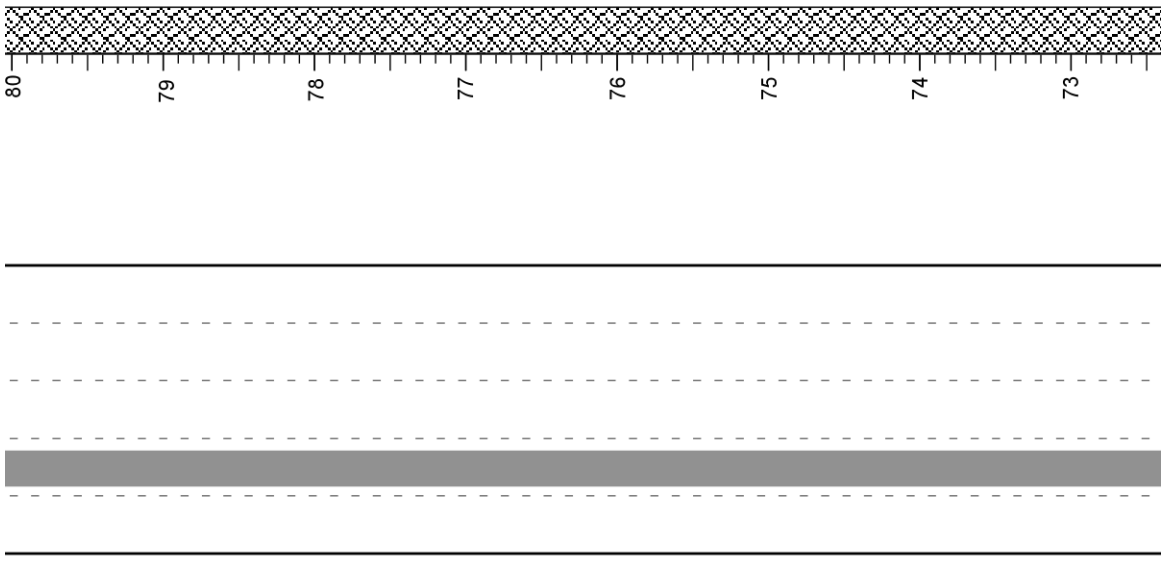
80
79
78
77
76
75
74
73

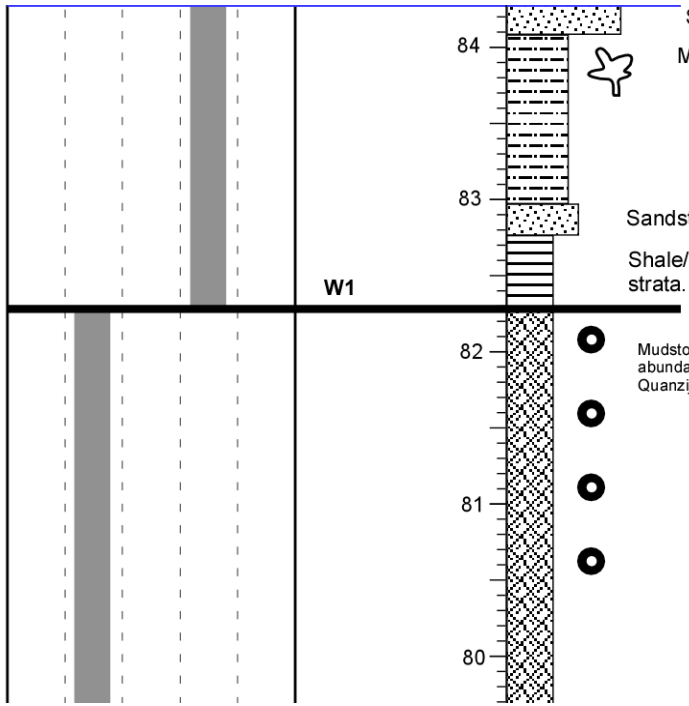

Sandstone, dark gray, c-vc lithic wacke.

Mudstone/shale, gray, silty, platy, weakly calcareous. Possible scattered plant debris.

Top of Quanzhijie Fm., as indicated by change of color from reddish purple to gay, absence of paleosols, and appearance of plant debris.

Sandstone, gray, f-vf, moderately sorted.

Shale/mudstone, purplish gray, blocky to platy. Gradational color and textural changes with the underlying strata.

Upper QZJ-Wutonggou LC boundary

Mudstone, reddish purple with lenses of dark grayish red layers. Weakly calcareous. No major sandstones. Partially covered. Common + abundant Fe-pisoids, some clay coats + slickensides. Red mudstone seen ~3 m from top. The top boundary is very close to the top of Quanzijie Fms.

North Tarlong Section

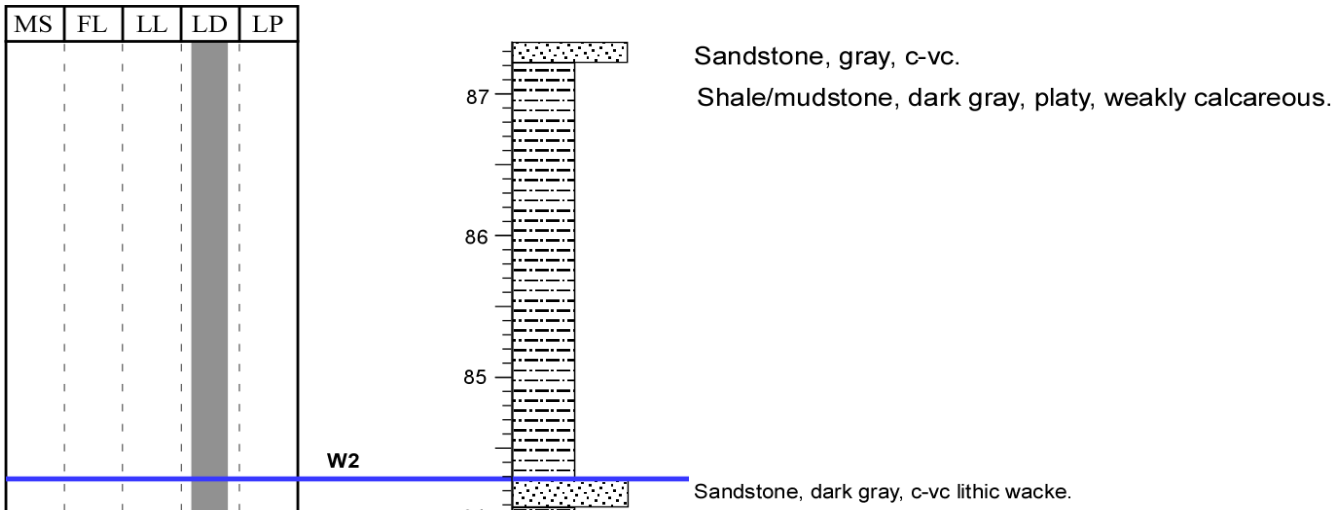

APPENDIX C
NORTH-CENTRAL TARLONG SECTION

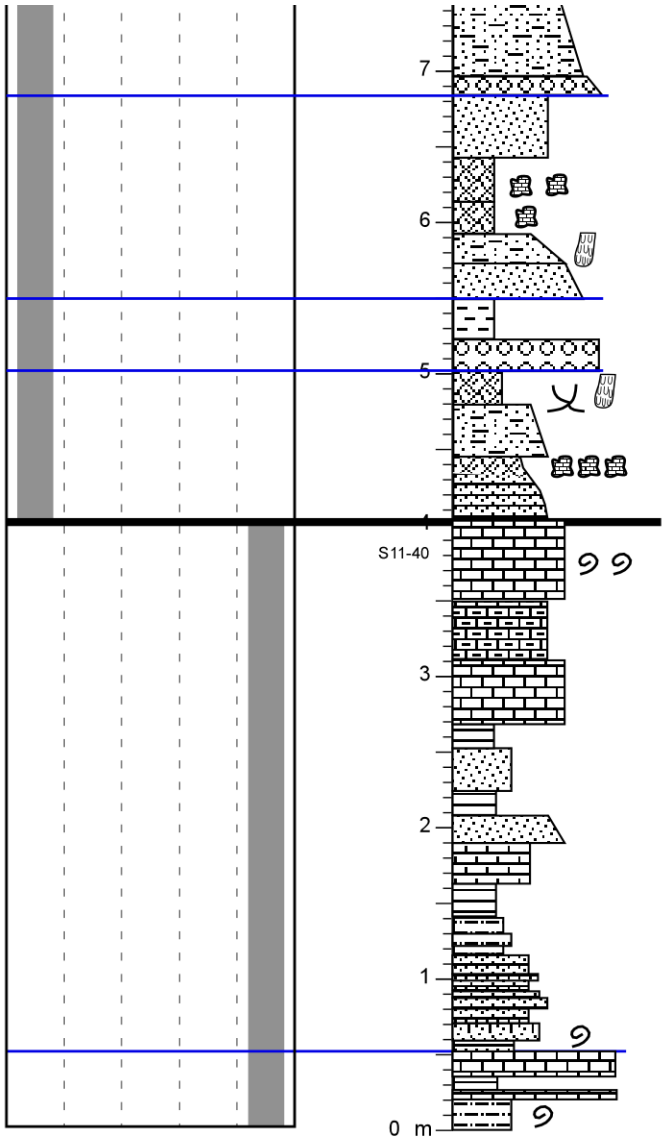

LA/LSA to LW. No grain size trend. Some parts contains granule and pebble size grains. Variegated with brown/maroon, light brown, slightly to non-calc throughout. Some parts very fissile. Sharp upper contact.

Mudstone, brown, thinly laminated in places, variably sandy and silty throughout. Calcitic nodules throughout. Sharp upper contact.

Finning upward from a gravely LA/LSA, light brown, f-vc, with granule size grains, subangular to subrounded. Upward changing to LW, brown, f-c, highly calc, subangular to subrounded. Some illuvial clays. Upward changing to vf-f sandy mudstone. Sand is rounded, calc. Upward changing to mudstone, clean, brown with calcitic nodules, scattered, rounded, gray. Gradational upper contact.

Finning upward from a conglomerate, gray, greenish gray, granule to fine pebble, subrounded to rounded. Upward changing to a mudstone, clean, with occasional floating scarce granule size grains, brown. Upward increasing in plant remains. Conglomerate is igneous dominant. Sharp upper contact.

Crudely finning upward from LSA/LW, grayish brown, f-m, subrounded to rounded, slightly calc. Upward changing to sandy mudstone, vf-f sand grains with some coarse grains. Moderately clay coated and slickensided. Some parts contains more sand than others. Sharp/erosional upper contact.

LA/LSA, crudely finning upward from a m-f, green greenish gray, olive green, well sorted and well rounded, upward changing to a vf/f LSA/LW, upward increasing in mud, brown/maroon, well sorted and rounded. Top part ~10 cm of calcitic nodules, rounded, gray, light greenish gray. Calcitic nodules are floating in the LA. Sharp upper contact.

Hongyanchi - Lower QZJ LC boundary

Limestone, gray, micritic to wackestone (15), some detrital granules. Thick-med beds, middle part, a 40 cm interval of shaly limestone. Upmost 30 cm, rich in choncostracans + sandy. No stromatolitic zone here below QZJ.

Shale, silty, dark purple, well laminated.

Siltstone, vf sandstone, thin-thick laminated, brownish gray.

Shale, silty, w-laminated, purple.

LSA, gray, very calcareous, m-c, mw sorted to well sorted, subrd to rd.

Micritic, clayey, greenish gary, platy, sandy.

Shale, purple, pure, very thinly laminated.

Lower 10 cm, LSA, light gray, very calcareous, f-m, laminated. Transgressive? Upward changing to LSA, green-gray, m-f, finning upward, siltstone, silty shale. Gradational upper contact.

Lower 20 cm, shale, platy, sandy, shell debris, dk purple. Upward changing to 5 cm of limestone, micritic. Upward changing to 10 cm of shale, thin laminated, dark purple, pure. Upward changing to 25 cm of micrite, sparse detritus, single bed, light gray. Upward changing to shale, silty, siltstone, purple, some ostracods, laminated.

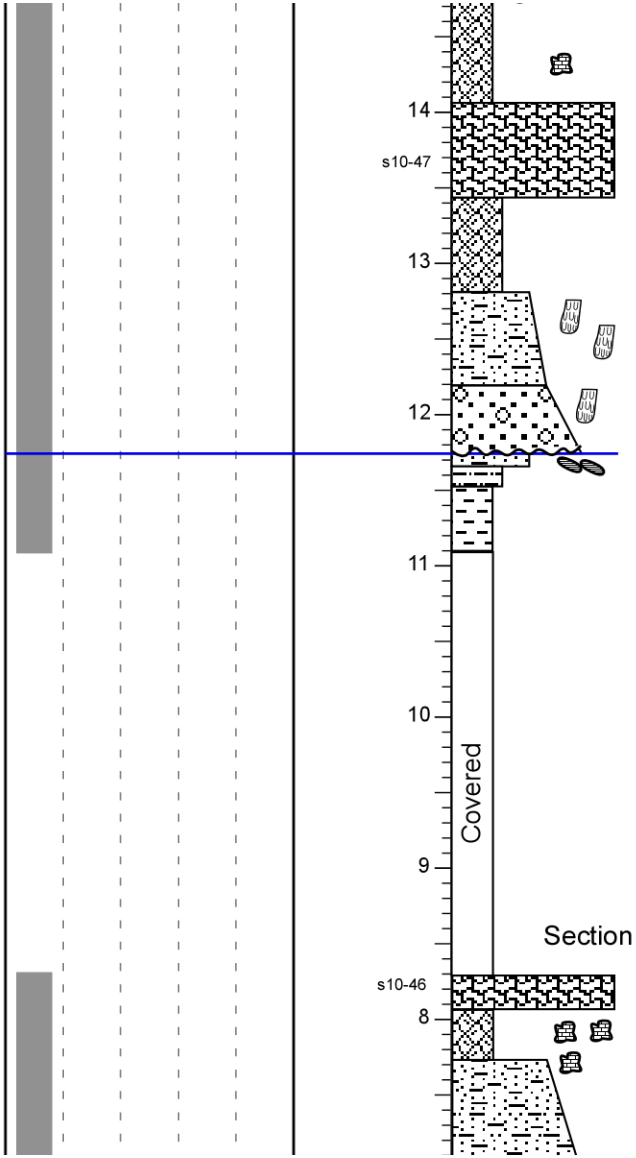

Calcrete, white light gray. Massive bed. Some seem to be rounded. Calcitic nodules? Gradational upper contact.

Conglomeratic LA/LSA, gray, dark gray, f-c/vc, with granule size, subrounded to rounded. Illuvial clays throughout. Upward changing to LW/LSA, vf-c, purplish gray, illuvial clays, subrounded to rounded, moderately sorted. Upward increasing in clay content. Sandy mudstone. Sharp upper contact.

Mudstone, brown, maroon, pure, non-calc. No other structure. Upward changing to a sandy mudstone, light brown, upward increasing in sand content, maybe LW on top. LW is f, subangular to rounded. LW contains abundant mud chips. Sharp/erosional upper contact.

Section covered for 280 cm.

Crudelly finning upward from a conglomerate, ~10 cm, granule and fine pebble, greenish gray, gray, subangular to rounded. Upward changing to LW, m-c/vc, brown, subrounded to rounded. Upward changing to sandy mudstone, brown/maroon, vf-m subangular to well rounded. Some granules floating. Upper part contains calcite nodules increasing in appearance in the last 20 cm. Rounded grains. Top most part, calcrete layer, discontinuous.

Calcrete layer seems to be weathered extremely. Dont know if this is just calcrete nodules or a bed. The section is poorly exposed. There seems to be another calcrete layer on top, consistent for about 20 m. Two layers of calcrete?

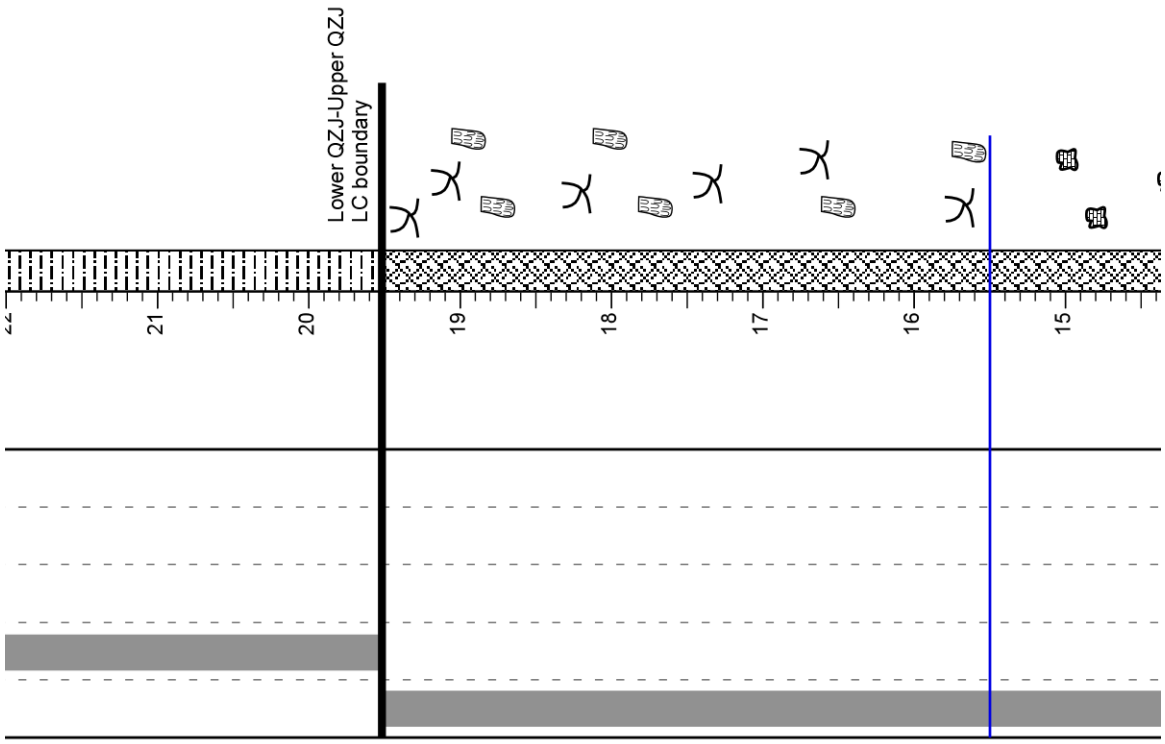
Lower QZJ-Upper QZJ
LC boundary
21
20
19
18
17
16
15

North-Central Tarlong Section

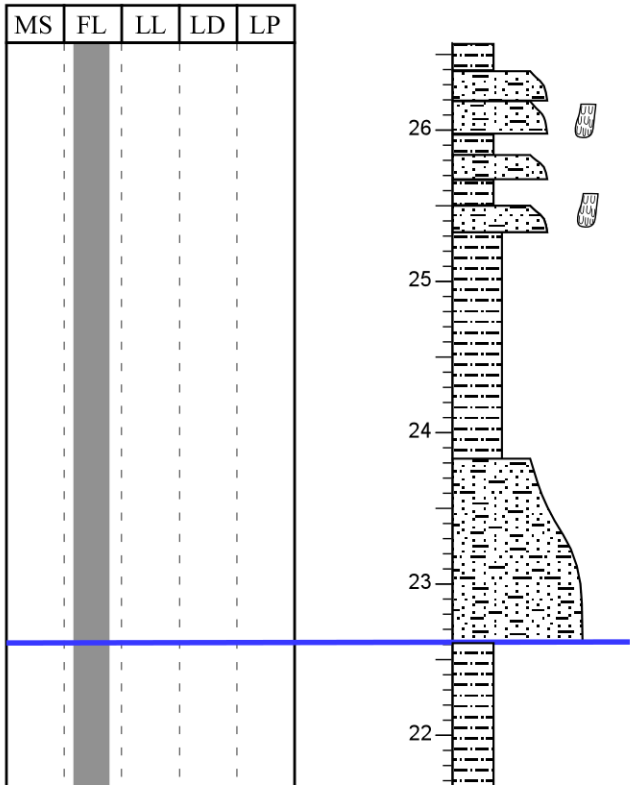

Same finning upward sequence as bellow. LA/LSA, m-c/vc on botton, upward changing to LW, f-vf, upward changing to a sandy mudstone. Covered at the top.

LA/LSA at the bottom, m-c/vc grayish maroon, brown, well sorted and rounded. Changing to a LSA/LW f/vf-m, Brown/maroon, well sorted and well rounded. Some illuvial clays. Sharp upper contact.

LW at the bottom m-f/ vf, upward changing to a sandy mudstone, cleaning upward. Sharp upper contact.

LW, f-c/vc, brown/maroon, gray. Changing to a sandy mudstone, brown, variably gray. Illuvial clays. Non-calc. Sharp upper contact.

Lower part, LW, brown/maroon, light brown, f-c/vc, subrounded to rounded. Upward changing to sandy mudstone, brown/maroon. Upward changing to mudstone, variably sandy and silty, mostly clean, brown/maroon, throughout but scattered. Sharp upper contact.

Mudstone, brown/maroon throughout, very clean. Bottom part, scattered calcite nodules, clay coating with slickensides. Middle part, increases in clay coating and slickensides, abundant. No calcite nodules. Upper part, very clean mudstone, no other structures. Monotonic. Sharp upper contact.

APPENDIX D
TAODONGGOU SECTION

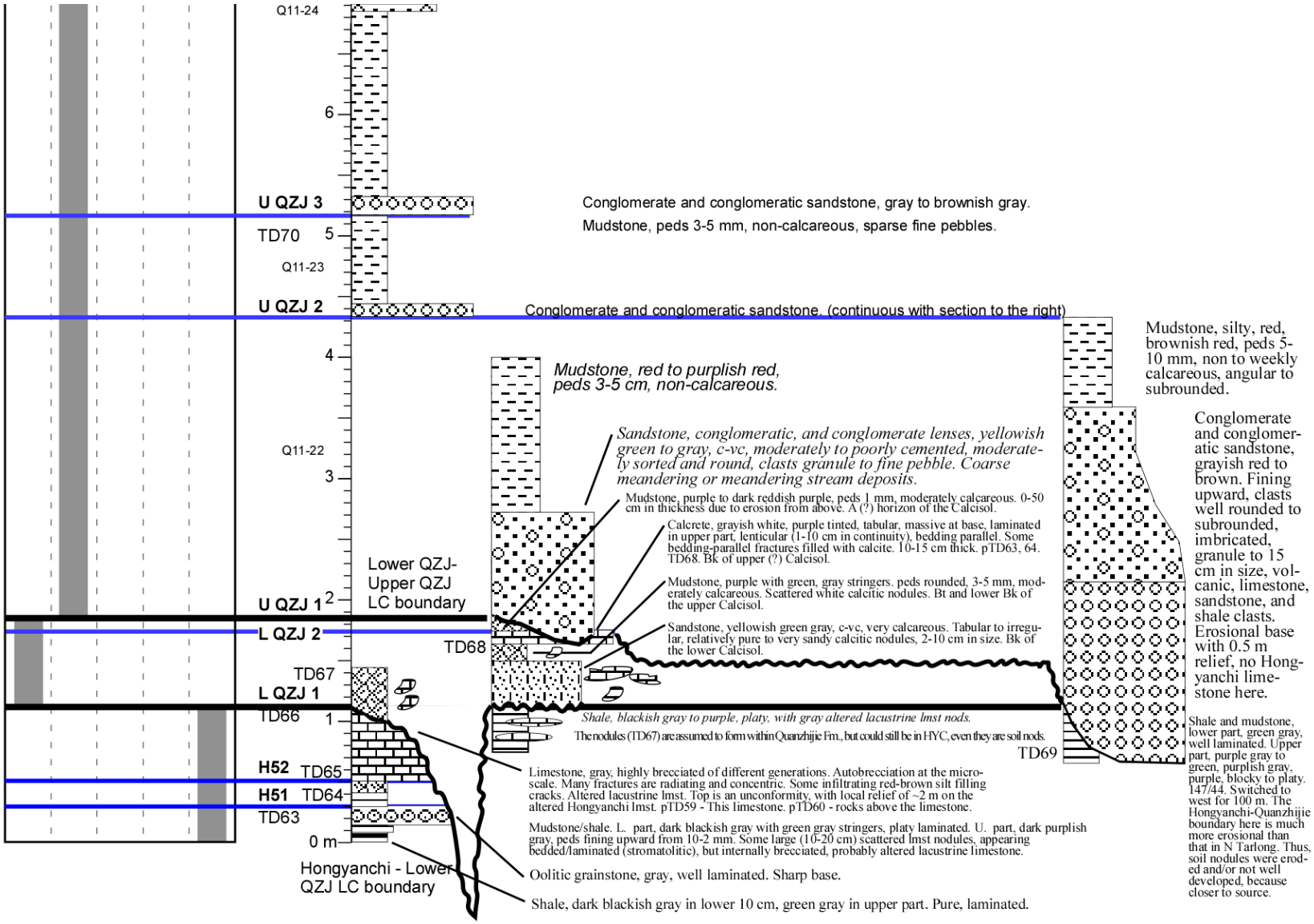
Q11-24
6
U QZJ 3
TD70
5
Q11-23
U QZJ 2
4
Q11-22
3
Lower QZJ-
Upper QZJ
LC boundary
U QZJ 1
2
L QZJ 2
TD68
TD67
L QZJ 1
TD66
1
H52
TD65
H51
TD64
TD63
0 m
Hongyanchi - Lower
QZJ LC boundary
Conglomerate and conglomeratic sandstone, gray to brownish gray.
Mudstone, peds 3-5 mm, non-calcareous, sparse fine pebbles.
Conglomerate and conglomeratic sandstone. (continuous with section to the right)
Mudstone, red to purplish red,
peds 3-5 cm, non-calcareous.
Sandstone, conglomeratic, and conglomerate lenses, yellowish green to gray, c-vc, moderately to poorly cemented, moderately sorted and round, clasts granule to fine pebble. Coarse meandering or meandering stream deposits.
Mudstone, purple to dark reddish purple, peds 1 mm, moderately calcareous. 0-50 cm in thickness due to erosion from above. A (?) horizon of the Calcisol.
Calcrete, grayish white, purple tinted, tabular, massive at base, laminated in upper part, lenticular (1-10 cm in continuity), bedding parallel. Some bedding-parallel fractures filled with calcite. 10-15 cm thick. pTD63, 64. TD68. Bk of upper (?) Calcisol.
Mudstone, purple with green, gray stringers. peds rounded, 3-5 mm, moderately calcareous. Scattered white calcitic nodules. Bt and lower Bk of the upper Calcisol.
Sandstone, yellowish green gray, c-vc, very calcareous. Tabular to irregular, relatively pure to very sandy calcitic nodules, 2-10 cm in size. Bk of the lower Calcisol.
Shale, blackish gray to purple, platy, with gray altered lacustrine lmst nods.
The nodules (TD67) are assumed to form within Quanzhijie Fm., but could still be in HYC, even they are soil nods.
TD69
Limestone, gray, highly brecciated of different generations. Autobrecciation at the micro-scale. Many fractures are radiating and concentric. Some infiltrating red-brown silt filling cracks. Altered lacustrine lmst. Top is an unconformity, with local relief of ~2 m on the altered Hongyanchi lmst. pTD59 - This limestone. pTD60 - rocks above the limestone.
Mudstone/shale. L. part, dark blackish gray with green gray stringers, platy laminated. U. part, dark purplish gray, peds fining upward from 10-2 mm. Some large (10-20 cm) scattered lmst nodules, appearing bedded/laminated (stromatolitic), but internally brecciated, probably altered lacustrine limestone.
Oolitic grainstone, gray, well laminated. Sharp base.
Shale, dark blackish gray in lower 10 cm, green gray in upper part. Pure, laminated.
Mudstone, silty, red, brownish red, peds 5-10 mm, non to weekly calcareous, angular to subrounded.
Conglomerate and conglomeratic sandstone, grayish red to brown. Fining upward, clasts well rounded to subrounded, imbricated, granule to 15 cm in size, volcanic, limestone, sandstone, and shale clasts. Erosional base with 0.5 m relief, no Hongyanchi limestone here.
Shale and mudstone, lower part, green gray, well laminated. Upper part, purple gray to green, purplish gray, purple, blocky to platy. 147/44. Switched to west for 100 m. The Hongyanchi-Quanzhijie boundary here is much more erosional than that in N Tarlong. Thus, soil nodules were eroded and/or not well developed, because closer to source.

14
13
Q11-28
12
11
Q11-27
10
Q11-26
9
8
Q11-25
7
Q11-24

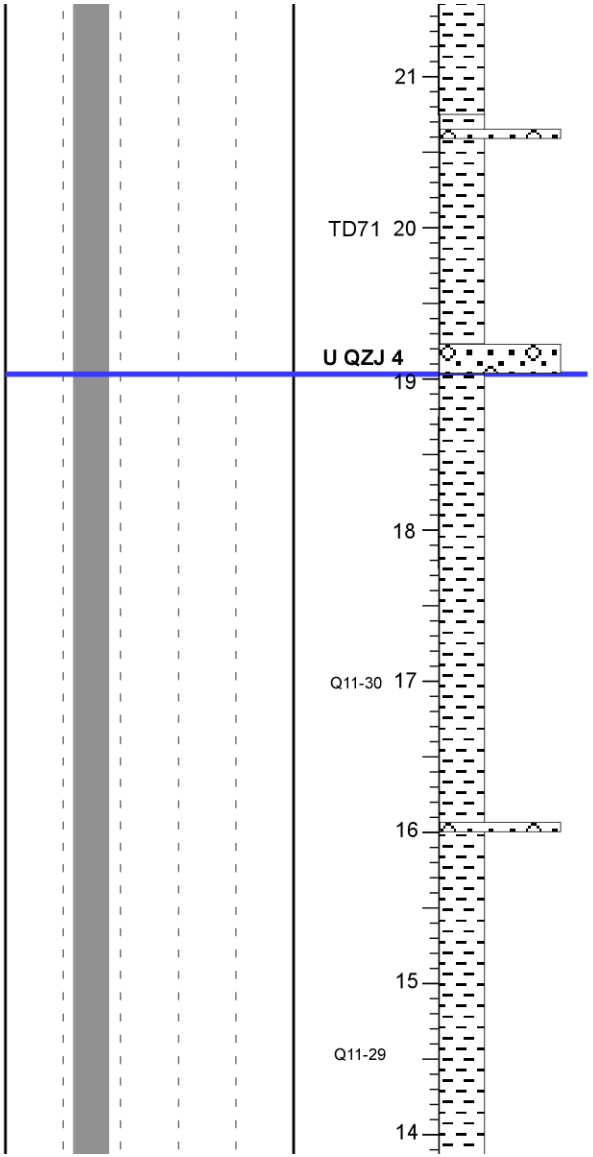

Mudstone, similar to below.

Conglomeratic sandstone, gray, poorly sorted.

Mudstone, purplish red, peds 1-3 mm, subrounded to rounded. Very few stringers (<10 cm) conglomeratic sandstone. Fine-ped soil intervals intercalated with shitly shale and sparse f lithic wackes. Weekly to no-calcareous.

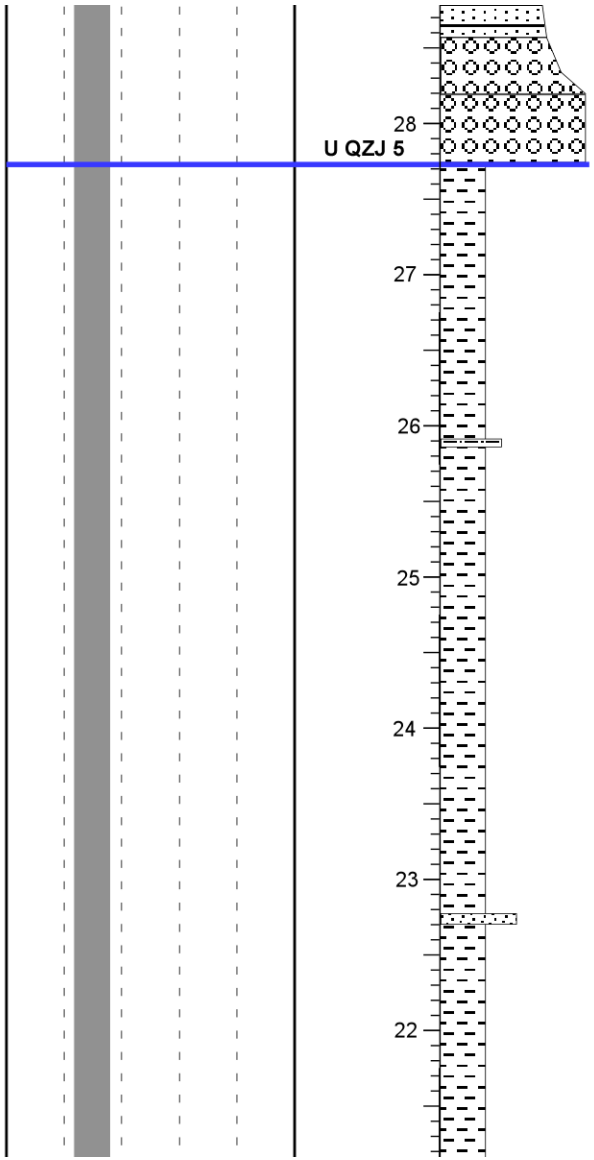

Conglomerate and conglomeratic sandstone, c-vc, poorly sorted, clasts subrounded to rounded, including sandstone and volcanic clasts,
max. 5 cm.

Mudstone, similar to below. Sharp top.

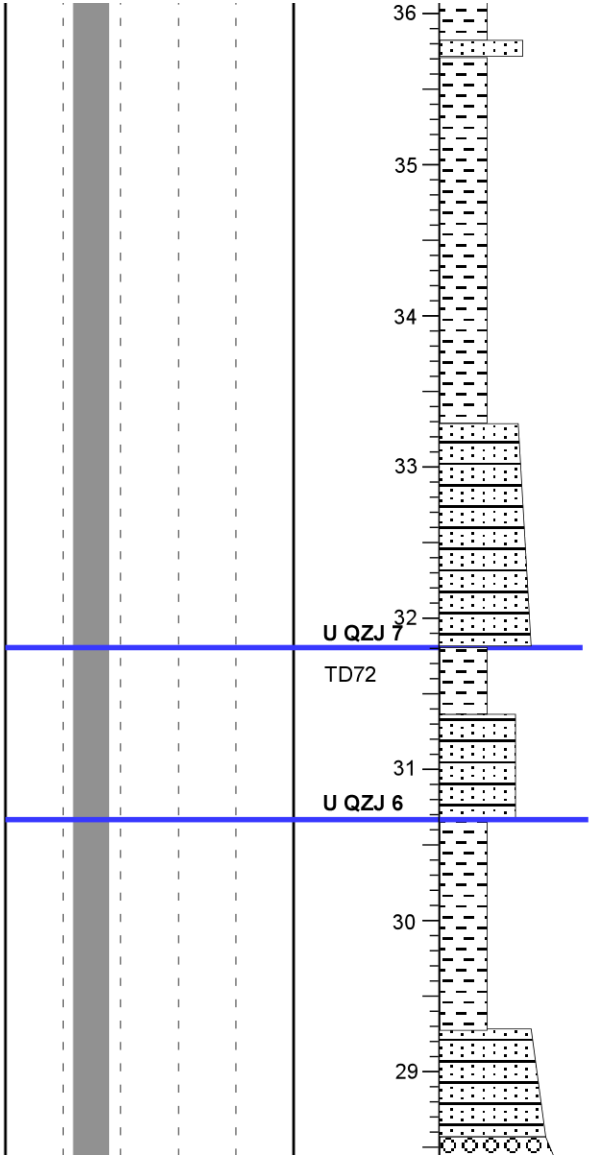

Mudstone, fine peds.

Sandstone, grayish brown to red, fining upward from m to f, lithic wacke to subarenite. Sharp base, gradational top.

Mudstone/shale, platy, peds 5-10 mm.

Sandstone, grayish purple, f, lithic subarenite, well sorted.

Mudstone, peds sub mm to 2 mm, rounded, non to weekly calcareous.

Sandstone, purple red, m-vc, poorly sorted, lithic wacke.

Conglomerate and conglomeratic sandstone, c-vc, poorly sorted, clasts subrounded to rounded, including

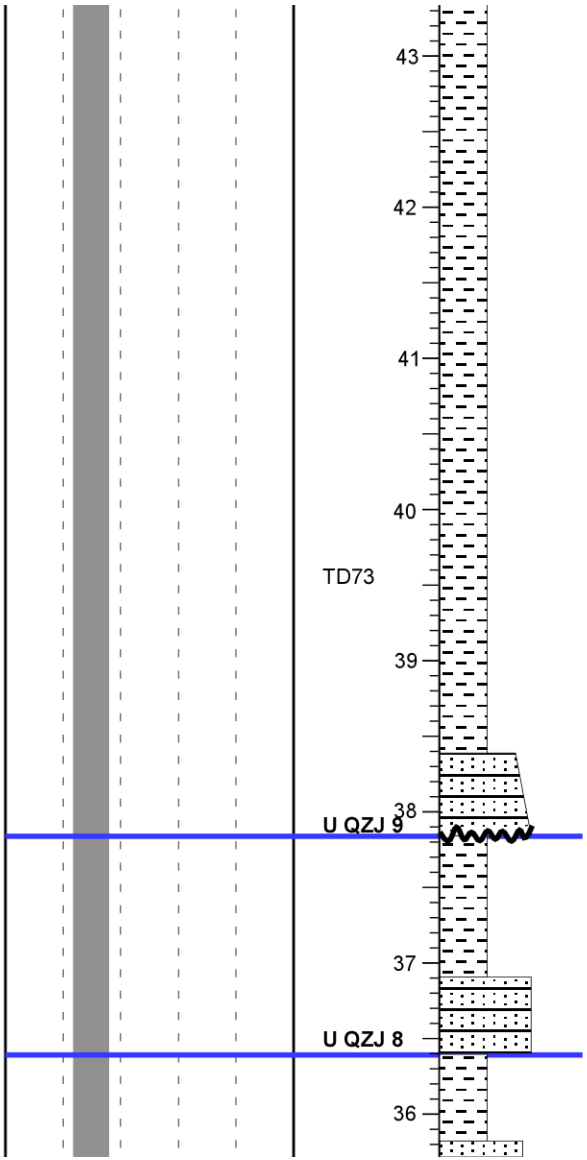

Sandstone, pale bluish gray to brown, m-f.

Mudstone, fine peds. Gradational base, sharp to erosional top.

Sandstone, pale bluish gray to brown, moderately calcareous, m-f.

Lower 15 cm, f-m lithic wacke. Upper part mudstone, vf peds (<1 mm). Sharp base and top.

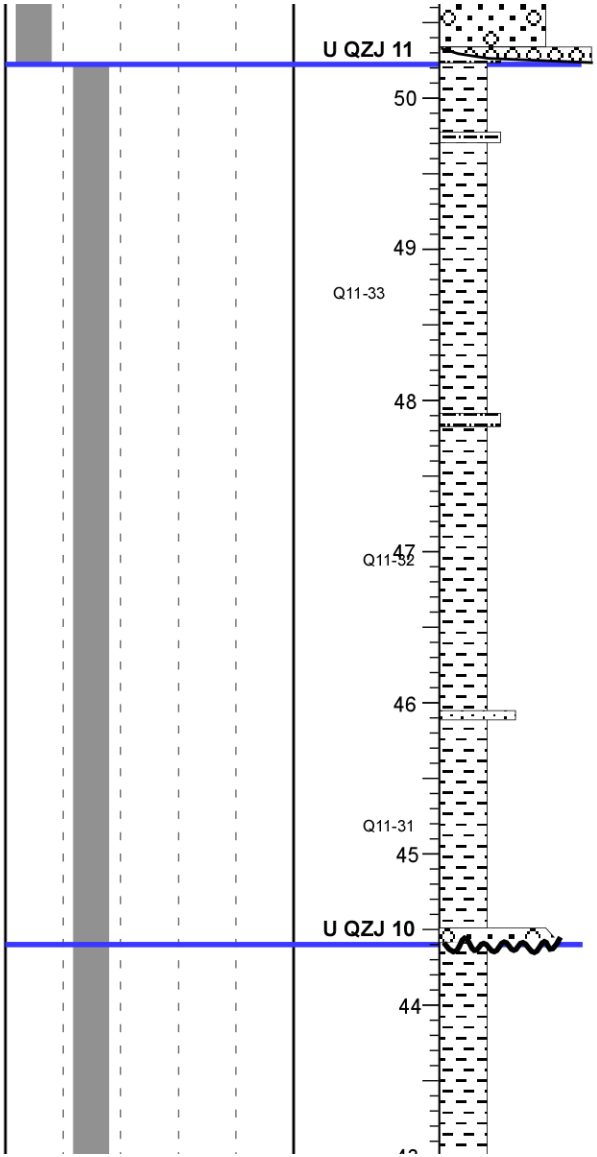

Conglomerate and conglomeratic sandstone, volcanic clasts, 10 cm max. Platy silty shale laterally.

Mudstone, dark brownish red, greenish red, variegated, with f sandstone and silty shale stringers, peds f-c, weekly to non-calcareous.

Conglomeratic sandstone and sandstone, fining upward from c-vc, 5 cm max. clasts. Erosional/sharp base, gradational top. This is the edge of a laterally very thick channel fill.

Mudstone, purplish red, thick (1-2 m) intervals of paleosols with well rounded, fine peds interbedded with thin (10s cm) intervals of paleosols with coarse (1-5 mm), subrounded peds.

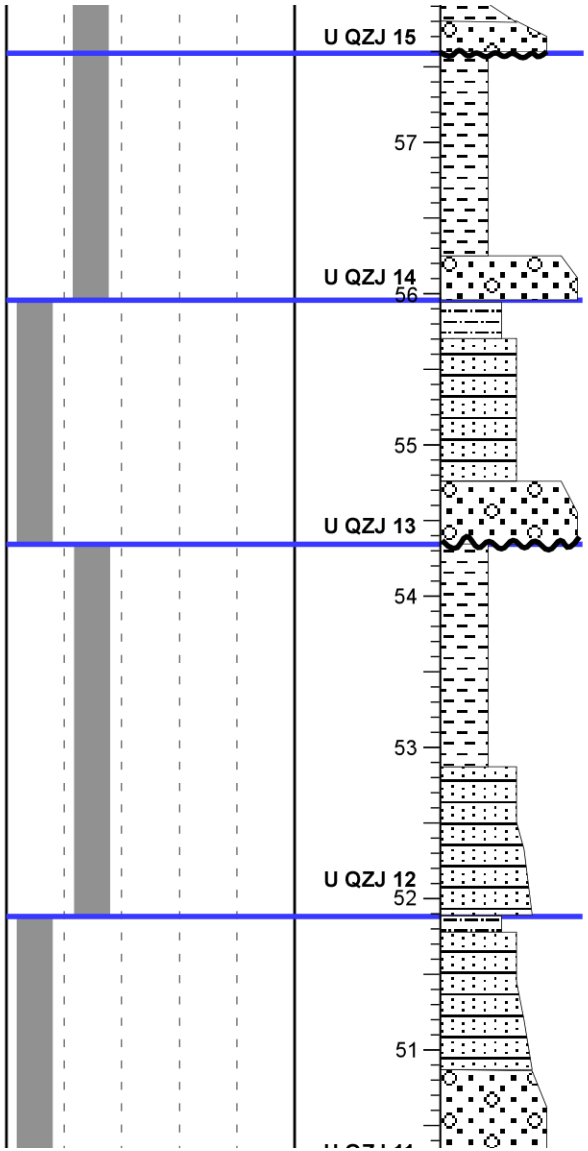

Mudstone, c-m-f peds. Less paleosols than in Tarlong section, closer to the source area, faster/more frequent sedimentation.

Sandstone, f, to silty shale. No soil. Overall fining upward.

Conglomerate and conglomeratic sandstone, clasts 10 cm max.

Mudstone, coarse peds.

Sandstone, reddish gray to dark reddish purple, fining upward from m-f. Sharp base, gradational top.

Conglomeratic sandstone, sandstone, silty shale. Fining upward from c to f. No soil in this cycle. Braided stream or coarse meandering stream.

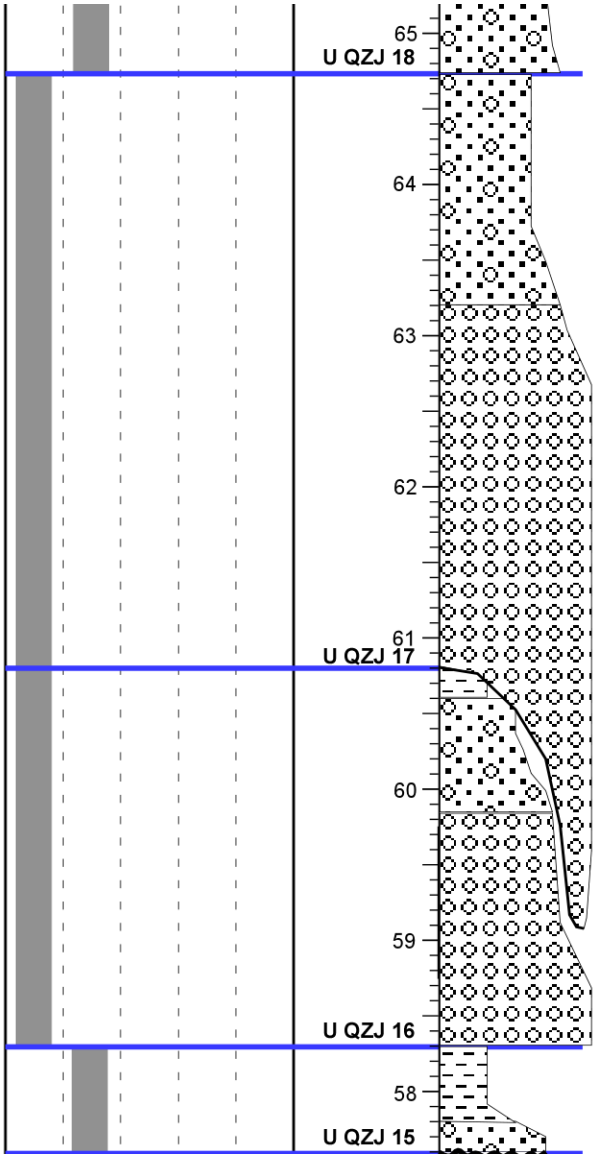

Conglomerate and conglomeratic sandstone, grayish brown, conglomerate dominant, clasts 10 cm max., volcanic dominant, limestone, sandstone clasts. Basal part 50 cm probably coarsening upward. Overall fining upward. Basal surface erosional with 1-2 m relief.

Conglomeratic sandstone, fining upward into m-f sandstone, silty shale, and coarse paleosol. Upper 20 cm mudstone, dark brownish red, peds coarse, angular to subrounded, weekly to non-calcareous.

Conglomerate, 25 cm max. clasts, volcanic, red sandstone (like those in Hongyanchi Fm.), rounded. Fining upward. Sharp base.

Conglomeratic sandstone in lower part, reddish brown, m-c, granular, Wacke. Gradational to the upper part, paleosol with m (2-5 mm) peds.

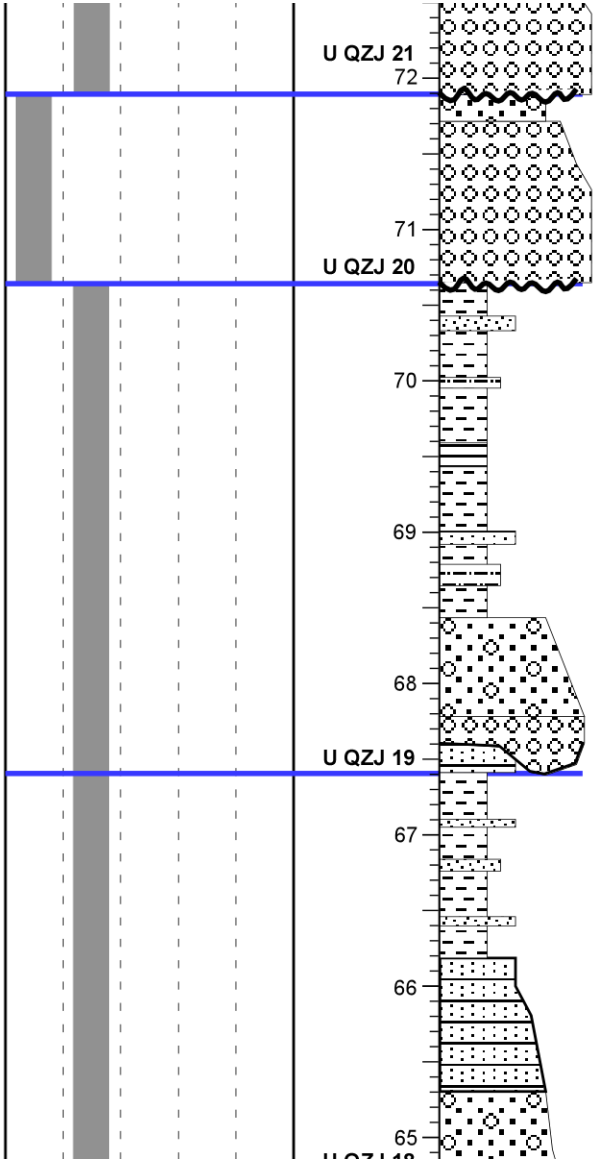

Conglomerate dominant, grayish brown, conglomeratic sandstone in uppermost part, granule to fine pebble clasts. Fining upward trend.

Shale, silty shale, and mudstone, f sandstone, purplish red, peds m-c. A mud plug, suggesting meandering stream environment. Sharp base.

Conglomerate and conglomeratic sandstone, brownish gray, granule to fine pebble clasts. Conglomeratic sandstone dominant. Clasts 5 cm max. Basal 20 cm f wacke, purplish red to gray.

Mudstone, peds m-f, interbedded with f sandstone and silty mudstone.

Sandstone, dark brownish red to purple, fining upward from conglomeratic sandstone, c-vc to f sandstone, wacke-subarenite. Most channel-fill conglomerates in this interval extend 10-50 m laterally. Coarse meandering streams.

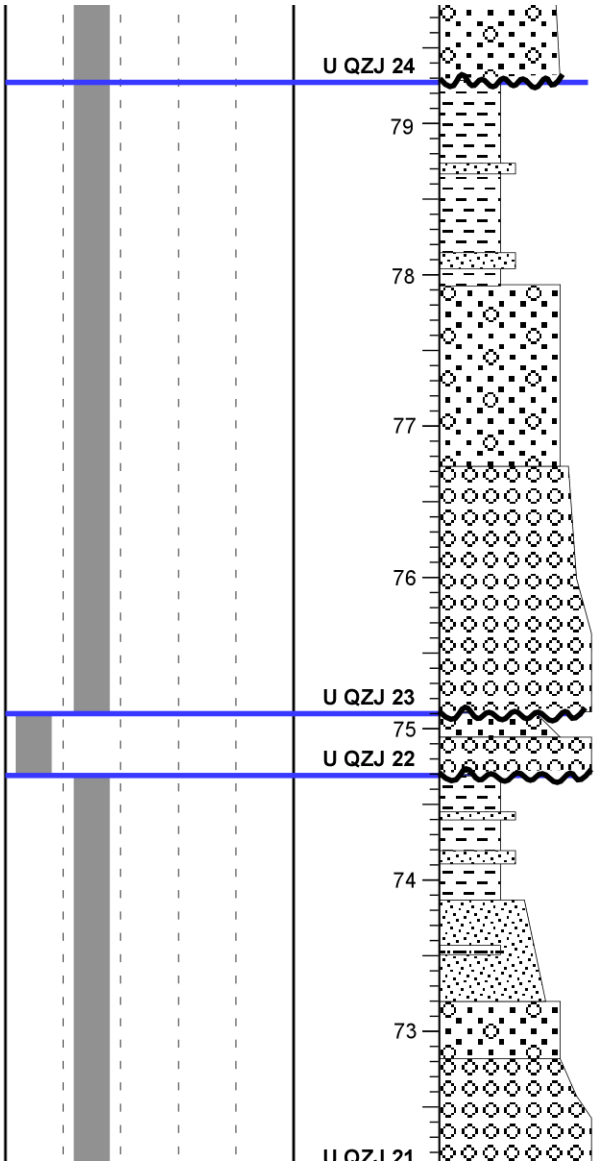

Mudstone, silty and sandy, some f sandstone, purplish red. Peds f-m.

Conglomeratic sandstone, greenish gray. Common greenish gray shale clasts (HYC) and volcanic clasts. Gradational base and top.

Conglomerate, brownish gray to grayish brown, 10 cm max. clast size. Fining upward. Gradational top.

Conglomerate and conglomeratic sandstone, brownish gray, granule to fine pebble clasts. Fining upward.

Mudstone, silty and f sandstone, peds m-c. Gradational base, erosional top.

Sandstone, purplish red, peds c, stringers of silty shale and coarse wacke. Overall fining upward, gradational base.

Conglomerate and conglomeratic sandstone, brownish gray, clasts 15 cm max., fining upward into conglomeratic sandstone. Some limestone and red sandstone, and conglomerate (HYC) clasts.

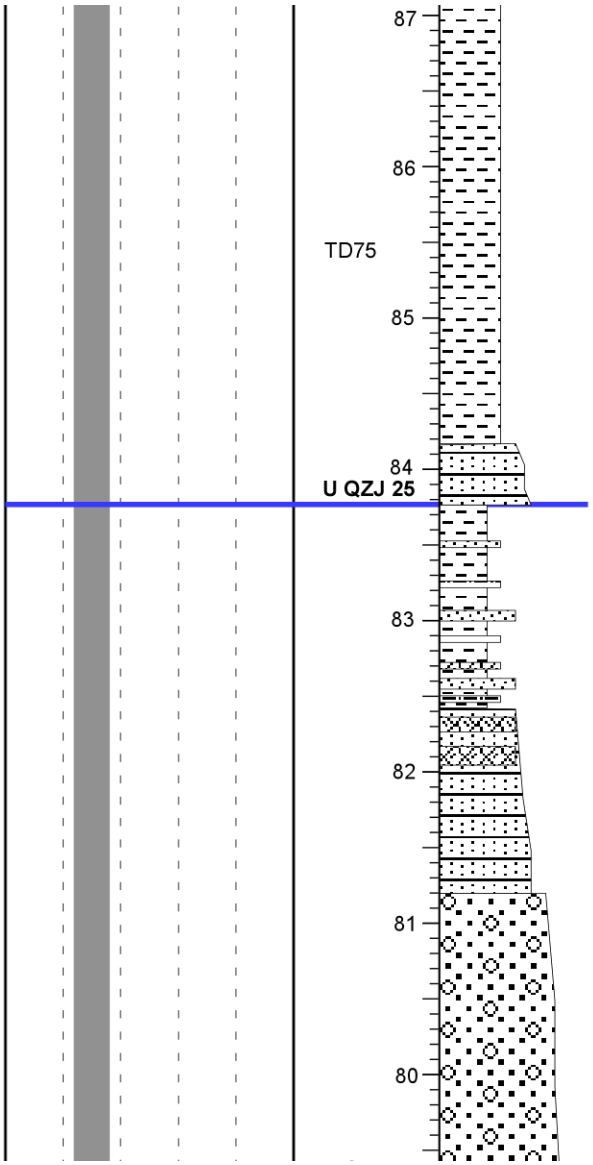

Sandstone, grayish purple, m-f, slightly conglomeratic with granules. Sharp base, gradational top.

Mudstone, siltstone, f sandstone, grayish brown to purple, platy to c peds, non-calcareous. Intercalated with siltstone and shale.

Sandstone, dark purplish gray, m-f, lithic wacke, platy to c peds. Gradational base.

Sandstone, brownish gray, c-vc, granule to fine pebble clasts.

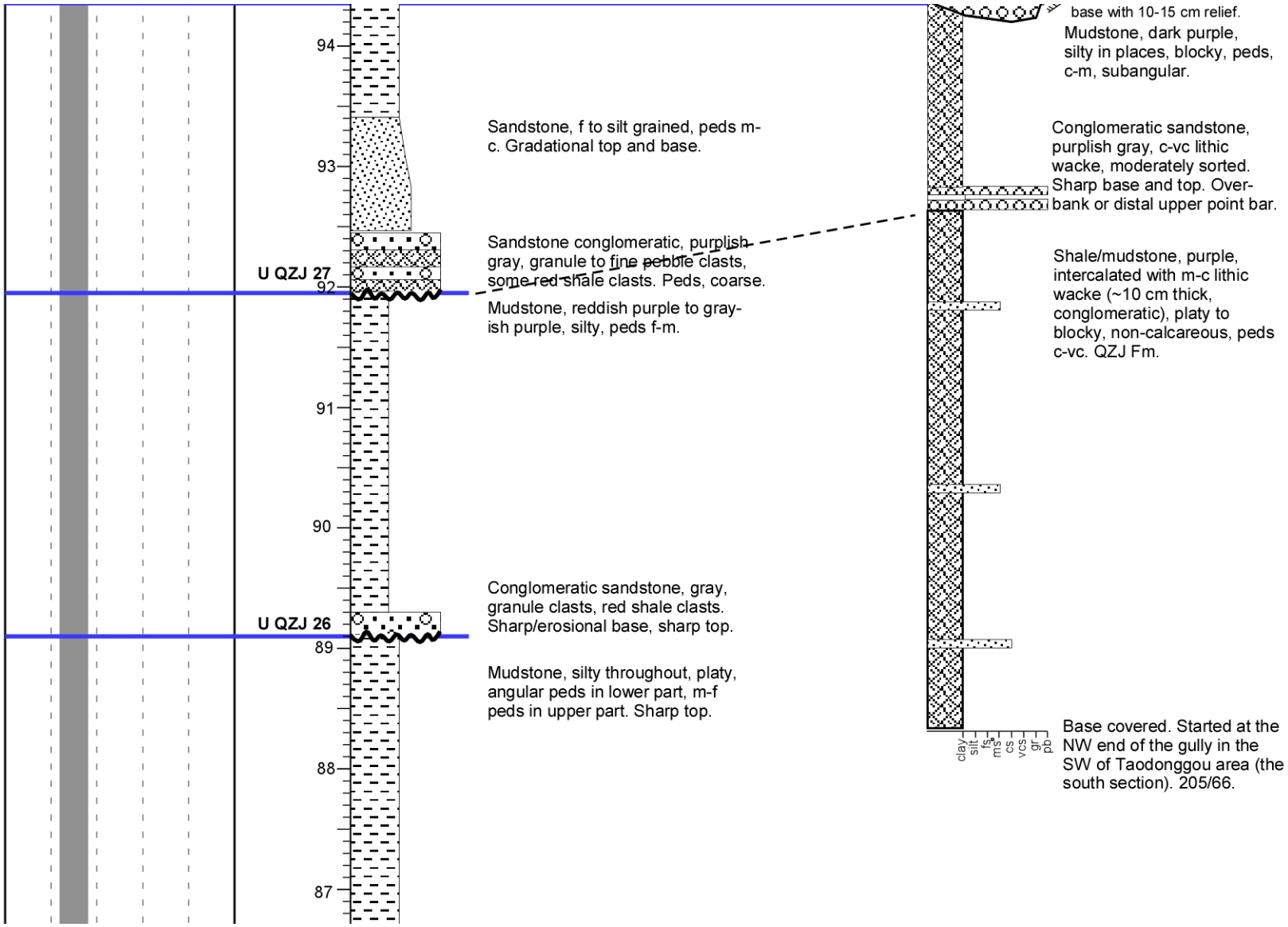
94
93
92
91
90
89
88
87
U QZJ 27
U QZJ 26
Sandstone, f to silt grained, peds m-c. Gradational top and base.
Sandstone conglomeratic, purplish gray, granule to fine pebble clasts, some red shale clasts. Peds, coarse.
Mudstone, reddish purple to gray-ish purple, silty, peds f-m.
Conglomeratic sandstone, gray, granule clasts, red shale clasts. Sharp/erosional base, sharp top.
Mudstone, silty throughout, platy, angular peds in lower part, m-f peds in upper part. Sharp top.
base with 10-15 cm relief.
Mudstone, dark purple, silty in places, blocky, peds, c-m, subangular.
Conglomeratic sandstone, purplish gray, c-vc lithic wacke, moderately sorted. Sharp base and top. Over-bank or distal upper point bar.
Shale/mudstone, purple, intercalated with m-c lithic wacke (~10 cm thick, conglomeratic), platy to blocky, non-calcareous, peds c-vc. QZJ Fm.
clay
silt
fs
ms
cs
vcs
gr
pb
Base covered. Started at the NW end of the gully in the SW of Taodonggou area (the south section). 205/66.

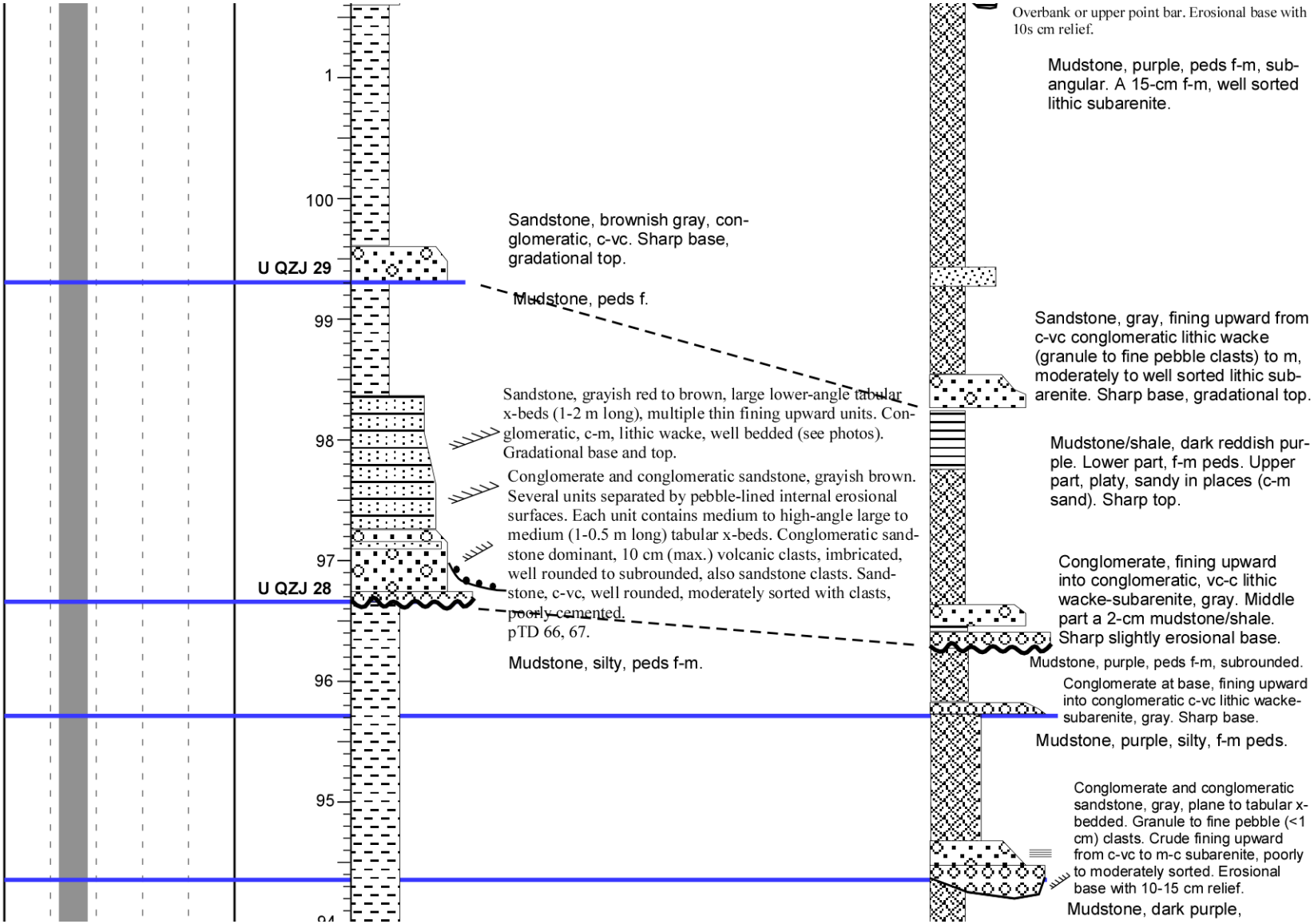
1
100
99
98
97
96
95
U QZJ 29
U QZJ 28
Sandstone, brownish gray, conglomeratic, c-vc. Sharp base, gradational top.
Mudstone, peds f.
Sandstone, grayish red to brown, large lower-angle tabular x-beds (1-2 m long), multiple thin fining upward units. Conglomeratic, c-m, lithic wacke, well bedded (see photos). Gradational base and top.
Conglomerate and conglomeratic sandstone, grayish brown. Several units separated by pebble-lined internal erosional surfaces. Each unit contains medium to high-angle large to medium (1-0.5 m long) tabular x-beds. Conglomeratic sandstone dominant, 10 cm (max.) volcanic clasts, imbricated, well rounded to subrounded, also sandstone clasts. Sandstone, c-vc, well rounded, moderately sorted with clasts, poorly-cemented.
pTD 66, 67.
Mudstone, silty, peds f-m.
Overbank or upper point bar. Erosional base with 10s cm relief.
Mudstone, purple, peds f-m, subangular. A 15-cm f-m, well sorted lithic subarenite.
Sandstone, gray, fining upward from c-vc conglomeratic lithic wacke (granule to fine pebble clasts) to m, moderately to well sorted lithic subarenite. Sharp base, gradational top.
Mudstone/shale, dark reddish purple. Lower part, f-m peds. Upper part, platy, sandy in places (c-m sand). Sharp top.
Conglomerate, fining upward into conglomeratic, vc-c lithic wacke-subarenite, gray. Middle part a 2-cm mudstone/shale. Sharp slightly erosional base.
Mudstone, purple, peds f-m, subrounded.
Conglomerate at base, fining upward into conglomeratic c-vc lithic wacke-subarenite, gray. Sharp base.
Mudstone, purple, silty, f-m peds.
Conglomerate and conglomeratic sandstone, gray, plane to tabular x-bedded. Granule to fine pebble (<1 cm) clasts. Crude fining upward from c-vc to m-c subarenite, poorly to moderately sorted. Erosional base with 10-15 cm relief.
Mudstone, dark purple,

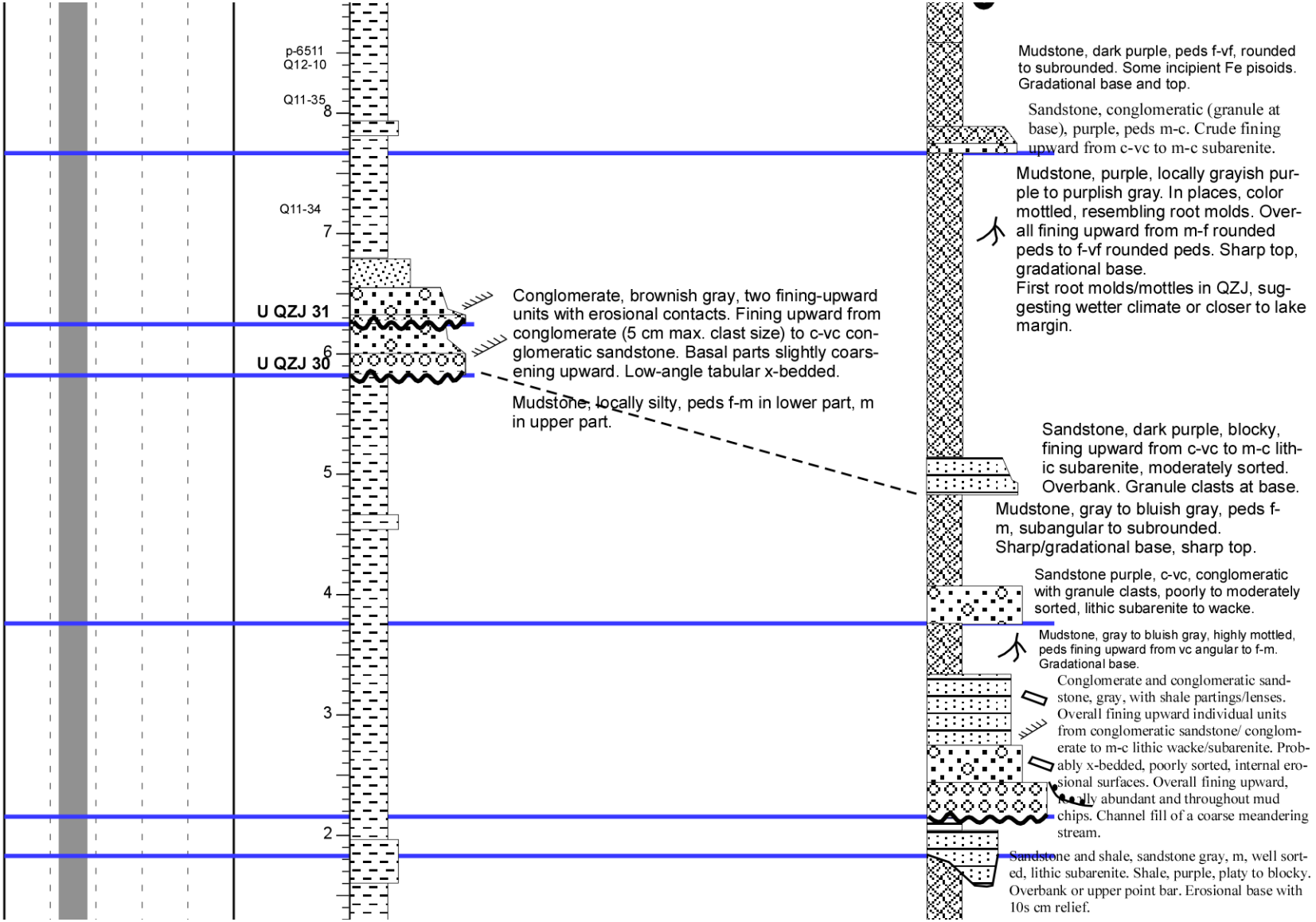
p-6511
Q12-10
Q11-35
8
Q11-34
7
U QZJ 31
6
U QZJ 30
5
4
3
2
Conglomerate, brownish gray, two fining-upward units with erosional contacts. Fining upward from conglomerate (5 cm max. clast size) to c-vc conglomeratic sandstone. Basal parts slightly coarsening upward. Low-angle tabular x-bedded.
Mudstone, locally silty, peds f-m in lower part, m in upper part.
Mudstone, dark purple, peds f-vf, rounded to subrounded. Some incipient Fe pisoids. Gradational base and top.
Sandstone, conglomeratic (granule at base), purple, peds m-c. Crude fining upward from c-vc to m-c subarenite.
Mudstone, purple, locally grayish purple to purplish gray. In places, color mottled, resembling root molds. Overall fining upward from m-f rounded peds to f-vf rounded peds. Sharp top, gradational base.
First root molds/mottles in QZJ, suggesting wetter climate or closer to lake margin.
Sandstone, dark purple, blocky, fining upward from c-vc to m-c lithic subarenite, moderately sorted. Overbank. Granule clasts at base.
Mudstone, gray to bluish gray, peds f-m, subangular to subrounded. Sharp/gradational base, sharp top.
Sandstone purple, c-vc, conglomeratic with granule clasts, poorly to moderately sorted, lithic subarenite to wacke.
Mudstone, gray to bluish gray, highly mottled, peds fining upward from vc angular to f-m. Gradational base.
Conglomerate and conglomeratic sandstone, gray, with shale partings/lenses. Overall fining upward individual units from conglomeratic sandstone/ conglomerate to m-c lithic wacke/subarenite. Probably x-bedded, poorly sorted, internal erosional surfaces. Overall fining upward, locally abundant and throughout mud chips. Channel fill of a coarse meandering stream.
Sandstone and shale, sandstone gray, m, well sorted, lithic subarenite. Shale, purple, platy to blocky. Overbank or upper point bar. Erosional base with 10s cm relief.

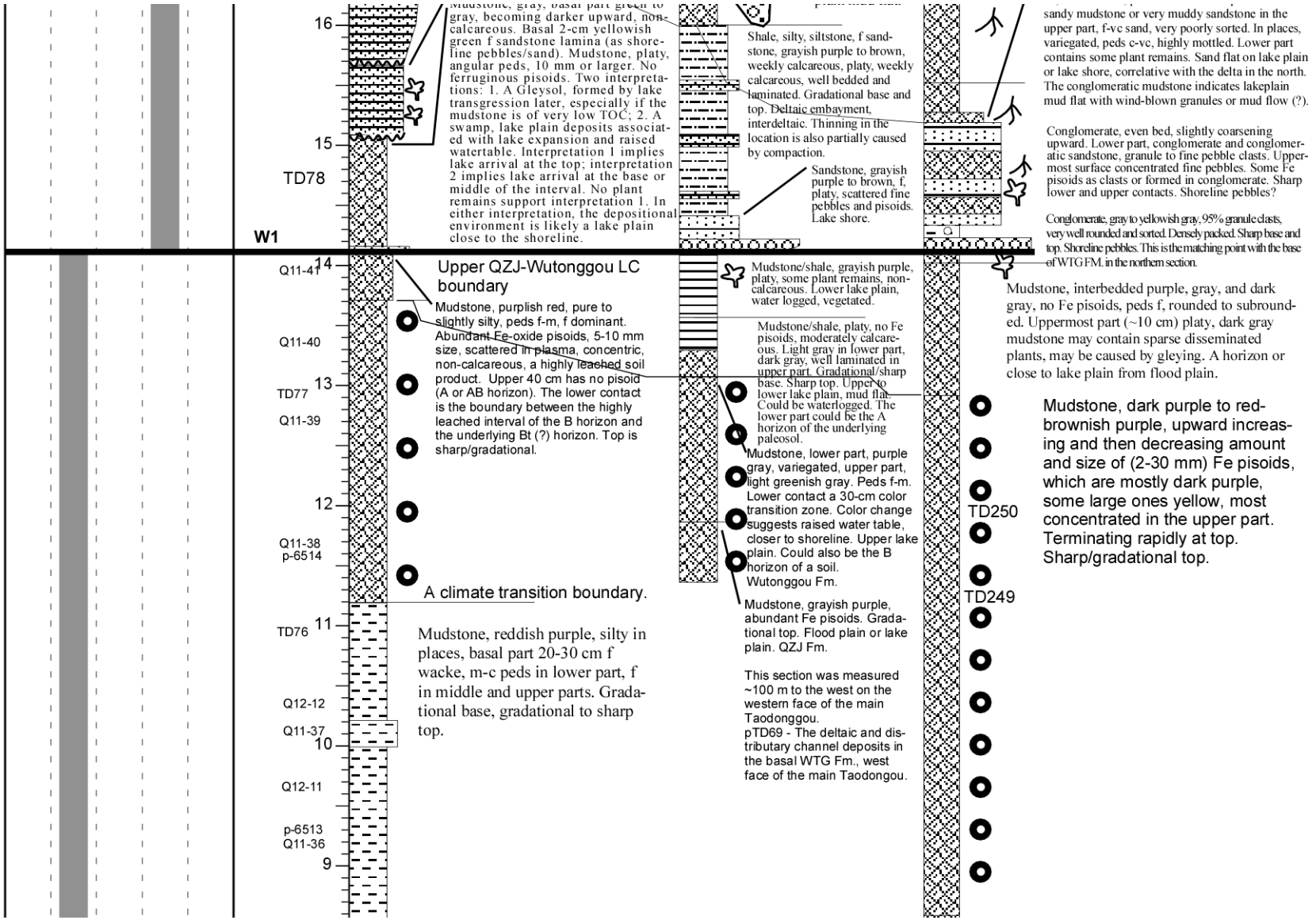
16
15
TD78
W1
14
Q11-41
Q11-40
13
TD77
Q11-39
12
Q11-38
p-6514
11
TD76
Q12-12
Q11-37
10
Q12-11
p-6513
Q11-36
9
Mudstone, gray, basal part green to gray, becoming darker upward, non-calcareous. Basal 2-cm yellowish green f sandstone lamina (as shoreline pebbles/sand). Mudstone, platy, angular peds, 10 mm or larger. No ferruginous pisoids. Two interpretations: 1. A Gleysol, formed by lake transgression later, especially if the mudstone is of very low TOC; 2. A swamp, lake plain deposits associated with lake expansion and raised watertable. Interpretation 1 implies lake arrival at the top; interpretation 2 implies lake arrival at the base or middle of the interval. No plant remains support interpretation 1. In either interpretation, the depositional environment is likely a lake plain close to the shoreline.
Upper QZJ-Wutonggou LC boundary
Mudstone, purplish red, pure to slightly silty, peds f-m, f dominant. Abundant Fe-oxide pisoids, 5-10 mm size, scattered in plasma, concentric, non-calcareous, a highly leached soil product. Upper 40 cm has no pisoid (A or AB horizon). The lower contact is the boundary between the highly leached interval of the B horizon and the underlying Bt (?) horizon. Top is sharp/gradational.
A climate transition boundary.
Mudstone, reddish purple, silty in places, basal part 20-30 cm f wacke, m-c peds in lower part, f in middle and upper parts. Gradational base, gradational to sharp top.
Shale, silty, siltstone, f sandstone, grayish purple to brown, weekly calcareous, platy, weekly calcareous, well bedded and laminated. Gradational base and top. Deltaic embayment, interdeltaic. Thinning in the location is also partially caused by compaction.
Sandstone, grayish purple to brown, f, platy, scattered fine pebbles and pisoids. Lake shore.
Mudstone/shale, grayish purple, platy, some plant remains, non-calcareous. Lower lake plain, water logged, vegetated.
Mudstone/shale, platy, no Fe pisoids, moderately calcareous. Light gray in lower part, dark gray, well laminated in upper part. Gradational/sharp base. Sharp top. Upper to lower lake plain, mud flat. Could be waterlogged. The lower part could be the A horizon of the underlying paleosol.
Mudstone, lower part, purple gray, variegated, upper part, light greenish gray. Peds f-m. Lower contact a 30-cm color transition zone. Color change suggests raised water table, closer to shoreline. Upper lake plain. Could also be the B horizon of a soil. Wutonggou Fm.
Mudstone, grayish purple, abundant Fe pisoids. Gradational top. Flood plain or lake plain. QZJ Fm.
This section was measured ~100 m to the west on the western face of the main Taodonggou.
pTD69 - The deltaic and distributary channel deposits in the basal WTG Fm., west face of the main Taodongou.
sandy mudstone or very muddy sandstone in the upper part, f-vc sand, very poorly sorted. In places, variegated, peds c-vc, highly mottled. Lower part contains some plant remains. Sand flat on lake plain or lake shore, correlative with the delta in the north. The conglomeratic mudstone indicates lakeplain mud flat with wind-blown granules or mud flow (?).
Conglomerate, even bed, slightly coarsening upward. Lower part, conglomerate and conglomeratic sandstone, granule to fine pebble clasts. Uppermost surface concentrated fine pebbles. Some Fe pisoids as clasts or formed in conglomerate. Sharp lower and upper contacts. Shoreline pebbles?
Conglomerate, gray to yellowish gray, 95% granule clasts, very well rounded and sorted. Densely packed. Sharp base and top. Shoreline pebbles. This is the matching point with the base of WTG FM. in the northern section.
Mudstone, interbedded purple, gray, and dark gray, no Fe pisoids, peds f, rounded to subrounded. Uppermost part (~10 cm) platy, dark gray mudstone may contain sparse disseminated plants, may be caused by gleying. A horizon or close to lake plain from flood plain.
TD250
TD249
Mudstone, dark purple to red-brownish purple, upward increasing and then decreasing amount and size of (2-30 mm) Fe pisoids, which are mostly dark purple, some large ones yellow, most concentrated in the upper part. Terminating rapidly at top. Sharp/gradational top.

Taodonggou Section

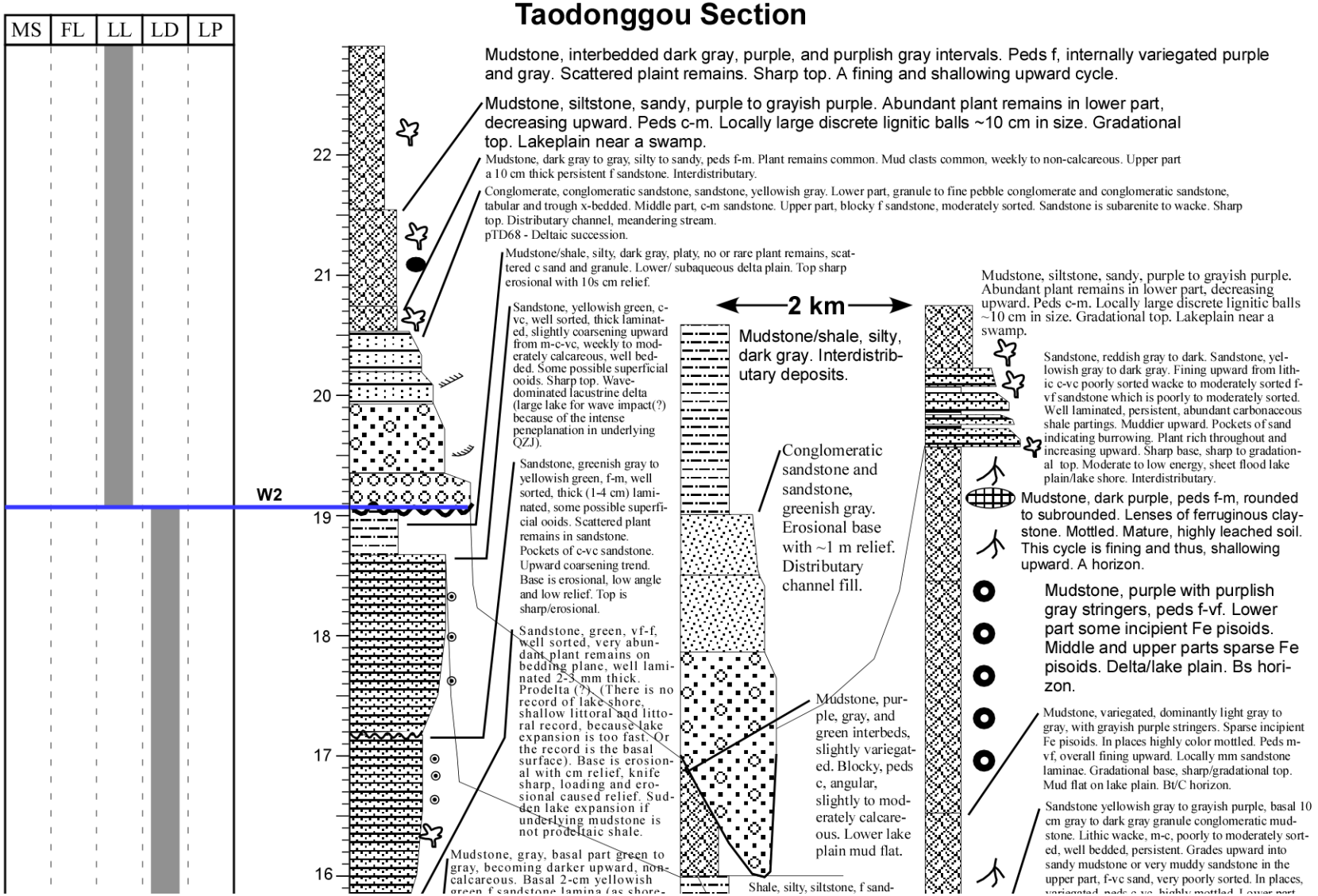

APPENDIX E
SOUTHWEST TARLONG SECTION

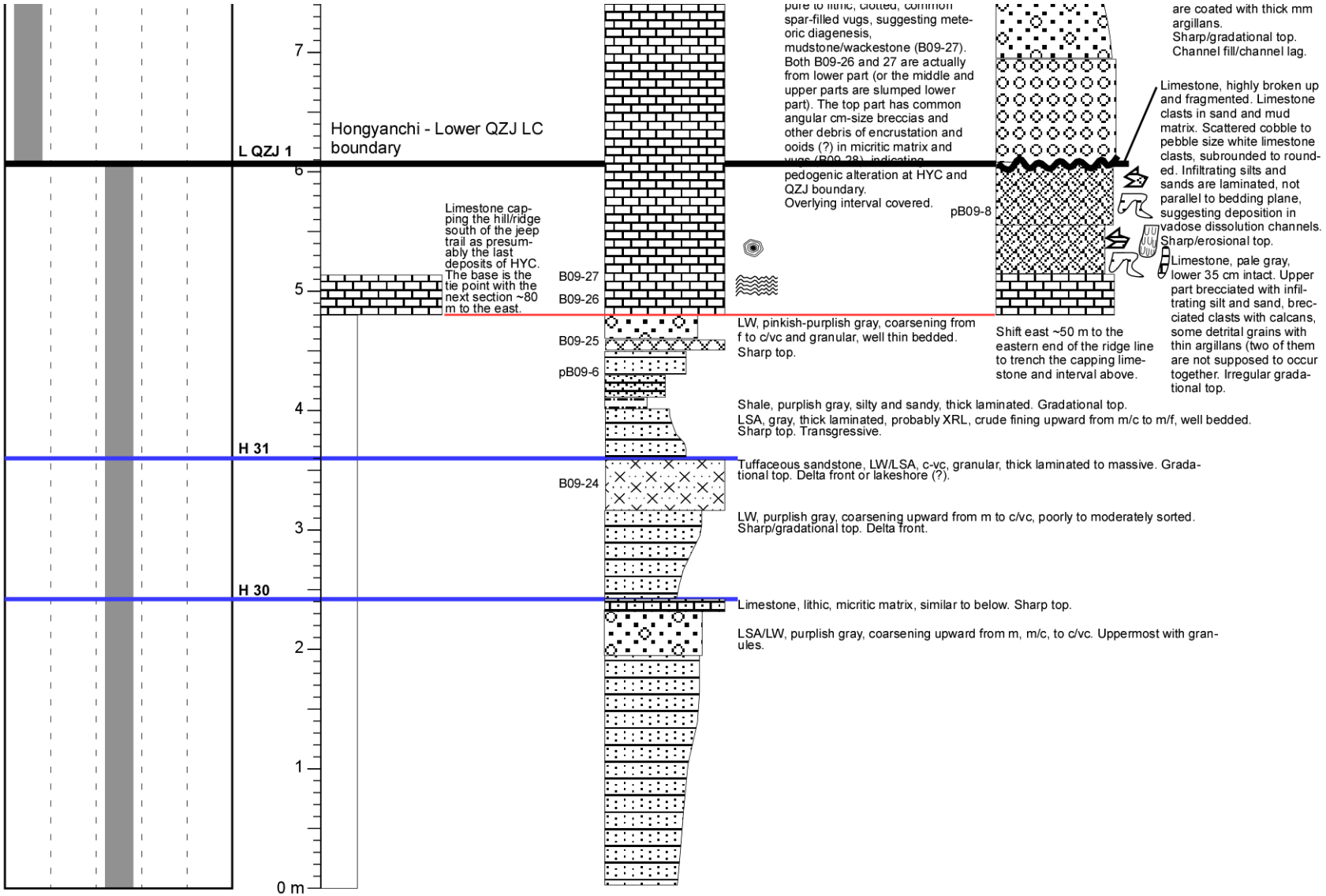
Hongyanchi - Lower QZJ LC boundary
L QZJ 1
H 31
H 30
0 m
1
2
3
4
5
6
7
Limestone capping the hill/ridge south of the jeep trail as presumably the last deposits of HYC. The base is the tie point with the next section ~80 m to the east.
B09-27
B09-26
B09-25
pB09-6
B09-24
pB09-8
pedogenic alteration at HYC and QZJ boundary.
Overlying interval covered.
LW, pinkish-purplish gray, coarsening from f to c/vc and granular, well thin bedded. Sharp top.
Shale, purplish gray, silty and sandy, thick laminated. Gradational top.
LSA, gray, thick laminated, probably XRL, crude fining upward from m/c to m/f, well bedded. Sharp top. Transgressive.
Tuffaceous sandstone, LW/LSA, c-vc, granular, thick laminated to massive. Gradational top. Delta front or lakeshore (?).
LW, purplish gray, coarsening upward from m to c/vc, poorly to moderately sorted. Sharp/gradational top. Delta front.
Limestone, lithic, micritic matrix, similar to below. Sharp top.
LSA/LW, purplish gray, coarsening upward from m, m/c, to c/vc. Uppermost with granules.
Shift east ~50 m to the eastern end of the ridge line to trench the capping limestone and interval above.
are coated with thick mm argillans. Sharp/gradational top. Channel fill/channel lag.
Limestone, highly broken up and fragmented. Limestone clasts in sand and mud matrix. Scattered cobble to pebble size white limestone clasts, subrounded to rounded. Infiltrating silts and sands are laminated, not parallel to bedding plane, suggesting deposition in vadose dissolution channels. Sharp/erosional top.
Limestone, pale gray, lower 35 cm intact. Upper part brecciated with infiltrating silt and sand, brecciated clasts with calcans, some detrital grains with thin argillans (two of them are not supposed to occur together. Irregular gradational top.

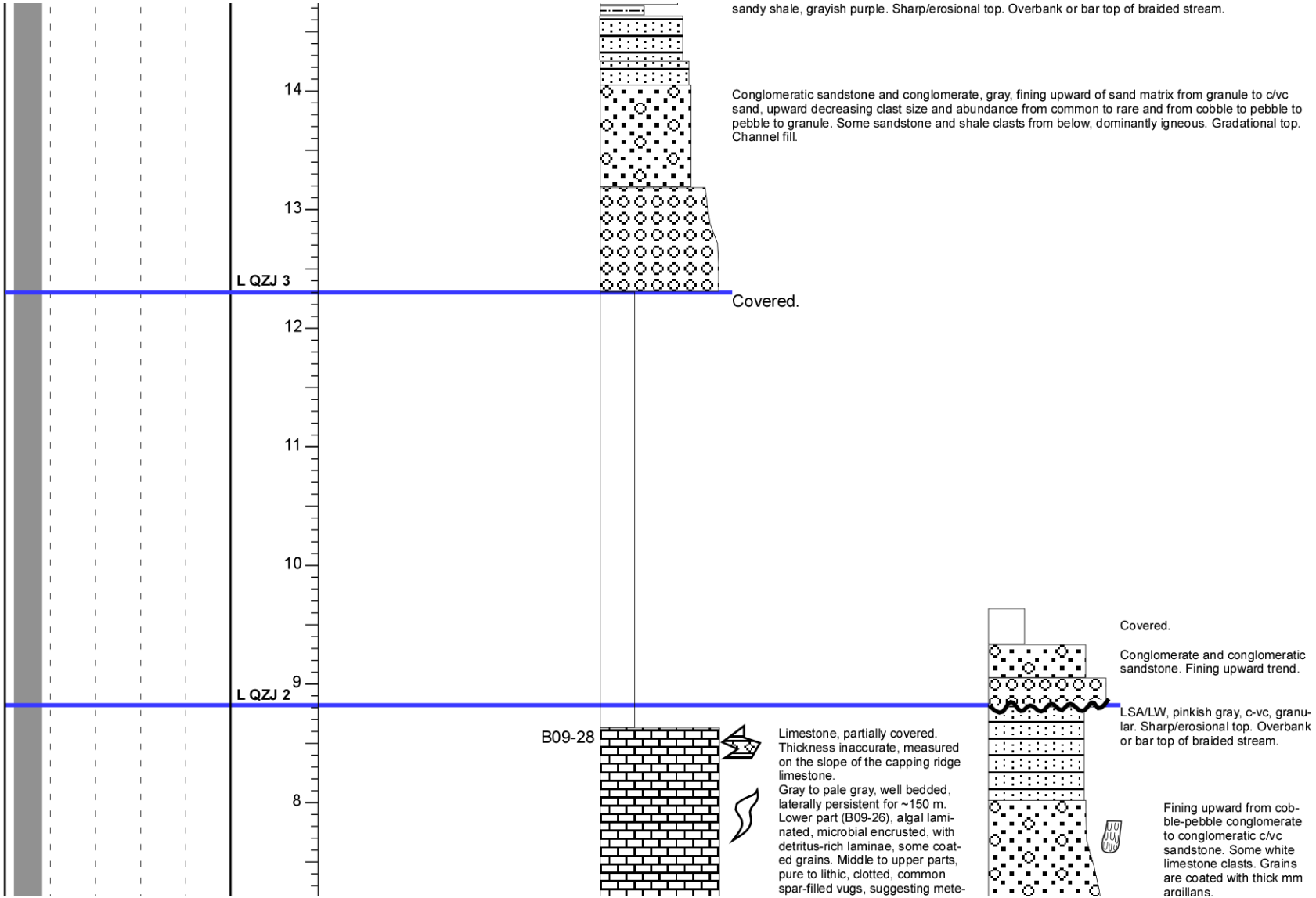
14
13
12
11
10
9
8
L QZJ 3
L QZJ 2
B09-28
sandy shale, grayish purple. Sharp/erosional top. Overbank or bar top of braided stream.
Conglomeratic sandstone and conglomerate, gray, fining upward of sand matrix from granule to c/vc sand, upward decreasing clast size and abundance from common to rare and from cobble to pebble to pebble to granule. Some sandstone and shale clasts from below, dominantly igneous. Gradational top. Channel fill.
Covered.
Limestone, partially covered. Thickness inaccurate, measured on the slope of the capping ridge limestone.
Gray to pale gray, well bedded, laterally persistent for ~150 m. Lower part (B09-26), algal laminated, microbial encrusted, with detritus-rich laminae, some coated grains. Middle to upper parts, pure to lithic, clotted, common spar-filled vugs, suggesting mete-
Covered.
Conglomerate and conglomeratic sandstone. Fining upward trend.
LSA/LW, pinkish gray, c-vc, granular. Sharp/erosional top. Overbank or bar top of braided stream.
Fining upward from cobble-pebble conglomerate to conglomeratic c/vc sandstone. Some white limestone clasts. Grains are coated with thick mm argillans.

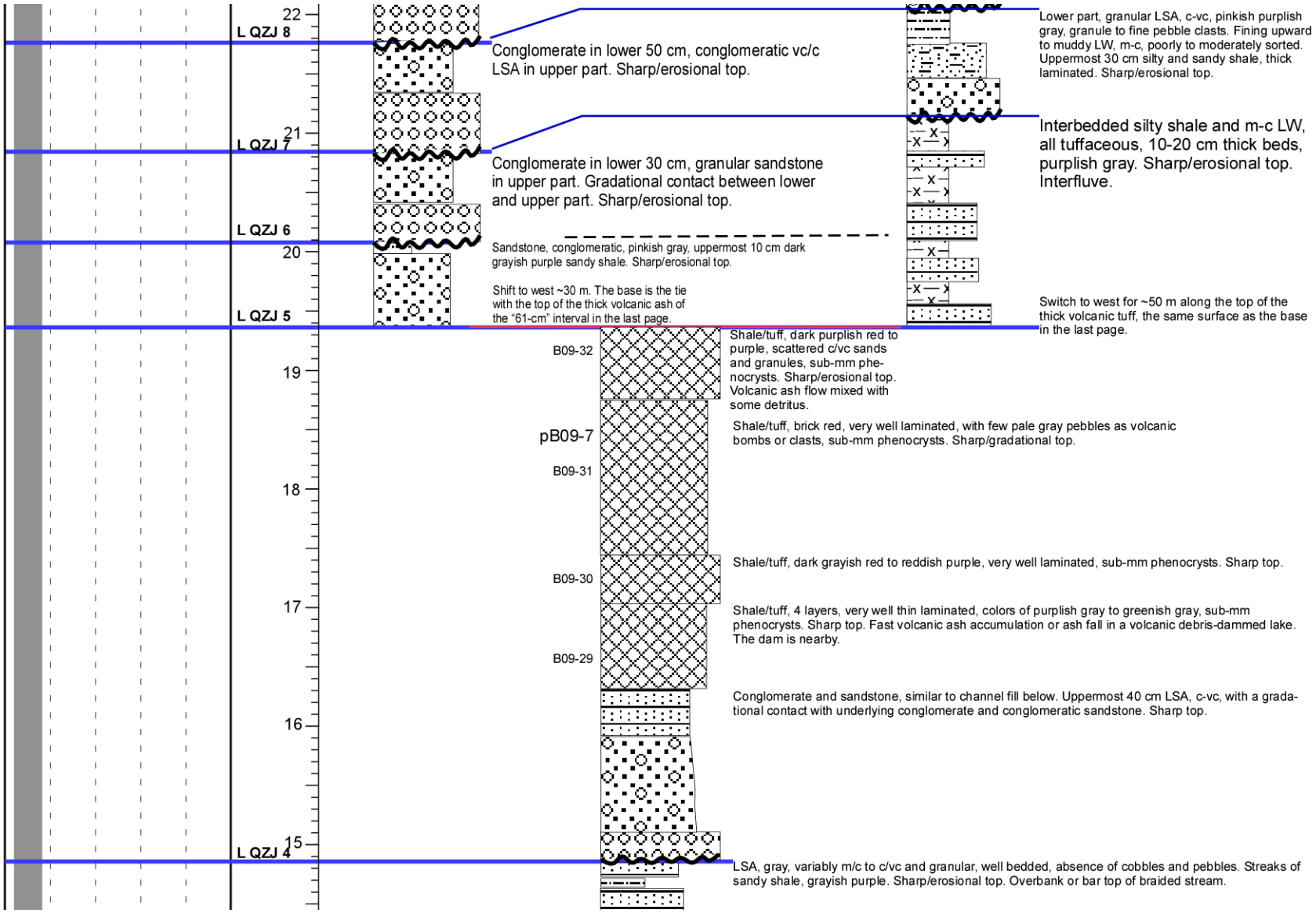
22
21
20
19
18
17
16
15
L QZJ 8
L QZJ 7
L QZJ 6
L QZJ 5
L QZJ 4
Conglomerate in lower 50 cm, conglomeratic vc/c LSA in upper part. Sharp/erosional top.
Conglomerate in lower 30 cm, granular sandstone in upper part. Gradational contact between lower and upper part. Sharp/erosional top.
Sandstone, conglomeratic, pinkish gray, uppermost 10 cm dark grayish purple sandy shale. Sharp/erosional top.
Shift to west ~30 m. The base is the tie with the top of the thick volcanic ash of the "61-cm" interval in the last page.
Lower part, granular LSA, c-vc, pinkish purplish gray, granule to fine pebble clasts. Fining upward to muddy LW, m-c, poorly to moderately sorted. Uppermost 30 cm silty and sandy shale, thick laminated. Sharp/erosional top.
Interbedded silty shale and m-c LW, all tuffaceous, 10-20 cm thick beds, purplish gray. Sharp/erosional top. Interfluve.
Switch to west for ~50 m along the top of the thick volcanic tuff, the same surface as the base in the last page.
B09-32
Shale/tuff, dark purplish red to purple, scattered c/vc sands and granules, sub-mm phenocrysts. Sharp/erosional top. Volcanic ash flow mixed with some detritus.
pB09-7
Shale/tuff, brick red, very well laminated, with few pale gray pebbles as volcanic bombs or clasts, sub-mm phenocrysts. Sharp/gradational top.
B09-31
B09-30
Shale/tuff, dark grayish red to reddish purple, very well laminated, sub-mm phenocrysts. Sharp top.
B09-29
Shale/tuff, 4 layers, very well thin laminated, colors of purplish gray to greenish gray, sub-mm phenocrysts. Sharp top. Fast volcanic ash accumulation or ash fall in a volcanic debris-dammed lake. The dam is nearby.
Conglomerate and sandstone, similar to channel fill below. Uppermost 40 cm LSA, c-vc, with a gradational contact with underlying conglomerate and conglomeratic sandstone. Sharp top.
LSA, gray, variably m/c to c/vc and granular, well bedded, absence of cobbles and pebbles. Streaks of sandy shale, grayish purple. Sharp/erosional top. Overbank or bar top of braided stream.

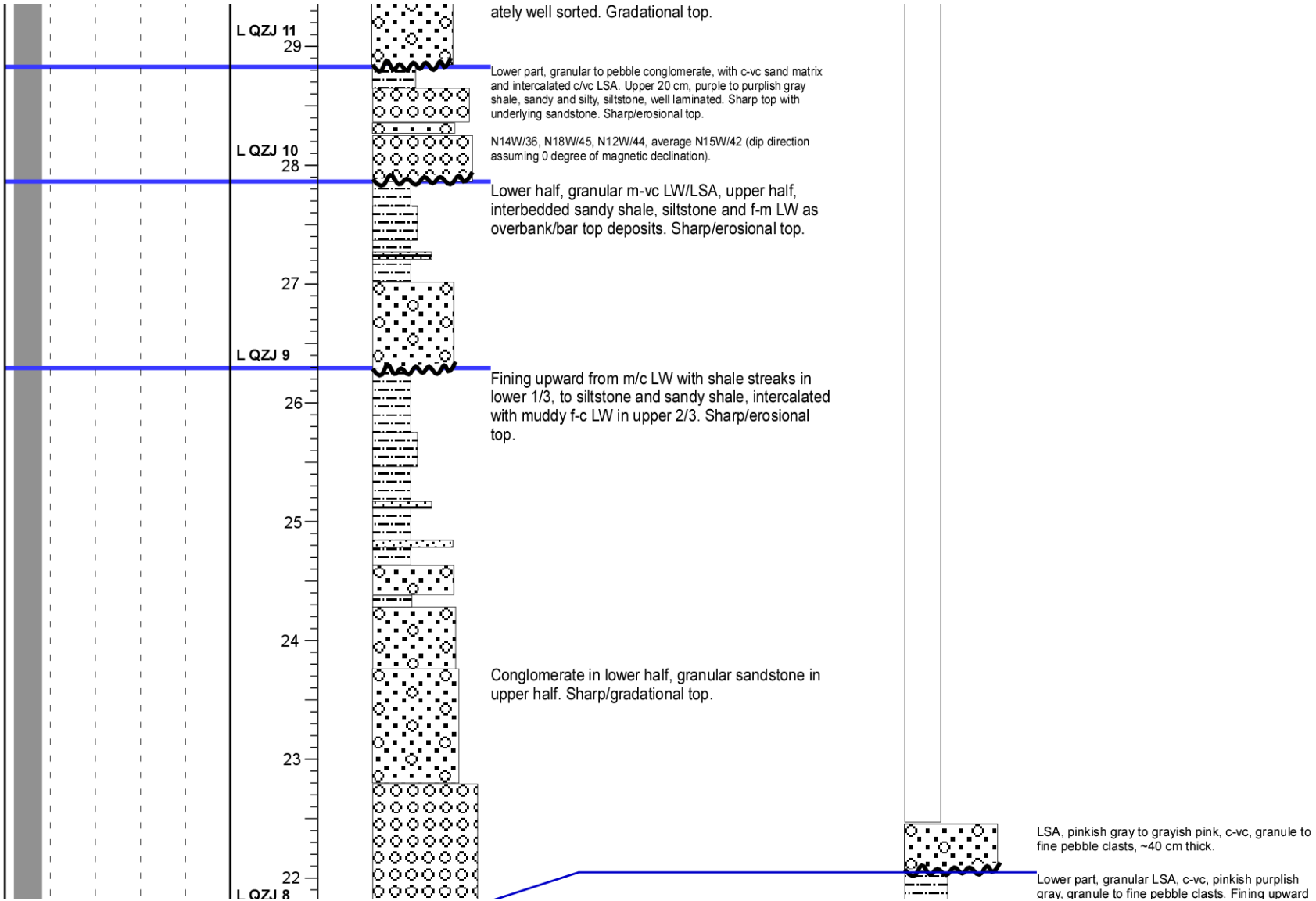
ately well sorted. Gradational top.
L QZJ 11
29
Lower part, granular to pebble conglomerate, with c-vc sand matrix and intercalated c/vc LSA. Upper 20 cm, purple to purplish gray shale, sandy and silty, siltstone, well laminated. Sharp top with underlying sandstone. Sharp/erosional top.
N14W/36, N18W/45, N12W/44, average N15W/42 (dip direction assuming 0 degree of magnetic declination).
L QZJ 10
28
Lower half, granular m-vc LW/LSA, upper half, interbedded sandy shale, siltstone and f-m LW as overbank/bar top deposits. Sharp/erosional top.
27
L QZJ 9
Fining upward from m/c LW with shale streaks in lower 1/3, to siltstone and sandy shale, intercalated with muddy f-c LW in upper 2/3. Sharp/erosional top.
26
25
24
Conglomerate in lower half, granular sandstone in upper half. Sharp/gradational top.
23
22
L QZJ 8
LSA, pinkish gray to grayish pink, c-vc, granule to fine pebble clasts, ~40 cm thick.
Lower part, granular LSA, c-vc, pinkish purplish gray, granule to fine pebble clasts. Fining upward

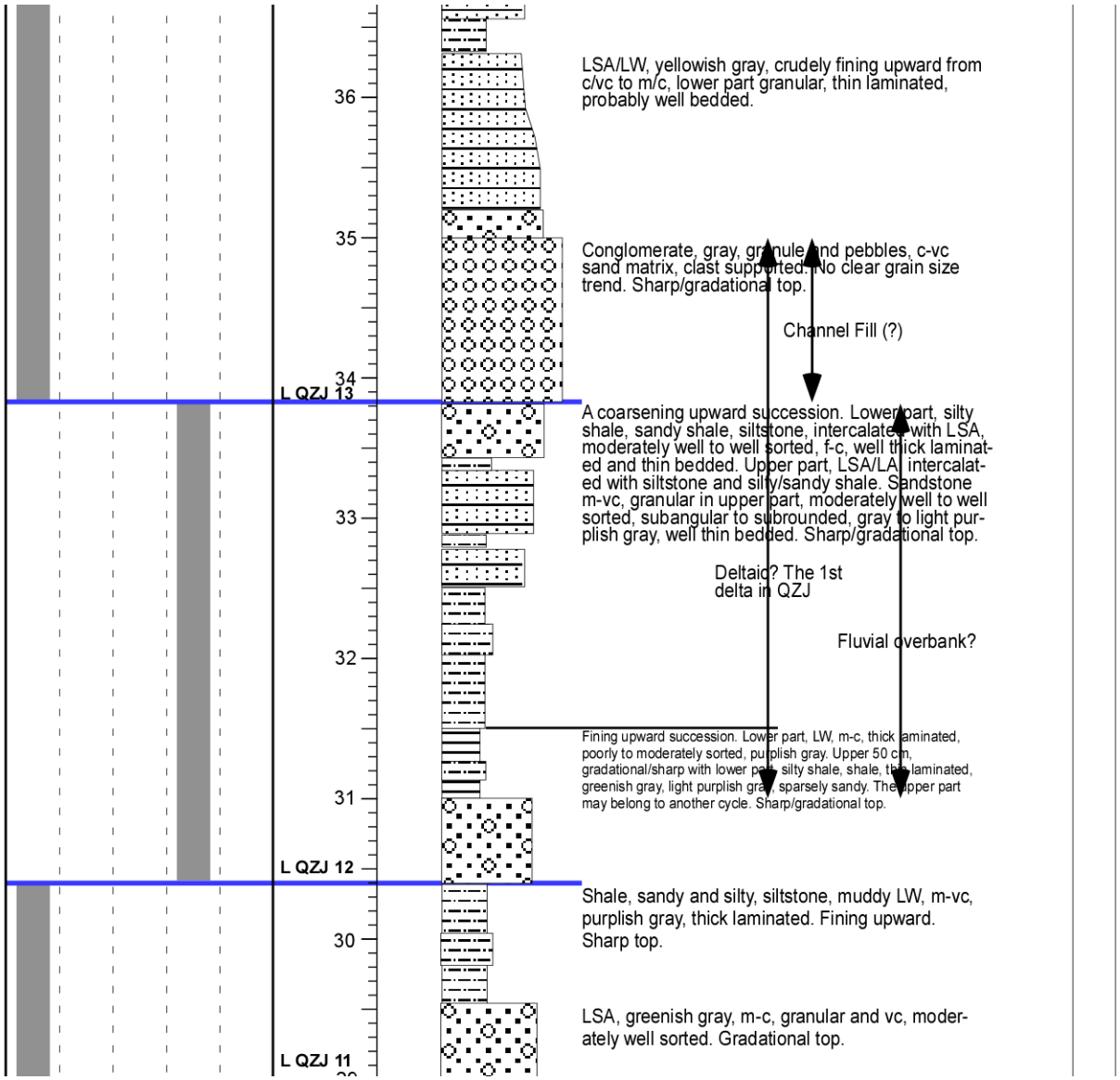
36
35
34
33
32
31
30
L QZJ 13
L QZJ 12
L QZJ 11
LSA/LW, yellowish gray, crudely fining upward from c/vc to m/c, lower part granular, thin laminated, probably well bedded.
Conglomerate, gray, granule and pebbles, c-vc sand matrix, clast supported. No clear grain size trend. Sharp/gradational top.
Channel Fill (?)
A coarsening upward succession. Lower part, silty shale, sandy shale, siltstone, intercalated with LSA, moderately well to well sorted, f-c, well thick laminated and thin bedded. Upper part, LSA/LA intercalated with siltstone and silty/sandy shale. Sandstone m-vc, granular in upper part, moderately well to well sorted, subangular to subrounded, gray to light purplish gray, well thin bedded. Sharp/gradational top.
Deltaic? The 1st delta in QZJ
Fluvial overbank?
Fining upward succession. Lower part, LW, m-c, thick laminated, poorly to moderately sorted, purplish gray. Upper 50 cm, gradational/sharp with lower part, silty shale, shale, thin laminated, greenish gray, light purplish gray, sparsely sandy. The upper part may belong to another cycle. Sharp/gradational top.
Shale, sandy and silty, siltstone, muddy LW, m-vc, purplish gray, thick laminated. Fining upward. Sharp top.
LSA, greenish gray, m-c, granular and vc, moderately well sorted. Gradational top.

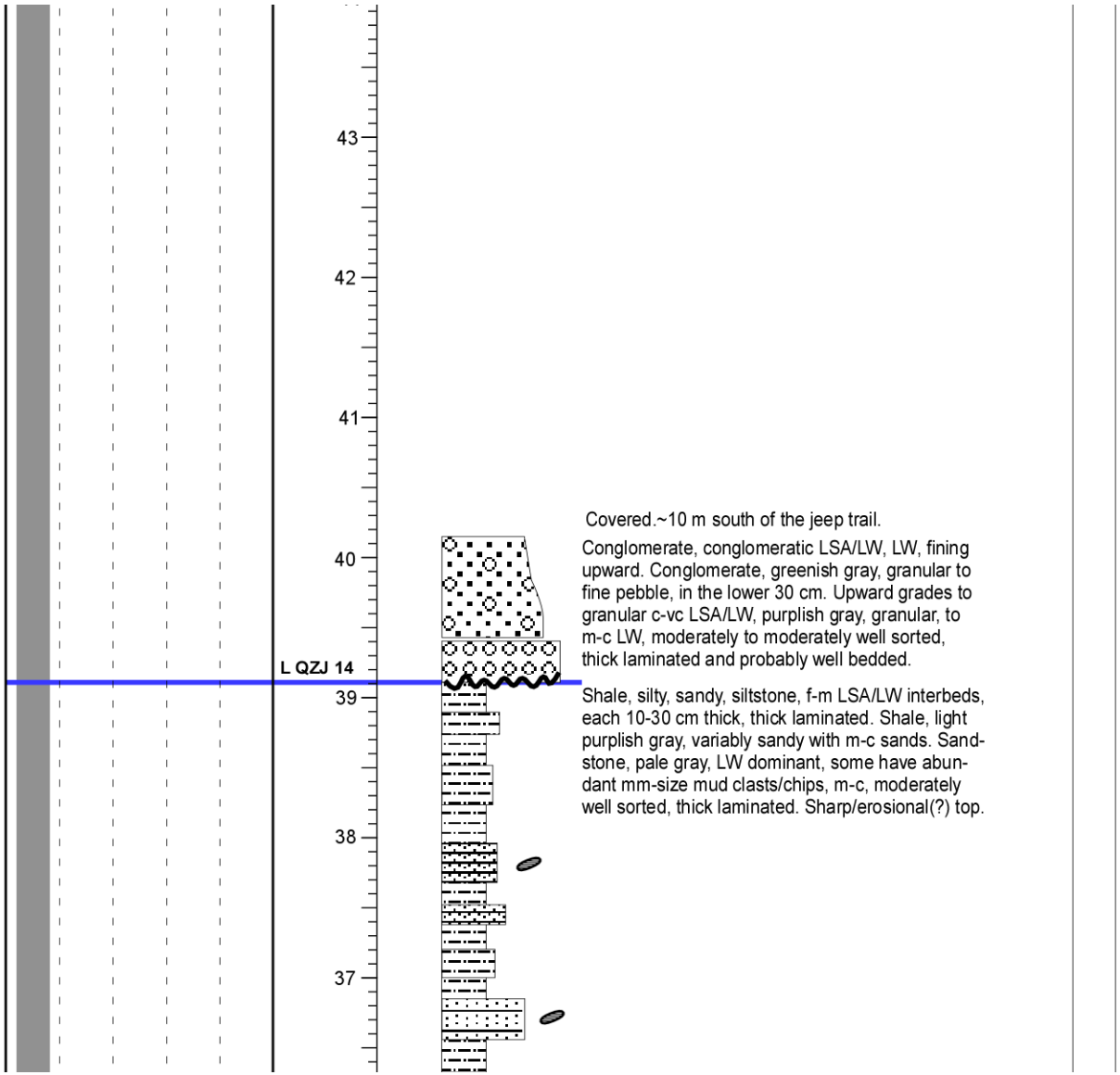
43
42
41
40
L QZJ 14
39
38
37
Covered.~10 m south of the jeep trail.
Conglomerate, conglomeratic LSA/LW, LW, fining upward. Conglomerate, greenish gray, granular to fine pebble, in the lower 30 cm. Upward grades to granular c-vc LSA/LW, purplish gray, granular, to m-c LW, moderately to moderately well sorted, thick laminated and probably well bedded.
Shale, silty, sandy, siltstone, f-m LSA/LW interbeds, each 10-30 cm thick, thick laminated. Shale, light purplish gray, variably sandy with m-c sands. Sandstone, pale gray, LW dominant, some have abundant mm-size mud clasts/chips, m-c, moderately well sorted, thick laminated. Sharp/erosional(?) top.

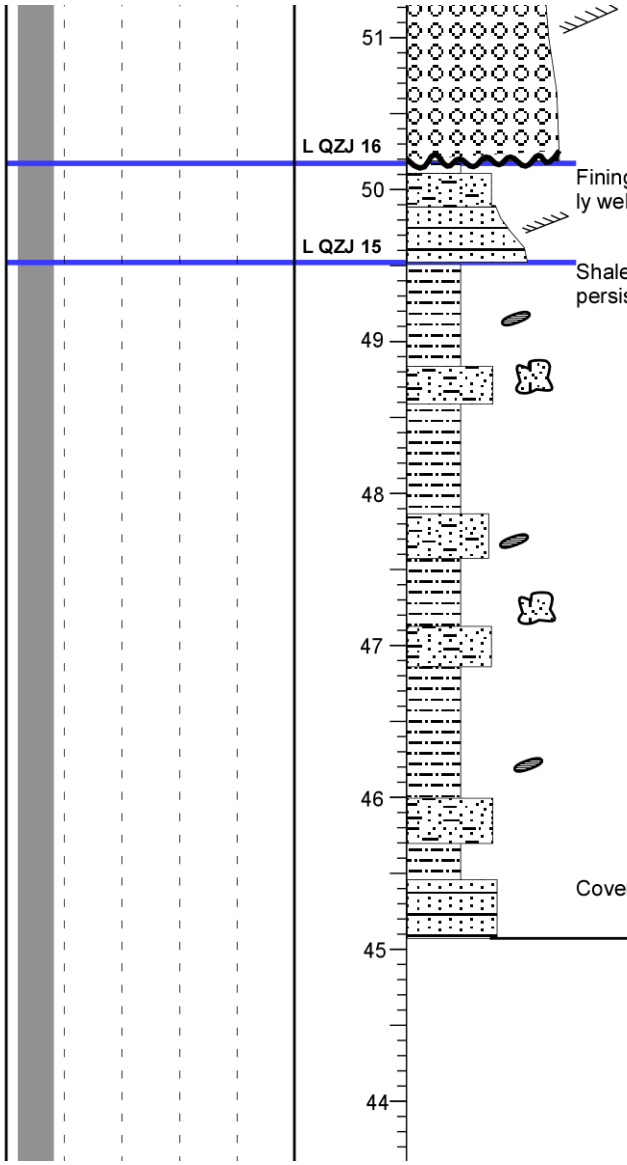

Fining upward from c-vc LSA to m-c LW, to muddy LW, to ~5 cm sandy shale at top. Angular platy, dense, moderately well to poorly sorted, thick laminated, probably XRL. Sharp/erosional, irregular top.

Shale, sandy, silty, intercalated with muddy LW, dense, angular platy, noncalcareous. 2 layers of discontinuous but persistent calcareous nodular (sandy) layers, each 10-20 cm thick. Common mm-size mud chips. Sharp top

Covered. Uppermost part LW, f-c, poorly sorted, none to weakly calcareous.

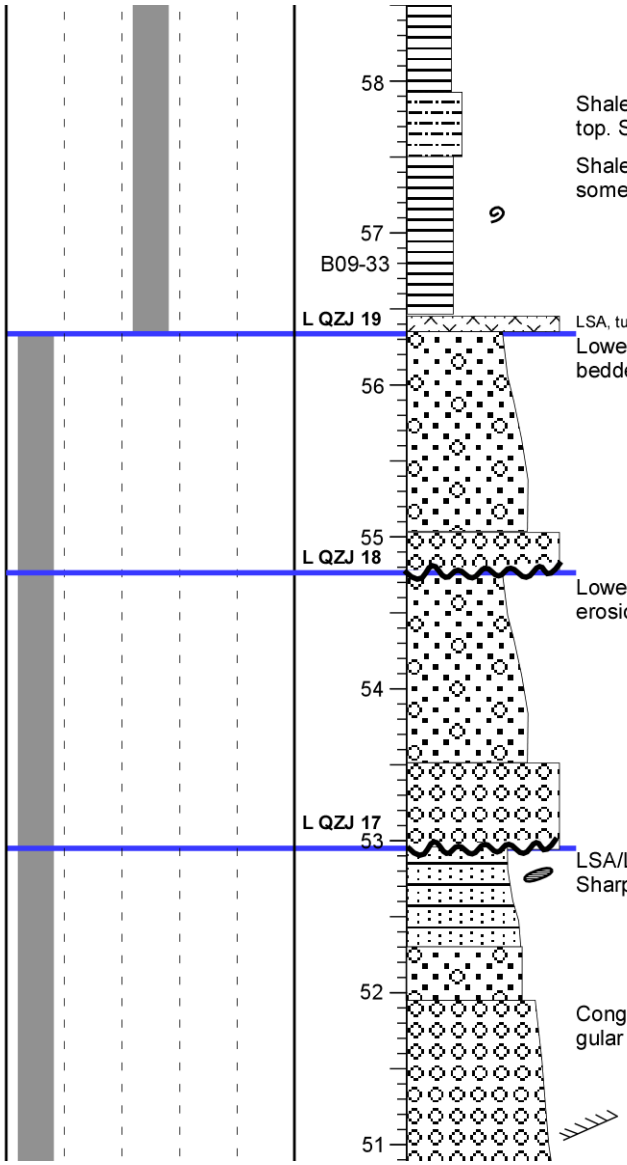

Shale, light purplish gray, silty, common m sand grains, rare granules, well thin laminated, weakly calcareous. Sharp top. Shallowing upward from the underlying bed.

Shale, greenish gray (rare in QZJ), pure, noncalcareous, platy to fissile, rare f-m sand grains, possible ostracods, some ash crystals. Sharp top. Lake deposits in a volcanically dammed lake.

LSA, tuffaceous, brick red, m, well sorted. Sharp top.

Lower 1/4, cobble to pebble conglomerate, grades into c-vc LSA, m-c LW, poorly to moderately sorted, probably well bedded. Sharp top.

Lower 1/3, cobble to pebble conglomerate, clast supported, upper 2/3, grades into pebble to granular c-vc LSA/LW, erosional base, laterally stacking channel fill. Sharp/erosional top.

LSA/LW, purplish gray, fining upward from granular vc to c/vc, thick laminated, well bedded, some mud chips. Sharp/erosional top. Upper point bar.

Conglomerate, pale gray, well cemented, crude upward fining from cobble-pebble to pebble-granule, clasts subangular to subrounded, imbricated, probably tabular x-bedded, some sandstone and shale clasts. Gradational top.

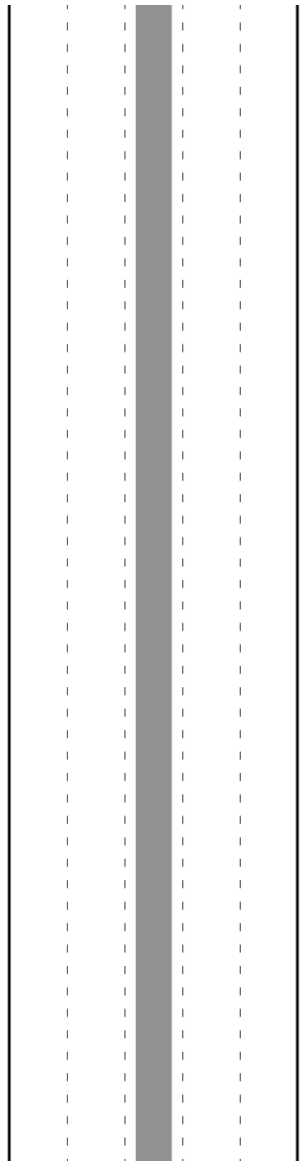

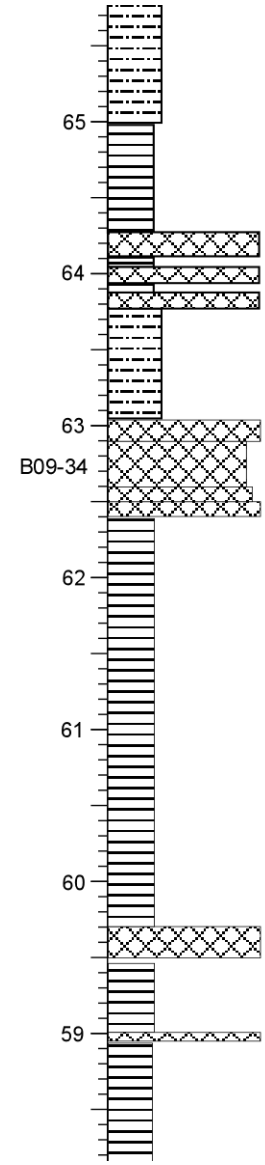

Lower part, dark olive gray, shale, silty, sparsely sandy. Elongate platy. Sharp contact with the upper part, 10 cm of fissile dark, gray tuff. Uppermost ~30 cm of pink, fissile shale/tuff mixed with white modern salt. Sharp upper contact.

To be switched ~100 m to the west to the eastern slope of the Quaternary alluvial plateau in summer of 2010.

4 layers of volcanic deposits. Lower part, coarse crystalline, red, well laminated tuff, upward to black, thin laminated, fine crystalline tuff, upward to fissile, pink tuff. Top part, clayey tuff, thick laminated. Sharp/gradational top.

Shale, greenish gray to gray, abundant ash fall particles, sparse sand grains. Lower part, 1-2 1-cm thick calcareous shale of same composition. Sharp top.

Lower part, reddish black tuff or welded tuff, upper part, bentonite, platy, thick clay coats, purplish gray. Gradational top.

Shale, greenish gray, some sand grains, abundant ash particles. Sharp top.

Tuff, rick red, abundant sub-mm phenocrysts, some vitrous mm-thick bands. Sharp top. 5 cm thick.

Shale, greenish gray, well laminated, pure, upward increasing sand grains, f-m from sparse to common, some ashfall particles. Sharp top.

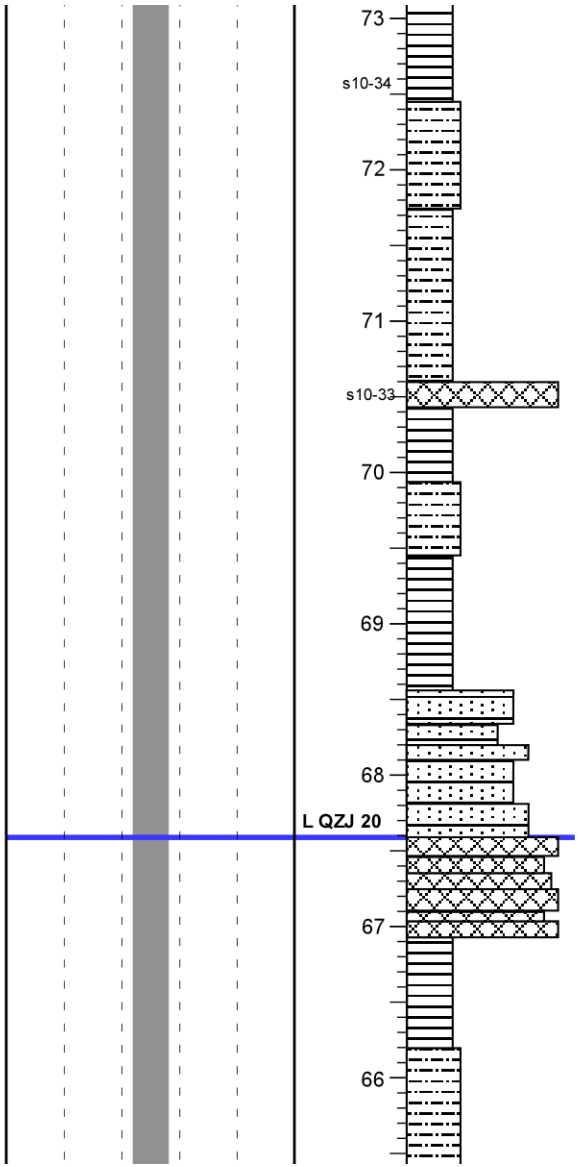

Shale, light gray to greenish gray, thin platy to fissile. Plate surfaces uneven, even when it is fissile. Variable amount of sand, f-vc, subrounded to rounded, scattered in most cases and phenocrysts. Tuffaceous shale to muddy and sandy ashflow tuff. Gradational upper contact. Lacustrine.

S10-33: From a very thin bed of tuff with large phenocrysts.

Lower part, LSA, vf-c/vc, well rounded, brown/maroon. Upward changing to a LW, m-vc, brown at the bottom changing to purplish red at the top. Gradational upper contact.

6 layers of fissile tuff, upward from purple, light green, pink, reddish pink, green, olive gray. Thin platy to fissile. Indicating multiple episodes of volcanism. Scattered phenocrysts, mixed with white modern salt. The uppermost part has common coarse sands. Sharp upper contact.

3 parts. Lower part, olive gray, platy mudstone. Middle part, light pink, gray, fissile. Upper part gray, thin platy, variable amount of sand grains. Some euhedral crystals, some black minerals (anhedral-euhedral), some organic/plant remains, platy, uneven, weakly to noncalcareous. They are a mixture of mud and tuff at varying degrees (tuffaceous shale). Sharp upper contact. Water-laid tuff, ashfall, or short-distance ashflow in a volcanics-dammed lake.

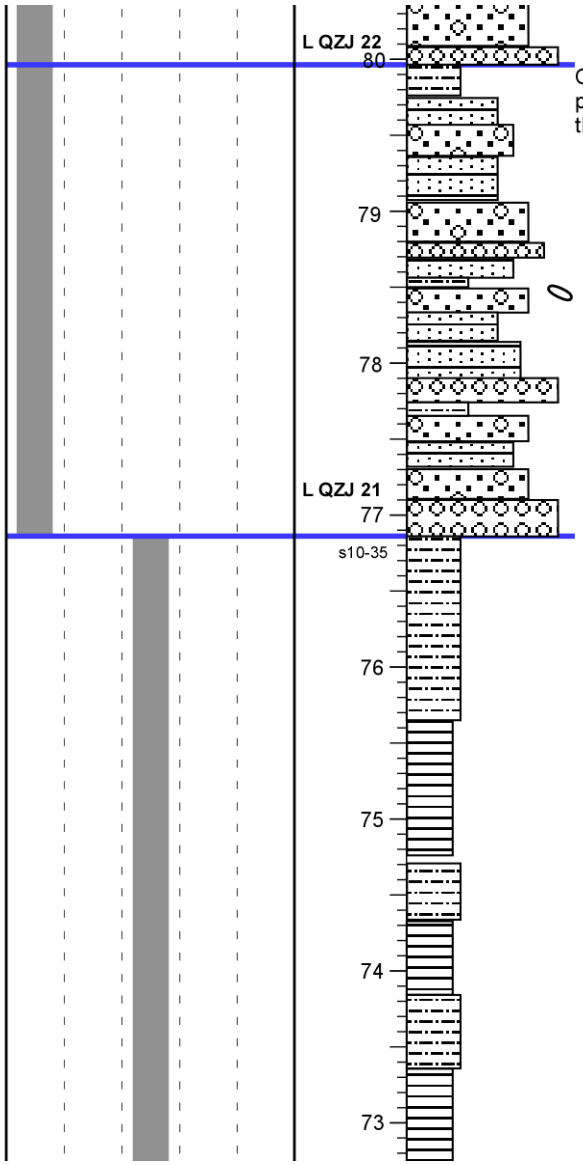

Overall finning upward from granule-fine pebble conglomerate, gravelly c-vc LW, to m-c LW, poorly sorted, subangular to rounded. Some siltstone stringers. Maroon. Multiple units 10s cm thick. Uppermost 20 cm, silty, sandy mudstone/shale. Sharp upper contact.

Shale, variegated, greenish gray, olive, purple, upward increasingly to dark purple, silty, sandy, tuffaceous at varying degrees, thin-thick platy. Upward increasing in silt. Some scattered sand and granules, locally concentrated. Sharp top. Still lake or mud flat deposits.

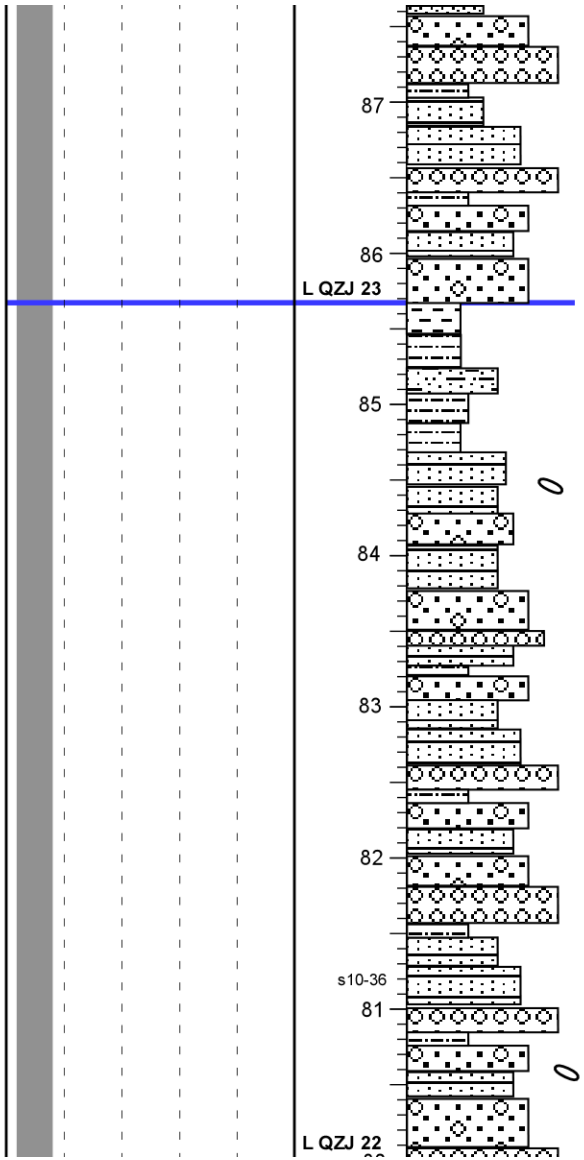

Similar to below, multiple 10 cm thick fining upward units, from granular c-vc LW to m-c LW, may be capped by sandy mudstone/shale stringers. As sandy braided stream or sheet-flow sand flat deposits. Uppermost ~1 m sandy mudstone/shale, siltstone, sandy, and muddy LW. Sparse maroon mudstone/shale clasts, sand to pebble size, angular to subrounded. The break is artificial in a large degree. Sharp upper contact.

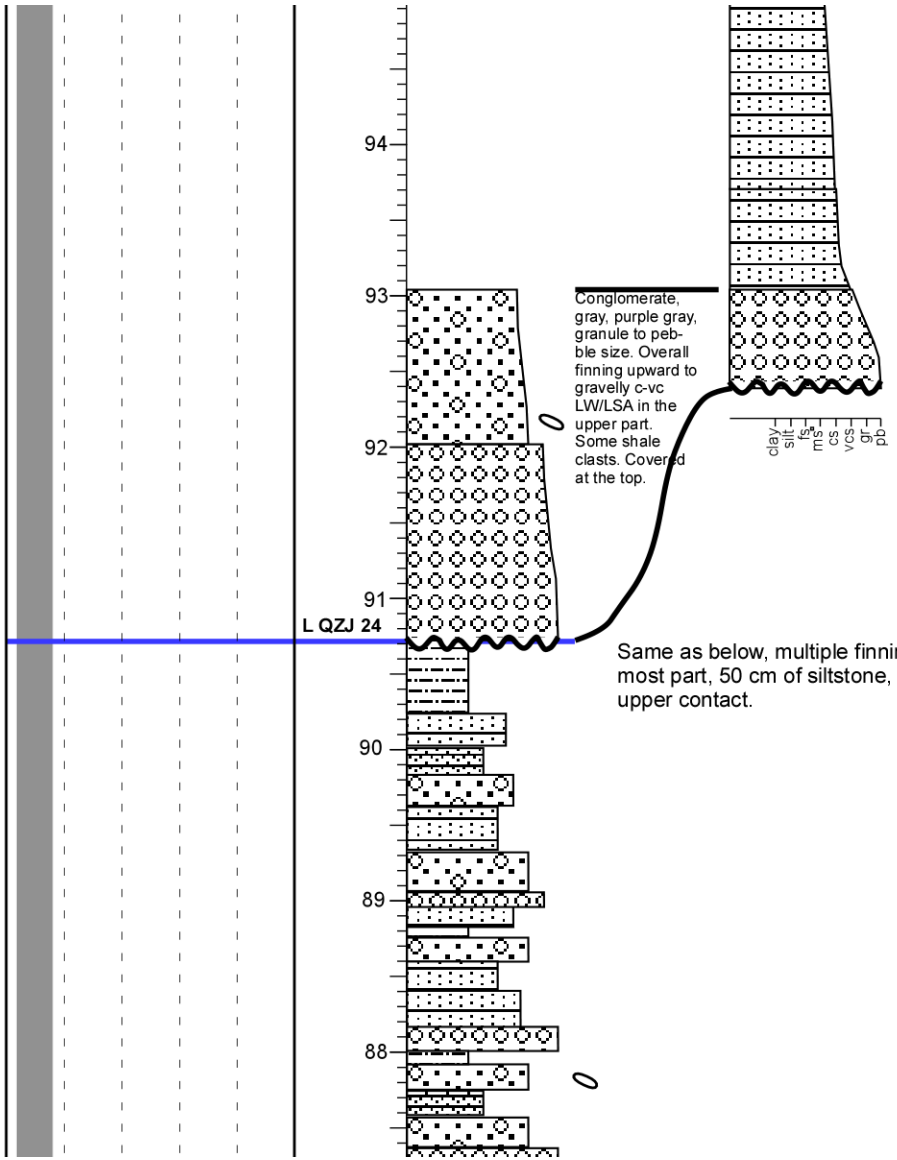
94
93
92
91
90
89
88
L QZJ 24
Conglomerate, gray, purple gray, granule to pebble size. Overall finning upward to gravelly c-vc LW/LSA in the upper part. Some shale clasts. Covered at the top.
clay
slt
fs
ms
cs
vcs
gr
pb
Conglomerate, similar to that 80 m to the west, but much thinner. Gradational top.
Shift to east for ~80 m, starting at the base of the channel lag conglomerate.
Same as below, multiple finning upward units of c-vc LSA/LW to f-c muddy LW. Uppermost part, 50 cm of siltstone, sandy, maroon. Poorly to moderately sorted. Erosional upper contact.

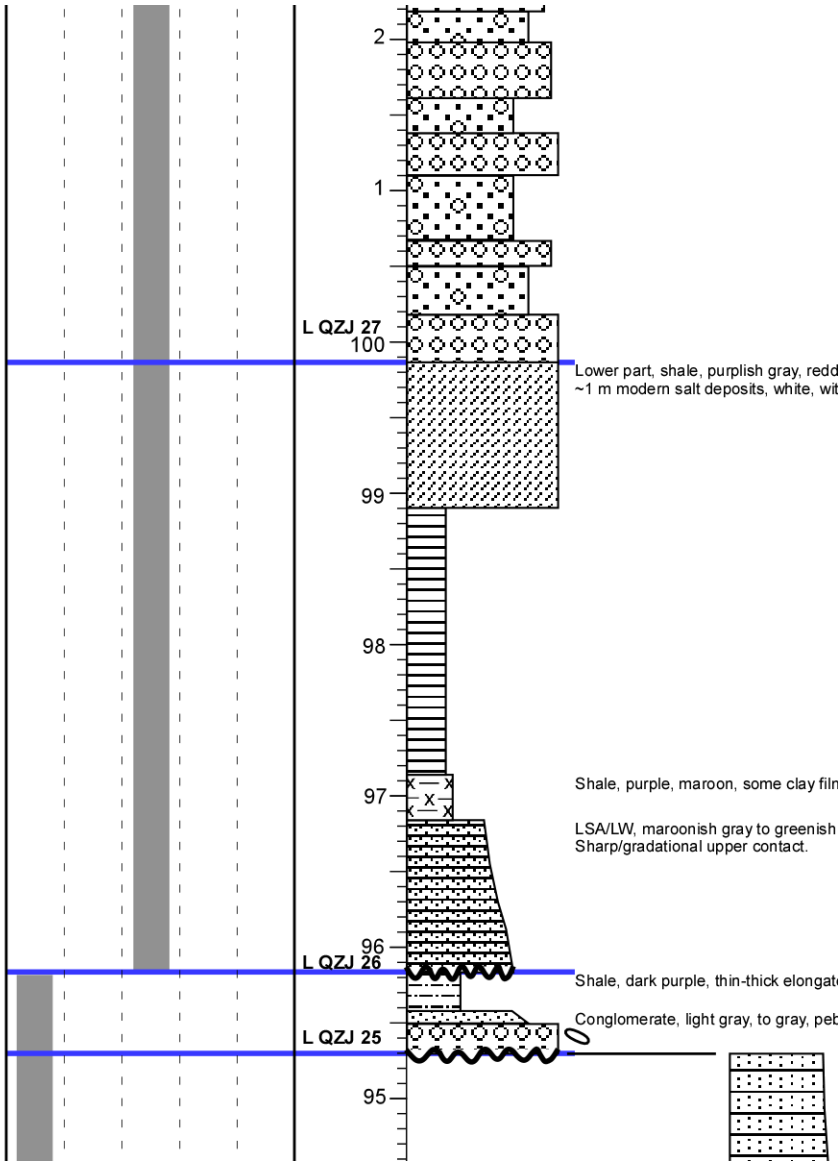

Lower part, shale, purplish gray, reddish gray, fissile, very thin laminated, pure. Lacustrine (volcanic damned). Upper part, ~1 m modern salt deposits, white, with flimsy of fissile shale, probably bentonitic. Sharp upper contact.

Shale, purple, maroon, some clay films, slickensides, secondary calcite plates. Probably a mixed bentonite.

LSA/LW, maroonish gray to greenish gray, well bedded and laminated, moderately well sorted, finning upward from c to f/m grains. Sharp/gradational upper contact.

Shale, dark purple, thin-thick elongated platy, scattered vc sand grains. Sharp/erosional (?) upper contact.

Conglomerate, light gray, to gray, pebble. Uppermost part, LW, c-vc, some mud clasts. Sharp/gradational upper contact.

LSA/LW, gray to reddish green gray. Overall fining upward and better sorted upward, from vc, moderately sorted to m-c, moderately well sorted. Sharp/erosional upper contact.

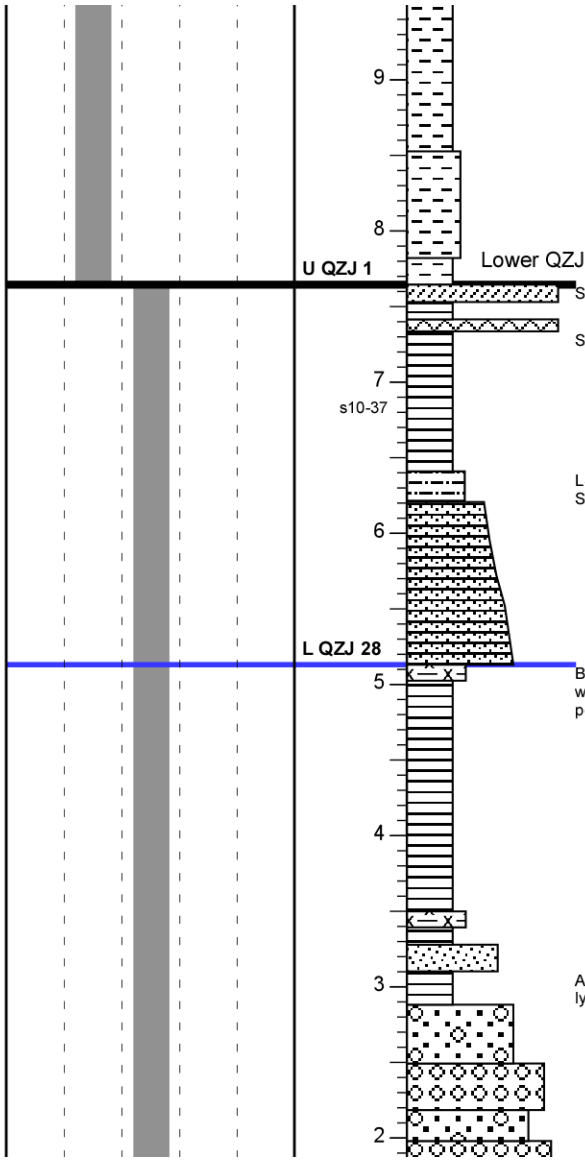

Lower QZJ-Upper QZJ LC boundary

Shale, grayish purple, fissile, possible volcanic ash fall, tuffaceous shale, white modern salt is dominant. Sharp upper contact.

Shale, grayish, purple, thinly laminated. Gradational top. Lake(?).

LSA/LA, olive gray, well laminated. Overall, crudely finning upward from c to m-f to a 20 cm siltstone, sandy mudstone. Sand flat. Sharp upper contact.

Basal 20 cm, LA, well sorted, greenish gray, with a gradational contact with overlying bed (transgressive?). 30 cm above, highly weathered, maybe tuffaceous. The rest is maroon, purple fissile shale. Uppermost 10 cm, pale gray with common phenocrysts, possibly tuffaceous shale. Sharp upper contact.

A succession of LW/LSA, gravelly, conglomerate 10s cm thick each, no definite grain size trend, olive gray, sharp contact with overlying shale. Uppermost 20 cm, a dark purple thin platy shale, deposits in a pond? Sharp upper contact.

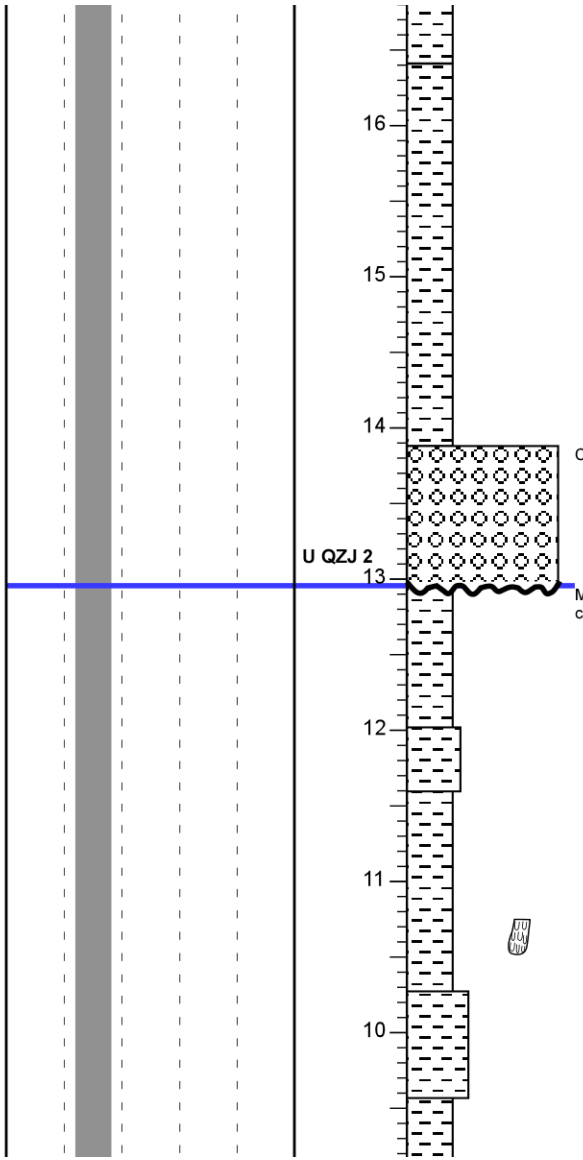

Conglomerate, light gray, granule-f pebble clasts. Sharp/gradational upper contact.

Mudstone, maroon, uniform color, no ped structure, weathered to granular (granular peds?), blocky short plates, rare sparse small clay films, structureless. Variably silty and sandy. Sharp/erosional upper contact.

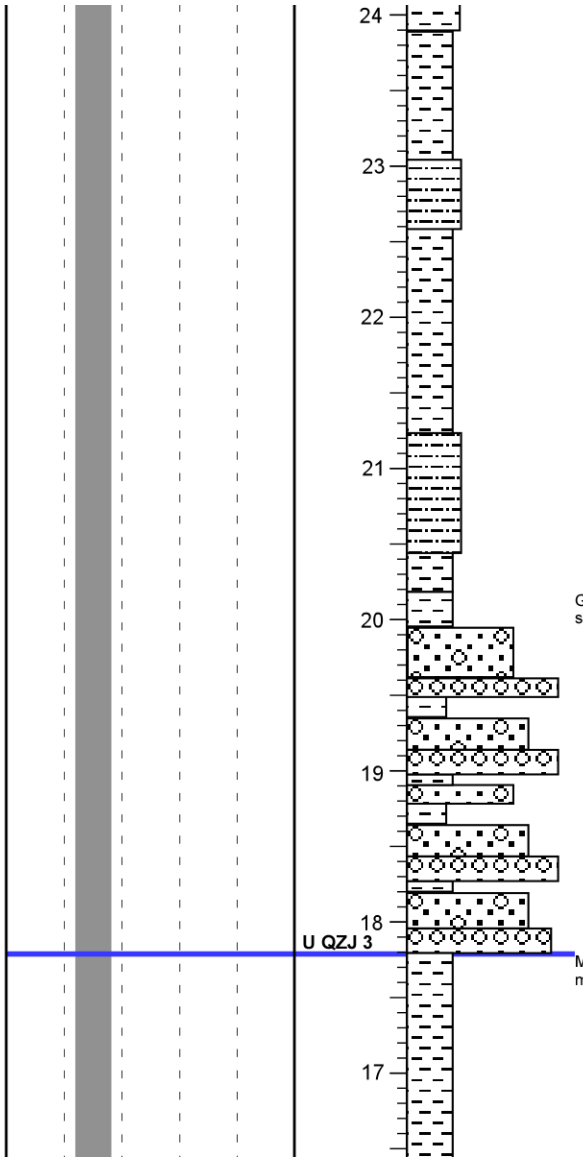

Gravelly LW/LSA and conglomerate, overall fining upward due to upward increase in intercalated and interbedded maroon mudstone. Gradational upper contact.

Mudstone, maroon, similar to below. Poorly developed soil structure than that in NE Tarlong, indicating faster deposition (?) on a mud flat. Sharp/erosional upper contact.

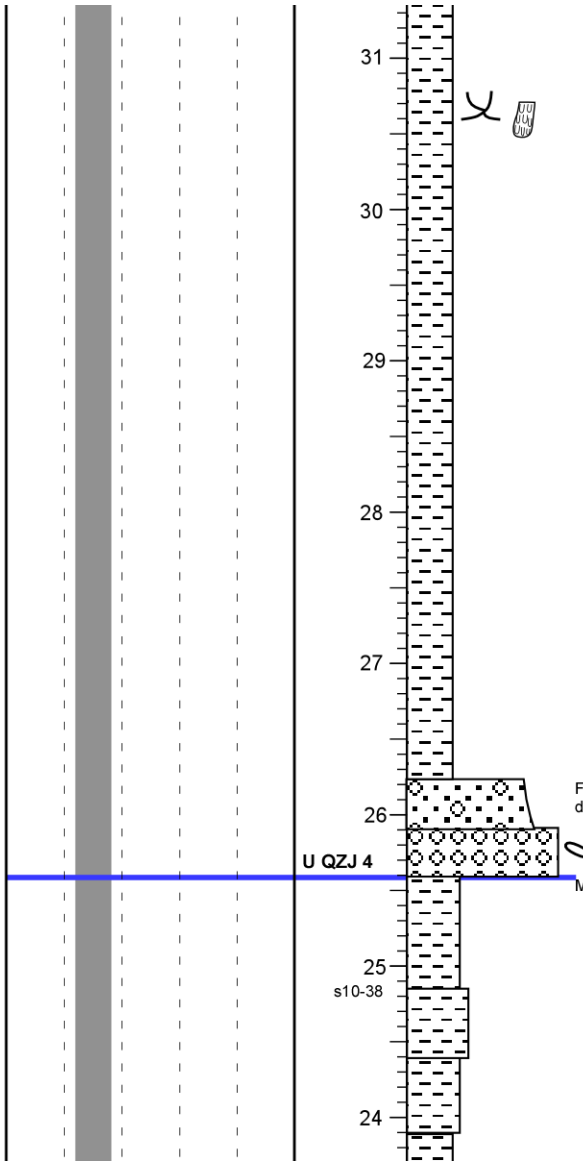

Fining upward from pebble-cobble conglomerate to granular LW/LSA. Common mudstone and shale clasts in conglomerate. Gradational upper contact.

Mudstone, maroon, similar to below, variably blocky to platy, and sandy and silty. Sharp/erosional upper contact.

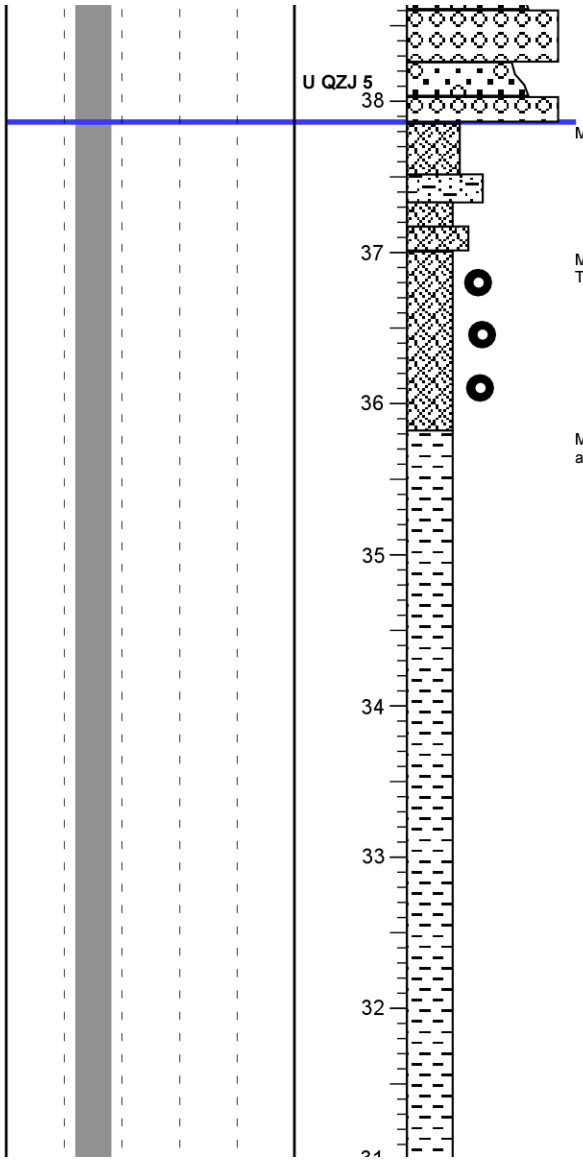

Mudstone, sandy siltstone, to muddy LW, vf-f, rounded, olive gray, maroon, sandy, blocky. Sharp upper contact.

Mudstone, maroon to dark reddish purple, common 1-3 mm Fe-pisoids. They are small, indicating moderately developed Gleysol. The first appearance of pisoids here seems earlier than in other parts of Tarlong. Sharp/gradational upper contact.

Mudstone, maroon, variegated with greenish gray, steel gray, pinkish red, similar to below. In the middle, a ~20 cm interval with abundant clay films and slickensides. Weathered granular blocks. Sharp/gradational upper contact.

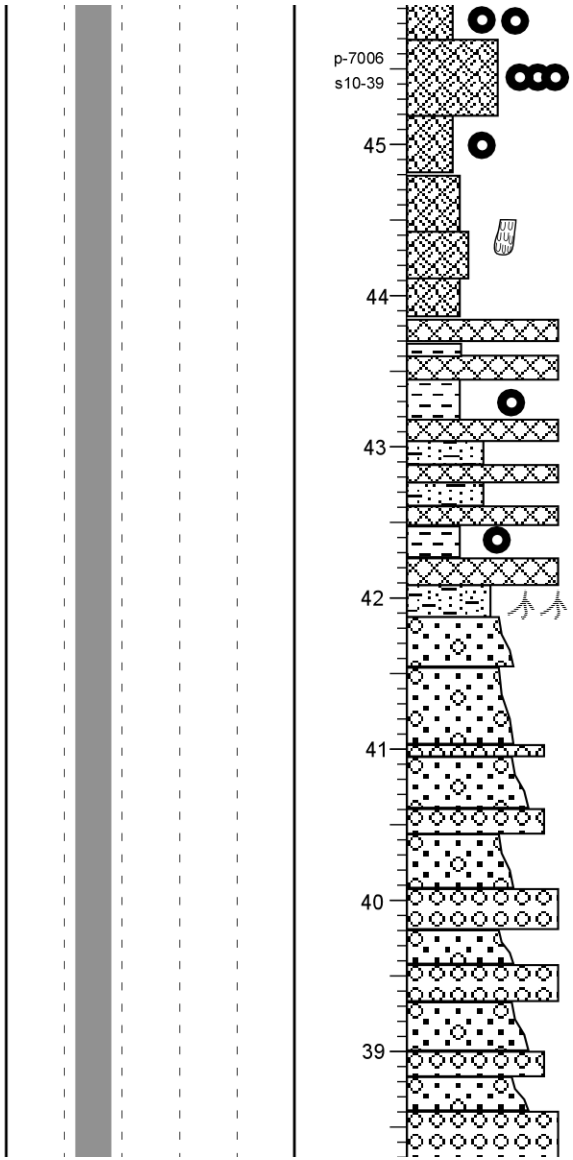

Mudstone, sandy, silty, maroon to dark maroon, minimal discontinuous clay coatings. Sharp upper contact.

An interval of 6 beds of green bentonites interbedded with maroon sandy mudstone, muddy LW, silty, which contains scattered small Fe-pisoids. In basal f-m LW, locally abundant clay-cutan-filled rootlets, subvertical to horizontal, 1 mm wide, 10s mm long. Sharp upper contact. Correlative to NE Tarlong.

From a distant overview of SW Tarlong, this contact is the line separating the yellowish green succession (presumably WTG) from the underlying reddish purple interval of the QZJ LC. Thus, this surface may be the WTG-QZJ LCB.

Fining upward from pebble-cobble conglomerate to gravelly m-c/vc LW interbeds. Light green to gray and maroon, upward increasingly maroon. Well-stratified with internal erosional surfaces. Many fining units, ~10s cm thick. Sharp/gradational upper contact.

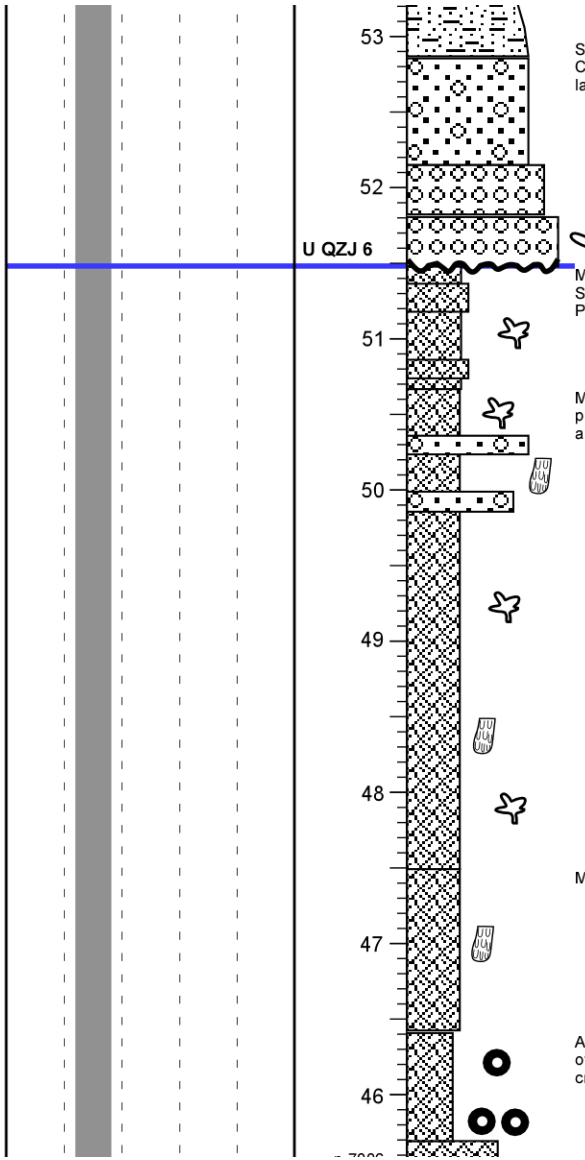

Shift 30 m to the east.
Conglomerate, brownish gray, finning upward from pebble-cobble conglomerate to gravelly LW/LSA, Basal 30 cm with some large mudstone and sandstone cobbles from below (many are LWs). Well stratified. Gradational to sharp upper contact.

Mudstone, dark maroon, blocky to platy, appears to be the topmost horizon of a soil profile, silty, siltstone. Sparse plant remains. Sharp/Erosional upper contact.
Photos.

Mudstone, silty, sandy, blocky, some platy, 2 ~10 cm thick LW and gravelly LW in upper part. Variegated in matrix and in beds (see photo), gray, green, yellow, maroon, dark gray. Rare, sparse, discontinuous clay films. Sparse plant remains throughout. Gradational top.

Mudstone, maroon, dark maroon, sparse, thin clay films, blocky, silty. Sharp upper contact.

An interval with Fe pisoids, yellowish re to maroon. Basal 40, upward increasing in pisoids. Upward to a 40-50 cm thick iron-crete of cemented pisoids. Cemented in yellowish maroon mud, weakly calcareous. Above, upward decreasing pisoids to sparse. Fe-crete indicates more intense water-logged condition (?) here. Gradational upper contact.

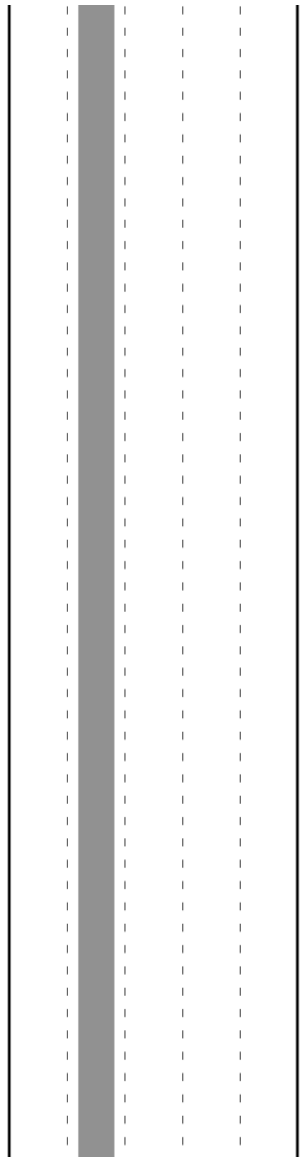

Variegated mudstone, silty, sandy, blocky to platy. 1 stringer of C LW, maroon, light gray, steel gray, purple. Lower part, 3-4 stringers of bentonites. Sharp upper contact.

LW/LSA, maroon, muddy, well laminated, elongate platy, fining upward from c/vc to f/vf, contains 4-5 bentonites, each 5-20 cm thick, light grayish green, thinly laminated to fissile, with phenocrysts. Gradational upper contact.

Shift 30 m to the east.

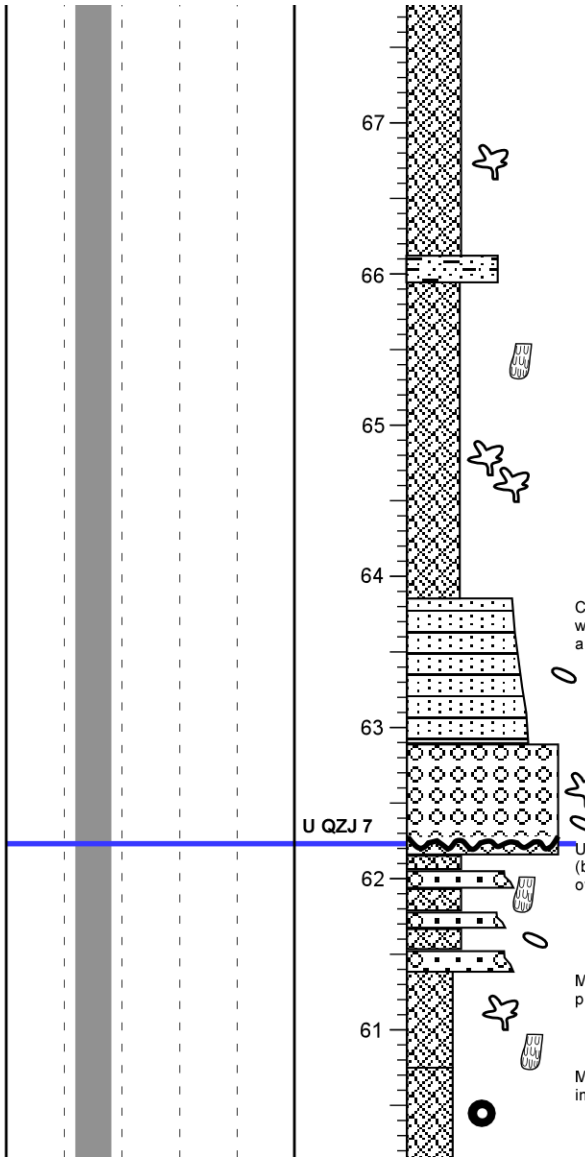

Conglomerate, pale gray, fining upward from cobble - pebble to c-vc LW, uppermost part, grayish green. Some large carbonized wood fragments in lower part, some mud clasts and chips. Sharp upper contact. Carbonized plant may indicate the end of QZJ and beginning of WTG.

Units of finning upward from granular LW/LSA to sandy mudstone. Upper part, a 5 cm thick, thinly laminated pure shale (bentonitic?). 10s cm thick beds. Some illuvial clay, some maroon mud chips. Sharp/erosional upper contact. Channel edge or overbank deposits.

Mudstone, variegated, maroon, purple, gray, platy to blocky, small (2 cm) rounded peds, with poorly developed clay coats, sparse plant remains. Sharp upper contact.

Mudstone, lower part, yellow, gray to yellow, greenish gray, upper part, gray to dark gray and maroonish to purplish gray, upward increasing then upward decreasing in Fe pisoids, fine block, peds ~1-5 mm in diameter. Gradational upper contact.

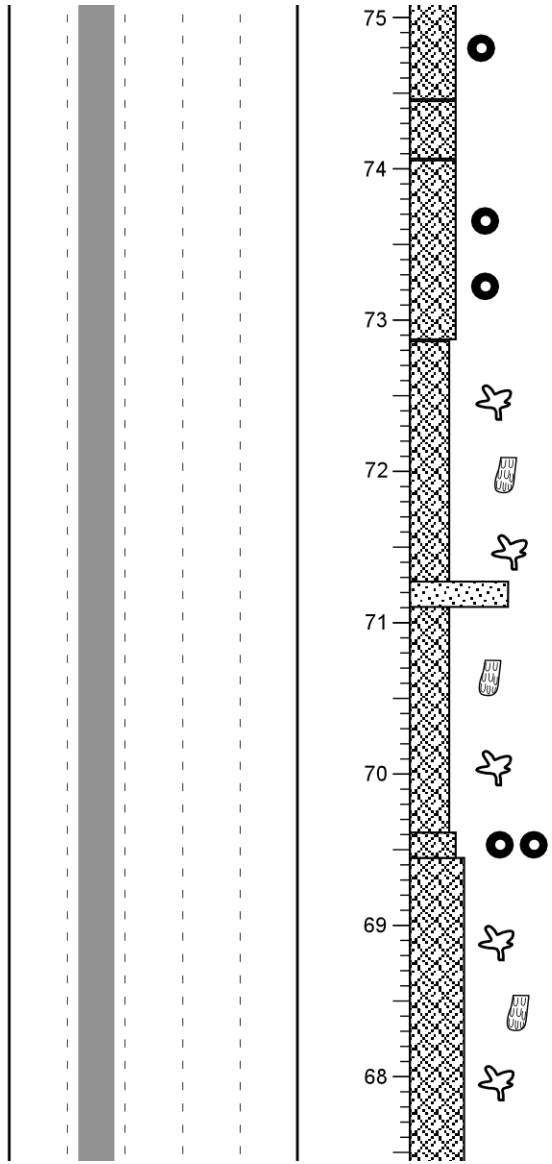

Mudstone, steel gray, no Fe pisoids. Sharp upper contact.

Mudstone, maroon to greenish gray, scattered common small mm-size Fe pisoids. Sharp upper contact.

Mudstone, olive gray, light gray, greenish gray, interbedded, scattered discontinuous clay films, 1 ~20 cm thick LW, c-m. Scattered plant remains, blocky. Lower part contains a very thin bed with small Fe pisoids. Sharp upper contact.

Mudstone, yellowish green, common mm-size Fe pisoids. Gradational top.

Mudstone, olive gray, maroonish gray, greenish gray, variable clay films, common and variably amount of plant remains. Variably sandy and silty. 1 stringer of ~ 10 cm muddy LW. 15 m to the west, the basal 0.5 m, dark gray shale containing cm-size carbonized leaves on bedding plane, highly carbonized. Sharp top. Lake plain/margin of WTC away from delta depocenter.

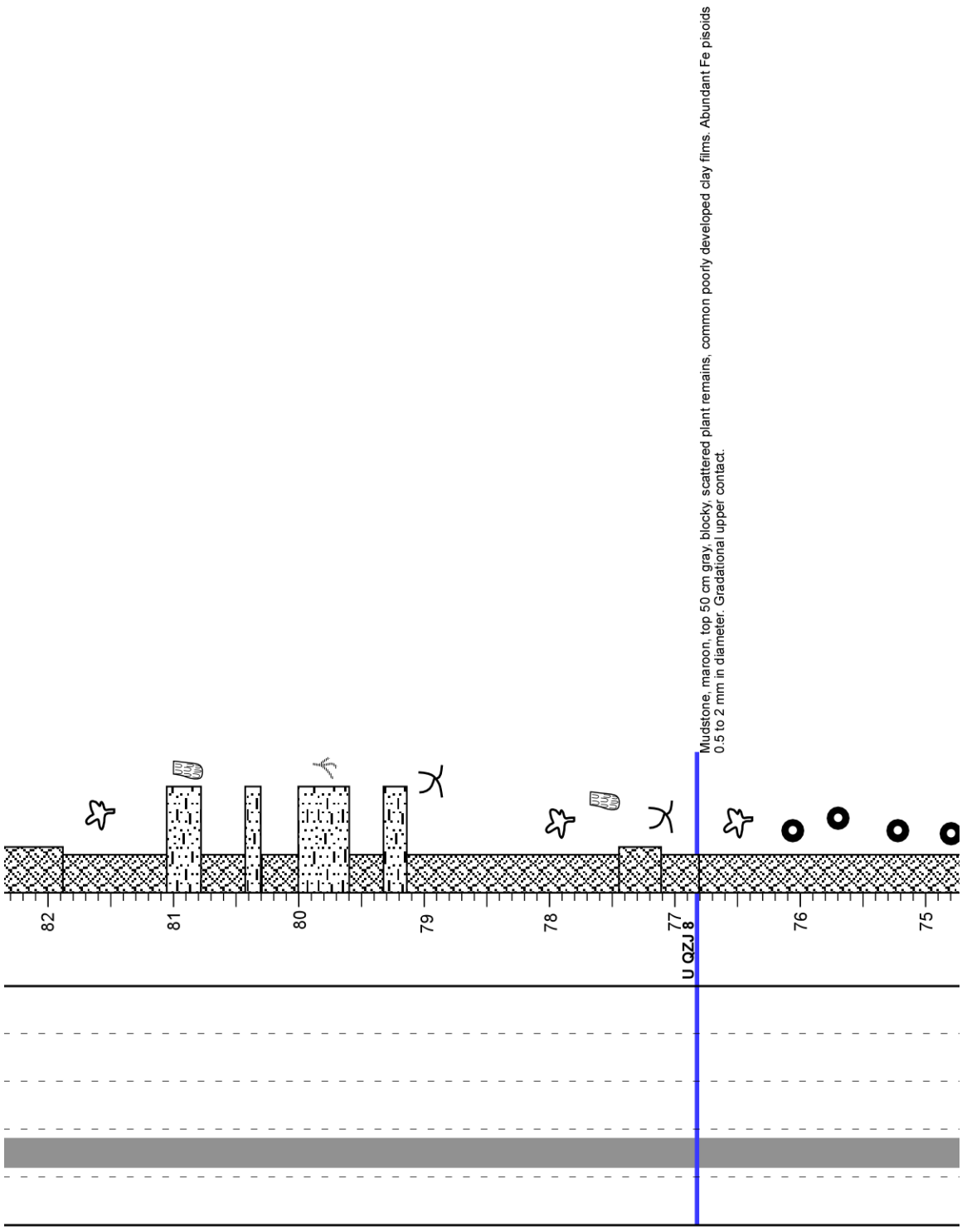
Mudstone, maroon, top 50 cm gray, blocky, scattered plant remains, common poorly developed clay films. Abundant Fe pisoids
0.5 to 2 mm in diameter. Gradational upper contact.
82
81
80
79
78
77
76
75
U QZJ 8

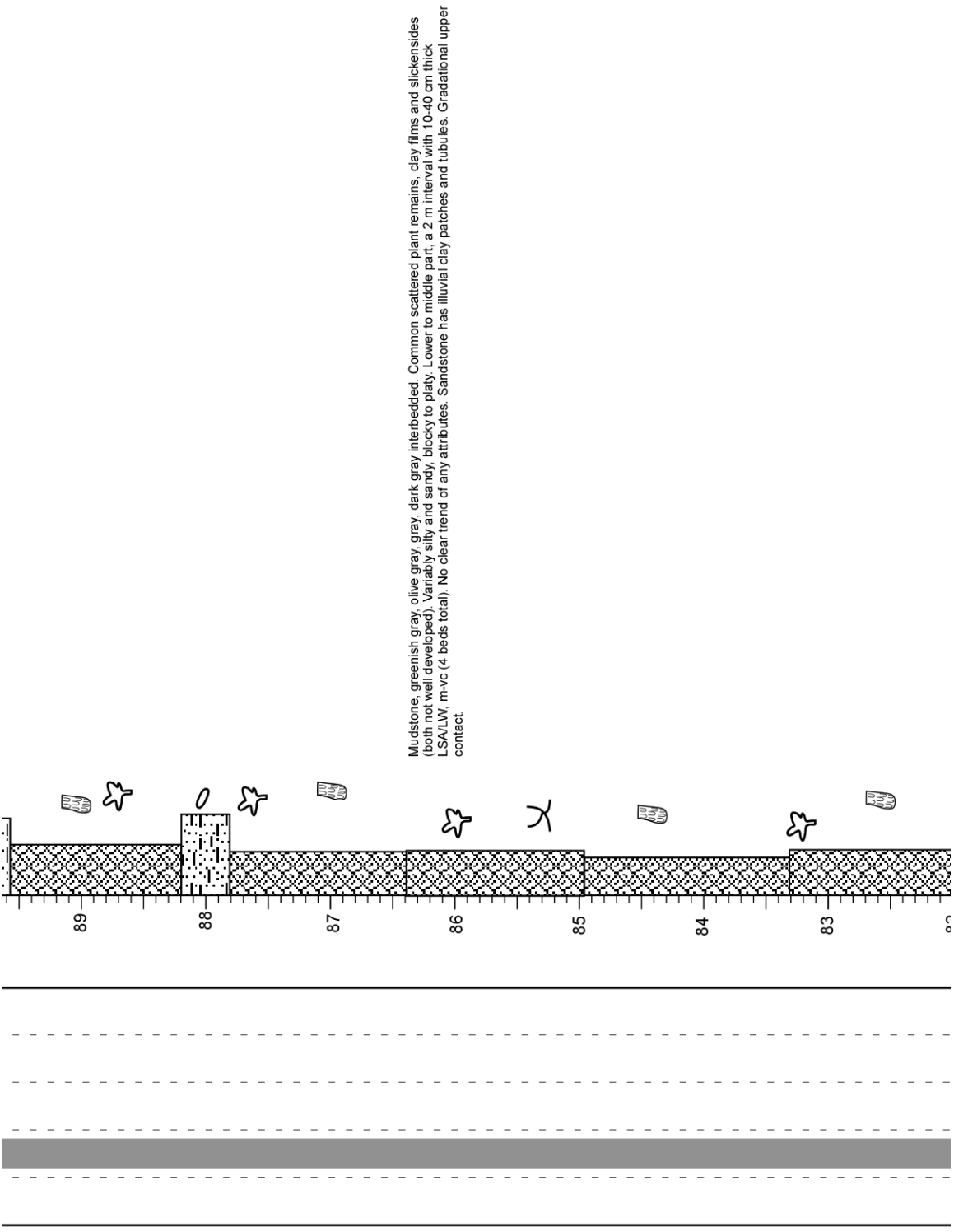
Mudstone, greenish gray, olive gray, gray, dark gray interbedded. Common scattered plant remains, clay films and slickensides (both not well developed). Variably silty and sandy, blocky to platy. Lower to middle part, a 2 m interval with 10-40 cm thick LSA/LW, m-vc (4 beds total). No clear trend of any attributes. Sandstone has illuvial clay patches and tubules. Gradational upper contact.
89
88
87
86
85
84
83

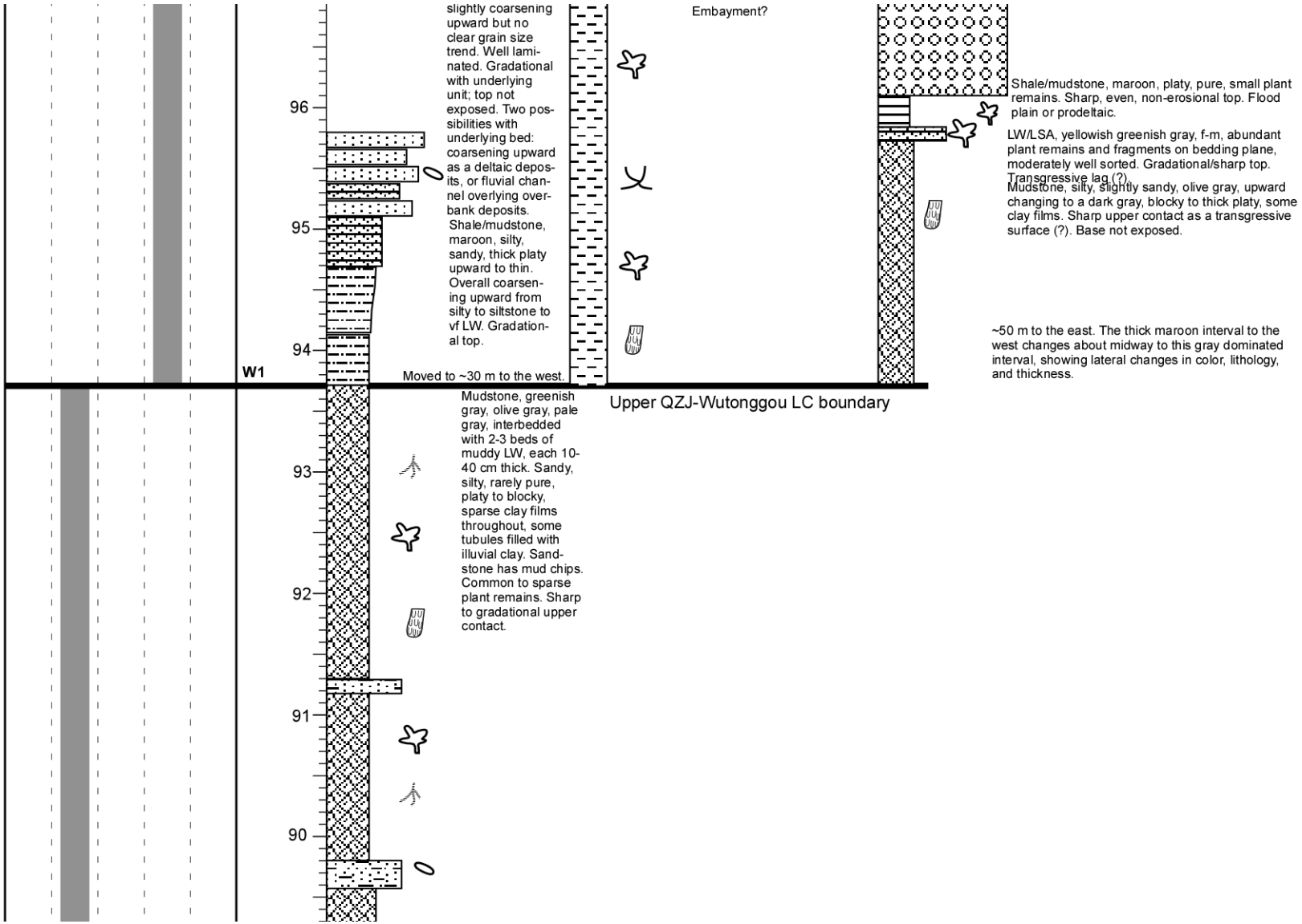
96
95
94
93
92
91
90
W1
slightly coarsening upward but no clear grain size trend. Well laminated. Gradational with underlying unit; top not exposed. Two possibilities with underlying bed: coarsening upward as a deltaic deposits, or fluvial channel overlying overbank deposits.
Shale/mudstone, maroon, silty, sandy, thick platy upward to thin. Overall coarsening upward from silty to siltstone to vf LW. Gradational top.
Moved to ~30 m to the west.
Mudstone, greenish gray, olive gray, pale gray, interbedded with 2-3 beds of muddy LW, each 10-40 cm thick. Sandy, silty, rarely pure, platy to blocky, sparse clay films throughout, some tubules filled with illuvial clay. Sandstone has mud chips. Common to sparse plant remains. Sharp to gradational upper contact.
Embayment?
Upper QZJ-Wutonggou LC boundary
Shale/mudstone, maroon, platy, pure, small plant remains. Sharp, even, non-erosional top. Flood plain or prodeltaic.
LW/LSA, yellowish greenish gray, f-m, abundant plant remains and fragments on bedding plane, moderately well sorted. Gradational/sharp top. Transgressive lag (?).
Mudstone, silty, slightly sandy, olive gray, upward changing to a dark gray, blocky to thick platy, some clay films. Sharp upper contact as a transgressive surface (?). Base not exposed.
~50 m to the east. The thick maroon interval to the west changes about midway to this gray dominated interval, showing lateral changes in color, lithology, and thickness.

Southwest Tarlong Section

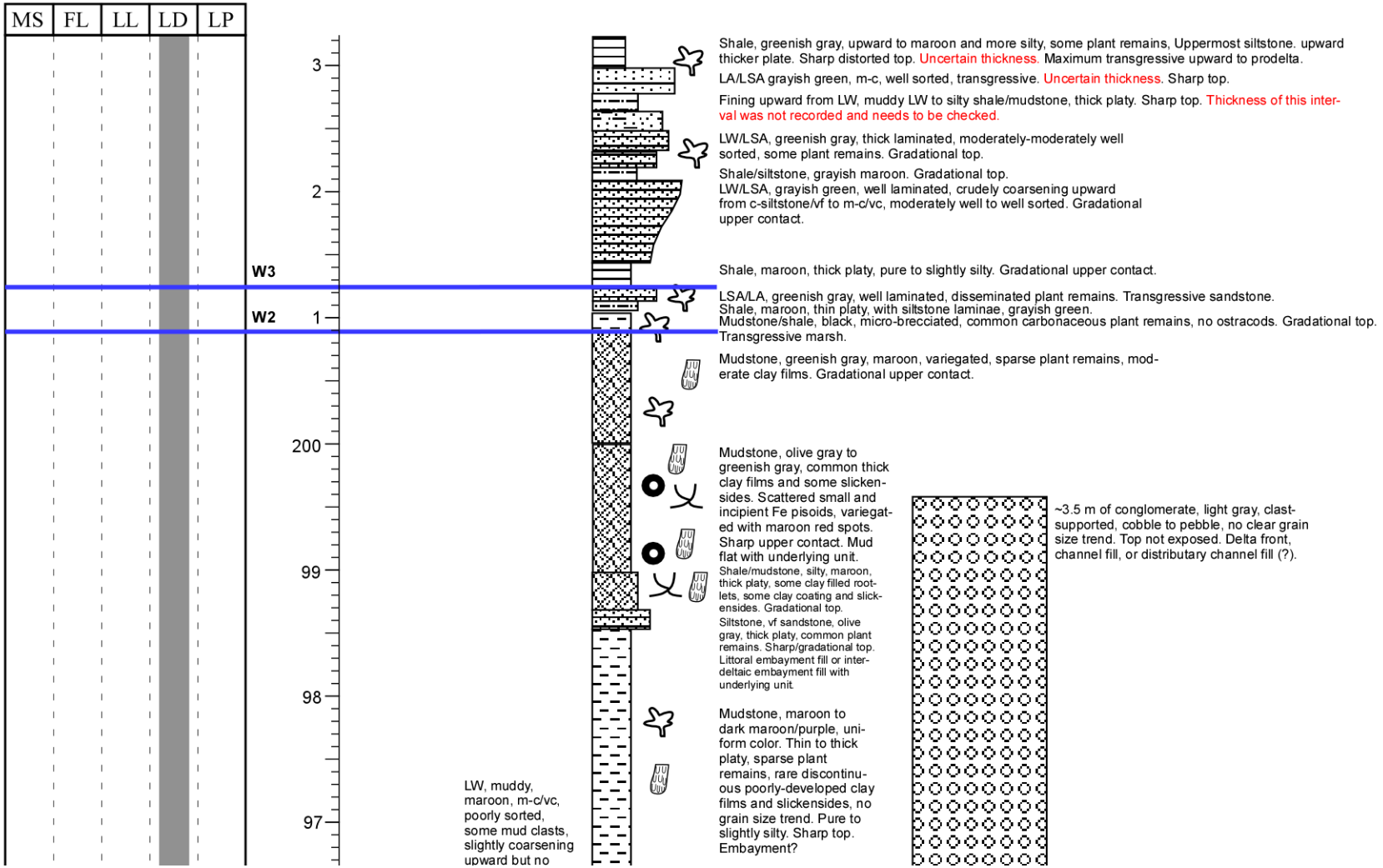

APPENDIX F
SOUTHEAST TARLONG SECTION

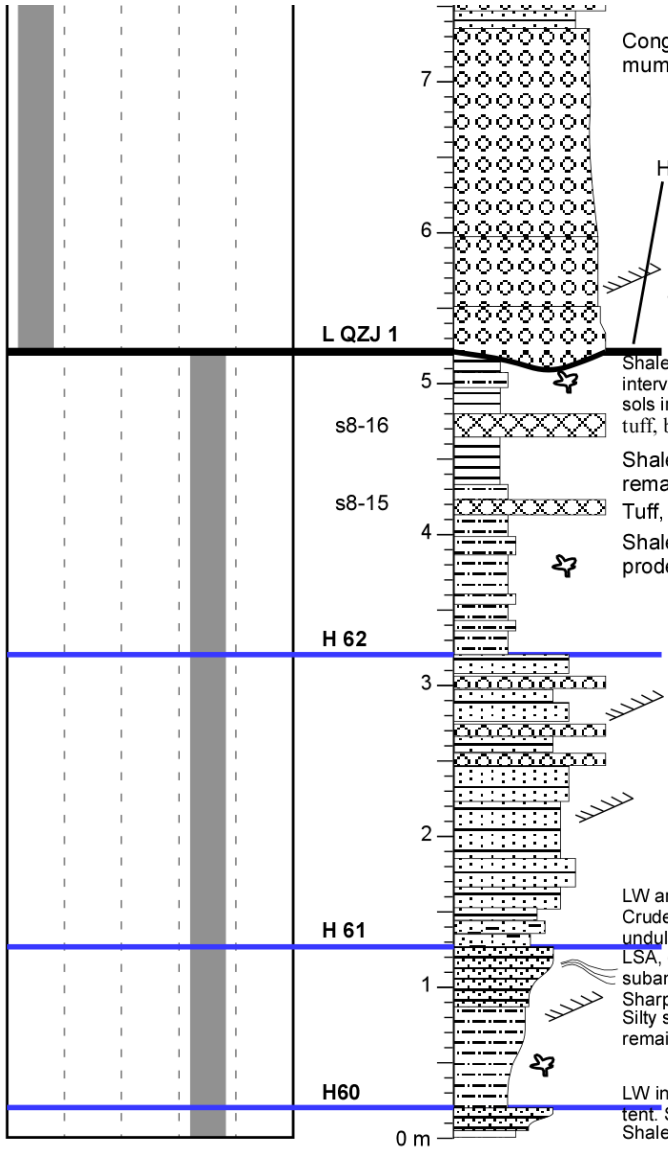

Conglomerate, gray, c-vc sand matrix, clasts well rounded to subrounded, 0.2-2 cm dominant, 5-cm maximum. Crudely fining upward from 2-3 cm to 1-2 cm. Clast supported. Gradational top.

Hongyanchi - Lower QZJ LC boundary

p8-8 - tuffs and channel lags

Conglomerate, greenish gray, well bedded, laterally persistent for at least 150 m. Lower 20-30 cm crudely fining upward from 5-cm to 2-1 cm pebbles. No bedding, some grains are imbricated or parallel to bedding plane, some are randomly oriented (as channel lag). Upper part, clasts 30 cm to granule, dominantly 3-6, mostly imbricated or parallel to bedding (both large and small clasts), crude low-angle large tabular x-beds, as bar deposits. Clast-supported, mostly rounded to subrounded, igneous clasts dominant, moderately to moderately well sorted. Sharp top. Channel lag of coarse-grained meandering stream.

Shale, pure-silty, gray to olive gray, well thin laminated, noncalcareous, some to common plant remains. The entire shale interval has no clear grain size trend. Erosional top with 1-10 cms relief. As HYC-QZJ low-order cycle boundary. The Calcisols in Northern Tarlong are eroded.

tuff, brick red, coarse silt to vf sand-size grains, thick laminated, sharp top and base. Uppermost 1 cm reddish black.

Shale, silty to pure, lower part greenish gray, upper part olive, noncalcareous, well laminated, some plant remains. Sharp top. Sublttoral or prodeltaic.

Tuff, light grayish red, basal 2 cm black, thin laminated, may not be as pure as overlying one. Sharp top.

Shale, silty, siltstone, basal part sandy, noncalcareous, well thin laminated, some plant remains. Sublittoral, prodeltaic.

LA dominant, brownish gray, some LSA lenses/laminae, c/vc, some conglomerate laminae with granule to 5-cm pebble clasts, well rounded, parallel to bedding or imbricated, gradational or sharp top and base, clast size overall increases upward. LA, c/vc, well sorted, subrounded to rounded, well cemented, noncalcareous, common red minerals, shifting lenticular bodies in upper 50 cm separated by m/c LSA. Large low-angle tabular x-beds dominant. Laterally persistent for ~100 m. Sharp top. Attitude: 9/40.

LW and LSA, thick interlaminated, f-c, well bedded and laminated. LW dominant in lower part, LSA mainly in upper part. Crudely coarsening upward. Some-sparse plant remains, poorly to moderately well sorted, subrounded to rounded. Sharp, undulating top. 10-40 cm thick. Delta front fringe.

LSA, gray, crudely coarsening upward from f/m to m/c, moderately well to well sorted, angular to subangular in lower part; subangular to rounded in upper part, well bedded, medium-large low-angle tabular x-beds, probably HCS, multi-directional. Sharp undulating top. 30-40 cm thick. Coarsening upward from underlying bed.

Silty shale, siltstone, vf sandstone, olive gray, overall crudely coarsening upward, rare m-sandstone laminae, some plant remains, noncalcareous. thick laminated, platy. Sharp/gradational undulating, wavy top with 10s of cm relief.

LW in basal and lower part, LSA in upper part, coarsening upward from f/m LW to m/c LSA. Well bedded, laterally persistent. Sharp top. Wave-dominated delta front.

Shale, olive gray, silty, siltstone.

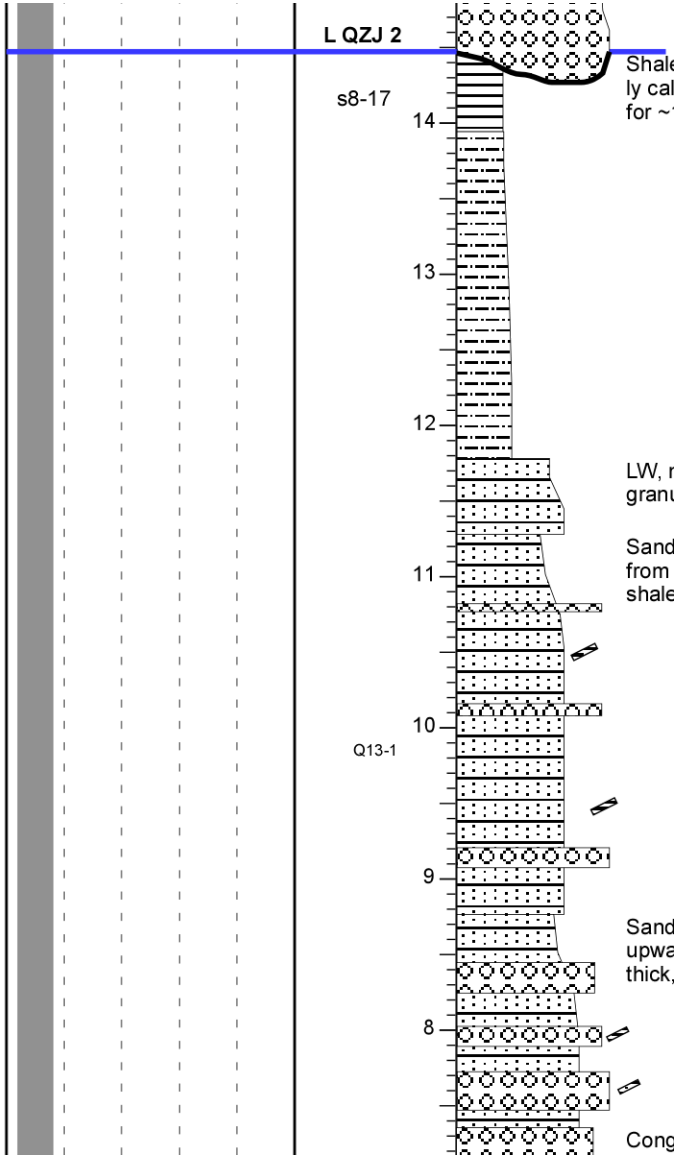

Shale, maroon, grayish maroon, sandy in lower part, upward less sandy. Upper ~50 cm pure. Non to weekly calcareous. No plant remains seen. Thick laminated. erosional top with 10s cm relief, laterally persistent for ~100 m. Upper part of coarse-grained meandering stream (not braided stream).

LW, muddy, maroon, m-c, fining upward, very poorly sorted, non to weekly calcareous, some scattered granules and 1-cm pebbles, thick laminated. Gradational top.

Sandstone, intercalated with 1-10 cm thick conglomerate, grayish maroon. Sandstone, LSA, fining upward from c-m to m/f LS, thick laminated. Conglomerate: granule to 1 cm. Non to weekly calcareous. Few sandy shale laminae. Few plant remains. Common angular, sand-granule size mud chips. Sharp/gradational top.

Sandstone and conglomerate interbeds, olive gray. Sandstone, LSA/LA, moderately well sorted, fining upward from c/vc to m-c crudely, well laminated. Conglomerate: granule to 2-cm, interbeds 10-30 cm thick, common angular mud chips. Gradational top.

Conglomerate, gray, c-vc sand matrix, clasts well rounded to subrounded, 0.2-2 cm dominant, 5-cm maxi-

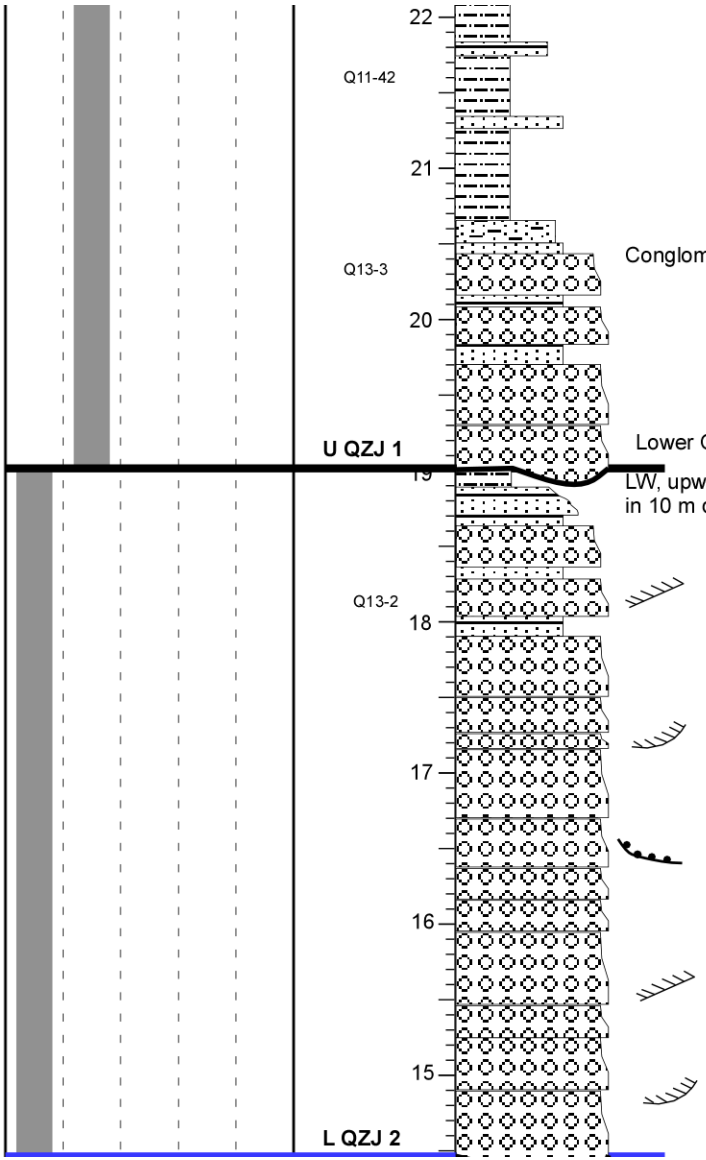

Conglomerate, same as below, subrounded to rounded, igneous clasts dominant. Sharp/gradational top.

Lower QZJ-Upper QZJ LC boundary

LW, upward to sandy shale, well thick laminated, well bedded, m-vc, granular. Variable thickness 20-50 cm in 10 m distance. Sharp erosional top.

Conglomerate, reddish gray, clast supported, granule to 20 cm (max.), 2-5 cm median, m-vc sand matrix, imbricated and parallel to bedding. Fining upward indicated by less abundant large pebbles. Rare m-vc LSA/LW stringers, 1-10 cm thick, in upper part. Large low-angle tabular and trough x-beds in lower part (p8-9), few internal erosional surface. Individual fining upward units 20-30 cm thick. Sharp/gradational top.

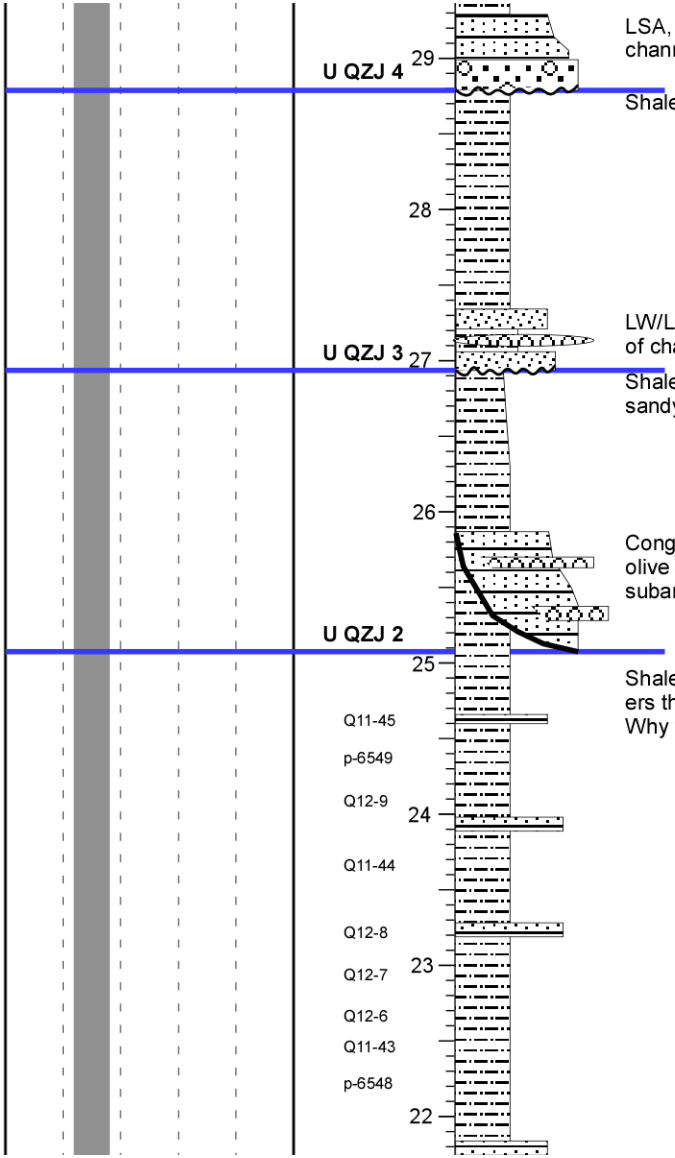

LSA, conglomeratic with granules, upward to LW, m-vc, poorly to moderately sorted, subrounded, small channel fill. Gradational to sharp top.

Shale, maroon, sandy (m-c sand grains) throughout. Sharp/erosional top.

LW/LSA, conglomerate (granular) lenses, shale/siltstone stringers, gray. Sharp/gradational top. Side/edge of channel fill.

Shale, maroon, variably sandy, rare granules. Monotonic, noncalcareous, crudely fining upward (less sandy). Sharp/erosional top.

Conglomerate and conglomeratic sandstone, basal 15 cm, grayish red (probably tuffaceous). Middle part olive gray, upper part reddish gray. Granule to <1 cm pebbles. LW/LSA, m-vc, poorly to moderately sorted, subangular to subrounded. 0-80 cm thick. Sharp/gradational top.

Shale, maroon, variably sandy, basal 15 cm, m-c LW, noncalcareous, no plant remains. LW, m-c, as stringers throughout. Sharp/erosional top.
Why the shale is so monotonic??

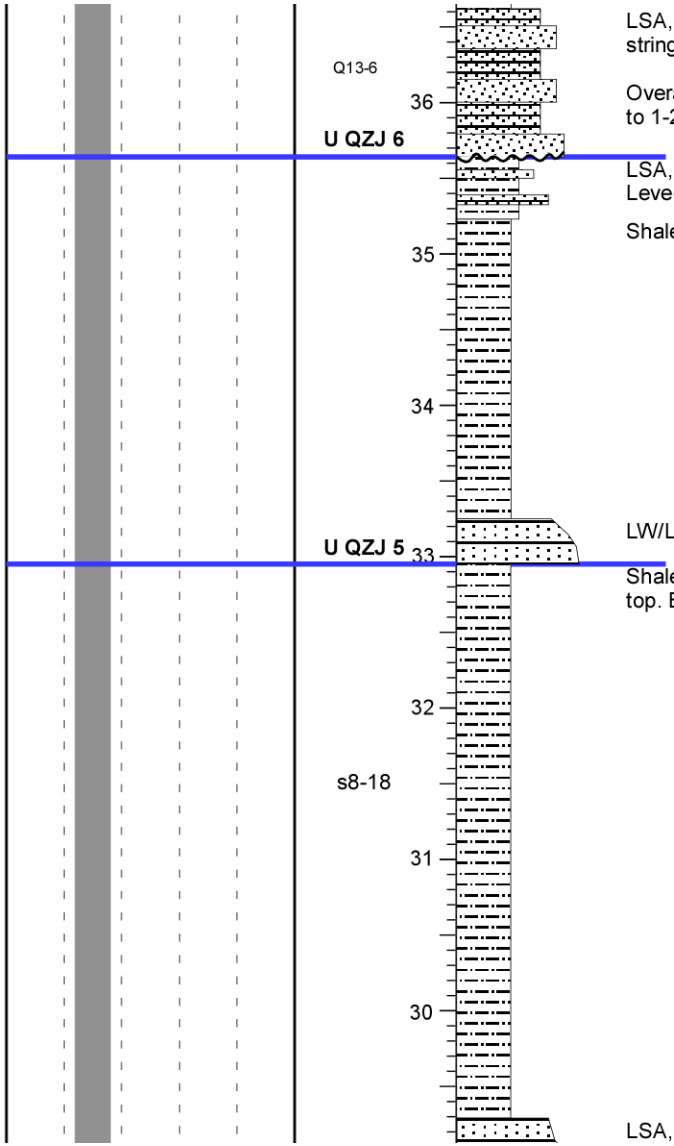

LSA, upward to LW, f-m, m-c, moderately to moderately well sorted, well bedded. A 10-cm thick siltstone stringer in upper part.

Overall, conglomerate to sandstone, c/vc sandstone to f-m sandstone, maximum clast size from 20-30 cm to 1-2 cm, in the QZJ LC.

LSA, siltstone, interbedded, maroon, f-m, moderately to moderately well sorted. Sharp/erosional top. Levee/crevasse deposits.

Shale, maroon, with floating rounded to subrounded, f-c sand grains. Sharp top.

LW/LSA, m-vc, poorly to moderately sorted. gradational top.

Shale, maroon, sandy with floating f-vc grains, rare granules and fine pebbles, thick laminated. Sharp top. Bay fill?

LSA, conglomeratic with granules, upward to LW, m-vc, poorly to moderately sorted, subrounded, small

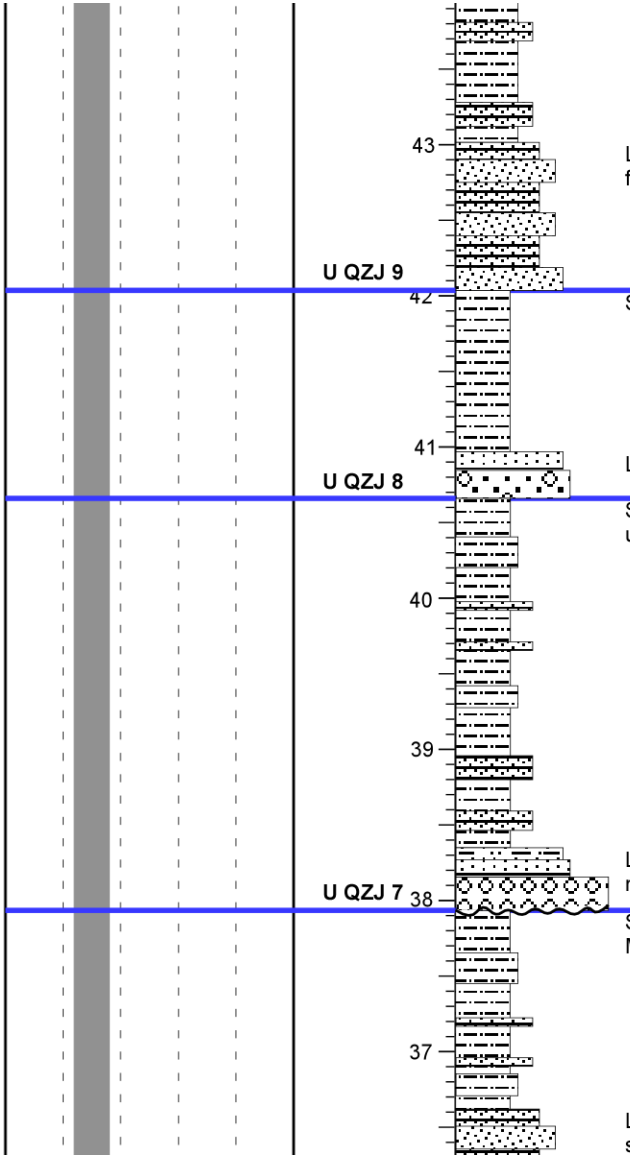

LSA, f-m, m-c, maroon and reddish gray, moderately to moderately well sorted, scattered granules and fine pebble, well laminated and bedded.

Shale, silty, maroon. Sharp top.

LSA/LW, reddish gray, m-vc, lower part some granule and fine pebble clasts. Gradational top.

Shale, silty, intercalated with LW and siltstone, maroon, platy, medium-thick laminated. Overall fining upward (less sandy and silty). Sharp top.

Lower 20 cm, pebbly granular conglomerate with c-vc sand matrix, upward to granular pebbly c-vc LSA, to muddy LW. Reddish gray. Poorly cemented (as all sandstone and conglomerate in QZJ). Gradational top.

Shale, sandy and silty, siltstone, f-m LW interbeds, silty shale dominant, intercalated with sandstone. Maroon. Crude fining upward trend. Sharp/erosional top.

LSA, upward to LW, f-m, m-c, moderately to moderately well sorted, well bedded. A 10-cm thick siltstone stringer in upper part.

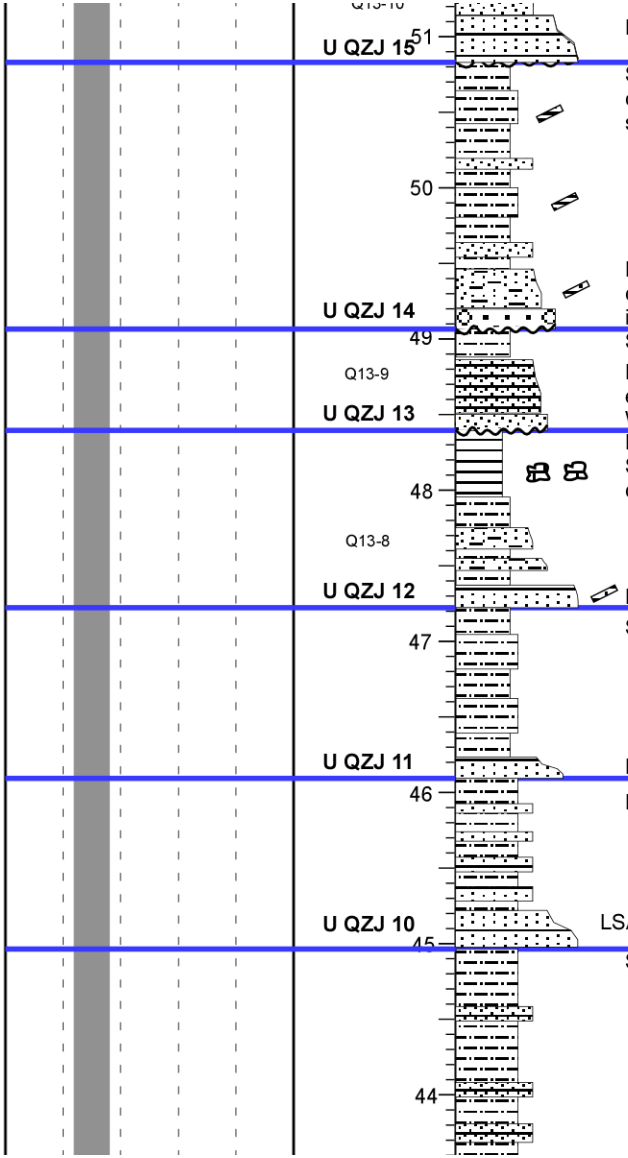

LA/LSA, gray, fining upward from c-vc to m-c, granular, well bedded, very calcareous. Sharp/gradational top.

Silty shale, sandy shale, siltstone, f LW interbeds, maroon, crudely fining upward, non to weekly calcareous. Possible scattered plant remains, well thick laminated. Scattered mud chips (also in many sandstones below). Sharp/erosional(?) top.

LSA, light gray, m-c, granule to fine pebble conglomeratic, moderately well sorted, subrounded, in lower 15 cm. Upward to LSA, LW, f-m, moderately to moderately well sorted, olive gray. Angular mud chips 1-10 mm in LW. Gradational/sharp top. Small channel fill.

Siltstone, silty shale, dark maroon. Noncalcareous. Sharp/erosional with 10s cm relief, concave top.

LA in lower 10 cm, m, upward to LSA, to LW, light to dark gray, moderately to very calcareous. LA, well sorted, subrounded to rounded, preferably calcite cemented to nodular. LSA/LW, f-m. Overall fining upward. Well bedded.

LW, muddy, very sandy shale in lower part, upward to sandy shale, to pure platy shale, dark maroon. Scattered 1-cm calcitic nodules, equant, in one laminae (diagenetic). Sharp/erosional, low-relief concave top.

LSA, grayish red, c-vc, subrounded to rounded, well bedded, common mud chips from below.

Shale, silty, sandy, siltstone, maroon. Sharp top.

LSA, upward to LW, f-c (m average), reddish gray.

LW, f, shale, sandy, siltstone interbeds. LW common, thick laminated, maroon. Sharp top.

LSA, c-vc in lower part, upward to m LW, grayish red to reddish gray. Sharp/gradational top. Crevasse splay?

Siltstone, sandy with f sands, f LW, interbeds, maroon. Sharp top.

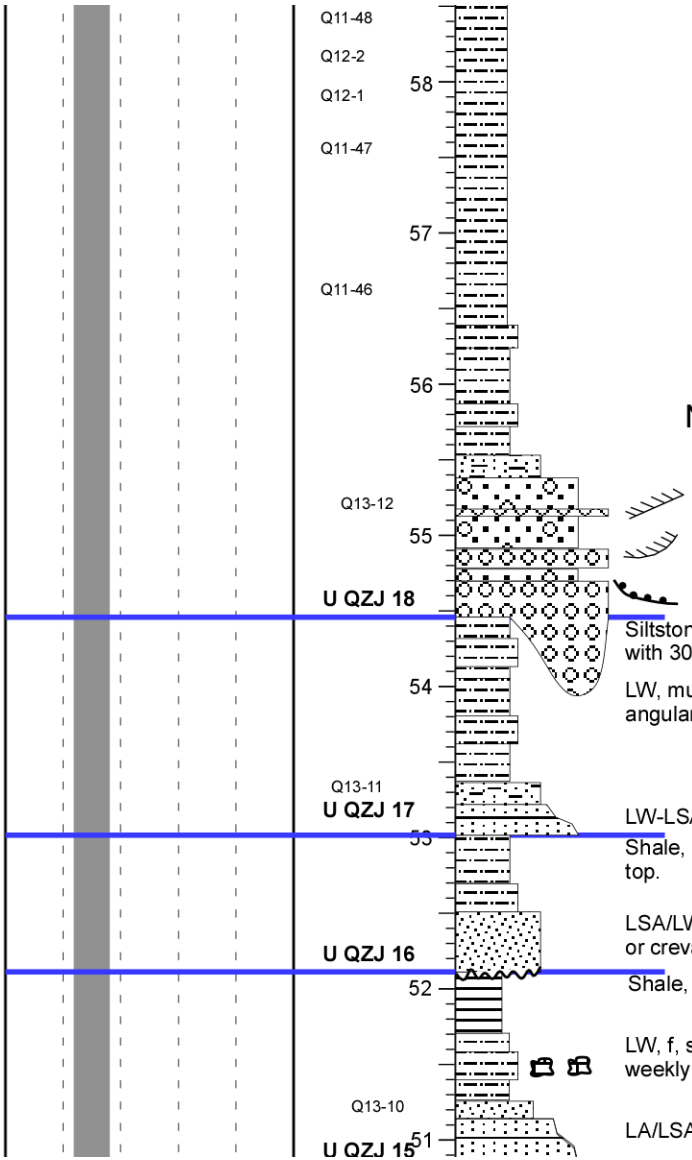

New attitude 022/ 52

Conglomerate and conglomeratic sandstone, reddish gray in lower part, gray in upper part. Overall fining upward, lower 50 cm conglomerate dominant, 5-cm (max.) pebbles, imbricated, low-angle tabular and trough large x-beds, internal erosional surfaces. Sandstone, conglomeratic, LSA/LW, c-vc, common mud chips, LSA upward to LW. Weakly calcareous. Sharp/gradational top.
A major channel fill, underlying thin couplets of possible overbank deposits.
A positive relationship between thickness of coarse-grain vs. upper fine-grained intervals, vs. total cycle thickness? Something to look into.

Siltstone, silty shale, not sandy, maroon, uniform, noncalcareous, medium-thick laminated. Erosional top with 30-50 cm relief.

LW, muddy, very sandy shale, and siltstone, maroon, thick laminated, noncalcareous. Sand grains m-vc, angular to rounded. Gradational top.

LW-LSA, olive gray, m-vc, poorly to moderately sorted, noncalcareous. Gradational top.

Shale, sandy to very sandy, siltstone, thick laminated, some possible plant remains, noncalcareous. Sharp top.

LSA/LW, f-m, light gray, moderately well to well sorted, noncalcareous. Gradational top. Small channel fill or crevasse splay.

Shale, maroon, pure, platy well laminated, noncalcareous. Sharp, low-relief erosional surface.

LW, f, siltstone, silty and sandy shale interbeds, platy, sparse scattered possible plant remains, non to weekly calcareous, some lines of scattered 1-2 cm equant calcitic nodules (diagenetic). Gradational top.

LA/LSA, gray, fining upward from c-vc to m-c, granular, well bedded, very calcareous. Sharp/gradational top.

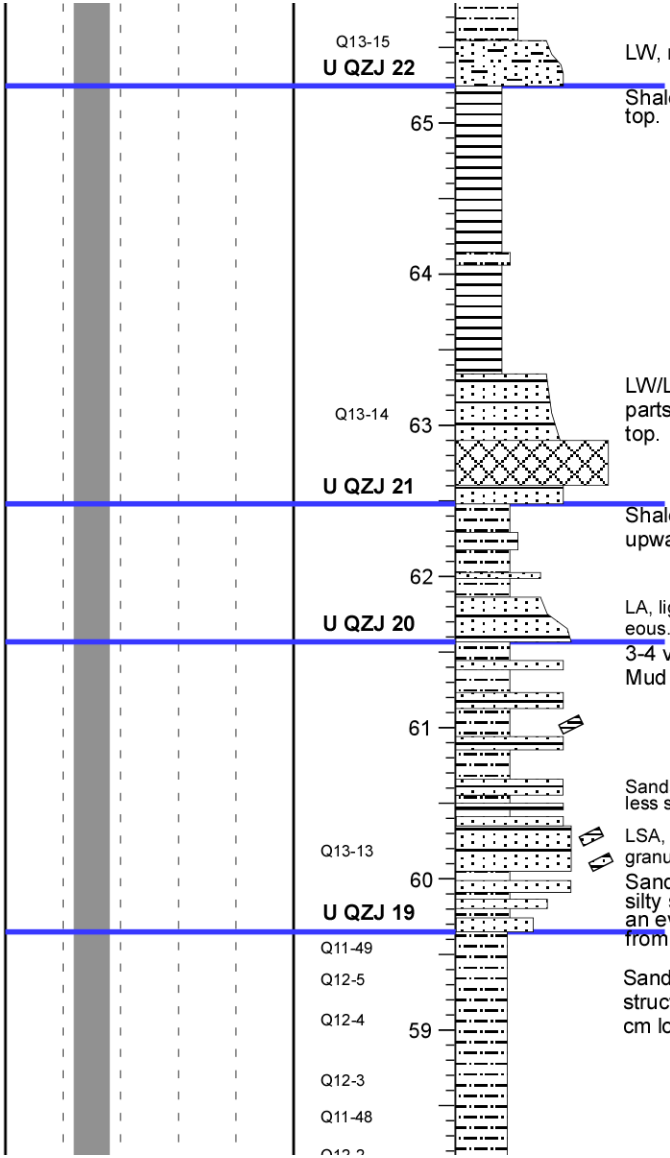

LW, muddy, greenish gray, fining upward from c/vc to m/c. Gradational top.

Shale, maroon, pure to silty, monotonic, rare (1) cm thick sandy shale stringer. Noncalcareous, sharp top.

LW/LSA, m-c muddier upward, light gray in basal 10 cm, maroon-olive gray in upper part. Lower-middle parts ~30 cm slippery, ductile, maroon, maybe fault gouge or bentonite. Overall fining upward. Gradational top.

Shale, sandy, siltstone, maroon, 1-2 cm thick LW, f-m, stringers as overbank deposits. Sharp top. Fining upward with underlying bed.

LA, light gray, c-vc, well sorted in lower 10 cm, fining upward to f-m LSA, to LW, thick laminated, well bedded, noncalcareous. Gradational top. Another crevasse event or fringe of a channel fill?

3-4 very sandy shale/muddy LW and silty shale/pure shale couplets. Maroon, thick to thin laminated, platy. Mud chips in sandy shale/LW. Sharp top. Fining upward from the underlying 3 beds.

Sandstone-shale couplets, 10-15 cm thick each. Thick laminated. Shale, maroon, 5-10 cm thick, silty, very sandy, upward less sandy, into overlying monotonic pure shale. Sandstone, LW, m-vc, gray. Sharp to gradational top.

LSA, light gray, c-vc, small to large (cms) mud chips, moderately well sorted, moderately calcareous. Some floating granule-fine pebble. Sharp top. Overbank deposits of a major flood event.

Sandstone-shale couplets, 5-10 cm thick each. Sandstone, LW/LSA, c-vc, gray, capped by 1-2 cm thick silty shale to sandy shale. Each couplet has sharp base and top with internal gradational contact, indicating an event of waning flow, representing one overbank event. thickness variable. Overall coarsening upward from f to m/c. Sharp top.

Sandy shale, siltstone, muddy LW in lower 1 m. Upper part, monotonic silty shale, no other textural and structural features, medium-thick laminated, thinner upward. Noncalcareous. Maroon. Sharp top, 1-10 cm low relief. Back to featureless shale.

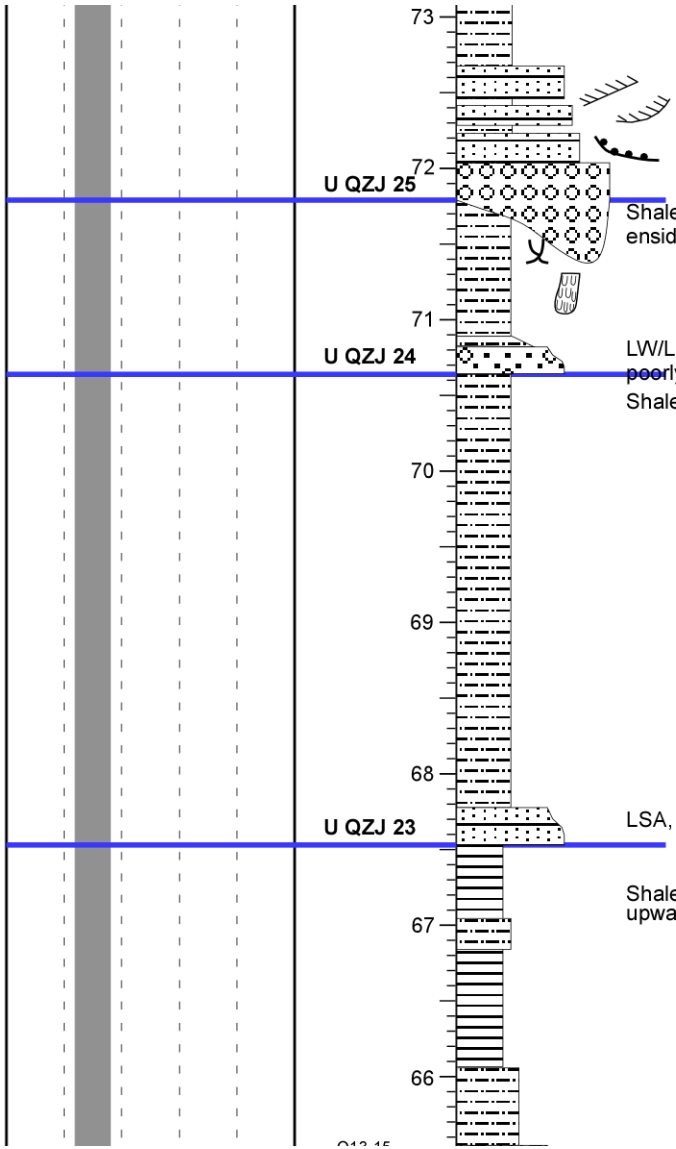

Conglomerate, granular, some fine pebbles, gray to olive gray; Sandstone, LSA/LA-LW, c-vc, sub-rounded to round. Probably large tabular and trough x-beds, internal erosional surfaces. Some sandy shale stringers. Sharp/gradational top.

Shale, maroon, silty, slightly to variably sandy, platy to blocky, common small (mm-cm) multi-faceted slick-ensides with maroon clay coats. Erosional top, concave, 10s cm relief)

LW/LSA, some granules and fine pebbles, olive gray, m-vc, upward to LW, to sandy shale, moderately to poorly sorted. Gradational top.

Shale, maroon, silty, variably sandy, noncalcareous, largely monotonic. Sharp top.

LSA, light gray upward to olive gray, c/vc, upward to m/c LW, well bedded. Gradational/sharp top.

Shale, maroon, lower 50 cm, very sandy to sandy, upper part silty to pure, variably sandy. Overall fining upward. Sharp top.

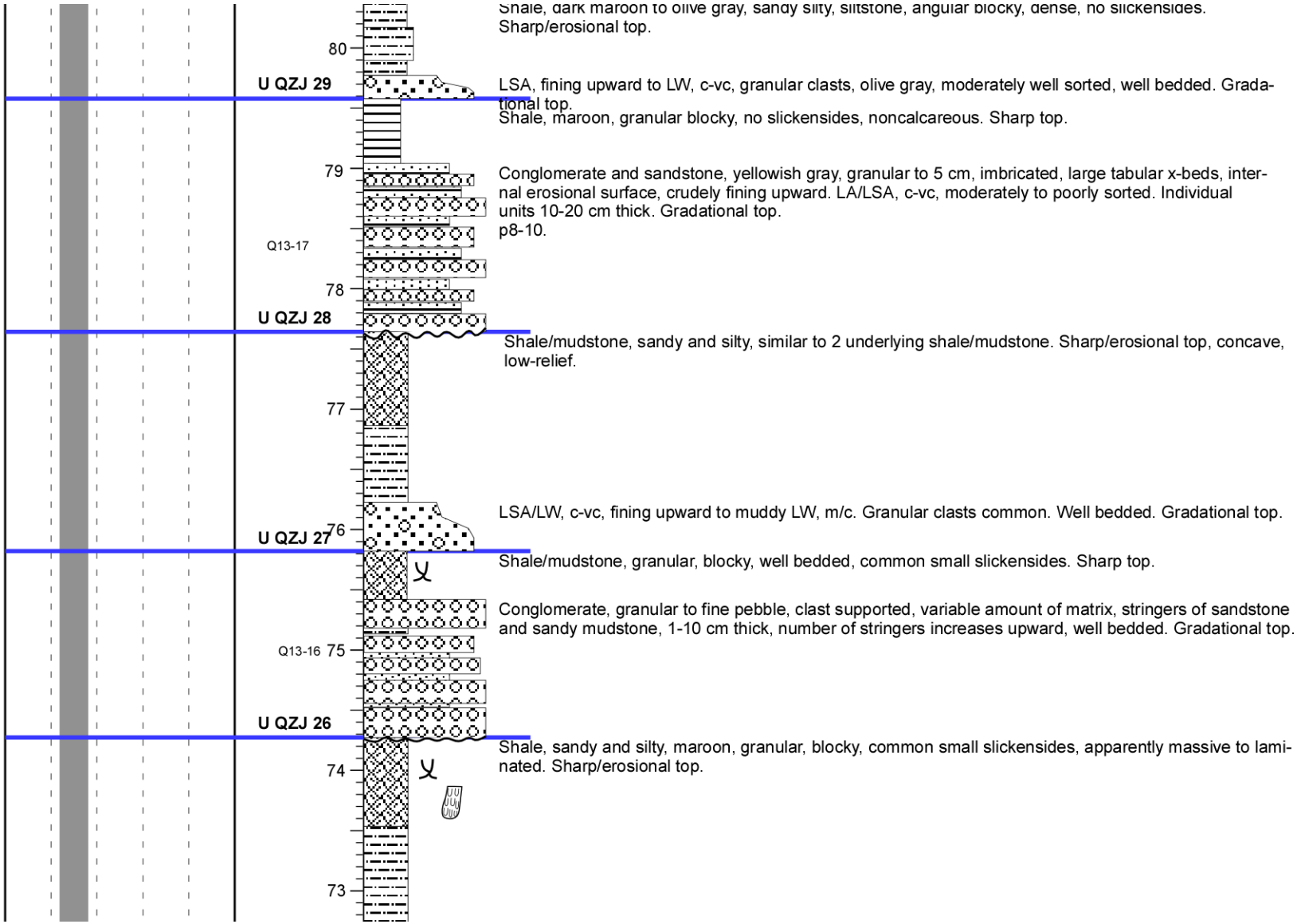

Shale, dark maroon to olive gray, sandy silty, siltstone, angular blocky, dense, no slickensides. Sharp/erosional top.

LSA, fining upward to LW, c-vc, granular clasts, olive gray, moderately well sorted, well bedded. Gradational top.

Shale, maroon, granular blocky, no slickensides, noncalcareous. Sharp top.

Conglomerate and sandstone, yellowish gray, granular to 5 cm, imbricated, large tabular x-beds, internal erosional surface, crudely fining upward. LA/LSA, c-vc, moderately to poorly sorted. Individual units 10-20 cm thick. Gradational top.

p8-10.

Shale/mudstone, sandy and silty, similar to 2 underlying shale/mudstone. Sharp/erosional top, concave, low-relief.

LSA/LW, c-vc, fining upward to muddy LW, m/c. Granular clasts common. Well bedded. Gradational top.

Shale/mudstone, granular, blocky, well bedded, common small slickensides. Sharp top.

Conglomerate, granular to fine pebble, clast supported, variable amount of matrix, stringers of sandstone and sandy mudstone, 1-10 cm thick, number of stringers increases upward, well bedded. Gradational top.

Shale, sandy and silty, maroon, granular, blocky, common small slickensides, apparently massive to laminated. Sharp/erosional top.

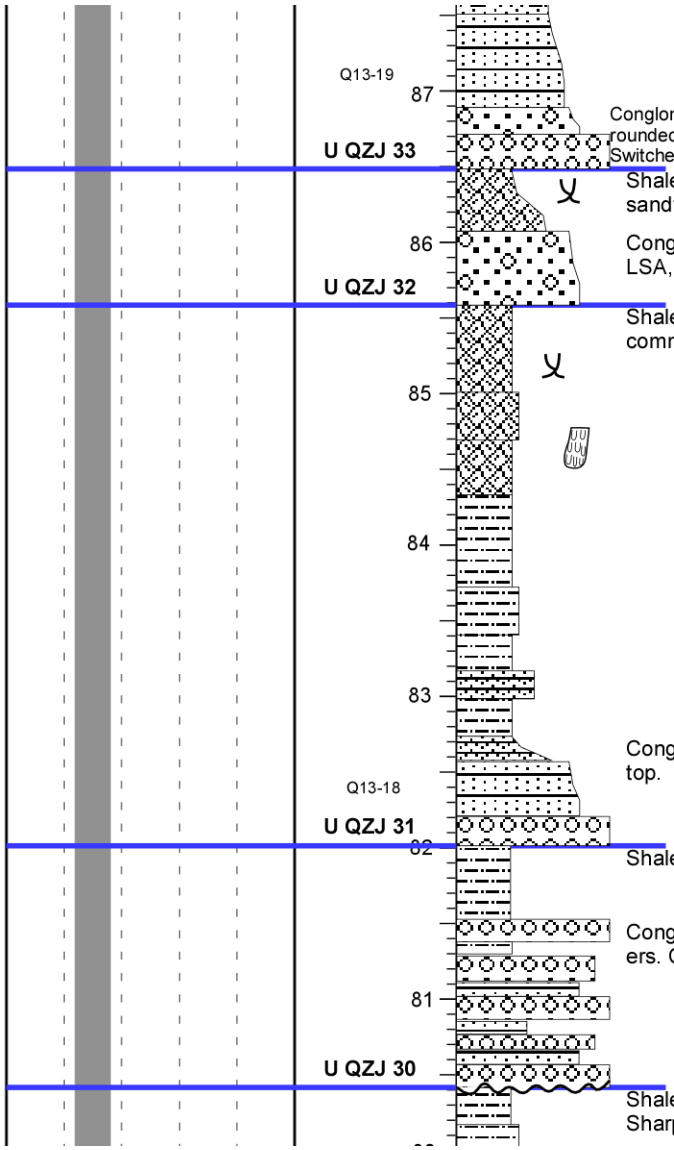

Conglomerate, light gray, granular to fine pebble in c/vc sand matrix. Upward to conglomeratic LSA/LA, c-vc, subrounded to rounded, moderately well sorted. Gradational top.
Switched to west over the ridge to the west side of the slope facing the Quaternary alluvium. Section at lower 1/3 of the slope.

Shale/mudstone, olive gray, blocky to platy, common slickensides, very sandy. Fining upward from LW to sandy shale. Erosional top.

Conglomeratic LSA (c-vc), gray, fining upward from LSA to LW, well rounded, moderately well sorted in LSA, subrounded to rounded. Gradational top.

Shale/mudstone, maroon, few stringers of sandy shale/LW, 10-20 cm thick. Mudstone, granular blocky, common multi-directional slickensides and clay films. Non to weakly calcareous. Sharp top. Proto Argillisol.

Conglomerate in lower 20 cm, fining upward to LSA/LA, c-vc, granular, to LW/sandy shale. Gradational top.

Shale, silty, sandy, scattered granules, maroon. No slickensides. Sharp top.

Conglomerate and sandstone, gray, granule to fine pebble, LSA, c-vc. Few sandy shale and LW, f-m, stringers. Crudely fining upward. Sharp/gradational top.

Shale, dark maroon to olive gray, sandy silty, siltstone, angular blocky, dense, no slickensides. Sharp/erosional top.

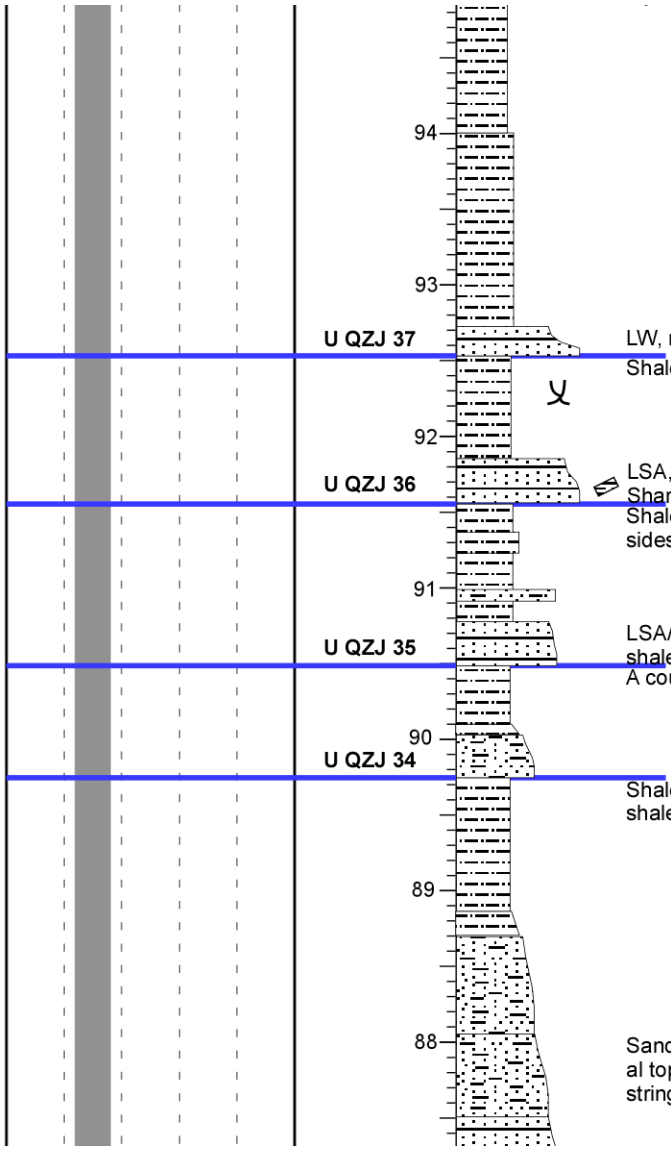

LW, maroon, m-vc, muddy, poorly sorted. Gradational top.
Shale, maroon, angular platy, noncalcareous, sandy, silty, sparse local slickensides. Sharp/gradational top.

LSA, olive gray, upward to LW, c-vc, moderately to moderately well sorted, some mud chips, well bedded. Sharp/gradational top.
Shale, maroon, silty, sandy, siltstone, muddy m-c LW interbeds. Thick platy, noncalcareous, no slickensides. Crudely fining upward. Sharp top.

LSA/LW, maroon, thick laminated, platy, m-c, poorly to moderately sorted, subangular to subrounded. Few shale stringers. Gradational top.
A couplet similar to the couplet below. No slickensides. Sharp top.

Shale, grayish maroon. Lower 1/2, sandy shale, muddy LW, f-m, overall fining upward. Upper 1/2, silty shale, siltstone, not sandy, platy. Noncalcareous, no slickensides. Gradational top.

Sandstone, in the upper 1/3, maroon, angular platy, LW, f-m, muddy, subangular to subrounded, gradational top. In the middle 1/3, maroon, platy, LSA upward to LW, m-c, subangular to subrounded, few f LW stringers. Gradational top. The lower 1/3 is the conglomerate below.

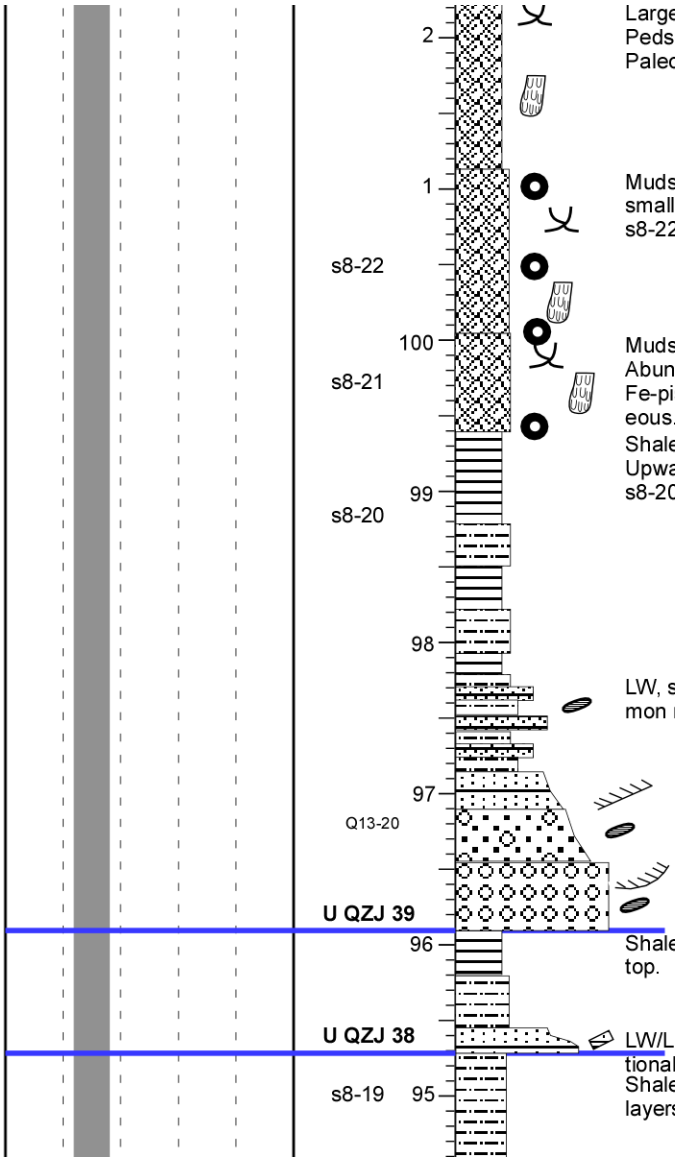

Large, thick slickensided surfaces with thick clay films and rounded corners, slickensides smaller upward. Peds rounded to subrounded, cm in size, upward decreasing in size, weakly calcareous. Sharp top. Top of Paleosol. BS (stacked Spodosol and Argillisol?).

p8-11: Bentonite

Mudstone, gray to dark gray, angular to subangular peds, cms in size, abundant 1-10 mm Fe-pisoids, small slickensides (cm) common. Thick clay films than below. sharp top. Gleyed in phreatic conditions?
s8-22: 50 cm above base.

Mudstone, light maroon upward to grayish maroon, to gray, a color transition zone. Pervasively slickensided. Abundant multi-directional slickensides, cm-size, illuvial clay films lining slickensides. First appearance of Fe-pisoids, dark gray to brownish yellow, 1-10 mm, sparse/rare at base, upward to common. Weakly calcareous. Peds elongate to wedge, cms in size. Slightly silty shale as parent rock. Gradational top.

Shale, maroon, silty vs pure interbeds, granular, angular 1-5 cm blocks, noncalcareous, no slickensides. Upward less silty. Sharp top.
s8-20: 50 cm below the top.

LW, sandy shale, siltstone interbeds, maroon, thick laminated, LW poorly to moderately well sorted. Common mud chips. Gradational top.

Conglomerate, granule to fine pebble, upward to conglomeratic LSA, c-vc, to LSA/LW, m-vc, rounded mud chips throughout. Light gray, olive gray in upper 30 cm. Fining upward in sand and clast size and abundance. Well bedded, large, low-angle, tabular and trough x-beds. Sharp/gradational top.

Shale, pure to silty, maroon, thin platy to small blocky, noncalcareous, no slickensides. Sharp/erosional (?) top.

LW/LSA, maroon, thick laminated, some mud chips, moderately to moderately well sorted, m-vc. Gradational top.

Shale, maroon, platy and sandy in lower part, more blocky and dominantly silty or pure in upper part. Local layers with sparse slickensides, not in upper part. Sharp top.

Southeast Tarlong Section

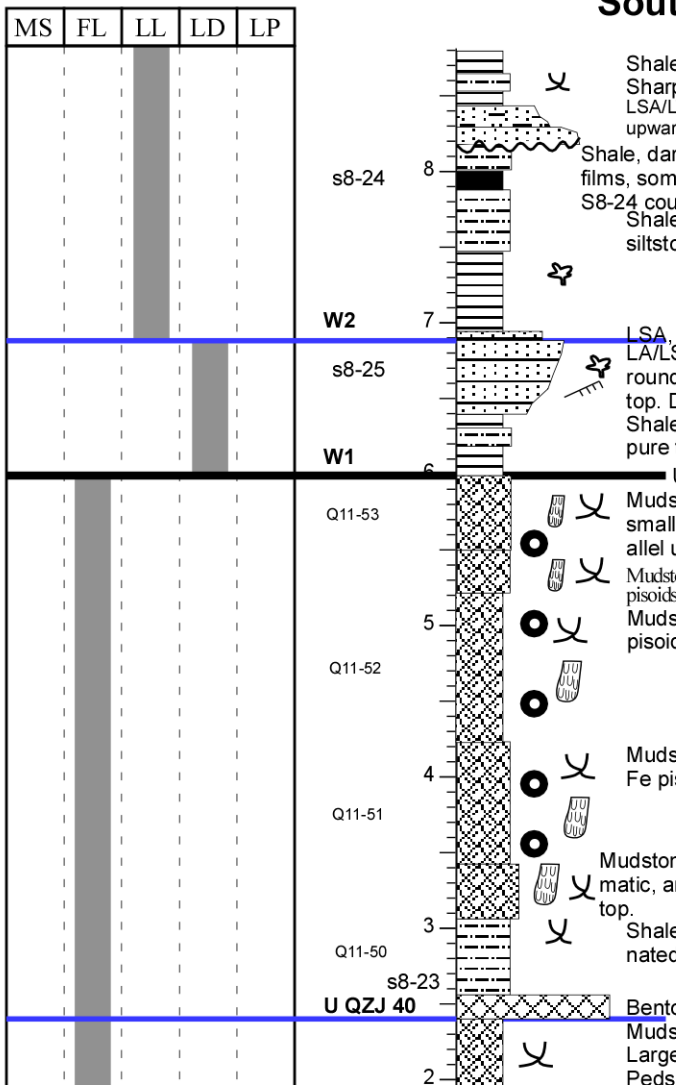

Shale, maroon, sparse small slickensides, sparse plant remains, thick, short plates. Locally silty and sandy. Sharp top. Delta plain.

LSA/LW, olive gray, f-c/vc, poorly to moderately sorted, upward to muddy LW, thick laminated, sparse plant remains. Fining upward. Gradational top. Delta plain, distributary channel, crevasse splay.

Shale, dark gray, grayish black in lower part, upward to dark gray, to gray, very well laminated, common carbon films, some discontinuous poorly-defined slickensides. Upward siltier. Sharp/erosional (?) top. Delta plain.

S8-24 could well be a bentonite.

Shale, maroon to olive gray, well laminated. Lower part pure, thin laminated, upward to slightly sandy to siltstone, some plant remains. Gradational top. Delta plain.

LSA, brownish gray, well laminated, f/m, well sorted. Gradational top. Transgressive (?).

LA/LSA, gray, very well thin laminated, coarsening upward from vf, f, m, m/c, to c/m, very well sorted, sub-rounded to rounded, noncalcareous. Probable ripple laminated. Possible tiny plant remains. gradational top. Distal delta front or delta front fringe.

Shale, olive gray to maroonish gray, thin laminated, upward to medium-thick laminated, very well laminated, pure to slightly silty, possible sparse plant remains. Gradational top.

Upper QZJ-Wutonggou LC boundary

Mudstone, gray to dark gray, uniform color, rare small Fe pisoids, thick discontinuous clay films, common small slickensides. Peds 1-2 cm, subrounded. AB(?), Gleyed? Sharp, undulating erosional surface as a parallel unconformity separating QZJ and WTG LCs.

Mudstone, variegated maroon, purple, green, gray, wedge-prismatic-columnal peds, 1-10 cm in size, weakly to noncalcareous. Common Fe pisoids (less than below), thick clay films, but less prominent, smaller slickensides than below. Sharp/gradational top.

Mudstone, gray to purplish gray, sparse small slickensides, less and thinner clay films. Still abundant Fe pisoids. Peds smaller (?) than below. Sharp/gradational top. Gleyed Spodosol (?).

Mudstone, maroon, purple, variegated with green. Large slickensides, angular, cm-size peds, abundant Fe pisoids. Sharp/gradational top.

Mudstone, variegated maroon, green, gray, lower part, shale/mudstone, pervasively slickensided, peds prismatic, angular, 1-10 cm in size. Illuvial clay lining ped surfaces. Basal part with remnant bedding. Gradational top.

Shale, silty, slightly variegated maroon and greenish gray, spare/rare small slickensides. Medium-thin laminated. Some plant remains. Gradational top.

Bentonite, olive greenish gray, basal 2 cm black, flaky, slippery, ductile, heterogeneous. Sharp top.

Mudstone, greenish, maroonish gray, not dark gray as below (lower vadose?), variegated. No Fe pisoids. Large, thick slickensided surfaces with thick clay films and rounded corners, slickensides smaller upward. Peds rounded to subrounded, cm in size, upward decreasing in size, weakly calcareous. Sharp top. Top of

APPENDIX G
DALONGKOU SECTION

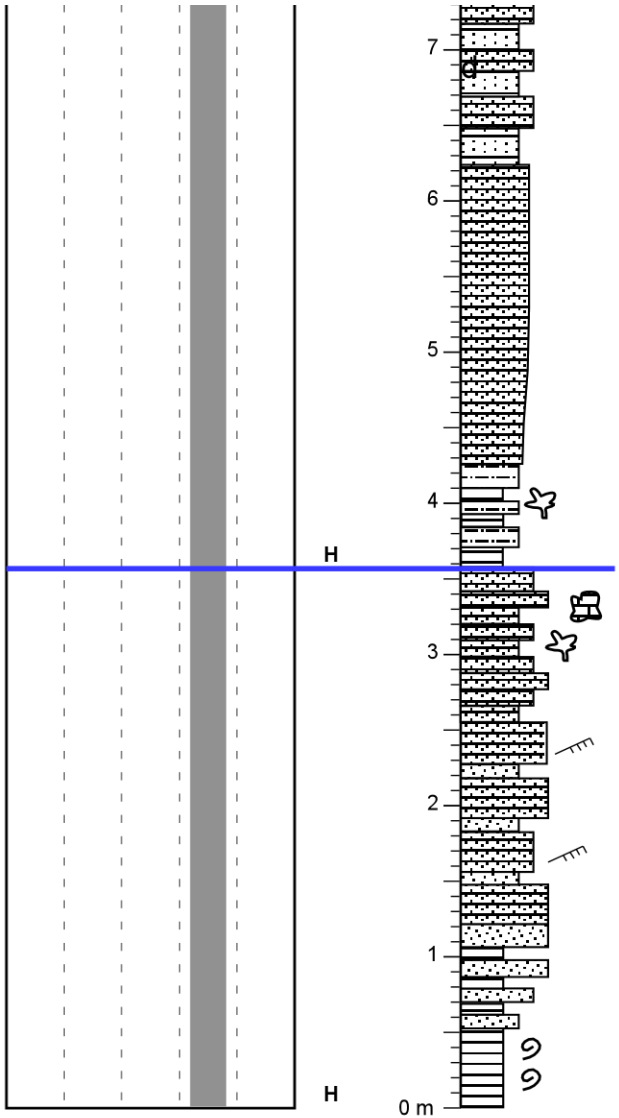

Siltstone, vf to f LW, gray, dark gray, mainly olive gray. Thick laminated to platy, well bedded.

Siltstone, gray to dark gray, papery, silty shale, some plant remains, non-calcareous.

Coarse siltstone, vf/f LW, thick platy to thick laminated, common to sparse plant remains. Contains boulder-size calcitic nodules (diagenetic). Sharp upper contact.

Lower part, shale, black, pure to silty, thinly laminated, non-calcareous with sparse ostracods. Base unseen. Changing upward to sandstone and shale interbeds, shale similar as below, sandstone is yellowish gray, very fine to medium, coarsening upward. Upward decreasing in shale laminae. Sandstone beds are silty to fine/medium, LW, sharp contact. Uppermost part, LW/LSA, yellowish gray, well laminated, climbing ripple laminated, well bedded, sparse siltstone laminae, moderately to moderately well sorted, rounded. In mid part, a 10 cm thick dark gray well laminated siltstone/vf sandstone, non-calcareous. Delta front or distal delta front, or littoral to sub littoral. Sharp to gradational upper contact.

QZJ Section, Dalongkou area, Summer 2011.
Dip direction: S74W
Dip Angle: 71

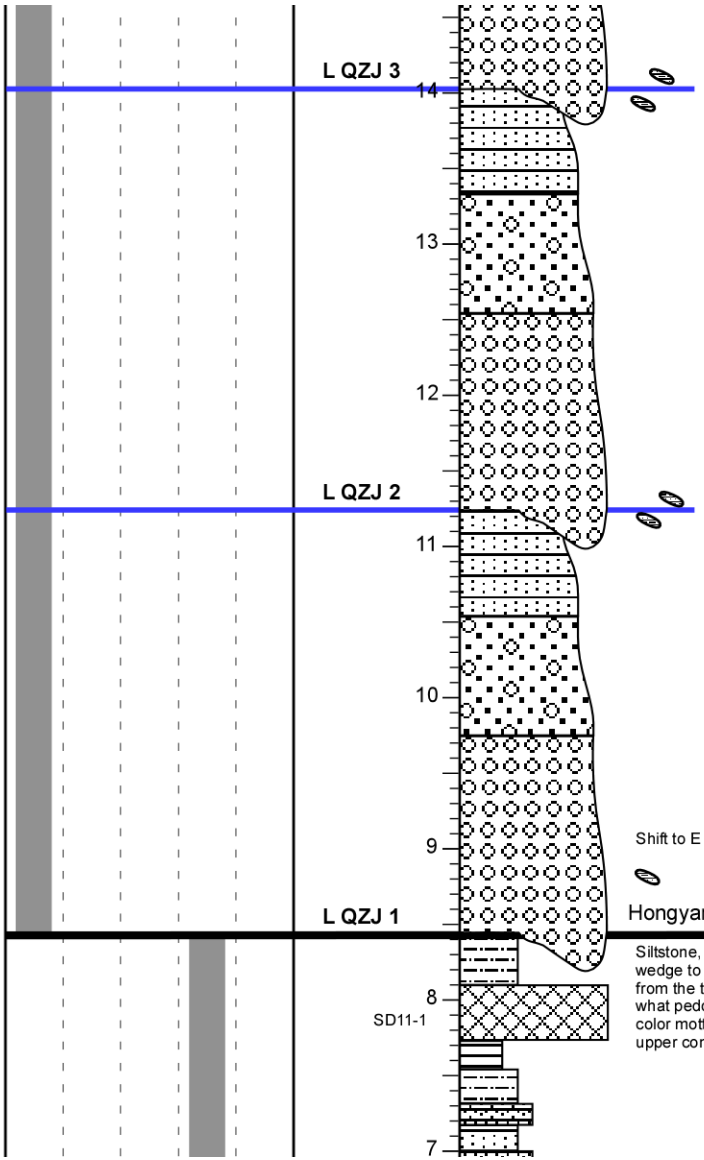

Shift to E for ~ 20 m below the base of the channel.

Hongyanchi - Lower QZJ LC boundary

Siltstone, vf LW, mainly gray to dark gray, thick platy to thick laminated, wedge to blocky in places, silty shale to shale/mudstone in upper part. 30 cm from the top, a possible bed of bentonite, black, ~ 40 cm thick. Maybe somewhat pedogenically altered, may not. Upmost 30 cm, variegated with purple, color mottled, maybe due to overlying fluvial channeling. Erosional, high relief upper contact.

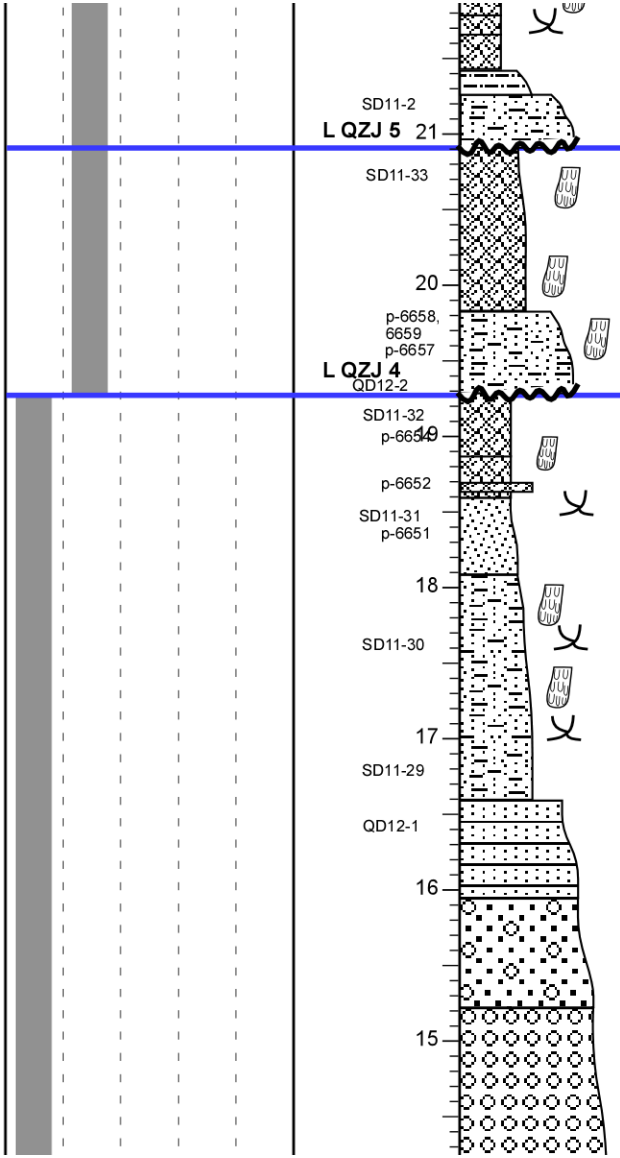

LW/LSA, maroon to olive gray, thick platy, moderately to poorly sorted, c to granule size, fining upward to muddy LW, sandy mudstone/shale. Gradational upper boundary.

Switched to E for ~ 10 m.

Mudstone, sandy, silty, dark gray to dark purple, mottled, 1-5 cm peds, discontinuous common clay films. Upmost part, a possible bentonite, angular peds, platy to blocky. Protosol. Sharp to erosional upper contact.

LW, olive gray to green gray, thick bedded, common illuvial clay (making it muddy), crudely fining upward from c-vc to c-m, non-calcareous, moderately to poorly sorted, subrounded to rounded, platy to blocky. Channel-edge or overbank deposits. Gradational upper boundary.

Mudstone/shale. Basal part, fining upward from muddy LW to sandy mudstone, platy to blocky, variegated red, olive, gray, maroon, color mottled, variable clay films, wedge-shaped peds; clay films and slickensides are more common in lower part. Silty mudstone/shale, siltstone, vf/f sandstone (minor) alternates, non-calcareous. Sharp to erosional upper boundary. Argillaceous Protosol with evidence of soil horizonation.

3-4 fining upward successions from conglomerate to sandstone, purple to dark purple to pinkish purple. Conglomerate to sandstone is 80-20 or 90-10%. Conglomerate is well rounded, imbricated, clast supported (80-90%) in c-vc sand matrix, well to moderately well sorted, pebble to boulder size, mainly pebble-cobble, igneous dominated, some sedimentary clasts (sandstone and shale), 10-20%, large and common in basal lags, probably from below. Sandstone is dark purple, well bedded, LSA, c-vc/granular, moderately well sorted, subrounded to subangular. Large scale (10s m) lateral accretionary bodies of fining upward trends. Each succession has an erosional base. Significant lateral changes in thickness in ~ 100 m. Similar to coarse-grained meandering stream deposits in SE Tarlong. Sharp to gradational upper boundary.

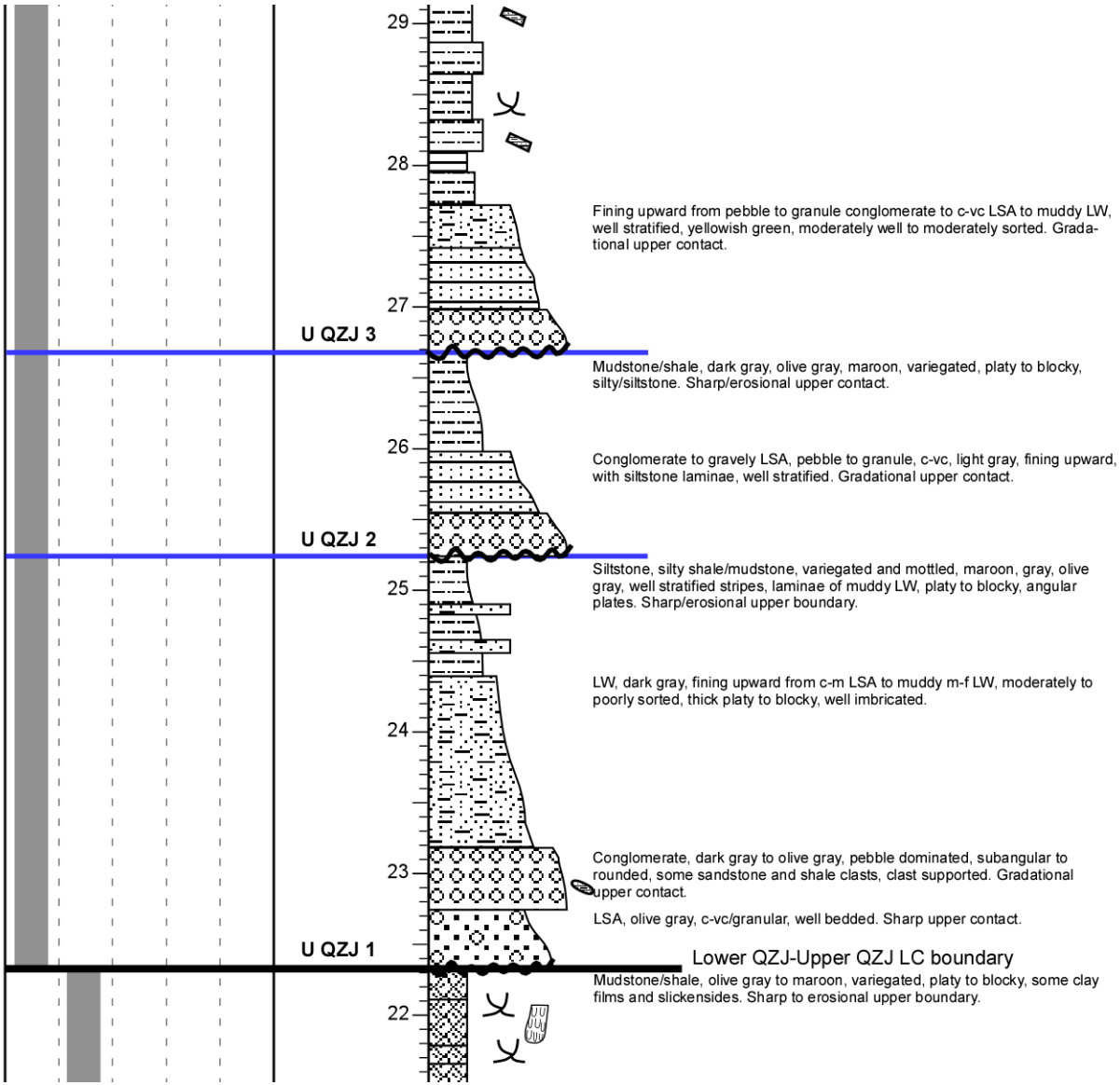
29
28
27
26
25
24
23
22
U QZJ 3
U QZJ 2
U QZJ 1
Fining upward from pebble to granule conglomerate to c-vc LSA to muddy LW, well stratified, yellowish green, moderately well to moderately sorted. Gradational upper contact.
Mudstone/shale, dark gray, olive gray, maroon, variegated, platy to blocky, silty/siltstone. Sharp/erosional upper contact.
Conglomerate to gravely LSA, pebble to granule, c-vc, light gray, fining upward, with siltstone laminae, well stratified. Gradational upper contact.
Siltstone, silty shale/mudstone, variegated and mottled, maroon, gray, olive gray, well stratified stripes, laminae of muddy LW, platy to blocky, angular plates. Sharp/erosional upper boundary.
LW, dark gray, fining upward from c-m LSA to muddy m-f LW, moderately to poorly sorted, thick platy to blocky, well imbricated.
Conglomerate, dark gray to olive gray, pebble dominated, subangular to rounded, some sandstone and shale clasts, clast supported. Gradational upper contact.
LSA, olive gray, c-vc/granular, well bedded. Sharp upper contact.
Lower QZJ-Upper QZJ LC boundary
Mudstone/shale, olive gray to maroon, variegated, platy to blocky, some clay films and slickensides. Sharp to erosional upper boundary.

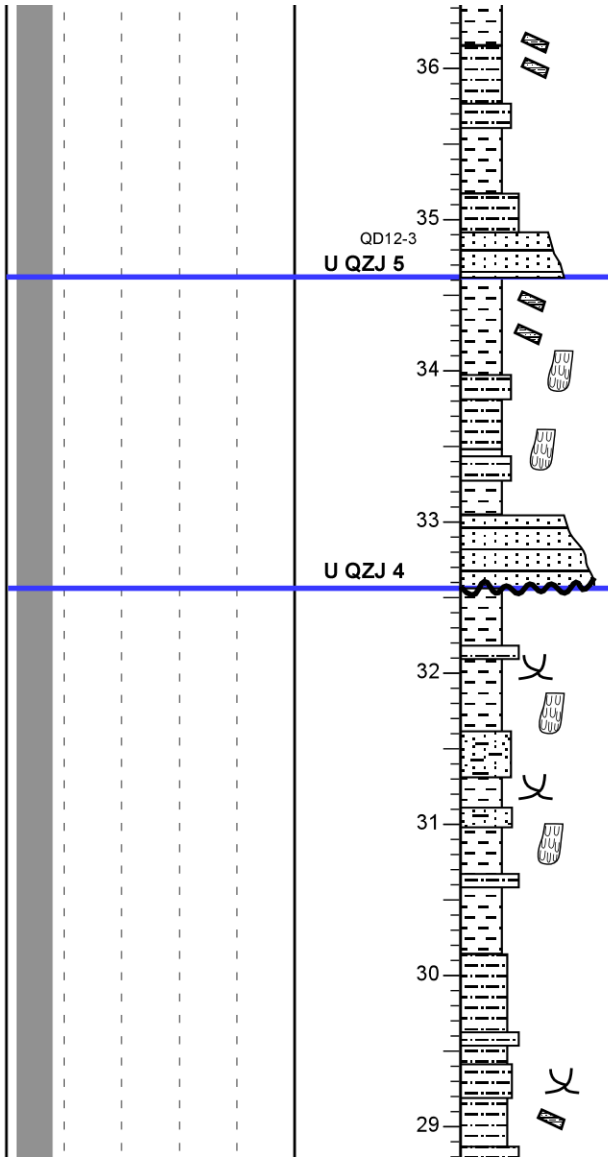

LSA/LW, greenish gray, m-c, moderately well sorted, laminated. Gradational upper contact.

Mudstone/shale, silty, siltstone, in places sandy, maroon and gray layers, blocky to thick platy, sparse and discontinuous clay films, non-calcareous. A 30 cm thick dark gray layer near top with some mud breccias (mm size), angular, sharp top, diffuse to gradational base.

LSA, fining upward from c-vc/granular to muddy m-c LW, yellowish green, well bedded, moderately to moderately well sorted.

Mudstone, maroon, variegated with gray. Upmost 50 cm gray to dark gray. Blocky, coarse peds, angular, no or sparse thin discontinuous clay films and slickensides, variably silty and locally sandy. Sharp/erosional upper contact.

Mudstone/shale, variably silty, variegated stripes/layers/beds of maroon, gray, brown, color mottled, platy to blocky, dense, non-calcareous, with scattered slickensides. Upmost 40 cm, a layer of dark steel gray to dark gray, platy silty shale/mudstone, with sharp top and gradational base, maybe a gleyed horizon, some angular mm size mud breccias. Sharp upper contact.

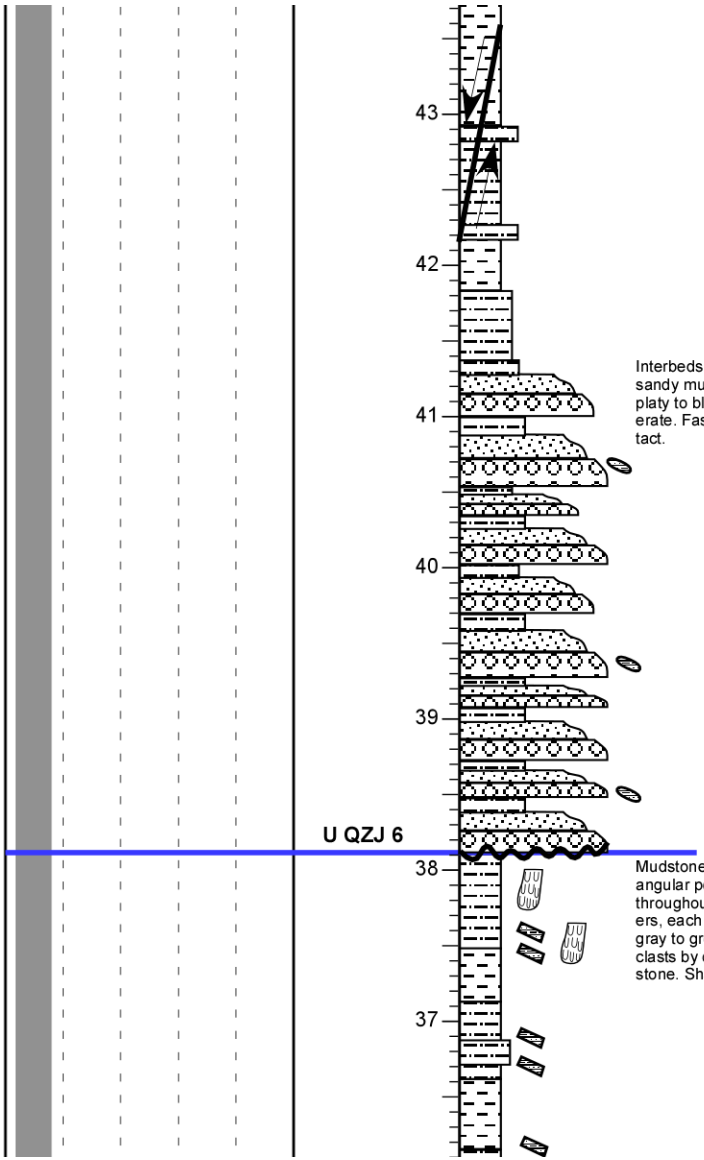

Interbeds of conglomerate (pebble), gravelly LSA/LW, m-vc, muddy LW and sandy mudstone/shale, each 10-30 cm thick, maroon, olive gray, gray, dark gray, platy to blocky, angular, dense,. Mud clasts common in sandstone and conglomerate. Fast shifting, poorly defined, shallow stream beds. Gradational upper contact.

Mudstone/shale, variegated maroon and dark gray layers, thick platy to blocky, angular peds, sandy in lowermost part, silty, siltstone, scattered c-vc sand grains throughout, sparse and discontinuous clay films in upper part. 3-4 dark gray layers, each 20-30 cm thick, contain common scattered mm-size (up to 1 cm) light gray to green silty mud breccias, floating in mud matrix. They may be rip up mud clasts by currents. If so, defies a loess or eolian origin of the silty mud and siltstone. Sharp/erosional upper contact.

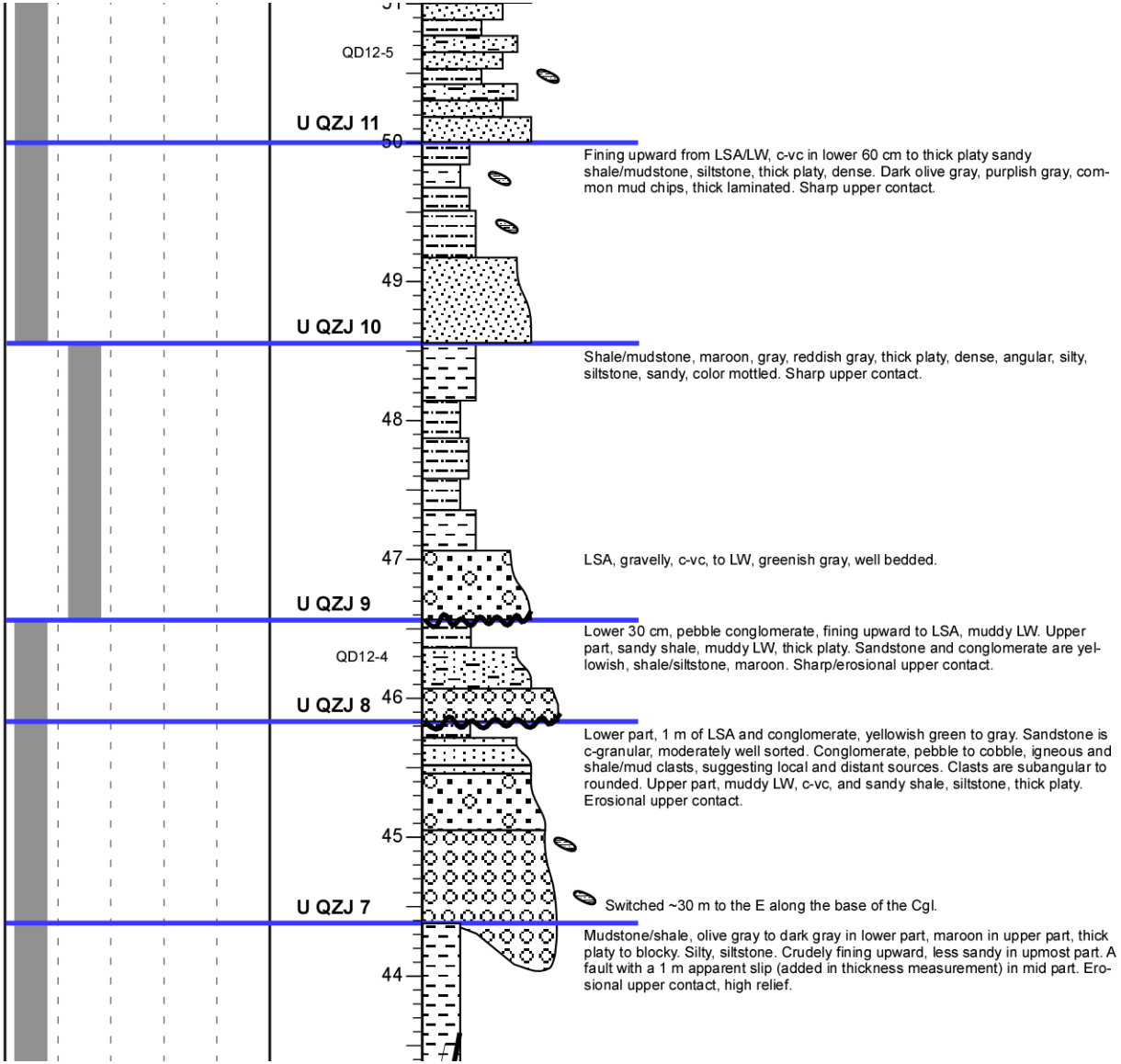
QD12-5
U QZJ 11
50
Fining upward from LSA/LW, c-vc in lower 60 cm to thick platy sandy shale/mudstone, siltstone, thick platy, dense. Dark olive gray, purplish gray, common mud chips, thick laminated. Sharp upper contact.
49
U QZJ 10
Shale/mudstone, maroon, gray, reddish gray, thick platy, dense, angular, silty, siltstone, sandy, color mottled. Sharp upper contact.
48
47
LSA, gravelly, c-vc, to LW, greenish gray, well bedded.
U QZJ 9
Lower 30 cm, pebble conglomerate, fining upward to LSA, muddy LW. Upper part, sandy shale, muddy LW, thick platy. Sandstone and conglomerate are yellowish, shale/siltstone, maroon. Sharp/erosional upper contact.
QD12-4
46
U QZJ 8
Lower part, 1 m of LSA and conglomerate, yellowish green to gray. Sandstone is c-granular, moderately well sorted. Conglomerate, pebble to cobble, igneous and shale/mud clasts, suggesting local and distant sources. Clasts are subangular to rounded. Upper part, muddy LW, c-vc, and sandy shale, siltstone, thick platy. Erosional upper contact.
45
Switched ~30 m to the E along the base of the Cgl.
U QZJ 7
Mudstone/shale, olive gray to dark gray in lower part, maroon in upper part, thick platy to blocky. Silty, siltstone. Crudely fining upward, less sandy in upmost part. A fault with a 1 m apparent slip (added in thickness measurement) in mid part. Erosional upper contact, high relief.
44

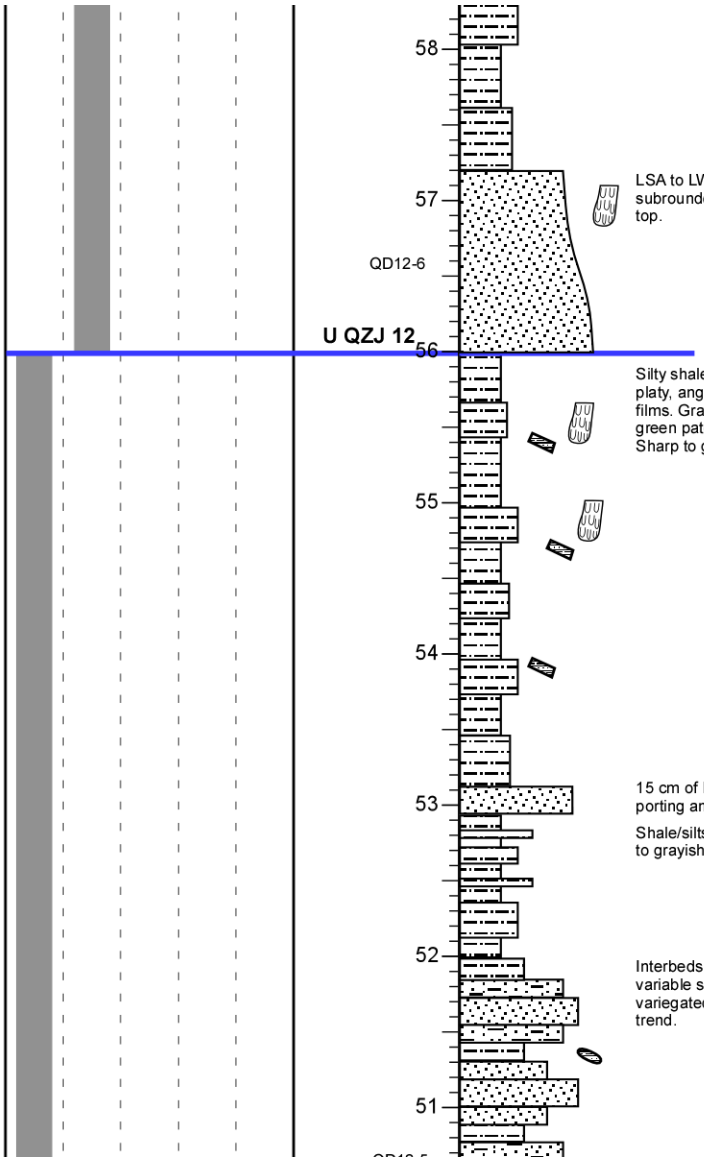

LSA to LW, maroon to olive gray, c-vc, granular, poorly to moderately sorted, subrounded, thick platy, dense, non-calcareous. Some illuvial clays. Gradational top.

Silty shale, sandy mudstone, siltstone, maroon, with 1-2 dark gray beds, thick platy, angular. Upward changing to black with sparse, thin discontinuous clay films. Gray beds have common mud breccias. Common color mottling, rounded green patches may be root halos. Sparse granule and fine pebbles troughout. Sharp to gradational upper contact.

15 cm of LW, greenish gray, muddy, c-vc, common 1-5 mm rd mud chips, supporting an overbank origin.

Shifted ~10 m to the W along the top of mudstone.

Shale/siltstone, sandy, silty, thick platy, dense, dark olive, gray changing upward to grayish maroon, variably sandy, local muddy LW. Sharp upper contact.

Interbeds of LSA, LW, muddy LW, sandy mudstone/shale, thick angular plates, variable sorting and roundness, common mud chips, grayish purple, olive gray, variegated. Fast shifting stream beds (shallow, poor defined). No clear grain size trend.

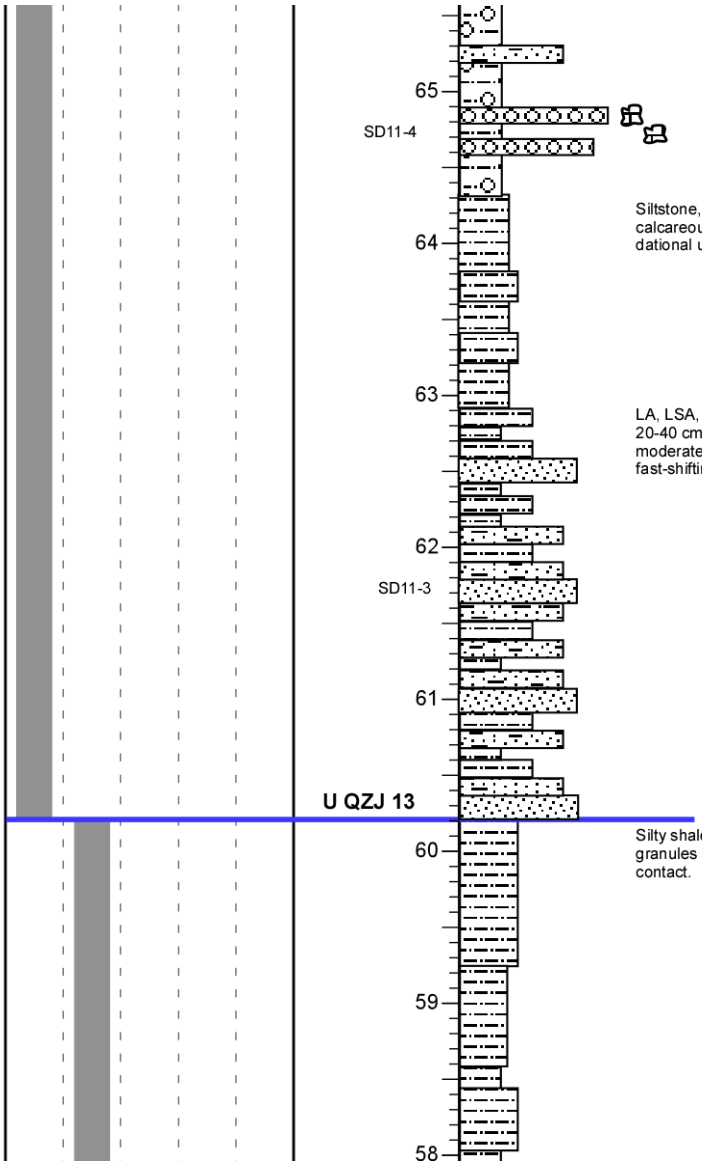

Siltstone, shale, olive gray to gray shale, maroon, thick platy, sandy, non-calcareous, common halos and tubes of color, suggesting rooting. Sharp to gradational upper contact.

LA, LSA, LW, with intercalated muddy LW, sandy shale, siltstone, each bed is 20-40 cm, olive gray, greenish gray, dark purplish gray, variably sorted, overall moderately to moderately well sorted, subrounded to rounded. Poorly defined, fast-shifting streams of shallow depth, close to sheet flows (?).

Silty shale, mudstone, siltstone, similar to that below. Root halos common, c-granules scattered throughout, variably silty and sandy, thick platy. Sharp upper contact.

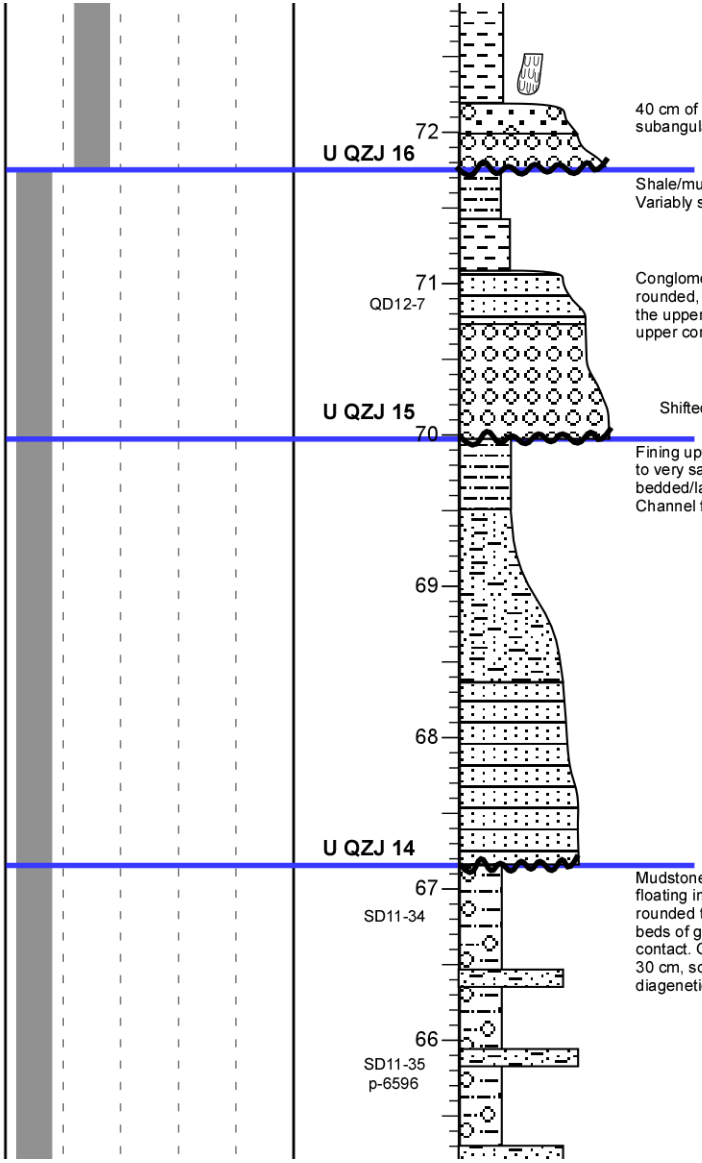

40 cm of conglomerate, pebble size, greenish gray, well rounded and imbricated, subangular to subrounded, fining upward to c-vc muddy LW.

Shale/mudstone, olive gray to purplish gray, thick platy, non-calcareous, dense. Variably sandy and gravelly. Sharp/erosional upper contact.

Conglomerate, reddish gray, pebble to cobble, well imbricated, subangular to rounded, clast supported, intercalated with c-vc LW. Fining upward to c-vc LW in the uppermost 30 cm, well bedded. Gray to olive gray. Gradational to sharp upper contact.

Shifted ~5 m to the E along the base of the cgl.

Fining upward from LA, c-vc, to LSA, LW, muddy LW, greenish gray to olive gray, to very sandy mudstone/shale in upmost 40 cm. Sandstone is well bedded/laminated, variably sorted, subangular to subrounded, non-calcareous. Channel fill. Erosional upper contact.

Mudstone, shale, gravelly, variable amount of well rounded granule and pebbles floating in silt and mud matrix, and sand grains of variable sizes, gravels are sub rounded to well rounded. Rare LW beds of 10-20 cm thick, c-vc, poorly sorted. 2 beds of granule to fine pebble conglomerate in lower part, 10 cm each in sharp contact. Gravel rich mud flat with mud flow deposits. Calcareous throughout. Basal 30 cm, some scattered equant and elongated calcitic nodules. May be rhizoliths or diagenetic. Sharp erosional upper contact.

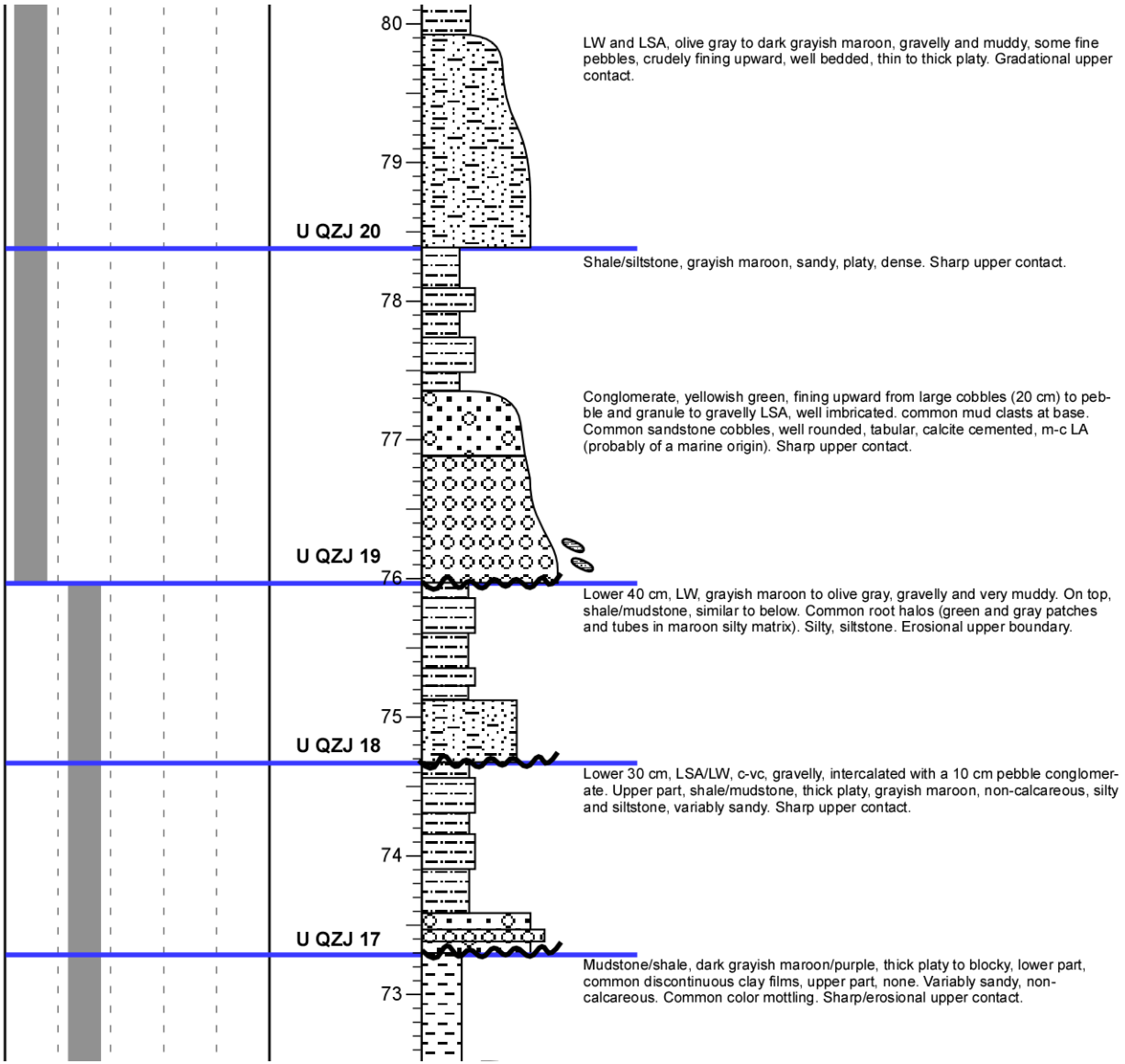
80
79
78
77
76
75
74
73
U QZJ 20
U QZJ 19
U QZJ 18
U QZJ 17
LW and LSA, olive gray to dark grayish maroon, gravelly and muddy, some fine pebbles, crudely fining upward, well bedded, thin to thick platy. Gradational upper contact.
Shale/siltstone, grayish maroon, sandy, platy, dense. Sharp upper contact.
Conglomerate, yellowish green, fining upward from large cobbles (20 cm) to pebble and granule to gravelly LSA, well imbricated. common mud clasts at base. Common sandstone cobbles, well rounded, tabular, calcite cemented, m-c LA (probably of a marine origin). Sharp upper contact.
Lower 40 cm, LW, grayish maroon to olive gray, gravelly and very muddy. On top, shale/mudstone, similar to below. Common root halos (green and gray patches and tubes in maroon silty matrix). Silty, siltstone. Erosional upper boundary.
Lower 30 cm, LSA/LW, c-vc, gravelly, intercalated with a 10 cm pebble conglomerate. Upper part, shale/mudstone, thick platy, grayish maroon, non-calcareous, silty and siltstone, variably sandy. Sharp upper contact.
Mudstone/shale, dark grayish maroon/purple, thick platy to blocky, lower part, common discontinuous clay films, upper part, none. Variably sandy, non-calcareous. Common color mottling. Sharp/erosional upper contact.

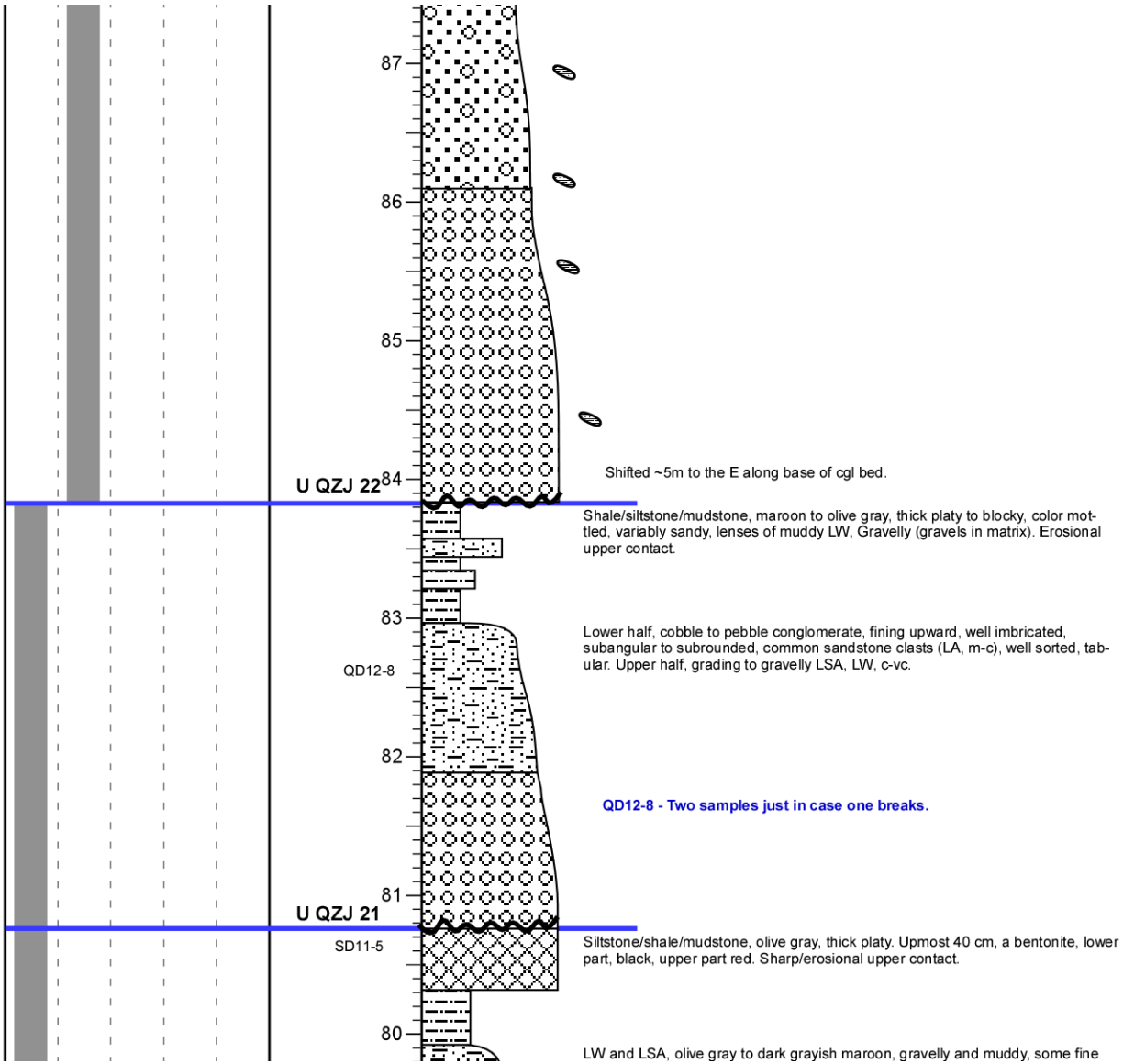
87
86
85
84
83
82
81
80
U QZJ 22
U QZJ 21
QD12-8
SD11-5
Shifted ~5m to the E along base of cgl bed.
Shale/siltstone/mudstone, maroon to olive gray, thick platy to blocky, color mottled, variably sandy, lenses of muddy LW, Gravelly (gravels in matrix). Erosional upper contact.
Lower half, cobble to pebble conglomerate, fining upward, well imbricated, subangular to subrounded, common sandstone clasts (LA, m-c), well sorted, tabular. Upper half, grading to gravelly LSA, LW, c-vc.
QD12-8 - Two samples just in case one breaks.
Siltstone/shale/mudstone, olive gray, thick platy. Upmost 40 cm, a bentonite, lower part, black, upper part red. Sharp/erosional upper contact.
LW and LSA, olive gray to dark grayish maroon, gravelly and muddy, some fine

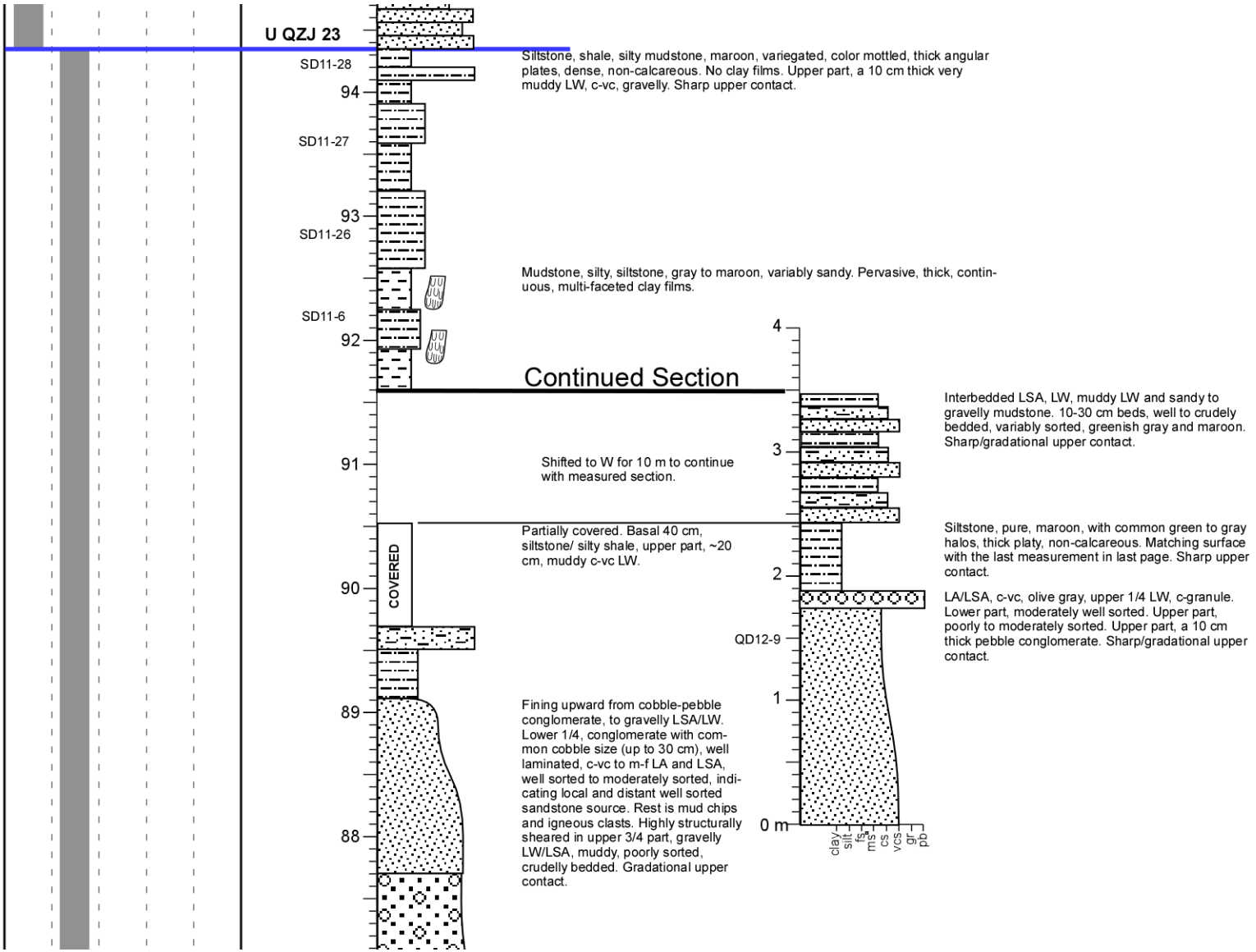
U QZJ 23
SD11-28
94
SD11-27
93
SD11-26
SD11-6
92
91
90
89
88
COVERED
Siltstone, shale, silty mudstone, maroon, variegated, color mottled, thick angular plates, dense, non-calcareous. No clay films. Upper part, a 10 cm thick very muddy LW, c-vc, gravelly. Sharp upper contact.
Mudstone, silty, siltstone, gray to maroon, variably sandy. Pervasive, thick, continuous, multi-faceted clay films.
Continued Section
Shifted to W for 10 m to continue with measured section.
Partially covered. Basal 40 cm, siltstone/ silty shale, upper part, ~20 cm, muddy c-vc LW.
Fining upward from cobble-pebble conglomerate, to gravelly LSA/LW. Lower 1/4, conglomerate with common cobble size (up to 30 cm), well laminated, c-vc to m-f LA and LSA, well sorted to moderately sorted, indicating local and distant well sorted sandstone source. Rest is mud chips and igneous clasts. Highly structurally sheared in upper 3/4 part, gravelly LW/LSA, muddy, poorly sorted, crudely bedded. Gradational upper contact.
4
3
2
1
0 m
QD12-9
clay
silt
fs
ms
cs
vcs
gr
pb
Interbedded LSA, LW, muddy LW and sandy to gravelly mudstone. 10-30 cm beds, well to crudely bedded, variably sorted, greenish gray and maroon. Sharp/gradational upper contact.
Siltstone, pure, maroon, with common green to gray halos, thick platy, non-calcareous. Matching surface with the last measurement in last page. Sharp upper contact.
LA/LSA, c-vc, olive gray, upper 1/4 LW, c-granule. Lower part, moderately well sorted. Upper part, poorly to moderately sorted. Upper part, a 10 cm thick pebble conglomerate. Sharp/gradational upper contact.

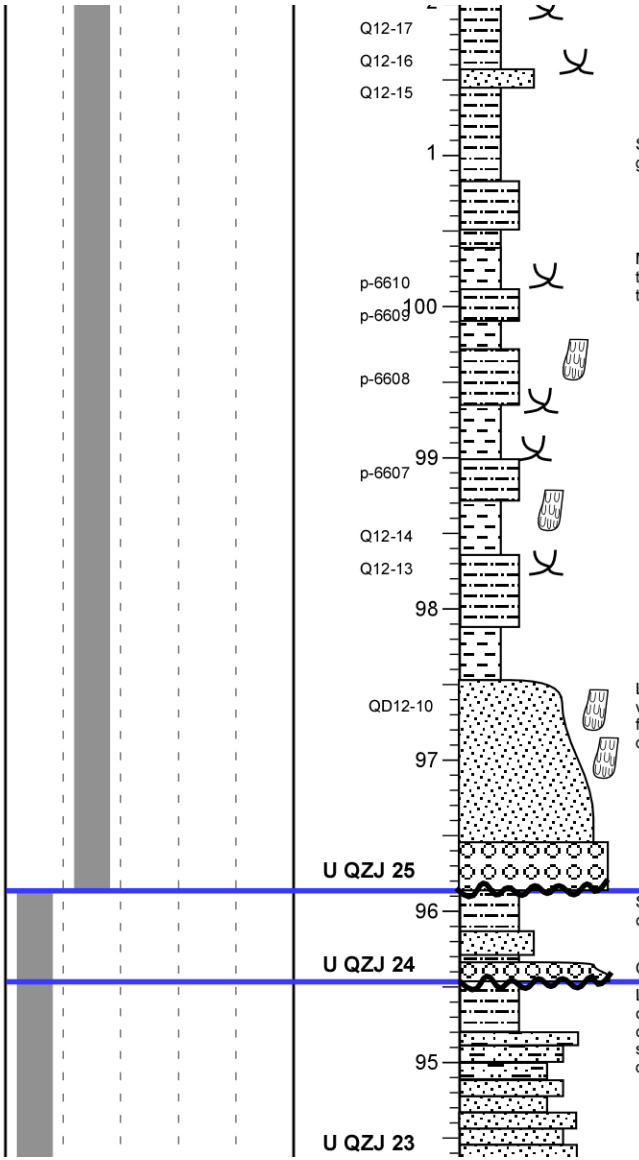

Siltstone, silty, sandy shale, yellowish gray-maroonish gray, thick platy, c-vc and granule grains common. Bedded. No clay films. Sharp upper contact.

Shifted ~20 m to the E.

Mudstone, siltstone, silty, slightly sandy. Grayish maroon, well developed thick continuous clay films and slickensides, color mottled. 1-5 cm wedge peds, subangular to rounded. Argillisol. Sharp upper contact.

Lower 30 cm, conglomerate, pebbly, light gray. Fining upward to LW, muddy to very muddy upward. Thick platy to blocky, well developed continuous, thick, multifaceted clay films, very poorly to poorly sorted, m-granule, some mud chips. Gradational upper contact.

Siltstone, maroon, thick platy, sandy at lower part, pure in upper part, non-calcareous. Sharp/erosional upper contact.

Conglomerate, fine pebble to granule, single bed, close to 10 cm thick.

Lower part, 90 cm of LA/LSA, color mottled, sparse discontinuous clay films, m-c, c-vc beds, moderately well to well sorted, well stratified, no clear grain size change, muddier upward, variably sorted, poorer sorting upward. Upper 30 cm, siltstone/silty shale/mudstone, maroon, thick platy, moderately to very sandy, dense. Sharp/erosional upper contact.

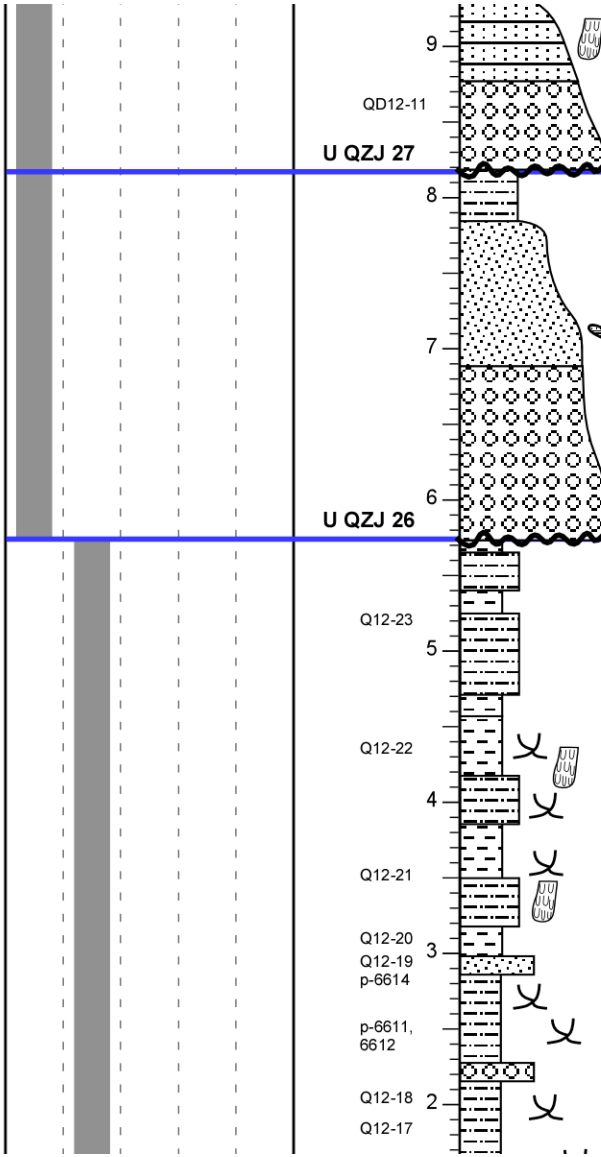

Conglomerate, cobble to pebble, yellowish gray, common mudstones (few below), sandstone, igneous clasts. Fining upward to LSA and muddy LW. Upmost 20 c,, siltstone, gravelly and very muddy LW. Sharp/erosional upper contact.

Siltstone/mudstone, maroon, dense, blocky, sandier than below, color mottled. A(?) of Argillisol, or an episode of faster overbank deposits. Sharp/erosional upper contact.

Siltstone/mudstone, dark gray to grayish maroon, common thick continuous clay films and slickensides, 1-2 cm subangular to subrounded peds. Color and texturally mottled. B horizon of Argillisol. Gradational upper contact.

Interbedded conglomerate (f pebble), muddy LW, LSA, c-vc, common granules, thick platy, upward changing to blocky, with sparse clay films. Crudely fining upward, with intercalated sandy shale/mudstone. Olive gray. Gradational upper contact.

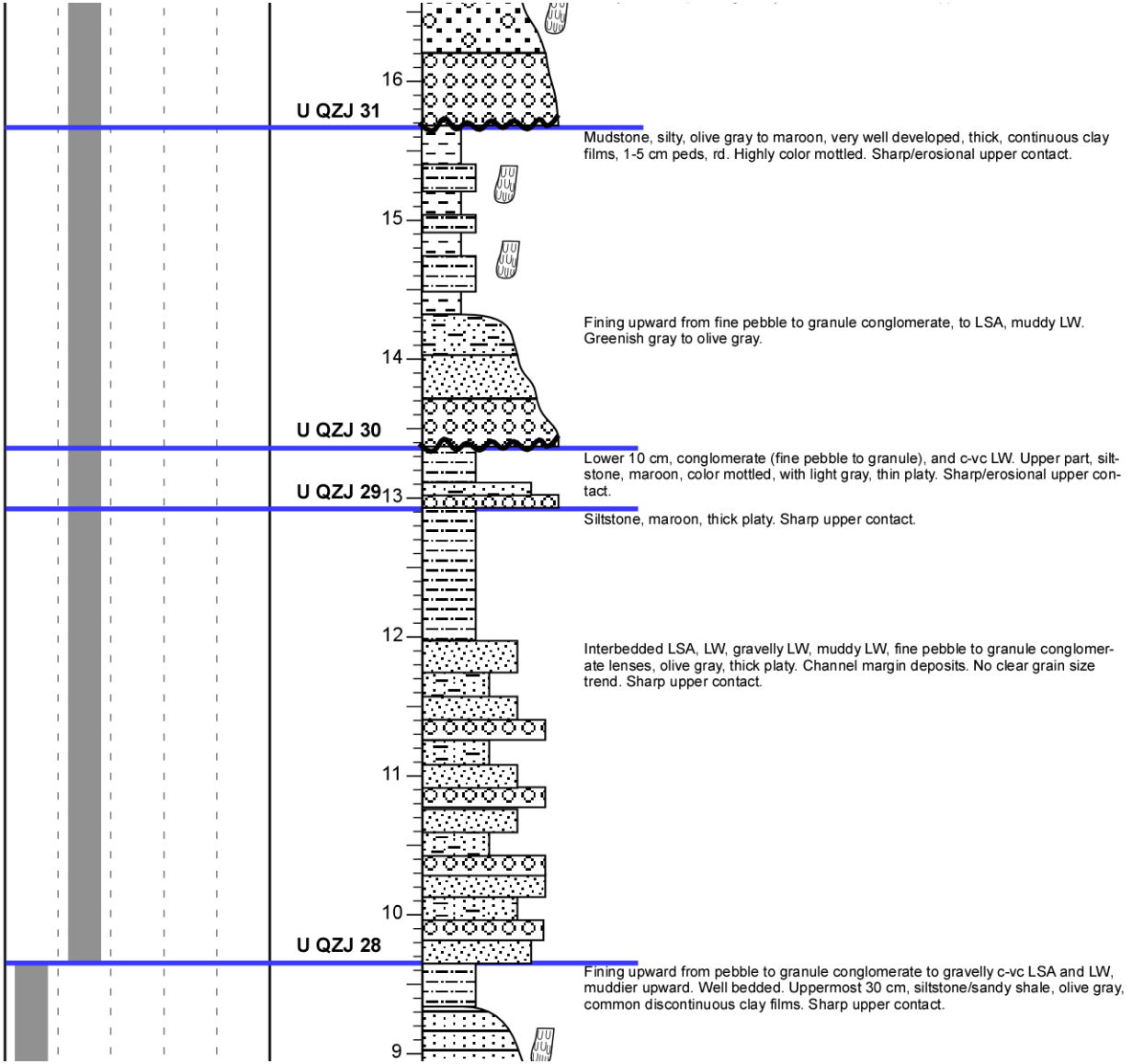
16
U QZJ 31
15
14
U QZJ 30
U QZJ 29
13
12
11
10
U QZJ 28
9
Mudstone, silty, olive gray to maroon, very well developed, thick, continuous clay films, 1-5 cm peds, rd. Highly color mottled. Sharp/erosional upper contact.
Fining upward from fine pebble to granule conglomerate, to LSA, muddy LW. Greenish gray to olive gray.
Lower 10 cm, conglomerate (fine pebble to granule), and c-vc LW. Upper part, siltstone, maroon, color mottled, with light gray, thin platy. Sharp/erosional upper contact.
Siltstone, maroon, thick platy. Sharp upper contact.
Interbedded LSA, LW, gravelly LW, muddy LW, fine pebble to granule conglomerate lenses, olive gray, thick platy. Channel margin deposits. No clear grain size trend. Sharp upper contact.
Fining upward from pebble to granule conglomerate to gravelly c-vc LSA and LW, muddier upward. Well bedded. Uppermost 30 cm, siltstone/sandy shale, olive gray, common discontinuous clay films. Sharp upper contact.

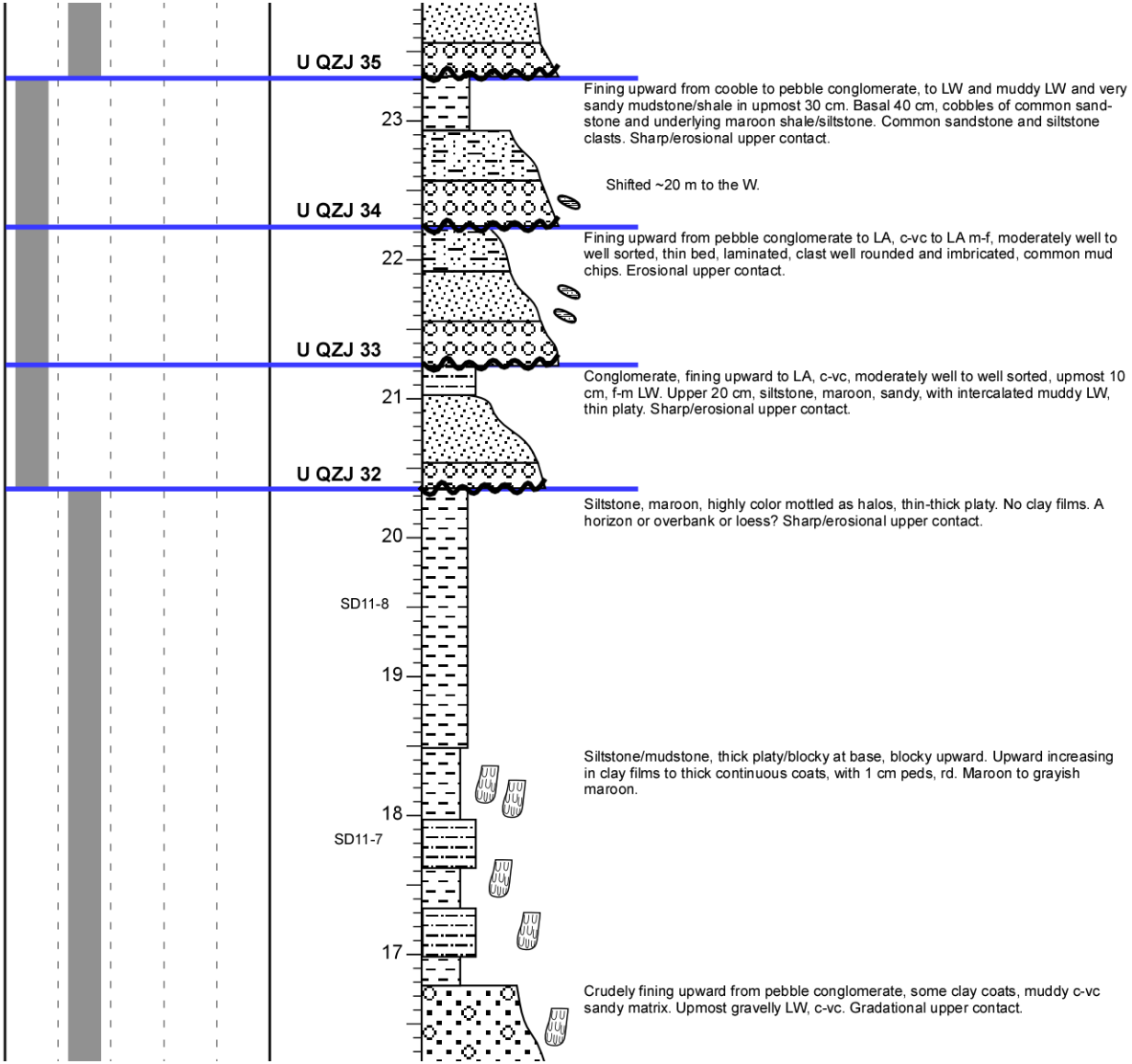
U QZJ 35
23
Fining upward from cooble to pebble conglomerate, to LW and muddy LW and very sandy mudstone/shale in upmost 30 cm. Basal 40 cm, cobbles of common sandstone and underlying maroon shale/siltstone. Common sandstone and siltstone clasts. Sharp/erosional upper contact.
Shifted ~20 m to the W.
U QZJ 34
22
Fining upward from pebble conglomerate to LA, c-vc to LA m-f, moderately well to well sorted, thin bed, laminated, clast well rounded and imbricated, common mud chips. Erosional upper contact.
U QZJ 33
21
Conglomerate, fining upward to LA, c-vc, moderately well to well sorted, upmost 10 cm, f-m LW. Upper 20 cm, siltstone, maroon, sandy, with intercalated muddy LW, thin platy. Sharp/erosional upper contact.
U QZJ 32
Siltstone, maroon, highly color mottled as halos, thin-thick platy. No clay films. A horizon or overbank or loess? Sharp/erosional upper contact.
20
SD11-8
19
Siltstone/mudstone, thick platy/blocky at base, blocky upward. Upward increasing in clay films to thick continuous coats, with 1 cm peds, rd. Maroon to grayish maroon.
18
SD11-7
17
Crudely fining upward from pebble conglomerate, some clay coats, muddy c-vc sandy matrix. Upmost gravelly LW, c-vc. Gradational upper contact.

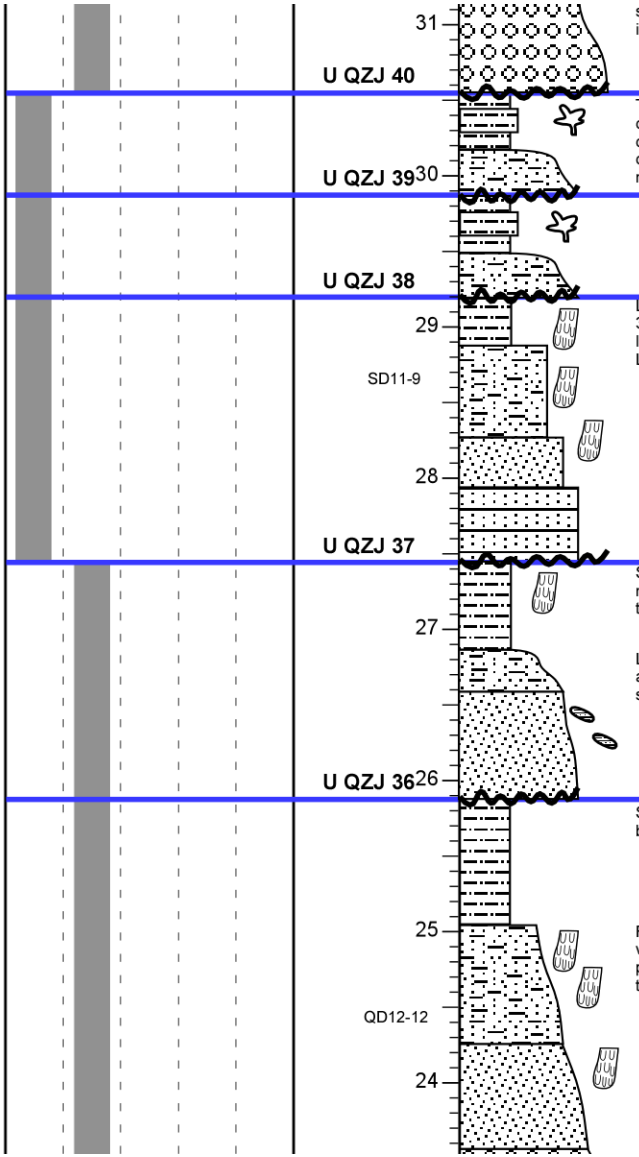

sandstone clasts. Shale clasts black and red/maroon. Clasts imbricated. Overall fining upward. Gradational upper contact.

Switched ~10 m to the E.

Two fining upward successions of about same thickness. Fining upward from LW, green, c-vc to muddy LW to sandy shale/siltstone. Well bedded and laminated. No clay films, common color mottling in finer parts, moderately well sorted. In some siltstone, possible carbonized plant remains parallel to bedding plane Sheet flow or lake margin? Too muddy to be lake shore. Fluvial? Sharp/erosional upper contact.

LA, upward changing to LSA, changing to LW, then to sandy mudstone in upmost 30 cm. Upward increasing in clay coats and overall abundant thick, sheet and tabular clay films, except basal 30 cm. Overall fining upward. Olive gray to maroon. Lower part, well bedded. Sharp/erosional upper contact.

Siltstone/silty shale, maroon, thick platy, variably sandy, color mottles of roots common throughout. Upmost 20 cm, sparse discontinuous clay films. Sharp upper contact.

LA/LSA, yellowish gray to maroon, c-vc, granular, fining upward to m-c to f-m LW and muddy LW, thick platy. Variably sorted. Common maroon mud chips (granular size). Gradational upper contact.

Siltstone, pure, maroon, apparently leached, dense, very angular, thick platy to blocky. Basal part, sandy. No clay films. A horizon? Sharp/erosional upper contact.

Fining upward from pebble conglomerate to granule, changing to LSA, gravelly, c-vc, changing to LW, then to muddy LW. Upward increasing in clay films from rare to pervasive, thick, continuous, some tubular clay fills. Thick platy to blocky. Gradational upper contact.

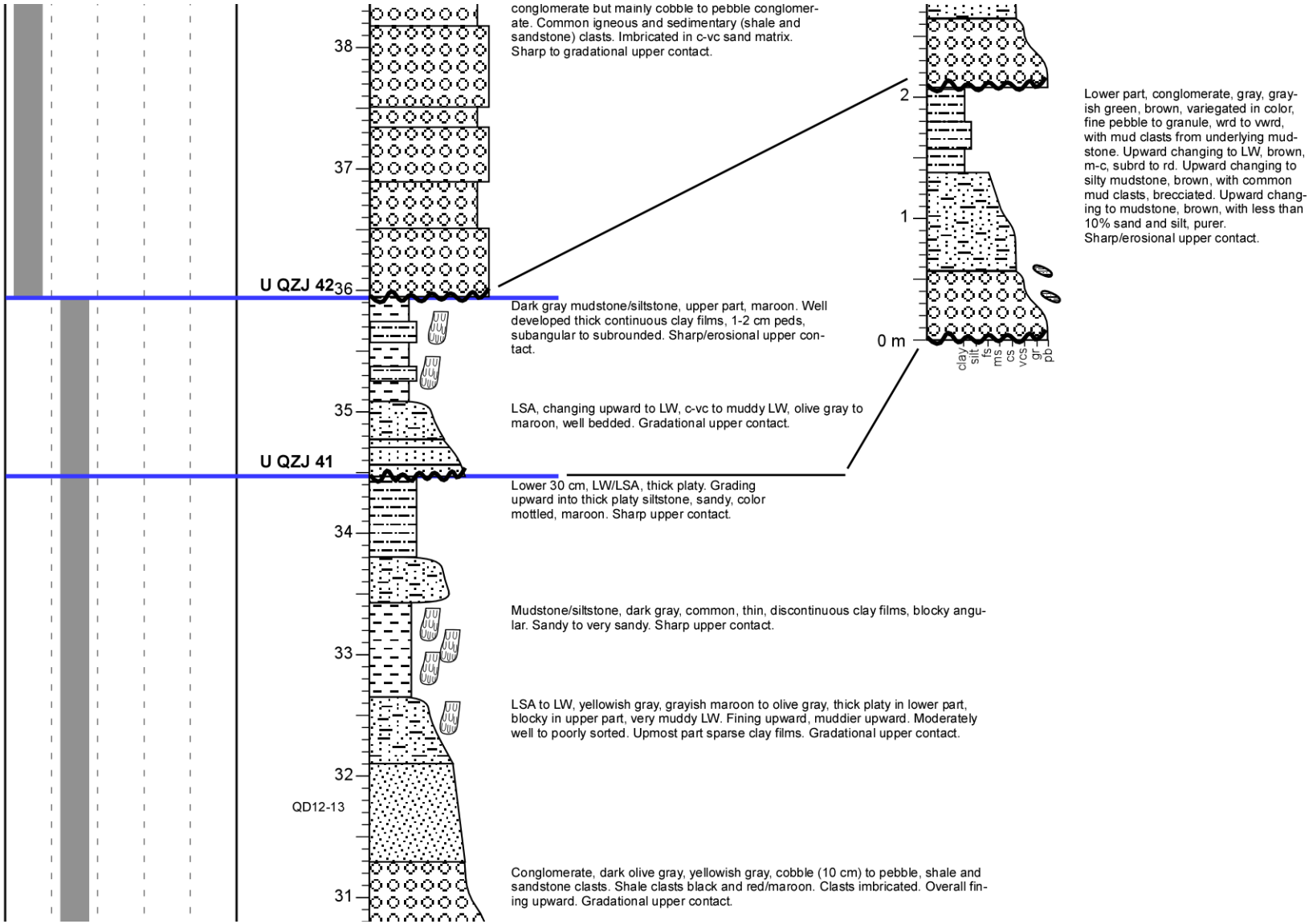
38
37
36
35
34
33
32
31
U QZJ 42
U QZJ 41
QD12-13
conglomerate but mainly cobble to pebble conglomerate. Common igneous and sedimentary (shale and sandstone) clasts. Imbricated in c-vc sand matrix. Sharp to gradational upper contact.
Dark gray mudstone/siltstone, upper part, maroon. Well developed thick continuous clay films, 1-2 cm peds, subangular to subrounded. Sharp/erosional upper contact.
LSA, changing upward to LW, c-vc to muddy LW, olive gray to maroon, well bedded. Gradational upper contact.
Lower 30 cm, LW/LSA, thick platy. Grading upward into thick platy siltstone, sandy, color mottled, maroon. Sharp upper contact.
Mudstone/siltstone, dark gray, common, thin, discontinuous clay films, blocky angular. Sandy to very sandy. Sharp upper contact.
LSA to LW, yellowish gray, grayish maroon to olive gray, thick platy in lower part, blocky in upper part, very muddy LW. Fining upward, muddier upward. Moderately well to poorly sorted. Upmost part sparse clay films. Gradational upper contact.
Conglomerate, dark olive gray, yellowish gray, cobble (10 cm) to pebble, shale and sandstone clasts. Shale clasts black and red/maroon. Clasts imbricated. Overall fining upward. Gradational upper contact.
2
1
0 m
clay
silt
fs
ms
cs
vcs
gr
pb
Lower part, conglomerate, gray, grayish green, brown, variegated in color, fine pebble to granule, wrd to vwrd, with mud clasts from underlying mudstone. Upward changing to LW, brown, m-c, subrd to rd. Upward changing to silty mudstone, brown, with common mud clasts, brecciated. Upward changing to mudstone, brown, with less than 10% sand and silt, purer. Sharp/erosional upper contact.

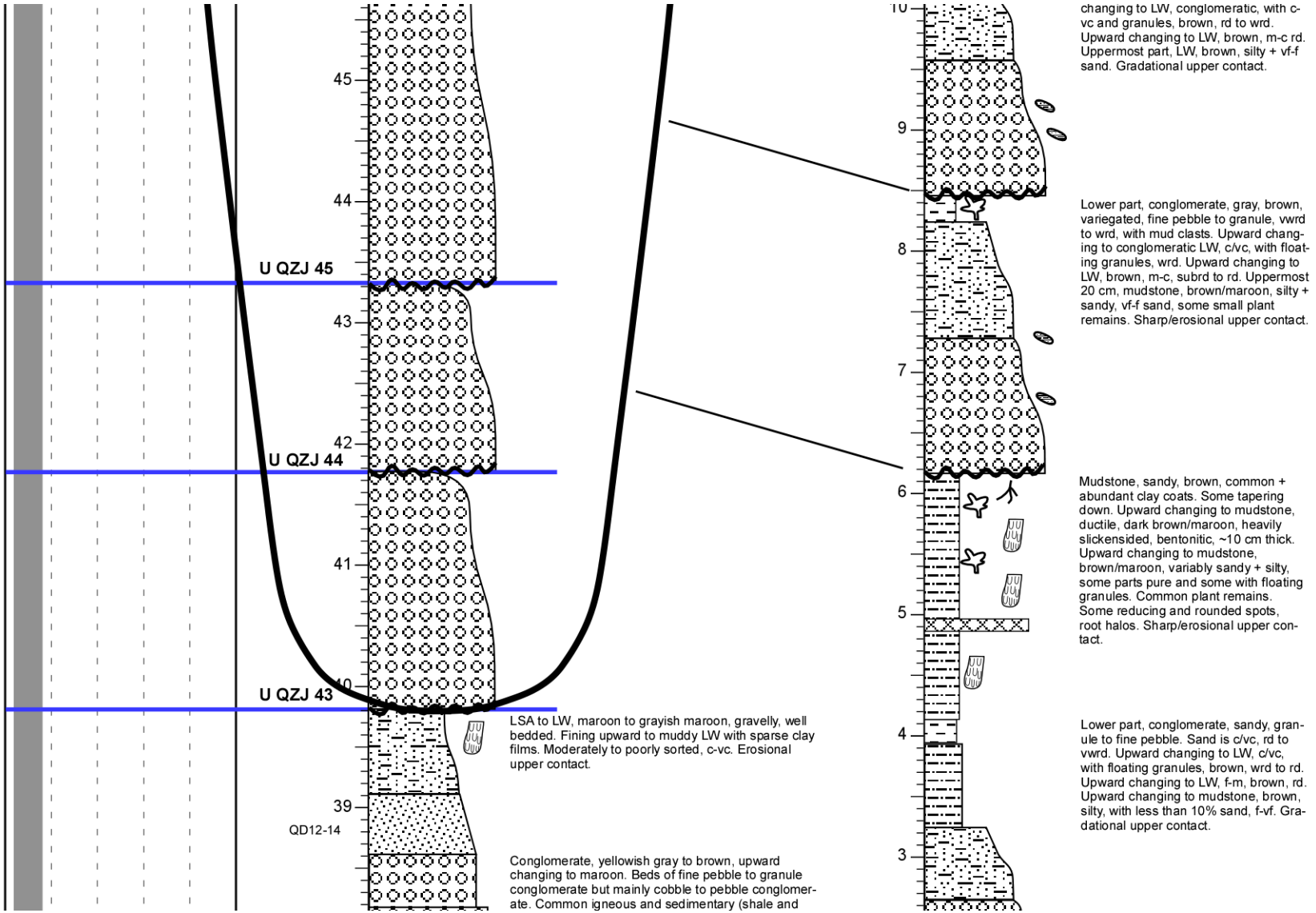
45
44
43
42
41
40
39
U QZJ 45
U QZJ 44
U QZJ 43
QD12-14
10
9
8
7
6
5
4
3
changing to LW, conglomeratic, with c-vc and granules, brown, rd to wrd. Upward changing to LW, brown, m-c rd. Uppermost part, LW, brown, silty + vf-f sand. Gradational upper contact.
Lower part, conglomerate, gray, brown, variegated, fine pebble to granule, vwrd to wrd, with mud clasts. Upward changing to conglomeratic LW, c/vc, with floating granules, wrd. Upward changing to LW, brown, m-c, subrd to rd. Uppermost 20 cm, mudstone, brown/maroon, silty + sandy, vf-f sand, some small plant remains. Sharp/erosional upper contact.
Mudstone, sandy, brown, common + abundant clay coats. Some tapering down. Upward changing to mudstone, ductile, dark brown/maroon, heavily slickensided, bentonitic, ~10 cm thick. Upward changing to mudstone, brown/maroon, variably sandy + silty, some parts pure and some with floating granules. Common plant remains. Some reducing and rounded spots, root halos. Sharp/erosional upper contact.
Lower part, conglomerate, sandy, granule to fine pebble. Sand is c/vc, rd to vwrd. Upward changing to LW, c/vc, with floating granules, brown, wrd to rd. Upward changing to LW, f-m, brown, rd. Upward changing to mudstone, brown, silty, with less than 10% sand, f-vf. Gradational upper contact.
LSA to LW, maroon to grayish maroon, gravelly, well bedded. Fining upward to muddy LW with sparse clay films. Moderately to poorly sorted, c-vc. Erosional upper contact.
Conglomerate, yellowish gray to brown, upward changing to maroon. Beds of fine pebble to granule conglomerate but mainly cobble to pebble conglomerate. Common igneous and sedimentary (shale and

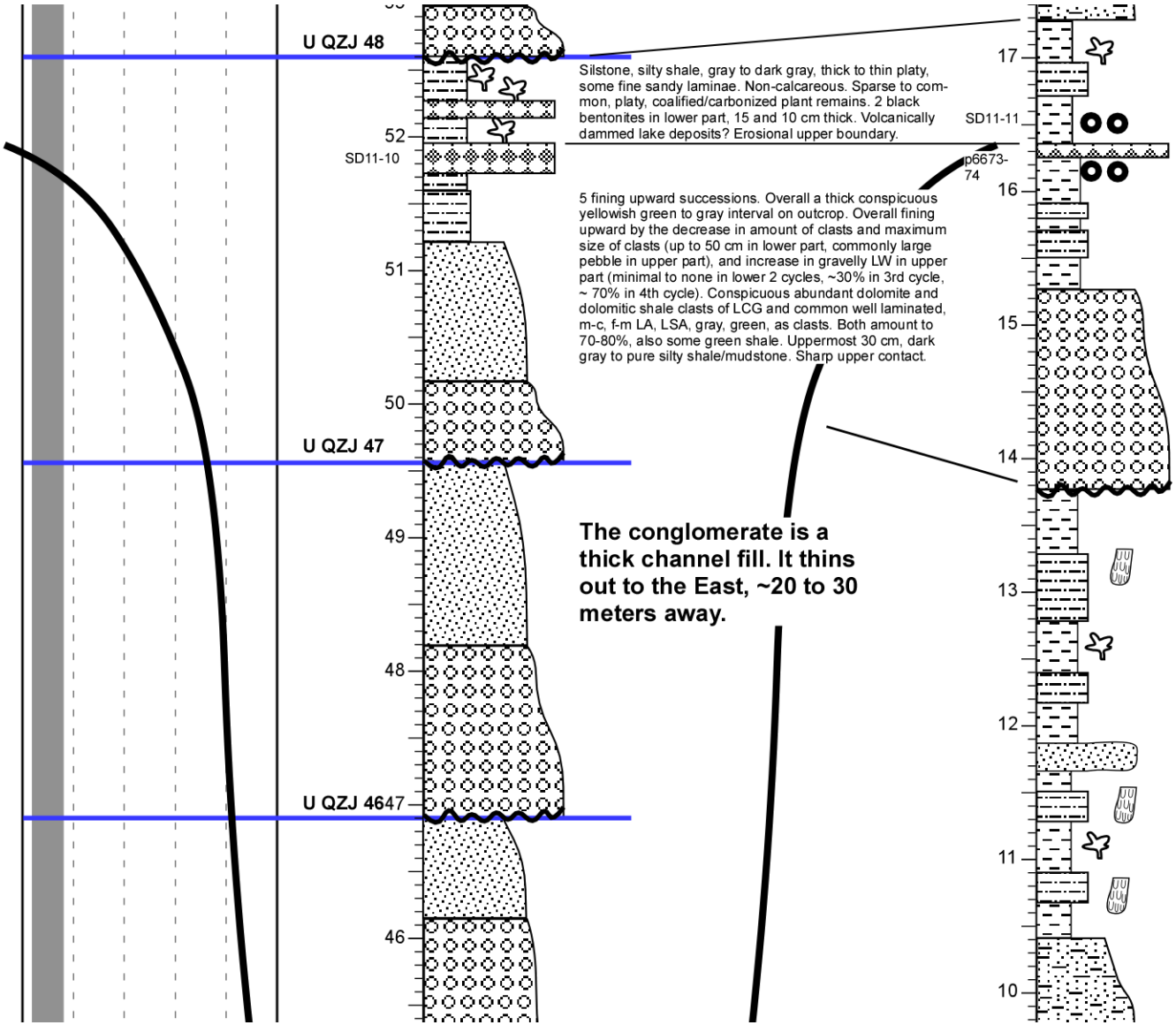
U QZJ 48
U QZJ 47
U QZJ 46
52
51
50
49
48
47
46
SD11-10
SD11-11
p6673-74
17
16
15
14
13
12
11
10
Silstone, silty shale, gray to dark gray, thick to thin platy, some fine sandy laminae. Non-calcareous. Sparse to common, platy, coalified/carbonized plant remains. 2 black bentonites in lower part, 15 and 10 cm thick. Volcanically dammed lake deposits? Erosional upper boundary.
5 fining upward successions. Overall a thick conspicuous yellowish green to gray interval on outcrop. Overall fining upward by the decrease in amount of clasts and maximum size of clasts (up to 50 cm in lower part, commonly large pebble in upper part), and increase in gravelly LW in upper part (minimal to none in lower 2 cycles, ~30% in 3rd cycle, ~ 70% in 4th cycle). Conspicuous abundant dolomite and dolomitic shale clasts of LCG and common well laminated, m-c, f-m LA, LSA, gray, green, as clasts. Both amount to 70-80%, also some green shale. Uppermost 30 cm, dark gray to pure silty shale/mudstone. Sharp upper contact.
The conglomerate is a thick channel fill. It thins out to the East, ~20 to 30 meters away.
Lower 10 cm, bentonite, correlation marker. On top, a 20 cm mudstone, dark blackish gray, to grayish maroon. Common 1-3 mm size Fe pisoids, thick continuous clay films. Above, mudstone, similar to below, no pisoids, blocky, thick clay films. May have a bentonite lamina. Common plant remains. Sharp upper contact.
Lower part, 150 cm of conglomerate, f-pebble to pebble, rd to wrd, sedimentary dominant. Upward changing to mudstone, sandy, with abundant clay coats and slickensides. Uppermost 50 cm, mudst, light brown to brown, with abundant Fe pisoids, 5 mm to 1 cm. Sharp upper contact. Same pisoids bed as pic 6673 and 74
Lower part, 20 cm of LA/LSA, a stringer?, m-c, with common clay tubules, tapering down, greenish gray. Upward changing to mudstone, brown, variably sandy + silty,, abundant clay tubules + scattered plant remains. Thick overbank deposits after the 50 cm conglomerate bed. Sharp/erosional upper contact.
Mudstone, variably sandy + silty, sand m-c, brown/gray/maroon, variegated. Common clay coats + clay tubules. Some reducing color spots. Scattered plant remains. Sharp upper contact.
Lower part, conglomerate, gray, greenish gray, granule to fine pebble, rd to wrd, common mud clasts. Upwrad changing to LW, conglomeratic, with c-vc and granules, brown, rd to wrd.

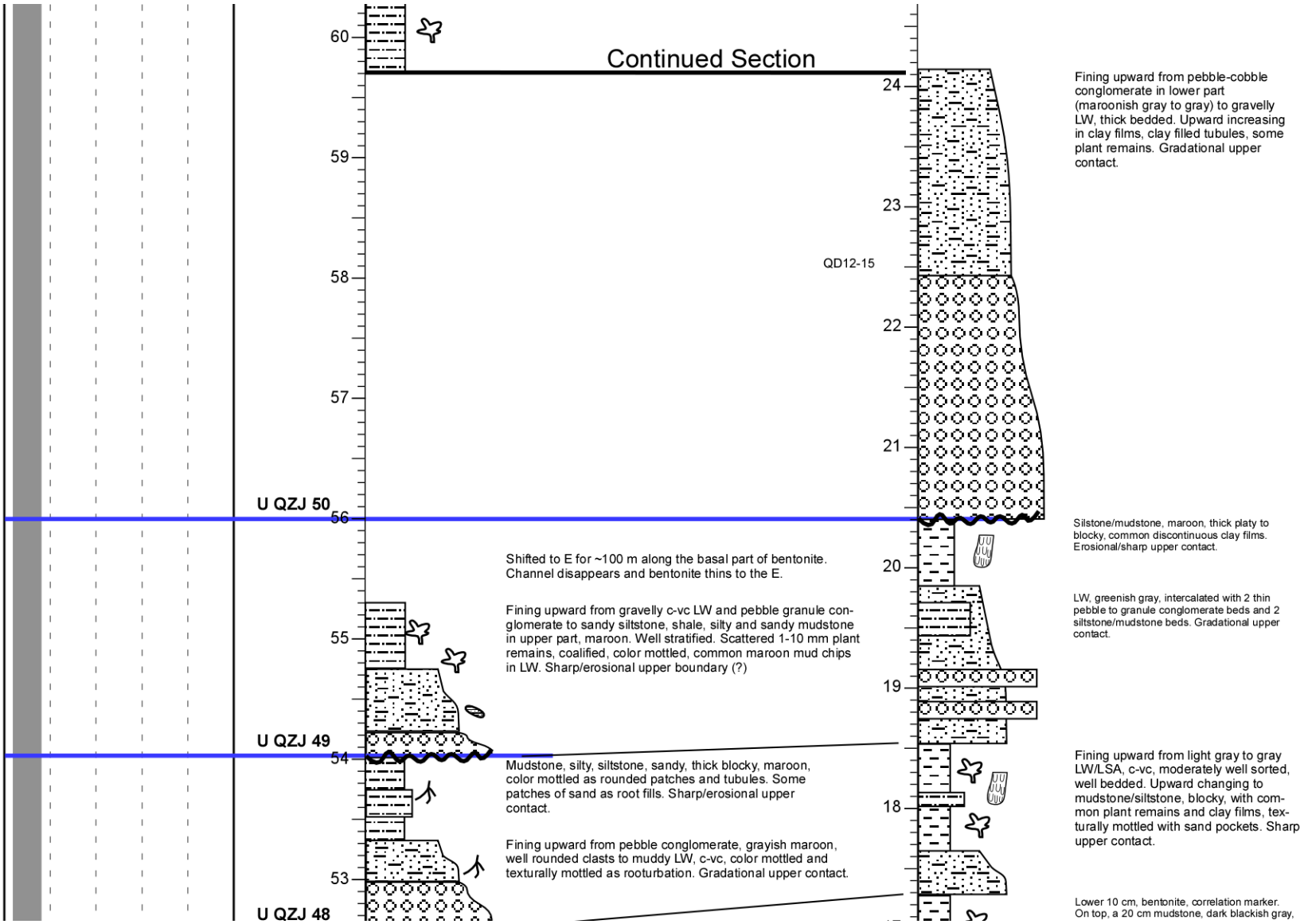
Continued Section
60
59
58
57
56
55
54
53
24
23
22
21
20
19
18
QD12-15
U QZJ 50
U QZJ 49
U QZJ 48
Shifted to E for ~100 m along the basal part of bentonite. Channel disappears and bentonite thins to the E.
Fining upward from gravelly c-vc LW and pebble granule conglomerate to sandy siltstone, shale, silty and sandy mudstone in upper part, maroon. Well stratified. Scattered 1-10 mm plant remains, coalified, color mottled, common maroon mud chips in LW. Sharp/erosional upper boundary (?)
Mudstone, silty, siltstone, sandy, thick blocky, maroon, color mottled as rounded patches and tubules. Some patches of sand as root fills. Sharp/erosional upper contact.
Fining upward from pebble conglomerate, grayish maroon, well rounded clasts to muddy LW, c-vc, color mottled and texturally mottled as rooturbation. Gradational upper contact.
Fining upward from pebble-cobble conglomerate in lower part (maroonish gray to gray) to gravelly LW, thick bedded. Upward increasing in clay films, clay filled tubules, some plant remains. Gradational upper contact.
Silstone/mudstone, maroon, thick platy to blocky, common discontinuous clay films. Erosional/sharp upper contact.
LW, greenish gray, intercalated with 2 thin pebble to granule conglomerate beds and 2 siltstone/mudstone beds. Gradational upper contact.
Fining upward from light gray to gray LW/LSA, c-vc, moderately well sorted, well bedded. Upward changing to mudstone/siltstone, blocky, with common plant remains and clay films, texturally mottled with sand pockets. Sharp upper contact.
Lower 10 cm, bentonite, correlation marker. On top, a 20 cm mudstone, dark blackish gray,

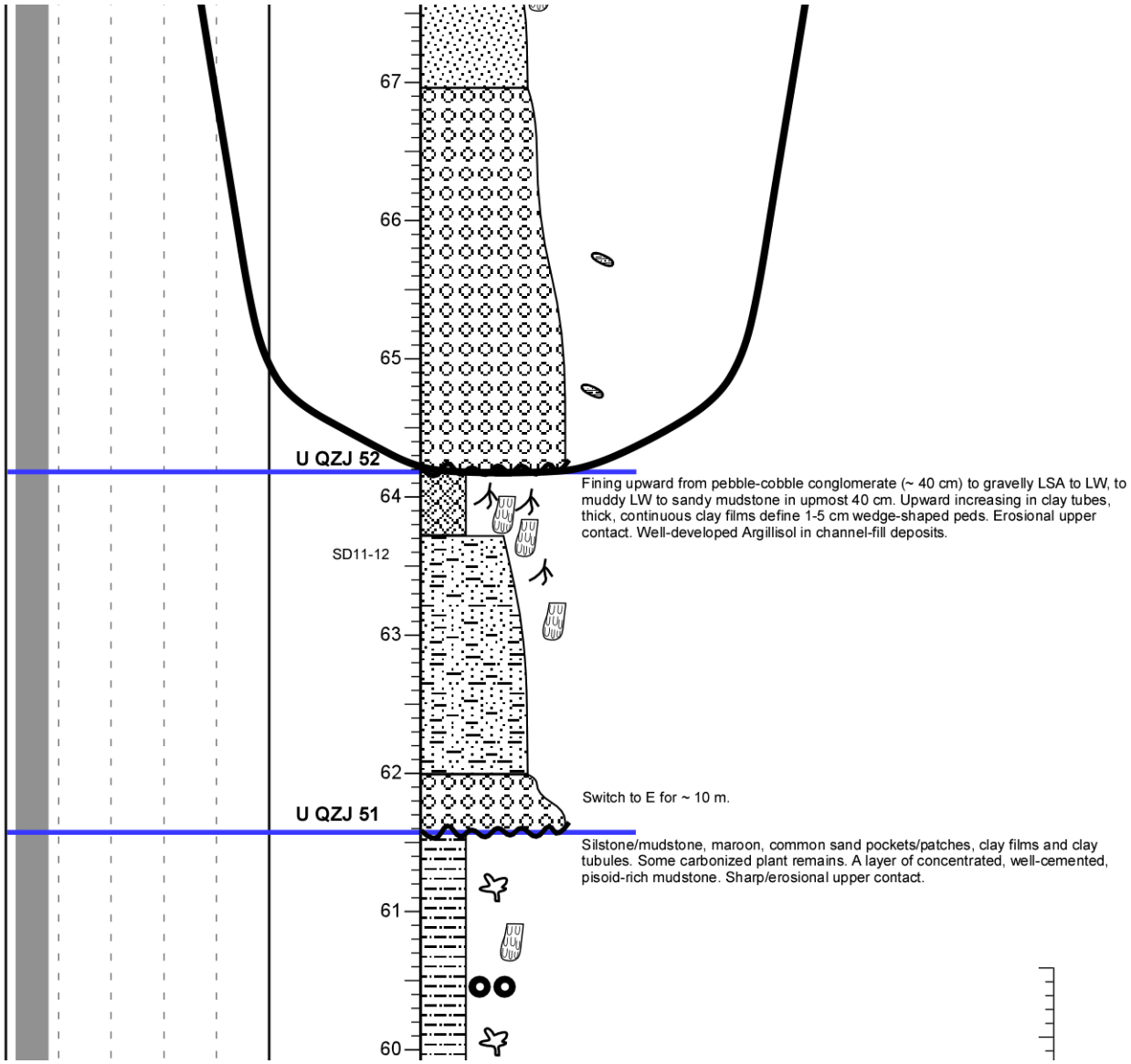
67
66
65
U QZJ 52
64
SD11-12
63
62
U QZJ 51
61
60
Fining upward from pebble-cobble conglomerate (~ 40 cm) to gravelly LSA to LW, to muddy LW to sandy mudstone in upmost 40 cm. Upward increasing in clay tubes, thick, continuous clay films define 1-5 cm wedge-shaped peds. Erosional upper contact. Well-developed Argillisol in channel-fill deposits.
Switch to E for ~ 10 m.
Silstone/mudstone, maroon, common sand pockets/patches, clay films and clay tubules. Some carbonized plant remains. A layer of concentrated, well-cemented, pisoid-rich mudstone. Sharp/erosional upper contact.

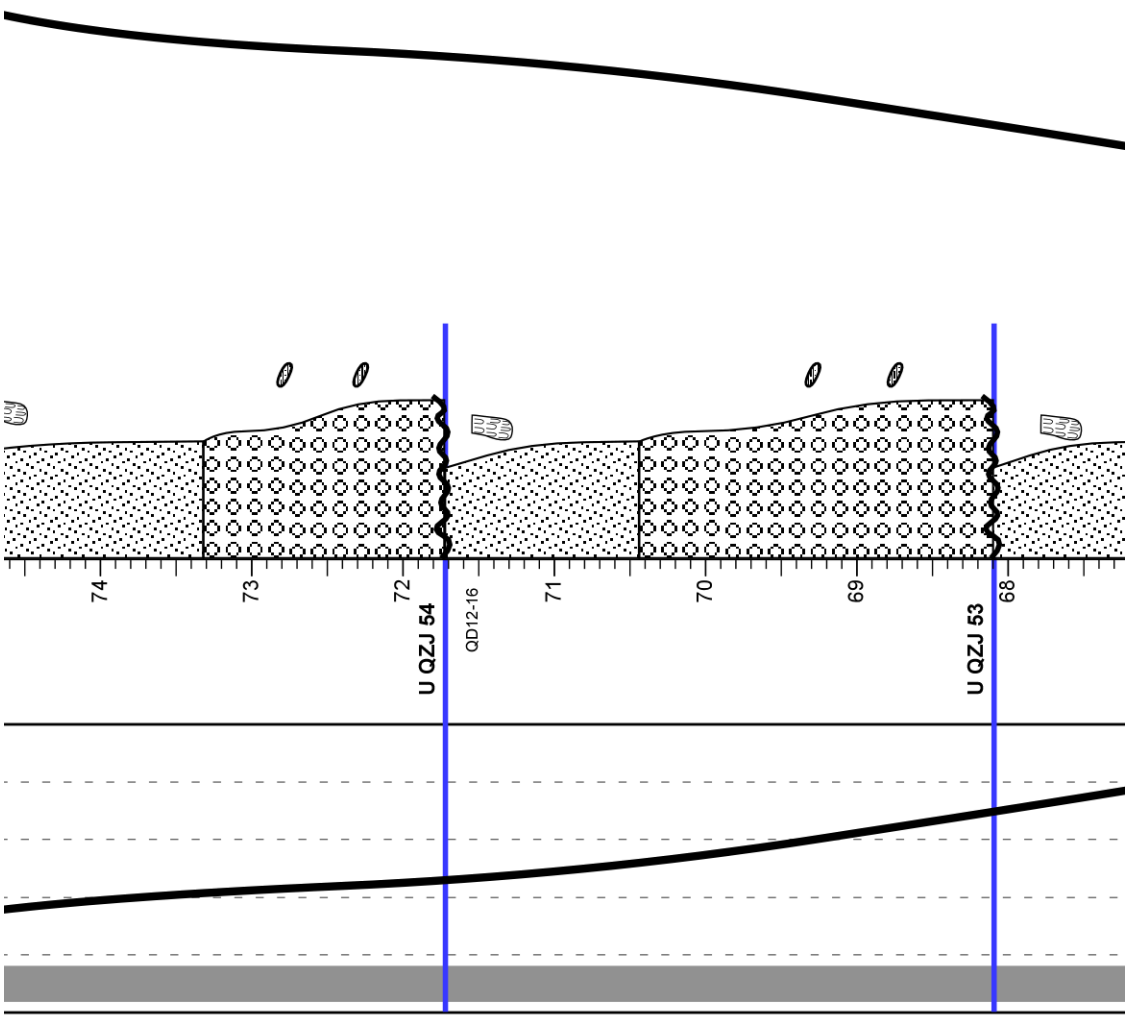
74
73
72
U QZJ 54
QD12-16
71
70
69
U QZJ 53
68

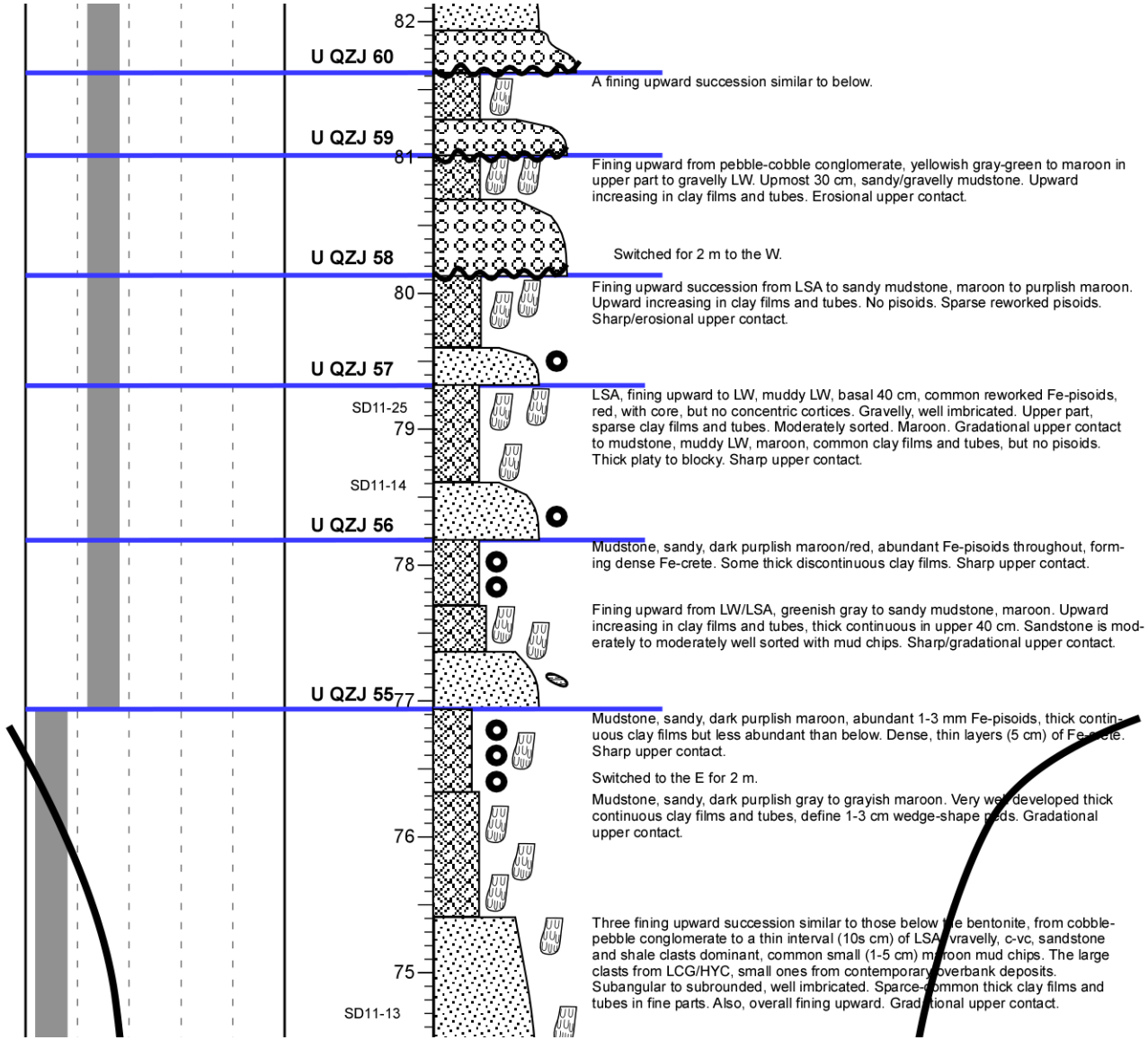
82
U QZJ 60
A fining upward succession similar to below.
U QZJ 59
81
Fining upward from pebble-cobble conglomerate, yellowish gray-green to maroon in upper part to gravelly LW. Upmost 30 cm, sandy/gravelly mudstone. Upward increasing in clay films and tubes. Erosional upper contact.
Switched for 2 m to the W.
U QZJ 58
Fining upward succession from LSA to sandy mudstone, maroon to purplish maroon. Upward increasing in clay films and tubes. No pisoids. Sparse reworked pisoids. Sharp/erosional upper contact.
80
U QZJ 57
SD11-25
LSA, fining upward to LW, muddy LW, basal 40 cm, common reworked Fe-pisoids, red, with core, but no concentric cortices. Gravelly, well imbricated. Upper part, sparse clay films and tubes. Moderately sorted. Maroon. Gradational upper contact to mudstone, muddy LW, maroon, common clay films and tubes, but no pisoids. Thick platy to blocky. Sharp upper contact.
79
SD11-14
U QZJ 56
Mudstone, sandy, dark purplish maroon/red, abundant Fe-pisoids throughout, forming dense Fe-crete. Some thick discontinuous clay films. Sharp upper contact.
78
Fining upward from LW/LSA, greenish gray to sandy mudstone, maroon. Upward increasing in clay films and tubes, thick continuous in upper 40 cm. Sandstone is moderately to moderately well sorted with mud chips. Sharp/gradational upper contact.
U QZJ 55
77
Mudstone, sandy, dark purplish maroon, abundant 1-3 mm Fe-pisoids, thick continuous clay films but less abundant than below. Dense, thin layers (5 cm) of Fe-crete. Sharp upper contact.
Switched to the E for 2 m.
Mudstone, sandy, dark purplish gray to grayish maroon. Very well developed thick continuous clay films and tubes, define 1-3 cm wedge-shape peds. Gradational upper contact.
76
Three fining upward succession similar to those below the bentonite, from cobble-pebble conglomerate to a thin interval (10s cm) of LSA, gravelly, c-vc, sandstone and shale clasts dominant, common small (1-5 cm) maroon mud chips. The large clasts from LCG/HYC, small ones from contemporary overbank deposits. Subangular to subrounded, well imbricated. Sparce-common thick clay films and tubes in fine parts. Also, overall fining upward. Gradational upper contact.
75
SD11-13

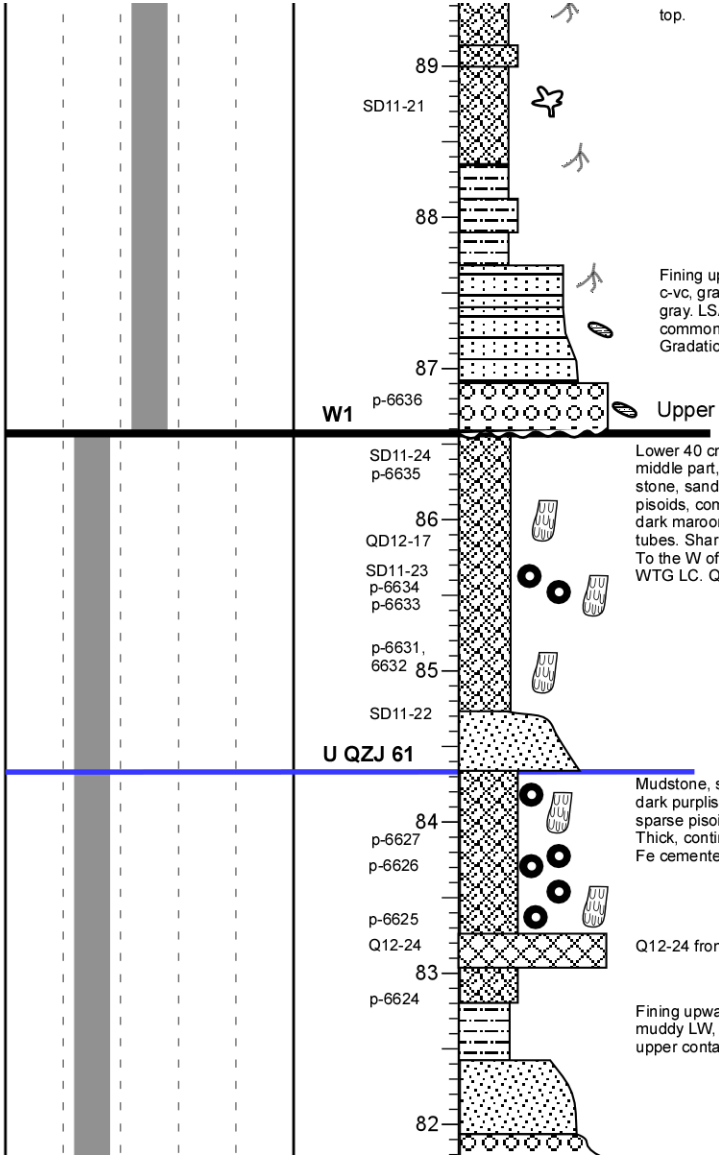

top.

Fining upward from pebble conglomerate, well sorted and imbricated, to LSA and LW, c-vc, gravelly, sparse reworked pisoids, uppermost part some clay tubules, greenish gray. LSA and conglomerate well to moderately sorted, subangular to subrounded, common 0.1-2 cm red mud chips. Basal surface flat, laterally persistent, low relief. Gradational top. Beach to littoral deposits.

Upper QZJ-Wutonggou LC boundary

Lower 40 cm, LW, grayish maroon, c-vc, muddy, sparse clay coats and tubes. Lower middle part, 20 cm mudstone, variegated, rich in clay coats. Above, 80 cm of mudstone, sandy, dark purplish maroon, upward increasing then upward decreasing in Fe pisoids, common clay films and tubes. Upper part, mudstone, sandy, silty, siltstone, dark maroon to purplish maroon, blocky, thin, discontinuous clay coats, common tubes. Sharp/erosional upper contact. A horizon.
To the W of measured section, a Fe-crete right below the littoral sandstone of the WTG LC. QD12-17 from the Fe-crete bed. See pic 6693, 6695, 6696+97 of Fe-crete.

Mudstone, sandy, gravelly and very muddy LW, no clear grain size trend. Maroon to dark purplish maroon (where Fe crete and pisoids most abundant) Lower 30 cm, sparse pisoids, upward increasing in abundance, upmost 40 cm, common to sparse. Thick, continuous clay coats throughout, lesses in upper 40 cm. Peds 1-5 cm. Dense, Fe cemented. Sharp upper contact.

Q12-24 from a bentonite. Contains some big carbonized plant remains.

Fining upward from cobble-pebble-granule conglomerate, maroon, to LW, very muddy LW, gravelly. Clast sandstone pebble-cobble, LA, well sorted. Gradational upper contact.

Dalongkou Section

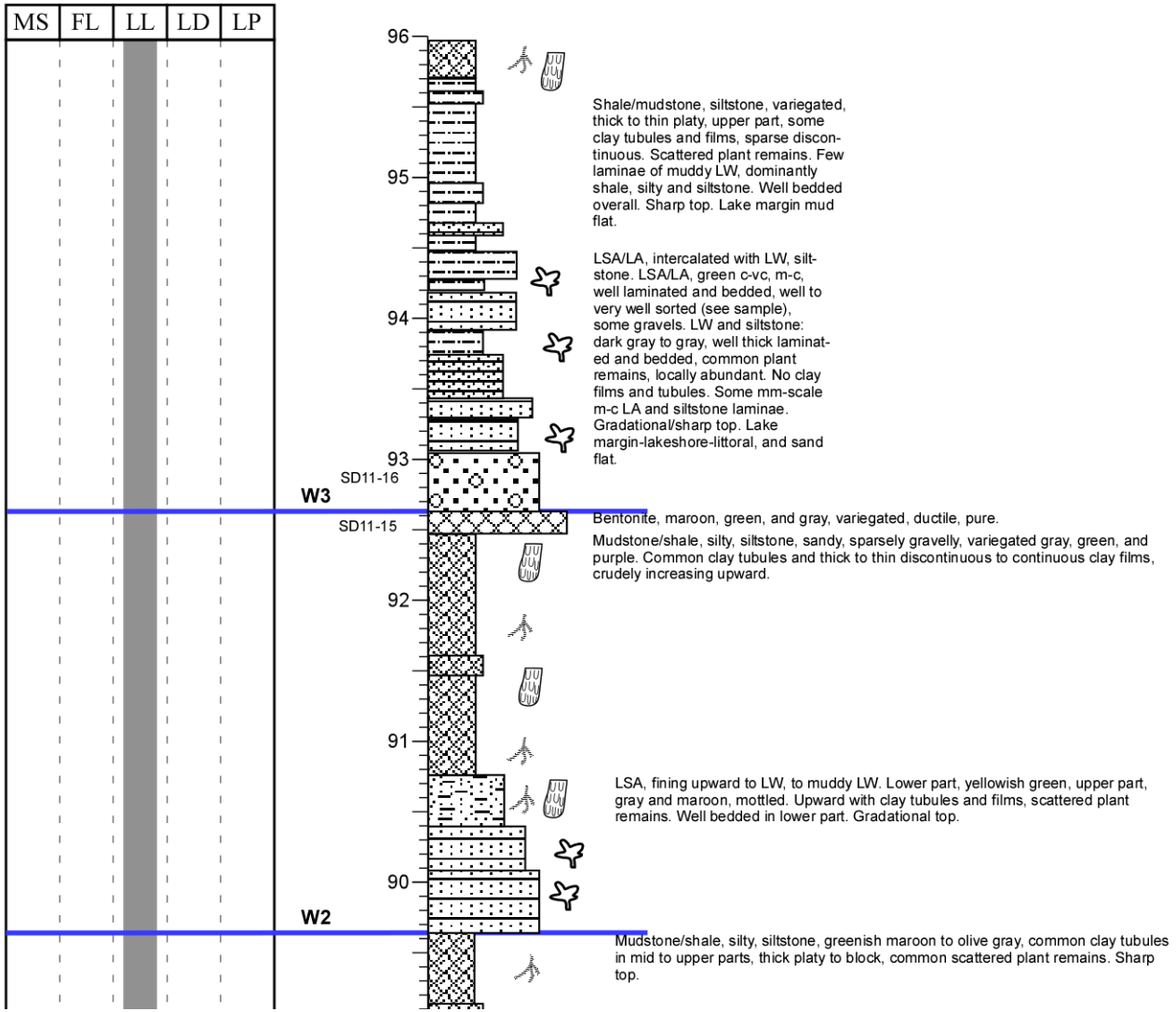

APPENDIX H
PALEOCURRENT

Paleocurrent indicator: Imbricated pebbles
Attitude (for structural correction in strike/dip):130/29

Section: Northeast Tarlong
Cycle: LQZJ 1

Vector: 219.9
Mean Vector Length: 25.55
Magnitude of Resultant Vector: 51.10

Dip	Dip direction	Corrected dip	Corrected dip direction
40	215	78.6	23.5
37	196	72	40
33	010	70.8	81.7
51	060	78.6	92.1
37	235	72.7	131.4
45	045	85.2	134.4
13	132	73.4	141.6
18	171	72.3	146.3
29	257	56.6	158.4
45	238	59.2	177.3
39	199	24.9	180.3
37	167	69.7	181
27	185	47.7	182.7
38	205	53	185.7
47	220	82.3	186.1
44	185	63.9	187.8
23	231	35.9	194.1
57	160	70.3	197.5
23	045	59.9	197.7
15	285	30.3	201.6
31	290	44.2	201.8
45	345	67.2	205
18	005	45.2	205.4
40	075	63	205.7
21	296	77.4	206.5
20	318	37.5	206.5
12	235	72.3	209.8
48	125	36	220.5
13	255	38.1	222.5
30	254	16.1	223.7
17	230	21.4	228.3
25	105	66	231.1
20	359	11.3	235.7
59	110	27.4	242.9
26	145	24.5	243.9
37	075	58.9	245.8
09	260	66.1	249.7
40	052	44.9	252.7
14	164	68.5	259.4
29	230	57.3	271.5
25	041	18	277.9
07	180	76	280.6
33	253	33.6	282.8
11	306	73.7	287.7
18	265	60.9	301.7
25	014	42.8	318
25	190	64.8	330.5
07	287	74.8	330.9
25	325	74.7	341.3
30	355	77.8	350.9

Rose Diagram

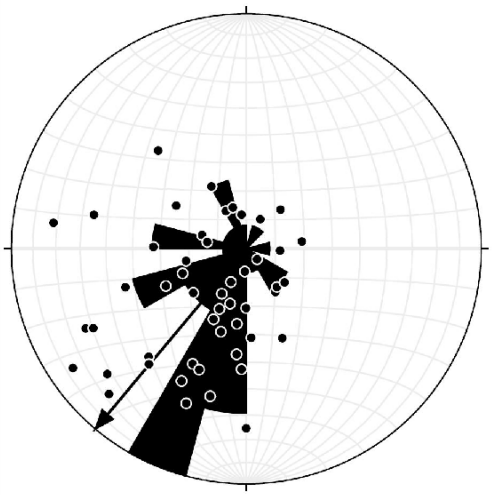

Paleocurrent indicator: Imbricated pebbles
Attitude (for structural correction in strike/dip):130/29

Section: Northeast Tarlong
Cycle: UQZJ 5

Vector: 140
Mean Vector Length: 9.58
Magnitude of Resultant Vector: 43.54

Dip	Dip direction	Corrected dip	Corrected dip direction
35	265	65.9	136
36	257	69.3	127
24	250	75.9	163.5
62	238	54.9	68.3
36	155	55.9	291.8
33	267	66	141.6
44	224	74.8	50.7
22	231	81.6	190.8
52	250	60.4	92.9
48	236	68.7	74.3
35	206	80.5	342.9
37	255	69.6	122.7
32	272	64.1	146.8
17	280	65.1	183
37	268	63.3	134.5
22	193	76.6	267.2
22	262	71.1	169.4
25	260	71.7	159.9
61	263	47.2	101.5
38	283	55.6	144.1
17	100	50	243.2
37	179	66.7	311.5

Rose Diagram

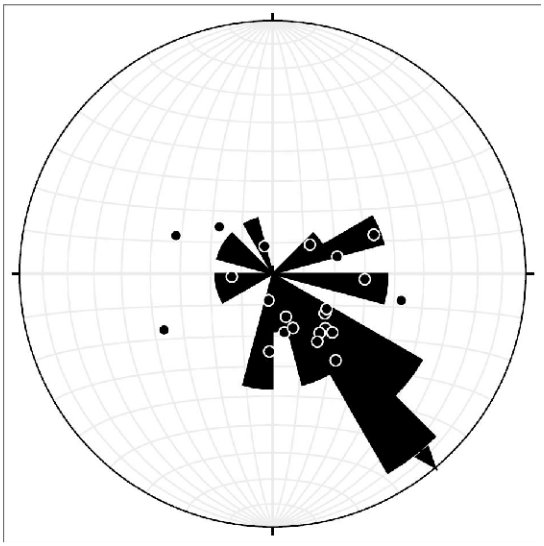

Paleocurrent indicator: Imbricated pebbles
Attitude (for structural correction in strike/dip):130/29

Section: Northeast Tarlong
Cycle: UQZJ 17

Vector: 210.2
Mean Vector Length: 8.03
Magnitude of Resultant Vector: 30.8

Dip	Dip direction	Corrected dip	Corrected dip direction
35	147	52.9	285.5
39	200	75.1	343.1
21	310	54.7	181.6
39	220	80	40
55	195	59.5	357
23	261	71.5	166.3
21	228	81.3	200.7
42	302	44	152.8
14	236	74	206
30	277	62.8	153.4
18	243	75.9	190.4
13	130	58.5	245.5
56	226	62.7	50.9
26	207	83.3	277.8
39	225	79.6	57.7
38	186	69.5	320.6
16	205	75.9	237
28	223	88.3	166.2
30	189	74.8	300.1
29	230	85.2	134.4
17	268	68.6	183.4
35	290	54.2	152.7
22	223	82.9	210.9
12	170	67	244
34	200	78.5	326.8
14	250	71.8	197.2

Rose Diagram

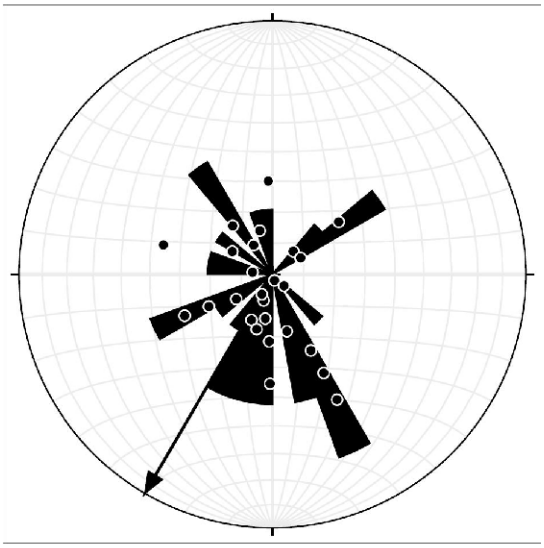

Paleocurrent indicator: Imbricated pebbles
Attitude (for structural correction in strike/dip):57/44

Section: Taodonggou
Cycle: UQZJ 1

Vector: 131.3
Mean Vector Length: 13.4
Magnitude of Resultant Vector: 66.9

Dip	Dip direction	Corrected dip	Corrected dip direction
36	165	76	98.4
46	118	69.5	232.1
43	116	68.8	223
39	156	82.2	100.3
36	155	80.5	117.3
34	160	77.1	112.6
13	159	58.6	141.8
45	153	85.7	45.8
23	128	66.8	165.8
26	128	69.1	170.6
32	142	77.6	159.4
39	188	62.7	82.6
20	121	62.8	166.2
40	156	82.8	93.9
24	160	68.8	132.3
33	198	57.3	95.4
39	137	81.7	196.3
25	110	62.4	180.3
37	175	70.7	88.4
46	203	51.2	75

Rose Diagram

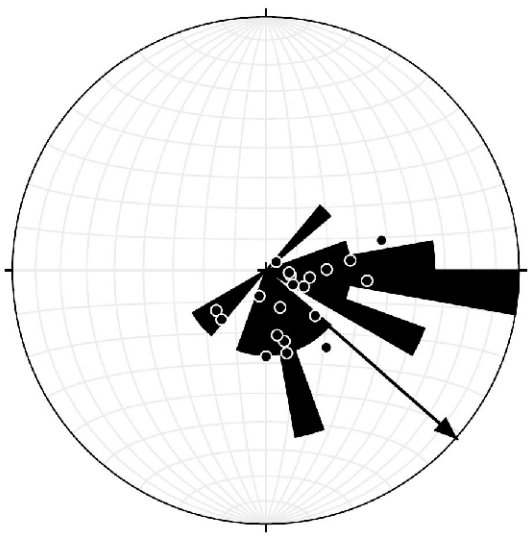

Paleocurrent indicator: Imbricated pebbles
Attitude (for structural correction in strike/dip):57/44

Section: Taodonggou
Cycle: UQZJ 17

Vector: 44.3
Mean Vector Length: 6.6
Magnitude of Resultant Vector: 33.1

Dip	Dip direction	Corrected dip	Corrected dip direction
35	140	80	170.7
48	148	85.9	337.5
52	157	79.1	13.3
45	156	83.6	51.2
68	176	56.4	21.3
62	135	69.7	295.1
49	160	79.3	33.7
55	170	69.5	32.8
35	130	76	190.9
52	140	80.5	291.6
37	175	70.7	88.4
64	119	60.1	269.3
46	175	70.2	61.3
43	212	46.6	82.9
29	166	71.4	117.4
45	195	56.9	73
33	169	72.6	104.1
55	159	75.7	10.7
47	145	86.7	300.9
34	144	79.8	156.5

Rose Diagram

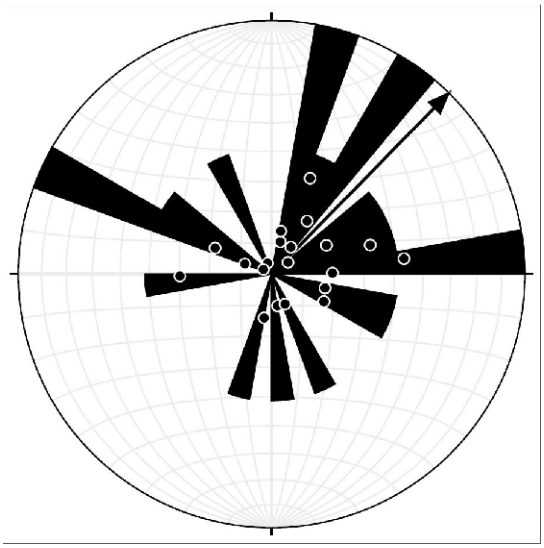

Paleocurrent indicator: Imbricated pebbles
Attitude (for structural correction in strike/dip): 57/44

Section: Taodonggou
Cycle: UQZJ 28

Vector: 78.0
Mean Vector Length: 9.25
Magnitude of Resultant Vector: 71.2

Dip	Dip direction	Corrected dip	Corrected dip direction
25	225	45.5	110.9
27	207	53	106.2
23	190	59.4	115.4
55	196	51.8	58.1
60	187	55.1	43.9
35	203	54.3	92.4
29	180	65.7	107
37	190	61.7	87.1
63	185	54.5	37.9
52	156	79.6	10
50	145	83.8	312.6
41	178	69	76.5
24	160	68.8	132.3

Rose Diagram

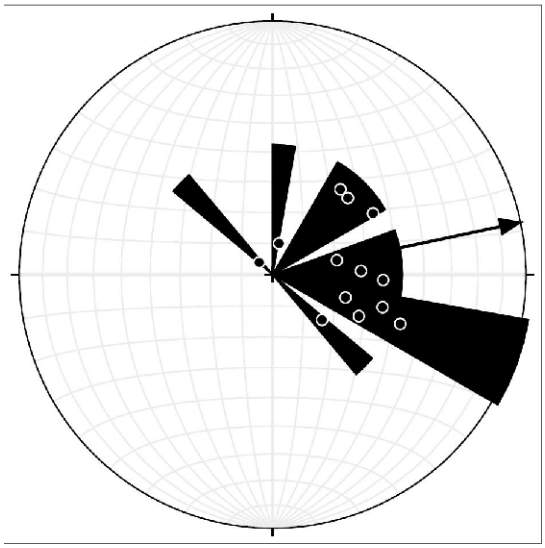

Paleocurrent indicator: Imbricated pebbles
Attitude (for structural correction in strike/dip): 255/42

Section: Southwest Tarlong
Cycle: LQZJ 1

Vector: 22.7
Mean Vector Length: 7.2
Magnitude of Resultant Vector: 48.0

Dip	Dip direction	Corrected dip	Corrected dip direction
28	260	43.1	24.8
59	337	71.9	142.4
24	275	50.5	22
36	305	64.5	46.3
39	352	84.6	291
44	305	63	64.1
56	325	69.5	110.8
43	331	80.5	75.8
40	354	83.8	277.1
44	316	70.2	69.9
39	000	79.8	277.7
27	311	66.1	23.7
12	280	51.8	2.7
32	356	78	315.8
14	246	44.1	4.4

Rose Diagram

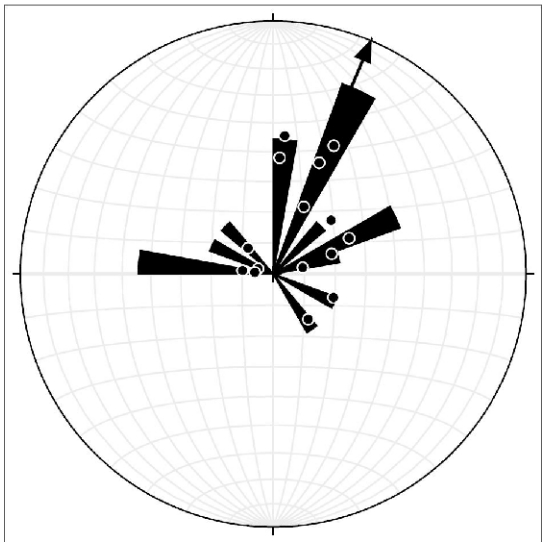

Paleocurrent indicator: Imbricated pebbles
Attitude (for structural correction in strike/dip): 255/42

Section: Southwest Tarlong
Cycle: LQZJ 18

Vector: 36.7
Mean Vector Length: 3.2
Magnitude of Resultant Vector: 53.4

Dip	Dip direction	Corrected dip	Corrected dip direction
39	333	81.7	49.4
26	314	66.8	20
58	345	74	165
37	329	78.7	42.8
38	330	79.6	46.8
40	348	87.2	301.6

Rose Diagram

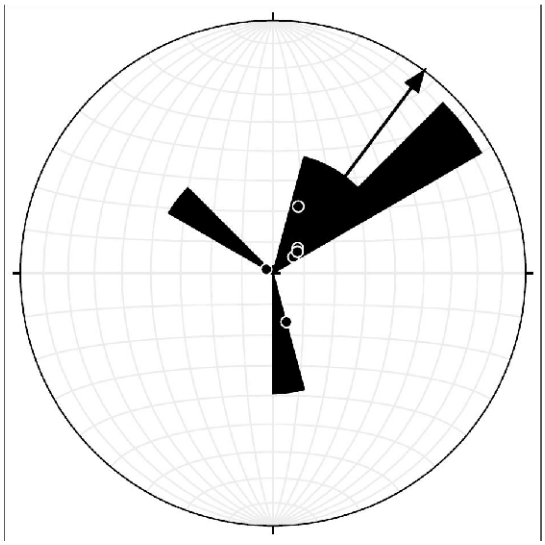

Paleocurrent indicator: Imbricated pebbles
Attitude (for structural correction in strike/dip): 255/42

Section: Southwest Tarlong
Cycle: UQZJ 2

Vector: 329.3
Mean Vector Length: 7.2
Magnitude of Resultant Vector: 72.3

Dip	Dip direction	Corrected dip	Corrected dip direction
31	352	78.3	327
45	315	69.3	72.1
15	270	49.7	7.7
26	329	71.8	7.7
29	002	73.8	314.5
20	017	63.2	321.3
40	354	83.8	277.1
16	330	63.2	354.1
34	014	70.6	290.2
38	020	67.4	278.4

Rose Diagram

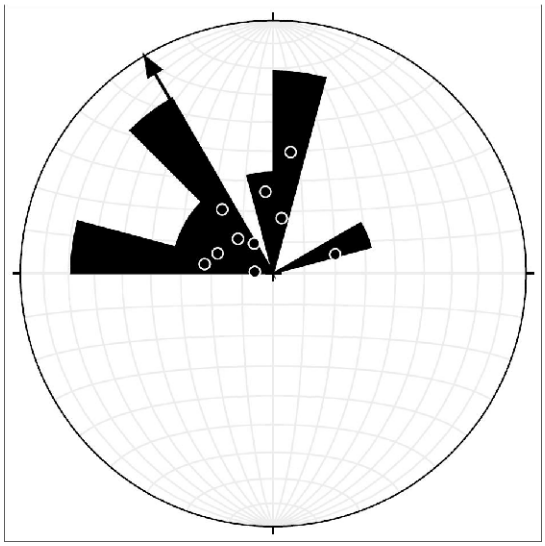

Paleocurrent indicator: Imbricated pebbles
Attitude (for structural correction in strike/dip): 292/52

Section: Southeast Tarlong
Cycle: LQZJ 1

Vector: 30.8
Mean Vector Length: 14.9
Magnitude of Resultant Vector: 74.8

Dip	Dip direction	Corrected dip	Corrected dip direction
35	101	36.2	337.8
48	087	41.3	318.4
27	020	65	24.1
41	061	60	326.2
30	044	64	356.7
07	061	43.3	16
23	013	60.6	29.1
48	058	62.3	311.8
34	310	40.3	66.2
22	257	23.7	41.6
54	348	62.9	105.7
32	293	32	60.6
44	345	61.6	83.7
13	289	36.2	38.2
30	358	63.3	48.9
23	032	60.5	14.1
24	000	59.3	39.3
50	348	63.7	96.9
37	357	67.1	62.9
46	022	84	22

Rose Diagram

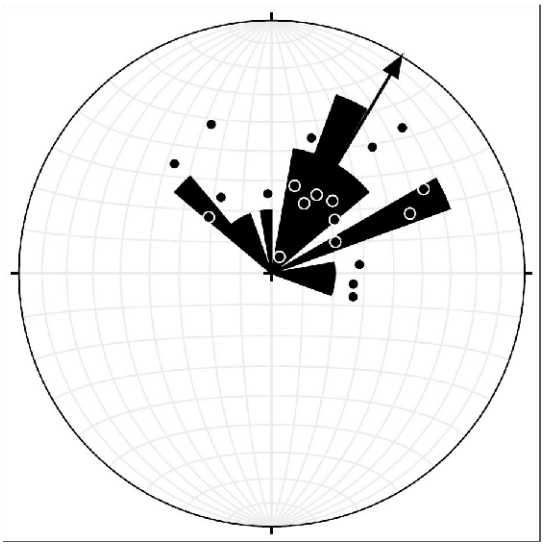

Paleocurrent indicator: Imbricated pebbles
Attitude (for structural correction in strike/dip): 292/52

Section: Southeast Tarlong
Cycle: LQZJ 2

Vector: 54.5
Mean Vector Length: 16.5
Magnitude of Resultant Vector: 82.5

Dip	Dip direction	Corrected dip	Corrected dip direction
34	140	17.7	350.8
46	354	68.2	87.2
60	355	66.3	123.6
35	350	62.6	63.3
28	351	59.4	50.4
59	359	69.9	125.4
37	338	56.4	71
36	001	68.5	57.1
21	021	59	22.7
41	017	78.4	38.6
28	350	59	50.9
45	347	63.1	85.7
55	000	72.1	114.9
04	350	41.4	24.8
31	021	69	23.4
24	347	55.6	46.4
25	008	61.8	34.5
25	358	59.6	41.8
19	025	57	20.2
26	355	59.4	45

Rose Diagram

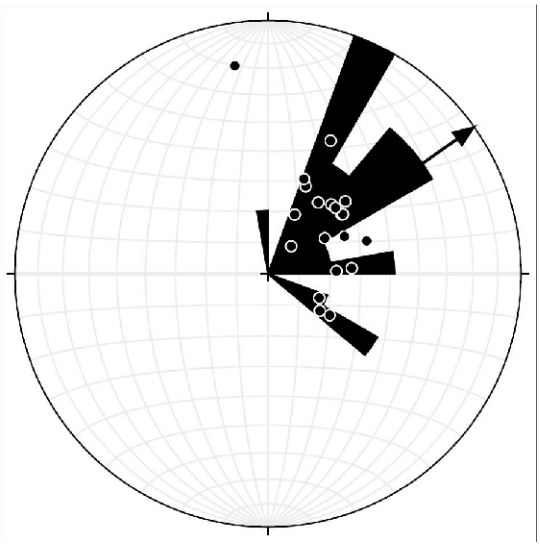

Paleocurrent indicator: Imbricated pebbles
Attitude (for structural correction in strike/dip): 292/52

Section: Southeast Tarlong
Cycle: UQZJ 18

Vector: 46.2
Mean Vector Length: 11.9
Magnitude of Resultant Vector: 59.5

Dip	Dip direction	Corrected dip	Corrected dip direction
28	015	65.6	30
33	311	41	65
43	014	79.3	52.6
45	022	83	22
39	007	73.2	56.4
48	043	73.5	312.6
23	043	58.7	6.4
46	355	68.9	86.9
32	024	70	18.9
50	055	64.4	306.9
54	075	48.2	306.2
50	004	75.9	98.2
46	018	83.3	47.4
51	350	65.1	99.7
48	355	69	92.5
55	034	79.9	278.4
45	013	80.3	63
56	003	74.1	120.8
35	012	71.7	40.5
51	014	83.7	100.4

Rose Diagram

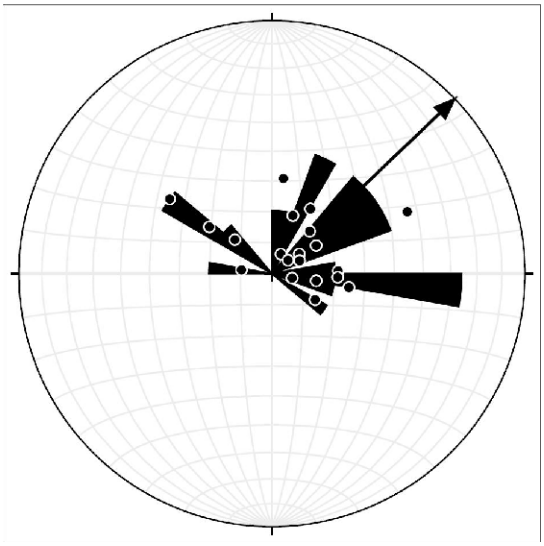

Paleocurrent indicator: Imbricated pebbles
Attitude (for structural correction in strike/dip): 174/71

Section: Dalongkou
Cycle: LQZJ 1

Vector: 77.4
Mean Vector Length: 18.8
Magnitude of Resultant Vector: 75.3

Dip	Dip direction	Corrected dip	Corrected dip direction
48	320	37.6	212.9
56	80	36.9	79.9
53	86	34	85.9
24	86	5	84.8
33	35	3.7	59.7
37	50	12.2	63.9
40	51	15.1	62.7
16	94	3.2	266.7
43	75	23.5	77.3
31	83	12	83.5
46	74	26.3	76
50	71	29.8	72.5
60	86	41	86.3
56	60	32.3	60.5
31	54	8.2	68.9
35	69	14.9	75.2
42	49	16	60.5
38	65	17.1	71.9
32	96	12.4	90.5
36	104	15	96
17	65	2.9	258.5
35	82	16	82.8
32	60	10.5	71.3
57	62	33.9	61.8
61	100	39.6	102.2

Rose Diagram

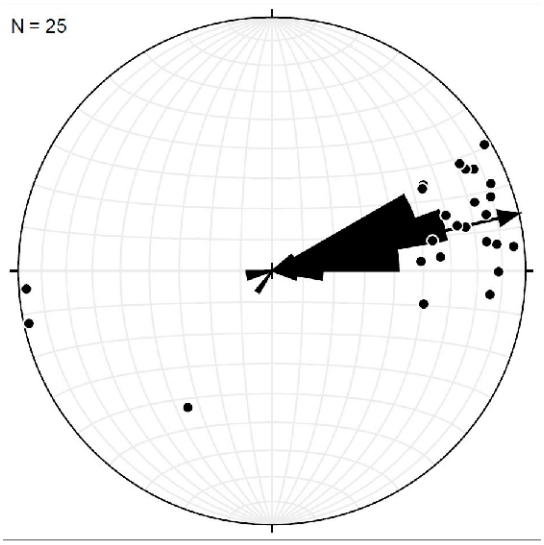

Paleocurrent indicator: Imbricated pebbles
Attitude (for structural correction in strike/dip): 174/71

Section: Dalongkou
Cycle: UQZJ 22

Vector: 52.0
Mean Vector Length: 7.6
Magnitude of Resultant Vector: 38.3

Dip	Dip direction	Corrected dip	Corrected dip direction
17	42	6.1	252.7
47	54	22.1	60.7
46	61	23.6	66.1
50	35	15.4	47.1
18	46	4.6	253
40	350	17	221.9
53	31	15	42.7
43	39	12.6	54.4
54	61	30.8	62.4
42	34	9.5	52.7
54	25	11.7	38.9
48	46	19.6	54.9
43	76	23.6	78.1
42	142	5.4	118.7
13	215	27.2	275
49	57	25	61.8
14	47	7.7	255.6
11	332	22.8	252.9
44	20	3.1	45.3
36	67	15.6	73.7

Rose Diagram

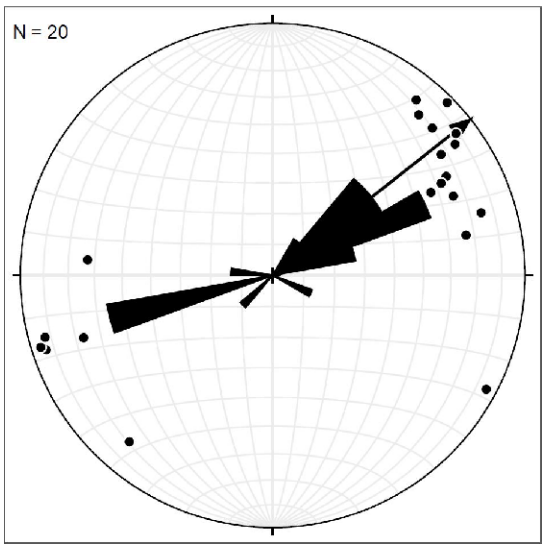

Paleocurrent indicator: Imbricated pebbles
Attitude (for structural correction in strike/dip): 174/71

Section: Dalongkou
Cycle: UQZJ 43

Vector: 29.1
Mean Vector Length: 13.7
Magnitude of Resultant Vector: 68.8

Dip	Dip direction	Corrected dip	Corrected dip direction
45	55	20.8	62.5
54	210	39.9	322.5
24	343	21.8	238.5
68	224	52.5	342.3
74	240	66.9	357.7
51	38	17.8	48
68	71	47.1	66.2
57	34	19.4	41.1
81	209	35.9	356.6
52	45	22.2	51.6
71	235	62.6	349.2
80	35	33.7	20.7
45	33	11	50
55	60	31.4	61
65	50	34.9	45.8
51	45	21.5	52.3
59	75	39.3	74
58	266	76.9	256.5
81	50	46.3	30.9
66	55	38.5	49.5

Rose Diagram

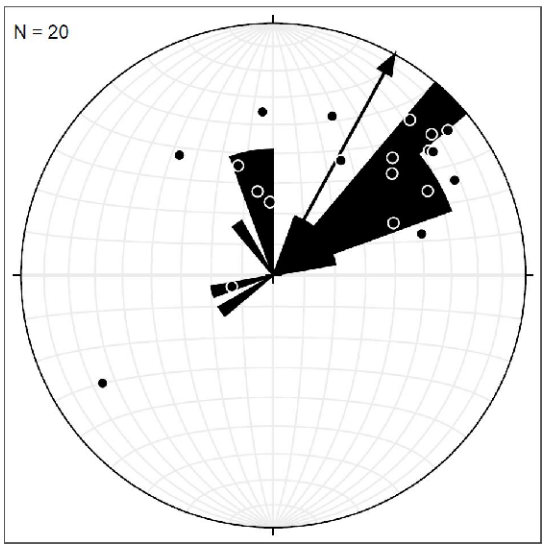

Paleocurrent indicator: Imbricated pebbles
Attitude (for structural correction in strike/dip): 174/71

Section: Dalongkou
Cycle: UQZJ 60

Vector: 66.3
Mean Vector Length: 18.26
Magnitude of Resultant Vector: 91.3

Dip	Dip direction	Corrected dip	Corrected dip direction
44	19	2.5	44.9
50	127	18.7	117.5
35	98	15	92.3
70	232	59.9	346.7
44	71	23.9	74.2
55	95	35	95
51	69	30.3	70.5
65	56	38.2	51.2
57	77	37.6	76.6
75	66	51.7	55.2
57	82	38	81.9
55	58	30.6	59.3
66	70	44.9	65.8
45	48	18.1	58.1
58	75	38.3	74.3
71	65	47.7	56.8
65	49	34.4	45
65	65	42.3	60.5
61	70	40.1	67.9
49	76	29.5	77.1

Rose Diagram

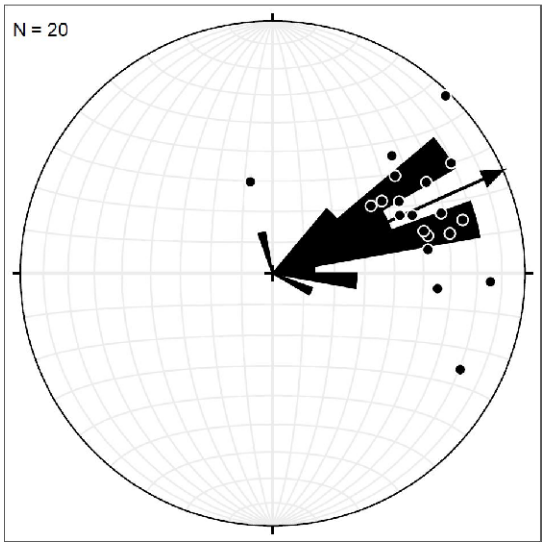

APPENDIX I

CLAST COUNTING

	NE Tarlong			SE Tarlong			Taodonggou			SW Tarlong			Dalongkou			
	LQZJ 1	UQZJ 5	UQZJ 7	LQZJ 1	UQZJ 18	UQZJ 39	UQZJ 1	UQZJ 17	UQZJ 28	LQZJ 1	LQZJ 18	UQZJ 2	LQZJ 1	UQZJ 22	UQZJ 43	UQZJ 60
Volcanic																
Intermediate	59	56	27	49	40	20	42	30	41	27	66	25	2	3	9	6
Mafic	12	10	1	31	23	0	1	24	16	5	10	1	0	0	0	0
Unknown	13	16	6	18	20	22	27	10	8	18	0	0	2	0	0	0
Sedimentary																
Sandstone	21	13	69	6	11	53	25	34	31	54	24	74	106	96	79	98
Mudstone	0	1	1	2	1	0	4	0	3	5	1	0	0	0	1	1
Limestone	0	0	0	0	0	0	0	0	0	9	0	3	1	4	0	1
Chert	0	5	1	0	5	7	1	2	1	2	0	3	1	0	0	0
Shale	0	0	0	0	0	0	0	0	0	0	0	0	0	0	14	0
Metamorphic	0	0	0	0	0	0	0	11	7	0	0	0	0	0	0	0

APPENDIX J
PARTICLE SIZE ANALYSIS

METHODS

Particle size analysis was carried out in the Beckman-Coulter Particle Size Characterization Laboratory in Miami, FL. In 150 mL beakers, one mL of 1M HCl was added to ~2g of sample to loosen and disperse it. Approximately 60 mL of DIW and one mL of 10% sodium hexametaphosphate (Calgon) were added and probe-sonicated for four minutes at 100 W. The preparation beaker was placed into a 500 mL beaker with water to prevent boiling by prolonged sonication. The entire content was added and rinsed into the Beckman Coulter Laser Diffraction Particle Size Analyzer (LS 13 320) Aqueous Liquid Module and run with standard operating procedures. Each sample was run through the machine three times and the results obtained are presented as an average of the three measurements.

In addition, reliability test were done to test sample representation. Two large samples weighing close to 10 g from were split into five smaller pieces and disaggregated following the aforementioned procedure. Each sample was treated in different beakers, making it a total of 10 pieces. Each sample was run separately for three times. The results showed small variations but a similar distribution throughout, indicating that smaller pieces are representative enough for an entire sample.

Particle Size
NE Tarlong Section
Cycle: UQZJ 3
Results in volume %

Size µm	S10-8	Q11-1	Q11-2	Q11-3	Q11-4	S10-9	Q11-5	S10-10	Q11-6	S10-11
0.393033	0.265	0.252	0.3206	0.229	0.238	0.245	0.281	0.2821	0.315	0.2542
0.431458	0.47	0.446	0.5666	0.404	0.421	0.433	0.497	0.499	0.556	0.4497
0.473639	0.704	0.663	0.8429	0.606	0.626	0.645	0.735	0.7414	0.825	0.6721
0.519944	1.041	0.97	1.2321	0.896	0.915	0.945	1.061	1.0804	1.201	0.9898
0.570777	1.373	1.261	1.6024	1.185	1.192	1.233	1.357	1.3986	1.553	1.3012
0.626578	1.71	1.546	1.9626	1.48	1.462	1.516	1.631	1.7042	1.889	1.6135
0.687836	2.06	1.832	2.3222	1.786	1.733	1.802	1.893	2.0055	2.218	1.9341
0.755082	2.434	2.13	2.6959	2.114	2.017	2.102	2.156	2.315	2.555	2.2741
0.828903	2.815	2.425	3.0644	2.452	2.301	2.403	2.404	2.6148	2.881	2.6177
0.90994	3.18	2.699	3.4029	2.778	2.567	2.684	2.619	2.8839	3.173	2.9443
0.9989	3.512	2.939	3.6942	3.075	2.803	2.934	2.795	3.1089	3.415	3.2371
1.09656	3.79	3.131	3.9203	3.325	2.998	3.137	2.926	3.276	3.593	3.4773
1.20376	4.003	3.271	4.075	3.514	3.145	3.287	3.015	3.3812	3.701	3.6544
1.32145	4.128	3.344	4.1413	3.626	3.233	3.369	3.05	3.4108	3.726	3.751
1.45064	4.156	3.346	4.1124	3.649	3.254	3.376	3.031	3.3613	3.662	3.7594
1.59246	4.083	3.276	3.9871	3.579	3.207	3.306	2.959	3.2343	3.509	3.678
1.74815	3.923	3.144	3.7807	3.427	3.1	3.167	2.845	3.0443	3.282	3.5184
1.91906	3.692	2.97	3.52	3.211	2.948	2.979	2.705	2.8133	3.006	3.3022
2.10667	3.418	2.776	3.2392	2.963	2.773	2.767	2.555	2.569	2.714	3.0594
2.31263	3.132	2.593	2.9787	2.72	2.602	2.562	2.417	2.3453	2.445	2.8281
2.53872	2.869	2.449	2.7747	2.519	2.46	2.395	2.311	2.1726	2.238	2.644
2.78692	2.66	2.367	2.6585	2.391	2.371	2.294	2.258	2.0768	2.123	2.5368
3.05939	2.518	2.358	2.6453	2.355	2.346	2.273	2.265	2.0686	2.115	2.5199
3.35849	2.447	2.422	2.7317	2.41	2.384	2.332	2.331	2.1448	2.211	2.5904
3.68682	2.431	2.539	2.8887	2.536	2.471	2.453	2.441	2.2849	2.385	2.7265
4.04726	2.448	2.679	3.0632	2.693	2.579	2.6	2.569	2.4525	2.591	2.8882
4.44294	2.465	2.797	3.1879	2.824	2.667	2.724	2.681	2.6004	2.764	3.0226
4.87731	2.447	2.853	3.2022	2.877	2.697	2.779	2.743	2.6807	2.844	3.0762
5.35414	2.37	2.819	3.0762	2.82	2.649	2.736	2.732	2.6647	2.795	3.016
5.87759	2.224	2.697	2.8182	2.654	2.528	2.599	2.646	2.5513	2.623	2.8426
6.45221	2.027	2.509	2.4672	2.412	2.36	2.399	2.5	2.3675	2.371	2.5896
7.08301	1.805	2.29	2.0729	2.138	2.176	2.172	2.319	2.1488	2.091	2.3013
7.77547	1.581	2.061	1.682	1.867	1.993	1.946	2.124	1.9224	1.819	2.0097
8.53563	1.367	1.838	1.3353	1.623	1.815	1.731	1.927	1.7023	1.572	1.7268
9.37012	1.168	1.627	1.0635	1.419	1.642	1.537	1.734	1.4971	1.353	1.4562
10.2862	1	1.447	0.8828	1.269	1.486	1.379	1.567	1.3312	1.18	1.2202
11.2918	0.894	1.326	0.7833	1.187	1.375	1.284	1.454	1.2351	1.079	1.0564
12.3958	0.884	1.286	0.7299	1.181	1.336	1.273	1.427	1.2382	1.078	1.0022
13.6076	0.983	1.333	0.6722	1.242	1.377	1.35	1.499	1.346	1.18	1.0691
14.938	1.17	1.44	0.5698	1.342	1.481	1.485	1.638	1.5192	1.341	1.22
16.3984	1.372	1.554	0.4307	1.434	1.603	1.62	1.781	1.6883	1.484	1.3693
18.0016	1.486	1.612	0.3072	1.47	1.685	1.689	1.835	1.7642	1.514	1.3995
19.7615	1.438	1.569	0.2456	1.42	1.682	1.652	1.745	1.7049	1.388	1.2387
21.6935	1.226	1.423	0.2603	1.284	1.583	1.511	1.539	1.5439	1.152	0.9256
23.8143	0.923	1.206	0.3335	1.09	1.407	1.311	1.285	1.345	0.893	0.5727
26.1425	0.628	0.972	0.4199	0.879	1.19	1.102	1.077	1.1822	0.699	0.3132
28.6983	0.408	0.769	0.4511	0.693	0.976	0.923	0.961	1.08	0.599	0.1935
31.504	0.276	0.622	0.3895	0.557	0.794	0.789	0.917	1.0126	0.571	0.1788
34.584	0.207	0.535	0.2512	0.478	0.662	0.693	0.906	0.9402	0.572	0.2359
37.9652	0.165	0.494	0.1113	0.45	0.579	0.615	0.846	0.8049	0.533	0.2957
41.6768	0.122	0.474	0.0288	0.452	0.532	0.54	0.617	0.5411	0.384	0.2609
45.7513	0.069	0.367	0.0037	0.406	0.496	0.417	0.313	0.2554	0.19	0.1454
50.2242	0.026	0.2	0.0002	0.318	0.446	0.28	0.074	0.0575	0.044	0.0361
55.1343	0.005	0.049	0	0.185	0.343	0.145	0.008	0.0057	0.005	0.0039
60.5245	4E-04	0.005		0.087	0.2	0.062	0	0	0	0
66.4417	0	0		0.02	0.076	0.013	0	0	0	0
72.9374	0	0		0.002	0.015	0.001				
80.0681				0	0.001	0				
87.8959				0	0	0				
96.4892					0					

Particle Size
NE Tarlong Section
Cycle: UQZJ 8
Results in volume %

Size µm	S10-13	Q11-8	Q11-9	S10-14	Q11-10	S10-15
0.393033	0.27938	0.26068	0.25171	0.30456	0.26691	0.19994
0.431458	0.49414	0.46119	0.44538	0.53985	0.47218	0.35395
0.473639	0.73712	0.68986	0.66465	0.80089	0.70077	0.52917
0.519944	1.08232	1.01787	0.97629	1.16083	1.01946	0.77913
0.570777	1.41621	1.3415	1.27836	1.48847	1.31658	1.02312
0.626578	1.74644	1.66813	1.57849	1.7968	1.60042	1.26777
0.687836	2.0806	2.00477	1.88396	2.09616	1.87914	1.51904
0.755082	2.43102	2.36285	2.20616	2.40108	2.1649	1.78626
0.828903	2.77976	2.72608	2.52928	2.68969	2.44115	2.05642
0.90994	3.10362	3.07255	2.83346	2.9439	2.68905	2.31391
0.9989	3.3846	3.3838	3.10381	3.15632	2.89759	2.54676
1.09656	3.60319	3.63873	3.3237	3.32006	3.05547	2.74171
1.20376	3.74976	3.82509	3.48471	3.43576	3.16011	2.89152
1.32145	3.80652	3.92425	3.57065	3.49007	3.19918	2.98256
1.45064	3.76615	3.92797	3.57493	3.48219	3.16941	3.00903
1.59246	3.6276	3.83428	3.49639	3.41514	3.07169	2.96954
1.74815	3.40462	3.65504	3.34669	3.3048	2.91854	2.87326
1.91906	3.12181	3.41382	3.14588	3.16532	2.72847	2.73504
2.10667	2.81216	3.14396	2.92114	3.01313	2.52465	2.57499
2.31263	2.51668	2.88801	2.70666	2.86821	2.33583	2.41793
2.53872	2.27342	2.68523	2.53457	2.75007	2.1885	2.28754
2.78692	2.11447	2.56771	2.43248	2.67669	2.10627	2.20476
3.05939	2.05471	2.54974	2.41301	2.65391	2.10058	2.18035
3.35849	2.0926	2.62824	2.47407	2.67783	2.17117	2.2147
3.68682	2.20628	2.77995	2.59549	2.73275	2.30281	2.29521
4.04726	2.35528	2.96049	2.74115	2.79796	2.46665	2.39848
4.44294	2.48612	3.11066	2.86383	2.84797	2.62358	2.49352
4.87731	2.54537	3.16881	2.91577	2.85685	2.73318	2.54953
5.35414	2.50176	3.09788	2.86729	2.80505	2.76882	2.54638
5.87759	2.35636	2.89997	2.71679	2.68601	2.72622	2.48063
6.45221	2.14199	2.61501	2.49177	2.5095	2.62253	2.36509
7.08301	1.90075	2.29481	2.23103	2.29495	2.4829	2.22083
7.77547	1.66479	1.97225	1.96639	2.06178	2.32642	2.06883
8.53563	1.44931	1.66267	1.7152	1.82248	2.16244	1.9263
9.37012	1.25896	1.37239	1.48544	1.58711	1.99792	1.80767
10.2862	1.11154	1.13264	1.29598	1.37329	1.84905	1.72658
11.2918	1.03044	0.99056	1.17232	1.20948	1.74162	1.69453
12.3958	1.04184	0.97701	1.14038	1.12496	1.6991	1.71642
13.6076	1.15394	1.0966	1.20718	1.13285	1.72675	1.78739
14.938	1.33471	1.28254	1.34032	1.21643	1.79954	1.89027
16.3984	1.52126	1.41959	1.47585	1.32359	1.86515	1.99769
18.0016	1.62303	1.38045	1.52582	1.37808	1.8611	2.07579
19.7615	1.5896	1.11044	1.43723	1.31583	1.74264	2.09007
21.6935	1.44434	0.67042	1.23216	1.12337	1.50648	2.01485
23.8143	1.24821	0.27012	0.97718	0.84442	1.1914	1.84236
26.1425	1.08025	0.05793	0.75714	0.55508	0.86336	1.59023
28.6983	0.97665	0.00538	0.61631	0.32465	0.58953	1.3015
31.504	0.92106	8.8E-05	0.54377	0.17875	0.4074	1.02858
34.584	0.88054	0	0.51184	0.10409	0.3196	0.81329
37.9652	0.79065	0	0.46254	0.06939	0.3051	0.67178
41.6768	0.55831		0.33045	0.04901	0.33451	0.59068
45.7513	0.27675		0.16456	0.02901	0.32533	0.53886
50.2242	0.06437		0.03841	0.01129	0.25847	0.47887
55.1343	0.00667		0.00399	0.00216	0.14333	0.3347
60.5245	0		0	0.00015	0.06342	0.16385
66.4417	0		0	0	0.01416	0.03715
72.9374	0			0	0.00145	0.00366
80.0681					0	0
87.8959					0	0

Particle Size
NE Tarlong Section
Cycle: UQZJ 19 and 20
Results in volume %

Size µm	Q11-11	Q11-12	Q11-13	Q11-14	Q11-15	Q11-16	Q11-17	Q11-18	Q11-19	Q11-20	Q11-21	S10-25	S10-26	S10-27	S10-28
0.393033	0.202	0.293	0.283	0.341	0.275	0.362	0.278	0.2472	0.227	0.231	0.2319	0.2129	0.3341	0.3305	0.2623
0.431458	0.358	0.519	0.5	0.604	0.486	0.64	0.492	0.4371	0.402	0.409	0.4104	0.3768	0.5911	0.5845	0.4638
0.473639	0.536	0.771	0.743	0.903	0.728	0.95	0.734	0.6532	0.603	0.61	0.613	0.5644	0.8792	0.864	0.6924
0.519944	0.794	1.122	1.084	1.33	1.079	1.382	1.076	0.9621	0.894	0.8943	0.9015	0.8342	1.2839	1.2483	1.0189
0.570777	1.05	1.449	1.405	1.747	1.43	1.785	1.405	1.2647	1.185	1.1673	1.1819	1.102	1.667	1.5966	1.3384
0.626578	1.312	1.762	1.714	2.162	1.787	2.169	1.729	1.5678	1.483	1.437	1.4617	1.3743	2.038	1.9187	1.6582
0.687836	1.585	2.07	2.019	2.585	2.157	2.544	2.054	1.8783	1.794	1.7103	1.7476	1.6574	2.4065	2.2253	1.9858
0.755082	1.878	2.385	2.334	3.029	2.552	2.928	2.393	2.2074	2.128	1.998	2.0502	1.961	2.7871	2.5313	2.3332
0.828903	2.179	2.689	2.64	3.47	2.956	3.297	2.728	2.5396	2.468	2.285	2.3547	2.2718	3.1585	2.8166	2.6849
0.90994	2.47	2.959	2.915	3.876	3.34	3.624	3.036	2.8542	2.796	2.5543	2.6428	2.5724	3.4949	3.0593	3.0196
0.9989	2.738	3.185	3.145	4.222	3.68	3.894	3.3	3.1342	3.092	2.7943	2.9008	2.8482	3.7785	3.2493	3.3203
1.09656	2.966	3.354	3.315	4.481	3.949	4.089	3.502	3.3613	3.336	2.9921	3.1136	3.0826	3.991	3.3773	3.5678
1.20376	3.145	3.462	3.419	4.638	4.13	4.206	3.634	3.5252	3.515	3.1417	3.2733	3.2653	4.1255	3.4451	3.7514
1.32145	3.259	3.495	3.442	4.669	4.2	4.229	3.68	3.6088	3.611	3.2293	3.3648	3.3804	4.1644	3.4406	3.8532
1.45064	3.3	3.45	3.379	4.565	4.146	4.153	3.633	3.6044	3.615	3.2504	3.382	3.4202	4.1015	3.3624	3.8639
1.59246	3.267	3.33	3.229	4.328	3.962	3.979	3.496	3.5099	3.524	3.2049	3.3242	3.3825	3.937	3.2136	3.7799
1.74815	3.169	3.149	3.006	3.979	3.662	3.725	3.284	3.3372	3.352	3.1042	3.2024	3.2765	3.6867	3.0104	3.6112
1.91906	3.022	2.928	2.734	3.552	3.278	3.421	3.023	3.1085	3.119	2.9646	3.0345	3.1196	3.376	2.7756	3.3788
2.10667	2.849	2.691	2.445	3.094	2.857	3.102	2.745	2.8543	2.858	2.8075	2.8445	2.9368	3.0382	2.5353	3.1125
2.31263	2.681	2.469	2.174	2.66	2.455	2.809	2.491	2.6126	2.605	2.6594	2.662	2.7597	2.7133	2.3223	2.8506
2.53872	2.544	2.29	1.959	2.302	2.125	2.58	2.295	2.4191	2.396	2.5455	2.5151	2.6186	2.4379	2.1661	2.6297
2.78692	2.463	2.18	1.829	2.062	1.913	2.445	2.186	2.3044	2.263	2.4874	2.4277	2.5395	2.2431	2.0937	2.4813
3.05939	2.451	2.151	1.8	1.954	1.845	2.419	2.178	2.2836	2.22	2.4945	2.4107	2.5357	2.144	2.1159	2.4215
3.35849	2.506	2.199	1.871	1.975	1.921	2.498	2.266	2.3555	2.266	2.5643	2.4624	2.6072	2.1402	2.2281	2.4505
3.68682	2.615	2.307	2.02	2.094	2.111	2.652	2.426	2.4989	2.383	2.6806	2.566	2.7382	2.2131	2.4045	2.5484
4.04726	2.751	2.448	2.2	2.264	2.352	2.825	2.613	2.6736	2.537	2.816	2.6919	2.8981	2.326	2.6017	2.6759
4.44294	2.877	2.583	2.355	2.417	2.557	2.951	2.773	2.8264	2.682	2.9352	2.8013	3.0449	2.4298	2.7659	2.7805
4.87731	2.955	2.675	2.432	2.487	2.644	2.967	2.85	2.9046	2.77	3.0014	2.8553	3.1351	2.4756	2.845	2.8095
5.35414	2.959	2.694	2.402	2.428	2.572	2.844	2.815	2.8761	2.772	2.9899	2.8287	3.1398	2.4352	2.8096	2.7321
5.87759	2.884	2.633	2.266	2.241	2.351	2.59	2.666	2.7398	2.682	2.8956	2.7185	3.0541	2.3098	2.6609	2.5511
6.45221	2.747	2.507	2.054	1.966	2.03	2.244	2.433	2.5253	2.525	2.7352	2.5443	2.8972	2.1255	2.4337	2.3009
7.08301	2.571	2.342	1.81	1.66	1.67	1.858	2.16	2.2738	2.331	2.5354	2.335	2.6974	1.9136	2.1754	2.0255
7.77547	2.378	2.162	1.575	1.367	1.33	1.481	1.885	2.0207	2.128	2.3188	2.1146	2.4758	1.6957	1.927	1.7572
8.53563	2.179	1.977	1.383	1.109	1.056	1.159	1.638	1.7865	1.926	2.0985	1.8961	2.2417	1.4848	1.7113	1.5097
9.37012	1.982	1.789	1.251	0.894	0.876	0.927	1.435	1.5797	1.732	1.8822	1.6886	2.0019	1.2929	1.5289	1.2873
10.2862	1.805	1.612	1.185	0.744	0.809	0.796	1.289	1.4149	1.558	1.6881	1.5081	1.7742	1.1397	1.3844	1.1061
11.2918	1.673	1.473	1.177	0.689	0.85	0.753	1.213	1.3072	1.428	1.5427	1.3795	1.5894	1.0419	1.28	0.991
12.3958	1.605	1.405	1.212	0.749	0.981	0.755	1.213	1.2722	1.367	1.4726	1.3274	1.4765	0.9991	1.2272	0.9673
13.6076	1.605	1.426	1.272	0.928	1.157	0.742	1.285	1.3097	1.381	1.4856	1.36	1.4423	0.9912	1.2338	1.04
14.938	1.649	1.507	1.348	1.168	1.308	0.666	1.398	1.3863	1.444	1.5525	1.4579	1.4601	0.9845	1.272	1.1769
16.3984	1.69	1.584	1.433	1.356	1.383	0.535	1.507	1.4511	1.503	1.6166	1.5721	1.473	0.9589	1.3069	1.3111
18.0016	1.673	1.563	1.523	1.371	1.359	0.413	1.553	1.4384	1.492	1.6049	1.6375	1.4165	0.9205	1.2748	1.355
19.7615	1.562	1.391	1.6	1.172	1.261	0.354	1.494	1.3175	1.372	1.4745	1.6019	1.253	0.8915	1.1485	1.2592
21.6935	1.356	1.109	1.639	0.811	1.152	0.385	1.335	1.1198	1.168	1.2448	1.452	0.9954	0.8907	0.9763	1.0514
23.8143	1.088	0.811	1.614	0.456	1.07	0.485	1.109	0.9015	0.94	0.9735	1.2183	0.6979	0.9058	0.817	0.8071
26.1425	0.805	0.601	1.521	0.237	1.048	0.6	0.872	0.7311	0.756	0.7336	0.9588	0.4233	0.8991	0.7485	0.612
28.6983	0.555	0.514	1.394	0.165	1.067	0.645	0.676	0.6363	0.649	0.5669	0.7285	0.2324	0.8262	0.7815	0.5046
31.504	0.365	0.526	1.281	0.158	1.084	0.572	0.53	0.599	0.607	0.466	0.5594	0.1324	0.6645	0.8846	0.4744
34.584	0.244	0.591	1.225	0.168	1.054	0.372	0.433	0.5882	0.604	0.4087	0.4558	0.0963	0.4212	0.9986	0.4933
37.9652	0.181	0.615	1.242	0.167	0.93	0.162	0.357	0.5448	0.583	0.3509	0.4006	0.0917	0.1898	1.0114	0.5033
41.6768	0.158	0.48	1.306	0.126	0.639	0.034	0.245	0.3949	0.482	0.2433	0.3687	0.1034	0.0492	0.7715	0.4335
45.7513	0.154	0.252	1.191	0.065	0.309	0.003	0.124	0.1993	0.299	0.1193	0.2752	0.122	0.0064	0.4016	0.2738
50.2242	0.122	0.06	0.912	0.015	0.071	0	0.029	0.0469	0.119	0.0276	0.1459	0.1097	0.0003	0.0962	0.1084
55.1343	0.068	0.006	0.504	0.002	0.007	0	0.003	0.0049	0.024	0.0029	0.0349	0.0669	0	0.0103	0.0217
60.5245	0.017	0	0.229	0	0		0	0	0.002	0	0.0036	0.0176		0	0.0019
66.4417	0.002	0	0.052	0	0		0	0	0	0	0	0.0019		0	0
72.9374	0		0.005								0	0			
80.0681	0		0									0			
87.8959			0												

Particle Size
Taodonggou Section
Cycle: UQZJ 31
Results in volume %

Size µm	Q12-10	Q12-11	Q12-12	TD76	TD77	TD78
0.393033	0.29191	0.3118	0.30114	0.30403	0.27884	0.29065
0.431458	0.5163	0.55147	0.53266	0.53766	0.49302	0.5142
0.473639	0.76445	0.81554	0.78715	0.79662	0.73536	0.76357
0.519944	1.10786	1.17938	1.13694	1.1562	1.07992	1.11183
0.570777	1.42328	1.51055	1.45369	1.48901	1.41381	1.43752
0.626578	1.71984	1.81889	1.74701	1.80432	1.74446	1.74954
0.687836	2.00684	2.11444	2.02667	2.11172	2.07954	2.05663
0.755082	2.2977	2.4115	2.30649	2.42511	2.4315	2.37189
0.828903	2.57494	2.69152	2.56866	2.72656	2.78298	2.67701
0.90994	2.81919	2.93439	2.79421	2.99548	3.1109	2.95085
0.9989	3.02069	3.13096	2.97507	3.22062	3.39715	3.18064
1.09656	3.16977	3.27239	3.10353	3.39034	3.62211	3.35325
1.20376	3.26622	3.35988	3.18154	3.50266	3.77596	3.4653
1.32145	3.29836	3.38202	3.19857	3.54415	3.84104	3.50288
1.45064	3.26382	3.33718	3.15351	3.51099	3.80952	3.46227
1.59246	3.16403	3.22749	3.04848	3.40368	3.67989	3.34466
1.74815	3.01243	3.06727	2.89706	3.23523	3.46559	3.1645
1.91906	2.82804	2.87606	2.71728	3.02541	3.19178	2.94309
2.10667	2.63402	2.67732	2.53056	2.79949	2.89272	2.70684
2.31263	2.45917	2.50035	2.36404	2.59003	2.61081	2.4881
2.53872	2.32979	2.37195	2.24236	2.42772	2.38541	2.31628
2.78692	2.26949	2.31626	2.18805	2.34002	2.24964	2.21722
3.05939	2.28824	2.34312	2.20972	2.33909	2.21916	2.20214
3.35849	2.3826	2.44846	2.30339	2.42223	2.29178	2.26842
3.68682	2.53152	2.61007	2.44806	2.56799	2.44283	2.39553
4.04726	2.69878	2.79017	2.60883	2.73863	2.62611	2.54755
4.44294	2.83835	2.94058	2.74143	2.88505	2.7808	2.67855
4.87731	2.90519	3.01374	2.80183	2.95749	2.8474	2.74301
5.35414	2.87319	2.98155	2.76479	2.92569	2.79198	2.71382
5.87759	2.74347	2.84471	2.6317	2.79003	2.61813	2.58987
6.45221	2.54417	2.63291	2.43264	2.58338	2.36496	2.39636
7.08301	2.31279	2.38583	2.20584	2.34922	2.08303	2.16821
7.77547	2.0795	2.13433	1.98029	2.11917	1.81224	1.93483
8.53563	1.86045	1.89278	1.76821	1.90158	1.57268	1.7147
9.37012	1.66257	1.66608	1.57007	1.68839	1.37045	1.51747
10.2862	1.5004	1.47021	1.40293	1.48549	1.21807	1.36115
11.2918	1.39327	1.33083	1.29214	1.31693	1.13098	1.26513
12.3958	1.36019	1.27531	1.27008	1.22131	1.12477	1.2476
13.6076	1.40351	1.31144	1.34985	1.22333	1.19701	1.31232
14.938	1.49199	1.40691	1.49748	1.30269	1.30895	1.42926
16.3984	1.57292	1.49691	1.64798	1.40012	1.39816	1.5493
18.0016	1.58072	1.49586	1.70484	1.41549	1.39041	1.60175
19.7615	1.48178	1.35377	1.6172	1.27488	1.25448	1.54225
21.6935	1.29743	1.09686	1.42406	0.99657	1.03202	1.38177
23.8143	1.07711	0.80036	1.2009	0.66671	0.79493	1.16219
26.1425	0.881	0.55502	1.04088	0.40371	0.61831	0.94948
28.6983	0.74039	0.40819	0.97311	0.26964	0.52841	0.78915
31.504	0.64563	0.34628	0.96743	0.24143	0.5046	0.68048
34.584	0.57648	0.34107	0.97081	0.29395	0.51299	0.61325
37.9652	0.49312	0.33547	0.89307	0.35088	0.49207	0.54066
41.6768	0.33813	0.25895	0.63453	0.30801	0.36496	0.38596
45.7513	0.16499	0.13692	0.31184	0.17479	0.18657	0.19705
50.2242	0.03805	0.03316	0.07201	0.04411	0.04418	0.04699
55.1343	0.00392	0.00356	0.00737	0.00495	0.00465	0.00509
60.5245	0	0	0	0	0	0
66.4417	0	0	0	0		

Particle Size
SE Tarlong Section
Cycle: UQZJ 1
Results in volume %

Size µm	Q12-6	Q12-7	Q12-8	Q12-9
0.393033	0.27643	0.24081	0.28561	0.25501
0.431458	0.48913	0.42619	0.50536	0.45134
0.473639	0.72352	0.62994	0.74838	0.66702
0.519944	1.04629	0.90917	1.08434	0.96245
0.570777	1.33994	1.16038	1.39242	1.22798
0.626578	1.61387	1.39208	1.68203	1.47259
0.687836	1.87728	1.6123	1.96239	1.70482
0.755082	2.14302	1.83225	2.24661	1.9365
0.828903	2.39451	2.03693	2.51732	2.15169
0.90994	2.61472	2.21186	2.7561	2.33507
0.9989	2.79655	2.35175	2.95417	2.48114
1.09656	2.93295	2.45196	3.10287	2.58507
1.20376	3.02527	2.51518	3.2025	2.64968
1.32145	3.06309	2.53344	3.242	2.66652
1.45064	3.04502	2.50675	3.21993	2.6357
1.59246	2.97284	2.4376	3.13864	2.56006
1.74815	2.85885	2.33754	3.01189	2.45208
1.91906	2.71849	2.2197	2.85772	2.32582
2.10667	2.57009	2.09891	2.69787	2.19713
2.31263	2.43729	1.99304	2.55924	2.08561
2.53872	2.342	1.91832	2.4662	2.00935
2.78692	2.30468	1.88983	2.44034	1.98539
3.05939	2.33316	1.91339	2.48977	2.02057
3.35849	2.42384	1.98617	2.6098	2.11246
3.68682	2.55823	2.09383	2.77946	2.2464
4.04726	2.70648	2.21344	2.96423	2.39891
4.44294	2.8311	2.31608	3.1203	2.54011
4.87731	2.89389	2.37385	3.2039	2.63991
5.35414	2.87121	2.36946	3.18771	2.6784
5.87759	2.76082	2.30168	3.06993	2.65189
6.45221	2.58529	2.18452	2.87474	2.57387
7.08301	2.3763	2.03838	2.63622	2.46517
7.77547	2.15915	1.88119	2.38138	2.3431
8.53563	1.94573	1.72522	2.12388	2.21642
9.37012	1.73764	1.58179	1.87123	2.08988
10.2862	1.55072	1.46489	1.64197	1.97468
11.2918	1.41011	1.39363	1.46457	1.89148
12.3958	1.34762	1.38453	1.36604	1.8642
13.6076	1.3799	1.44658	1.35149	1.90614
14.938	1.48	1.57615	1.38819	2.00558
16.3984	1.59378	1.75031	1.41518	2.12279
18.0016	1.63566	1.93276	1.36102	2.19738
19.7615	1.5564	2.07719	1.19027	2.17237
21.6935	1.38291	2.14203	0.93368	2.0223
23.8143	1.17742	2.11106	0.66092	1.76477
26.1425	1.02177	1.99556	0.44577	1.45598
28.6983	0.94757	1.84444	0.31997	1.16409
31.504	0.93144	1.71639	0.26621	0.93793
34.584	0.93064	1.65172	0.25622	0.79576
37.9652	0.86524	1.66331	0.24585	0.72329
41.6768	0.62493	1.71995	0.18521	0.68484
45.7513	0.31398	1.75124	0.09577	0.63848
50.2242	0.07358	1.6809	0.02282	0.49674
55.1343	0.00767	1.22873	0.0024	0.28668
60.5245	0	0.62486	0	0.09989
66.4417	0	0.14422	0	0.01811
72.9374		0.01463		0.00142
80.0681		0		0
87.8959		0		

Particle Size
SE Tarlong Section
Cycle: UQZJ 18
Results in volume %

Size µm	Q12-1	Q12-2	Q12-3	Q12-4	Q12-5
0.393033	0.37013	0.23697	0.29846	0.29737	0.27433
0.431458	0.65419	0.41928	0.52789	0.52587	0.48532
0.473639	0.96483	0.62301	0.78178	0.77937	0.71799
0.519944	1.38932	0.90829	1.13352	1.13175	1.03872
0.570777	1.7685	1.17699	1.45753	1.45854	1.33098
0.626578	2.11316	1.43687	1.76319	1.76871	1.60375
0.687836	2.43525	1.69548	2.05999	2.07155	1.86598
0.755082	2.75167	1.96391	2.36169	2.3807	2.13037
0.828903	3.04092	2.22792	2.65068	2.67861	2.38042
0.90994	3.27937	2.47132	2.90737	2.945	2.59873
0.9989	3.45768	2.68437	3.12168	3.16847	2.77753
1.09656	3.56812	2.85662	3.28334	3.33736	2.90933
1.20376	3.61573	2.98492	3.39176	3.44975	2.99537
1.32145	3.59016	3.05739	3.4349	3.4928	3.0256
1.45064	3.49081	3.07014	3.41015	3.46299	2.99891
1.59246	3.3208	3.02308	3.3186	3.36103	2.91748
1.74815	3.09702	2.92657	3.17331	3.20008	2.79448
1.91906	2.84306	2.7961	2.99352	3.00048	2.6473
2.10667	2.58571	2.6518	2.80319	2.78814	2.49655
2.31263	2.3569	2.51883	2.63227	2.59534	2.36778
2.53872	2.18436	2.42083	2.50788	2.45173	2.2842
2.78692	2.09332	2.37872	2.4538	2.38311	2.26703
3.05939	2.09497	2.40173	2.47995	2.40053	2.32467
3.35849	2.18598	2.48717	2.58254	2.50018	2.45311
3.68682	2.34265	2.6172	2.73977	2.65892	2.63139
4.04726	2.5218	2.76112	2.91328	2.836	2.82417
4.44294	2.66854	2.87937	3.05329	2.97869	2.98681
4.87731	2.732	2.93301	3.11084	3.03535	3.07485
5.35414	2.68722	2.89807	3.05769	2.97639	3.06109
5.87759	2.54214	2.77382	2.89626	2.80526	2.94295
6.45221	2.33042	2.58226	2.65723	2.5564	2.74393
7.08301	2.09166	2.35468	2.3797	2.27384	2.4982
7.77547	1.85579	2.11762	2.09298	1.99061	2.23613
8.53563	1.64354	1.88672	1.81315	1.72198	1.97843
9.37012	1.47129	1.67361	1.5522	1.47595	1.73871
10.2862	1.35513	1.4955	1.33409	1.27219	1.54097
11.2918	1.3032	1.37646	1.18758	1.13951	1.41143
12.3958	1.30168	1.33865	1.1307	1.10369	1.37414
13.6076	1.31518	1.38646	1.15611	1.16661	1.43432
14.938	1.29847	1.49841	1.22204	1.29103	1.55737
16.3984	1.22859	1.62484	1.26799	1.4058	1.68317
18.0016	1.12576	1.70376	1.23609	1.42783	1.72771
19.7615	1.03352	1.69099	1.10802	1.31756	1.64113
21.6935	0.98841	1.57953	0.92467	1.10675	1.44343
23.8143	0.99046	1.40148	0.74714	0.86685	1.19326
26.1425	1.00125	1.2066	0.62458	0.67065	0.97115
28.6983	0.96392	1.03393	0.55617	0.54767	0.82193
31.504	0.83583	0.90176	0.50877	0.4828	0.73704
34.584	0.61744	0.80506	0.4545	0.44446	0.69257
37.9652	0.34561	0.72225	0.36907	0.38903	0.62726
41.6768	0.13033	0.63132	0.23897	0.26805	0.45174
45.7513	0.02441	0.43746	0.11059	0.12861	0.22893
50.2242	0.0018	0.21566	0.02503	0.02916	0.05412
55.1343	0	0.04915	0.00253	0.00288	0.00573
60.5245		0.00491	0	0	0
66.4417		0		0	0
72.9374		0			

Particle Size
Dalongkou Section
Cycle: LQZJ 3
Results in volume %

Size µm	SD11-29	SD11-30	SD11-31	SD11-32	SD11-33
0.393033	0.18	0.14003	0.14786	0.18756	0.20405
0.431458	0.31847	0.24783	0.2616	0.33192	0.36114
0.473639	0.48068	0.37504	0.39599	0.50331	0.54571
0.519944	0.7201	0.56433	0.59619	0.75989	0.81894
0.570777	0.96912	0.76414	0.8079	1.03332	1.10456
0.626578	1.23289	0.97873	1.03545	1.32889	1.40842
0.687836	1.51612	1.21174	1.28265	1.65104	1.73559
0.755082	1.82694	1.46955	1.55633	2.00803	2.09506
0.828903	2.15401	1.7435	1.84734	2.38774	2.47361
0.90994	2.48018	2.02013	2.14129	2.77069	2.85127
0.9989	2.78794	2.28511	2.42266	3.13551	3.2074
1.09656	3.05666	2.52111	2.67297	3.45649	3.51748
1.20376	3.27108	2.7148	2.87803	3.71373	3.76335
1.32145	3.41283	2.85071	3.02145	3.88503	3.9237
1.45064	3.471	2.91942	3.09308	3.95701	3.98662
1.59246	3.44054	2.91621	3.08777	3.92343	3.94738
1.74815	3.32801	2.84549	3.01039	3.79147	3.81476
1.91906	3.1503	2.72006	2.87498	3.58115	3.6098
2.10667	2.93333	2.56033	2.70379	3.32384	3.36425
2.31263	2.71023	2.39268	2.52499	3.05995	3.11869
2.53872	2.51345	2.24301	2.36622	2.82897	2.91212
2.78692	2.37052	2.13337	2.25085	2.66417	2.77682
3.05939	2.29676	2.07619	2.1924	2.58346	2.72881
3.35849	2.2936	2.07343	2.1926	2.58825	2.76706
3.68682	2.34647	2.11466	2.23924	2.66063	2.87076
4.04726	2.42558	2.17737	2.30655	2.76433	3.00044
4.44294	2.49056	2.23024	2.35921	2.85015	3.10345
4.87731	2.5012	2.24118	2.36261	2.86749	3.12571
5.35414	2.43238	2.18973	2.29516	2.78396	3.0325
5.87759	2.28406	2.07481	2.15675	2.59682	2.82124
6.45221	2.07895	1.91299	1.96549	2.33376	2.52258
7.08301	1.84903	1.72776	1.74762	2.03544	2.18162
7.77547	1.62023	1.53821	1.5266	1.7371	1.83659
8.53563	1.40718	1.35736	1.31997	1.46131	1.51068
9.37012	1.22036	1.19727	1.14557	1.22214	1.2194
10.2862	1.07295	1.07545	1.01881	1.04217	0.99054
11.2918	0.98533	1.01229	0.95624	0.94482	0.85608
12.3958	0.97457	1.02059	0.96424	0.94922	0.84132
13.6076	1.04733	1.09958	1.03885	1.05477	0.94822
14.938	1.19205	1.22946	1.16939	1.22212	1.135
16.3984	1.3704	1.37807	1.33097	1.38013	1.31206
18.0016	1.52915	1.51263	1.50257	1.43891	1.36131
19.7615	1.61537	1.61136	1.65699	1.35299	1.21435
21.6935	1.59827	1.66989	1.76562	1.15637	0.91174
23.8143	1.48825	1.69366	1.8133	0.92327	0.56546
26.1425	1.32336	1.69215	1.78983	0.73709	0.30704
28.6983	1.16601	1.67875	1.7216	0.63347	0.18662
31.504	1.07089	1.6677	1.65886	0.59571	0.16961
34.584	1.0628	1.68022	1.64243	0.58973	0.22406
37.9652	1.14258	1.73504	1.7068	0.55239	0.28295
41.6768	1.27233	1.83634	1.83434	0.40274	0.25187
45.7513	1.38159	1.96707	1.95813	0.20337	0.14121
50.2242	1.39528	2.07942	1.98817	0.04778	0.03518
55.1343	1.05254	2.10164	1.73485	0.00497	0.00383
60.5245	0.54741	1.97024	1.18939	0	0
66.4417	0.12769	1.51968	0.57034	0	0
72.9374	0.01311	0.87001	0.16954		
80.0681	0	0.30883	0.02729		
87.8959	0	0.05688	0.00193		
96.4892		0.00457	0		
105.922		0	0		
116.278		0			

Particle Size
Dalongkou Section
Cycle: UQZJ 22
Results in volume %

Size µm	SD11-6	SD11-26	SD11-27	SD11-28
0.393033	0.26719	0.24757	0.1479	0.17278
0.431458	0.47232	0.43798	0.26166	0.30567
0.473639	0.71161	0.65427	0.39477	0.46038
0.519944	1.0631	0.96303	0.59119	0.68738
0.570777	1.42442	1.26491	0.79553	0.92113
0.626578	1.80168	1.56717	1.01227	1.16688
0.687836	2.20093	1.87679	1.24544	1.42941
0.755082	2.63383	2.20491	1.50196	1.71684
0.828903	3.08253	2.53611	1.77294	2.0187
0.90994	3.51931	2.85037	2.0449	2.31957
0.9989	3.91641	3.13168	2.30397	2.60427
1.09656	4.24273	3.36203	2.53358	2.85479
1.20376	4.4774	3.53136	2.72141	3.05808
1.32145	4.59511	3.62266	2.85226	3.19738
1.45064	4.5811	3.62825	2.91678	3.26269
1.59246	4.42968	3.54592	2.90999	3.249
1.74815	4.15397	3.38624	2.83618	3.16188
1.91906	3.78532	3.16906	2.70803	3.01602
2.10667	3.36822	2.92237	2.54584	2.83438
2.31263	2.95669	2.68188	2.37599	2.64671
2.53872	2.6012	2.48143	2.22464	2.48257
2.78692	2.34398	2.3497	2.1145	2.36769
3.05939	2.20798	2.30035	2.05895	2.31683
3.35849	2.19449	2.33225	2.06065	2.33215
3.68682	2.27903	2.42666	2.10918	2.40073
4.04726	2.41121	2.54877	2.18137	2.4952
4.44294	2.52462	2.65193	2.24465	2.57783
4.87731	2.55637	2.68869	2.266	2.61035
5.35414	2.47318	2.63015	2.22482	2.56836
5.87759	2.27989	2.47725	2.12062	2.45028
6.45221	2.01138	2.26064	1.97087	2.27573
7.08301	1.71292	2.01995	1.79961	2.07272
7.77547	1.425	1.78381	1.62615	1.86368
8.53563	1.18282	1.56301	1.46308	1.66124
9.37012	1.0102	1.36075	1.32213	1.47509
10.2862	0.91888	1.19548	1.21989	1.32106
11.2918	0.89881	1.09753	1.17625	1.22345
12.3958	0.91198	1.09902	1.20411	1.20464
13.6076	0.90828	1.2099	1.30139	1.27389
14.938	0.84728	1.39692	1.44647	1.41656
16.3984	0.74107	1.5866	1.60391	1.58936
18.0016	0.64667	1.6821	1.73914	1.73161
19.7615	0.61402	1.63095	1.83027	1.78821
21.6935	0.66718	1.45897	1.87241	1.73519
23.8143	0.77405	1.23661	1.87107	1.59083
26.1425	0.86486	1.04386	1.83401	1.40195
28.6983	0.85884	0.91573	1.77101	1.22636
31.504	0.72007	0.8361	1.69406	1.10517
34.584	0.4636	0.76947	1.62105	1.05145
37.9652	0.20867	0.66313	1.57164	1.05317
41.6768	0.05165	0.45022	1.55607	1.07458
45.7513	0.00609	0.21432	1.56816	1.0658
50.2242	0.00013	0.0484	1.58156	0.98496
55.1343	0	0.00479	1.5515	0.69708
60.5245		0	1.43503	0.34432
66.4417			1.11296	0.0782
72.9374			0.70557	0.00778
80.0681			0.32591	0
87.8959			0.12046	
96.4892			0.02412	
105.922			0.00216	
116.278			0	
127.646			0	

Particle Size
Dalongkou Section
Cycle: UQZJ 25
Results in volume %

Size µm	Q12-13	Q12-14	Q12-15	Q12-16	Q12-17	Q12-18	Q12-19	Q12-20	Q12-21	Q12-22	Q12-23
0.393033	0.20103	0.21697	0.2004	0.2166	0.2201	0.1694	0.2252	0.2077	0.2441	0.2009	0.1938
0.431458	0.35563	0.38376	0.3547	0.3833	0.3894	0.2997	0.3983	0.3675	0.4317	0.3556	0.3429
0.473639	0.53582	0.57624	0.5321	0.573	0.5844	0.4496	0.5968	0.5534	0.6467	0.534	0.515
0.519944	0.80042	0.85573	0.7887	0.8443	0.8671	0.6665	0.8831	0.8257	0.9567	0.7928	0.765
0.570777	1.07312	1.13774	1.0459	1.1105	1.1518	0.884	1.1685	1.1052	1.2662	1.0539	1.0178
0.626578	1.35971	1.42823	1.3099	1.3783	1.4448	1.1076	1.4597	1.398	1.5821	1.3235	1.2792
0.687836	1.66555	1.73294	1.5862	1.6541	1.7522	1.3424	1.763	1.7096	1.9116	1.6073	1.5549
0.755082	1.99979	2.06164	1.8842	1.9481	2.0841	1.596	2.0888	2.0495	2.266	1.9146	1.8537
0.828903	2.34991	2.40051	2.1911	2.2466	2.4268	1.8583	2.423	2.4045	2.6307	2.2328	2.1637
0.90994	2.69724	2.72981	2.49	2.5325	2.761	2.1152	2.7467	2.7556	2.9856	2.5446	2.4683
0.9989	3.0233	3.03138	2.7657	2.7923	3.0692	2.3545	3.0432	3.0842	3.3131	2.8347	2.7524
1.09656	3.30632	3.28448	3.001	3.0106	3.3313	2.5618	3.2934	3.3683	3.5928	3.085	2.9984
1.20376	3.53069	3.47551	3.1845	3.1786	3.5339	2.7279	3.4852	3.5924	3.8118	3.2834	3.1945
1.32145	3.67672	3.58589	3.2998	3.281	3.6584	2.8387	3.6007	3.736	3.951	3.4126	3.324
1.45064	3.73287	3.60548	3.3382	3.3105	3.6945	2.8867	3.6302	3.788	3.9999	3.4634	3.378
1.59246	3.69377	3.53024	3.2962	3.2649	3.6377	2.8687	3.5698	3.7434	3.9532	3.4321	3.3528
1.74815	3.56668	3.36931	3.1819	3.153	3.4966	2.7905	3.4283	3.6099	3.8189	3.3262	3.2557
1.91906	3.37007	3.14281	3.0113	2.991	3.2901	2.6649	3.2243	3.4062	3.6156	3.162	3.1028
2.10667	3.13201	2.8798	2.8082	2.8016	3.0461	2.5108	2.9851	3.1604	3.3712	2.9633	2.9177
2.31263	2.88861	2.61691	2.6029	2.6137	2.8005	2.3526	2.7457	2.9101	3.1216	2.761	2.7307
2.53872	2.67518	2.38943	2.4248	2.4552	2.588	2.2144	2.5402	2.6918	2.901	2.5851	2.5714
2.78692	2.52208	2.22761	2.2997	2.3503	2.4387	2.1173	2.3981	2.5372	2.7391	2.4619	2.4652
3.05939	2.44587	2.1477	2.2415	2.3116	2.3685	2.073	2.3353	2.4625	2.6525	2.4056	2.4257
3.35849	2.44771	2.15055	2.2516	2.3393	2.3784	2.0832	2.3526	2.469	2.6432	2.4172	2.4535
3.68682	2.51043	2.2188	2.3166	2.4183	2.4508	2.1375	2.4325	2.5394	2.6952	2.4825	2.5342
4.04726	2.59973	2.31798	2.4096	2.5207	2.5511	2.214	2.5409	2.6401	2.774	2.574	2.639
4.44294	2.66974	2.40228	2.4938	2.6091	2.633	2.2826	2.6317	2.7256	2.8327	2.6537	2.7292
4.87731	2.67483	2.42658	2.532	2.6457	2.6506	2.3123	2.6591	2.7485	2.8247	2.6834	2.7657
5.35414	2.5873	2.36377	2.5	2.6066	2.5762	2.2831	2.5949	2.6782	2.7239	2.6377	2.7233
5.87759	2.40748	2.21432	2.3955	2.4896	2.4104	2.193	2.439	2.5116	2.5338	2.5138	2.6001
6.45221	2.16236	2.00413	2.2372	2.3141	2.1808	2.0571	2.2178	2.2763	2.2822	2.3313	2.4165
7.08301	1.89	1.76943	2.0526	2.1086	1.9256	1.8972	1.9683	2.0115	2.0034	2.1196	2.2021
7.77547	1.62263	1.54073	1.8645	1.8969	1.6764	1.7316	1.7209	1.7492	1.7228	1.9034	1.9815
8.53563	1.38019	1.33704	1.687	1.694	1.4517	1.5723	1.4934	1.5054	1.4584	1.6974	1.7693
9.37012	1.17418	1.16906	1.5305	1.5107	1.2624	1.4317	1.2963	1.2829	1.2286	1.5117	1.5755
10.2862	1.01896	1.0479	1.4093	1.363	1.1218	1.3257	1.1442	1.1016	1.0552	1.362	1.4157
11.2918	0.93126	0.98637	1.3434	1.2724	1.0472	1.2745	1.0565	0.9868	0.9545	1.2703	1.3115
12.3958	0.92548	0.99476	1.3486	1.2578	1.0525	1.2918	1.0504	0.9699	0.9203	1.2573	1.2816
13.6076	1.00419	1.07494	1.4269	1.3239	1.1372	1.3773	1.1284	1.0644	0.9224	1.3272	1.3298
14.938	1.14704	1.21157	1.5582	1.4511	1.2776	1.5161	1.2685	1.2363	0.916	1.4597	1.4357
16.3984	1.30945	1.37155	1.7005	1.5966	1.4263	1.6781	1.423	1.4176	0.8714	1.6064	1.555
18.0016	1.43017	1.50956	1.8043	1.7042	1.5271	1.8332	1.5309	1.4989	0.8014	1.7059	1.633
19.7615	1.4595	1.58399	1.8306	1.7289	1.5422	1.954	1.5474	1.4178	0.7465	1.7132	1.6274
21.6935	1.38676	1.57581	1.7656	1.6577	1.4684	2.0192	1.4657	1.2197	0.7435	1.6181	1.5274
23.8143	1.24093	1.49439	1.6228	1.5107	1.3332	2.0174	1.3156	0.9929	0.7966	1.4489	1.3553
26.1425	1.08239	1.37697	1.4323	1.334	1.1791	1.9408	1.1492	0.8468	0.8685	1.2525	1.1536
28.6983	0.96603	1.27168	1.2311	1.1728	1.0395	1.8013	1.0104	0.813	0.8958	1.0681	0.9673
31.504	0.9197	1.21499	1.0505	1.055	0.9297	1.6333	0.9205	0.8618	0.8234	0.917	0.8256
34.584	0.94348	1.22123	0.9079	0.9865	0.8473	1.4785	0.8773	0.9346	0.6414	0.7989	0.7381
37.9652	1.0063	1.27623	0.8066	0.9506	0.7764	1.3806	0.8576	0.9167	0.3762	0.6966	0.696
41.6768	1.05603	1.33647	0.7352	0.9146	0.6971	1.3545	0.828	0.6815	0.1491	0.592	0.6759
45.7513	0.84901	1.18259	0.6705	0.6956	0.4979	1.3811	0.627	0.3453	0.029	0.4011	0.6483
50.2242	0.46772	0.8596	0.5894	0.3707	0.2522	1.4126	0.3317	0.0813	0.0023	0.1945	0.4866
55.1343	0.11464	0.44633	0.4075	0.0893	0.0588	1.3702	0.0794	0.0085	0	0.0438	0.2556
60.5245	0.01204	0.19163	0.1994	0.0093	0.006	1.1648	0.0082	0	0	0.0044	0.0607
66.4417	0	0.0423	0.0452	0	0	0.7497	0	0		0	0.0063
72.9374	0	0.00434	0.0045	0	0	0.3244	0			0	0
80.0681		0	0			0.0686					0
87.8959		0	0			0.0064					
96.4892						0					
105.922						0					

Particle Size
Dalongkou Section
Cycle: UQZJ 61
Results in volume %

Size µm	SD11-22	SD11-23	SD11-24
0.393033	0.32935	0.32787	0.30639
0.431458	0.5827	0.57917	0.54181
0.473639	0.86803	0.85739	0.80268
0.519944	1.27067	1.24414	1.16484
0.570777	1.65492	1.60283	1.49988
0.626578	2.03006	1.94249	1.81734
0.687836	2.40511	2.27356	2.127
0.755082	2.79422	2.61159	2.4432
0.828903	3.17549	2.93902	2.74828
0.90994	3.52209	3.23378	3.02212
0.9989	3.81475	3.48322	3.25386
1.09656	4.03299	3.67465	3.43256
1.20376	4.16797	3.80648	3.55724
1.32145	4.20101	3.86515	3.61523
1.45064	4.12625	3.84483	3.60277
1.59246	3.94542	3.74328	3.51966
1.74815	3.67686	3.57137	3.37797
1.91906	3.34992	3.34982	3.19665
2.10667	3.00235	3.10566	2.99949
2.31263	2.68027	2.87247	2.81585
2.53872	2.42552	2.68053	2.67193
2.78692	2.272	2.55693	2.59122
3.05939	2.23333	2.5155	2.58454
3.35849	2.30394	2.55556	2.64989
3.68682	2.45597	2.65614	2.76757
4.04726	2.64108	2.77548	2.90087
4.44294	2.79653	2.85868	3.00232
4.87731	2.85985	2.85482	3.02692
5.35414	2.79288	2.74146	2.95208
5.87759	2.59671	2.53316	2.78446
6.45221	2.31085	2.27121	2.55338
7.08301	1.9903	1.9967	2.29163
7.77547	1.67866	1.73175	2.02127
8.53563	1.39823	1.48205	1.75693
9.37012	1.16005	1.25139	1.51298
10.2862	0.98245	1.05925	1.31156
11.2918	0.89194	0.93082	1.17033
12.3958	0.90981	0.87821	1.08581
13.6076	1.03477	0.88938	1.03503
14.938	1.21987	0.92563	0.98112
16.3984	1.36947	0.94436	0.906
18.0016	1.37405	0.91848	0.8223
19.7615	1.18082	0.85249	0.75777
21.6935	0.8373	0.77813	0.73606
23.8143	0.44832	0.71793	0.74568
26.1425	0.16687	0.67444	0.74856
28.6983	0.03449	0.62444	0.6973
31.504	0.00346	0.5406	0.56434
34.584	8.5E-05	0.40518	0.34729
37.9652	0	0.26179	0.14574
41.6768		0.13698	0.02979
45.7513		0.05789	0.00253
50.2242		0.01265	0
55.1343		0.00123	
60.5245		0	

Reliability Results (in volume %)

Sample Q11-9

Size µm	Test 1	Test 2	Test 3	Test 4	Test 5
0.393033	0.251298	0.256954	0.267913	0.258361	0.264478
0.431458	0.444427	0.454582	0.473651	0.456636	0.467623
0.473639	0.665879	0.677892	0.705114	0.680712	0.698773
0.519944	0.985088	0.994703	1.032343	0.999271	1.02965
0.570777	1.30218	1.300727	1.346287	1.308177	1.354607
0.626578	1.623582	1.603643	1.654463	1.614557	1.680733
0.687836	1.955543	1.91094	1.964787	1.926017	2.015247
0.755082	2.309157	2.234273	2.289563	2.254613	2.370063
0.828903	2.667887	2.557693	2.613047	2.585283	2.728907
0.90994	3.008795	2.86125	2.914853	2.897633	3.069447
0.9989	3.311722	3.130043	3.18022	3.175777	3.373013
1.09656	3.554742	3.347637	3.393157	3.402187	3.61887
1.20376	3.725643	3.505963	3.546657	3.567873	3.795377
1.32145	3.806585	3.588993	3.625467	3.656037	3.88394
1.45064	3.789558	3.590113	3.622903	3.657953	3.875363
1.59246	3.673348	3.508003	3.53731	3.57013	3.76669
1.74815	3.47226	3.354113	3.379887	3.40251	3.569577
1.91906	3.213472	3.148547	3.171487	3.17619	3.307943
2.10667	2.933365	2.918607	2.94032	2.92115	3.015517
2.31263	2.674458	2.698723	2.721533	2.67552	2.73462
2.53872	2.474455	2.521087	2.54761	2.475843	2.50514
2.78692	2.363897	2.413367	2.446107	2.354103	2.360683
3.05939	2.357635	2.388383	2.429807	2.327357	2.318107
3.35849	2.453447	2.444317	2.49595	2.395703	2.376363
3.68682	2.626608	2.56112	2.62249	2.537303	2.51212
4.04726	2.829178	2.70234	2.769147	2.70852	2.680243
4.44294	2.99807	2.820167	2.883583	2.85089	2.820373
4.87731	3.07317	2.86668	2.915237	2.907413	2.873093
5.35414	3.020778	2.81305	2.836307	2.846097	2.804197
5.87759	2.842938	2.659677	2.652623	2.671347	2.617527
6.45221	2.570578	2.435793	2.400727	2.41973	2.351657
7.08301	2.245707	2.180397	2.126403	2.137467	2.056157
7.77547	1.908172	1.923797	1.86374	1.859707	1.768937
8.53563	1.595313	1.681307	1.627837	1.60493	1.50863
9.37012	1.344415	1.460103	1.42244	1.383333	1.283653
10.2862	1.187072	1.278853	1.257393	1.212987	1.110327
11.2918	1.137965	1.16326	1.15001	1.116397	1.01076
12.3958	1.184383	1.138213	1.118243	1.111153	1.004355
13.6076	1.283707	1.208447	1.16499	1.194347	1.090243
14.938	1.370857	1.340533	1.264127	1.329147	1.232427
16.3984	1.386092	1.471417	1.36382	1.452097	1.363443
18.0016	1.306835	1.520023	1.399067	1.490877	1.403877
19.7615	1.154305	1.441467	1.327953	1.40841	1.312257
21.6935	0.970414	1.258157	1.158	1.226257	1.113337
23.8143	0.790591	1.029613	0.933761	0.999976	0.872191
26.1425	0.627644	0.827898	0.718467	0.792647	0.662694
28.6983	0.481473	0.688987	0.557689	0.640162	0.52308
31.504	0.350786	0.602182	0.46221	0.541918	0.448245
34.584	0.242913	0.542738	0.423198	0.484109	0.414906
37.9652	0.168157	0.465008	0.411439	0.435091	0.382954
41.6768	0.123795	0.317263	0.389663	0.356012	0.309917
45.7513	0.08875	0.152596	0.290675	0.267991	0.191993
50.2242	0.053714	0.034828	0.149086	0.166295	0.077975
55.1343	0.015186	0.003531	0.035585	0.084776	0.01622
60.5245	0.002022	0	0.00368	0.020784	0.001491
66.4417	0	0	0	0.002233	0
72.9374	0	0	0	0	0

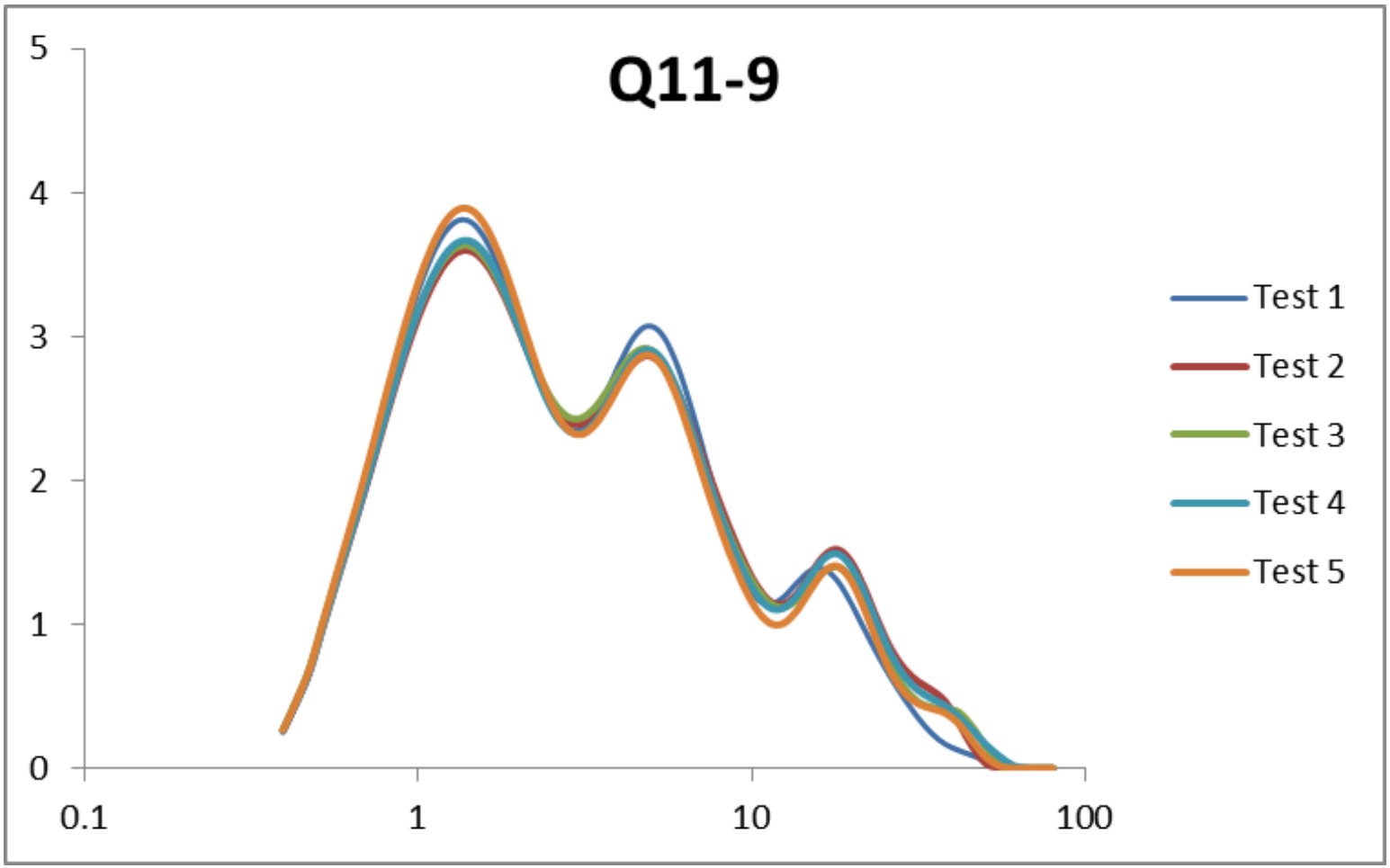
Q11-9
5
4
3
2
1
0
0.1
1
10
100
Test 1
Test 2
Test 3
Test 4
Test 5

Sample Q11-20

Size µm	Test 1	Test 2	Test 3	Test 4	Test 5
0.393033	0.246847	0.226686	0.225665	0.255822	0.22581
0.431458	0.436806	0.401303	0.399249	0.452905	0.399665
0.473639	0.650563	0.598465	0.59637	0.673205	0.596568
0.519944	0.952059	0.877406	0.87732	0.981024	0.876246
0.570777	1.23993	1.145547	1.150793	1.26943	1.147053
0.626578	1.52191	1.41052	1.423417	1.54721	1.416217
0.687836	1.805383	1.679347	1.701497	1.822467	1.69045
0.755082	2.101603	1.962513	1.995347	2.106947	1.980097
0.828903	2.395017	2.245613	2.290543	2.384053	2.270767
0.90994	2.667213	2.51205	2.568947	2.636043	2.545203
0.9989	2.905623	2.750433	2.81641	2.852753	2.79065
1.09656	3.096663	2.94811	3.017813	3.02347	2.99306
1.20376	3.2347	3.099183	3.16606	3.145293	3.145417
1.32145	3.305973	3.18996	3.247683	3.205443	3.233607
1.45064	3.305773	3.21552	3.25759	3.200867	3.25221
1.59246	3.234113	3.175443	3.195483	3.132927	3.20058
1.74815	3.10278	3.080063	3.073123	3.01435	3.089383
1.91906	2.930273	2.944913	2.910287	2.861817	2.935707
2.10667	2.74062	2.790403	2.732717	2.695727	2.762437
2.31263	2.563507	2.64246	2.57019	2.541577	2.597977
2.53872	2.42629	2.525557	2.448757	2.42303	2.468963
2.78692	2.352483	2.461257	2.389903	2.36132	2.39829
3.05939	2.35273	2.4592	2.403807	2.365083	2.39669
3.35849	2.424993	2.517947	2.488883	2.43169	2.462853
3.68682	2.551523	2.622807	2.627687	2.54479	2.58078
4.04726	2.70074	2.748297	2.78719	2.677723	2.72172
4.44294	2.831323	2.861237	2.923893	2.796773	2.847543
4.87731	2.901887	2.926813	2.996017	2.866877	2.91947
5.35414	2.8865	2.92167	2.979057	2.864307	2.912023
5.87759	2.783217	2.841113	2.872153	2.783373	2.82152
6.45221	2.61284	2.700987	2.69272	2.639373	2.665717
7.08301	2.404707	2.52539	2.464687	2.45736	2.47124
7.77547	2.182007	2.33302	2.21091	2.25895	2.26019
8.53563	1.957903	2.13254	1.95599	2.05682	2.045597
9.37012	1.742233	1.926813	1.731937	1.85751	1.838067
10.2862	1.55278	1.73168	1.57153	1.679053	1.655787
11.2918	1.41466	1.574613	1.49759	1.54877	1.524493
12.3958	1.349127	1.487323	1.506247	1.496773	1.467067
13.6076	1.360833	1.487483	1.56557	1.537707	1.488543
14.938	1.4277	1.55549	1.627937	1.645887	1.567213
16.3984	1.504803	1.643233	1.6484	1.763227	1.655763
18.0016	1.537197	1.67442	1.61008	1.801587	1.695137
19.7615	1.482983	1.589013	1.520397	1.695893	1.64008
21.6935	1.333453	1.384553	1.39078	1.4515	1.47886
23.8143	1.113193	1.103903	1.228367	1.127413	1.236313
26.1425	0.871992	0.824883	1.02403	0.817573	0.96301
28.6983	0.665089	0.612484	0.778354	0.594177	0.71142
31.504	0.527108	0.479592	0.522985	0.460852	0.517999
34.584	0.469415	0.420818	0.307411	0.400859	0.395413
37.9652	0.480782	0.389493	0.180792	0.356924	0.332605
41.6768	0.53453	0.325698	0.14566	0.26148	0.307574
45.7513	0.466494	0.209558	0.160939	0.135708	0.236784
50.2242	0.278993	0.085521	0.203856	0.03273	0.130574
55.1343	0.072117	0.018007	0.178984	0.003566	0.032141
60.5245	0.008028	0.001649	0.109364	0	0.003447
66.4417	0	0	0.027508	0	0
72.9374	0	0	0.003127	0	0
80.0681	0	0	0	0	0

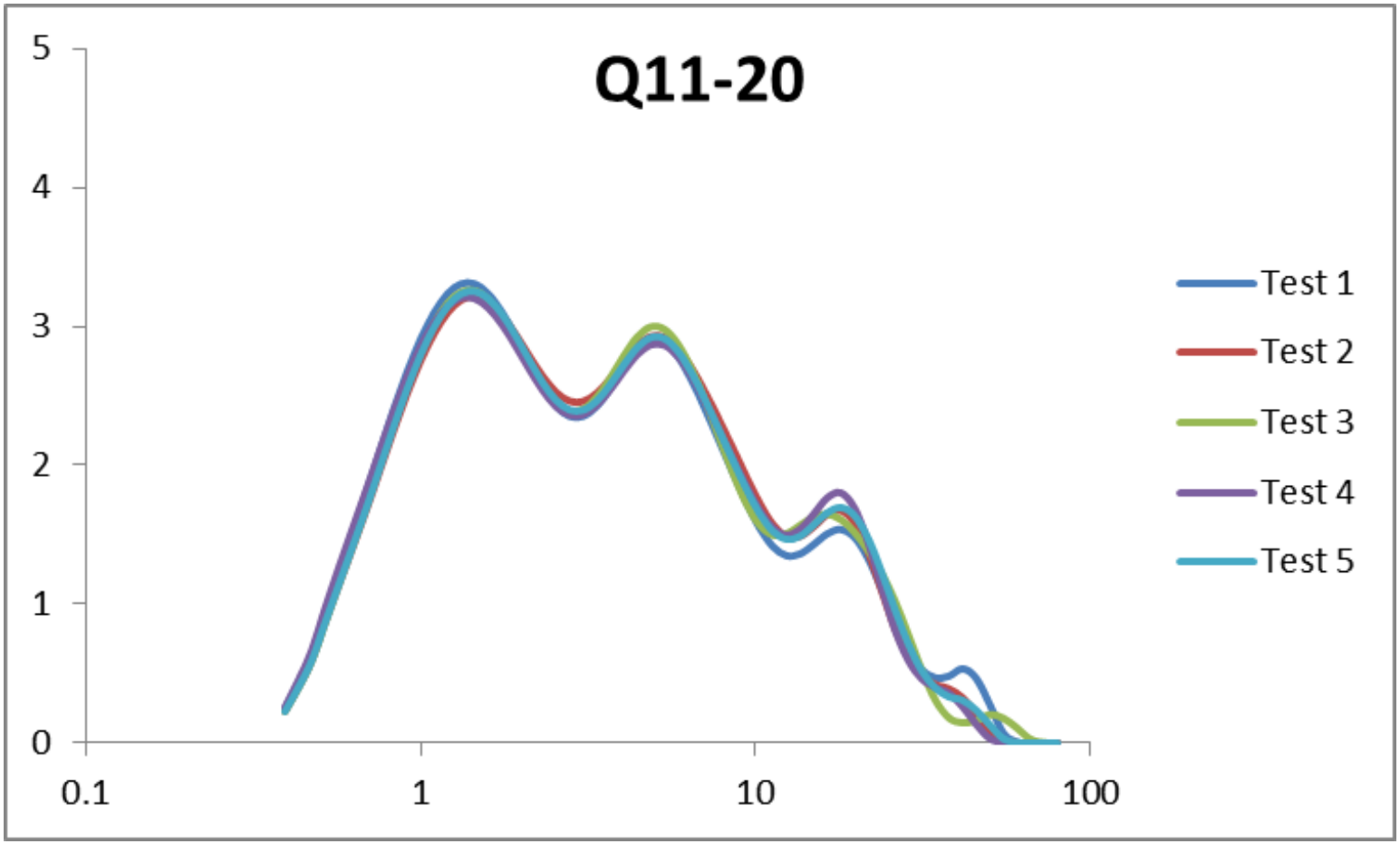
Q11-20
5
4
3
2
1
0
0.1
1
10
100
Test 1
Test 2
Test 3
Test 4
Test 5

APPENDIX K

CYCLE THICKNESS

Cycles types for all sections

Cycle Types	
MS	Meandering Stream
LD	Lacustrine Deltaic
LL	Lake plain Littoral
EFL	Ephemeral Fluvial-Loess
MFL	Meandering Fluvial-Loess

Northeast Tarlong Section

Northeast Tarlong									
Cycle	Channel			Bentonite	Overbank			Cycle	Cycle
	Total	Congl	Sand		Total	Loess	Floodp.	Thicknes	Type
LQZJ 1	1.52	0.54	0.98	0.00	0.00	0.00	0.00	1.52	MS
LQZJ 2	1.36	0.47	0.89	0.00	0.00	0.00	0.00	1.36	MS
LQZJ 3	1.27	0.45	0.83	0.00	1.11	0.00	1.11	2.38	MS
UQZJ 1	0.00	0.00	0.00	0.00	2.74	2.74	0.00	2.74	EFL
UQZJ 2	2.58	0.93	1.65	0.00	2.82	0.00	2.82	5.39	MS
UQZJ 3	0.51	0.51	0.00	0.00	7.67	6.21	1.46	8.18	EFL
UQZJ 4	0.95	0.00	0.95	0.00	1.84	1.84	0.00	2.80	EFL
UQZJ 5	1.44	0.69	0.75	0.00	2.19	2.19	0.00	3.63	EFL
UQZJ 6	0.63	0.31	0.32	0.00	0.99	0.99	0.00	1.63	MFL
UQZJ 7	0.40	0.00	0.40	0.00	1.70	1.70	0.00	2.10	MFL
UQZJ 8	0.78	0.00	0.78	0.00	4.34	4.34	0.00	5.11	EFL
UQZJ 9	0.51	0.00	0.51	0.00	1.69	1.69	0.00	2.20	EFL
UQZJ 10	0.56	0.00	0.56	0.00	2.00	2.00	0.00	2.56	EFL
UQZJ 11	0.62	0.23	0.39	0.21	1.79	1.79	0.00	2.62	EFL
UQZJ 12	0.95	0.00	0.95	0.00	3.34	3.34	0.00	4.30	MFL
UQZJ 13	0.62	0.22	0.40	0.00	0.80	0.80	0.00	1.42	EFL
UQZJ 14	0.71	0.22	0.50	0.23	2.54	2.54	0.00	3.48	EFL
UQZJ 15	1.06	0.00	1.06	0.00	1.25	1.25	0.00	2.31	MFL
UQZJ 16	0.77	0.00	0.77	0.00	1.23	1.23	0.00	2.00	EFL
UQZJ 17	1.68	0.28	1.40	0.31	7.07	7.07	0.00	9.06	EFL
UQZJ 18	0.93	0.27	0.66	0.00	0.28	0.28	0.00	1.21	EFL
UQZJ 19	1.06	0.00	1.06	0.00	6.66	6.66	0.00	7.71	EFL
UQZJ 20	0.00	0.00	0.00	0.00	5.30	5.30	0.00	5.30	EFL
UQZJ 21	0.00	0.00	0.00	0.59	2.96	2.96	0.00	3.55	EFL
UQZJ 22	0.00	0.00	0.00	0.00	1.73	1.73	0.00	1.73	EFL

North Tarlong Section

North Tarlong									
Cycle	Channel			Bentonite	Overbank			Cycle	Cycle
	Total	Congl	Sand		Total	Loess	Floodp.	Thicknes	Type
LQZJ 1	0.00	0.00	0.00	0.00	2.63	0.00	2.63	2.63	MS
LQZJ 2	0.00	0.00	0.00	0.00	0.66	0.00	0.66	0.66	MS
LQZJ 3	0.00	0.00	0.00	0.00	1.07	0.00	1.07	1.07	MS
LQZJ 4	0.00	0.00	0.00	0.00	1.95	0.00	1.95	1.95	MS
UQZJ 1	3.23	0.00	3.23	0.00	0.00	0.00	0.00	3.23	MS
UQZJ 2	1.06	0.00	1.06	0.00	0.67	0.00	0.67	1.73	EFL
UQZJ 3	0.19	0.00	0.19	0.00	8.62	8.62	0.00	8.81	EFL
UQZJ 4	2.80	0.00	2.80	0.00	6.25	6.25	0.00	9.05	EFL
UQZJ 5	1.82	0.00	1.82	0.00	1.51	1.51	0.00	3.34	EFL
UQZJ 6	1.16	0.00	1.16	0.00	12.29	12.29	0.00	13.45	EFL
UQZJ 7	0.00	0.00	0.00	0.00	15.83	15.83	0.00	15.83	EFL
UQZJ 8	0.00	0.00	0.00	0.00	11.00	11.00	0.00	11.00	EFL

North-Central Section

North Tarlong									
Cycle	Channel			Bentonite	Overbank			Cycle	Cycle
	Total	Congl	Sand		Total	Loess	Floodp.	Thicknes	Type
LQZJ 1	0.78	0.00	0.78	0.00	0.23	0.00	0.23	1.00	MS
LQZJ 2	0.18	0.18	0.00	0.00	0.29	0.00	0.29	0.47	MS
LQZJ 3	0.41	0.00	0.41	0.00	0.93	0.00	0.93	1.34	MS
LQZJ 4	0.89	0.12	0.77	0.00	3.99	0.00	3.99	4.88	MS
LQZJ 5	1.06	0.00	1.06	0.00	2.67	0.00	2.67	3.73	MS
LQZJ 6	0.00	0.00	0.00	0.00	3.92	0.00	3.92	3.92	MS
UQZJ 1	0.00	0.00	0.00	0.00	3.12	3.12	0.00	3.12	EFL
UQZJ 2	1.23	0.00	1.23	0.00	2.73	2.73	0.00	3.96	MFL

Taodonggou Section

Taodonggou									
Cycle	Channel			Bentonite	Overbank			Cycle	Cycle
	Total	Congl	Sand		Total	Loess	Floodp.	Thicknes	Type
LQZJ 1	0.38	0.00	0.38	0.00	0.23	0.00	0.23	0.61	MS
LQZJ 2	0.00	0.00	0.00	0.00	0.10	0.00	0.10	0.10	MS
UQZJ 1	0.84	0.00	0.84	0.00	1.60	1.60	0.00	2.44	MFL
UQZJ 2	0.11	0.11	0.00	0.00	0.71	0.71	0.00	0.82	EFL
UQZJ 3	0.16	0.16	0.00	0.00	13.48	13.48	0.00	13.64	EFL
UQZJ 4	0.20	0.00	0.20	0.00	8.34	8.34	0.00	8.54	EFL
UQZJ 5	1.55	0.83	0.72	0.00	1.36	1.36	0.00	2.91	EFL
UQZJ 6	0.70	0.00	0.70	0.00	0.43	0.43	0.00	1.13	EFL
UQZJ 7	1.46	0.00	1.46	0.00	3.06	3.06	0.00	4.52	EFL
UQZJ 8	0.50	0.00	0.50	0.00	0.90	0.90	0.00	1.40	EFL
UQZJ 9	0.55	0.00	0.55	0.00	5.91	5.91	0.00	6.46	EFL
UQZJ 10	0.12	0.00	0.12	0.00	5.62	5.62	0.00	5.74	EFL
UQZJ 11	1.63	0.00	1.63	0.00	0.00	0.00	0.00	1.63	MS
UQZJ 12	0.99	0.00	0.99	0.00	1.44	1.44	0.00	2.43	EFL
UQZJ 13	1.33	0.00	1.33	0.00	0.24	0.00	0.24	1.57	MS
UQZJ 14	0.30	0.00	0.30	0.00	1.31	1.31	0.00	1.61	EFL
UQZJ 15	0.20	0.00	0.20	0.00	0.52	0.52	0.00	0.72	EFL
UQZJ 16	2.24	1.52	0.72	0.00	0.24	0.00	0.24	2.48	MS
UQZJ 17	3.84	2.34	1.51	0.00	0.00	0.00	0.00	3.84	MS
UQZJ 18	1.44	0.00	1.44	0.00	1.20	1.20	0.00	2.64	MFL
UQZJ 19	1.02	0.37	0.65	0.00	2.16	2.16	0.00	3.17	MFL
UQZJ 20	1.25	1.07	0.18	0.00	0.00	0.00	0.00	1.25	MS
UQZJ 21	1.96	0.91	1.05	0.00	0.79	0.79	0.00	2.75	MFL
UQZJ 22	0.42	0.26	0.16	0.00	0.00	0.00	0.00	0.42	MS
UQZJ 23	2.77	1.58	1.20	0.00	1.32	1.32	0.00	4.09	MFL
UQZJ 24	3.11	0.00	3.11	0.00	1.31	1.31	0.00	4.42	MFL
UQZJ 25	0.41	0.00	0.41	0.00	4.85	4.85	0.00	5.26	EFL
UQZJ 26	0.19	0.00	0.19	0.00	2.64	2.64	0.00	2.83	EFL
UQZJ 27	0.46	0.00	0.46	0.00	4.12	4.12	0.00	4.58	EFL
UQZJ 28	1.67	0.00	1.67	0.00	0.95	0.95	0.00	2.62	EFL
UQZJ 29	0.30	0.00	0.30	0.00	6.13	6.13	0.00	6.43	EFL
UQZJ 30	0.42	0.00	0.42	0.00	0.00	0.00	0.00	0.42	EFL
UQZJ 31	0.29	0.00	0.29	0.00	7.44	7.44	0.00	7.73	EFL

Southwest Tarlong Section

Southwest										
Cycle	Channel			Bentonite	Overbank			Lake	Cycle Thicknes	Cycle Type
	Total	Congl	Sand		Total	Loess	Floodp.			
LQZJ 1	2.76	0.88	1.88	0.00	0.00	0.00	0.00	0.00	2.76	MS
LQZJ 2	3.47	0.22	3.25	0.00	0.00	0.00	0.00	0.00	3.47	MS
LQZJ 3	2.55	0.87	1.68	0.00	0.00	0.00	0.00	0.00	2.55	MS
LQZJ 4	1.46	0.24	1.21	3.05	0.00	0.00	0.00	0.00	4.51	MS
LQZJ 5	0.75	0.00	0.75	0.00	0.00	0.00	0.00	0.00	0.75	MS
LQZJ 6	0.76	0.31	0.44	0.00	0.00	0.00	0.00	0.00	0.76	MS
LQZJ 7	0.93	0.49	0.43	0.00	0.00	0.00	0.00	0.00	0.93	MS
LQZJ 8	2.86	1.02	1.84	0.00	1.64	0.00	1.64	0.00	4.50	MS
LQZJ 9	0.73	0.00	0.73	0.00	0.85	0.00	0.85	0.00	1.58	MS
LQZJ 10	0.78	0.78	0.00	0.00	0.17	0.00	0.17	0.00	0.95	MS
LQZJ 11	0.72	0.00	0.72	0.00	0.85	0.00	0.85	0.00	1.57	MS
LQZJ 12	1.56	0.00	1.56	0.00	1.88	0.00	1.88	0.00	3.44	LD
LQZJ 13	3.05	1.19	1.86	0.00	2.24	0.00	2.24	0.00	5.29	MS
LQZJ 14	6.36	0.29	6.06	0.00	4.05	0.00	4.05	0.00	10.41	MS
LQZJ 15	0.64	0.00	0.64	0.00	0.00	0.00	0.00	0.00	0.64	MS
LQZJ 16	2.78	1.79	0.99	0.00	0.00	0.00	0.00	0.00	2.78	MS
LQZJ 17	1.80	0.55	1.25	0.00	0.00	0.00	0.00	0.00	1.80	MS
LQZJ 18	1.56	0.26	1.29	0.00	0.00	0.00	0.00	0.00	1.56	MS
LQZJ 19	0.00	0.00	0.00	2.22	0.00	0.00	0.00	8.88	11.11	LL
LQZJ 20	0.98	0.00	0.98	0.00	0.00	0.00	0.00	8.26	9.24	LL
LQZJ 21	2.87	1.28	1.59	0.00	0.19	0.00	0.19	0.00	3.06	MS
LQZJ 22	4.70	2.64	2.06	0.00	0.98	0.00	0.98	0.00	5.68	MS
LQZJ 23	4.56	2.51	2.05	0.00	0.51	0.00	0.51	0.00	5.06	MS
LQZJ 24	4.55	2.32	2.23	0.00	0.00	0.00	0.00	0.00	4.55	MS
LQZJ 25	0.19	0.19	0.00	0.00	0.34	0.00	0.34	0.00	0.54	MS
LQZJ 26	0.99	0.00	0.99	0.96	0.00	0.00	0.00	2.06	4.01	LL
LQZJ 27	3.01	1.51	1.51	0.24	0.00	0.00	0.00	1.97	5.22	LL
LQZJ 28	1.06	0.00	1.06	0.25	0.00	0.00	0.00	1.19	2.50	LL
UQZJ 1	0.00	0.00	0.00	0.00	5.26	5.26	0.00	0.00	5.26	EFL
UQZJ 2	0.93	0.93	0.00	0.00	3.88	3.88	0.00	0.00	4.81	EFL
UQZJ 3	2.16	1.08	1.08	0.00	5.62	5.62	0.00	0.00	7.78	EFL
UQZJ 4	0.65	0.31	0.34	0.93	11.60	11.60	0.00	0.00	13.18	EFL
UQZJ 5	4.19	2.09	2.09	1.01	8.33	8.33	0.00	0.00	13.53	EFL
UQZJ 6	3.82	0.69	3.13	0.28	6.60	6.60	0.00	0.00	10.70	EFL
UQZJ 7	1.63	0.70	0.93	0.00	12.92	12.92	0.00	0.00	14.55	EFL
UQZJ 8	0.39	0.00	0.39	0.00	16.46	16.46	0.00	0.00	16.84	EFL

Southeast Tarlong Section

Southeast									
Cycle	Channel			Bentonite	Overbank			Cycle	Cycle
	Total	Congl	Sand		Total	Loess	Floodp.	Thicknes	Type
LQZJ 1	6.47	3.19	3.28	0.00	2.65	0.00	2.65	9.12	MS
LQZJ 2	4.36	4.12	0.24	0.00	0.12	0.00	0.12	4.48	MS
UQZJ 1	1.62	1.40	0.23	0.00	4.37	4.37	0.00	5.99	MFL
UQZJ 2	0.78	0.78	0.00	0.00	1.03	1.03	0.00	1.81	EFL
UQZJ 3	0.40	0.00	0.40	0.00	1.43	1.43	0.00	1.83	EFL
UQZJ 4	0.48	0.19	0.29	0.00	3.62	3.62	0.00	4.10	EFL
UQZJ 5	0.30	0.00	0.30	0.00	2.34	2.34	0.00	2.63	EFL
UQZJ 6	0.96	0.00	0.96	0.00	1.29	1.29	0.00	2.25	MFL
UQZJ 7	0.40	0.20	0.20	0.00	2.27	2.27	0.00	2.67	EFL
UQZJ 8	0.30	0.00	0.30	0.00	1.04	1.04	0.00	1.34	EFL
UQZJ 9	0.97	0.00	0.97	0.00	1.92	1.92	0.00	2.89	EFL
UQZJ 10	0.38	0.00	0.38	0.00	0.70	0.70	0.00	1.09	EFL
UQZJ 11	0.13	0.00	0.13	0.00	0.98	0.98	0.00	1.11	EFL
UQZJ 12	0.50	0.00	0.50	0.00	0.63	0.63	0.00	1.14	EFL
UQZJ 13	0.45	0.00	0.45	0.00	0.21	0.21	0.00	0.66	EFL
UQZJ 14	0.56	0.00	0.56	0.00	1.18	1.18	0.00	1.74	EFL
UQZJ 15	0.87	0.00	0.87	0.00	0.42	0.42	0.00	1.28	EFL
UQZJ 16	0.40	0.00	0.40	0.00	0.49	0.49	0.00	0.89	EFL
UQZJ 17	0.33	0.00	0.33	0.00	1.09	1.09	0.00	1.42	EFL
UQZJ 18	1.03	1.03	0.00	0.00	4.05	4.05	0.00	5.09	MFL
UQZJ 19	0.98	0.00	0.98	0.00	0.88	0.88	0.00	1.86	MFL
UQZJ 20	0.30	0.00	0.30	0.00	0.61	0.61	0.00	0.90	EFL
UQZJ 21	0.55	0.00	0.55	0.30	1.88	1.88	0.00	2.74	EFL
UQZJ 22	0.24	0.00	0.24	0.00	1.96	1.96	0.00	2.20	EFL
UQZJ 23	0.24	0.00	0.24	0.00	2.82	2.82	0.00	3.06	EFL
UQZJ 24	0.18	0.00	0.18	0.00	0.96	0.96	0.00	1.14	EFL
UQZJ 25	0.91	0.28	0.63	0.00	1.57	1.57	0.00	2.48	MFL
UQZJ 26	1.13	1.13	0.00	0.00	0.41	0.41	0.00	1.54	MFL
UQZJ 27	0.40	0.00	0.40	0.00	1.39	1.39	0.00	1.79	EFL
UQZJ 28	1.37	1.37	0.00	0.00	0.52	0.52	0.00	1.89	MFL
UQZJ 29	0.19	0.00	0.19	0.00	0.63	0.63	0.00	0.82	EFL
UQZJ 30	1.12	1.12	0.00	0.00	0.48	0.48	0.00	1.60	EFL
UQZJ 31	0.71	0.19	0.52	0.00	2.81	2.81	0.00	3.53	EFL
UQZJ 32	0.48	0.00	0.48	0.00	0.41	0.41	0.00	0.89	EFL
UQZJ 33	1.56	0.23	1.33	0.00	1.67	1.67	0.00	3.23	MFL
UQZJ 34	0.36	0.00	0.36	0.00	0.37	0.37	0.00	0.73	EFL
UQZJ 35	0.30	0.00	0.30	0.00	0.77	0.77	0.00	1.08	EFL
UQZJ 36	0.29	0.00	0.29	0.00	0.66	0.66	0.00	0.94	EFL
UQZJ 37	0.18	0.00	0.18	0.00	2.53	2.53	0.00	2.71	EFL
UQZJ 38	0.16	0.00	0.16	0.00	0.63	0.63	0.00	0.79	EFL
UQZJ 39	1.59	0.45	1.14	0.00	4.61	4.61	0.00	6.20	MFL
UQZJ 40	0.00	0.00	0.00	0.17	3.34	3.34	0.00	3.52	EFL

Dalongkou Section

Dalongkou									
Cycle	Channel			Bentonite	Overbank			Cycle	Cycle
	Total	Congl	Sand		Total	Loess	Floodp.	Thicknes	Type
LQZJ 1	2.82	1.33	1.49	0.00	0.00	0.00	0.00	2.82	MS
LQZJ 2	2.77	1.28	1.48	0.00	0.00	0.00	0.00	2.77	MS
LQZJ 3	2.56	1.20	1.36	0.00	2.67	0.00	2.67	5.23	MS
LQZJ 4	0.55	0.00	0.55	0.00	1.08	1.08	0.00	1.63	EFL
LQZJ 5	0.52	0.00	0.52	0.00	0.91	0.91	0.00	1.43	EFL
UQZJ 1	2.04	0.41	1.63	0.00	0.86	0.00	0.86	2.90	MS
UQZJ 2	0.73	0.29	0.43	0.00	0.69	0.00	0.69	1.42	MS
UQZJ 3	1.05	0.31	0.74	0.00	4.82	0.00	4.82	5.87	MS
UQZJ 4	0.49	0.00	0.49	0.00	1.57	0.00	1.57	2.05	MS
UQZJ 5	0.29	0.00	0.29	0.00	3.20	0.00	3.20	3.49	MS
UQZJ 6	3.16	1.52	1.64	0.00	3.09	0.00	3.09	6.25	MS
UQZJ 7	1.33	0.67	0.66	0.00	0.12	0.00	0.12	1.45	MS
UQZJ 8	0.53	0.23	0.29	0.00	0.20	0.00	0.20	0.73	MS
UQZJ 9	0.50	0.00	0.50	0.00	1.48	0.00	1.48	1.98	MFL
UQZJ 10	0.63	0.00	0.63	0.00	0.82	0.00	0.82	1.45	MS
UQZJ 11	1.98	0.00	1.98	0.00	3.98	0.00	3.98	5.96	MS
UQZJ 12	1.21	0.00	1.21	0.00	3.01	0.00	3.01	4.22	MFL
UQZJ 13	2.69	0.00	2.69	0.00	4.23	0.00	4.23	6.92	MS
UQZJ 14	2.34	0.00	2.34	0.00	0.46	0.00	0.46	2.80	MS
UQZJ 15	1.12	0.76	0.36	0.00	0.66	0.00	0.66	1.78	MS
UQZJ 16	0.44	0.23	0.21	0.15	1.07	0.00	1.07	1.66	EFL
UQZJ 17	0.31	0.00	0.31	0.00	1.08	0.00	1.08	1.40	EFL
UQZJ 18	0.45	0.00	0.45	0.00	0.84	0.00	0.84	1.29	EFL
UQZJ 19	1.38	0.91	0.47	0.00	1.03	0.00	1.03	2.41	MS
UQZJ 20	1.53	0.00	1.53	0.45	0.39	0.00	0.39	2.37	MS
UQZJ 21	2.21	1.12	1.08	0.00	0.85	0.00	0.85	3.06	MS
UQZJ 22	5.27	2.27	3.00	0.00	5.21	0.00	5.21	10.48	MFL
UQZJ 23	0.85	0.00	0.85	0.00	0.32	0.00	0.32	1.17	MS
UQZJ 24	0.14	0.14	0.00	0.00	0.47	0.00	0.47	0.61	MS
UQZJ 25	1.39	0.32	1.08	0.00	8.17	8.17	0.00	9.57	MFL
UQZJ 26	2.11	1.14	0.97	0.00	0.33	0.00	0.33	2.43	MS
UQZJ 27	1.15	0.59	0.57	0.00	0.31	0.00	0.31	1.47	MS
UQZJ 28	2.32	1.05	1.27	0.00	0.94	0.00	0.94	3.26	MFL
UQZJ 29	0.20	0.10	0.10	0.00	0.23	0.00	0.23	0.43	EFL
UQZJ 30	0.97	0.37	0.60	0.00	1.33	0.00	1.33	2.31	MFL
UQZJ 31	1.12	0.53	0.58	0.00	3.57	3.57	0.00	4.69	MFL
UQZJ 32	0.66	0.18	0.49	0.00	0.21	0.00	0.21	0.87	MS
UQZJ 33	0.99	0.32	0.67	0.00	0.00	0.00	0.00	0.99	MS
UQZJ 34	0.69	0.33	0.35	0.00	0.39	0.00	0.39	1.08	MS
UQZJ 35	1.72	0.25	1.48	0.00	0.83	0.00	0.83	2.56	MFL
UQZJ 36	0.98	0.00	0.98	0.00	0.56	0.00	0.56	1.55	MFL
UQZJ 37	1.43	0.00	1.43	0.00	0.32	0.00	0.32	1.75	MS
UQZJ 38	0.30	0.00	0.30	0.00	0.39	0.00	0.39	0.69	MS
UQZJ 39	0.28	0.00	0.28	0.00	0.38	0.00	0.38	0.66	MS
UQZJ 40	2.10	0.75	1.35	0.00	1.81	0.00	1.81	3.91	MFL
UQZJ 41	0.62	0.00	0.62	0.00	0.85	0.00	0.85	1.47	MFL
UQZJ 42	3.85	2.67	1.18	0.00	0.00	0.00	0.00	3.85	MS
UQZJ 43	1.94	1.94	0.00	0.00	0.00	0.00	0.00	1.94	MS
UQZJ 44	1.55	1.55	0.00	0.00	0.00	0.00	0.00	1.55	MS
UQZJ 45	3.55	2.81	0.74	0.00	0.00	0.00	0.00	3.55	MS
UQZJ 46	2.66	1.29	1.37	0.00	0.00	0.00	0.00	2.66	MS
UQZJ 47	1.64	0.60	1.03	0.38	1.01	0.00	1.01	3.03	MS
UQZJ 48	0.73	0.38	0.35	0.00	0.70	0.00	0.70	1.43	MS
UQZJ 49	0.72	0.19	0.53	0.00	1.23	0.00	1.23	1.95	MS
UQZJ 50	3.70	2.02	1.68	0.00	1.86	0.00	1.86	5.56	MS
UQZJ 51	2.15	0.43	1.72	0.00	0.46	0.00	0.46	2.60	MS
UQZJ 52	3.89	2.77	1.12	0.00	0.00	0.00	0.00	3.89	MS
UQZJ 53	3.62	2.35	1.28	0.00	0.00	0.00	0.00	3.62	MS
UQZJ 54	3.67	1.59	2.08	0.00	1.52	0.00	1.52	5.19	MS
UQZJ 55	0.41	0.00	0.41	0.00	0.83	0.00	0.83	1.24	MFL
UQZJ 56	0.42	0.00	0.42	0.00	0.71	0.00	0.71	1.13	MFL
UQZJ 57	0.27	0.00	0.27	0.00	0.54	0.00	0.54	0.81	MFL
UQZJ 58	0.56	0.56	0.00	0.00	0.33	0.00	0.33	0.88	MFL
UQZJ 59	0.26	0.26	0.00	0.00	0.35	0.00	0.35	0.60	MFL
UQZJ 60	0.79	0.31	0.49	0.32	1.59	0.00	1.59	2.70	MFL
UQZJ 61	0.38	0.00	0.38	0.00	1.84	0.00	1.84	2.22	MFL

APPENDIX L
CHANNEL GEOMETRY

Northeast Tarlong Section

Northeast Tarlong			
Cycle Number	Width	Depth	W/D Ratio
LQZJ 1	124.10	4.90	25.33
UQZJ 2	102.20	1.90	53.79
UQZJ 3	87.60	0.50	175.20
UQZJ 5	43.80	1.60	27.38
UQZJ 6	42.34	0.50	84.68
UQZJ 7	36.50	0.40	91.25
UQZJ 8	65.70	0.80	82.13
UQZJ 9	42.34	0.50	84.68
UQZJ 10	87.60	0.70	125.14
UQZJ 11	35.04	0.65	53.91
UQZJ 12	14.60	1.00	14.60
UQZJ 13	41.61	0.65	64.02
UQZJ 14	10.95	0.40	27.38
UQZJ 15	7.30	0.80	9.13
UQZJ 16	33.58	0.75	44.77
UQZJ 17	73.00	1.10	66.36
UQZJ 18	9.49	0.95	9.99
UQZJ 19	16.06	1.30	12.35

Dalongkou Section

Dalongkou			
Cycle Number	Width	Depth	W/D Ratio
UQZJ 1	134.00	2.10	63.81
UQZJ 5	115.00	0.60	191.67
UQZJ 6	124.00	3.25	38.15
UQZJ 9	143.00	0.50	286.00
UQZJ 13	77.00	2.50	30.80
UQZJ 14	28.00	2.30	12.17
UQZJ 15	53.00	1.10	48.18
UQZJ 17	28.00	0.30	93.33
UQZJ 19	120.00	1.40	85.71
UQZJ 21	27.00	2.20	12.27
UQZJ 22	84.00	5.30	15.85
UQZJ 23	53.00	0.85	62.35
UQZJ 25	27.00	1.40	19.29
UQZJ 26	16.00	2.10	7.62
UQZJ 27	7.00	1.10	6.36
UQZJ 31	29.00	1.10	26.36
UQZJ 33	69.00	1.00	69.00
UQZJ 35	66.00	1.75	37.71
UQZJ 36	61.00	0.95	64.21
UQZJ 37	57.00	1.40	40.71
UQZJ 42	61.00	3.85	15.84
UQZJ 47	182.00	1.60	113.75
UQZJ 50	61.00	3.75	16.27
UQZJ 52, 53, 54	258.00	11.20	23.04
UQZJ 58	58.00	0.60	96.67

APPENDIX M

DETRITAL ZIRCON GEOCHRONOLOGY

METHODS

Zircon grains were separated from rocks using standard techniques and annealed at 900^{o}C for 60 hours in a muffle furnace. Randomly selected grains were mounted in epoxy and polished until their centers were exposed. Cathodoluminescence (CL) images were obtained with a JEOL JSM-1300 scanning electron microscope and Gatan MiniCL. Zircon was analyzed by laser ablation inductively coupled plasma mass spectrometry (LA-ICPMS) using a ThermoElectron X-Series II quadrupole ICPMS and New Wave Research UP-213 Nd:YAG UV (213 nm) laser ablation system. In-house analytical protocols, standard materials, and data reduction software were used for acquisition and calibration of U-Pb dates and a suite of high field strength elements (HFSE) and rare earth elements (REE). Zircon was ablated with a laser spot of 25 μm wide using fluence and pulse rates of 5 J/cm^2 and 10 Hz, respectively, during a 45 second analysis (15 sec gas blank, 30 sec ablation) that excavated a pit ~25 μm deep. Ablated material was carried by a 1.2 L/min He gas stream to the nebulizer flow of the plasma. Dwell times were 5 ms for Si and Zr, 200 ms for ^{49}Ti and ^{207}Pb, 80 ms for ^{206}Pb, 40 ms for ^{202}Hg, ^{204}Pb, ^{208}Pb, ^{232}Th, and ^{238}U and 10 ms for all other HFSE and REE. Background count rates for each analyte were obtained prior to each spot analysis and subtracted from the raw count rate for each analyte. Ablations pits that appear to have intersected glass or mineral inclusions based on time-resolved Ti and P data. U-Pb dates from these analyses are considered valid if the time-resolved U-Pb ratios appear to have been unaffected by the inclusions. Analyses that appear contaminated by common Pb were rejected based on an intensity of mass 204 above baseline. For concentration calculations, background-subtracted count rates for each analyte were internally normalized to ^{29}Si and calibrated

with respect to NIST SRM-610 and -612 glasses as the primary standards. Temperature was calculated from the Ti-in-zircon thermometer. Because there are no constraints on the activity of TiO_2 in the source rocks, an average value in crustal rocks of 0.8 was used.

For U-Pb and $^{207}Pb/^{206}Pb$ dates, instrumental fractionation of the background-subtracted ratios was corrected and dates were calibrated with respect to interspersed measurements of the Plešovice zircon standard (Sláma et al., 2008). Two analyses of Plešovice were done for every 10 analyses of unknown zircon; a polynomial fit to the standard analyses yields each sample-specific fractionation factor. Signals at mass 204 were indistinguishable from zero following subtraction of mercury backgrounds measured during the gas blank (<1000 cps ^{202}Hg), and thus dates are reported without common Pb correction. Radiogenic isotope ratio and age error propagation for all analyses includes uncertainty contributions from counting statistics and background subtraction. For spot analyses that are individually interpreted (e.g., detrital zircon analyses), the uncertainty from the standard calibration is propagated into the error on each date. This uncertainty is the standard deviation of the time-varying U/Pb fractionation factor and the standard error of the mean of the time-invariant, smaller $^{207}Pb/^{206}Pb$ fractionation factor. Data were collected in five experiments in June 2013. Standard calibration uncertainties for $^{207}Pb/^{206}Pb$ dates ranged from 0.56 to 0.88% (2σ). Standard calibration uncertainties for $^{206}Pb/^{238}U$ dates ranged from 3.8% to 5.0% (2σ). Age interpretations are based on $^{207}Pb/^{206}Pb$ dates for >1000 Ma zircon. Analyses with >20% positive discordance and >10% negative discordance are not considered. The $^{206}Pb/^{238}U$ dates are used for <1000 Ma zircon. Errors on the $^{207}Pb/^{206}Pb$ and $^{206}Pb/^{238}U$ dates from individual analyses are given at 2σ.

Two zircon secondary reference materials were treated as unknowns to assess accuracy, interspersed as groups of two analyses for every 20 unknown analyses. Weighted mean dates are calculated using Isoplot 3.0 (Ludwig, 2003) from errors on individual dates that do not include the standard calibration uncertainties. However, errors on weighted mean dates include the standard calibration uncertainties within each experiment and are given at 2σ. Seiland zircon (530 Ma from unpublished chemical abrasion thermal ionization mass spectrometry (CA-TIMS) data, Boise State University) and Temora zircon (417 Ma from unpublished chemical abrasion thermal ionization mass spectrometry (CA-TIMS) data, Boise State University) yielded accurate $^{207}Pb/^{206}Pb$ and $^{206}Pb/^{238}U$ dates.

Results

SD11-31	±	SD11-23	±	SD11-11	±	QD12-16	±	QD12-14	±	QD12-1	±	Q11-17	±	Q11-7	±	Q11-5	±
275	7	240	11	247	8	262	8	271	10	270	11	259	8	271	11	254	14
282	9	242	7	264	13	268	10	274	8	275	9	260	11	271	13	264	14
284	9	243	9	268	11	273	10	278	8	276	10	268	12	273	10	271	10
284	13	243	8	271	11	275	9	278	14	280	11	273	10	274	10	290	11
285	12	245	7	272	9	275	8	279	9	282	10	296	10	284	10	292	11
288	9	245	8	276	12	276	10	280	13	285	13	304	15	286	10	294	10
290	9	245	9	279	11	278	12	280	8	286	8	304	11	286	12	295	15
290	8	248	8	281	15	279	8	283	11	286	10	306	11	287	8	297	12
292	10	249	10	284	11	280	9	283	9	287	9	318	15	291	9	297	14
292	8	250	8	285	14	280	11	284	12	289	14	321	11	292	9	298	12
293	9	251	9	286	11	281	9	285	8	291	9	324	13	292	10	299	9
293	9	253	9	286	9	281	11	285	9	292	7	328	13	292	10	302	15
294	12	253	8	286	9	281	11	287	12	295	11	328	10	293	10	308	11
295	10	253	8	292	10	282	8	287	14	296	11	333	13	299	12	315	13
295	11	253	10	294	8	282	8	288	9	296	11	347	11	300	9	316	12
297	11	254	9	294	12	282	9	290	8	297	10	427	15	300	15	318	10
298	9	254	10	294	11	283	9	290	10	298	11	790	25	300	12	321	12
298	9	255	9	296	9	283	10	290	11	298	11			301	11	322	11
298	8	256	10	297	13	283	10	291	9	299	10			301	12	323	14
298	11	257	11	300	12	283	10	291	10	300	11			303	11	324	12
299	11	257	12	301	14	283	10	292	9	301	9			305	9	366	22
300	8	257	10	301	14	283	9	292	10	302	10			305	11	400	14
301	10	260	12	303	10	284	10	293	14	303	8			306	10	425	15
302	9	261	10	303	16	285	8	294	10	306	10			307	10		
302	9	262	10	304	11	285	10	295	12	306	14			309	12		
303	12	263	11	304	12	286	13	295	11	306	10			309	17		
303	8	265	10	304	10	286	10	295	13	306	14			311	18		
304	8	267	10	306	11	287	7	295	14	307	12			312	12		
305	11	271	9	307	12	287	9	295	12	307	15			312	14		
305	10	272	12	307	14	287	9	296	11	308	9			313	12		
306	10	273	17	307	16	287	8	296	10	314	14			315	11		
306	10	278	11	308	11	288	11	296	11	315	10			339	15		
306	9	279	11	308	13	288	8	297	12	316	10			361	14		
306	9	280	12	308	12	288	10	298	12	318	11			362	16		
308	9	280	12	310	13	288	8	298	13	318	10			369	14		
309	12	282	10	310	11	289	10	298	15	318	12			387	19		
309	11	282	12	310	11	289	8	299	9	319	12			394	14		
309	9	282	11	310	10	289	8	300	15	323	10			414	16		
310	11	283	14	314	13	290	7	300	10	327	14			428	14		
312	12	284	11	314	10	290	9	300	11	329	14			457	24		
312	12	284	11	315	14	292	9	300	10	344	16			1094	21		
312	8	285	9	315	14	292	10	301	12	347	17						
312	11	286	12	316	10	292	11	301	12								
312	11	286	15	316	14	292	8	301	12								
313	13	287	14	316	12	292	10	301	10								
313	9	287	12	318	12	292	10	303	11								
313	10	287	11	320	11	293	8	303	11								
313	10	289	10	321	11	293	8	304	10								
313	9	291	10	323	15	294	9	305	12								
314	10	292	12	335	10	295	9	306	10								
314	12	292	14	335	14	295	14	306	8								
315	10	293	12	338	10	295	10	306	13								
315	13	294	9	339	12	296	9	307	10								
317	14	294	12	340	11	296	11	309	10								
319	12	295	10	363	15	296	11	310	10								
320	13	295	11	364	16	296	14	310	10								
320	15	298	18	378	13	297	12	310	9								
326	11	298	11	385	17	297	12	312	12								
327	11	298	10	440	12	298	12	312	11								
329	9	298	11	459	20	300	10	313	14								
330	15	298	10	475	17	300	8	314	21								
332	13	299	11	482	19	300	12	315	12								
333	12	299	12	1869	120	300	11	316	12								
340	12	301	12			301	11	317	12								
351	13	301	13			303	9	319	12								
353	15	301	15			303	12	321	11								
360	23	301	14			304	12	325	18								
364	10	307	11			305	10	326	14								
402	13	308	12			307	12	329	13								
417	12	308	10			307	11	331	11								
451	15	310	15			308	10	336	11								
556	18	310	11			308	13	338	16								
923	27	310	12			309	13	342	11								
		310	11			309	10	350	14								
		314	9			309	11	353	14								
		314	9			309	14	355	14								
		317	12			310	15	356	13								
		319	12			312	12	367	12								
		320	12			312	11	371	19								
		322	15			318	12	425	13								
		325	15			319	12	466	19								
		325	12			319	10	488	20								
		327	12			327	10	527	28								
		328	20			327	12	825	37								
		330	14			330	13	1839	26								
		330	12			330	13										
		333	12			330	15										
		335	13			331	10										
		342	16			341	14										
		346	16			344	9										
		412	17			391	13										
		417	23			394	15										
		481	20			441	17										
		485	21			454	12										
		487	23			470	18										
		489	16			475	14										
		491	25			499	21										
		534	22			505	25										
		1079	53			532	24										
						1811	52										
						1846	24										

APPENDIX N

X-RAY DIFFRACTION

Methods

Bulk Mineralogy: 20 grams of each sample is crushed using a mortar and pestle. The grounded samples are loaded as randomly oriented powder for X-ray diffraction (XRD) analysis using a PANalytical X'Pert Pro Multi-Purpose Diffractometer with Cu-Kα radiation from 4° to 80° 2Θ at a scanning speed of 2º 2Θ/min. The results are used to substantiate field observations and interpretations of mineral composition.

Clay Mineralogy: 20 grams of each sample studied is placed into a 100 mL beaker with 60 mL of deionized water (DIW). Stirring with a spatula is done to disaggregate the samples. Once the samples are disaggregated, the samples are allowed to settle for 30 seconds and decanted into another 100 mL beaker. 10 mL of sodium hexametaphosphate (Calgon) is added into the decanted fraction to prevent flocculation. Once the sample remains in suspension, a pipette is used to remove a portion of the suspended material and transferred into a glass slide and allowed to dry.

First scan – untreated sample is analyzed from 2° to 38° 2Θ at 2°2Θ/minute.

Second scan – sample is placed in an ethylene glycol chamber for 24 hours. The samples is removed from the chamber and placed into the XRD machine immediately. Sample is analyzed from 2° to 38° 2Θ at 2°2Θ/minute.

Third scan – sample is placed in an oven at 500° C for one hour after the ethylene glycol treatment. The sample then is analyzed from 2° to 38° 2Θ at 2°2Θ/minute.

Bulk Mineralogy

Sample S10-3 (Sandstone)
Section: NE Tarlong LQZJ 1

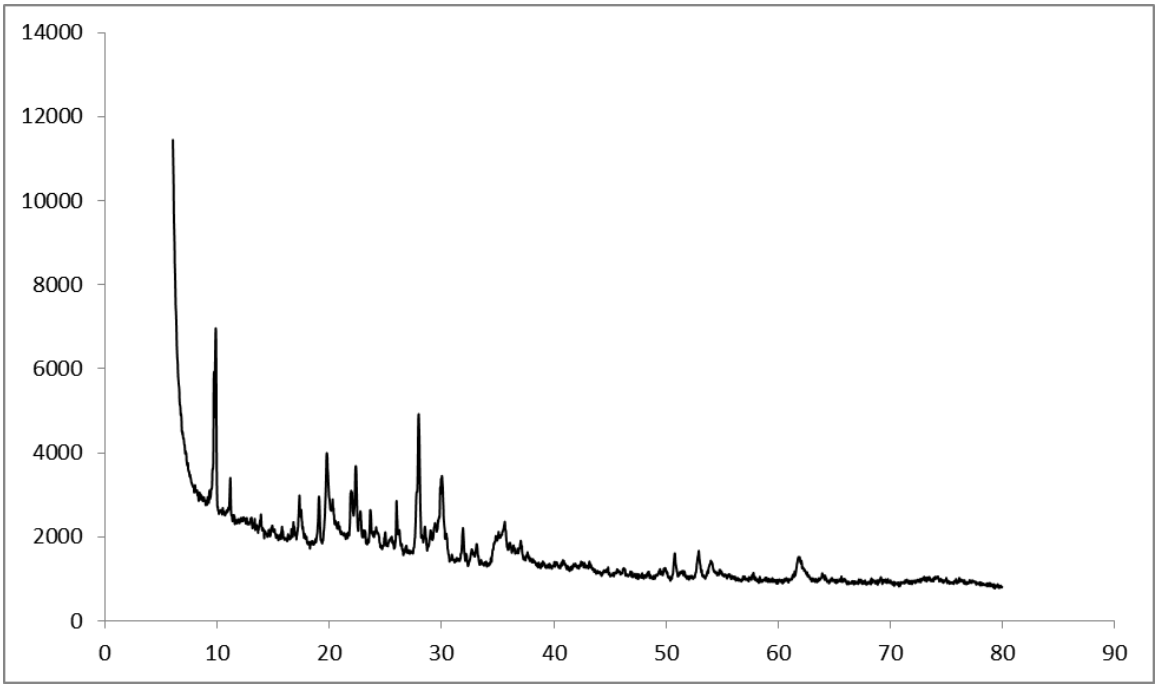

Sample S10-5 (Mudrock)
Section: NE Tarlong UQZJ 1

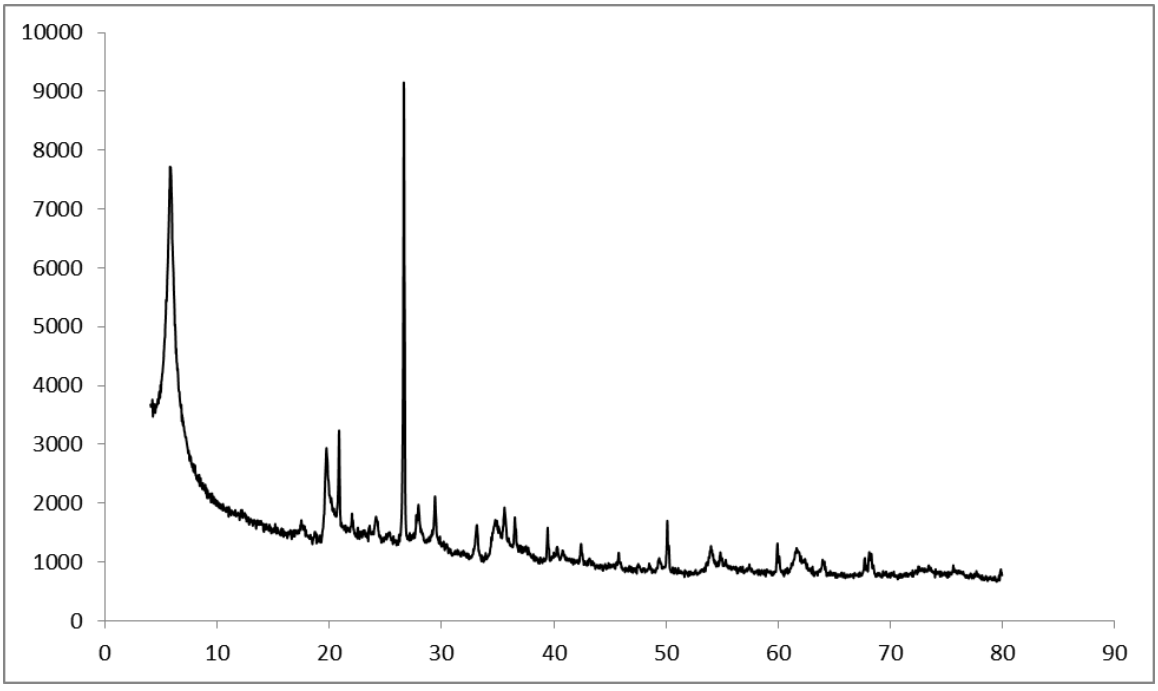

Sample S10-14 (Mudrock)
Section: NE Tarlong UQZJ 8

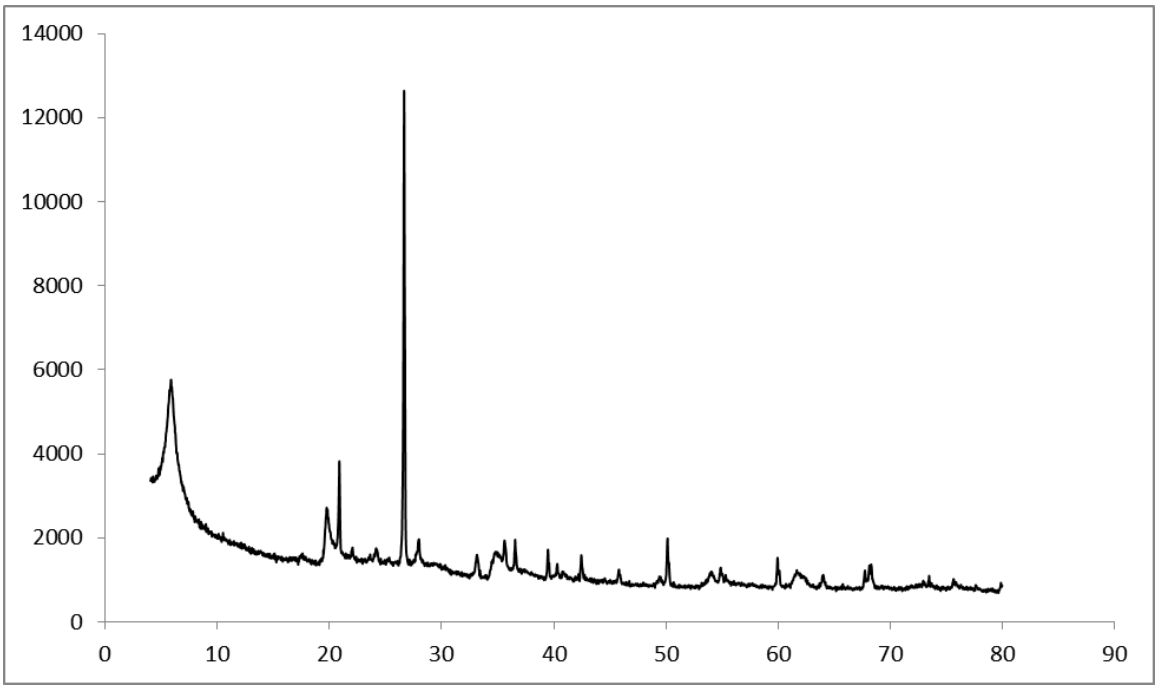

Sample Q11-18 (Mudrock)
Section: NE Tarlong UQZJ 19

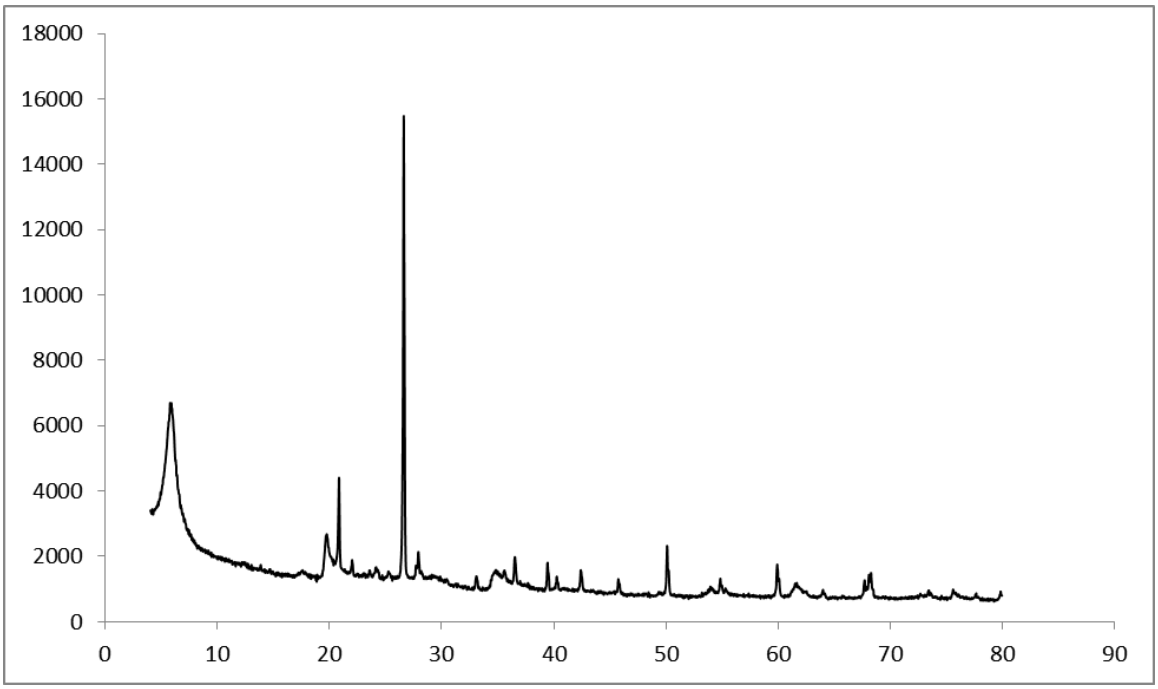

Sample Q13-12 (Sandstone)
Section: SE Tarlong UQZJ 18

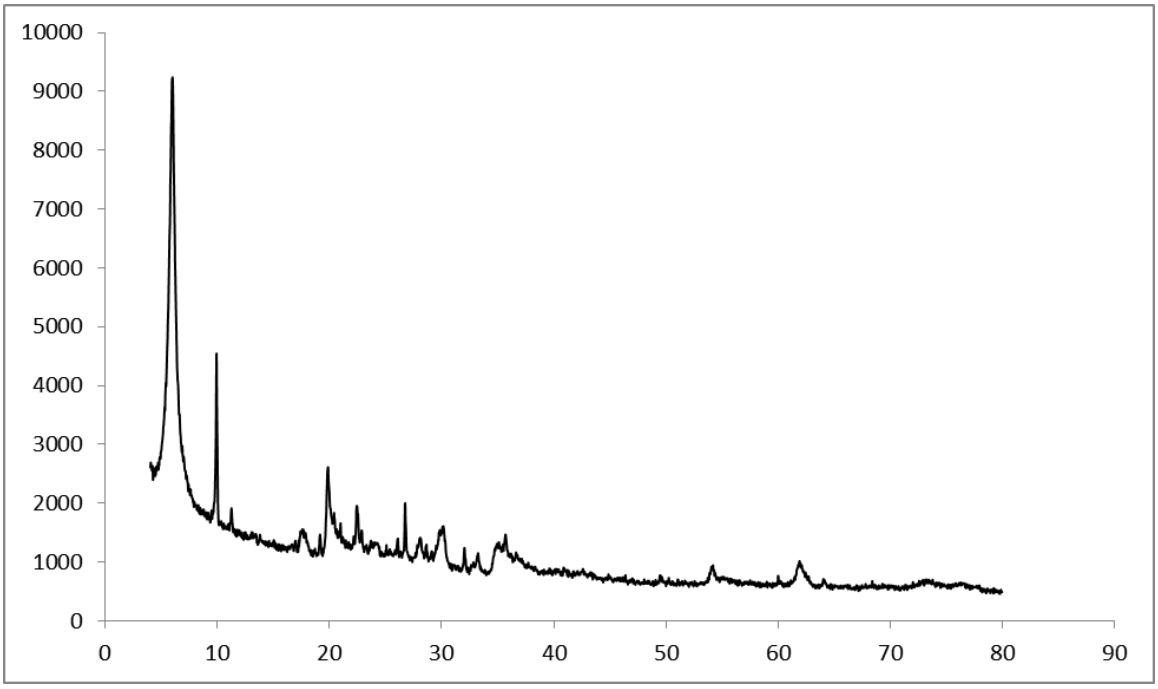

Sample Q11-48 (Mudrock)
Section: SE Tarlong UQZJ 18

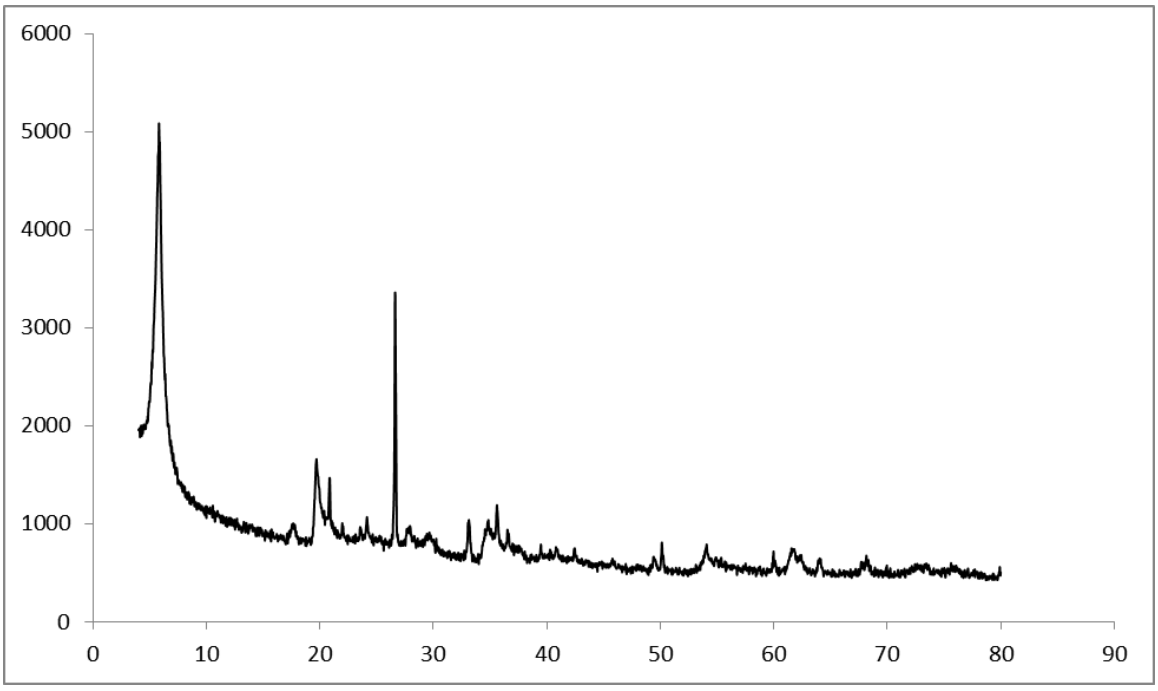

Sample Q12-5 (Mudrock)
Section: SE Tarlong UQZJ 18

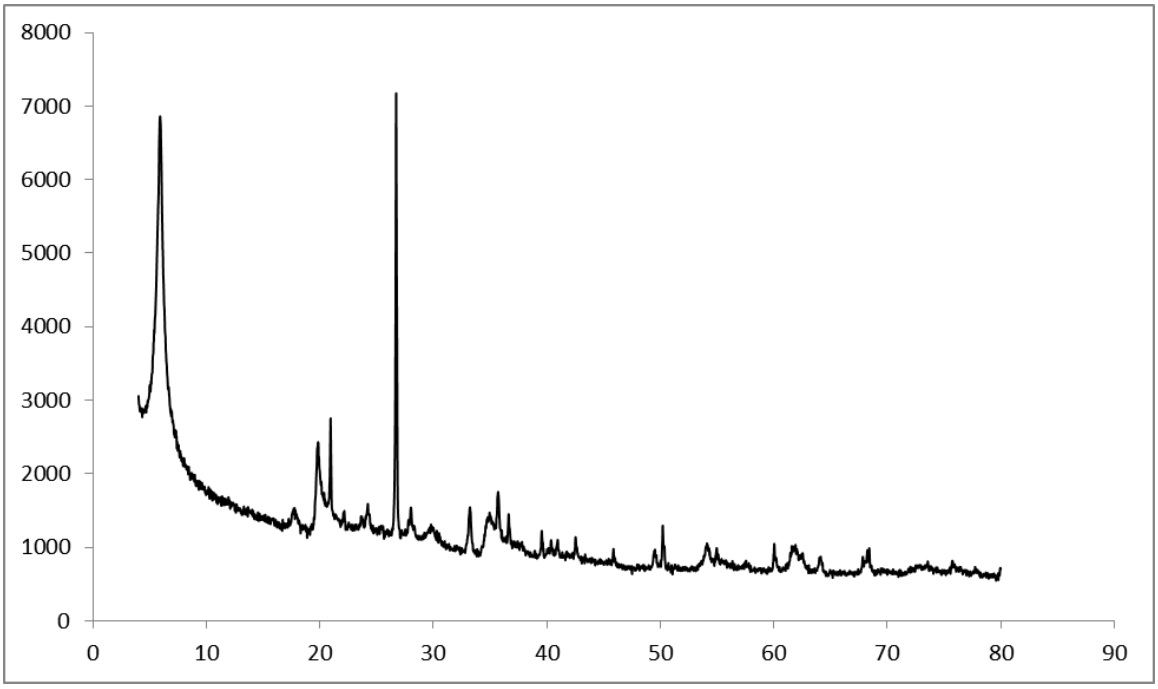

Sample SD11-31 (Mudrock)
Section: Dalongkou LQZJ 3

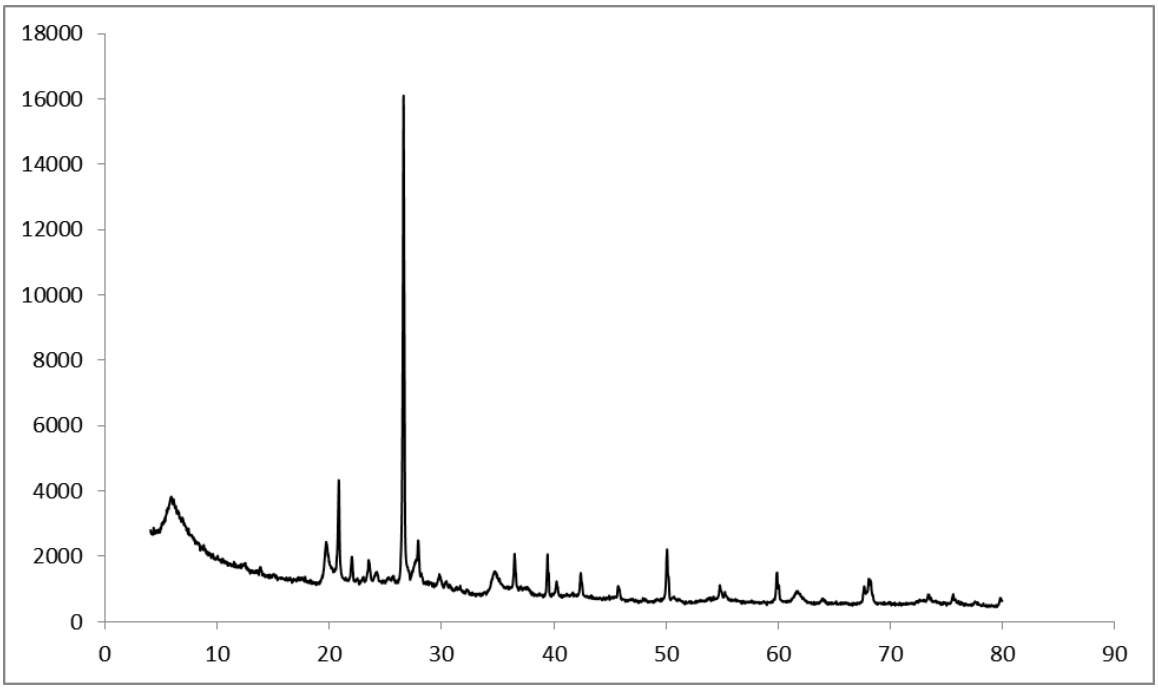

Sample SD11-27 (Mudrock)
Section: Dalongkou UQZJ 22

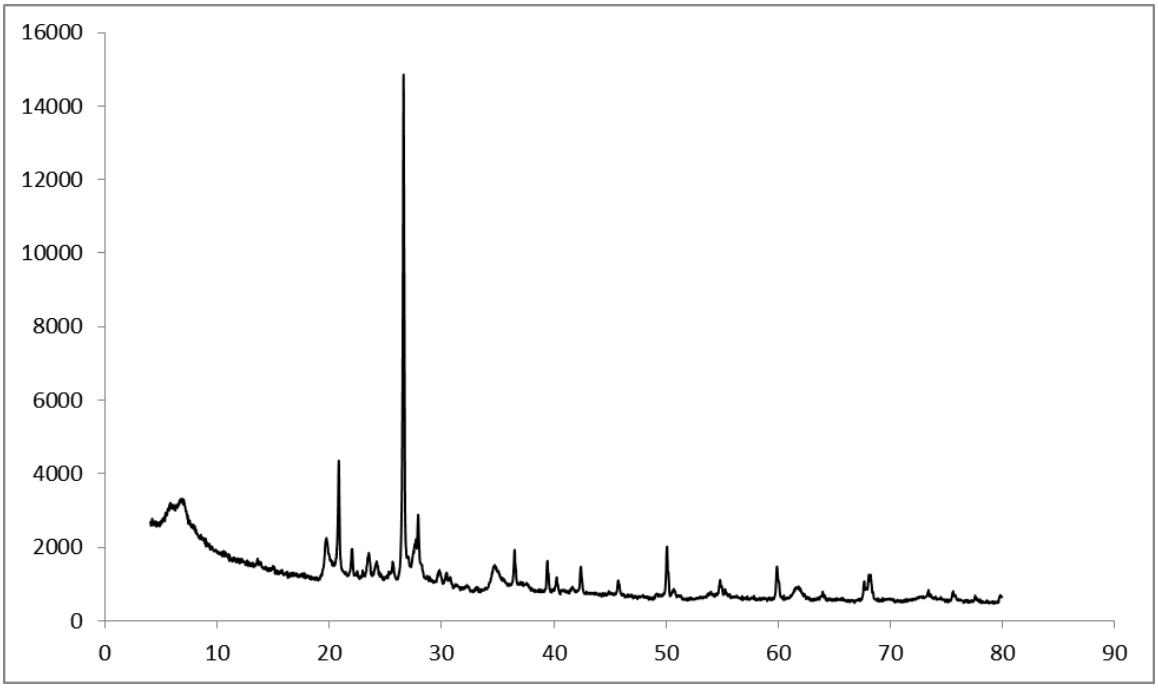

Sample SD11-22 (Mudrock)
Section: Dalongkou UQZJ 61

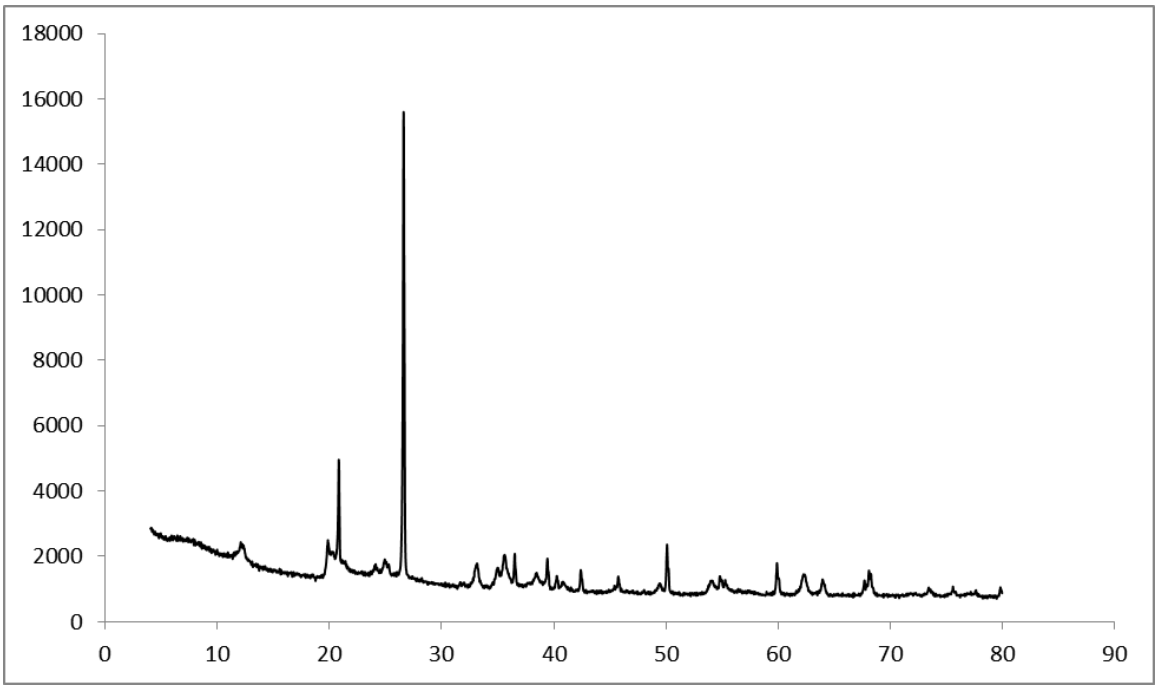

Clay Mineralogy

Sample S10-8 (Mudrock)
Section: NE Tarlong UQZJ 3

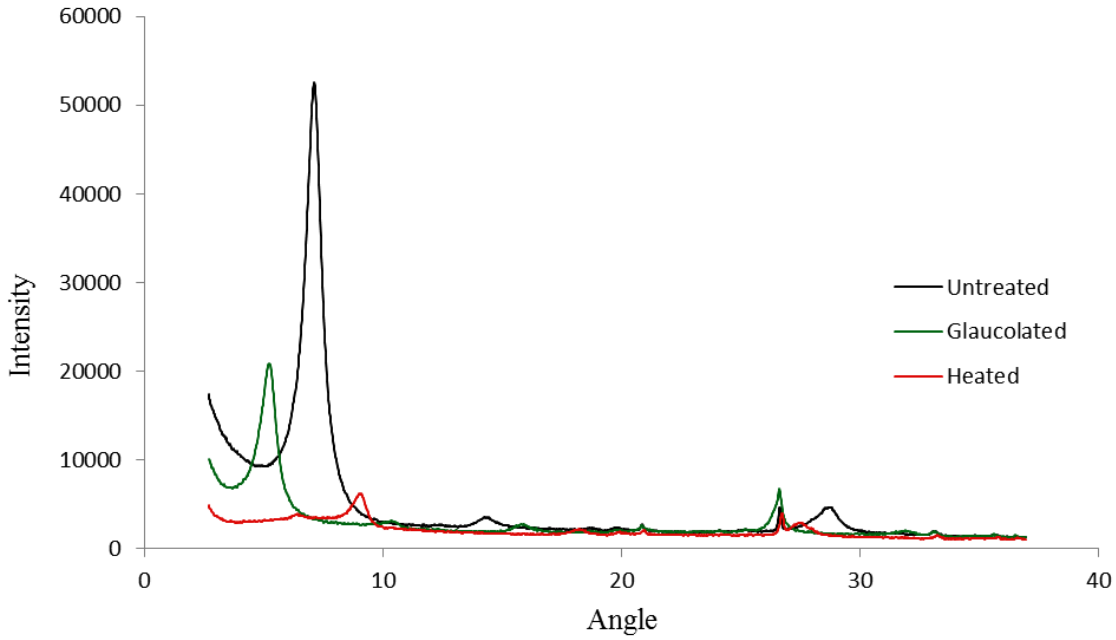

Sample Q11-1 (Mudrock)
Section: NE Tarlong UQZJ 3

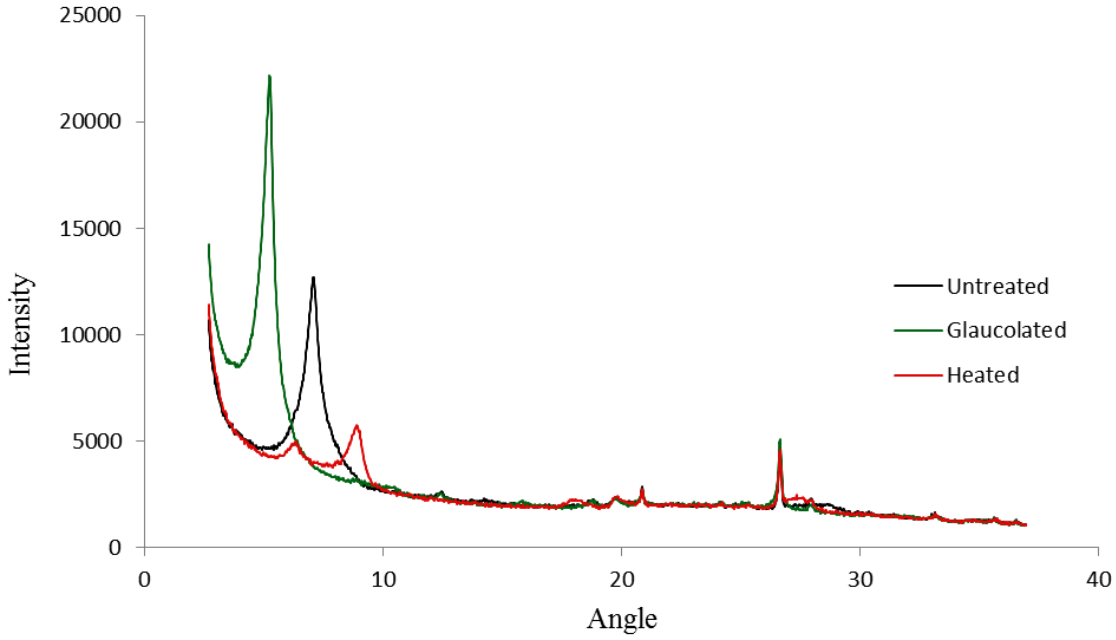

Sample Q11-2 (Mudrock)
Section: NE Tarlong UQZJ 3

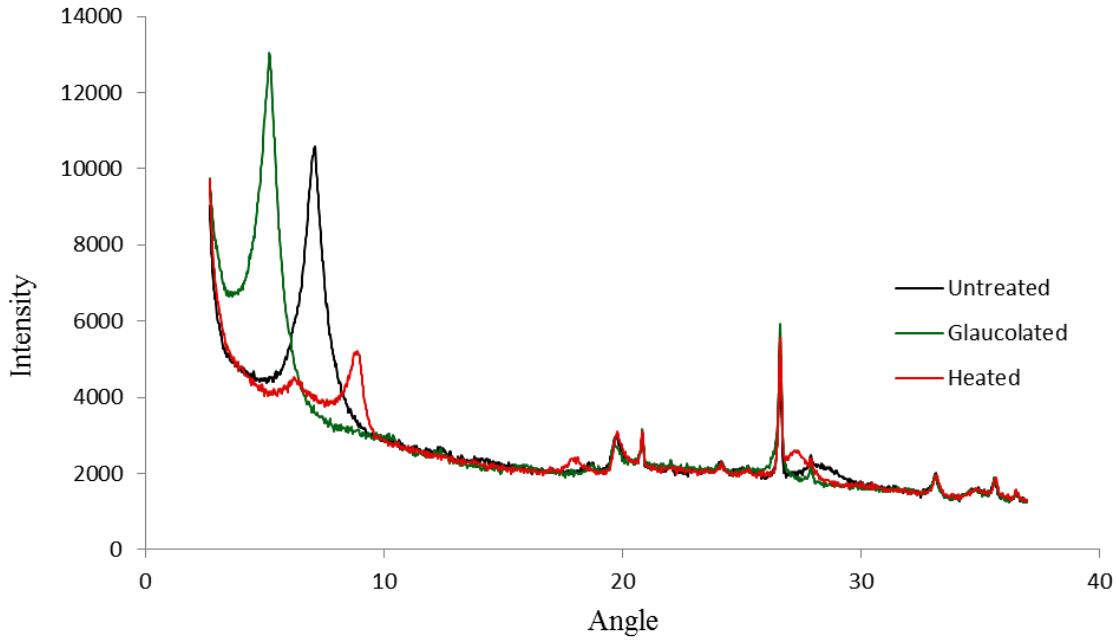

Sample Q11-3 (Mudrock)
Section: NE Tarlong UQZJ 3

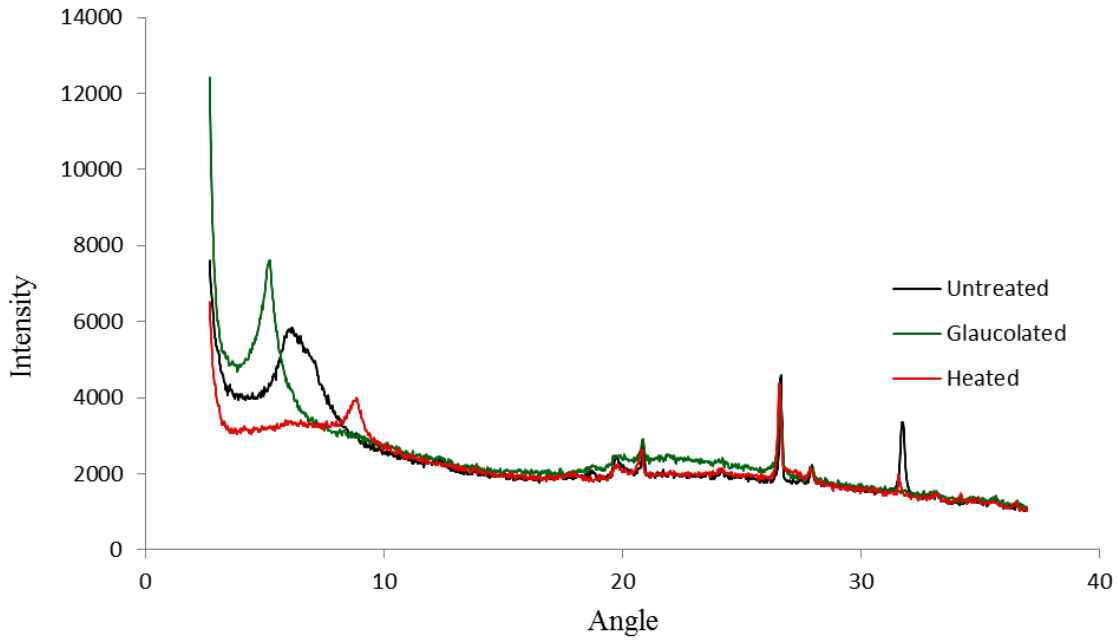

Sample Q11-4 (Mudrock)
Section: NE Tarlong UQZJ 3

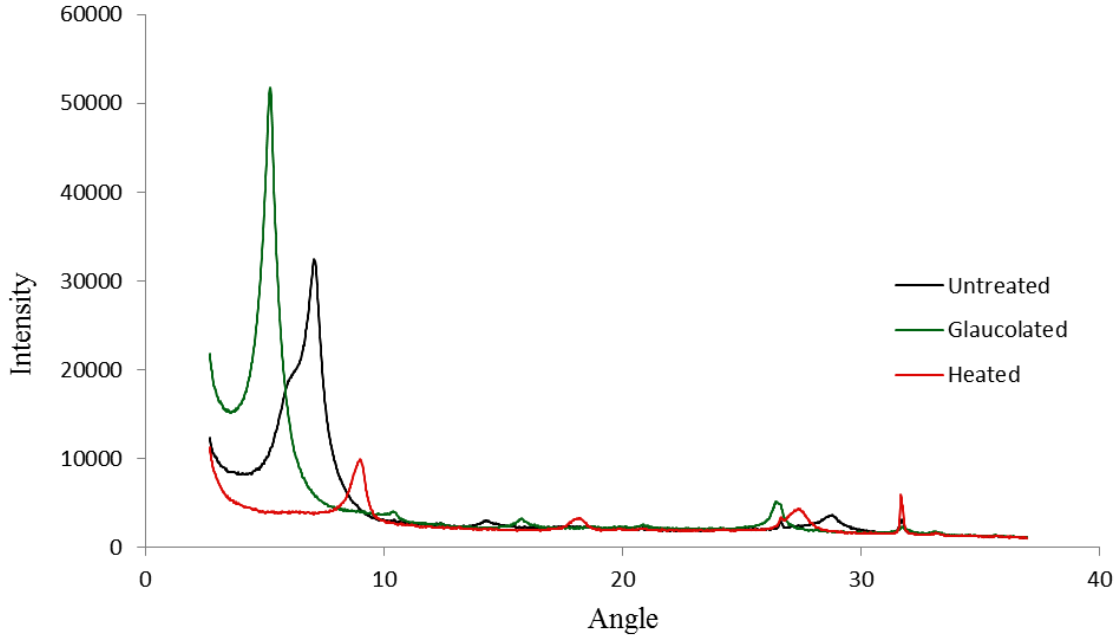

Sample S10-9 (Mudrock)
Section: NE Tarlong UQZJ 3

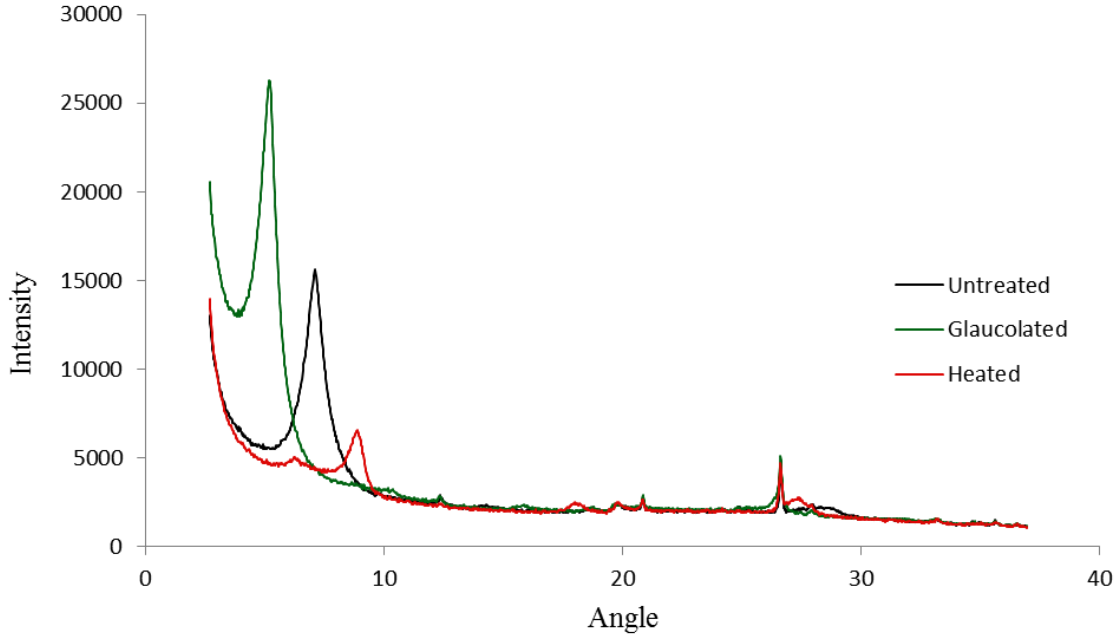

Sample Q11-5 (Mudrock)
Section: NE Tarlong UQZJ 3

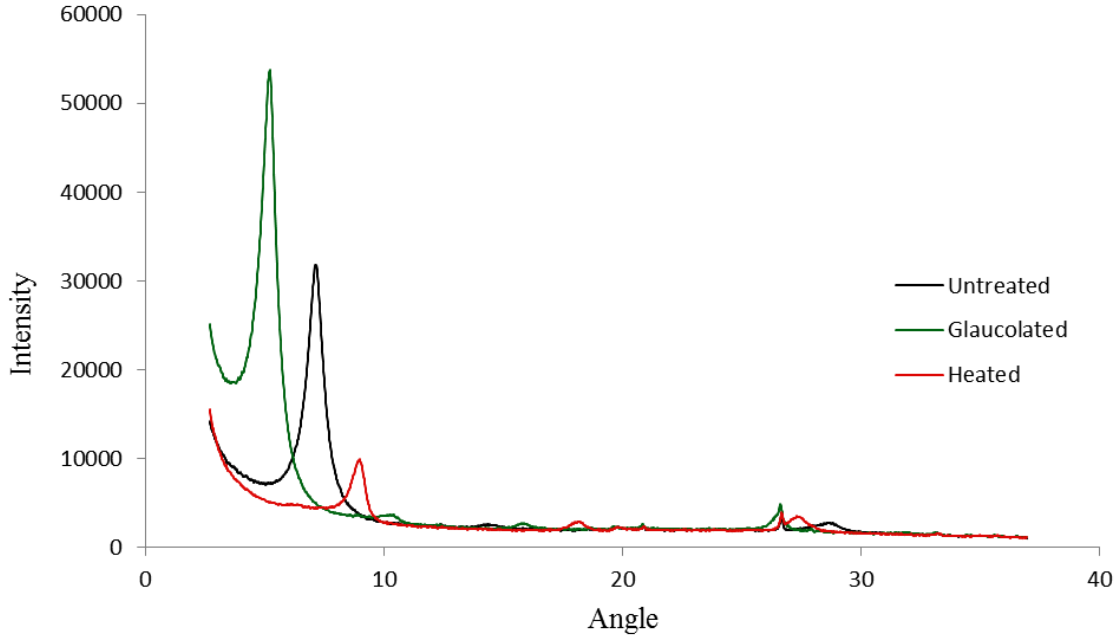

Sample S10-10 (Mudrock)
Section: NE Tarlong UQZJ 3

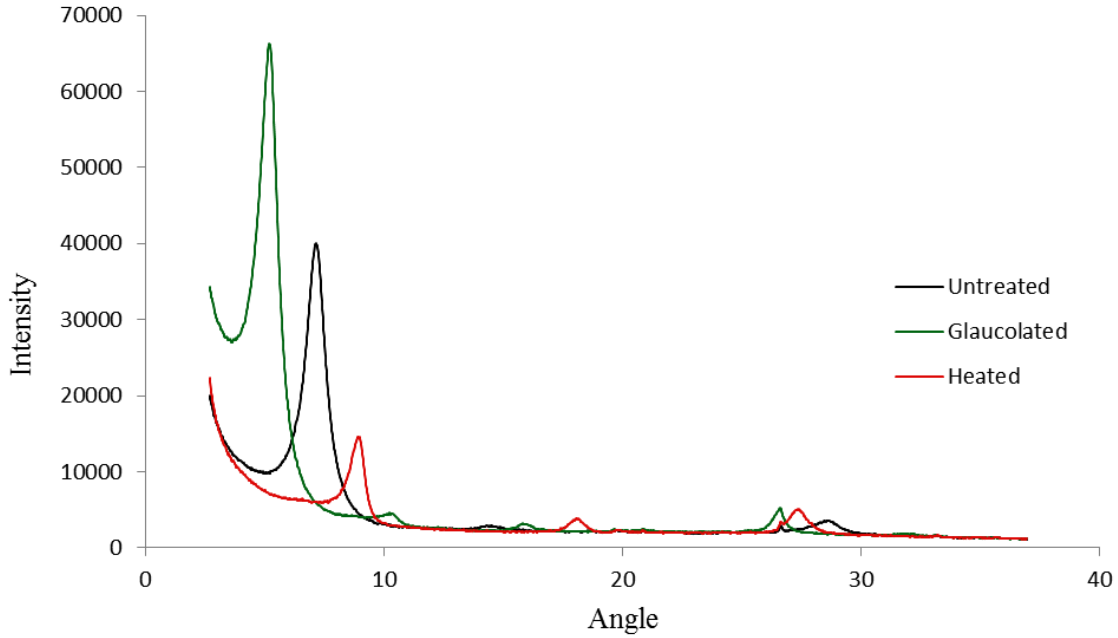

Sample Q11-6 (Mudrock)
Section: NE Tarlong UQZJ 3

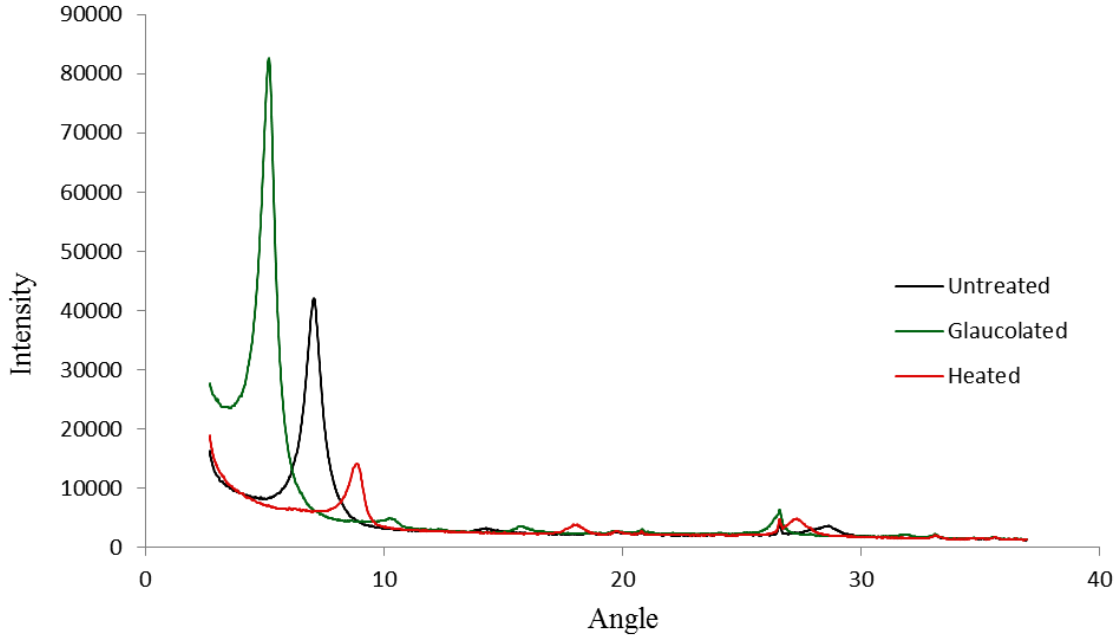

Sample S10-11 (Mudrock)
Section: NE Tarlong UQZJ 3

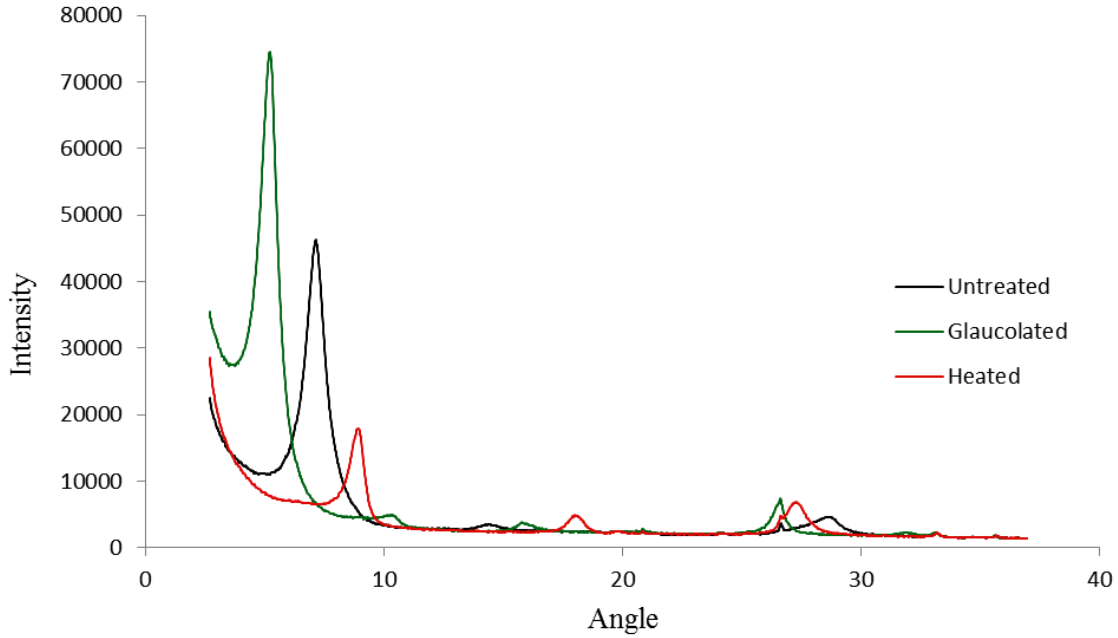

Sample S10-13 (Mudrock)
Section: NE Tarlong UQZJ 8

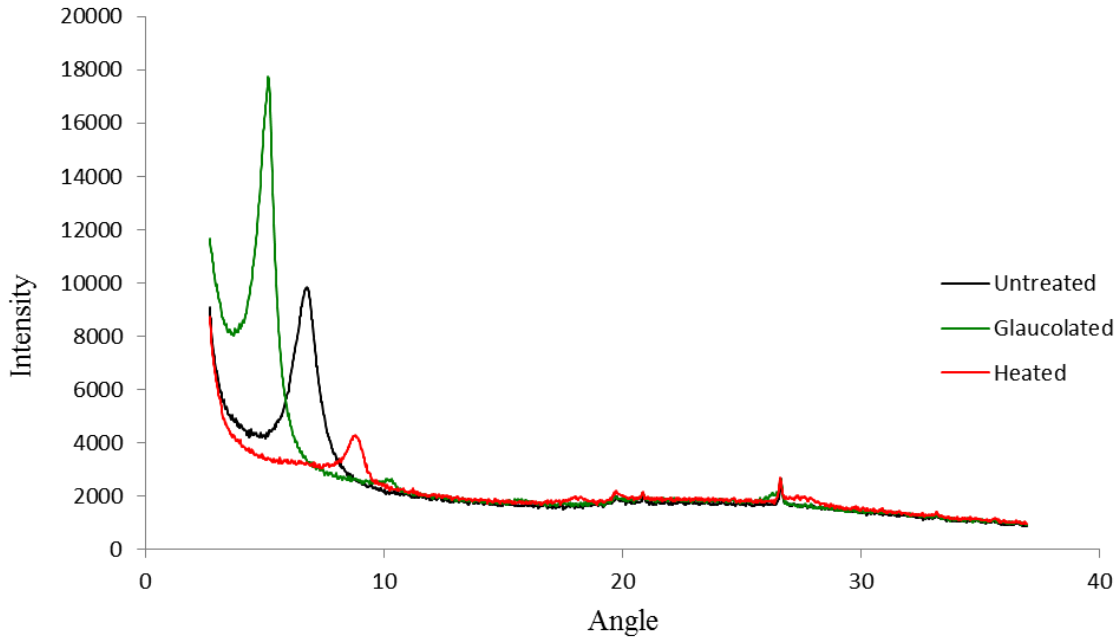

Sample Q11-8 (Mudrock)
Section: NE Tarlong UQZJ 8

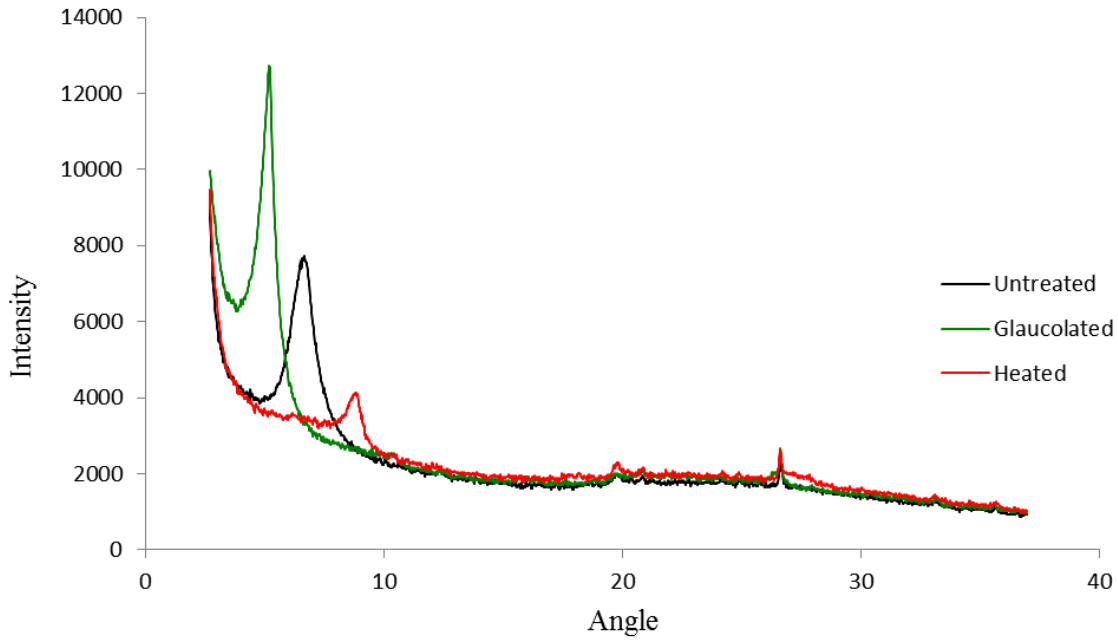

Sample Q11-9 (Mudrock)
Section: NE Tarlong UQZJ 8

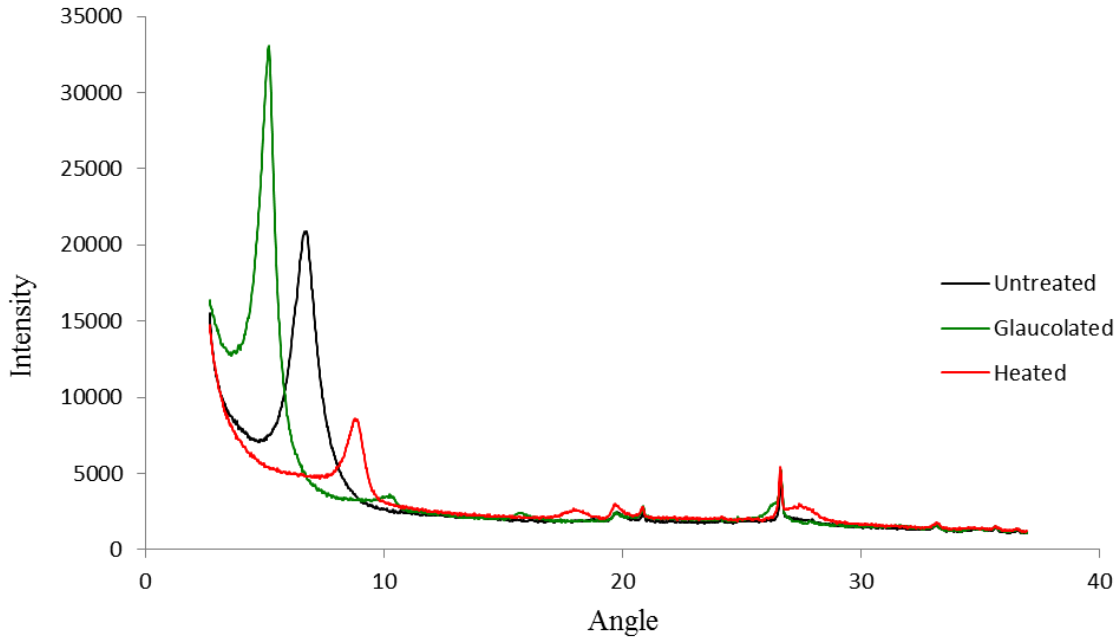

Sample S10-14 (Mudrock)
Section: NE Tarlong UQZJ 8

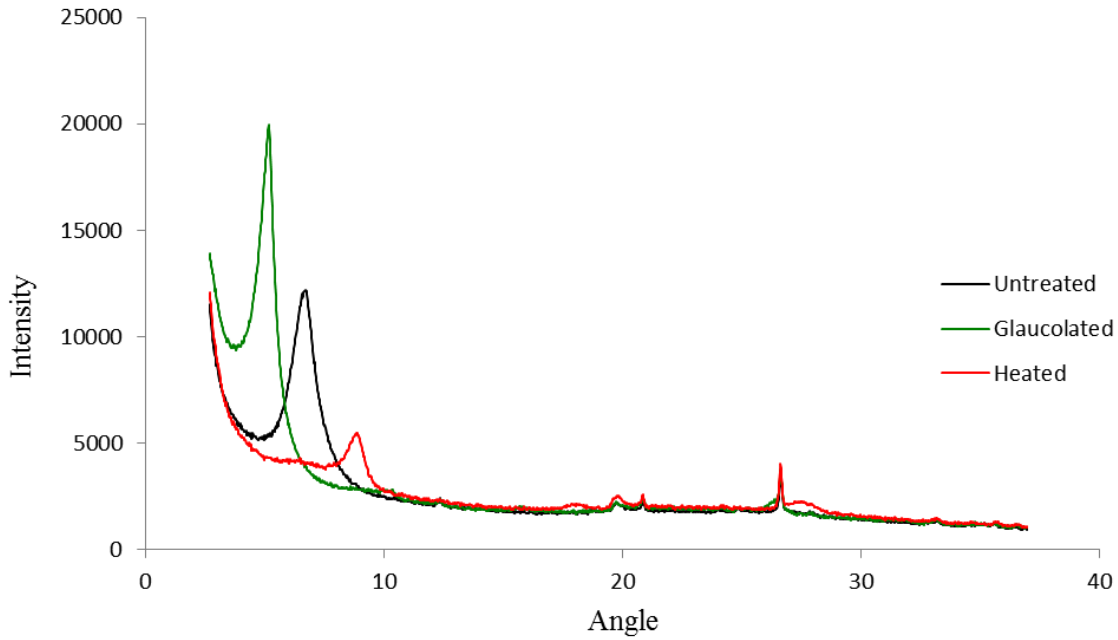

Sample Q11-10 (Mudrock)
Section: NE Tarlong UQZJ 8

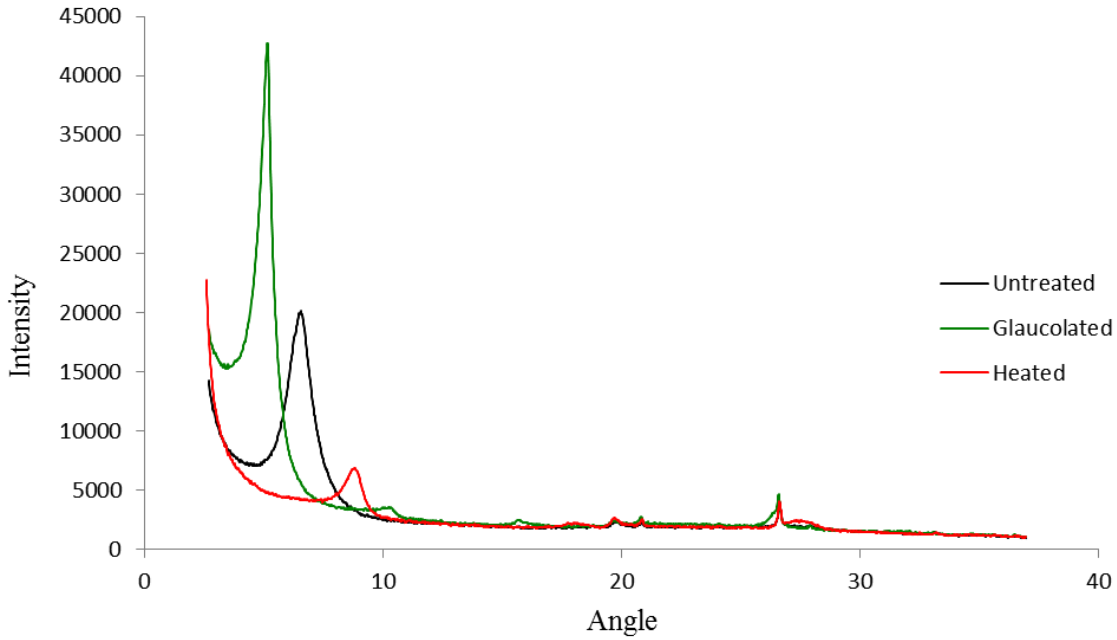

Sample S10-15 (Mudrock)
Section: NE Tarlong UQZJ 8

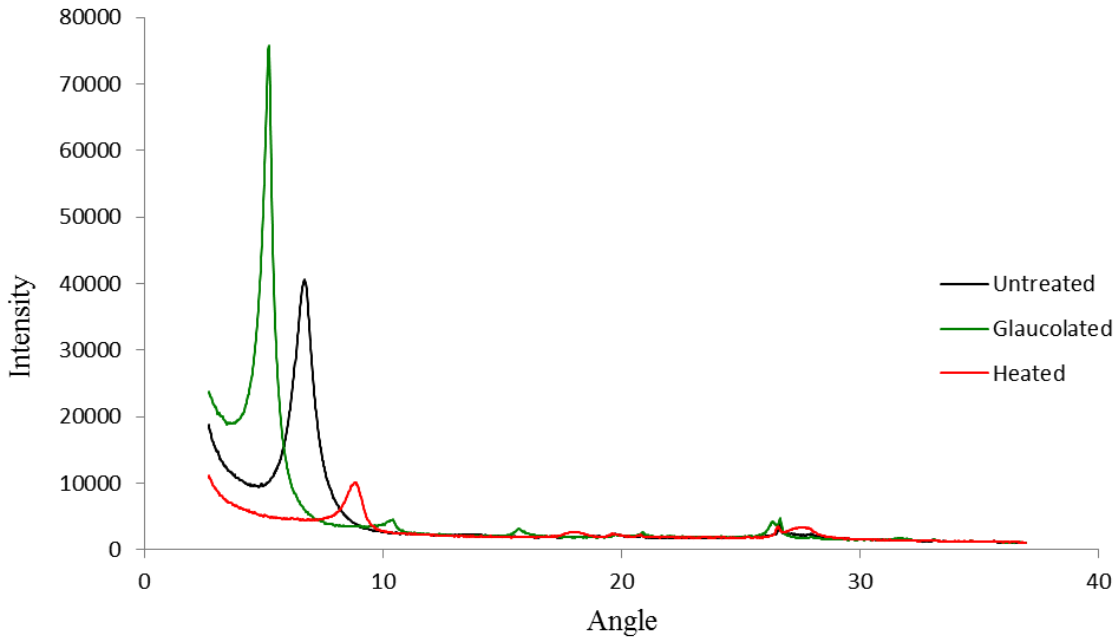

BIBLIOGRAPHY

Allen, M.B., Sengor, A.M.C., and Natal'in, B.A., 1995, Junggar, Turfan and Alakol basins as Late Permian to Early Triassic extensional structures in a sinistral shear zone in the Altaid orogenic collage, central Asia: Journal of the Geological Society, v. 152, p. 327-338.

Blum, M.D., and Törnqvist, T.E., 2000, Fluvial responses to climate and sea-level change: a review and look forward: Sedimentology, v. 47, p. 2-48.

Carroll, A.R., Graham, S.A., Hendrix, M.S., Ying, D., and Zhou, D., 1995, Late Paleozoic tectonic amalgamation of northwestern China: sedimentary record of the northern Tarim, northwestern Turpan, and southern Junggar Basins: Geological Society of America Bulletin, v. 107, p. 571-594.

Carroll, A.R., Graham, S.A., and Smith, M.E., 2010, Walled sedimentary basins of China: Basin Research, v. 2010, p. 17-32.

Carroll, A.R., Liang, Y., Graham, S.A., Xiao, X., Hendrix, M.S., Chu, J., and McKnight, C.L., 1990, Junggar basin, northwest China: trapped Late Paleozoic ocean: Tectonophysics, v. 183, p. 1-14.

Dickinson, W.R., 1985, Interpreting provenance relations from detrital modes of sandstones, *in* Zuffa, G.G., ed., Provenance of arenites: D. Reidel Publishing Company, p. 333-361.

Dickinson, W.R., Beard, L.S., Brakenridge, G.R., Erjavec, J.L., Ferguson, R.C., Inman, K.F., Knepp, R.A., Lindberg, F.A., and Ryberg, P.T., 1983, Provenance of North American Phanerozoic sandstones in relation to tectonic setting: Geological Society of America Bulletin, v. 94, p. 222-235.

Dickinson, W.R., and Suczek, C., 1979, Plate tectonics and sandstone composition: American Association of Petroleum Geologists Bulletin, v. 63, p. 2164-2182.

Fielding, C.R., Frank, T.D., Birgenheier, L.P., Rygel, M.C., Jones, A.T., and Roberts, J., 2008, Stratigraphic impring of the Late Paleozoic Ice Age in eastern Australia: a record of alternating glacial and nonglacial climate regime: Journal of the Geological Society, v. 165, p. 129-140.

Greene, T.J., Carroll, A.R., Wartes, M.A., Graham, S.A., and Wooden, J.L., 2005, Integrated provenance analysis of a complex orogenic terrane: Mesozoic uplift of the Bogda Shan and inception of the Turpan-Hami basin, NW China: Journal of Sedimentary Research, v. 75, p. 251-267.

Hsu, K.J., 1988, Relict back-arc basins: Principles of recognition and possible new examples from China, *in* Leinspell, K.L., and Paola, C., eds., New perspectives in basin analysis: Springer-Verlag, New York, p. 245-263.

Isbell, J.L., Fraiser, M.L., and Henry, L.C., 2008, Examining the complexity of environmental change during the late Paleozoic and early Mesozoic: Palaios, v. 23, p. 267-269.

Lowenstein, T.K., Hein, M.C., Bobst, A.L., Jordan, T.E., Ku, T.L., and Luo, S., 2003, An assessment of stratigraphic completeness in climate-sensitive closed-basin lake sediments: Salar de Atacama, Chile: Journal of Sedimentary Research, v. 73, p. 91-104.

Ludwig, K.R., 2003, User's Manual for Isoplot 3.00. Berkeley Geochronology Center: Berkeley, CA, 70 p.

Metcalfe, I., Foster, C.B., Afonin, S.A., Nicoll, R.S., Mundil, R., Xiaofeng, W., and Lucas, S.G., 2009, Stratigraphy, biostratigraphy and C-isotopes of the Permian-Triassic non-marine sequence at Dalongkou and Lucaogou, Xinjian Province, China: Journal of Asian Earth Sciences, v. 36, p. 503-520.

Miall, A.D., 1996, The geology of fluvial deposits: sedimentary facies, basin analysis, and petroleum geology: Springer, New York, 582 pp.

Olsen, P.E., 1997, Stratigraphic record of the Early Mesozoic breakup of Pangea in the Laurasia-Gondwana rift system: Annual Review of Earth and Planetary Sciences, v. 25, p. 337-401.

Shao, L., Stattegger, K., and Garbe-Schoenberg, C.-D., 2001, Sandstone petrology and geochemistry of the Turpan basin (NW China): implications for the tectonic evolution of a continental basin: Journal of Sedimentary Research, v. 71, p. 37-49.

Sheldon, N.D., Chakrabarti, R., Retallack, G.J., and Smith, R.M.H., 2014, Contrasting geochemical signatures on land from the Middle and Late Permian extinction events: Sedimentology, v. 61, p. 1812-1829.

Sláma, J., Košler, J, Condon, D.J., Crowley, J.L., Gerdes, A., Hanchar, J.M., Horstwood, M.S.A., Morris, G.A., Nasdala, L., Norberg, N., Schaltegger, U., Schoene, B. Tubrett, M.N, Whitehouse, M.J. 2008. Plešovice zircon - A new natural reference material for U–Pb and Hf isotopic microanalysis: Chemical Geology, v. 249, p. 1-35.

Suttner, L.J., and Dutta, P.K., 1986, Alluvial sandstone composition and paleoclimate, I. Framework mineralogy: Journal of Sedimentary Petrology, v. 56, p. 329-345.

Talbot, M.R., and Allen, P.A., 1996, Lakes, *in* Reading, H.G., ed., Sedimentary environments: processes, facies and stratigraphy: Blackwell Science, London, 83-124 pp.

Thomas, S.G., Tabor, N.J., Yang, W., Myers, T.S., Yang, Y., and Wang, D., 2011, Paleosol stratigraphy across the Permian-Triassic boundary, Bogda Mountains, NW China: implications for palaeoenvironmental transition through earth's largest mass extinction: Palaeogeography, Palaeoclimatology, Palaeoecology, v. 308, p. 41-64.

Wartes, M.A., Carroll, A.R., and Greene, T.J., 2002, Permian sedimentary record of the Turpan-Hami basin and adjacent regions, northwest China: constraints on postamalgamation tectonic evolution: Geological Society of America Bulletin, v. 114, p. 131-152.

Yang, W., Feng, Q., Liu, Y., Tabor, N., Miggins, D., Crowley, J.L., Lin, J., and Thomas, S., 2010, Depositional environments and cyclo- and chronostratigraphy of uppermost Carboniferous-Lower Triassic fluvial-lacustrine deposits, southern Bogda Mountains, NW China - A terrestrial paleoclimatic record of mid-latitude NE Pangea: Global and Planetary Change, v. 73, p. 15-113.

Yang, W., Liu, Y., Feng, Q., Lin, J., Zhou, D., and Wang, D., 2007, Sedimentary evidence of Early-Late Permian mid-latitude continental climate variability, southern Bogda Mountains, NW China: Palaeogeography, Palaeoclimatology, Palaeoecology, v. 252, p. 239-258.

VITA

Jonathan Obrist Farner obtained his B.A. in Psychology and B.S. in Geology from Wichita State University in May 2010. He obtained a M.S. in Geology and Geophysics in May 2012 and a Ph.D. in Geology and Geophysics in May 2015 from Missouri University of Science and Technology.